ADVANCING METHODS FOR APPORTIONING THE SOURCES OF SEDIMENT IN RIVERS: COMBINING SPECTROSCOPY AND STABLE ISOTOPES WITH BAYESIAN MIXING MODELS

BY

RICHARD JAMES COOPER

THESIS

Submitted to the School of Environmental Sciences,
University of East Anglia for the degree of

DOCTOR OF PHILOSOPHY

MAY 2015

I dedicate this thesis to the entire Wensum Alliance team

ABSTRACT

Sediment fingerprinting is a commonly employed technique for estimating sediment contributions from various eroding terrestrial sources to fluvial sediment load via a mixing model approach. However, there remain significant shortcomings in sediment fingerprinting practice, specifically relating to difficulties in producing high-temporal resolution apportionment estimates, inconsistencies in mixing model uncertainty representation, and a lack of attention given to organic matter provenance. Addressing these deficiencies, a combined X-ray fluorescence spectroscopy (XRFS) and diffuse reflectance infra-red Fourier transform spectroscopy (DRIFTS) approach is developed to rapidly, accurately and non-destructively analyse suspended particulate matter (SPM) geochemistry directly from sediment covered quartz fibre filter (QFF) papers at masses as low as 3 mg. An improved Bayesian source apportionment mixing model is then developed which allows for full characterisation of spatial geochemical variability, instrument precision and residual error, to yield a realistic and coherent assessment of the uncertainties associated with sediment fingerprinting estimates. Lastly, a novel application of a coupled molecular and $\delta^{2}H$ and $\delta^{13}C$ compound-specific isotope analysis (CSIA) of leaf wax *n*-alkane biomarkers is conducted to demonstrate the apportionment of plant-specific organic matter contributions to streambed sediments. Employing these developments in conjunction with automatic water samplers, high-temporal resolution SPM source apportionment estimates are derived throughout the progression of numerous storm events in a lowland agricultural catchment, revealing significant temporal variability in SPM provenance at 60- and 120-min resolution. Lower resolution, weekly, baseflow sampling is also performed, revealing distinct seasonal cycles in SPM geochemistry and sediment source apportionment over a 23-month period. Collectively, the developments presented in this thesis significantly advance sediment fingerprinting research by enabling organic and inorganic fluvial sediment fractions to be quantitatively apportioned at both low- and high-temporal resolution within realistic levels of uncertainty, thereby enhancing our understanding of sediment dynamics under a range of instream hydrological conditions.

THESIS CONTENTS

THESIS TABLES

THESIS FIGURES

ABBREVIATIONS

ACL	Average chain length
Al_{di}	Dithionate extractable aluminium
Al_{ox}	Oxalate extractable aluminium
ASE	Accelerated solvent extractor
CI	Credible interval
CLR	Centred log-ratio
C_{max}	Most abundant *n*-alkane
CPI	Carbon preference index
CSA	Critical source area
CSIA	Compound-specific isotope analysis
DAG	Directed acyclic graph
DOC	Dissolved organic carbon
DP	Dissolved phosphorus
DRIFTS	Diffuse reflectance infrared Fourier transform spectroscopy
DTC	Demonstration Test Catchment
DWPP	Diffuse water pollution plan
ELS	Entry level stewardship
EU	European Union
Fe_{di}	Dithionate extractable iron
Fe_{ox}	Oxalate extractable iron
FFD	Freshwater Fisheries Directive
GOF	Goodness-of-fit
GC-FID	Gas chromatography-flame ionisation detector
ICP-AES	Inductively coupled plasma atomic emission spectrometry
ICP-MS	Inductively coupled plasma mass spectrometry
ILR	Isometric log-ratio
KW	Kruskal-Wallis
LDA	Linear discriminant analysis
LOI	Loss-on-ignition
LOO	Leave-one-out
MC	Mean centred
MCMC	Markov chain Monte Carlo
MCF	Mass correction factor

MCSG	Mean centring and Savitzky-Golay smoothed
MSC	Multiplicative scatter correction
MVN	Multivariate normal
NPP	No pre-processing
NTU	Nephelometric turbidity units
OC	Organic carbon
OLS	Ordinary least squares
OM	Organic matter
OFAT	One-factor-at-a-time
PCA	Principal component analysis
PLS	Partial least squares
POC	Particulate organic carbon
PP	Particulate phosphorus
PSA	Particle size analysis
QFF	Quartz fibre filters
RMSEP	Root mean squared error of prediction
SAC	Special area of conservation
SEM	Scanning electron microscope
SIMM	Stable isotope mixing model
SG	Savitzky-Golay
SPM	Suspended particulate matter
SRP	Soluble reactive phosphorus
SS	Suspended sediment
SSA	Specific surface area
SSSI	Site of Special Scientific Interest
SSR	Sum of squared residuals
TAR	Terrestrial-to-aquatic ratio
TP	Total phosphorus
VE	Variance explained
VIF	Variance inflation factor
WFD	Water Framework Directive
XRFS	X-ray fluorescence spectroscopy

ACKNOWLEDGEMENTS

First and foremost, I have to thank my four fantastic supervisors for all the magnificent help and support they have given me over the past 3½ years, without which this thesis would never have got off the ground. Specifically, I thank Barry for his help during the early stages in getting the DRIFTS approach up and running and, perhaps more importantly, introducing me to R which has proved so invaluable. My thanks also go to Tobi, whose knowledge of all things Bayesian has helped me discover a whole new world of statistical modelling and uncertainty analysis. I have to sincerely thank Nikolai who kindly agreed to join my supervisory team late in the day and provided the inspiration for the stable isotope analysis. Finally, I express my deepest gratitude to Kevin for being a great primary supervisor, from the first day to the very last.

I reserve a special heartfelt thank you for the new friends made in the Wensum Alliance fieldwork team – Jenny, Zanist, Simon, Chris and Steve W. The endless 'banter', particularly during those long arduous days digging up porous pots, has made fieldwork a pleasure over the past 3 years, even during the coldest and wettest of days. I must also mention my great lab partner Ali, who helped get me through the long days and nights in the lab. My thanks go to the rest of the Wensum Alliance team – Faye, Gilla, Steve D., Ros, Andrew, Liz and Trudie – all fantastic people who have been a joy to get to know and work alongside. I must also thank Salle Farm Co. for their cooperation in granting land access to the Wensum DTC study area.

During my many hours working in UEA's laboratories I have been kindly helped by a number of technicians – Paul, Rob, John and Graham - to whom I am extremely grateful for the time and assistance they have given me. I am similarly very grateful for the help and time given by Gren and Andy whilst working at the BGS in Keyworth.

Lastly, I acknowledge the support of a NERC BGS Case studentship that helped fund this intellectual adventure.

Thank you to all for helping make my PhD journey an enjoyable one!

Chapter 1

INTRODUCTION

1.1 Research Rationale

During the past century, intensification of agriculture and extensive urbanisation have resulted in widespread sediment and nutrient enrichment of environmentally sensitive freshwater environments (Wilkinson, 2005; Cordell *et al*., 2009; Quinton *et al*., 2010). Fluvial systems affected by sustained high suspended particulate matter (SPM) concentrations experience an array of detrimental impacts which threaten sustainable ecosystem functioning. Elevated concentrations of fine clay and silt sized (<63 µm) sediment fractions increase water turbidity, restricting light penetration to underwater plants and thereby lowering rates of photosynthesis and dissolved oxygen concentrations. Sediments smother gravel salmonid spawning grounds and benthic habitats, reduce oxygen circulation through the streambed, clog fish gills and abrasively scour macrophytes, periphyton and small invertebrates (Acornley and Sear, 1999; Hilton *et al*., 2006; Bilotta and Brazier, 2008). SPM is also a major vector for the transport of nutrients and other potentially toxic pollutants due to its high surface area providing ample opportunity for the sorption of dissolved constituents (House *et al*., 1995; Russell *et al*., 1998; Evans *et al*., 2004). In fact, previous research has found that up to 90% of total phosphorus (TP) load is transported in association with the fine grained sediment fraction in rural UK catchments (He *et al*., 1995; Walling *et al*., 1997; Bowes *et al*., 2003). This means nutrient rich SPM plays an important role in the development of eutrophic conditions, fuelling blooms of phytoplankton, periphyton and neuro-toxin secreting cyanobacteria colonies, which can dramatically lower species diversity and lead to a fundamental breakdown of ecosystem functioning (Smith *et al*., 1999; Hilton *et al*., 2006; Wither and Jarvie, 2008). Ultimately, the degree of environmental degradation caused by elevated sediment concentrations is highly variable and known to be a function of sediment concentration, chemical composition, particle size, duration of exposure, species sensitivity and the seasonal timing of enrichment (Bilotta and Brazier, 2008; Bilotta *et al*., 2012).

Alongside ecological concerns there are also economic impacts to consider, with high rates of sedimentation reducing navigability, enhancing flood risk, increasing dredging requirements, increasing water treatment costs and reducing the lifetimes of dams and reservoirs (Pretty *et al*., 2003; Hilton *et al*., 2006; Owens *et al*., 2010).

Under national and international legislation, such as the US Clean Water Act (1972) and the EU Water Framework Directive (2000/60/EC), governments have an obligation to ensure that water bodies achieve good ecological and chemical status. Some legislation, such as the EU Freshwater Fisheries Directive (78/659/EEC; 2006/44/EC), sets a guideline of 25 mg L^{-1} of SPM in waters suitable for salmonid (e.g. salmon, trout, char) and cyprinid (e.g. carp, minnow, barbel) fish populations during normal flow conditions. Unfortunately, many fluvial systems across Europe are at risk of failing to achieve recommended standards in water quality due to excessively high sediment ingress from the eroding terrestrial environment (Environment Agency, 2009). Mitigation measures are therefore required to help reduce the amount of land-to-river sediment transfer. However, for these to be targeted effectively, it is essential to first understand the provenance of these fluvial sediments.

In response to this requirement, sediment source apportionment research has become increasingly common over recent years as a method for estimating the sediment contribution from various eroding terrestrial sources to fluvial sediment load via a mixing model approach (Figure 1.1). This technique relies on selecting appropriate markers or 'fingerprints' that are transported from the source to the target in a reliable manner through well understood biotic or abiotic pathways. It is important to recognise that the terms sediment 'tracing', sediment 'fingerprint' and sediment 'source apportionment' are frequently used interchangeably within the literature to describe this technique, but a distinction should be made to avoid confusion. Specifically, sediment 'tracing' more commonly refers to the process where known sediment sources are marked, for example with fluorescent dye, and their progression *downstream* to a certain point in the river is tracked. This differs from sediment 'fingerprinting' and 'source apportionment' which can be referred to as an *upstream* process, whereby the origin of fluvial sediments is unknown and has to be determined based on the known geochemistry of the target sediments and that of potential sediment source areas across the catchment (Koiter *et al*., 2013).

A variety of fingerprints have been used to help differentiate potential sediment source areas, including major and trace elements (Walling *et al*., 2008; Evrard *et al*., 2011;

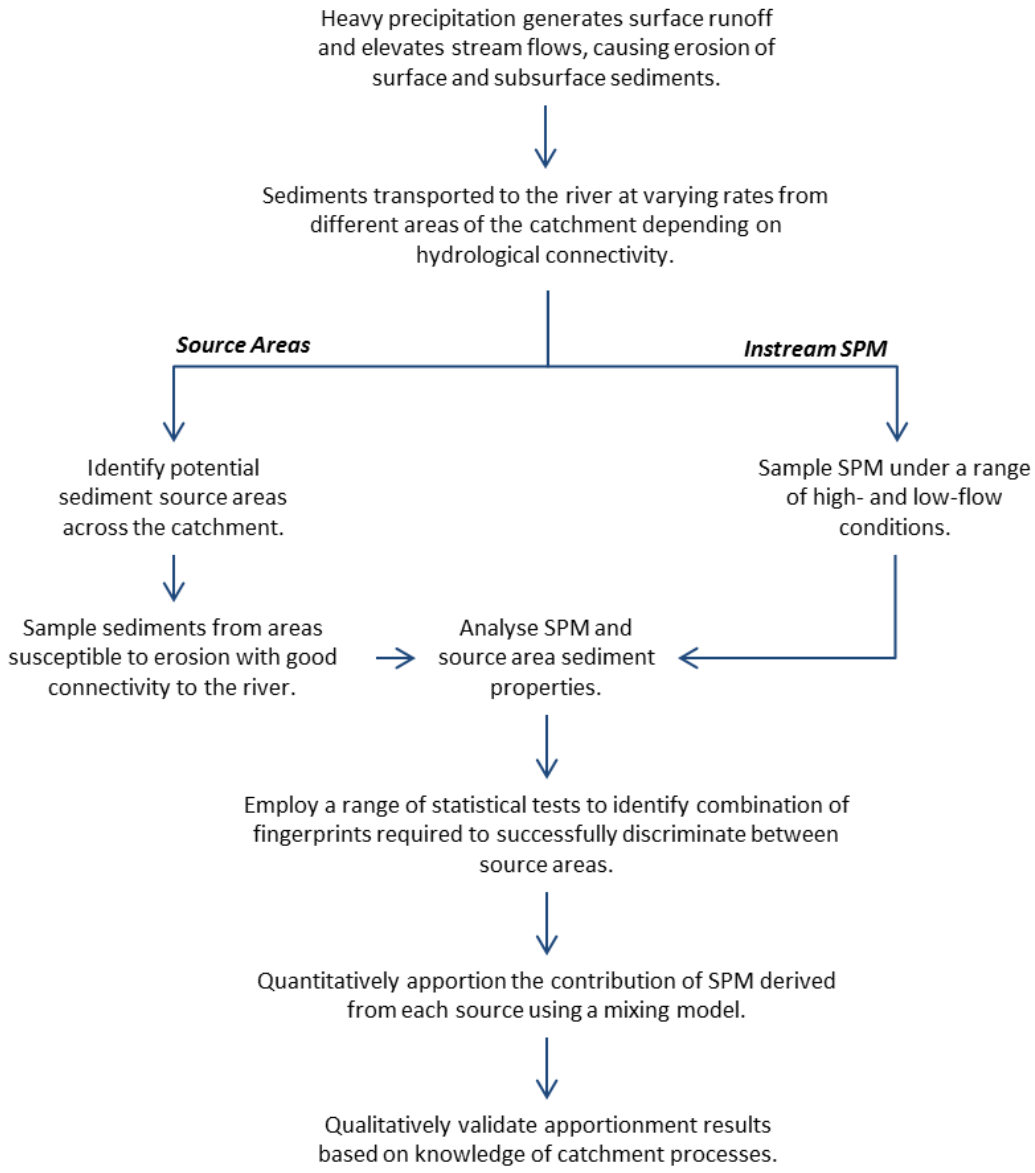

Figure 1.1: A conceptual diagram of the sediment source apportionment procedure.

Navratil *et al.*, 2012), colour coefficients (Martínez-Carreras *et al.*, 2010a), fallout radionuclides (Huisman and Karthikeyan, 2012; Olley *et al.*, 2013; Smith *et al.*, 2013; Theuring *et al.*, 2013), mineral magnetism (Russell *et al.*, 2001; Blake *et al.*, 2004), organic and inorganic carbon (Schindler Wildhaber *et al.*, 2012a; Slimane *et al.*, 2013) and compound-specific stable isotopes (Blake *et al.*, 2012; Hancock and Revill, 2013). These have helped to identify sediment contributions from a variety of sources, including arable topsoils (Collins and Walling, 2007; Martinez-Carreras *et al.*, 2010a), stream channel banks (Collins *et al.*, 2013b; Haddadchi *et al.*, 2014), forests and woodlands (Walling, 2005; Schuller *et al.*, 2013; Yao *et al.*, 2013), pasture and grassland (Russell *et al.*, 2001; Walling *et al.*, 2008), roads and road verges (Motha *et al.*, 2004; Collins *et al.*,

2010; 2013a), urban areas (Devereux *et al*., 2010; Franz *et al*., 2014), wildfire burned land (Blake *et al*., 2009; Smith *et al*., 2013; Stone *et al*., 2014) and geological provinces (Evrard *et al*., 2011; D'Haen *et al*., 2012; Navratil *et al*., 2012; Fryirs and Gore, 2013).

A wide range of mixing model approaches have also been employed to quantitatively assess sediment volumes derived from each source area, with models ranging in complexity from simple optimisation routines (e.g. Collins *et al*., 1997; Gruszowski *et al*., 2003) to more complex and comprehensive Bayesian uncertainty assessments (e.g. Fox and Papanicolaou, 2008; D'Haen *et al*., 2012). The large number of existing sediment fingerprinting studies indicates this technique is now a common analytical tool (Guzman *et al*., 2013; Walling, 2013). Importantly, because fingerprinting fluvial sediments allows the sources of sediment from across the entire catchment to be apportioned, it has significant advantages over more conventional erosion monitoring techniques (e.g. erosion pins, remote sensing, field surveys, profiling) which are considerably more localised and require a greater understanding of the sediment mobilisation and transportation linkages to be able to determine exported loads at the catchment outlet (Collins and Walling, 2004). However, there remain significant shortcomings in current fingerprinting practice which provided the motivation to advance sediment source apportionment methods. In this thesis, three main areas requiring further development were addressed, namely:

(i) **High-resolution monitoring**: With approximately 90% of SPM transported during less than 20% of the year during storm events (e.g. Horowitz, 2008; Bilotta *et al*., 2010; Oeurng *et al*., 2010, 2011), regular high-resolution monitoring is essential in order to obtain a detailed understanding of the geochemical processes occurring in these dynamic high-flow periods. In particular, understanding how the provenance of SPM changes during the course of a precipitation event, for example at hourly resolution, has the potential to yield important information for catchment managers looking to mitigate land-to-river sediment transfers (Legout *et al*., 2013). To date such studies have been rare because the required high-temporal resolution information is often too expensive and time consuming to collate (Walling, 2013). However, high-temporal resolution geochemical data are essential if one is to understand catchment processes sufficiently well to enable erosion mitigation measures to be targeted effectively. Recent progress has been made in this area with the development of infrared spectroscopy as a rapid, accurate and inexpensive technique to analytically determine fingerprint properties using relatively small volumes of sediment (e.g. Poulenard *et al*., 2009, 2012; Martínez-Carreras *et al*.,

2010b; Evrard *et al.*, 2013). However, further research is required into the effectiveness of different types of spectroscopy such that a wider suite of fingerprints can be determined.

(ii) Mixing model uncertainty: Considerable differences exist in the way previous sediment fingerprinting studies have incorporated sources of uncertainty into sediment mixing models. Earlier traditional, or so called 'frequentist', fingerprinting studies estimated sediment source contributions by optimising mixing model parameters using simply the means or medians of the input data constellations (e.g. Collins *et al*., 1997; Gruszowski *et al.*, 2003). This approach was of limited use as the omission of measurement error, source variability and residual model error meant that the mixing model failed to provide any measure of the uncertainties surrounding the 'optimal' source contribution. This failing encouraged more recent studies to couple the parameter optimisation with Monte-Carlo based stochastic sampling of input/output data constellations which reflect information on source and target sediment variability available through repeat measurements (e.g. Motha *et al.*, 2003; Collins *et al.*, 2013a; Wilkinson *et al*., 2013). However, these approaches can still be considered somewhat inconsistent since two different error assumptions are used (one for the Monte-Carlo simulation and one for the likelihood function to be maximised) thus making interpretation of uncertainties unrealistic. An alternative, consistent and flexible framework for dealing with all perceived uncertainties in sediment mixing models is available through Bayesian statistics (e.g. Fox and Papanicolaou, 2008; Palmer and Douglas, 2008; Rowan *et al.*, 2011; D'Haen *et al.*, 2012; Massoudieh *et al.*, 2012; Dutton *et al*., 2013). These Bayesian approaches are advantageous over traditional optimisation methods as they allow all known and residual uncertainties associated with the mixing model and the dataset to be coherently translated into parameter probability distributions. However, there still remain significant methodological differences in the Bayesian frameworks used, and further research is required to investigate the choice of appropriate error models.

(iii) Organic matter apportionment: The vast majority of sediment source apportionment studies have tended to focus solely on the inorganic sediment fraction by using inorganic fingerprints, such as major or trace metals, to identify sediment source areas (e.g. Collins *et al*., 2010; Thompson *et al*., 2013). This has meant the important organic matter component has largely been ignored, with only a handful of studies using stable isotopes of carbon to fingerprint organic matter contributing sources (Blake *et al.*, 2012; Hancock and Revill, 2013). As a result, apportionment

estimates which fail to account for this organic fraction may misrepresent the loads of organic material derived from each individual source, particularly if organic and inorganic material originates from difference sources. Soil organic carbon loss as a result of intensive arable cultivation represents a significant threat to long-term soil fertility and stability (Loveland and Webb, 2003), whilst organic matter within fluvial environments can significantly influence dissolved oxygen concentrations and the transport of phosphorus (P) and other contaminants which adsorb to its surface (Withers and Jarvie, 2008). Further research is therefore required to examine suitable methods for identifying and apportioning different sources of organic matter within stream sediments to enable a complete picture of both organic and inorganic sediment provenance to be obtained (Granger *et al*., 2007).

1.2 Primary Research Aim

To advance existing methods for apportioning the sources of fluvial sediment by combining spectroscopy and stable isotope analysis with Bayesian mixing models to improve the temporal resolution of source apportionment, the assessment of uncertainty and the identification of organic matter provenance.

1.3 Research Objectives

(i) To develop rapid, accurate, inexpensive and non-destructive methods for assessing the geochemistry of SPM at high-temporal resolution directly from sediment covered filter papers via a combined X-ray fluorescence spectroscopy (XRFS) and diffuse reflectance infra-red Fourier transform spectroscopy (DRIFTS) approach.

(ii) To improve existing source apportionment mixing models by formulating a consistent and flexible Bayesian mixing model framework that is able to provide a full and coherent characterisation of all perceived uncertainties associated with the sediment fingerprinting procedure.

(iii) To apportion, with uncertainty, the sources of SPM in a lowland, intensive arable, headwater catchment at high-temporal resolution under both low- and high-flow conditions.

(iv) To demonstrate how a novel, coupled, molecular and compound-specific carbon ($\delta^{13}C$) and hydrogen ($\delta^{2}H$) stable isotope analysis of plant lipid extracts can be used to identify and quantitatively apportion the origins of organic matter present in fine (<63 μm) streambed sediments.

(v) To explore the temporal dynamics of SPM geochemistry and sediment source apportionment at hourly-to-seasonal timescales, with specific emphasis upon the organo-mineral controls on particulate phosphorus (PP) variability under high- and low-flow conditions.

1.4 Broader Significance

This research was carried out as part of the wider UK Demonstration Test Catchment (DTC) project. The DTC platform represents a joint initiative between the Environment Agency, the Department for Environment, Food and Rural Affairs (Defra), and the Welsh Assembly Government, working in three UK catchments (River Avon, Hampshire; River Eden, Cumbria; River Wensum, Norfolk) to evaluate the extent to which on-farm mitigation measures can cost-effectively reduce the impacts of diffuse water pollution on river ecology while still maintaining food production capacity (Outram *et al*., 2014; Wensum Alliance, 2014). The project aims to build partnerships, foster stakeholder stewardship and enhance knowledge exchange by bringing together land owners, farmers, scientists, public agency officials and non-governmental organisations to help tackle the problem of catchment wide diffuse pollution from agriculture. Diffuse agricultural pollution is estimated to account for approximately 25% of phosphorus, 60% of nitrates and 70% of sediment inputs into UK rivers nationally (Edwards and Withers, 1998; Defra, 2011), and thus the advancements in sediment source apportionment presented here represent an important contribution to achieving the overall goals of the DTC project.

1.5 Thesis Outline

In Chapter 2, background information is presented on the study location for this research – the River Wensum catchment, Norfolk, UK. Specifically, details of the Wensum DTC monitoring network in the Blackwater sub-catchment are presented, alongside information on catchment land use, climate and the ecological significance of

this lowland, calcareous river system. Chapter 3 presents the important methodological development that is the direct spectroscopic analysis of sediment covered filter papers for high-temporal resolution monitoring of SPM geochemistry. Similarly, Chapter 4 presents the important development of a new and improved Bayesian sediment source apportionment mixing model and explores the impact of different model structures and uncertainty parameterisations via a one-factor-at-a-time (OFAT) sensitivity analysis. In Chapter 5, the methodological developments presented in Chapters 3 and 4 are applied to quantitatively apportion the sources of SPM at high-temporal resolution during a selection of heavy precipitation events. In Chapter 6, a novel, integrated molecular and compound-specific carbon and hydrogen stable isotope analysis of plant *n*-alkanes is conducted to identify and apportion the sources of organic matter present within streambed sediments over a 7-month period. Chapter 7 explores evidence for diel and seasonal cycles in SPM geochemistry and sediment source apportionment between May 2012 and March 2014, whilst also examining the role of organo-mineral relationships in controlling SPM P concentrations under high- and low-flow conditions. Finally, overall conclusions from this research are drawn together in Chapter 8.

Chapter 2

STUDY LOCATION: THE RIVER WENSUM CATCHMENT

2.1 The River Wensum

The River Wensum is a 78 km long, nutrient enriched, lowland calcareous river that rises near the village of South Raynham, west Norfolk (52°46'N, 0°47'E) ~75 m above sea level and flows southeast before merging with the River Yare south of Norwich (Figure 2.1). In 1993, a 71 km stretch of the Wensum from South Raynham to Hellesdon Mill was designated a whole river Site of Special Scientific Interest (SSSI) in recognition of it being one of the best examples of a lowland calcareous river in the UK (Sear *et al.*, 2006). In 2001, the Wensum was given further European Special Area of Conservation (SAC) status due to the diversity of its internationally important flora and invertebrate fauna. Under the conservation objectives of the SAC, habitat quality must be maintained in a favourable condition for water crowfoot (*Ranunculus fluitans*) and water starwort (*Callitriche palustris*) communities, as well as for populations of the protected Bullhead (*Cottus gobio*), Brook Lamprey (*Lampetra planeri*), white-clawed crayfish (*Austropotamobius pallipes*) and Desmoulin's whorl snail (*Vertigo moulinsiana*).

However, the ecological condition of the Wensum is in decline, with 99.4% of the protected habitat considered to be in an unfavourable or declining state due, primarily, to excessive sediment and nutrient loadings from agriculture and sewage treatment works (Grieve *et al*., 2002; Sear *et al.*, 2006). Morphologically, the river is also in poor condition having experienced a long history of anthropogenic modification in order to drain the surrounding land for agriculture. Over deepening, widening, straightening, regular dredging, impounding by mill structures and removal of riparian vegetation have resulted in the river becoming disconnected from its floodplain and being characterised by high nutrient concentrations, high rates of siltation and the loss of important fish spawning gravel bed habitats (Sear *et al.*, 2006; Coombes *et al.*, 2007).

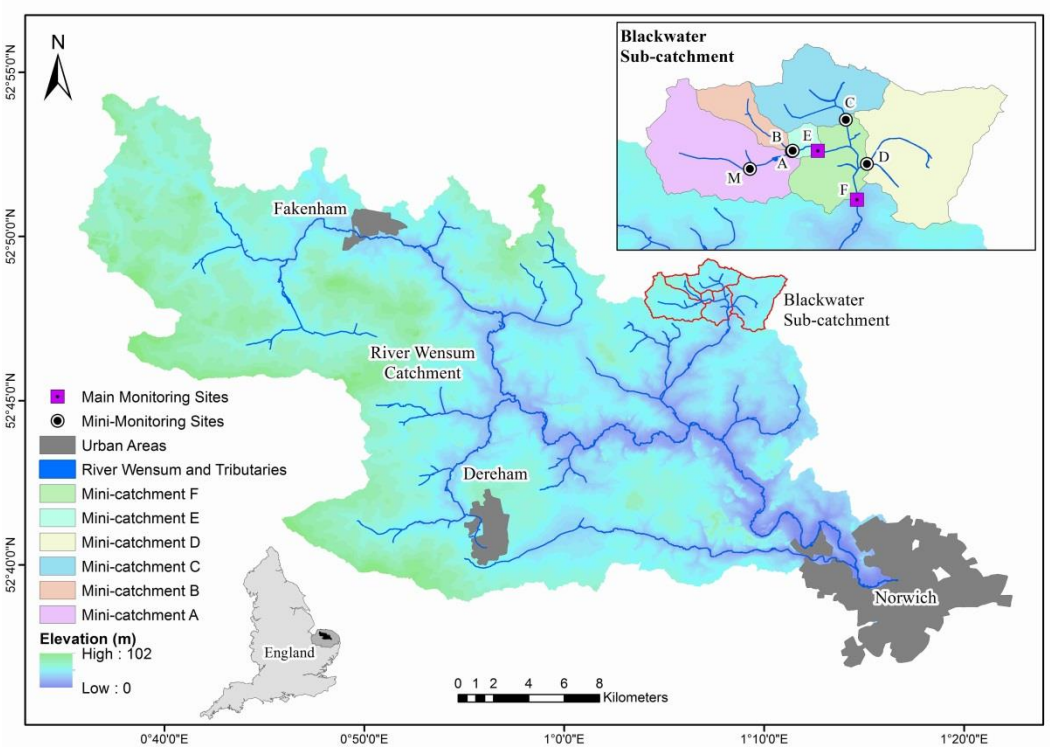

Figure 2.1: The River Wensum catchment, Norfolk. Inset displays the Blackwater sub-catchment which is being intensively monitored as part of the Demonstration Test Catchment project

2.2 The Blackwater Sub-catchment

The Wensum catchment drains an area of 593 km^2 that extends approximately 40 km east-to-west and 25 km north-to-south. The catchment is divided into 20 sub-catchments, one of which, the 20 km^2 lowland Blackwater sub-catchment, represents the area intensively studied as part of the River Wensum DTC. For monitoring purposes, the Blackwater sub-catchment is divided into six 'mini-catchments' A to F, with a seventh mini-catchment, M, nested within A. Each of these seven mini-catchments has a bankside kiosk at its outlet monitoring parameters including pH, turbidity, temperature, ammonium, chlorophyll, dissolved oxygen and electrical conductivity at 30 min resolution (Figure 2.2). These kiosks are referred to as Swanhills A (52^{o}47'14" N, 01^{o}07'44" E), Swanhills B (52^{o}47'15" N, 01^{o}07'44" E), Brakehills C (52^{o}47'35" N, 01^{o}08'49" E), Black Bridge D (52^{o}47'02" N, 01^{o}09'10" E), Stinton Hall Farm E (52^{o}47'13" N, 01^{o}08'16" E), Park Farm F (52^{o}46'38" N, 01^{o}08'58" E) and Merisons M (52^{o}47'03" N, 01^{o}06'53" E). Two main kiosks (Stinton Hall Farm E and Park Farm F) additionally measure nitrate, soluble reactive phosphorus (SRP) and total phosphorus (TP). Each kiosk encompasses an ISCO automatic water sampler (Teledyne ISCO, Lincoln, NE) containing 24, 1L polypropylene

sample bottles which are remotely activated via text message to sample stream water during heavy precipitation events. Each monitoring site also has a pressure transducer located in a stilling well which records river stage every 30 min (Table 2.1). Weather stations at Swanhills A and Black Bridge D record precipitation at 15 min intervals via tipping-bucking rain gauges, alongside measurements of temperature, wind speed, humidity and solar radiation.

Table 2.1: River stage (m) statistics for monitoring sites A, B and E. Data recorded between 1st April 2012 and 31st March 2014.

	Site A (m)	**Site B (m)**	**Site E (m)**
Min.	0.038	0.000	0.044
Median	0.227	0.066	0.157
Mean	0.258	0.099	0.183
Max.	1.000	0.737	1.000

This research focussed upon mini-catchments A, B and E, with data collection carried out between May 2012 and March 2014. The bedrock of these three mini-catchments is Cretaceous white chalk at a depth of ~20 m which serves as the principal aquifer for this region. This aquifer, which has a storage coefficient of 0.064, transmissivity of 685 m^2/d and effective fracture porosity of 1-2%, supplies approximately 40% of public water supply in East Anglia, rising to 90% in some rural areas of north Norfolk (Toynton, 1983; Hiscock *et al.*, 2001).

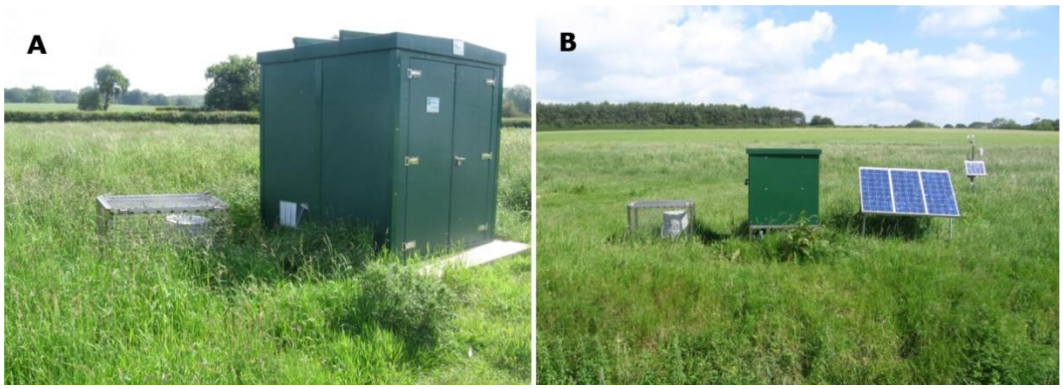

Figure 2.2: Images of the Blackwater sub-catchment showing the main and 'mini' bankside monitoring kiosks located at Stinton Hall Farm E (A) and Swanhills A (B), respectively. ISCO automatic samplers are visible in the metal cages to the left hand side of both kiosks. The weather station can be seen in the right hand side of image B. Further images of the Blackwater can be found in Appendix A.

Overlaying the chalk are superficial deposits of Mid-Pleistocene diamicton glacial tills, principally chalky, flint-rich boulder clays of the Sheringham Cliffs (0.2-0.5 m depth) and Lowestoft Formations (0.5-20 m depth). These are interspersed with layers of glaciofluvial and glaciolacustrine sands and gravels. The overlying deposits are of Late Pleistocene silty loess (cover loam) and Holocene-age alluvium and river terrace material. The principal surface soil types are clay loam to sandy clay loam soils to a depth of at least 0.2 m (Hiscock, 1993; Hiscock *et al.*, 1996; Lewis, 2011; Rawlins, 2011b).

2.3 Land Use

Topographically, the land in mini-catchments A, B and E is ideally suited to arable farming, being 30-50 m above sea level and having gentle slopes that rarely exceed 0.5^{o} of inclination. Of the 5.4 km^{2} of mini-catchment A, intensively farmed arable land constitutes 92%, with wheat, barley, sugar beet, oilseed rape and spring beans grown in a 7 year rotation. A further 5% of this headwater catchment is grassland, 1.5% is deciduous woodland, 0.5% is coniferous woodland and 1% constitutes rural settlements (Figure 2.3). A small amount of land is planted with maize to provide game bird cover.

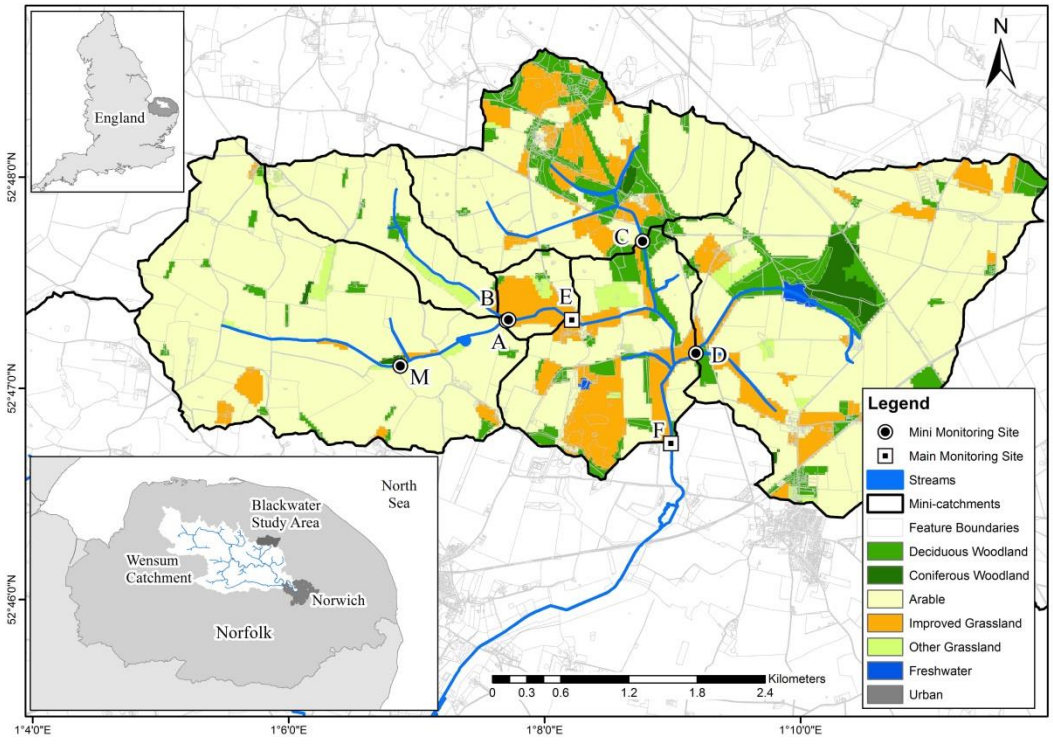

Figure 2.3: Land use across the six mini-catchments of the River Blackwater.

The 1.3 km^2 of mini-catchment B is similarly structured, with 89% arable land, 7% grassland, 3% mixed woodland and 1% rural settlements. At 0.42 km^2, mini-catchment E represents the smallest land unit within the Blackwater and it also has the largest proportion of land under grassland, at 55%. Of the remainder, 41% is under arable cultivation and 4% is deciduous woodland.

2.4 Mitigation Measures

As part of the River Wensum DTC goal to evaluate the extent to which on-farm mitigation measures can cost-effectively reduce the levels of diffuse agricultural pollution, nine arable fields within mini-catchments A were selected to trial different cultivation methods during 2013/14 (Figure 2.4). Seven of the nine fields had an oilseed radish cover crop planted over winter. Theoretically, cover crops help absorb excess nitrates that would otherwise leach through the soil into the river, whilst also protecting the soil surface from erosive winter rainfall events that carry sediments and P into the stream (Stevens and Quinton, 2009a, b).

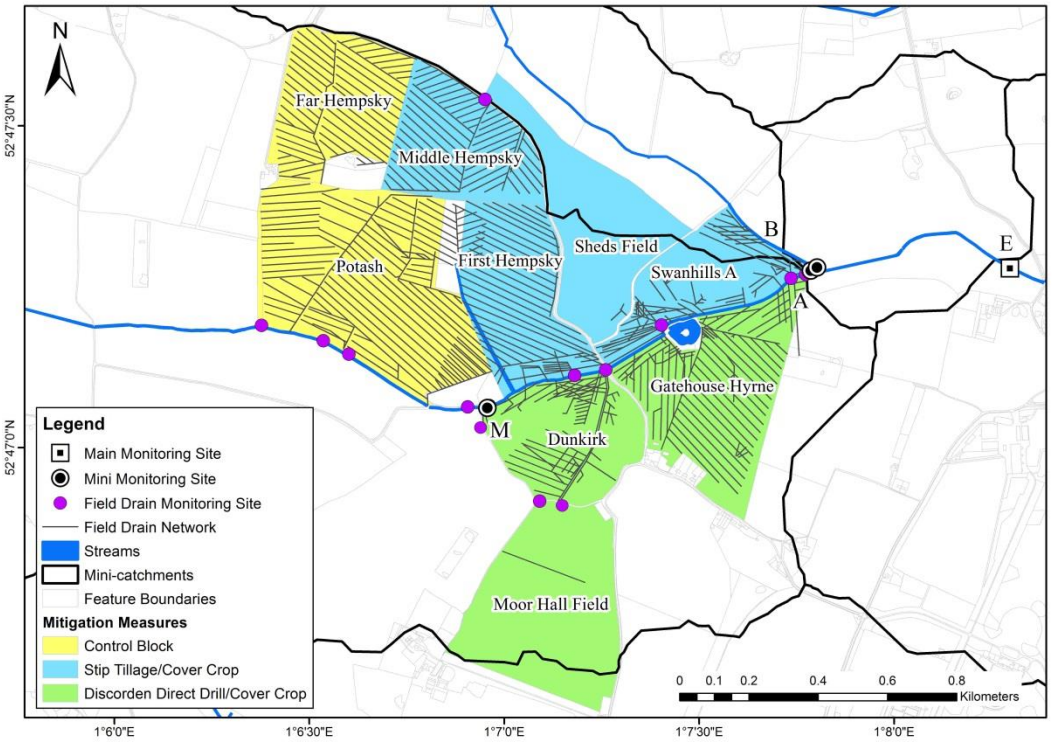

Figure 2.4: Map showing the nine fields in mini-catchment A that are trialling infield mitigation measures aimed at reducing the land-to-river transfer of nitrate, phosphorus and sediment. Also shown are the network of field drains under each field and the locations of regular field drain water quality monitoring.

Of these seven fields, four (Swanhills, First Hempsky, Middle Hempsky and Sheds Field) then underwent spring direct drilling with the planting of spring beans, whilst the other three (Gatehouse, Dunkirk and Moor Hall Field) were cultivated using a specialised Discordon cultivator and were then drilled with a Rapid drill. Both cultivation regimes represent a form of reduced, or minimum, tillage in which the soil receives little or no ploughing prior to seeding or after harvesting. Theoretically, minimum tillage increases the structural stability of the soil making it less susceptible to erosion, whilst also helping to increase soil organic matter content, enhance soil biota and lower cultivation costs for the farmer (Withers *et al*., 2007). Two of the fields (Far Hempsky and Potash) were kept as controls and underwent the normal practice of deep ploughing with no winter cover crop planted.

The effectiveness of these mitigation measures was assessed by monitoring the water quality of 12 subsurface agricultural field drains at 1-2 week intervals during the field trial period (Figure 2.4). Additionally, soil water collected in 90 porous pots buried 90 cm deep across the nine fields was also analysed several times per year to detect changes in soil water chemistry. Alongside these trialled cultivation measures, the farm (Salle estate) had 10-15 m wide grass buffer strips along most of the length of the stream channel prior to the onset of the DTC project as part of the farm's Entry Level Stewardship (ELS) scheme measures to reduce the direct transfer of soil from arable fields to the river.

2.5 Local Climate

The Wensum catchment experiences a temperate maritime climate, although it is situated within one of the driest regions of the UK – East Anglia. Between 1981 and 2010, mean annual temperatures recorded at the nearby Marham weather station were 10.0^{o}C, being highest in August (17.1^{o}C) and lowest in January (3.9^{o}C). Over the same period, mean annual precipitation totals were 653 mm, with mean monthly totals being highest during October (67.3 mm) and lowest during February (39.3 mm) (Meteorological Office, 2013). During the April 2012 to March 2014 fieldwork period, average annual temperatures recorded by the weather station in mini-catchment A were 8% lower (9.2^{o}C) than the 1981-2010 mean, with sustained below average temperatures observed throughout 2012 and 2013 (Figure 2.5). Winter 2013/14 saw above average temperatures return, with negligible snow fall compared with the previous winter. Average annual rainfall totals in mini-catchment A were 24% higher (808 mm) during this period, with

2012 proving to be a very wet year in comparison to the 1981-2010 mean. 2013 was a drier year, with the wet summer 2012 contrasting strongly with the dry summer 2013.

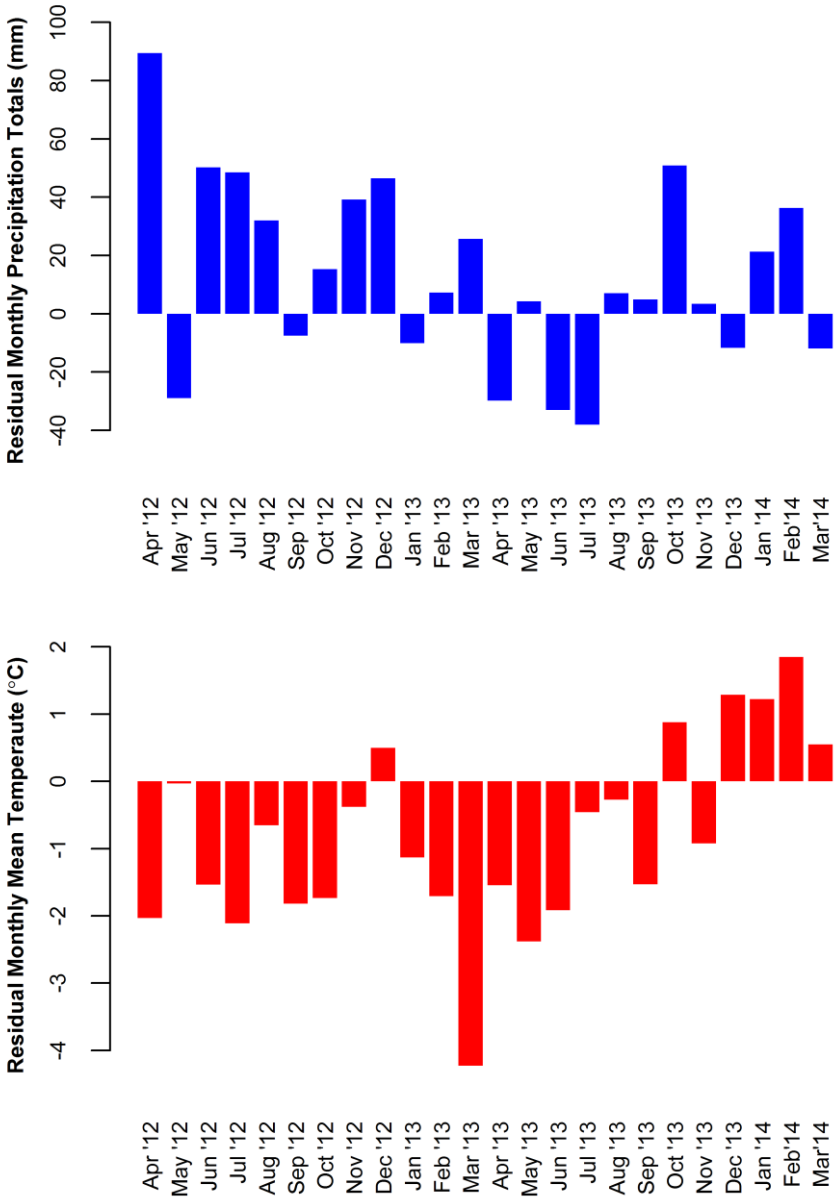

Figure 2.5: Monthly mean temperature and total monthly precipitation recorded at Swanhills A between April 2012 and March 2014. Values expressed as departures from the 1981-2010 mean climate data obtained from the nearby UK Meteorological Office weather station at Marham.

2.6 SPM Sampling Protocol

Sampling of SPM under baseflow conditions took place at weekly intervals throughout the 23-month period from May 2012 to March 2014 at kiosk sites A, B and E. High-density polyethylene (HDPE) bottles were used to collect 1-8 L grab samples of

stream water, with the volume collected at each site depending upon turbidity and a 25 mg target SPM mass (see Chapter 3). Upon return to the laboratory, all samples were kept in cold storage (5^{o}C) until they were processed. When >8 mm of precipitation was forecast (herein termed a storm event), the ISCO automatic water samplers were remotely activated to collect 1 L grab samples every 60- or 120-min depending on the duration of the event. A total of 14 storm events were captured at each kiosk site between September 2012 and February 2014. Automatic and manual grab samples were always taken from the same location and depth in the centre of the channel to ensure consistency between baseflow and storm event samples. Where possible, SPM samples were also collected at the same time of day to ensure consistency between weeks, with previous research having demonstrated significant diurnal variations in stream water geochemistry (Halliday *et al*., 2012). Whilst it is acknowledged that grab samples taken at a single location may not be wholly representative of SPM geochemistry over the entire cross-section of the stream channel, the spatial and temporal consistency of the sampling protocol employed here does ensure that all collected SPM samples are comparable.

Chapter 3

DEVELOPING FILTER PAPER BASED ANALYTICAL TECHNIQUES FOR MONITORING SPM GEOCHEMISTRY*

3.1 Chapter Summary

Many of the commonly used analytical techniques for assessing the properties of fluvial SPM are neither cost-effective nor time-efficient, making them prohibitive to long-term high-resolution monitoring. In this chapter, an in-depth methodology utilising two types of spectroscopy is presented which, when combined with automatic water samplers, can generate accurate, high-temporal resolution SPM geochemistry data, inexpensively and non-destructively, directly from sediment covered filter papers. A combined X-ray fluorescence spectroscopy (XRFS) and diffuse reflectance infrared Fourier transform spectroscopy (DRIFTS) approach is developed to estimate concentrations for a range of elements (Al, Ca, Ce, Fe, K, Mg, Mn, Na, P, Si, Ti) and organic and inorganic phases (particulate organic carbon (POC), dithionate extractable Al (Al_{di}) and Fe (Fe_{di}), oxalate extractable Al (Al_{ox}) and Fe (Fe_{ox})) within SPM trapped on quartz fibre filters (QFF) at masses as low as 3 mg. Calibration models with small prediction errors are derived, along with mass correction factor models to account for variations in retained SPM mass. Spectral pre-processing methods are shown to enhance the reproducibility of results for some compounds, and the importance of filter paper selection and homogeneous sample preparation in minimising spectral interference is emphasised. The geochemical signal from sediment covered filter papers is demonstrated to be time stable, enabling samples to be stored for several weeks prior to

* Published as: Cooper RJ, Rawlins BG, Lézé B, Krueger T, Hiscock KM. 2014a. Combining two filter paper-based analytical methods to monitor temporal variations in the geochemical properties of fluvial suspended particulate matter. *Hydrological Processes* **28:** 4042-4056. DOI*:* 10.1002/hyp.9945.

analysis. Example applications of this novel spectroscopic analysis technique during a selection of precipitation events in November 2012, September 2013 and February 2014, demonstrate this methodology has considerable potential to be utilized for high-resolution monitoring of SPM geochemistry under a range of instream hydrological conditions.

3.2 Background

SPM is operationally defined as the fine particulate fraction, commonly <63 µm in diameter, which cannot pass through a 0.7 µm membrane filter (Bilotta and Brazier, 2008). Much of this material will, however, be aggregated to larger flocs due to the cohesive electrostatic forces acting between clay mineral surfaces. The distinction between dissolved and particulate material at 0.7 µm is arbitrarily defined for operational convenience and is somewhat misleading, with very fine colloidal material known to exist down to 1 nm (Hens and Merckx, 2002; Gimbert *et al*., 2007). This is further complicated by the threshold between dissolved (DP) and particulate phosphorus (PP) being defined as 0.45 µm. Therefore, PP between 0.45 and 0.7 µm is effectively within the 'dissolved' sediment fraction (Haygarth *et al*., 2006).

SPM can be considered to consist of two components; an inorganic fraction composed of mineral matter eroded from parent rock, and an organic fraction derived originally from photosynthesis or chemosynthesis. In the literature, the term 'suspended sediments' (SS) is widely used to describe both the organic and inorganic fractions, but this term should solely be reserved for inorganic material. The organic fraction is more correctly termed 'volatile solids' (Bilotta and Brazier, 2008). 'Suspended particulate matter' (SPM) or 'suspended solids' are more appropriate terms for describing particulate material where no distinction is made between the organic and inorganic fractions. SPM is therefore referred to throughout this thesis when describing all suspended material.

As described in Chapter 1, high fluvial SPM concentrations are detrimental not only with respect to increased turbidity, but also due to the role fine sediment plays in the transport of P. Fundamentally, P sorption onto sediment surfaces can only occur across the water-sediment interface. As such, the specific surface area (SSA) of sediments strongly influences the rates of surface reactions and therefore the ability of sediments to adsorb P (Evans *et al*., 2004; Demars and Harper, 2005; Rawlins *et al*., 2010; Panuska *et al*., 2011). SPM is dominated by fine grained particulates that have large numbers of small intra- and inter-aggregate pores and rough mineral surfaces, thus giving SPM a high SSA

(Palmer-Felgate *et al*., 2009; Wagai *et al*., 2009). Consequently, SPM has greater capacity for P sorption than coarser streambed sediments and thereby has greater potential to influence water quality (Stutter *et al*., 2007). A detailed understanding of SPM geochemical and temporal dynamics under a range in instream hydrological conditions is therefore required if water quality issues, such as eutrophication, are to be tackled.

Previous investigations of SPM have typically used time-integrated samplers as a way of obtaining sufficiently large volumes of sediment (>10 g) to facilitate detailed analysis (e.g. Birgand *et al*., 2004; Panuska *et al*., 2011; Schindler Wildhaber *et al*., 2012b). Time-integrated samplers are essentially 1 m long PVC pipes ~10 cm in diameter with narrow 4 mm diameter inlet and outlet tubes to encourage sedimentation within the main body of the tube as water velocity reduces (Phillips *et al*. 2000). However, the problem with this technique is that the SPM properties are amalgamated over time making them unsuitable for resolving important catchment processes at high-resolution (e.g. Jordan *et al*., 2007). Phillips *et al*. (2000) also found that the material leaving time-integrated samplers is finer than the material entering it due to the preferential settling of coarser sediment fractions within the tube, thus allowing some of the geochemically important fine sediment fraction to be lost. Perks *et al*. (2014) also demonstrated that time-integrated samplers were unsuitable for estimating sediment fluxes due to them significantly underestimating sediment loads.

An alternative is to use automatic water samplers that can be programmed to capture samples at defined time intervals during high-flow storm events when SPM transport is greatest (e.g. Stutter *et al*., 2008a; Oeurng *et al*., 2010). Unfortunately, the masses of sediment captured are often too low (<100 mg) for traditional analysis such as loss-on-ignition (LOI), colorimetry, acid digestion and Inductively Coupled Plasma Mass Spectrometry (ICP-MS), techniques which also tend to be expensive, time-consuming and destructive. There is therefore a requirement for an alternative cost-effective and time-efficient technique capable of dealing with low SPM concentrations that can be used in conjunction with automatic water samplers to generate high-temporal frequency geochemistry data for a range of hydrological conditions (Evrard *et al*., 2011; Guzmán *et al*., 2013).

Two candidates for this role are X-ray fluorescence spectroscopy (XRFS) and diffuse reflectance infrared Fourier transform spectroscopy (DRIFTS). These spectrometers can be calibrated to directly estimate the properties of SPM trapped on filter papers with minimal prior preparation at masses as low as a few milligrams. Furthermore, because

XRFS is non-destructive, it can be used in conjunction with DRIFTS on a single SPM sample to generate an array of geochemical and mineralogical data. Several studies have demonstrated the capability of XRFS (Barnhisel *et al*., 1969; Cann and Winter, 1971) and infrared spectroscopy (Martínez-Carreras *et al*., 2010b; Tremblay *et al*., 2011) to analyse SPM directly on filter papers. However, until now there has been no detailed methodology published demonstrating how the two techniques can be used consecutively to yield a wider range of high-temporal resolution geochemical time-series. Addressing this shortcoming, the objectives of this chapter were:

(i) to present an in-depth methodology for a combined XRFS and DRIFTS analysis of SPM geochemistry directly from sediment covered filter papers;

(ii) to consider the sensitivity of XRFS and DRIFTS to methods of sample preparation, homogenisation and storage, sediment mass retention on filter papers, and the effects of spectral pre-processing on calibration model performance.

3.3 Methods

3.3.1 Selecting Filter Papers

Choosing the appropriate filter papers for direct spectral analysis is an important first step, since using filters with a complex chemical structure will increase the risk of spectral 'noise' originating from the filter paper overwhelming the signal derived from the trapped SPM. Traditionally, glass fibre filter papers made from 100% borosilicate glass are used for the laboratory filtration of stream water samples (e.g. Oeurng *et al*., 2011; Dawson *et al*., 2012). However, whilst it would still be possible to use these filters after careful calibration to remove background noise, we opted to use Millipore 100% quartz fibre filter (QFF) papers (Merck Millipore, Billerica, MA, USA) as their simple chemistry (only Si-O bonds) generates less spectral interference than typical glass fibres. Unfortunately, these QFF papers are traditionally sold as a filter for air pollution monitoring and therefore only had a particle retention rating for aerosolized Dioctyl Phthalate particles of 99.998% at 0.3 μm. It was therefore necessary to manually derive their retention rating for aquatic media. Initially, the microfiber structure of the QFF papers was compared against the traditional glass fibre filters under a scanning electron microscope (SEM) at 500 times magnification. This can be seen in Figure 3.1 for filters both with (B and D) and without (A and C) sediment trapped on the surface.

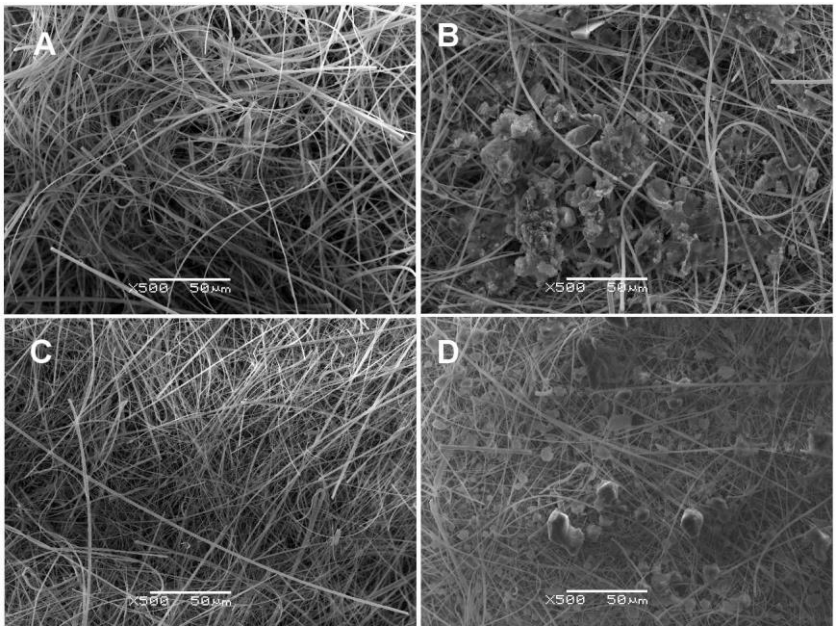

Figure 3.1: A series of scanning electron microscope (SEM) images of Millipore quartz fibre (A, B) and Sartorius glass fibre (C, D) filters at 500 times magnification, shown with (B, D) and without (A, C) trapped sediment.

Despite the random nature of the fibres, the structure and pore sizes of the QFF papers appears visually similar to the traditional glass fibre variety, so one could logically expect them to have a similar particle retention rating. Nevertheless, the average aqueous particle retention was then tested empirically by mixing 25 mg of a streambed sediment sample (Johnson *et al*., 2005) with 1 L of Milli-Q water (18.2 MΩ.cm; Merck Millipore, Billerica, MA, USA) which was then vacuum filtered through a single QFF paper. This process was repeated 40 times. The resulting 40 L of filtrate were bulked together and centrifuged at 5000 rpm for 15 min to concentrate the colloidal particles into a 500 mL solution. The concentrated filtrate was analysed in a Beckman Coulter LS13320 Laser Diffraction Particle Size Analyser (Beckman Coulter, CA, USA) with 20 drops of Calgon added and 2-min of sonication (18 W) used to disperse aggregated flocs. Total sediment mass retention was also determined gravimetrically by weighing all filters after oven drying at 105^{o}C for 2 hrs.

3.3.2 XRFS Calibration

X-ray fluorescence spectroscopy was chosen as the method for the geochemical analysis of SPM due to it being a highly accurate, non-destructive and reproducible analytical tool capable of estimating concentrations of all elements from sodium to

uranium in a sample down to ppm levels (Norrish and Hutton, 1969). Calibrations were made for a total of 10 major elements (Al, Ca, Fe, K, Mg, Mn, Na, P, Si and Ti) and the rare earth element cerium (Ce), using 42 certified laboratory sediment standards from various global locations to form a global calibration. Cerium was selected in addition to the majors as it is naturally enriched in P-bearing apatite minerals and is therefore also enriched in the inorganic phosphate fertilizers derived from these (Land *et al*., 1999; Reynard *et al*., 1999). Previous research by Rawlins (2011a), also found that variations in the streambed sediment concentration of Ce could explain 10.4% of the variability in streambed sediment P concentrations in rivers across a large region of eastern England.

25 mg of each standard was separately mixed into suspension with 1 L of Milli-Q water in a sealed flask and vacuum filtered through individual QFFs to yield 42 filter paper standards. Dispersing the sediment this way ensured that each QFF had a homogeneous covering of sediment after filtering. This is an essential step because surface roughness, uneven sediment distribution, differing densities and mixtures of different particle sizes can all produce spectra that deviate from the expected theory making them difficult to interpret quantitatively (Tiwari *et al*., 2005; Maruyama *et al*., 2008). The sediment loaded filters were dried at 105^{o}C for 2 hrs before being re-weighed to determine the mass of trapped sediment.

Each sediment covered filter paper was loaded into a wavelength-dispersive XRFS (Bruker S4 Pioneer, Bruker AXS, Germany) and bombarded with short wavelength X-rays for between 100-300 seconds per element. A blank filter paper was also loaded to provide a set of background counts at each X-ray peak position that could subsequently be subtracted from counts measured on the sediment covered filters. As the X-rays are emitted, some pass straight through the sample, some are back scattered by Compton or Rayleigh scattering when photons collide with electrons, whilst the rest is absorbed by the sediment. This absorbed fraction excites electrons within the sediment resulting in the ionisation of elemental constituents by ejecting one or multiple electrons from the inner K- and L-orbitals. This destabilises the electron structure causing the outer shells to collapse inwards filling in the vacancy left by the ejected electrons. The transition of electrons from higher to lower energy atomic shells releases X-ray fluorescence radiation with wavelengths and energies characteristic of the orbitals involved and the atoms present within the sample (Bruker, 2008). These fluorescence spectra were recorded and a mathematical ‘peak search’ technique was employed to find spectral peaks, whilst a ‘peak match’ procedure determined the elements to which each peak belonged by referring to a database of reference values (Brouwer, 2003).

Of the 42 prepared standards, 26 were used to develop the calibration model which took the general form (Equation 3.1; Brouwer, 2003):

$$(3.1) \quad C_x = (A_x + B_x * I_x) * M_x / MCF$$

where C_x is the estimated concentration of element x; A_x and B_x are the gradient and intercept determined by linear regression from the reference standards; and I_x is the measured intensity. M_x is the matrix correction factor which corrects for various effects that impact upon the number of photons being ejected from a sample (Enzweiler and Vendemiatto, 2004). These include the partial elemental absorption of X-rays attenuating the resulting fluorescent emission, as well as the enhancement of emission spectra by fluorescent X-rays of heavy elements stimulating further secondary fluorescence of lighter elements. Further corrections for Compton matrix scattering and spectral peak line overlaps (deconvolutions) were applied using the Bruker S4 Pioneer software, reviewed in more detail in Brouwer (2003). MCF is the mass correction factor which accounts for the inability to obtain exactly 25 mg of SPM (the calibration mass) on each filter paper every time a stream water sample is filtered. Barnhisel *et al*. (1969) and Cann and Winter (1971) previously demonstrated that individual mass correction adjustments are required for each element because the XRFS procedure assumes all samples are of equal mass. Therefore, deviations between the mass of SPM retained and the mass used for calibration will strongly impact upon elemental concentrations predicted by XRFS. Individual MCFs were developed for each element by dividing the estimated percentage concentration of four reference standards at a range of masses (3-60 mg) by the percentage concentration at the calibration mass (Equation 3.2):

$$(3.2) \quad MCF = C_x / C_{xCM}$$

where C_x is the estimated concentration of element x at any given mass, and C_{xCM} is the concentration of element x at calibration mass (i.e. 25 mg). This yields MCF fractions with values <1 for sediment masses below 25 mg and >1 for masses higher than 25 mg. A regression model was then formulated to explain the relationship between the MCF and sediment mass, from which adjustments could be made to the estimated concentration by dividing by the appropriate MCF value (Equation 3.1). Calibrations were subsequently verified against the remaining 16 independent standards using an iterative predictive model that works by first predicting element $n = 1$, then $n = 1, 2$, and so on continuously up to $n = 11$, with the final iteration taken as the elemental composition of the sample as this accounts for all of the various aforementioned matrix interactions between each element (Brouwer, 2003).

3.3.3 DRIFTS Calibration

3.3.3.1. Sample Selection

Alongside XRFS, diffuse reflectance infrared Fourier transform spectroscopy is proposed as a complementary, semi-destructive, analytical technique capable of determining concentrations of various compounds present within SPM. Covalently bonded molecules have a characteristic rotational-vibrational structure unique to the mass of the atoms and strength of the bonding between them. DRIFTS exploits this by targeting a beam of multi-frequency mid-infrared (4000-400 cm^{-1}) light onto a ground SPM sample, where upon infrared light that matches the resonant frequency of the molecular bonds is absorbed producing a characteristic absorption spectrum at a specific wavelength unique to the vibrational frequency of that particular bond. The remainder of the light is either reflected or refracted, with only the diffusely reflected fraction utilised in the DRIFTS procedure (Tremblay and Gagné, 2002).

Numerous studies have already demonstrated the effectiveness of infrared spectroscopy in the geochemical analysis of both soils (Viscarra Rossel *et al*., 2006; Rawlins, 2011b; Stumpe *et al*., 2011) and stream sediments (Poulenard *et al*., 2009 & 2012; Martínez-Carreras *et al*., 2010a, b; Rawlins, 2011a). The advantage here being it can be used directly on SPM covered filter papers after the elemental composition has been derived by XRFS. Calibrations were made for a total of 5 organic and inorganic phases (POC, Al_{di}, Al_{ox}, Fe_{di}, Fe_{ox}), selected based on the well documented organo-mineral associations that occur within soils and stream sediments (e.g. Evans *et al*., 2004; Wagai *et al*., 2009; Hartikainen *et al*., 2010). Specifically, Al and Fe oxyhydroxides are known to play an important role in organic matter (OM) stabilisation, through both the formation of organo-mineral complexes and via the sorption of OM onto metal oxide surfaces (Wagai and Mayer, 2007). Their large surface areas also give these metal oxyhydroxides a high P sorption capacity (McKeague and Day, 1966).

In contrast to XRFS, which can be accurately calibrated using globally derived certified standards, Minasny *et al.* (2009) demonstrated that the regional transferability of mid-infrared spectra measurements is relatively weak. Therefore, local calibrations had to be derived using a selection of 72 dry ground soils (Rawlins, 2011b) and streambed sediment samples (Johnson *et al*., 2005) from the River Blackwater catchment (Figure 3.2). Because the soil types within the catchment range from sandy and chalky boulder clays in the west, to sands and gravels in the east (Rawlins, 2011b), a reasonable degree of geochemical and mineralogical variability was provided for calibration.

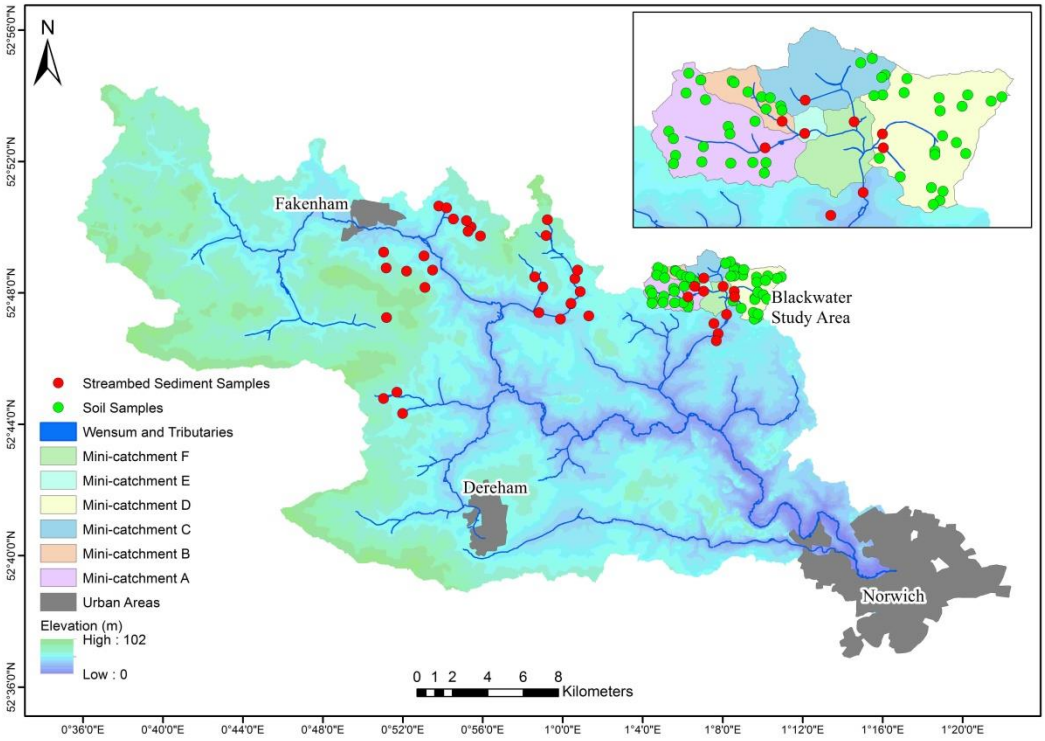

Figure 3.2: Map of the River Wensum catchment showing the location of soil and streambed sediment samples used to calibrate the DRIFTS procedure.

3.3.3.2 Particulate Organic Carbon and Metal Oxyhydroxide Extractions

Organic matter, which can be considered to be ~58% organic carbon (Broadbent, 1953; Howard and Howard, 1990), contains a complex mix of cellulose, lignin, carbohydrates and polysaccharides in variable proportions with relatively large amounts of labile P in the form of DNA, ATP and phospholipids available for liberation upon microbial mineralisation (Stumpe *et al.*, 2011). The POC contents for each calibration sample were derived gravimetrically following combustion of 1 g of dry ground sediment at 450^{o}C for 8 hrs, with POC taken to be 58% of the LOI. Crystalline Fe and Al oxyhydroxides, as well as much of the amorphous phase, were extracted via dithionite extraction (McKeague and Day, 1966). 1 g of sediment was weighed into a 30 mL centrifuge tube along with 20 mL of 25% (w/v) sodium citrate ($Na_3C_6H_5O_7.2H_2O$) and 5 ml of 10% (w/v) sodium dithionite (NaS_2O_4) and was shaken overnight. Samples were centrifuged at 2500 rpm for 20 min and a 15 mL aliquot of the supernatant was extracted and filtered through a 0.45 µm Whatman membrane syringe filter prior to ICP-AES analysis to determine the concentrations of Al_{di} and Fe_{di}. Amorphous Fe and Al mineral phase concentrations were determined via oxalate extraction (McKeague and Day, 1966). 25 mL of ammonium oxalate ($C_2H_8N_2O_4$; 0.2 M) and oxalic acid ($H_2C_2O_4$; 15.76 g/L)

were added to 1.5 g of sediment in a centrifuge tube. The resulting mixture was shaken for 2 hrs and processed via the same method used for the dithionite extraction to yield concentrations of Al_{ox} and Fe_{ox}.

3.3.3.3 Sample Preparation

Once POC and oxyhydroxide concentrations had been determined for all calibration samples (n = 58 for POC and n = 72 for oxyhydroxides), 25 mg of each sample was transferred onto individual QFF papers using the same procedure as for the XRFS calibration. Unlike infrared transparent potassium bromide (KBr), which is traditionally used as the sole background matrix for DRIFTS analysis not on filter papers, quartz fibres produce strong absorption features in the region 1200-1000 cm^{-1} (Masserschmidt *et al*., 1999). This can reduce infrared beam penetration depth to as little as 10 µm meaning only sediment at the sample cup surface will be analysed and spectral band intensities will be suppressed. Consequently, the way in which the absorbing matrix material is prepared will affect the degree of scatter, the amount of Fresnel reflectance and the interaction between sediment and infrared radiation, making it easy to misinterpret changes in the spectra due to matrix effects as genuine changes in the sediment chemical composition (Brimmer and Griffiths, 1986). There were therefore four key preparation factors that had to be considered in order to obtain good quality reproducible spectra with a high degree of interpretational accuracy (Pike Technologies, 2011):

(i) **Particle size**: large particles >50 µm result in major Fresnel reflection off particle surfaces, increasing scattering and yielding noisy spectra with wide bandwidths and low absorption intensities (Brimmer and Griffiths, 1986).

(ii) **Packing**: densely packed samples restrict infrared beam penetration depth and increase spectral distortions and irregularities caused by Fresnel reflections off compacted sample surfaces.

(iii) **Grinding**: the degree of grinding can affect spectral properties by destroying chemical bonds and thereby reducing the specific light absorption of those molecules (Stumpe *et al*., 2011).

(iv) **Homogeneity**: spectra from non-homogeneous samples will be severely affected by matrix scattering causing spectra to lose crucial reproducibility and making them difficult to quantitatively interpret.

With these points in mind, each sediment covered filter paper was uniformly ground for 50 seconds into a fine homogeneous powder using a ShakIR steel ball mill (Pike

Technologies, Madison, WI, USA). A small amount of KBr was added to act as an infrared transmitting matrix and an effective abrasive agent helping to reduce particle sizes. The resulting powders were lightly hand packed into steel sample cup holders being careful to avoid surface compaction. Samples were then scanned 40 times at 4 cm^{-1} resolution across the wave-number range 4000-400 cm^{-1} in a BIO-RAD Excalibur Series FTS-3000 FTIR (Cambridge, MA, USA) fitted with an AutoDiff^{TM} automated diffuse reflectance accessory (Pike Technologies, Madison, WI, USA). Sample cups were rotated through 90^{o} after the first scan and rescanned another 40 times so that spectra could be averaged to offset any potential spectral reflectance noise generated by the orientation of the powdered particles. A background spectrum of the QFF paper and KBr matrix was also collected and subtracted from all subsequent sample scans to isolate the sediment signal using Resolutions Pro spectral processing software (Agilent Technologies, CA, USA).

3.3.3.4 Chemometrics

Having carefully prepared and scanned all samples, a multivariate partial least squares (PLS) regression model with leave-one-out (LOO) cross-validation was developed using the '*pls*' package (Mevik *et al*., 2011) in the *R* environment (R Development Core Team, 2014). Such multivariate model calibration is beneficial over univariate regression as the wavelength at which the signal is present does not have to be generated exclusively by the target compound. Instead, PLS regression models exploit the fact that different compounds have different absorbance at a range of wavelengths which can then be used to decipher information from multiple overlapping spectral bands without prior band assignment (Alaoui *et al*., 2011). Because concentration estimates derived from DRIFTS are a reflection of the relative proportion of ground SPM to filter paper within the sample cup, MCFs had to be developed for DRIFTS using the same method as that developed for the XRFS procedure.

3.3.3.5 Spectral Pre-processing

A potential limitation of using DRIFTS on filter papers is the inability to obtain highly reproducible spectra when considerable noise is generated from the quartz fibre matrix. Four methods of spectral pre-processing were therefore assessed to determine whether applying certain filters or corrections prior to developing the PLS regression would enhance model strength and, more specifically, whether it would enhance the

reproducibility of the resulting concentration estimates. These four methods were (a) no pre-processing; (b) mean centring and 15-point, first-order, Savitzky-Golay (SG) filtering (Savitzky and Golay, 1964; Martínez-Carreras *et al*., 2010a); (c) multiplicative scatter correction (MSC); and (d) mean centring, SG filtering and MSC (Figure 3.3). SG filtering was applied using the '*signal'* package in the *R* environment (Short, 2011) to reduce high frequency variations associated with matrix noise whilst still preserving the line shape and lower frequency trends associated with the sediment signal. Prior to applying the low-pass filter, the spectra were mean centred such that they all had a common baseline, thereby removing any potential drift effects of the spectrometer. MSC was applied using the '*pls*' package and, theoretically, distinguishes between and separates absorption features of the actual sediment from the random light-scattering noise generated by the background matrix (Martens *et al*., 2003).

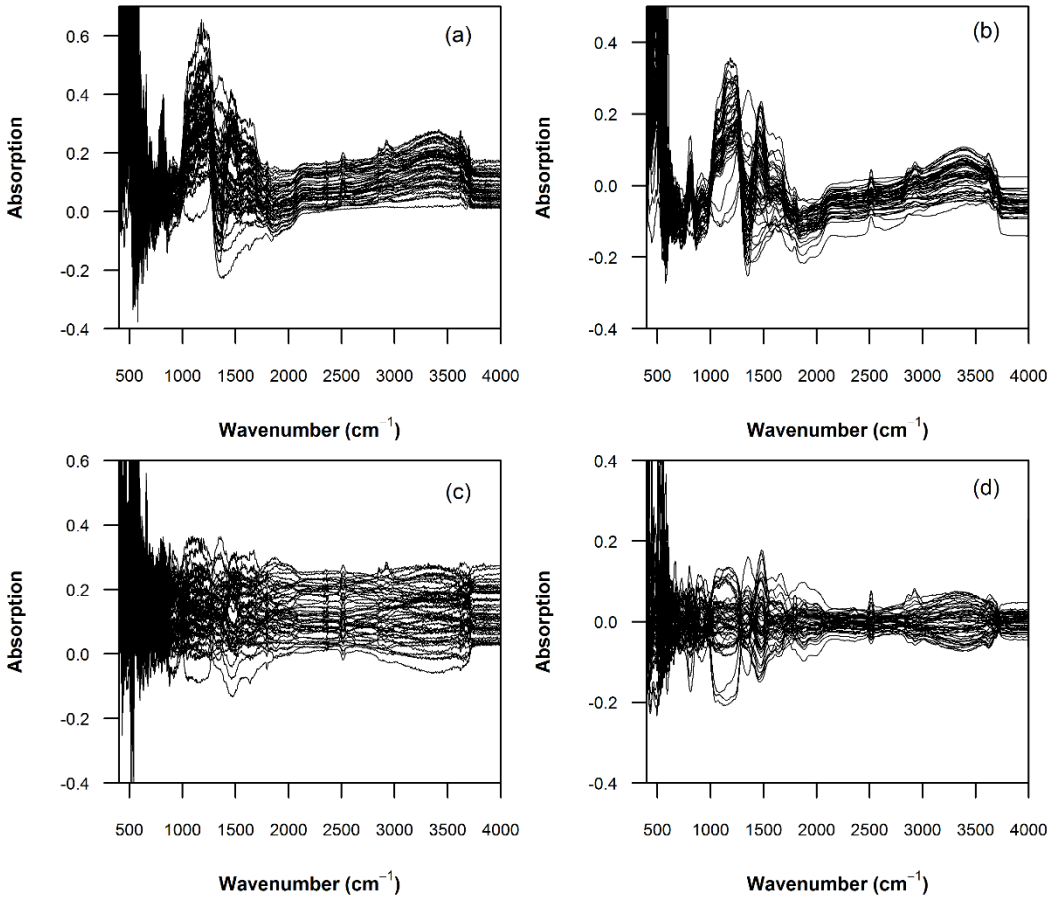

Figure 3.3: Mid-infrared (4000-400 cm-1) DRIFT spectra for 92 River Blackwater catchment standards showing the impact of various spectral pre-processing methods on the resulting spectral shape. (a) No pre-processing; (b) mean centred and Savitzky-Golay smoothed; (c) multiplicative scatter corrected; (d) multiplicative scatter corrected, mean centred and Savitzky-Golay smoothed.

3.3.4 Temporal Degradation

An advantage of utilising both XRFS and DRIFTS directly on filter papers is that, once dried, large numbers of samples from automatic samplers can be stored for an extended period of time prior to analysis, thereby removing the need for analytical facilities to be immediately available once the stream water samples have been returned to the laboratory. Whilst it is known that oven dried sediment samples can be stored for many months, or even years, prior to elemental analysis without degrading (e.g. USEPA, 2001), we decided to test whether this remains the case when only a few milligrams of sediment is distributed across a filter paper. The reason being, that a small mass of sediment exposed on the relatively large surface area of the filter paper could make the samples more susceptible to biological or chemical degradation than traditionally stored bulk sediment samples with lower surface area to mass ratios. For XRFS, this was tested by re-analysing three of the calibration standards at 39, 68, 80, 94, 109 and 122 days after the filters were initially prepared. The results for the three standards were then averaged together and the concentrations expressed relative to the day the standards were prepared. During this time, the oven dried sediment-covered filters were individually stored at room temperature in a sealed air-tight box with silica gel desiccant beads. For DRIFTS, it was not possible to re-analyse the initial calibration samples as, once ground, the resulting powders readily absorb water which alters the resulting spectra. As such, two new calibration standards were prepared at 49, 42, 29, 22 and 4 days prior to DRIFTS analysis. The results where then averaged to offset any variability in concentration estimates arising from slight differences in the preparation of these new samples. Once prepared, these standards were stored in the dark at room temperature in individual air-tight polyethylene bags.

3.4 Results and Discussion

3.4.1 Filter Papers

The bulked particle size distribution of the filtrate revealed an average aqueous particle retention rating of 99.26% at 0.45 µm (99.04% at 0.7 µm) for the 40 QFF papers (Figure 3.4), with an average mass retention of 94.5 ± 5.2%. This confirms the suitability of these filters for SPM investigation with respect to their ability to retain nearly all clay and silt-sized fractions from suspension. Importantly, this includes particulates at 0.7 µm, operationally defined as the threshold between SPM (0.7-63 µm) and dissolved

constituents (<0.7 µm), as well at 0.45 µm which marks the transition between DP and PP fractions. Very fine colloidal material (1-100 nm) may still pass through, although as the pores become blocked by larger particles, retention of colloids will be enhanced.

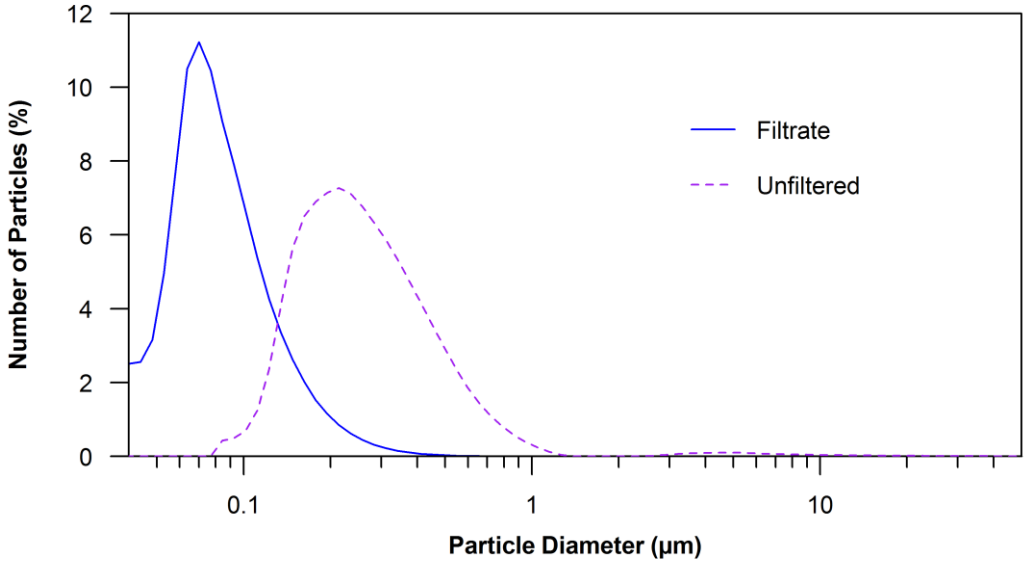

Figure 3.4: Average particle size distributions of the Millipore quartz fibre filtrate and the unfiltered streambed sediment sample.

3.4.2 XRFS

The XRFS calibration results are displayed in Figure 3.5 as the actual versus predicted percentage concentrations of all 11 elements. Of the 26 prepared calibration standards, a few provided weak correlations and were therefore rejected from the final regression model. In most cases, rejected standards had either visibly uneven sediment distribution or poor sediment retention (i.e. filters had retained less than 25 mg of sediment), with some elements (e.g. Fe) more affected by this inhomogeneity in sample preparation than others. All calibrations, derived from between 13 to 25 standards, were statistically significant (p<0.001) with adjusted variance explained (R^2) statistics ranging from 93.4% for Si to 99.7% for K (Table 3.1). All validation estimates were also statistically significant (p<0.001), with adjusted R^2 values ranging from 63.9% for Si to 95.9% for Ca. The weaker validation shown for Si arises from the imperfect removal of the Si-rich QFF paper background and, as such, caution has to be exercised when using the Si data. As is typical with regressions of this type, the uncertainty around the calibration increased towards the upper end of the concentration range where there were fewer reference standards, particularly for Mn and P where validation samples deviated

substantially from expected values. Despite this, the 95% confidence intervals were relatively narrow and the majority of the validation samples fell within a small range of the calibration line.

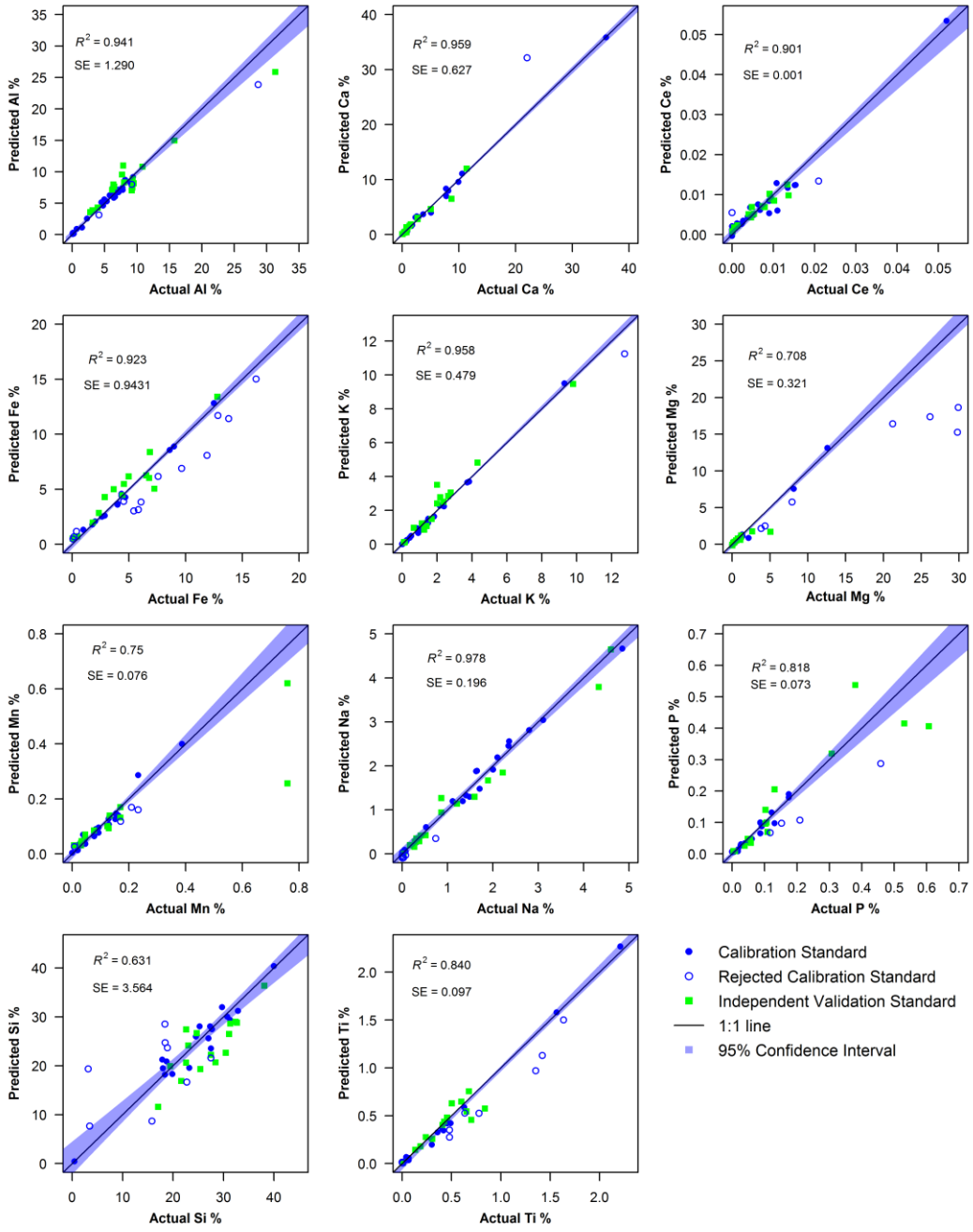

Figure 3.5: XRFS calibration and validation plots for the percentage concentration of 11 elements (Al, Ca, Ce, Fe, K, Mg, Mn, Na, P, Si, Ti) in 42 sediment standards. 95% confidence intervals refer to the regression calibration. Adjusted R^2 and standard error (*SE*) statistics refer to the validation dataset.

Table 3.1: Summary XRFS calibration and validation statistics for the percentage concentration of 11 elements (Al, Ca, Ce, Fe, K, Mg, Mn, Na, P, Si, Ti) in 42 certified sediment standards determined directly on filter papers. *n* standards refer to the fraction of available standards used. *SE* is the standard error.

	Calibration			Validation			
Element	***n* standards**	**Adjusted R^2**	***SE* (%)**	***n* standards**	**Adjusted R^2**	***SE* (%)**	***p*-value**
Al	22/26	0.971	0.494	16/16	0.941	1.290	$3.5e^{-10}$
Ca	25/26	0.996	0.418	16/16	0.959	0.627	$2.2e^{-11}$
Ce	24/26	0.966	0.001	14/16	0.901	0.001	$1.3e^{-7}$
Fe	13/26	0.994	0.264	16/16	0.923	0.943	$2.1e^{-9}$
K	25/26	0.997	0.106	16/16	0.958	0.479	$3.0e^{-11}$
Mg	19/26	0.988	0.345	15/16	0.707	0.320	$5.1e^{-5}$
Mn	22/26	0.951	0.019	14/16	0.749	0.076	$3.8e^{-5}$
Na	20/26	0.985	0.143	16/16	0.978	0.196	$3.1e^{-13}$
P	22/26	0.947	0.012	15/16	0.818	0.073	$2.2e^{-6}$
Si	18/26	0.934	2.128	16/16	0.639	3.564	$1.2e^{-4}$
Ti	16/26	0.996	0.038	16/16	0.840	0.097	$3.6e^{-7}$

For the mass correction factors (MCFs), strong, positive logarithmic (Al, Mg, Na, P) and power law (Ca, Ce, Fe, K, Ti) relationships were established for 9 out of 11 elements, being strongest for Ca (R^2 = 0.992) and weakest for Ce (R^2 = 0.934) (Figure 3.6). The non-linearity between sediment mass and the MCF arises because as the sediment mass on the filter paper increases, the intensity of fluorescent X-ray generation from each element per milligram of sediment declines due to an increasing influence of matrix attenuation. As such, increases in sediment at small masses have a greater impact on fluorescent X-ray generation than an increase in sediment at large masses. In contrast, Si exhibited a strong negative logarithmic relationship with increasing sediment mass which reflects the fact that smaller sediment masses are associated with increased X-ray penetration depth and therefore enhanced fluorescence generation originating from the QFF paper. For Mn, the relationship between sediment mass and the MCF was much weaker and best fitted by a linear relationship. It is not clear why the Mn MCF regression performed poorly in comparison with the other elements, but it may relate to stronger matrix interactions with other elements. The results demonstrate that variations in SPM mass can be corrected by simple MCF regression models.

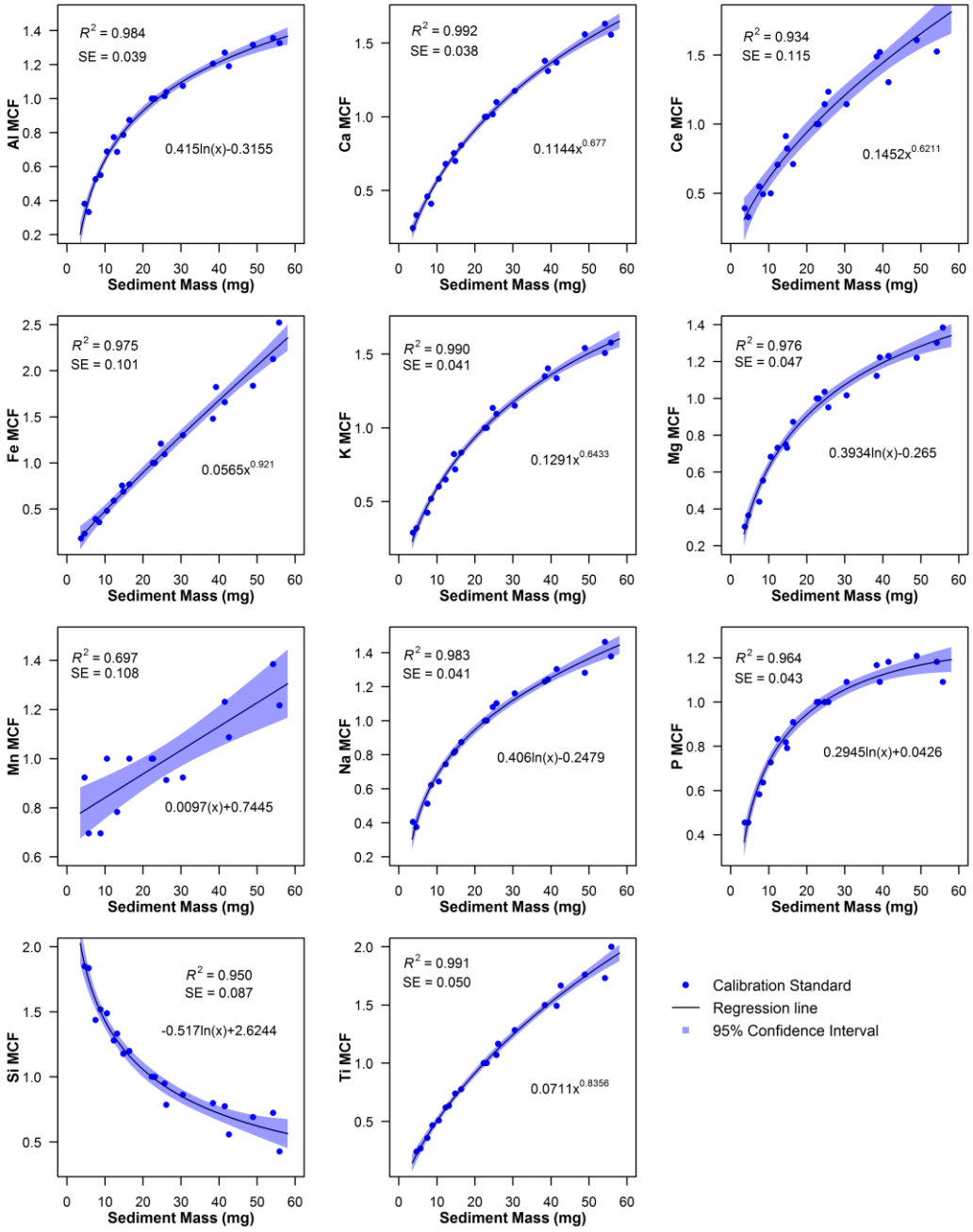

Figure 3.6: XRFS mass correction factor (MCF) calibration plots for 11 elements (Al, Ca, Ce, Fe, K, Mg, Mn, Na, P, Si, Ti) in four certified sediment standards of varying mass.

3.4.3 DRIFTS

The impact of applying various spectral pre-processing techniques to the DRIFTS spectra can be seen in Figure 3.7, which shows the concentration estimates for POC, Al_{di}, and Fe_{di} in six batches of the same sediment standard. No plots are shown for either Al_{ox} or Fe_{ox} as these exhibited near identical patterns to Al_{di} and Fe_{di}, respectively. Both no

pre-processing (NPP) and mean centring and Savitzky-Golay filtering (MCSG) methods yielded significantly higher reproducibility than multiplicative scatter correction (MSC) or a combination of all methods (ALL). Whilst several authors have used MSC as a pre-processing tool in infrared spectroscopy (e.g. Vogel *et al*., 2008; Martínez-Carreras *et al*., 2010), the simplicity of the technique means that it can erroneously remove spectral signals derived from the sediment chemical bonds, thereby yielding poorly representative spectra that worsen the multivariate model calibration, as has occurred here. For both POC and, in particular, the Fe compounds, MCSG yields higher reproducibility and was therefore chosen as the spectral pre-processing method for these compounds. For both Al_{di} and Al_{ox}, there was little difference in the performance of NPP and MCSG, however NPP yielded a stronger calibration model (lower root mean squared error of prediction (RMSEP)), negating the need to pre-process the spectra for Al compounds. Also shown is the reproducibility of spectra prepared by hand grinding the filter papers in an agate pestle and mortar as opposed to the ShakIR ball mill. The wide variability in concentration estimates emphasises the importance of producing homogeneously ground and mixed sample powders prior to analysis if precise results are to be obtained, something that manual hand grinding was unable to achieve.

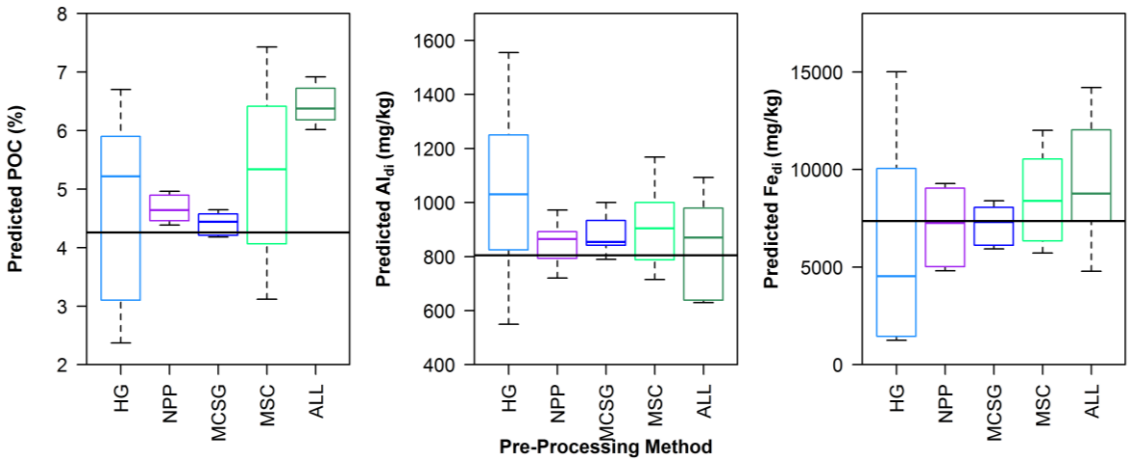

Figure 3.7: Box-plots demonstrating the impact of various DRIFTS spectral pre-processing methods on the reproducibility of concentration estimates for POC, Aldi, and Fedi in six batches of a calibration sample. HG are hand ground samples with no pre-processing. The others are ShakIR ball mill ground samples, whereby NPP is no pre-processing; MCSG is mean centred and Savitzky-Golay filtered; MSC is multiplicative scatter correction; ALL is MCSG and MSC combined. The solid black line is the measured concentration in the calibration sample, the solid line at the centre of the box is the median, the top and bottom of the boxes represent the interquartile range and the whiskers are the maximum and minimum values.

The DRIFT model calibrations are displayed (Figure 3.8) as measured versus predicted concentrations for POC, Al_{di}, Al_{ox}, Fe_{di}, and Fe_{ox} with leave-one-out cross validation. Rather than allow the PLS model to be run over the full spectrum (4000-400 cm^{-1}), discrete spectral regions were selected for each compound to enhance model calibrations. For POC (3975-1300 cm^{-1}) this included a very strong absorption feature in a band around 2950-2845 cm^{-1} caused by symmetric and asymmetric stretching and vibration of various aliphatic and aromatic C-H bonds, as well as bands around 1300-1125 cm^{-1} associated with ester, ether and phenol groups and at 2035-1975 cm^{-1} due to aromatic rings (Alaoui *et al*., 2011; Tremblay *et al*., 2011). For Fe_{di} (3704-3189 cm^{-1}) and Fe_{ox} (1727-1320 cm^{-1}) this included numerous absorption features in the regions 2500-1666 cm^{-1} and 3800-3200 cm^{-1} associated with Fe bearing minerals such as hematite, maghemite, lepidocrocite, goethite and magnetite (Namduri and Nasrazandani, 2008). For Al_{di} (3903-2202 cm^{-1}) and Al_{ox} (3849-2879 cm^{-1}) the major absorption features occur in a band around 3800-3200 cm^{-1} associated with the stretching of O-H bonds in aluminosilicates (Tremblay *et al*., 2011). Although other relevant absorption features are known to occur in the region 1200-400 cm^{-1}, this band was avoided because it was dominated by matrix noise from the QFF that made quantitative interpretation impossible.

The optimum number of principal model components selected for each calibration (n = 7 to 10) was based on the lowest achievable RMSEP following leave-one-out cross-validation. All five calibrations were statistically significant, with variance explained statistics for the cross-validated models ranging from 74.6% for Al_{ox} to 96.6% for POC (Table 3.2). However, the limited number of high Fe_{di} and Fe_{ox} concentration standards does increase model uncertainly at higher concentrations for these compounds.

Table 3.2: Summary DRIFTS PLS calibration and validation statistics for 5 organic and inorganic phases in calibration samples determined directly on filter papers. *n* stand. are the number of standards; *n* PC are the number of principal components selected; RMSEP is the root mean square error of prediction; MC is mean centred; and SG is Savitzky-Golay smoothed.

Compound	*n* stand.	Pre-processing	Spectral region (cm^{-1})	*n* PC	Calibration		Validation	
					R^2	RMSEP	R^2	RMSEP
POC (%)	58	MC, SG	3975-1300	10	0.990	0.326	0.966	0.589
Al_{di} (mg/kg)	72	None	3903-2202	10	0.978	67.46	0.842	179.97
Al_{ox} (mg/kg)	72	None	3849-2879	10	0.993	33.79	0.746	211.51
Fe_{di} (mg/kg)	72	MC, SG	3704-3189	10	0.971	970.20	0.893	1865.10
Fe_{ox} (mg/kg)	72	MC, SG	1727-1320	7	0.945	536.90	0.823	956.90

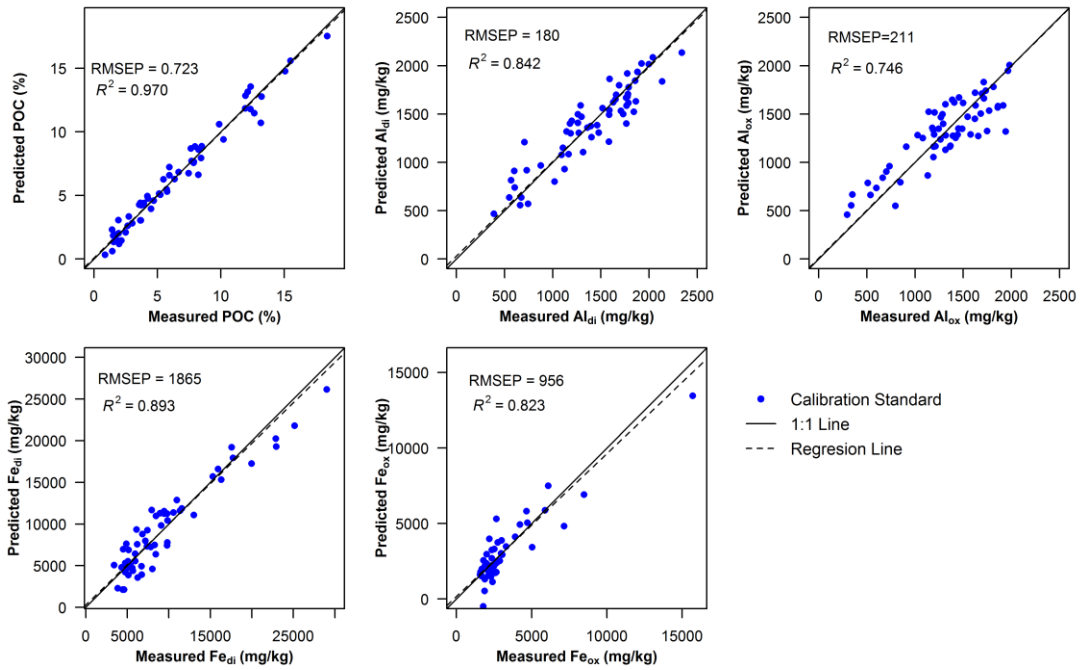

Figure 3.8: DRIFTS PLS calibration plots with leave-one-out (LOO) cross-validation for POC, Al_{di}, Al_{ox}, Fe_{di}, and Fe_{ox}.

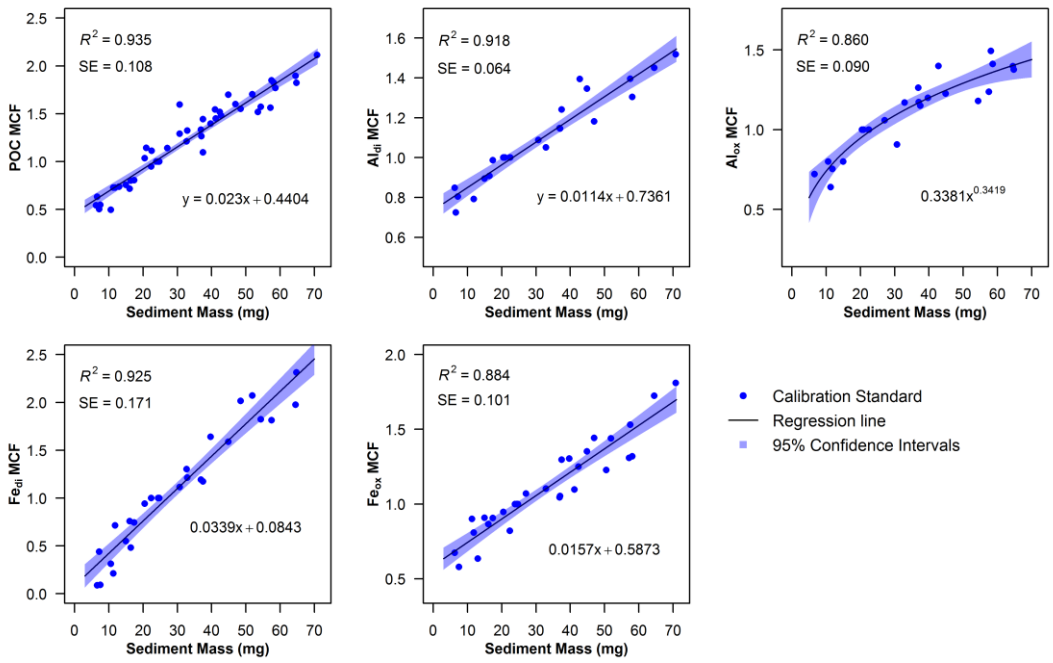

Figure 3.9: DRIFTS mass correction factor (MCF) calibration plots for five compounds (POC, Al_{di}, Al_{ox}, Fe_{di}, Fe_{ox}) in four calibration samples of varying mass.

Strong linear regression MCF models with narrow confidence intervals were developed for POC (R^2 = 0.935), Al_{di} (R^2 = 0.918), Fe_{di} (R^2 = 0.925) and Fe_{ox} (R^2 = 0.884) (Figure 3.9). As with the XRFS, uncertainty increased towards the extremes of the concentration range. A weaker association was established between Al_{ox} and sediment mass (R^2 = 0.860) that was best fitted by a power law relationship. This likely arises due to the weaker PLS calibration model derived for Al_{ox} and, as such, there is greater uncertainty in adjusting for retained SPM mass for this compound. Despite this, the strong regression models developed here demonstrate the ability of the DRIFTS MCF values to adjust for fluctuating instream SPM concentrations.

The importance of the MCF can be seen in Figure 3.10, which shows mid-infrared spectral estimates of POC concentration (%) for two bed sediment reference samples across a range of different masses (5-60 mg). When no MCF is applied, estimated POC concentration increases linearly with increasing sediment mass as the amount of POC within the sample is effectively increased. This yields estimates of POC that deviate significantly from the actual value obtained at calibration mass (i.e. 25 mg). However, application of the MCF can be seen to remove this mass associated trend, producing estimates for POC much closer to the actual concentrations.

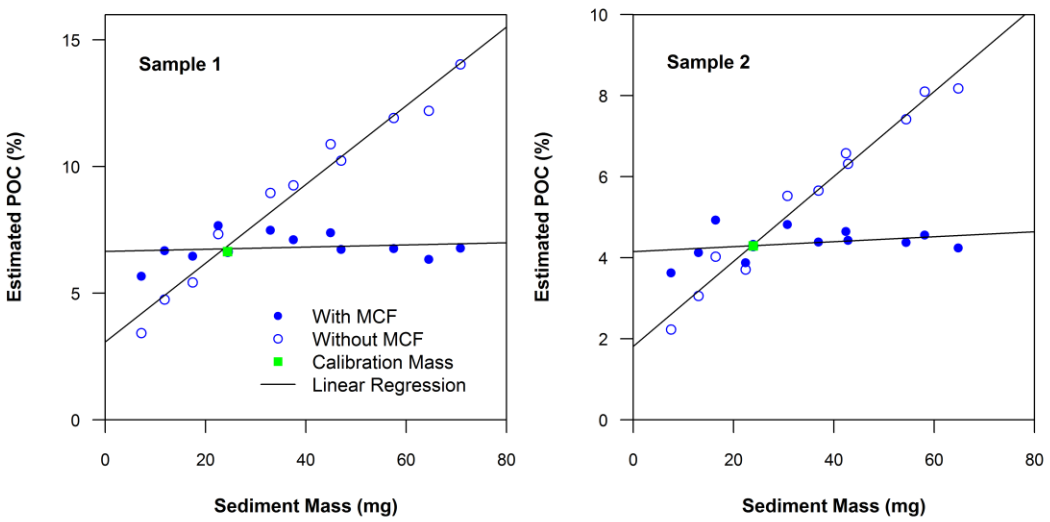

Figure 3.10: The impact of the mass correction factor (MCF) on the predicted concentrations of POC (%) for two River Wensum streambed sediment reference samples. The green squares represent the estimated POC concentration at calibration mass (25 mg).

3.4.4 Temporal Stability

Relative concentrations for the XRFS standards varied by less than 5% for all elements expect Mn during the 122 day period over which they were analysed (Figure 3.11). This level of variability was within the range of the calibration uncertainty, which, along with the absence of any apparent temporal trends in the data, strongly suggests the filter paper standards do not degrade over time. The largest amount of temporal variability occurred for Ce and P, although this reflects small changes in the estimated actual concentrations of these low abundance elements (Ce = ~0.0062% and P = ~0.068%) having a comparatively large impact on their estimated relative concentrations. For the organic and inorganic phases determined by DRIFTS, relative concentrations varied by less than 8.5% during the 49 day period over which they were analysed, with no longer term trends apparent in the data. Although temporal variability was greater than observed for XRFS, it was within the range of calibration uncertainty. The higher DRIFTS variability reflects that the same calibration samples are not being analysed each time and, as such, some noise was introduced by sample preparation. We can therefore conclude that once oven dried at 105^{o}C for 2 hrs, sediment covered filters can be reliably stored at room temperature in an air-tight environment for several months without risk of degradation.

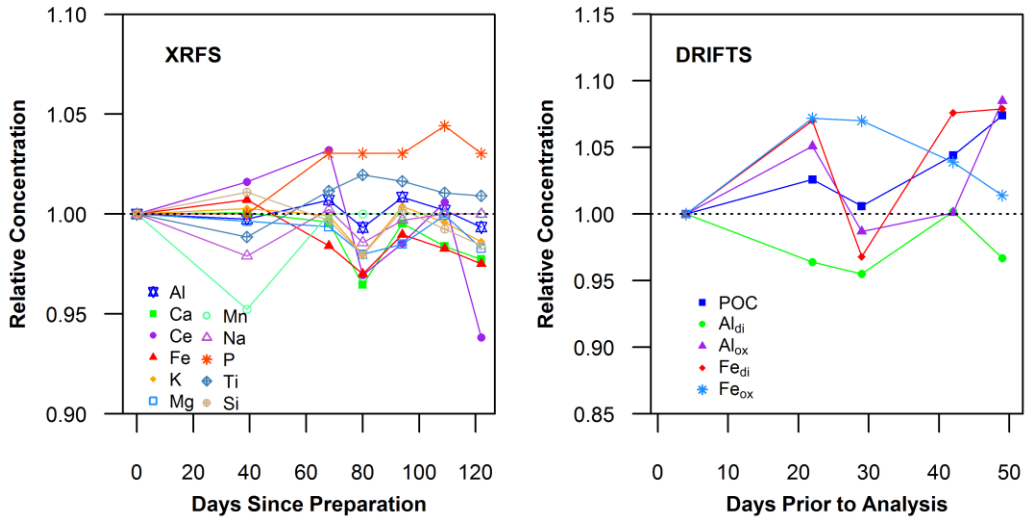

Figure 3.11: Time-series plots showing relative geochemical concentration in 16 calibration samples versus the number of days between filter paper preparation and analysis. XRFS concentrations are expressed relative to the day the filter paper standards were prepared, whilst DRIFTS concentrations are expressed against filter paper standards prepared four days prior to analysis.

3.4.5 Example Applications

The effectiveness of these two, direct, spectroscopic techniques is demonstrated using geochemical data from a selection of heavy precipitation events that occurred at sites A, B and E during September 2013, February 2014 and November 2012 respectively (Figures 3.12 to 3.14). For each event, ISCO automatic water samplers were remotely activated via text message to sample 1 L of water every 60- or 120-min depending on the forecasted duration of precipitation. All stream water samples were then returned to the laboratory and vacuum filtered through the Millipore QFF papers to extract the SPM. Once oven dried at 105^{o}C for 2 hrs, SPM covered filters were weighed to determine sediment mass retention and then analysed directly by XRFS and DRIFTS following the procedures described above.

The resulting geochemical time-series reveal the passage of rainfall across the Blackwater catchment is usually associated with increases in the concentrations of both SPM and clay mineral associated elements (e.g. Al, Mg and K). In fact, with the exception of Ca, all elements determined by XRFS analysis were observed to increase as precipitation commenced in the catchment, thus generating 'spiky' geochemical time-series. This is most pronounced for Al, with concentrations rising by up to 6% during the events presented here. By contrast, Ca concentrations were strongly depleted during precipitation relative to the other elements, with concentrations declining by up to 10% compared to pre-event conditions. These trends strongly indicate the existence of co-dependencies between most of the major elements within SPM (see Chapter 7 for further details). It is known that the distributions of many cations (e.g. Fe^{3+}, Mg^{2+}, Mn^{2+}, K^{+}) are usually correlated with increasing clay mineral accumulation (White, 2006), and thus these trends indicate an increase in the clay mineral content of SPM during rainfall events.

Temporal variations in the concentrations of organic and inorganic phases determined by DRIFTS were not as strongly associated with rainfall events. For example, whilst POC concentrations do display some degree of positive response to rainfall during the November 2012 events at site E (Figure 3.12), such behaviour is not so obvious during September 2013 (Figure 3.13) and February 2014 (Figure 3.14) at sites A and B, respectively. POC concentrations do, however, decline over time by up to 5% across all of the events presented here, although this pattern is not representative of every event recorded during the 23-month monitoring period. This trend in POC depletion has been observed in other studies and linked to an initial flushing of POC from the system during the early stages of an event, as well as sediments being supplied from increasingly POC

impoverished sources as the event progresses (e.g. Cerro *et al*., 2014). POC concentrations in SPM across all sites under both baseflow and storm event conditions were generally between 10-20%, which is within the range recorded in previous studies for chalk streams in southern England (Acornley and Sear, 1999) and in upland streams in the Scottish Highlands (Dawson *et al*., 2012). Concentrations of Fe and Al oxyhydroxides appear more variable than other recorded parameters, with Al_{ox} in particular showing a rapid rise in concentration towards the later stages of the November 2012 event (Figure 3.12).

From these high-frequency time-series it is possible to explore how quickly SPM geochemistry responds to changing catchment conditions. For example, during the September 2013 event (Figure 3.13), major peaks in element concentrations occurred 4-6 hrs after the onset of the initial rainfall, whilst concentrations of SPM peaked within the first 2 hrs. Similarly, during the November 2012 event (Figure 3.12), response in some element concentrations to the first rainfall band is delayed by 2-4 hrs relative to rainfall, whereas the response occurs concurrently with precipitation during later events. From such response times it is possible to detect evidence of the catchment wetting up, with the wetter catchment during later events resulting in a more rapid response in SPM geochemistry. Clearly, sampling at a lower resolution (e.g. weekly or monthly) using time-integrated samplers would have missed this dynamic temporal geochemical variability. Consequently, the examples presented here provide us with an invaluable detailed insight into the behaviour of SPM geochemistry before, during and after precipitation events at hourly resolution. Such accurate, high-frequency time-series would be difficult to generate using traditional sediment sampling methods and the geochemical data would be more expensive and time consuming to collate if traditional laboratory techniques were employed.

3.4.6 Experimental Limitations

Despite the strong calibration results for both XRFS and DRIFTS, there are limitations to analysing SPM geochemistry directly on filter papers. Principally, when using time-integrated samplers, a sufficiently large mass of SPM (>10g) can be captured, sieved and fractionated, thereby enabling the importance of the colloidal, clay, silt and sand fractions, as well as algal and detrital material, to be assessed independently. Clearly, when analysing masses of 25 mg in-situ on filter papers, such size fractionation is impossible. However, given that the majority of SPM is <63 µm in diameter (averaging

~86% by volume in mini-catchments A, B and E under both high- and low-flow conditions), this is not a major analytical limitation.

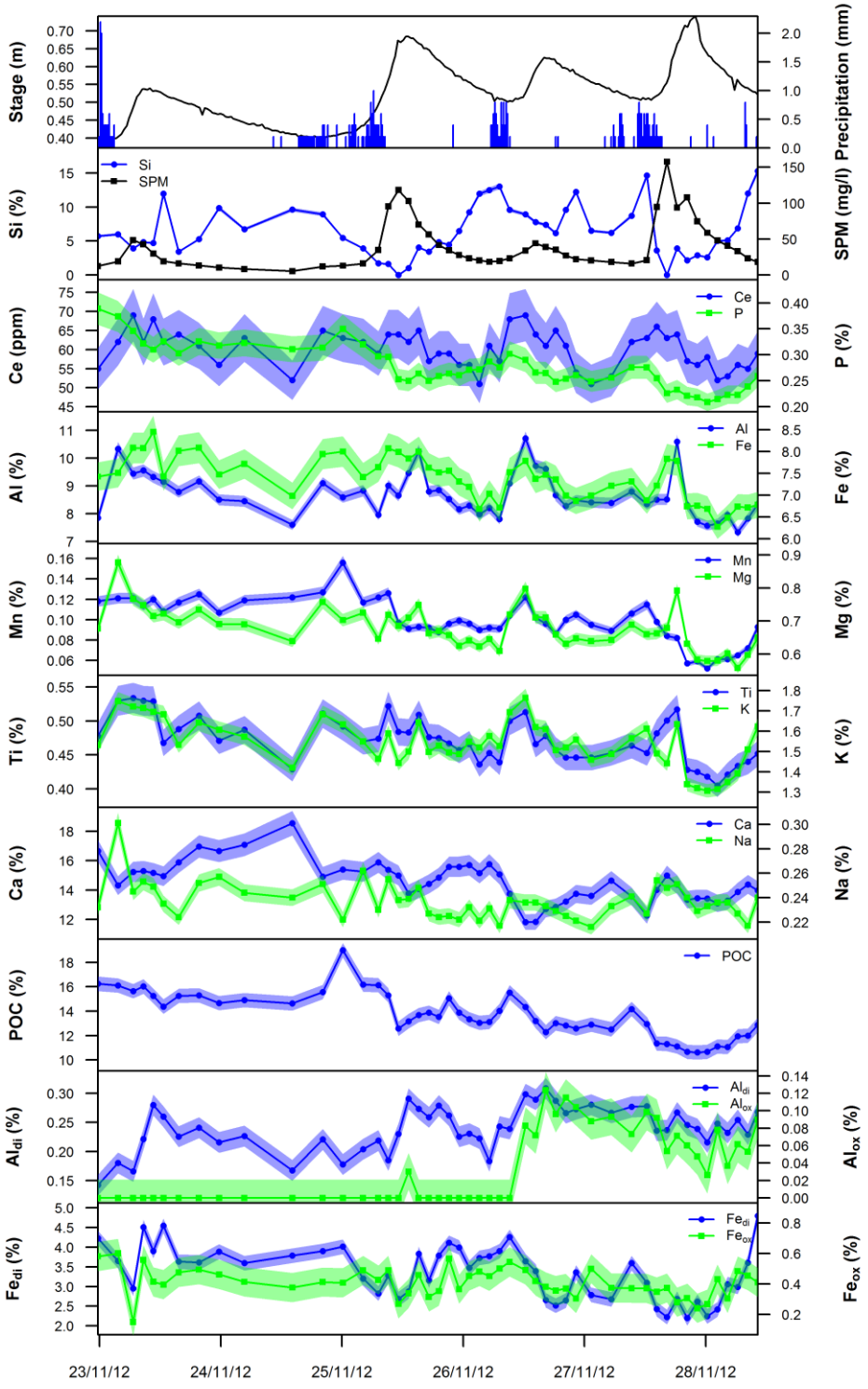

Figure 3.12: Time-series plots of SPM geochemistry (% by weight) at site E recorded at 120-min intervals during a succession of heavy rainfall events (46 mm total) in November 2012. Points relate to the times the automatic water sampler captured samples. Shading represents instrumental precision (2 St. Dev.) based on 46 repeat analyses of a standard.

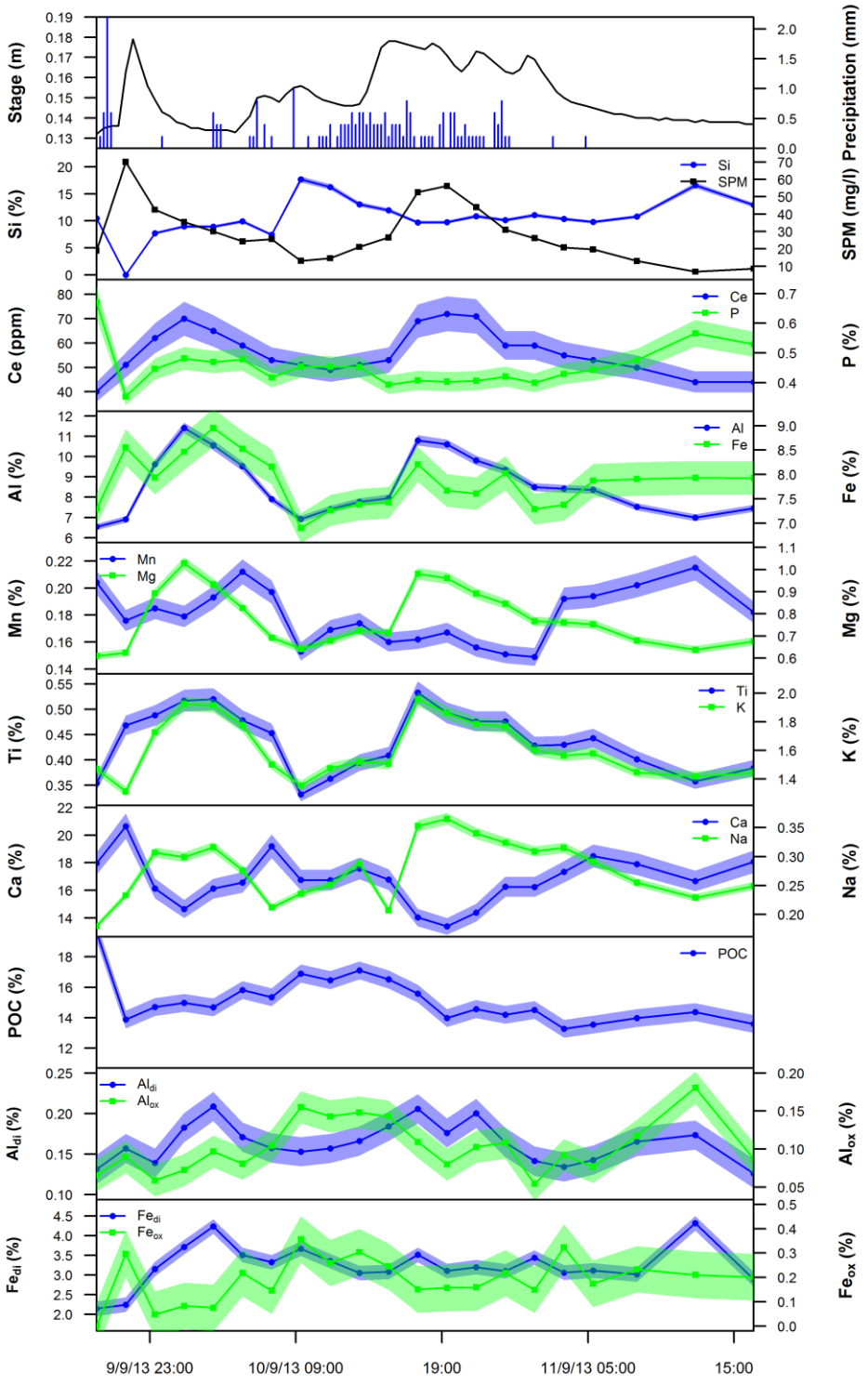

Figure 3.13: Time-series plots of SPM geochemistry (% by weight) at site A recorded at 120-min intervals during a heavy rainfall (26.2 mm) event in September 2013. Points relate to the times the automatic water sampler captured samples. Shading represents instrumental precision (2 St. Dev.) based on 46 repeat analyses of a standard.

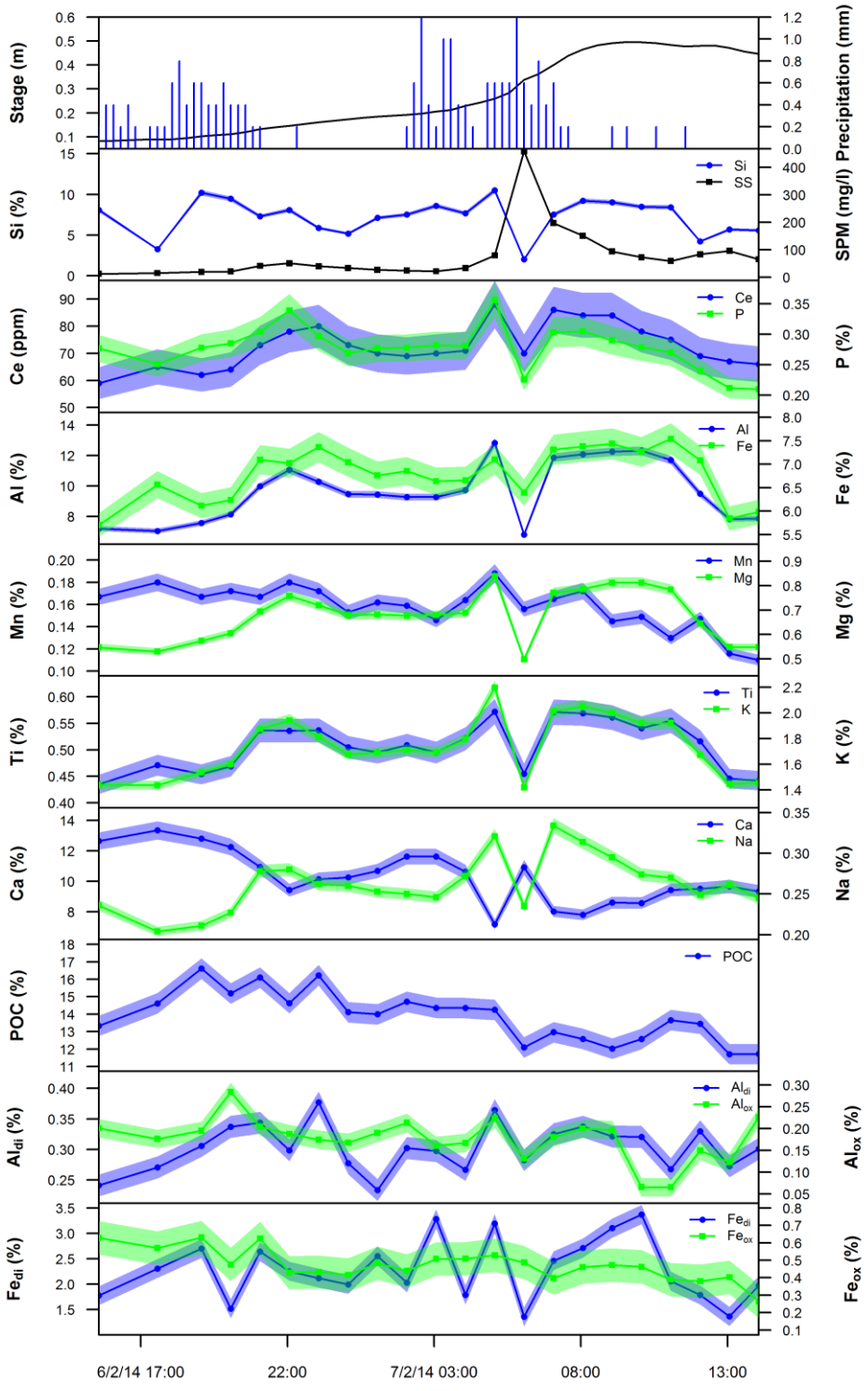

Figure 3.14: Time-series plots of SPM geochemistry (% by weight) at site B recorded at 60-min intervals during a heavy rainfall event (21.8 mm) in February 2014. Points relate to the time the automatic water sampler captured samples. Shading represents instrumental precision (2 St. Dev.) based on 46 repeat analyses of a standard.

Another potential issue with using very small sediment masses for geochemical analysis is that it only takes a few grains of material with an unusual chemical composition to majorly influence SPM geochemistry and lead to non-reproducible and unrepresentative analytical results. Horowitz (2008) therefore advises collecting as much sediment as feasibly possible to reduce the risk of generating unrepresentative data and, where small masses are unavoidable, to consider merging samples into a larger composite. This composite approach was adopted throughout this thesis by aiming to collect, where possible, 25 mg of SPM on each filter paper even when instream SPM concentration were very low (<5 mg/L). During storm events, this meant ISCO automatic water samples from successive time-steps were merged together when sediment concentrations were less than ~20 mg/L, whilst under baseflow conditions up to eight 1 L water samples were collected at any one time and merged to generate a single composite SPM sample.

Finally, unlike XRFS which is a truly non-destructive analytical technique, the DRIFTS procedure outlined here is best described as semi-destructive. Whilst the grinding of SPM covered QFFs does not affect the chemistry of the sample (which can still be analysed by other laboratory methods), the fact that it has been ground into a powder does prohibit the same samples from being reanalysed by XRFS using the same procedure. The DRIFTS procedure also uses a regional specific calibration and thus to apply this technique further afield would require the addition of samples from catchments local to other study regions (Minasny *et al.*, 2009).

3.5 Conclusions

Many commonly used methods for determining the properties of SPM, both in the field (e.g. time-integrated samplers) and in the laboratory (e.g. ICP-AES, LOI), are neither cost-effective nor time-efficient, making them prohibitive for long-term high-resolution monitoring. In this chapter, we have demonstrated an alternative method using two types of spectroscopy applied directly to sediment covered filter papers to quickly generate accurate geochemistry data without altering the SPM chemistry. By utilising a combination of XRFS and DRIFTS, it is possible to obtain concentration estimates for a range of elements (Al, Ca, Ce, Fe, K, Mg, Mn, Na, P, Si, Ti) and organic and inorganic phases (POC, Al_{di}, Al_{ox}, Fe_{di}, and Fe_{ox}) from a single SPM covered filter paper at masses as low as a 3 mg, thereby removing the requirement for the collection of large sample volumes in the field. When combined with automatic water samplers, large numbers of SPM covered filter paper discs can be cheaply produced via simple vacuum filtering,

thereby enabling hydrologically dynamic storm events to be monitored in high-resolution. We have demonstrated that QFF papers are appropriate for this type of analysis by minimising spectral interference and retaining nearly all SPM greater than 0.45 µm. Homogeneous sample preparation was shown to be essential if accurate and reproducible results are to be obtained, whilst local DRIFTS calibration is necessary for the technique to be applied in other catchments due to the weak regional transferability of mid-infrared spectral measurements. Pre-processing the infrared spectra by mean centring and Savitzky-Golay filtering prior to developing PLS regression models proved to be the most effective way to generate reproducible concentration estimates for both POC and iron oxyhydroxide complexes, whilst spectra for Al compounds did not require processing. The development of property-specific mass correction factor (MCF) models enables variations in retained SPM mass from that used during calibration to be corrected for by simple regression. The temporal stability of filter paper standards prepared up to 122 days prior to analysis indicates that it is possible to store batches of sediment covered filters for several months if necessary. The example applications presented here demonstrate considerable potential for a combined XRFS and DRIFTS approach to be used in conjunction with automatic water samplers as a tool for the high-resolution analysis of SPM geochemistry under a range of fluvial conditions.

Chapter 4

ASSESSING THE SENSITIVITY OF SOURCE APPORTIONMENT ESTIMATES TO MIXING MODEL STRUCTURE: A BAYESIAN MODEL COMPARISON[†]

4.1 Chapter Summary

Mixing models have become increasingly common tools for apportioning fluvial sediment load to various sediment sources across catchments. However, the lack of a common model framework has resulted in a wide variety of Bayesian and frequentist modelling approaches being employed. In this chapter, an improved Bayesian mixing model is developed which allows for full characterisation of spatial geochemical variability, instrument precision and residual error to yield a realistic and coherent assessment of the uncertainties associated with source apportionment estimates. It is then demonstrated how different Bayesian and frequentist model setups can impact upon resulting source apportionment estimates via a one-factor-at-a-time (OFAT) sensitivity analysis. 13 versions of a mixing model are formulated, each with different error assumptions and model structural choices. These are then applied to sediment geochemistry data from mini-catchment A to apportion sediment contributions from three sources (arable topsoils, road verges and subsurface soils) under baseflow conditions between August 2012 and August 2013. Whilst all 13 models estimate subsurface sources to be the largest contributor of SPM (median ~76%), comparison of

[†] Chapter published as: Cooper RJ, Krueger T, Hiscock KM, Rawlins BG. 2014b. Sensitivity of fluvial sediment source apportionment to mixing model assumptions: A Bayesian model comparison. *Water Resources Research* **50**: 9031-9047. DOI: 10.1002/2014WR016194.

apportionment estimates reveals varying degrees of sensitivity to changing priors, inclusion of covariance terms, incorporation of time-variant distributions and methods of proportion characterisation. Differences in apportionment results are also demonstrated between a full and an empirical Bayesian setup, and between a Bayesian and a frequentist Maximum Likelihood optimisation approach. This OFAT sensitivity analysis reveals that mixing model structural choices and error assumptions can significantly impact upon sediment source apportionment results, with estimated median contributions in this study varying by up to 21% between model versions. Users of mixing models are therefore strongly advised to carefully consider and justify their choice of model structure prior to conducting sediment source apportionment investigations.

4.2 Background

Source apportionment mixing models have been employed across a range of scientific disciplines to estimate the proportions of various sources that feed into a particular mixture or 'target' of interest. They are all based on the fundamental assumption that the composition of the target being studied, whether that be hair samples from mammals (Darimont *et al*., 2009) or sediment from rivers (Thompson *et al*., 2013), is a function of the composition of potential sources multiplied by their proportional contribution to the target. This approach relies on selecting appropriate markers or 'fingerprints' that can be traced from the source to the target in a reliable manner through well understood biotic or abiotic pathways. In ecology, stable isotope mixing models (SIMMs) have been used extensively to investigate the dietary intake of organisms by comparing the stable isotopic composition (typically $\delta^{13}C$ and $\delta^{15}N$ ratios) of some part of an organism's body against the isotopically distinct food sources it is believed to consume (Ogden *et al*., 2005; Tarroux *et al*., 2012; Hindell *et al*., 2013). Similarly, within the geosciences, a wide variety of fingerprints, ranging from compound-specific stable isotopes (Fox *et al.*, 2010; Puttock *et al*., 2012), to fallout radionuclides (Blake *et al*., 2009; Kim *et al*., 2013; Schuller *et al.*, 2013; Slimane *et al.*, 2013) and major and trace elements (Sutter *et al*., 2009; Evrard *et al.*, 2013; Fryirs and Gore, 2013; Yao *et al.*, 2013), have all been used to estimate the contribution of various terrestrial sediment sources to fluvial sediment load.

The ability of any mixing model to accurately represent source contributions to a mixture will ultimately be determined by the error assumptions and model structural choices made by the modeller. Two overarching statistical approaches are commonly employed in model formulation. The first is traditional Maximum Likelihood optimisation which

has been widely used in sediment fingerprinting studies for the past 15-20 years (Gruszowski *et al*., 2003; Walling *et al*., 2003; Motha *et al.*, 2003; Martínez-Carreras *et al.*, 2010; Walling, 2013). These frequentist models commonly minimise the sum of squared residuals as outlined by Collins *et al*. (1997), with more recent approaches typically coupling parameter optimisation with Monte Carlo based stochastic sampling to represent uncertainties associated with source area and target sediment variability (Collins *et al.*, 2013a; Wilkinson *et al*., 2013). However, these models are often inconsistent in their uncertainty representation and they lack the structural flexibility to coherently translate all sources of error into model results.

Consequently, Bayesian mixing models have come to increasing prominence over the last 5-10 years as a more robust alternative for comprehensively incorporating uncertainty into models (Fox and Papanicolaou, 2008; Palmer and Douglas, 2008; Rowan *et al*., 2011; Massoudieh *et al*., 2012; D'Haen *et al*., 2013; Dutton *et al*., 2013; Nosrati *et al*., 2014). Fundamentally, the Bayesian approach is advantageous over frequentist methods as it enables all known and residual uncertainties associated with the mixing model and the dataset to be coherently translated into parameter probability distributions in a hierarchical framework. However, due to the lack of an accepted model framework, a wide variety of Bayesian model setups have been employed, with previous studies differing in the choice of prior parameter distributions, the inclusion of covariance terms, the incorporation of time-variant distributions, the methods of proportion characterisation and whether full or empirical Bayesian formulations are used.

Therefore, the objectives of this chapter were:

- **(i)** to develop an improved Bayesian mixing model capable of providing full characterisation of spatial geochemical variability, instrument precision and residual error;
- **(ii)** to assess the sensitivity of source apportionment estimates to variations in mixing model structure and uncertainty representation via a one-factor-at-a-time (OFAT) sensitivity analysis of 13 mixing model versions.

This OFAT sensitivity analysis was conducted using SPM and sediment source area geochemistry data collected under baseflow conditions from mini-catchment A over a 12-month period between August 2012 and August 2013.

4.3 Methods

4.3.1 M1: The benchmark model

The first stage was to create a 'benchmark' Bayesian mixing model (M1), against which 12 other versions, each with at least one differing structural element, could be compared. This benchmark model represents a modified version of the empirical Bayesian mixing model developed by Parnell *et al.* (2013) for quantifying the dietary intake of Brent geese. The model follows Bayes' theorem (Equation 4.1):

$$\mathrm{P}(A|B) = \frac{\mathrm{P}(B|A)\,\mathrm{P}(A)}{\mathrm{P}(B)} \quad (4.1)$$

which states that the probability (P) of *A* given *B* (P(*A*|*B*) – the posterior) is a function of prior belief in *A* (P*(A)*) and a quotient that represents the support knowledge of *B* provides to *A* (P*(B*|*A)*/P*(B)*). This model is succinctly summarised by the Directed Acyclic Graph (DAG; Lunn *et al*., 2000) in Figure 4.1, which links together sets of random variable parent nodes with their conditional child node dependencies. Symbol meanings are as follows: *Y* is the measured concentration of fingerprints in SPM; Y^s and *S* are the measured and modelled concentrations of fingerprints in source area sediments, respectively; *P* and Φ are the sediment contributions of each source area in original and ILR-transformed space (see below); μ^{sg} and σ^{2sg} are hyper-prior guesses at the source means; Y^z is the measured instrument error; *j* and *k* are the fingerprint and source indices, respectively; Σ are covariance matrices; σ^2 are variances; μ are means; *i* is the model time-step index; and MVN, N, Dirch, Inv-W and Inv-Γ represent multivariate normal, normal, Dirichlet, inverse multivariate Wishart and inverse gamma distributions, respectively.

The core model formula is a mass balance whereby the concentration of each fingerprint in SPM (*Y*) is derived from the concentration of that fingerprint in each source area (*S*) multiplied by the proportional sediment contribution from that source (*P*).Accordingly, the likelihood function is (Equation 4.2):

$$\mathrm{L}(S, P \mid Y) \quad (4.2)$$

which essentially asks 'what is the likelihood of *S* and *P* given our knowledge of *Y*?' The solution is solved via a Markov Chain Monte Carlo (MCMC) sampling procedure of the full parameter distributions.

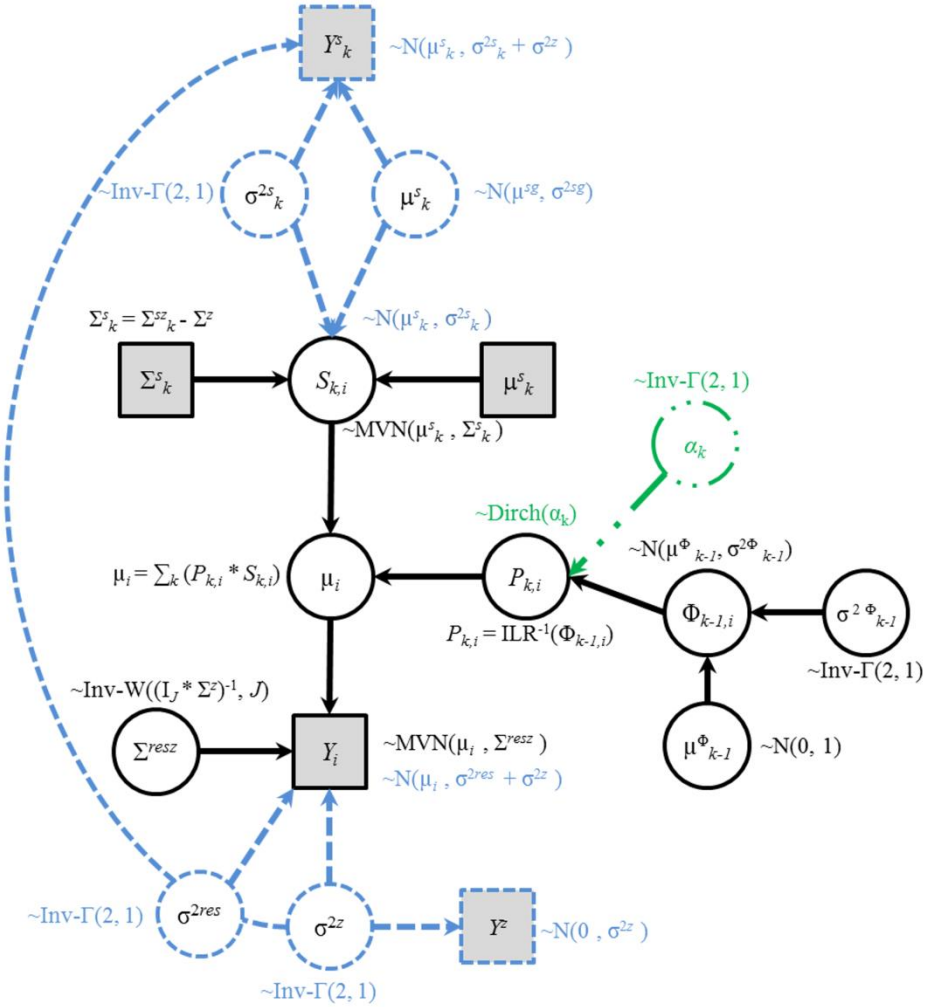

Figure 4.1: A Directed Acyclic Graph (DAG) of the benchmark Bayesian mixing model (M1; solid black lines), with extension to the Dirichlet distribution parameterisation (M11; green dot-dash lines) and the full Bayesian model (M12; blue dash). Squares indicate nodes with observed data, whilst circles indicate random variables estimated by the Markov Chain Monte Carlo (MCMC) procedure. Prior distributions and deterministic link equations are noted alongside.

Prior distributions for the sources (*S*) are estimated via an empirical Bayesian approach, whereby multivariate normal distributions are parameterised using the actual measured means (μ^s) and covariance matrices (Σ^s) of fingerprints in all source area samples. For the prior probability on the proportions (*P*), the procedure of Parnell *et al.* (2013) was adopted by applying a geometric transformation to the data – in this instance the isometric log-ratio (ILR) transform (Egozcue *et al.*, 2003). Transforming the compositional data in this way ensures that all proportions are independent (orthogonal) in transformed space on the complete real scale, thus allowing univariate normal priors, while all proportions are positive and sum to unity in the original space. The ILR transformation is specified as (Equation 4.3):

$$(4.3) \quad \Phi_i = \mathrm{ILR}(P_i) = V^T \log \left[\frac{P_{i1}}{g(P_i)}, \ldots, \frac{P_{ik}}{g(P_i)}\right]$$

where V is a *k-1 x k* triangular Helmert matrix and $g(Pi)$ is the geometric mean of the proportions, defined as (Equation 4.4):

$$(4.4) \quad g(P_i) = \left(\prod_{i=1}^{k} P_{ik}\right)^{\frac{1}{k}}$$

The reverse transformation of Φ to return real P values occurs by exponentiation and re-normalisation (Equation 4.5; Egozcue *et al*., 2003):

$$(4.5) \quad P_i = \mathrm{ILR}^{-1}(\Phi_i)$$

The Φ values are estimated by prior hyper-parameter distributions of μ^{Φ} and $\sigma^{2\Phi}$ that are assigned weakly informative normal and inverse gamma distributions, respectively. Combined instrument precision and residual error (Σ^{resz}) was incorporated into the model via a semi-informative, inverse Wishart distribution – the conjugate prior of the multivariate normal (Barnard *et al*., 2000; Sun and Berger, 2006). Here, the Wishart scale matrix (Ω) is represented by the product of an uninformative identity matrix (I_J) for residual error and an informative covariance matrix (Σ^{z}) for instrument error. Σ^{z} was derived empirically from 42 repeat analyses of a sediment standard. Inclusion of the residual error term accounts for uncertainties not explicitly incorporated into the model.

The complete Bayesian posterior distribution can be written in condensed form as (Equation 4.6):

(4.6)

$$p(\Sigma^{resz}, \mu, S, P, \Phi, \mu^{\Phi}, \sigma^{2\Phi} \mid Y) \propto p(Y \mid \mu, \Sigma^{resz}) \times p(S \mid \mu^{s}, \Sigma^{s}) \times p(\Phi \mid \mu^{\Phi}, \sigma^{2\Phi}) \times p(\Sigma^{resz}) \times p(\mu^{\Phi}) \times p(\sigma^{2\Phi})$$

4.3.2 OFAT sensitivity analysis

Twelve variants to the benchmark model were formulated (Table 4.1). Models 2-5 (M2-M5) assess the impact of altering the mean and variance hyper-parameter terms for the prior proportion distributions. Models 6-8 (M6-M8) evaluate modifications in covariance structure. Model 9 (M9) considers changes in the temporal variability of

source distributions. Models 10 (M10) and 11 (M11) assess the impact of proportion characterisation. Model 12 (M12) contrasts the empirical with the full Bayesian approach. And finally, model 13 (M13) assesses the frequentist optimisation technique.

Table 4.1: Comparison of the structure and parameters of the 13 different mixing model formulations. Differences from the benchmark model (M1) are emphasised in bold. ~N and ~Inv-Γ refer to normal and inverse gamma distributions, respectively. Square brackets denote distributions or parameters that vary with each source (*k*) or time-step (*i*).

Model Version	**Inference**	**Full or Empirical**	**Source Distribution (*S*)**	**Source Covariance (Σ^s)**	**Residual/ Instrument Covariance (Σ^{resz})**	**Proportion Method (*P*)**	**Proportion Mean (μ^{Φ})**	**Proportion Variance ($\sigma^{2\Phi}$)**
M1	Bayesian	Empirical	[*i*,*k*]	Yes	Yes	ILR	~N(0,1)	[*k*] ~Inv-Γ(2,1)
M2	Bayesian	Empirical	[*i*,*k*]	Yes	Yes	ILR	~N(0,1)	[*k*] **~Inv-Γ(0.001,0.001)**
M3	Bayesian	Empirical	[*i*,*k*]	Yes	Yes	ILR	**~N(0,1000)**	[*k*] ~Inv-Γ(2,1)
M4	Bayesian	Empirical	[*i*,*k*]	Yes	Yes	ILR	**0**	[*k*] ~Inv-Γ(2,1)
M5	Bayesian	Empirical	[*i*,*k*]	Yes	Yes	ILR	~N(0,1)	**~Inv-Γ(2,1)**
M6	Bayesian	Empirical	[*i*,*k*]	**No**	Yes	ILR	~N(0,1)	[*k*] ~Inv-Γ(2,1)
M7	Bayesian	Empirical	[*i*,*k*]	Yes	**No**	ILR	~N(0,1)	[*k*] ~Inv-Γ(2,1)
M8	Bayesian	Empirical	[*i*,*k*]	**No**	**No**	ILR	~N(0,1)	[*k*] ~Inv-Γ(2,1)
M9	Bayesian	Empirical	**[*k*]**	Yes	Yes	ILR	~N(0,1)	[*k*] ~Inv-Γ(2,1)
M10	Bayesian	Empirical	[*i*,*k*]	Yes	Yes	**CLR**	~N(0,1)	[*k*] ~Inv-Γ(2,1)
M11	Bayesian	Empirical	[*i*,*k*]	Yes	Yes	**Dirichlet**	N/A	N/A
M12	Bayesian	**Full**	[*i*,*k*]	**No**	**No**	ILR	~N(0,1)	[*k*] ~Inv-Γ(2,1)
M13	**Frequentist**	N/A	**[*k*]**	Yes	Yes	N/A	N/A	N/A

4.3.2.1 Hyper-parameters

Hyper-parameters are an important component of Bayesian inference and are one of the main differences to the frequentist approach. By setting informative hyper-parameters on model priors one is able to incorporate prior knowledge of the system into the model, whilst setting uninformative hyper-parameters allows the modeller to relax assumptions that the system being modelled has been fully understood (Fox and Papanicolaou *et al*., 2008). Here, we tested mixing model sensitivity to changing hyper-parameter distributions on the transformed proportions (Φ). In M1, the mean (μ^{Φ}) and variance ($\sigma^{2\Phi}$) parameters of Φ were assigned normal and inverse gamma distributions of N(0,1) and Inv-Γ(2,1), respectively, where the Inv-Γ employs a shape-rate parameterisation and ensures positivity (Plummer, 2003). In M2, Φ was assigned a more informative distribution through the selection of a narrower inverse-gamma distribution on the variance ($\sigma^{2\Phi}$~Inv-Γ(0.001,0.001)). In M3, Φ was assigned a less informative distribution through a wider normal distribution on the mean (μ^{Φ} ~N(0,1000)). In M4, μ^{Φ} was fixed to zero which equates to a more rigid prior assumption of 33.33% mean

contribution from each source (e.g. Parnell *et al.*, 2013). And finally, a common $\sigma^{2\Phi}$ for all sources (*k*) was tested in M5 (e.g. Hopkins and Ferguson, 2012).

4.3.2.2 Covariance terms

Covariation between the geochemical properties of soils and sediments is well known (e.g. Rawlins, 2011a). Incorporating correlation between input parameters into models is also known to have considerable implications for estimated uncertainties, thus making it an important part of both frequentist and Bayesian inference (Dilks *et al*., 1992; Smith *et al.*, 1992). This was achieved in M1 through the use of MVN distributions to parameterise source and target variability (Σ^{s} and Σ^{resz}), with an inverse-Wishart prior on the combined residual and instrument error term (Σ^{resz}). Model sensitivity to the inclusion of covariance terms was then assessed by first removing covariation between source area fingerprints (M6 and M8) and then removing it from the combined residual and instrument error term (M7 and M8) by setting the off-diagonal elements of these covariance matrices to zero. For M7 and M8, this involved replacing the inverse-Wishart prior on Σ^{resz} with an inverse-gamma prior Inv-Γ(2,1) on the variance terms (the diagonal elements of Σ^{resz}).

4.3.2.3 Time-variable sources

In M1, data are drawn from new source distributions (*S*) at each time-step, thereby enabling temporal variability in sediment source geochemistry to be incorporated into the model. This is important because it allows the model to implicitly account for the erodability and connectivity of different locations within any given source classification (Fox and Papanicolaou *et al*., 2008), whilst also enabling the model to account for transient sediment storage within the fluvial system. We assessed model sensitivity to the inclusion of temporal source variability by removing the temporal component in M9, thus ensuring source area distributions were kept constant for each SPM sample. Other researchers (e.g. Brewer *et al*., 2011; Parnell *et al*., 2013) have included more explicit temporal source components in their mixing models, such as using splines to model autocorrelation within the dataset. These features can allow specific knowledge of temporal relationships to be incorporated into the model (e.g. specific bed sediment storage parameters). This aspect represents a promising area of mixing model development which warrants separate investigation and, as such, was not explored further

here. This would provide a useful focus for future research into mixing model development.

4.3.2.4 Characterising proportions

Logically, the posterior distribution of the proportions should conform to positivity and unity requirements, such that contributions from any one source must be between zero and one, and the contribution from all sources must sum to one. Such assumptions can be met through the selection of appropriate parameterisations of *P*. As discussed above, this is achieved in the benchmark model through the ILR transformation. Another transformation for compositional data is the centered log-ratio transformation (CLR) (Aitchison, 1986), which has been applied in previous mixing model studies (Semmens *et al.*, 2009; Hopkins and Ferguson, 2012). The CLR transformation, tested in M10, may be favoured in some instances because, in contrast to the ILR, it does not lose the direct one-to-one relationship between the original proportions and the transformed Φ values, thereby making interpretation somewhat simpler (Pawlowsky-Glahn and Egozcue, 2006). The CLR is defined as (Equation 4.7):

$$\Phi_i = \mathrm{CLR}(P_i) = \log\left[\frac{P_{i1}}{g(P_i)}, \ldots, \frac{P_{ik}}{g(P_i)}\right] \quad (4.7)$$

where $g(P_i)$ is the geometric mean of the proportions (Equation 4.4). An alternative to transformation is to use a Dirichlet prior on the untransformed proportions (M11). Being a multivariate generalisation of the Beta distribution, the Dirichlet is defined on the interval (0, 1) in the simplex and therefore conforms to the unity requirements (Lingwall *et al*., 2008; Massoudieh *et al*., 2012; Erhardt and Bedrick, 2013). The Dirichlet shape parameters (α) were assigned weakly informative hyper-parameters with prior Inv-Γ(2, 1).

4.3.2.5 Full versus empirical Bayes

The distinguishing feature of empirical Bayesian approaches (M1) is that some prior distributions are estimated offline using deterministic data, meaning that the parameters of the prior distributions are essentially fixed at the Maximum Likelihood estimate (Carlin and Louis, 1996). This has the advantage of reducing model complexity and correlation between parameters, however it also reduces model flexibility and can lead to biased estimates where the data are unrepresentative - a particular problem with

small sample sizes (e.g. <20) (Ward *et al.*, 2010). The alternative is a full Bayesian approach (Palmer and Douglas, 2008; Hopkins and Ferguson, 2012) where hyper-parameters are themselves treated as random variables with prior distributions and all priors are integrated out during the numerical solution (Fox and Papanicolaou *et al.*, 2007, 2008). This is true to the Bayesian paradigm, whereas empirical Bayes is an approximation for numerical tractability. We tested the sensitivity to a full Bayesian approach in M12, where the prior means of the sources (*S*) were assigned informative MVN(μ^{sg},Σ^{sg}) distributions to aid convergence, while weakly informative Inv-Γ(2,1) distributions were assigned to the source variances (Figure 4.1). Covariation was omitted from the full Bayesian formulation due to numerical difficulties in ensuring all covariance matrices met the required positive-definiteness criteria. The empirical Bayes equivalent of M12 is thus M8.

4.3.2.6 Frequentist models

Bayesian mixing models and frequentist Maximum Likelihood optimisation differ fundamentally in the way they use probability. In Bayesian models, the parameters are treated as unknown random variables and are determined probabilistically (Lunn *et al.*, 2000). In frequentist approaches, the model parameters are deterministic and only their estimates are random (Carlin and Louis, 1996). To understand the impact of selecting Bayesian or Maximum Likelihood approaches on source apportionment estimates, we compared M1 against M13 – a modified version of the least squares regression sediment fingerprinting model presented by Collins *et al.* (1997, 2013a). The model solution was determined by optimisation through minimising the sum of squared residuals (SSR) (Equation 4.8):

$$\text{SSR} = \sum_{j=1}^{J}\left(Y_j - \sum_{k=1}^{K} S_{j,k}P_k\right)^2 \quad (4.8)$$

whilst satisfying the following constraints:

$$\sum_{k=1}^{K} P_k = 1$$

and

$$P_k \geq 0$$

Similar to Collins *et al*. (2013a), source and target variability were incorporated by nesting the optimisation step within an ordinary Monte Carlo iteration that sampled from the source and target distributions. As with the Bayesian approach, source area fingerprints (*S*) were parameterised via multivariate normal distributions to account for covariance. Instrument precision, as determined via repeat analysis of sediment standards, was incorporated via the covariance parameter of the multivariate normal distribution used to parameterise the target (*Y*) values. Following standard practice, the robustness of the source apportionment estimates was evaluated via the goodness-of-fit (GOF) criterion presented by Martínez-Carreras *et al.* (2010b) (Equation 4.9), with a tolerance criterion for acceptance set to $\geq$0.95, as recommended by Motha *et al*. (2003):

$$\text{GOF} = 1 - \left\{ \frac{1}{J} \left[\sum_{j=1}^{J} \left(Y_j - \sum_{k=1}^{K} S_{j,k} P_k \right) / Y_j \right] \right\} \quad (4.9)$$

4.3.2.7 Particle size and organic matter corrections

This frequentist model (M13) approach differs from that presented by Collins *et al*. (2013a) in that no correction factors for particle size or organic matter (OM) were incorporated within the model. Such corrections have previously been applied to source and target sediment fingerprint values based on the assumption that downstream selective transport preferentially carries more of the finer, organic-rich material downstream (Walling and Moorehead, 1989; Collins *et al*., 1997; Collins *et al*., 2012; Koiter *et al*., 2013). Therefore, if the target SPM is finer or richer in OM than the corresponding source areas as a result of this downstream selective transport, then concentrations of certain fingerprints within SPM may be higher as a result. This could skew the mixing model results as this geochemical variation would be apportioned to changes in source area contribution rather than differences driven by preferential transport. These corrections typically take the form (Equation 4.10):

$$\frac{Y_x}{S_{xk}} \times S_{jk} \quad (4.10)$$

where Y_x is the OM concentration or specific surface area (SSA) of SPM; S_{xk} is the mean OM concentration or SSA for each source area (*k*); and S_{jk} is the mean concentration of each fingerprint (*j*) in each source area (Collins *et al*., 1997). This represents a very simplistic correction, with the ratio of Y_x:S_x applied to all fingerprints. Any fingerprint specific associations with SSA or OM are neglected (Russell *et al*., 2001). Previous

research by Smith and Blake (2014) found that the relationships between OM, particle size and sediment geochemistry is complex and generalising these relationships through simplistic, one size fits all correction factors carries the inherent risk of miscorrecting the data and thereby generating additional unknown levels of uncertainty. This complex relationship can be seen in Figure 4.2, which shows correlations between POC and eight other elements in SPM samples collected under both high- and low-flow conditions at site A between May 2012 and March 2014. It is apparent that associations are, for the most part, weak and inconsistent in direction across the eight fingerprints (R^2 = -0.105 to 0.308). Whilst concentrations of most elements do increase with the increasing OM content of SPM, the weak and variable nature of the associations clearly render the application of a single correction factor to all fingerprints inappropriate and unnecessary.

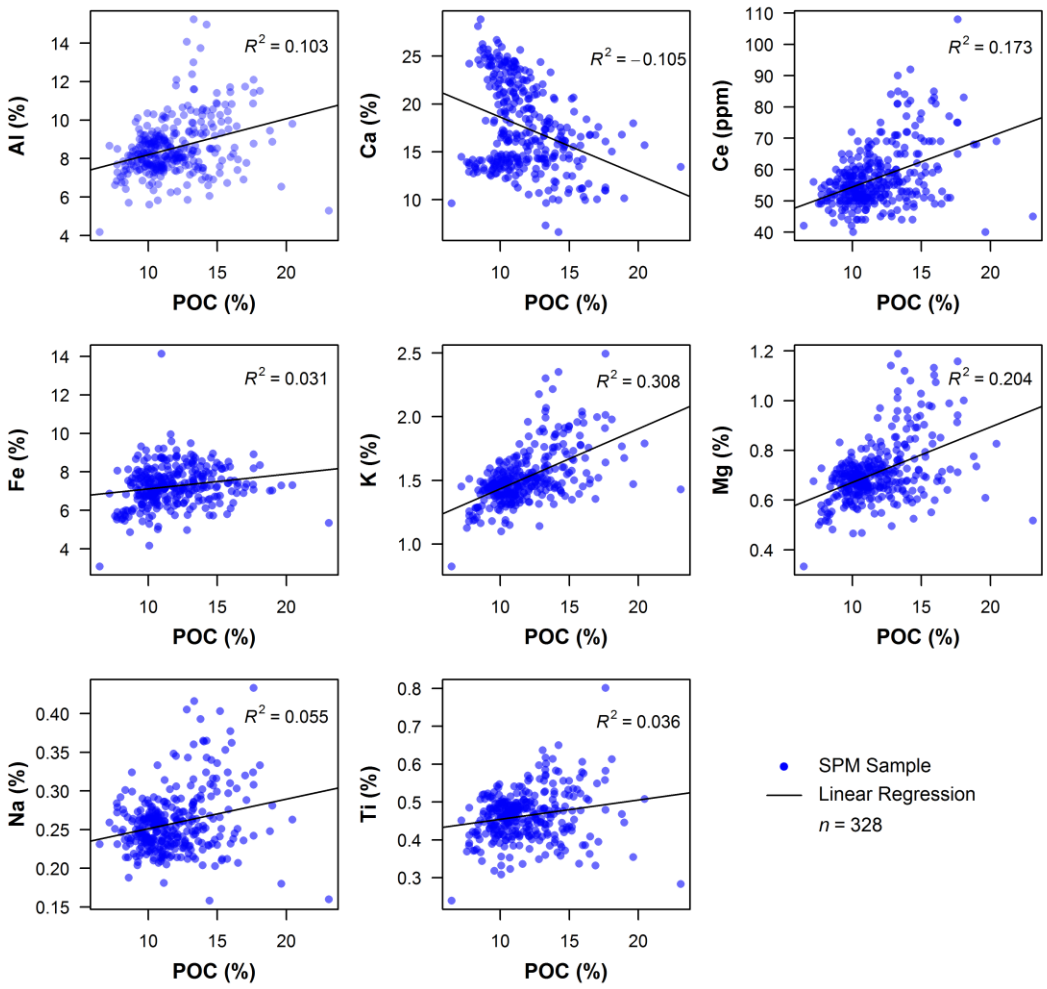

Figure 4.2: Correlation plots of POC versus eight elements selected as fingerprints for site A. SPM samples were collected under high- and low-flow conditions between May 2012 and March 2014.

Correcting for both OM and particle size could also result in an over-correction of the mixing model, as the two parameters are likely to be inter-related (i.e. fine material tends to be organic rich). For example, Smith and Blake (2014) found that applying corrections to fallout radionuclide data from surface and subsurface soils resulted in a complete and nonsensical inversion of radionuclide concentrations with depth. Furthermore, as Smith and Blake (2014) highlight, differences in OM content and SSA between sources and target are unlikely to solely reflect downstream selective transport. Some of this variation likely reflects genuine differences in OM content and SSA between source groups and thus applying corrections would remove a potentially helpful discriminatory characteristic. Such corrections also fail to account for the fact that a potentially significant proportion of OM present in stream sediments would have been generated by autochthonous sources (e.g. bacteria, algae, macrophytes) and would therefore not relate to the preferential transport of terrestrial sediments. For all of the above reasons, explicit OM and particle size correction factors were omitted from the mixing model. If the actual source mixing processes that occurred in this study required such corrections, this model error would be implicitly wrapped up in the residual error distribution (Σ^{resz}) in the results.

4.3.3 Sample Collection and Processing

Comprehensive details of the fieldwork and laboratory procedures employed are presented in Chapter 5 and can also be found in Cooper *et al*. (2015a). However, to summarise briefly here, three potential sediment contributing source areas where identified across mini-catchment A. Namely, arable topsoils, damaged road verges and a combined stream channel bank and agricultural field drain 'subsurface' source. Previous studies have demonstrated that by merging sources with similar properties, as was true here for channel bank and field drain sediments, the resulting reduction in the number of potential sources can significantly improve source apportionment performance (Parnell *et al.*, 2010; Ward *et al*., 2011). Thirty samples of both topsoil and road verge material were collected as <50 mm surface scrapes from areas susceptible to erosion that had potentially high connectivity to the stream channel. Channel bank sediments were sampled as surface scrapes at depths of 10, 30 and 50 cm above the streambed at 10 locations along a 2.9 km stretch of the river in mini-catchment A to yield 30 samples. Sediments discharging from field drains were collected by bulking together grab samples taken from 120 drains identified across the mini-catchment to yield 30 samples for analysis. For the target mixture data, instream SPM was collected as 1-8 L grab samples

under baseflow conditions at approximately weekly intervals between 7th August 2012 and 6th August 2013, yielding a total of 40 samples.

All SPM samples were vacuum filtered through QFF papers to extract particulate matter. Consolidated source area material was first sonicated for 7-min in a water bath and wet sieved to <63 µm before being vacuum filtered onto QFF papers to ensure that particle size distributions, and thus geochemistry, of sources and SPM were comparable (Legout *et al.*, 2013). The geochemistry of all the sediment covered QFF papers was then assessed directly by XRFS following the methods presented in Chapter 3, yielding concentrations for 11 major elemental fingerprints (Table 4.2).

Table 4.2: Summary geochemistry data for SPM and source area sediments. µ is the mean; σ is the standard deviation.

Source Areas	Statistic	Concentrations (weight %)							
		Al	**Ca**	**Ce**	**Fe**	**K**	**Mg**	**Na**	**Ti**
SPM	µ	8.17	22.51	0.0051	8.08	1.43	0.70	0.23	0.47
(n = 40)	σ	0.57	1.76	0.0003	0.68	0.09	0.04	0.02	0.03
Channel Banks	µ	6.97	35.47	0.0036	5.04	1.19	0.61	0.19	0.45
(n = 30)	σ	2.34	7.65	0.0013	1.65	0.44	0.18	0.06	0.09
Field Drains	µ	6.89	17.50	0.0049	8.21	1.12	0.51	0.26	0.38
(n = 30)	σ	2.49	8.23	0.0015	5.14	0.39	0.17	0.09	0.11
Road Verges	µ	10.40	6.63	0.0086	6.12	2.08	1.01	0.48	0.61
(n = 30)	σ	0.99	1.32	0.0007	0.48	0.11	0.09	0.05	0.02
Topsoils	µ	14.07	3.97	0.0091	6.93	2.45	0.88	0.41	0.66
(n = 30)	σ	1.17	2.00	0.0008	0.62	0.23	0.07	0.04	0.02

4.3.4 Discriminating Source Areas

Before including any fingerprints in the model, the mixing space geometry of source area geochemistry was examined via a principal components analysis (PCA). The Kruskal-Wallis *H*-test, which is the non-parametric alternative to the one-way-analysis-of-variance (ANOVA), was then applied to identify which of the fingerprints were significantly different between at least two source groups and thereby able to discriminate between them. A stepwise linear discriminant analysis (LDA) variable selection procedure based on the minimisation of the Wilk's Lambda criterion with leave-one-out cross validation was also employed to quantitatively determine the proportion of source area samples that could be correctly classified (Collins *et al.*, 1997).

LDA explicitly looks for linear combinations of fingerprints that best explain differences between the source classes and can therefore be used to identify the optimum combination of fingerprints for differentiating source areas. From these tests, the resultant suite of eight elements (Al, Ca, Ce, Fe, K, Mg, Na, Ti) was selected for the mixing models (Figure 4.3; Table 4.3).

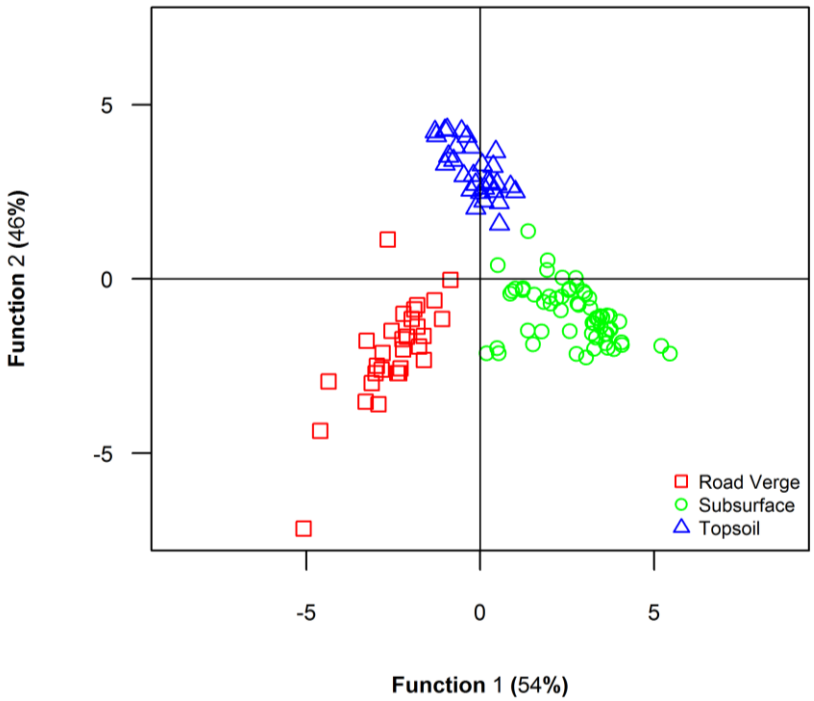

Figure 4.3: Linear discriminant analysis (LDA) plot showing separation of the three source areas by the eight elemental fingerprints.

Table 4.3: Kruskal-Wallis one-way analysis of variance and minimisation of Wilks-Lambda fingerprint discrimination statistics.

	Kruskal-Wallis		**Minimisation of Wilks-Lambda**			
Fingerprint property	***H*-value**	***p*-value**	**Selection step**	**Wilks-Lambda**	**Cumulative *p*-value**	**Cumulative % of sources correctly classified**
Ca	101.96	<0.001	1	0.1724	<0.001	79.2
K	96.42	<0.001	2	0.0499	<0.001	85.0
Mg	82.41	<0.001	3	0.0195	<0.001	93.3
Al	88.76	<0.001	4	0.0103	<0.001	96.7
Ce	91.85	<0.001	5	0.0086	<0.001	97.5
Fe	25.91	<0.001	6	0.0075	<0.001	97.5
Na	90.37	<0.001	7	0.0075	<0.001	97.5
Ti	93.55	<0.001	8	0.0066	<0.001	97.5

Such combinations of multi-property fingerprints are typically utilised because different elements can have different mobilisation and transport dynamics, thus helping to improve source area differentiation. Additionally, using multi-property fingerprints helps avoid potentially spurious matches between source area and target sediments that commonly arise when using a single diagnostic property (Collins *et al*., 1998; Russell *et al*., 2001). Furthermore, previous research has demonstrated that, provided fingerprints are legitimate, maximising the number of tracers can help to significantly improve differentiation and reduce model uncertainties (Small *et al*., 2002; Dutton *et al*., 2013). In this respect, the LDA tracer reduction step was not strictly necessary. However, we chose to employ it here in order to aid numerical efficiency and improve model convergence by reducing the number of variables present, whilst still maintaining sufficient data to facilitate discrimination.

4.3.5 Conservative Fingerprint Behaviour

Implicit within the sediment fingerprinting procedure is the assumption of conservative fingerprint behaviour during mobilisation and transport of sediments from source areas to the stream channel. Conservative behaviour is important because any alterations in chemical or physical state could jeopardise the ability of the particular geochemical properties to serve as accurate fingerprints for sediment sources (Motha *et al*., 2002; Walling, 2005). As discussed above, the selective transport of fine, OM rich material is one such way in which the assumption of conservative transport can be violated. However, past research has indicated that there are also many other physical, chemical and biological processes that can act upon sediments during mobilisation, transport and storage, modifying their fingerprint properties (Koiter *et al*., 2013). For example, biologically mobile elements (e.g. P and K) may be assimilated by plants, other elements may be diluted as a result of leaching through the soil profile, whilst some fingerprints, particularly those at the soil surface (e.g. fallout radionuclides), may be concentrated as surface runoff mobilises only the upper most soil layers (Koiter *et al*., 2013). Precipitation, dissolution and adsorption processes can also alter sediment characteristics, especially with regard to the finer particulate fraction. For these reasons, it has been recommended that the most suitable fingerprints are those that are environmentally benign and thus less susceptible to modification (Zhang *et al*., 2001). One simple, albeit not overly robust, method of assessing whether sediment geochemistry exhibits conservative behaviour is to examine the geochemical mixing space to see whether target sediments extend outside the range of values observed across the

respective source areas. This was carried out here, but further research is required to better understand how the mobilisation and transport of sediments affects geochemistry.

4.3.6 Running the Models

All Bayesian modelling was carried out using the open source software JAGS version 3.3.0 (Just Another Gibbs Sampler; (Plummer, 2003)) within the R environment (R Development Core Team, 2014). JAGS performs hierarchical Bayesian inference using a Gibbs sampling Markov Chain Monte-Carlo (MCMC) algorithm on the prior probability distributions and the likelihood function to estimate the posterior distribution. All mixing models were run for 750,000 iterations, with a 100,000 sample burn-in and jump length of 225 to minimise autocorrelation between runs and ensure low density regions of the distributions were adequately sampled. To confirm convergence of the MCMC random walk on the equilibrium distribution, three MCMC chains were run in parallel from different starting conditions and trace plots of the parameter distributions were inspected for evidence of mixing. Convergence diagnostics were performed via the R package 'coda' (Plummer *et al.*, 2006). The frequentist M13 was run using the 'limSolve' R package (Van den Meersche *et al*., 2009) and was afforded 750,000 iterations to converge on the optimum solution.

4.4 Results

4.4.1 Apportioning sources of SPM

The posterior proportion estimates of the benchmark model reveal subsurface material to be the dominant source of SPM under baseflow conditions throughout the period from August 2012-August 2013 (Figure 4.4). Estimated median sediment contributions derived from the combined channel bank and field drain source areas vary between 71-80% (51-92% at the 95% credible interval), with median contributions of 6-9% (1-27%) for arable topsoils and 12-17% (4-38%) for road verges. The dominance of subsurface sediment contribution, particularly during the summer months when field drains cease flowing, indicates that erosion of the lower section of stream channel banks is the primary mechanism of SPM generation under baseflow conditions. Relatively low contributions from topsoils and road verges indicate limited surface land-to-river sediment transfer outside of heavy precipitation events, as intuitively would be expected.

With negligible surface runoff occurring, the continued contribution of road verge and topsoil material to SPM indicates the resuspension of material from these sources deposited on the streambed during prior precipitation events. Temporal fluctuations in this surface source contribution, which is not correlated to either stage or SPM concentration (Figure 4.4), likely reflects both the degree of bed disturbance prior to sampling and the antecedent sediment delivery conditions – i.e. whether a rainfall event had delivered topsoil and road verge material to the stream in the days preceding sample collection (Cooper *et al.*, 2015a).

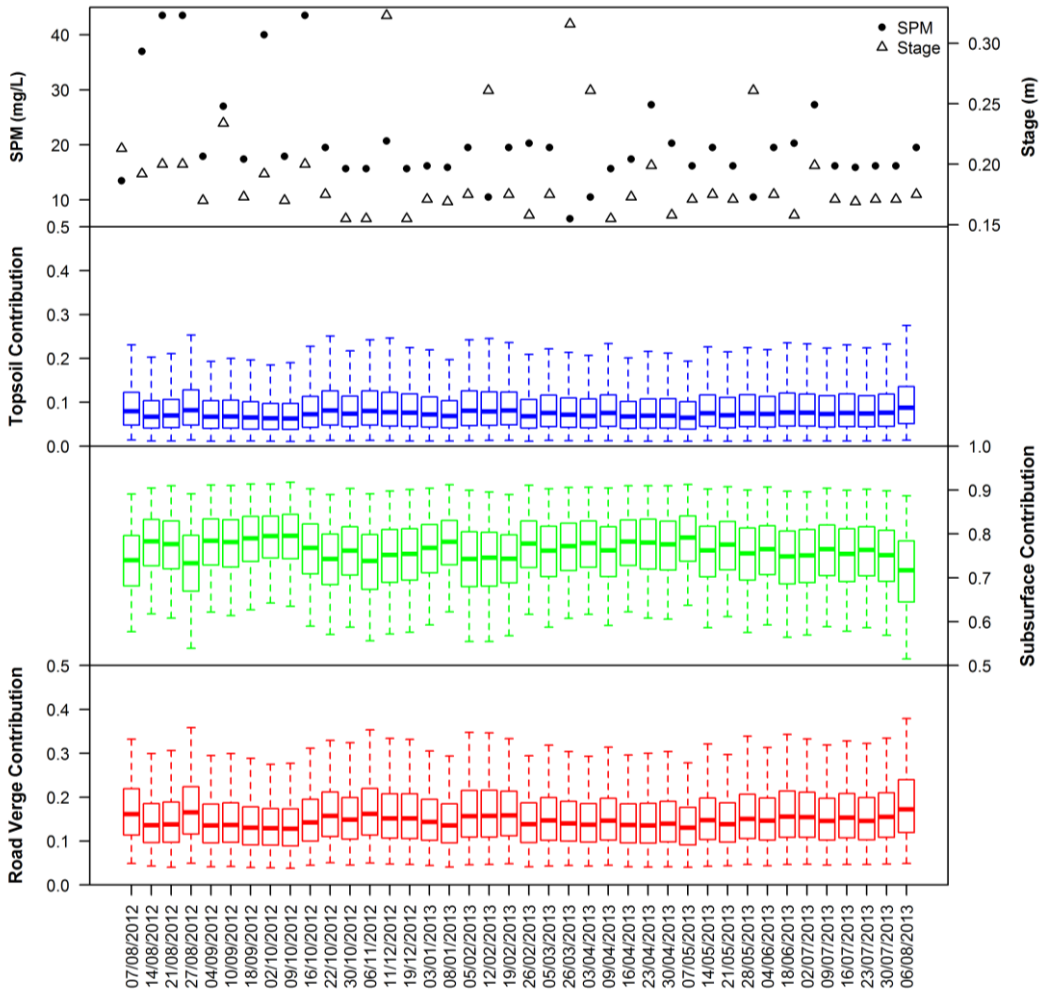

Figure 4.4: Model 1 source apportionment estimates under baseflow conditions for the period August 2012-August 2013. The solid central line and the end of the boxes and whiskers represent the median, 50% and 95% Bayesian credible intervals, respectively.

4.4.2 Model Sensitivity

Source apportionment results for the 13 model versions are summarised in Figure 4.5 as the temporal average across all 40 SPM samples. Whilst all models estimate

subsurface sediments to be the dominant source of SPM in the River Blackwater, significant differences exist in the median contributions and width of credible intervals (CI). These departures from the benchmark model results are explored in turn. Note, depending upon the shape of the posterior distributions, the median contributions across sources do not necessarily sum to unity.

Models 2-5: Selection of a more informative hyper-parameter distribution for the variance on Φ in M2 had a major impact upon estimated uncertainties, reducing CI widths by 6.7%, 18.2% and 11.8% for topsoils, subsurface sources and road verges, respectively, relative to the benchmark model. The impact upon the median source contributions was less pronounced, varying by <2.6% across all sources. The reverse situation arises with M3, where the selection of a vague prior hyper-parameter distribution for the mean on Φ resulted in a reduction of estimated median topsoil contribution by 5.6%, whilst subsurface material and road verge contributions increased by 0.5% and 5.2%, respectively. The range of 95% CIs were also impacted, although not as strongly as for M2. For M4, fixing the prior mean of Φ at zero resulted in some of the largest deviations in median apportionment, with increases of 7.1% and 2.0% estimated for topsoils and subsurface material, respectively, and a decline of 8.9% in estimated road verge contribution. This reversed the order of importance of topsoil and road verge sediment contributions. M4 topsoil and subsurface source CI widths were also ~15% wider compared with the benchmark model. Lastly, fixing the variance parameter of M5 across sources had limited impact on model results, with median contributions and CI ranges varying by less than 0.9% and 1.9%, respectively, across all sources.

Models 6-8: Omitting source covariance from M6 resulted in a 2.8% and 2.5% increase in estimated median subsurface and topsoil contributions, respectively, whilst road verge contribution declined by 5.3%. Additionally, the 95% credible interval ranges decreased by 5.6% and 6.6% for subsurface and road verges, respectively. Removing covariance from the combined residual and instrument error term (M7) had a less pronounced effect, with median proportions varying by less than 2.7% across all sources and credible interval ranges varying by a maximum of 4.8%. Removal of all covariance (M8) impacted most strongly upon median road verge contribution, which declined by 5.4%, and subsurface credible interval width, which narrowed by 6.2% - overall similar to the behaviour of M6, indicating that the mixing model results are more sensitive to the parameterisation of source covariance than of instrument and residual covariance.

Model 9: Making the source distributions time-invariable impacted upon the estimated apportionment uncertainty, which increased significantly for both subsurface (5.1%) and

topsoil (6.8%) sources. Estimated median proportions were also affected, increasing by 6.6% for the subsurface and declining by 5.9% and 0.6% for road verges and topsoils, respectively.

Models 10-11: Application of the CLR transformation (M10) had only minor influence on the posterior distributions relative to M1. Median proportions varied by less than 1.1% across all sources, whilst the credible interval ranges increased across all sources by a maximum of just 2.1%. Similarly, application of the Dirichlet distribution (M11) also had limited impact on the median proportions which varied by less than 0.5%. Credible interval ranges did, however, increase for all sources by up to 6.2%.

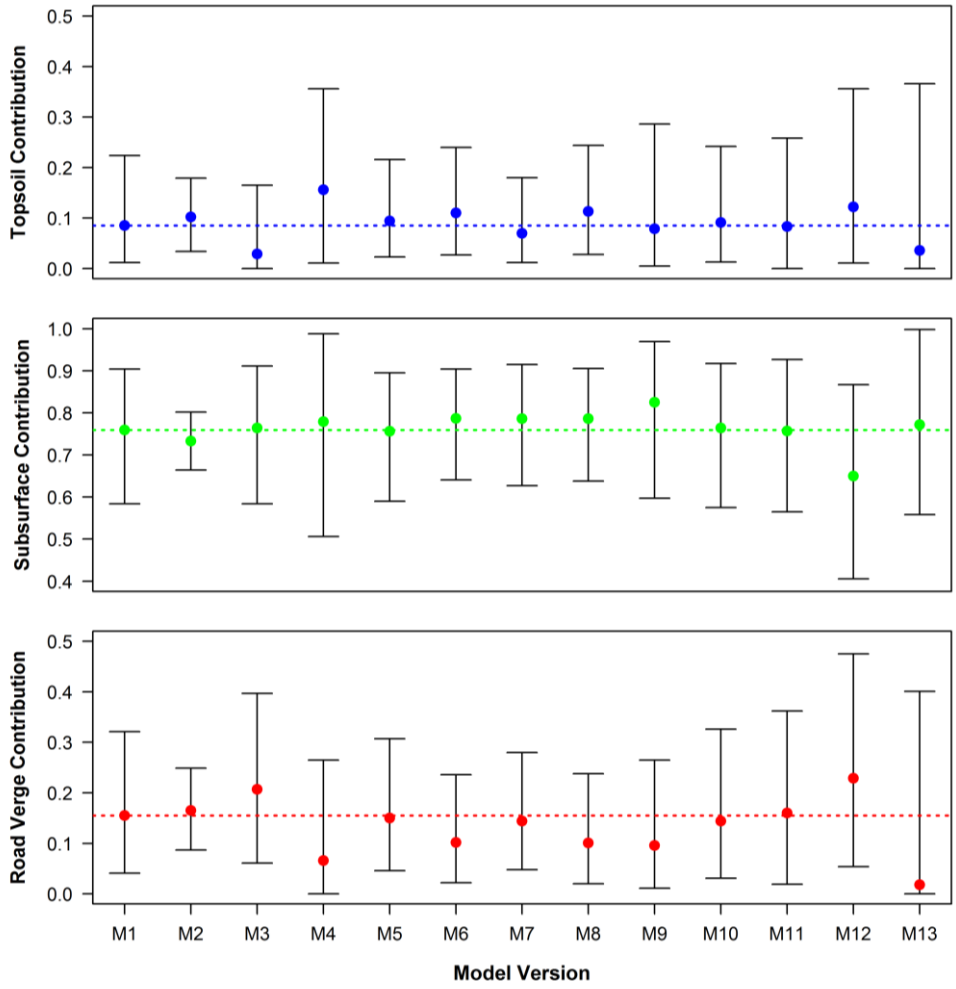

Figure 4.5: Comparison of sediment source apportionment as estimated by 13 mixing model versions. Results displayed as the average of 40 SPM samples spanning August 2012-August 2013. Points represent median contributions with associated 95% credible interval error bars, whilst dashed lines represent the median contribution estimated by the benchmark model.

Model 12: The full Bayesian model had a major impact upon estimated uncertainties relative to M1, increasing credible interval widths by 13.2%, 14.1% and 14.2% for

topsoil, subsurface and road verges, respectively. Estimated median contributions were also significantly impacted, reducing by 10.9% for subsurface and increasing by 3.7% and 7.4% for topsoils and road verges, respectively.

Model 13: Median subsurface apportionment of the frequentist optimisation differed by just 1.3% compared to the M1, despite the major differences in model structure. However, topsoil and road verge contributions were heavily impacted, declining by 4.9% and 13.7%, respectively, and having strongly positively skewed distributions (Figure 4.5). Additionally, the 95% confidence intervals were considerably wider, increasing by 15.4%, 12.0% and 12.1% for topsoil, subsurface and road verge sources, respectively.

4.4.3 Model Runtimes

Runtimes for Bayesian models 1-11 were all comparable at between 289-402 seconds to complete 750,000 iterations of each model time-step (Figure 4.6). Relative to the benchmark model (393 s), M9 had the shortest runtime (289 s), reflecting that, with source distributions being time-invariable, fewer nodes had to be modelled. Similarly, the runtime for M11 (345 s) was reduced due to the inclusion of fewer nodes in the parameterisation of the proportions. Setting less informative priors on the proportions (M3) slightly increased runtimes (403 s) as the MCMC procedure had to explore a larger parameter space.

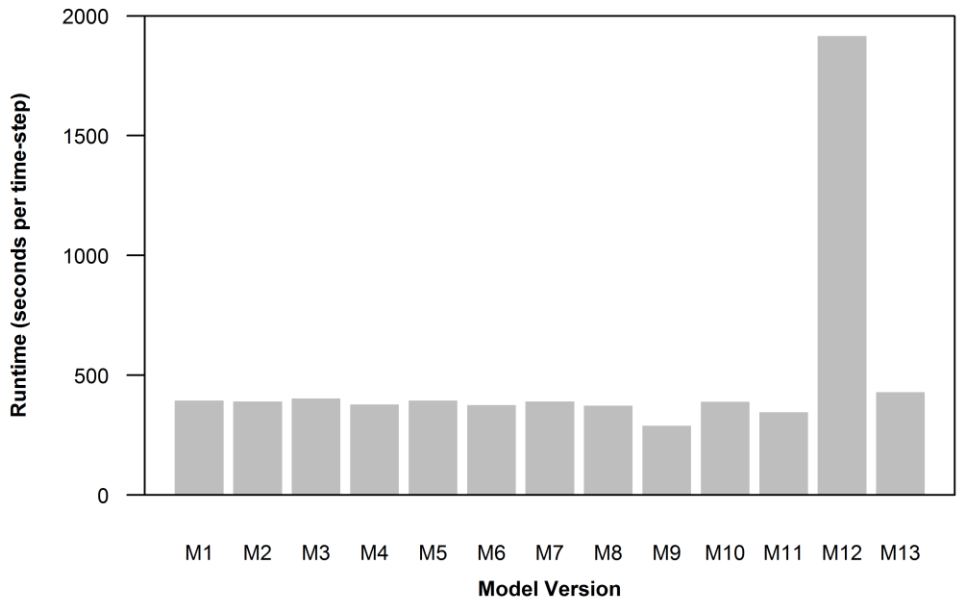

Figure 4.6: Model runtimes for the 13 different model versions, displayed as seconds taken to run each model time-step.

A significantly longer runtime was recorded for the full Bayesian procedure (M12, 1915 s) due to the greater number of hyper-parameters that had to be estimated. The runtime of the frequentist optimisation (M13, 429 s) did not differ significantly from that of the benchmark model.

4.5 Discussion

4.5.1 Hyper-parameters

It is generally understood that the more data that is entered into Bayesian models, the less weight the choice of prior hyper-parameters will have on the resulting posterior distributions (Moore and Semmens, 2008; Van den Meersche *et al*., 2008). Despite the number of fingerprints (eight) included in our model being greater than that commonly used in source apportionment studies (e.g. Fox and Papanicolaou *et al*., 2008), it was still relatively small compared to the number of parameters that had to be estimated. As a result, the model results demonstrate considerable sensitivity to the choice of hyper-parameter values.

The narrower hyper-parameter distribution used in M2 essentially states that the modeller has greater prior certainty (lesser uncertainty) about the shape the posterior distribution should take, hence the reduction in credible interval width. Similarly, the shifts in posterior median sediment contributions for M3 intuitively make sense, because the selection of a wider prior normal distribution to parameterise the mean on Φ has afforded the posterior proportion distributions greater flexibility to vary over a wider range of possible values. However, not all proportions respond in the same direction due to co-dependencies and interactions between the parameters. In M4, the reversal in the order of importance for topsoil and road verge contribution highlights that these two sources occupy similar source geometry in mixing space. This allows for a wider range of possible model solutions, thereby making differentiation difficult and highly dependent upon prior specification (Moore and Semmens, 2008). Previous research has demonstrated that, provided fingerprints are legitimate, maximising the number of tracers can help to significantly improve differentiation and reduce model uncertainties (Small *et al*., 2002; Dutton *et al*., 2013), and this approach would need to be explored here. The increased credible intervals of M4 seem to reflect that as the proportions are pulled toward an unrealistic range around 33.33% a priori, the model is then uncertain where to move next given the limited information content of the data. In fact, all the results appear to demonstrate that sources with high data information content (e.g. subsurface clearly

distinguished by a strong calcium signature; Table 4.2) are less affected by the choice of prior.

Overall, these results correspond with the findings of other mixing model studies (e.g. Franco-Trecu *et al*., 2013) and strongly imply that where hyper-parameters are to be used, they must be carefully selected to prevent model output being biased by poorly chosen priors. In particular, a balance must be struck between setting overly informative priors, that may impart bias onto results if the system being modelled is not fully understood, and setting overly vague priors that may result in the solution remaining undetermined due to the model failing to converge (Sun and Berger, 2006; Van den Meersche *et al*., 2008).

4.5.2 Covariance terms

The considerable sensitivity demonstrated to the inclusion of covariance terms is consistent with previous studies (Dilks *et al*., 1992; Hopkins and Ferguson, 2012; Laceby and Olley, 2014). The narrowing of the uncertainty ranges around apportionment estimates is the result of the narrower source and combined residual-instrument error distributions that occur when covariance terms are omitted from the priors (Figure 4.7). This occurs most strongly for geochemical fingerprints that display a high degree of correlation, and thus covariation, with other elements (e.g. Pearson correlation between Al and Mg = 0.93 here). Thus, as the model degrees of freedom increase with the inclusion of covariance terms, the uncertainty around apportionment estimates also increase. Lower sensitivity is exhibited to the inclusion of residual-instrument error covariance because, as is often the case (Phillips and Gregg, 2001), instrument error is small in comparison with source area variability. Overall, the smaller precision of apportionment estimates when covariance is included is balanced by greater accuracy where covariation does exist. By omitting covariance for either term, one is essentially stating that source fingerprint concentrations are linearly independent and that residual-instrument error is random and uncorrelated (Christensen and Gunst, 2004), conditions not satisfied by the data used here. This false assumption thus translates into unrealistically narrow uncertainty intervals around apportionment estimates.

We can therefore state that whilst modelling of covariance can be difficult due to issues of dimensionality and positive-definiteness constraints (Barnard *et al*., 2000), its inclusion within mixing models is essential if posterior distributions are to accurately represent important co-dependencies between fingerprints (Hopkins and Ferguson, 2012;

Erhardt and Bedrick, 2013). Until now, such covariation has been largely ignored in sediment fingerprinting studies (e.g. D'Haen *et al*., 2013).

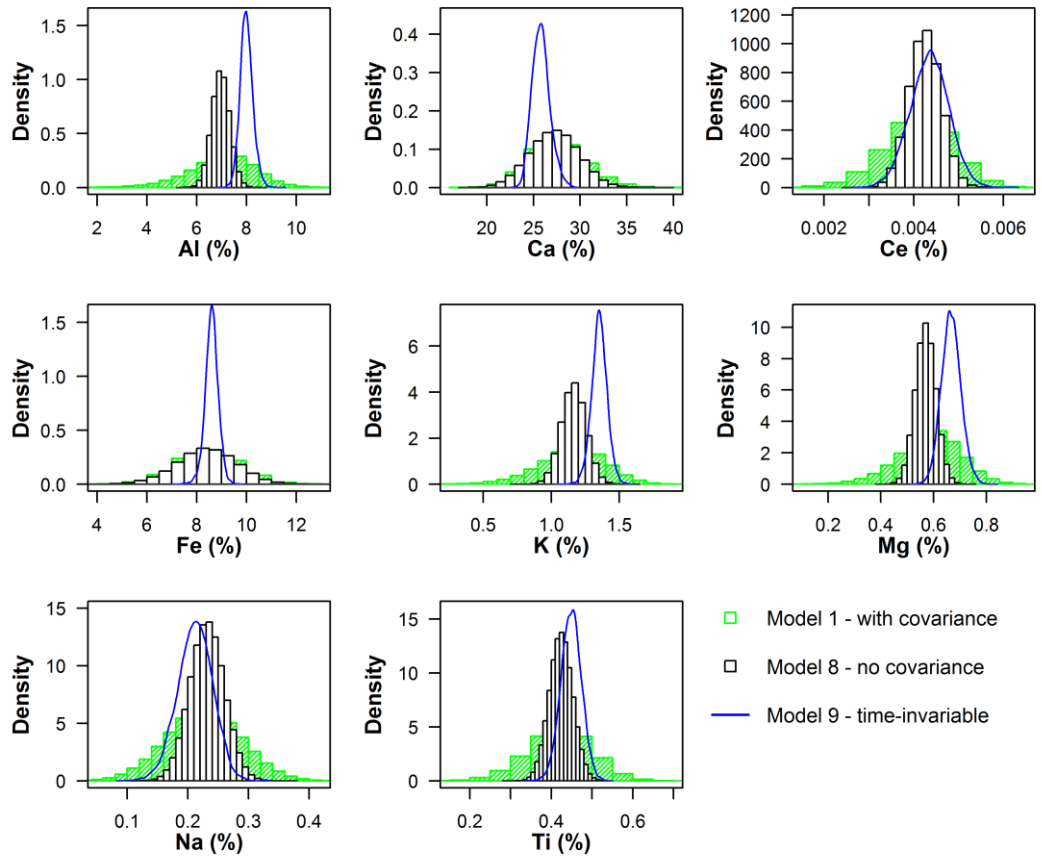

Figure 4.7: Histograms of the combined posterior subsurface source fingerprint concentrations for all 40 model time-steps. Shown for models run with (M1) and without (M8) covariance terms and with time-invariable source distributions (M9).

4.5.3 Time-variability

The consequence of keeping source distributions fixed between time-steps in M9 is that, over the 40 time-steps, source area distributions were less variable than those observed in M1 (Figure 4.7). This also meant that there are fewer degrees of freedom in the model, thus limiting the choice of feasible values that could fit all time-steps. Consequently, the location of proportion distributions was shifted and the uncertainty around apportionment estimates increased. It is also important to recognise that by omitting time-variable sources (e.g. Semmens *et al.*, 2009; D'Haen *et al*., 2012; Erhardt and Bedrick, 2013), mixing models are unable to account for important temporal factors, such as the transient delivery of sediment to the river channel, or the erodability and

connectivity of different sediments at different times within each source area (Fox and Papanicolaou *et al*., 2008). The approach taken in the benchmark model is therefore favoured on mechanistic grounds as these influential variables are implicitly accounted for through more flexible posterior source distributions (Figure 4.7).

4.5.4 Dirichlet distribution and CLR transformation

Out of all mixing model versions, sensitivity was lowest to the selection of either a Dirichlet distribution or a CLR-transformation to characterise the prior proportions. Whilst this implies any method is suitable, previous research has strongly indicated that geometric transformations are preferable (Semmens *et al*., 2009; Parnell *et al*., 2013). This is because the compositional data of the proportions are in a closed form (i.e. must be positive and sum to unity) meaning that any increase in one source will inevitably result in a decrease in another source due to cross-dependencies, regardless of whether there is any mechanistic link between them (Moore and Semmens, 2008; Nosrati *et al*., 2014). Under such circumstances, traditional statistical methods are not appropriate as they are designed to work in independent infinite space, not in situations where there are strong negative covariances between elements (Pawlowsky-Glahn and Egozcue, 2006). Selection between the ILR and CLR transformations appears more subjective, although the ILR can be considered a more sub-compositionally coherent transformation due to the orthogonal nature of the data (Egozcue *et al.*, 2003).

4.5.5 Full Bayes

The high sensitivity exhibited to the adoption of a full Bayes approach arises because the fixed hyper-parameters of the benchmark empirical model are replaced with more uninformative hyper-parameters that are treated as random variables with prior distributions. This increases both the degrees of freedom and the variability of source distributions, thereby allowing a greater range of potential solutions. In essence, it represents the opposite of M2 where more informative priors substantially reduced the estimated uncertainty by narrowing the range of potential *P* values. Whilst the sensitivity exhibited here supports the results of Ward *et al.* (2010), who similarly found increased variability in source contributions when employing a full Bayesian approach, it is in contrast to Parnell *et al*. (2013) who found little difference between the two formulations. This seems to indicate that the implications of approximating full with empirical

Bayesian methods are data specific and may therefore vary between source apportionment studies. The decision on which approach to adopt may come down to how much prior knowledge the modeller has on the system being studied, particularly in relation to how well catchment wide variability in source area geochemistry is captured by the sediment samples obtained in the field. If source distributions are unrepresentative, due to the poor sampling of within-class source area geochemical variability, apportionment via the full Bayesian approach would likely prove less biased by such unreliable data. Similarly, where source mixing space geometry is poor due to overlapping source distributions, the increased flexibility of the full Bayesian approach may help to capture this ambiguity more accurately (Ward *et al.*, 2010). However, such full methods increase model complexity and can lead to correlation between estimated proportions and estimated source means as the model updates prior distributions based on the information in the data (Ward *et al.*, 2010). Whilst this increased correlation is not mechanistically incorrect, it can cause numerical problems for convergence, as emphasised here by a runtime five times greater than that of the benchmark model. Ultimately, the modeller will have to weigh up the trade-off between model accuracy and slow convergence (full Bayesian), and potential bias (empirical Bayes) (Ward *et al.*, 2011).

4.5.6 Frequentist Optimisation

Large apportionment differences between frequentist and Bayesian approaches, which have similarly been recorded in other studies (e.g. Nosrati *et al.*, 2014), can primarily be explained by the type of inference employed. The frequentist method employed here only carries out 'point' optimisation, whereby single random draws are made from the source and target distributions at each iteration of the Monte Carlo wrapper. It is therefore unable to yield full distributions for all of the underlying parameters. A direct consequence is that the optimisation can produce heavily skewed proportion distributions whereby the best fit arises when one source supplies 100% of the sediment and the other sources supply 0% (Figure 4.8). Such skewed distributions are commonly seen in other fingerprinting studies that adopt similar pseudo-uncertainty approaches to optimisation (e.g. Collins *et al.*, 2012) and it can lead to a high solution rejection rate by the GOF criterion, with as few as 10-20% of the solutions being accepted. This situation does not arise in Bayesian inference because the entire distributions of all parameters are fully explored together, resulting in more realistic posterior distributions (Schmelter and Stevens, 2013).

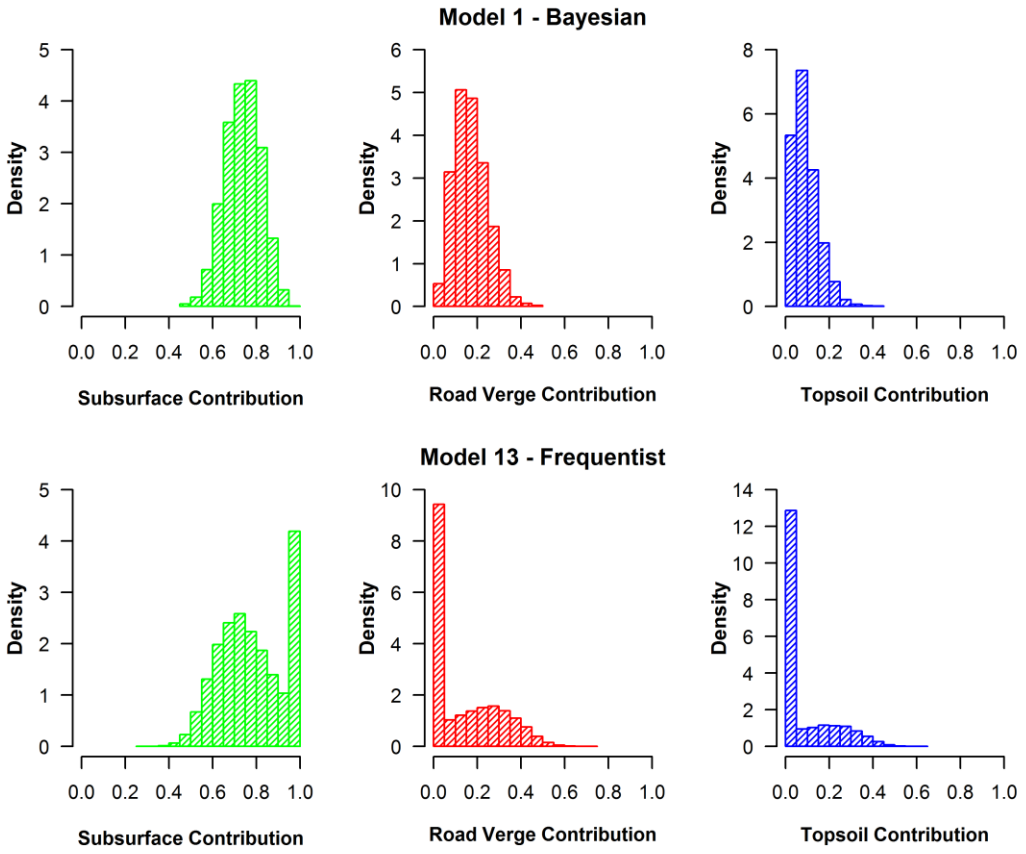

Figure 4.8: Source apportionment histograms for the first time-step, showing the heavily skewed distributions that result from the frequentist optimisation (M13) compared with the Bayesian approach (M1).

To further investigate the performance of the two approaches, M1 and M13 were re-run on four known laboratory mixtures (Figure 4.9). Namely, (a) a pure subsurface sediment; (b) a 50:50 subsurface-topsoil mix; (c) a 33.3% mix of all three sources; and (d) a 75% subsurface, 12.5% road verge and 12.5% topsoil sediment mixture. The results show that whilst both models can unmistakably identify pure subsurface sediments (A), the frequentist model yielded more accurate median contributions. This apparent unique solution might suggest superiority of the frequentist approach. However, as demonstrated in Figure 4.8, this is an artefact of 'point' optimisation within a Monte Carlo wrapper where 100% apportionment from one source is a common result. When the target samples fall between source regions within the mixing space (as occurs in reality and with the other mixtures shown here) the greater accuracy and precision of the Bayesian approach becomes clear once more, particularly with mixtures C and D.

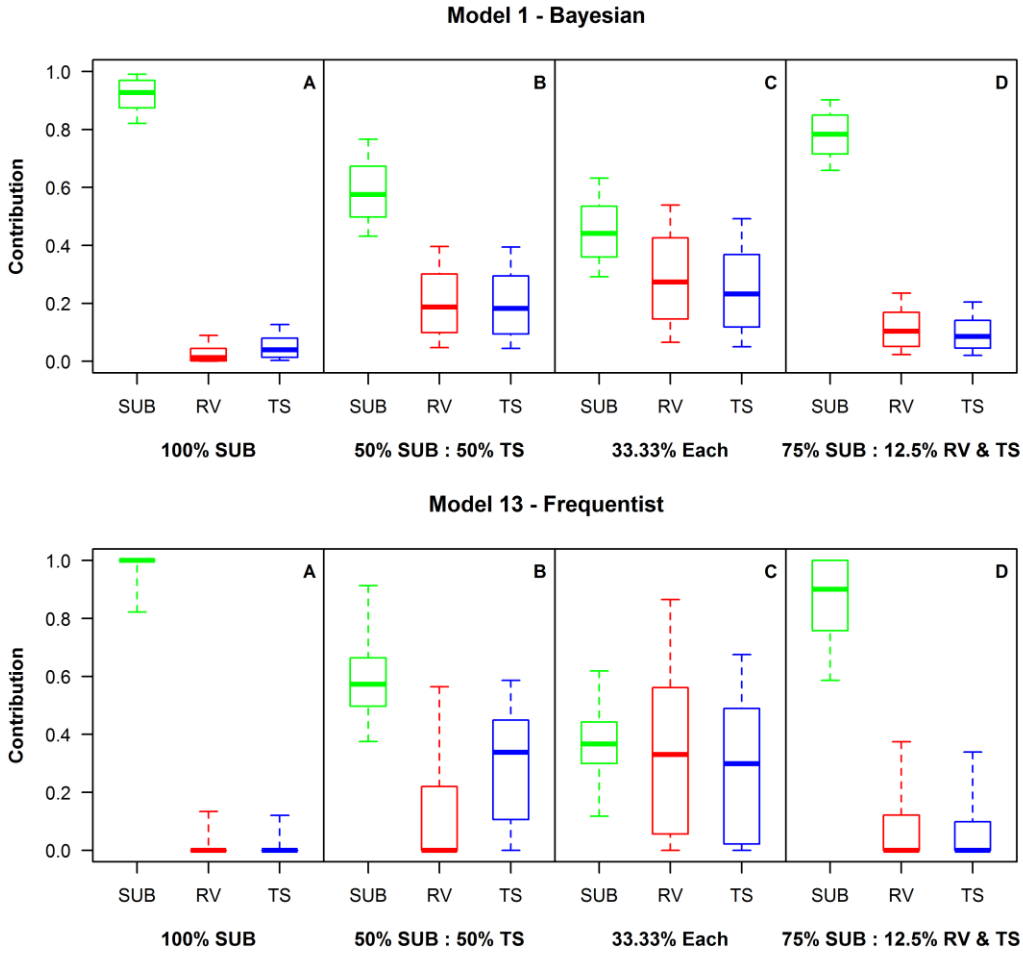

Figure 4.9: Comparing how Bayesian (M1) and frequentist (M13) mixing models perform in identifying sediment samples derived from (A) 100% subsurface sediment, (B) a 50:50 subsurface-topsoil mix, (C) a 33.33% mix of all 3 sources and (D) a 75% subsurface, 12.5% road verge, 12.5% topsoil mix. The solid central line, boxes and whiskers represent the median, 50% and 95% credible intervals, respectively.

4.5.7 Implications and Recommendations

The results of this OFAT sensitivity analysis, which are supported by very similar findings from a four end-member mixing model for the neighbouring mini-catchment B (Figure B1, Appendix B), clearly demonstrate that differences in mixing model structure can impact significantly upon the resulting source apportionment estimates. Without exception, all model versions estimated subsurface sediment sources to be the major contributor of SPM to the River Blackwater under baseflow conditions. However, there existed considerable variation in CI widths and estimated median proportions when one considers that all models used the same empirical data. Indeed, source apportionment

results proved particularly sensitive to the selection of frequentist and full or empirical Bayesian approaches, especially with respect to the estimated uncertainty.

Across the 13 model versions, median contributions (95% CI ranges) varied between 2.9-15.6% (14.5-36.6%) for topsoils, 1.8-22.9% (16.2-42.1%) for road verges and 65.0-82.5% (13.8-48.2%) for subsurface sources, thus yielding a maximum median apportionment variation of 21.1% between models (Figure 4.6). To put this in context with other sources of fingerprinting uncertainty, Smith and Blake (2014) found that the commonly applied particle size correction shifted mean source apportionment by 0-11% relative to the uncorrected model, whilst correcting for both organic matter content and particle size shifted mean apportionment by 0-45%. Similarly, Laceby and Olley (2014) found median source apportionment differences of 0-97% between models with or without tracer discriminatory and source variation weightings. It is therefore apparent that differences in mixing model structure play an equally important role in influencing source apportionment results as applying weighting factors or correcting for particle size and organic matter content. This has significant implications for the interpretation of results from other fluvial sediment fingerprinting investigations. If previous frequentist fingerprinting studies were to be repeated within a Bayesian framework, the results presented here indicate that apportionment results, and the conclusions based upon them, may be different.

It is therefore recommend that users of sediment fingerprinting mixing models carefully consider and justify their choice of model structure and error assumptions when conducting source apportionment studies. Specifically, we advocate a Bayesian approach to mixing model formulation as it provides a robust and flexible framework in which all known and residual uncertainties associated with the mixing model and the dataset can be fully and coherently translated into parameter probability distributions. Furthermore, we recommend the inclusion of covariance terms to ensure that models accurately represent co-dependencies between selected fingerprints and thereby minimise the risk of obtaining unrealistic uncertainty intervals around proportion estimates. We also advise that source distributions are time-variable to enable models to account for differences in source area erodability, connectivity and transient sediment storage. Mechanistic extensions of the mixing model to account for the same effects should be an area of further research, but would require more data for parameterisation. Finally, we recommend that, where possible, uninformative hyper-parameters should be used within a full Bayesian framework to stay true to the Bayesian paradigm and minimise the risk of unrepresentative data biasing results, particularly when fingerprints are poorly defined. However, we acknowledge that convergence issues can arise when model priors are set

too vague, and therefore empirical Bayes methods can provide a pragmatic approximation.

4.6 Conclusions

In this chapter, the sensitivity of fluvial sediment source apportionment estimates to changing mixing model structure has been assessed via a one-factor-at-a-time (OFAT) sensitivity analysis. Thirteen model versions were developed, each with slightly different structures and error assumptions. All 13 models were then applied to SPM geochemistry data from mini-catchment A to apportion sediment contributions from three sources (arable topsoils, road verges and subsurface sediments) under baseflow conditions for the period August 2012-August 2013. Whilst all models estimated subsurface sediments to be the largest contributor of SPM (median ~76%), comparison of apportionment estimates across model versions reveals varying degrees of sensitivity to changing priors, inclusion of covariance terms, incorporation of time-variant distributions and methods of proportion characterisation. In particular, we have demonstrated substantial differences in apportionment results between full and empirical Bayesian approaches and between Bayesian and frequentist frameworks, with median apportionment varying by up to 21% between model versions. Mixing model structure thus impacts heavily upon the resulting source apportionment estimates. This has notable implications for the interpretation of results from other sediment fingerprinting investigations which, due to the lack of a coherent modelling framework, employ a wide variety of modelling approaches that often incorporate source and target uncertainty *ad hoc*. We therefore conclude that users of sediment mixing models should fully consider what impact their choices of model structure and error assumptions have on the resulting source apportionment estimates prior to conducting sediment fingerprinting investigations.

Chapter 5

HIGH-TEMPORAL RESOLUTION SEDIMENT SOURCE APPORTIONMENT[‡]

5.1 Chapter Summary

It has repeatedly been demonstrated that ~90% of fluvial SPM is exported during high-flow storm events that occur for less than 20% of annual duration, with minimal sediment transported during low-flow regimes (e.g. Horowitz, 2008; Bilotta *et al*., 2010; Oeurng *et al*., 2010, 2011). Identifying the sources of SPM during these high-flow periods is therefore crucial if mitigation measures aimed at improving water quality are to be targeted effectively. In this chapter, we demonstrate how the analytical and modelling techniques developed in Chapters 3 and 4 can be applied to quantitatively apportion, with uncertainty, the sources of fluvial SPM at high-temporal resolution throughout the duration of numerous precipitation events. Coupling automatic water samplers with direct XRFS and DRIFTS analyses of SPM covered QFF papers, large numbers of SPM samples were rapidly, accurately and inexpensively analysed at 60- and 120-min resolution for 5 and 6 storm events in mini-catchments A and B, respectively. The Bayesian mixing model was then applied to apportion sediment contributions from eroding arable topsoils, damaged road verges, agricultural field drains and channel bank sources at high-temporal resolution. Calcium-rich sediments from subsurface channel banks and agricultural field drains were found to dominate SPM supply before and after storm events, whilst clay mineral and metal oxide-rich contributions from topsoils and road verges increased within a few hours of rainfall onset as surface runoff was initiated. The results presented in this chapter successfully demonstrate how combining Bayesian mixing models with the direct spectroscopic analysis of SPM-covered filter papers can produce high-temporal resolution source apportionment estimates that can assist with the

[‡] Chapter published as: Cooper RJ, Krueger T, Hiscock KM, Rawlins BG. 2015a. High-temporal resolution fluvial sediment source fingerprinting with uncertainty: a Bayesian approach. *Earth Surface Processes and Landforms* **40**: 78-92. DOI: 10.1002/esp.3621.

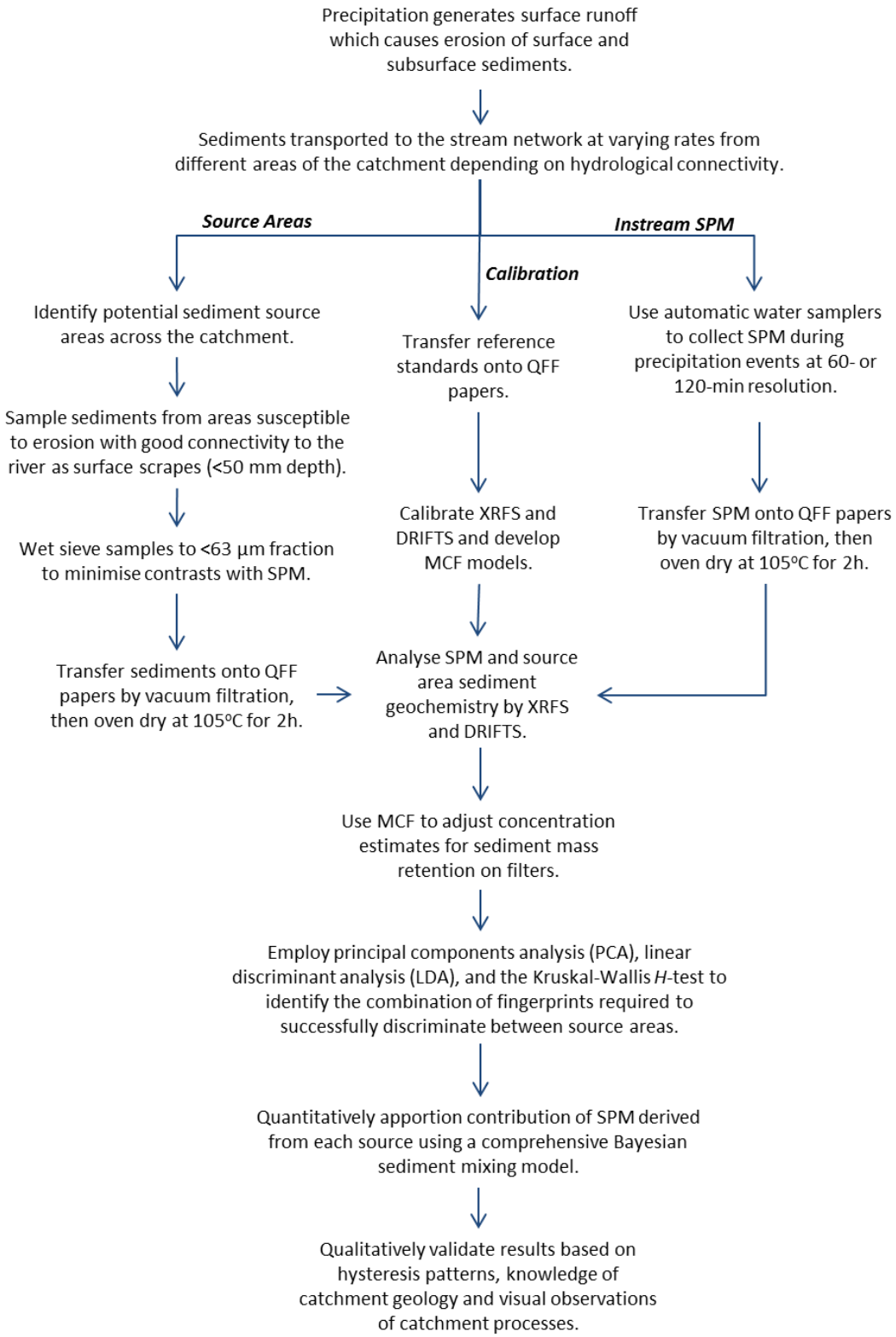

Figure 5.1: Conceptual diagram of the Bayesian sediment source apportionment procedure employed in this chapter.

appropriate targeting of sediment pollution mitigation measures at a catchment level. The conceptual diagram presented in Figure 5.1 summarises the approach taken to Bayesian sediment source apportionment in this chapter.

5.2 Methods

5.2.1 Source Area Sampling

At the beginning of the field sampling campaign, catchment walk over surveys were carried out under both wet and dry conditions to identify potential sediment contributing areas in the Blackwater catchment. Stream channel banks, agricultural field drains, damaged road verges and arable topsoils were identified as the four main sediment source areas within both mini-catchments A and B. Whilst it was not possible to completely rule out sediment contributions from other sources, such as woodland, grassland or windblown dust, our observations and knowledge of catchment land use suggested any such inputs were negligible. Source area sampling was carried out twice in both catchments; during April and October 2013 in mini-catchment A and during August 2013 and March 2014 in mini-catchment B (Figure 5.2).

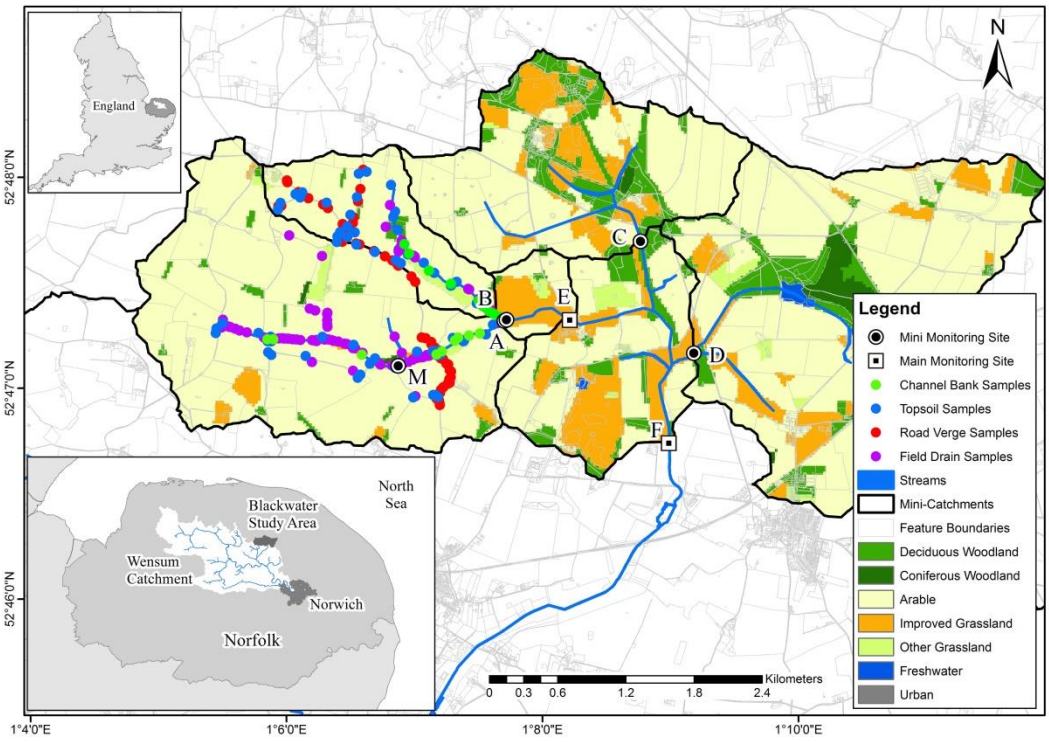

Figure 5.2: Locations of sediment source area sampling in mini-catchments A and B, with land use for the River Blackwater catchment also shown.

5.2.1.1 Surface Sources

Surface soils become a source of fluvial SPM during precipitation events when the kinetic energies of rain splash and overland flow exceed the soil shear strength, detaching and entraining sediments and transporting them to streams via a combination of vertical percolation, diffuse surface sheets and concentrated rill erosion down tramlines and furrows left by agricultural machinery. The total amount of sediment physically mobilised and transported during each storm event is known to vary spatially and temporally depending on the intensity of precipitation, evapotranspiration rates, soil texture and porosity, topography, crop types, the hydraulic connectivity of the field drainage system and the potential for flow interception by vegetation (Johnes and Hodgkinson, 1998; Dougherty *et al*., 2004; Withers *et al*., 2006; Wilson *et al*., 2012).

Here, for both topsoils and road verges, 30 samples of ~100 g were collected from each source area in each mini-catchment. Each sample was collected as <50 mm depth surface scrapes across 1 m long transects using a non-magnetic trowel. Sampling focused upon areas which appeared susceptible to erosion and which potentially had good connectivity to the stream channel. This primarily meant sampling narrow road sections (Figure 5.3A), field entrances (Figure 5.3B), gateways, infield tramlines and road bridges where soil surfaces become damaged by heavy vehicular use and act as critical source areas (CSAs) for sediment ingress into the river. In particular, samples were collected from areas in close proximity to impervious metalled roads as these had been observed to increase land-to-river connectivity by channelling sediment-laden water during precipitation events. Additionally, two topsoil samples were collected from a small copse of deciduous trees in mini-catchment B through which the stream flowed. Although there was no visible evidence of soil erosion in this area due to a thick, protective, leaf litter layer, the fact that the stream flowed directly through the middle of this copse justified the collection of a limited number of samples.

Differences in the geochemistry between topsoil and road verge material likely reflect two factors: soil management and sediment deposition. Arable topsoils are modified by intensive cultivation, frequent fertilizer application, addition of crop residues, and are a mixture of deep and shallow soils as a consequence of soil inversion during ploughing. Conversely, uncultivated road verges represent solely surface soil and experience enhanced deposition of material from vehicles and salt inputs from winter road gritting. To ensure actual road verge material was sampled and not transient sediments from other sources deposited on the road during prior precipitation events, the outermost layer of verge sediment was brushed away to expose fresh material for sampling.

Figure 5.3: Eroding road verges (A) and damaged field entrances (B) represent two of the critical sediment source areas in mini-catchments A and B.

5.2.1.2 Channel Banks

Due to the Blackwater catchment being an intensive arable landscape, stream channels have been extensively straightened and deepened to reduce water residence times (Figure 5.4A). This has resulted in the complete disconnection of the river from its floodplain, with channel banks typically rising >2 m above the bed at an angle of 20-30^{o} to form deep V-shaped channels. At ten locations along the 2.9 km stream reach in mini-catchment A, channel bank material was collected as surface scrapes at three depths (10, 30 and 50 cm above the streambed) such that 30 samples of ~100 g were collected. The same procedure was carried out at seven locations along the 1.7 km reach in mini-catchment B, yielding 20 samples for analysis (one sample removed due to contamination). As with road verge samples, the outermost layer (few mm) of channel bank sediments were gently scrapped away to expose fresh material for sampling. The position 0-50 cm above the bed represents the zone most actively eroded by the stream, with stage lower than 50 cm for 95% of the April 2012 to March 2014 monitoring period at site A, and for 99% of the time at site B. This lower channel bank section is located within the chalky, flint-rich, boulder clay deposits of the Lowestoft Formation and the transition into the overlying carbonate depleted deposits can be clearly seen in both catchments (Figure 5.4B). Above 50 cm, banks become densely vegetated with grasses and ground elder (*Aegopodium podagraria*), stabilising the upper sections (Figure 5.4A). Upper banks were therefore not considered to be a major sediment source, likely only becoming important during episodes of periodic slumping or channel dredging operations, of which none were observed during the study period.

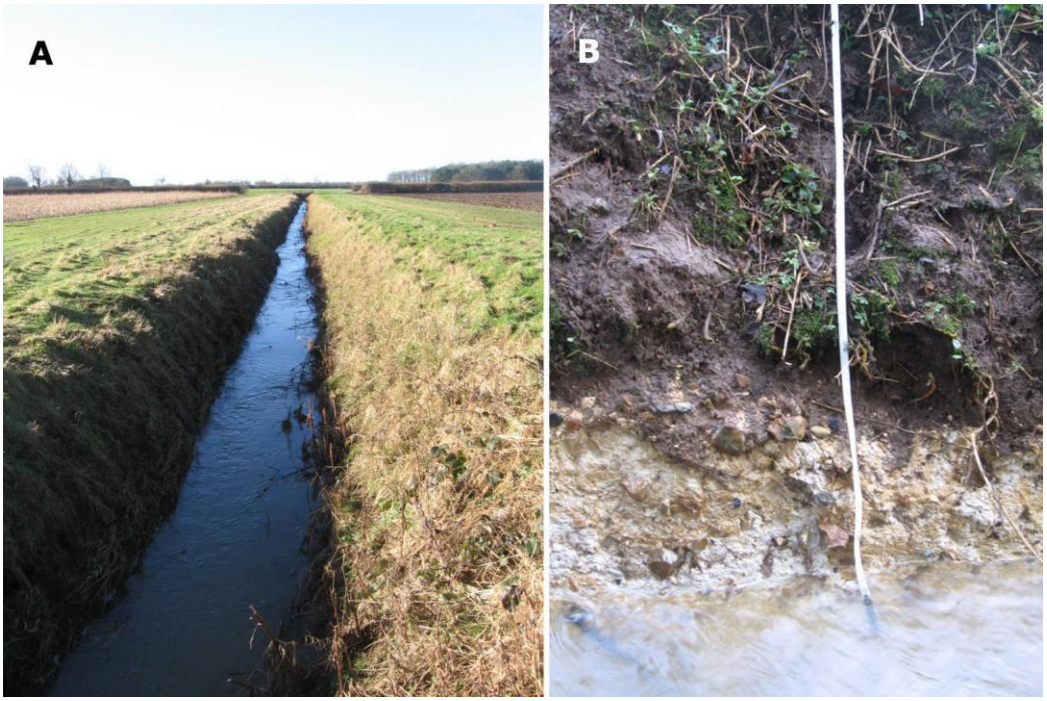

Figure 5.4: Channel banks of the River Blackwater. (A) The straightened and deepened channel profile typical of the Blackwater catchment. The top of the channel is ~4 m wide. (B) Cross-section of the channel bank showing the transition between the grey, calcium carbonate-rich boulder clays found in lower ~50 cm of the bank and the overlying darker, calcium-depleted surface soils situated above. Image view is ~80 cm top-to-bottom.

5.2.1.3 Field Drains

Most of the arable land in the Blackwater catchment is extensively under-drained by a dense network of plastic (Figure 5.5A), concreate (Figure 5.5B) and clay agricultural field drains installed in a herringbone layout at depths of 1-1.5 m during numerous phases of land drainage over the past 60-70 years (Figure 2.4). A substantial body of research has highlighted that the high connectivity of such dense drainage networks has the potential to facilitate the rapid and preferential transfer of particulates and associated pollutants from the soil directly into the stream channel, bypassing opportunities for natural attenuation (e.g. Kronvang *et al*., 1997; Haygarth and Jarvis, 1999; Laubel *et al*., 1999; Stutter *et al.*, 2008a; Withers *et al*., 2009). Whilst the percolation of water through the soil matrix can filter out coarser particulates and thereby lower sediment concentrations in field drain discharges compared to surface runoff (Schelde *et al*., 2006; Stutter *et al*., 2008a), the flow rates of field drains can also be much higher over the duration of a rainfall event and therefore the total sediment loads exported from field drains can still be substantial (Deasy *et al*., 2009a; Frey *et al*., 2012).

Figure 5.5: Plastic (A), concrete (B) and clay agricultural field drains underlie most of mini-catchments A and B. The majority are situated 1-1.5 m below the surface and discharge directly into the stream. Diameter of both drains shown is ~10 cm.

Across the study area, 143 drains were identified discharging directly into the stream. 125 of these drains were in mini-catchment A, with a further 18 in mini-catchment B. The discharge from each drain varied considerably depending on the season, antecedent weather conditions, stage of crop growth and the catchment area drained by the individual pipes. The fastest recorded flows exceeded 1 L s^{-1} during the winter months, with most drains drying up completely between June and September. Grab samples (1 L) taken from each flowing drain were collected over several months and bulked together, necessary due to low sediment concentrations at the time of sampling (typically <3 mg/L). In total, 30 bulked sediment samples were collected from mini-catchment A and 18 were collected from mini-catchment B. It is likely the sediments discharging from these drains represent a composite of material eroded from the soil surface and material entrained from deeper within the soil profile. Inspection of field drain geochemistry certainly supports this theory, with concentrations of most geochemical parameters falling between that of surface topsoils and subsurface channel bank material (section 5.3.1).

5.2.2 SPM Sampling

The bankside ISCO automatic samplers at the outlets to mini-catchments A and B were remotely activated via text message to collect 1 L stream water grab samples every 60- or 120-min for the duration of 14 moderate-to-heavy precipitation events (>8 mm rainfall over the entire event) that occurred between September 2012 and February 2014. Results for five of these events (5th October 2012; 24th, 26th and 27th November 2012; 14th February 2013) are presented in this chapter - selected because they encompassed a range of low-, medium- and high-flow conditions. As explained in Chapter 3, the principal advantage of using automatic samplers as opposed to the time-integrated samplers commonly employed in sediment fingerprinting studies (Phillips *et al.*, 2000) is the increased temporal resolution, and thereby understanding of catchment processes, that can be achieved by sampling at regular short intervals. Stage at both site A and B was recorded every 30 min by pressure transducers, whilst precipitation was recorded at 15 min intervals via a tipping-bucking rain gauge.

5.2.3 Laboratory Analysis

All stream water samples were returned to the laboratory and immediately vacuum filtered through QFF papers to extract the particulate matter. The SPM-covered filters were subsequently oven dried at 105^{o}C for 2 hrs before being weighed to determine sediment mass retention. Source area samples were initially air dried at room temperature for 48-72 hrs before being lightly disaggregated with a pestle and mortar. To ensure these more consolidated source area materials had particle size distributions, and thus geochemistry (Horowitz and Elrick, 1987; Horowitz, 2008), comparable to fluvial SPM, a 10 g aliquot of each source sample was mixed with Milli-Q water (18.2 MΩ.cm; Merck Millipore, Billerica, MA, USA) and placed in an ultrasonic bath for 7 min to disaggregate clasts. These source area sediments were then wet sieved to <63 µm to minimise contrasts with SPM and ~25 mg of material was transferred onto QFF papers by vacuum filtration before oven drying for 2 hrs.

The geochemistry of all sediment-covered filter papers was analysed directly by XRFS and DRIFTS using the methods presented in Chapter 3. As previously discussed, this direct spectroscopic analysis of filter papers has many advantages over other analysis techniques commonly employed in fingerprinting studies, such as ICP-MS/AES, colorimetry, acid-digestion and loss-on-ignition. The principal benefit being that large numbers of samples can be rapidly and cheaply analysed, non-destructively, from small

sediment masses (as little as 3 mg of material required) to yield a wide array of geochemical and mineralogical data with a high degree of accuracy. This makes such spectroscopic analysis conducive to high-temporal resolution monitoring programmes such as the one presented here. Concentrations of 10 major (Al, Ca, Fe, K, Mg, Mn, Na, P, Si, Ti) and one minor (Ce) elemental fingerprints were determined for this part of the analysis, alongside additional estimates for the five organic and inorganic phases calibrated in Chapter 3 (POC, Al_{di}, Al_{ox}, Fe_{di}, Fe_{ox}).

A Beckman Coulter LS13320 laser diffraction particle size analyser (Beckman Coulter, CA, USA) was used to determine the grain size distribution of both SPM samples and the 63 µm sieved source area sediments. Because complete disaggregation of material is essential for an accurate assessment of particle sizes, all samples were mixed with Calgon (10% w/w) and underwent 2 min of sonication (18 W) prior to analysis to disperse any re-aggregated flocs.

5.2.4 Discriminating Source Areas

Following the procedures set out in Chapter 4, the mixing space geometry of source area fingerprints was examined via a PCA. The Kruskal-Wallis *H*-test was applied to identify which of the fingerprints were significantly different between at least two source groups and thereby able to discriminate between them. The stepwise LDA variable selection procedure based on the minimisation of the Wilk's Lambda was then employed to quantitatively determine the proportion of source area samples that could be correctly classified by the selected fingerprints (Collins *et al*., 1997). Prior to this statistical discrimination, Si was removed as a potential fingerprint because noise originating from the QFF paper reduced the accuracy of these measurements during XRFS analysis (see Chapter 3).

5.2.5 Bayesian Mixing Model

The benchmark empirical Bayesian mixing model (M1) presented in Chapter 4 was employed here to quantitatively apportion sediment source contributions for mini-catchments A and B. The mixing model was run using JAGS in the R environment for 750,000 iterations, with a 100,000 sample burn-in and jump length of 225 to minimise autocorrelation between runs. To confirm whether the MCMC random walk had converged on the equilibrium distribution, three MCMC chains were run in parallel from

different starting conditions so that trace plots of the parameter distributions could be inspected for evidence of mixing. The 'coda' package (Plummer *et al.*, 2006) was then used to perform convergence diagnostics.

5.3 Results

5.3.1 Source Area Geochemistry

Boxplots of source area geochemistry for mini-catchments A and B are presented in Figures 5.6 and 5.7, respectively. The main observation to make here is the increase in Ca concentrations with depth, from topsoils (<0.05 m), to field drains (1-1.5 m), to channel banks (2-3 m) at both sites. This is assumed to relate to a typical carbonate weathering profile (e.g. Tye *et al.*, 2013) and it provides the main distinction between source areas in the Blackwater catchment. Other points to note are the similarities between road verge and topsoil geochemistry, with both these surface sources being enriched in metal oxides and clay mineral associated elements (i.e. Al, K, Mg, Na and Ti) compared with the more Ca-rich subsurface channel bank and field drain sediments. It is also notable that field drain sediment geochemistry is the most variable of the four sources, with concentrations of most elements and compounds between that of channel banks and topsoils. These field drain sediments also have the highest recorded Fe concentrations, with concentrations up to 22% recorded at several locations within mini-catchment A. On numerous occasions Fe-rich material was observed discharging from some of the older clay and concreate field drains (Figure 5.8), although there was no obvious spatial pattern or depth association with these discharges. This likely indicates the localised oxidation and release of iron sulphides from the glacial till deposits (Marttila *et al*., 2013).

Importantly, the concentrations of P, POC, Fe_{di} and Fe_{ox} in SPM at site A, and POC, Al_{di} and Fe_{di} in SPM at site B, extend outside the range of values observed in the four respective source areas, thus breaking the conservative transport assumption (assuming all sources have been correctly identified). For POC and P, this SPM enrichment can be explained by these components being generated instream via phytoplankton and macrophyte production (i.e. autochthonous sources), whilst POC also tends to be enriched in SPM due to its lower specific gravity compared with inorganic material (Schindler Wildhaber *et al.*, 2012a). The effect of this POC enrichment is particularly evident at site B, where SPM POC concentrations are ~5% higher in SPM than any of the four source areas (Figure 5.7).

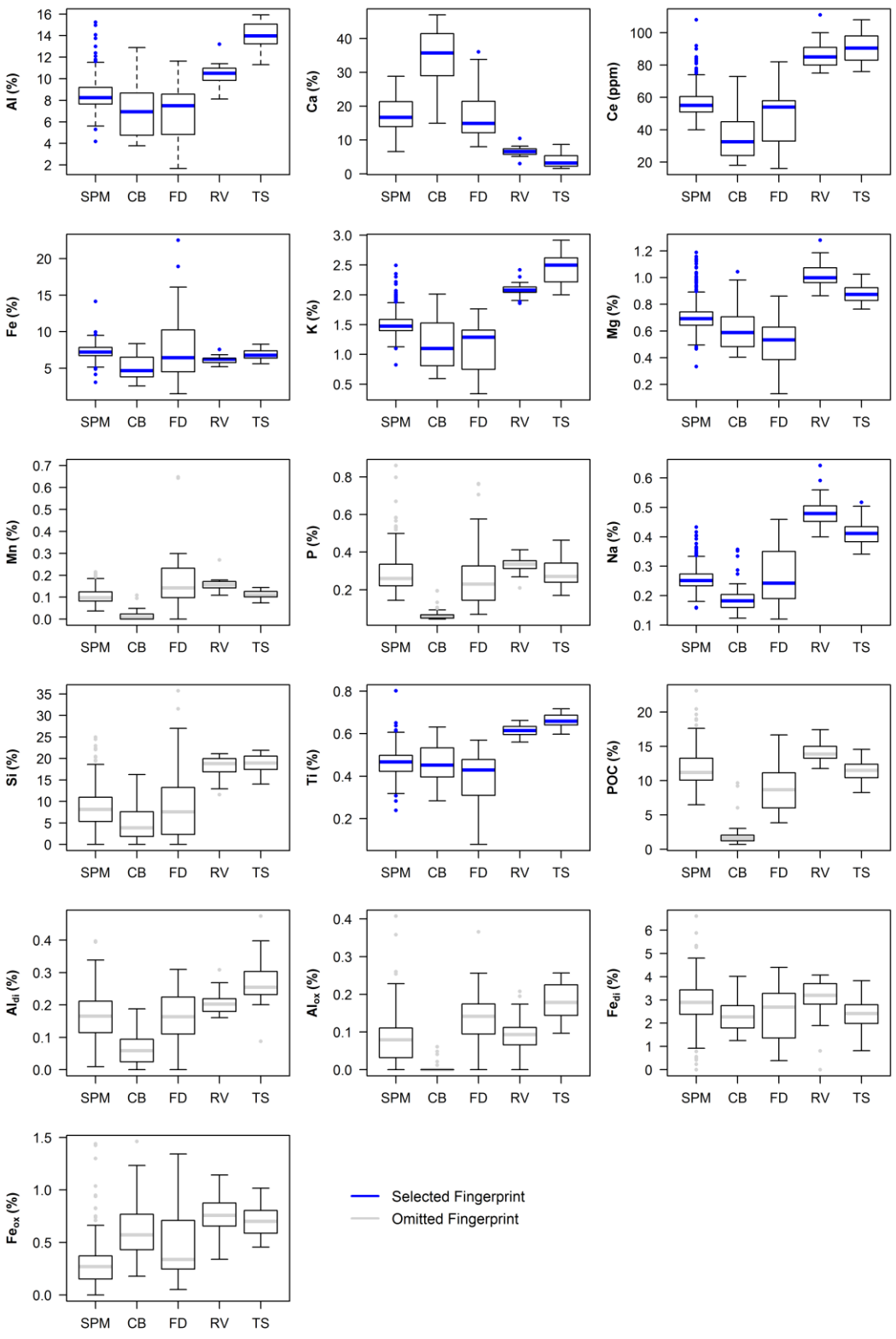

Figure 5.6: Boxplots of SPM and source area geochemistry for mini-catchment A. Blue (dark) boxes represent fingerprints selected for the mixing model, whilst grey (light) boxes indicate those omitted. SPM refers to all 328 storm and baseflow samples obtained from May 2012 to March 2014. Summary statistics can be found in Table C1 (Appendix C).

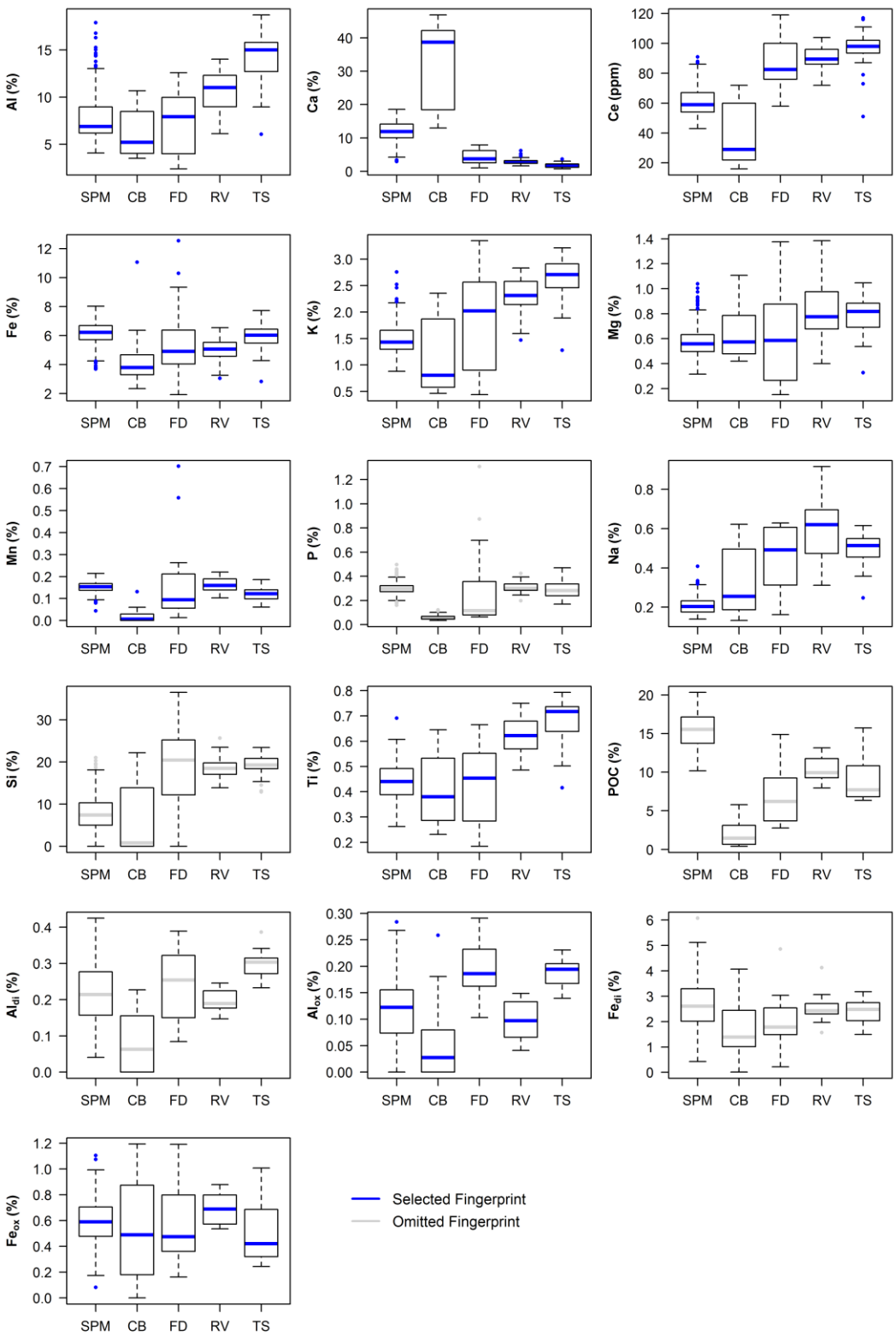

Figure 5.7: Boxplots of SPM and source area geochemistry for mini-catchment B. Blue (dark) boxes represent fingerprints selected for the mixing model, whilst grey (light) boxes indicate those omitted. SPM refers to all 325 storm and baseflow samples obtained between May 2012 and March 2014. Summary statistics can be found in Table C2 (Appendix C).

Whilst the flexible Bayesian modelling procedure can partly address these issues through wider source area distributions and through the inclusion of a residual error term (see Chapter 4), these compounds were omitted as potential fingerprints as a precaution.

Figure 5.8: Iron-rich material discharging from a clay agricultural field drain within mini-catchment A in February 2014.

5.3.2 Particle Size Distributions

Particle size analysis results for 27 SPM samples collected from sites A and B revealed that almost all had either a silt or silty loam texture under both low- and high-flow conditions. SPM from site E (added here for comparison) also had a very similar silt/silt loam texture (Figure 5.9). Particle size distributions for three bulked samples of each source area sediment revealed that, once sieved down to <63 μm, all bar one (channel bank sediments from mini-catchment A) of these source area samples also fell within the silt or silty loam categories. This enables us to be reasonably confident that geochemical differences between sediment source groups and target SPM were not purely a manifestation of particle size differences.

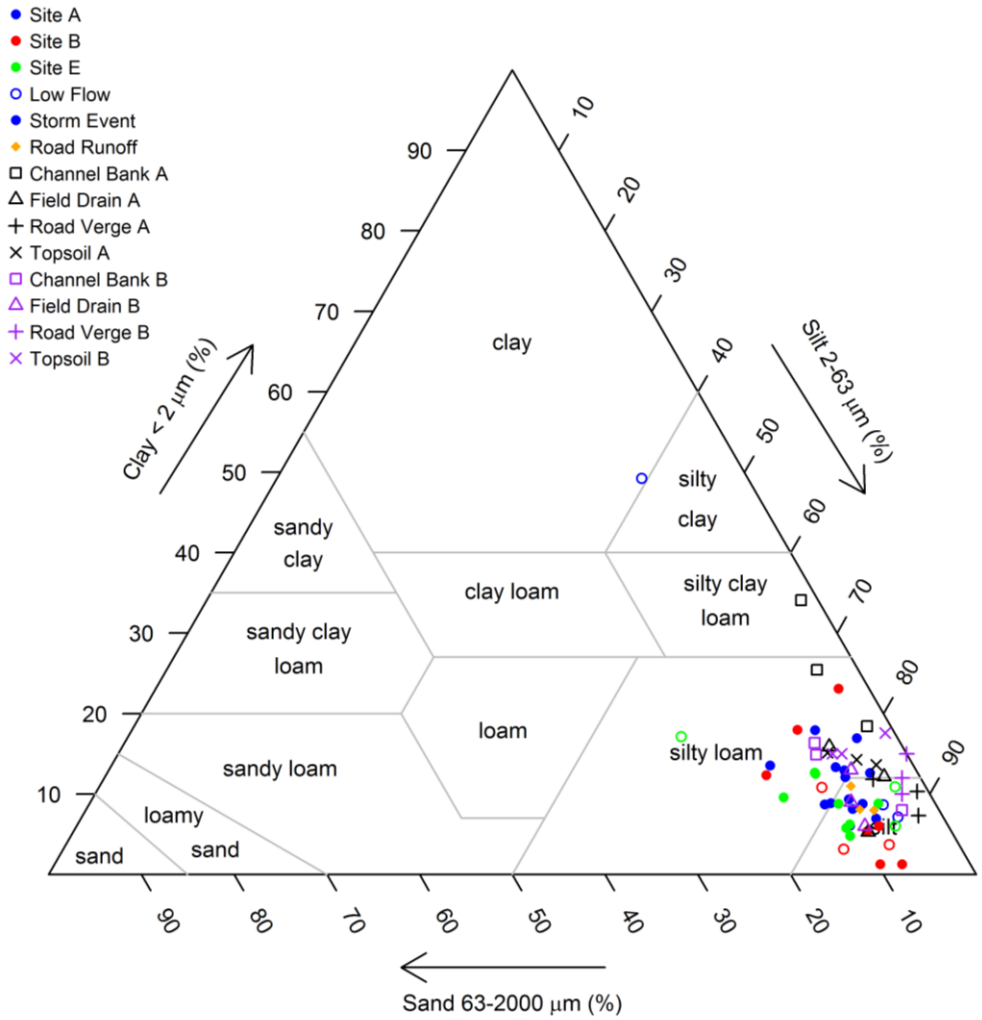

Figure 5.9: Texture triangle for SPM collected at sites A, B and E and for <63 µm source area sediments collected within mini-catchments A and B. The divisions are based upon the United States Department of Agriculture (USDA) classification.

5.3.3 Discriminating Sources

5.3.3.1 Mini-catchment A

For mini-catchment A, PCA revealed strong contrasts between the geochemistry of surface and subsurface sediment sources that could largely be explained by the first two components (Figure 5.10). PC1 (which explained 75.05% of data variance) highlighted Ca as the most powerful discriminator of surface and sub-surface sediments. This reflects the increase in Ca concentration with depth through the geological transition from the weathered carbonate-depleted surface deposits to the chalky, less weathered, boulder clays at depths exceeding 0.5 m. The second PC (which explained 12.79% of data

variance) emphasised the importance of Fe concentrations in differentiating between channel bank and field drain, and road verge and topsoil sediments, respectively. Despite this, there remained a significant overlap in the geochemical ranges of both channel bank and field drain sediments which made differentiation difficult. The geochemical data for channel banks and field drains were therefore merged into a combined 'subsurface' sediment source prior to running the apportionment model. The third PC (5.34% of the variance) weighed most heavily on Na as a discriminator of topsoil and road verge sources, and possibly reflects the higher Na concentrations in road verge sediments as a consequence of winter road gritting with salts.

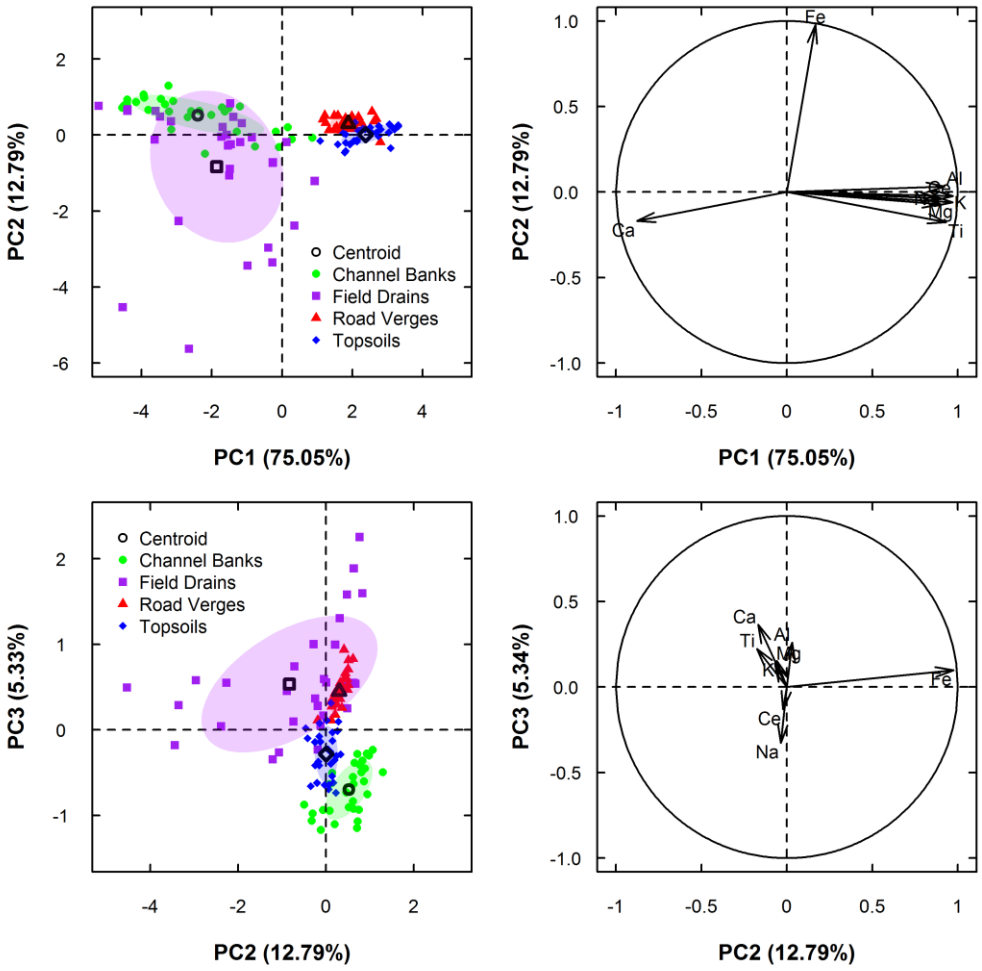

Figure 5.10: PCA plots of mini-catchment A source area samples (left) and fingerprint loadings (right) for the first three principal components. Shaded ellipsoids cover 50% of the source area range.

The Kruskal-Wallis *H*-test and LDA revealed that eight geochemical fingerprints (Al, Ca, Ce, Fe, K, Mg, Na, Ti) were significantly different between at least two source areas and were therefore carried forward to the mixing model. Ca was the strongest discriminator,

capable of successfully differentiating 79.2% of source area samples (Table 5.1). Combined with the other seven elements, 97.5% of source area samples could be correctly identified. Whilst inclusion of Fe, Na and Ti did not improve the power of source discrimination, these additional fingerprints were still included in the mixing model because previous research has demonstrated that maximizing the number of tracers in Bayesian mixing models can help to significantly improve differentiation and reduce model uncertainties (Parnell *et al*., 2010).

Table 5.1: Assessing the ability of the geochemical fingerprints to differentiate between topsoil, road verge and subsurface sediment source areas in mini-catchment A via the Kruskal-Wallis *H*-test and minimisation of Wilks-Lambda.

Fingerprint property	Kruskal-Wallis		Minimisation of Wilks-Lambda			
	H-value	*p*-value	Selection step	Wilks-Lambda	Cumulative *p*-value	Cumulative % of source areas correctly classified
Ca	101.96	<0.001	1	0.1724	<0.001	79.2
K	96.42	<0.001	2	0.0499	<0.001	85.0
Mg	82.41	<0.001	3	0.0195	<0.001	93.3
Al	88.76	<0.001	4	0.0103	<0.001	96.7
Ce	91.85	<0.001	5	0.0086	<0.001	97.5
Fe	25.91	<0.001	6	0.0075	<0.001	97.5
Na	90.37	<0.001	7	0.0075	<0.001	97.5
Ti	93.55	<0.001	8	0.0066	<0.001	97.5

5.3.3.2 Mini-catchment B

For mini-catchment B, PC1 (which explained 51.74% of the variance) once again revealed Ca to be a powerful discriminator between surface and subsurface sediment sources (Figure 5.11). Importantly, however, PC2 (which explained 18.67% of the variance) revealed that lower Ca concentrations and higher concentrations of Mn, Fe and Ce in field drain sediments helped to better differentiate this material from channel bank sediments. As a result, it was not necessary to merge these two subsurface sources for this catchment. Whilst topsoil and road verge material displayed significant overlap for PC1 and PC2, PC3 (which explained 9.1% of the variance) revealed good differentiation, with differences in Al_{ox}, Fe_{ox}, Fe and Na concentrations proving to be important source

discriminators (Figure 5.11). Winter road gritting is again likely to be responsible for the higher Na concentrations observed in road verge material.

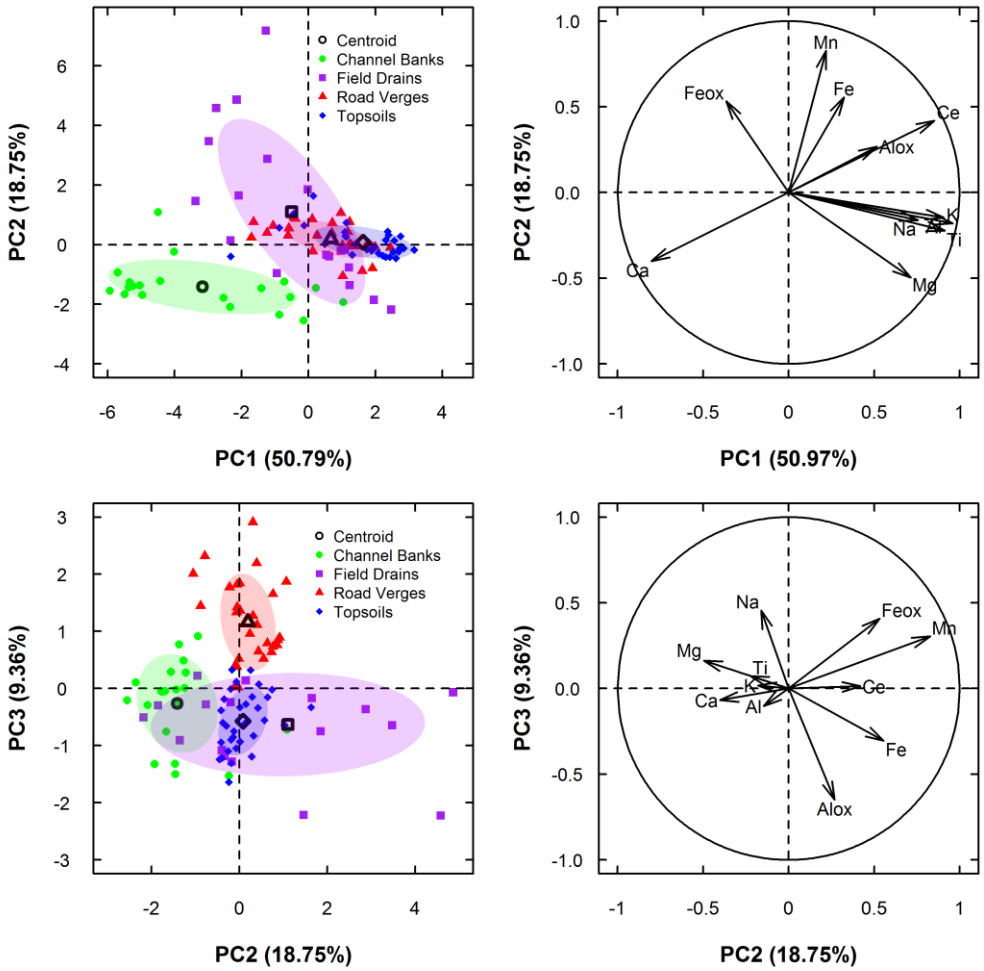

Figure 5.11: PCA plots of mini-catchment B source area samples (left) and fingerprint loadings (right) for the first three principal components. Shaded ellipsoids cover 50% of the source area range.

Application of the Kruskal-Wallis *H*-test and LDA with minimisation of Wilks-Lambda revealed that 11 geochemical fingerprints (Al, Ca, Ce, Fe, K, Mg, Mn, Na, Ti, Al_{ox}, Fe_{ox}) were significantly different between at least two of the four source areas and these elements and compounds were therefore carried forward to the mixing model for mini-catchment B (Table 5.2). As with mini-catchment A, Ca was the strongest discriminator, capable of correctly classifying 53% of source area samples. The addition of a further 7 fingerprints (Al_{ox}, Ti, Fe_{ox}, Al, Mg, K, Ce) allowed up to 95% of source area samples to be correctly identified. Na, Mn and Fe did not statistically improve source differentiation but, as with mini-catchment A, these elements were included in the Bayesian mixing model in order to maximise the number of tracers.

Table 5.2: Assessing the ability of the geochemical fingerprints to differentiate between road verge, topsoil, field drain and channel bank sediment source areas in mini-catchment B via the Kruskal-Wallis *H*-test and minimisation of Wilks-Lambda.

Fingerprint property	Kruskal-Wallis		Minimisation of Wilks-Lambda			
	H-value	*p*-value	Selection step	Wilks-Lambda	Cumulative *p*-value	Cumulative % of source areas correctly classified
Ca	69.09	<0.001	1	0.1859	<0.001	53.0
Al_{ox}	60.94	<0.001	2	0.1018	<0.001	74.0
Ti	55.03	<0.001	3	0.0521	<0.001	82.0
Fe_{ox}	15.81	0.001	4	0.0310	<0.001	85.0
Al	58.15	<0.001	5	0.0237	<0.001	90.0
Mg	10.27	0.016	6	0.0154	<0.001	94.0
K	43.04	<0.001	7	0.0135	<0.001	94.0
Ce	50.92	<0.001	8	0.0119	<0.001	95.0
Na	27.50	<0.001	9	0.0114	<0.001	95.0
Mn	53.91	<0.001	10	0.0113	<0.001	95.0
Fe	26.42	<0.001	11	0.0110	<0.001	95.0

5.3.4 Low-flow Apportionment: October 2012

The first precipitation event investigated in this chapter occurred during low-flow conditions on the 4th-5th October 2012, when stage was <0.25 m at site A and <0.05 m at site B. During the event 10.2 mm of rainfall fell over 7 hrs resulting in the approximate export of 31.8 kg of SPM from mini-catchments A and 5.9 kg from mini-catchment B, as calculated via stage-discharge rating curves (Figure 5.12). This equated to a sediment loss of 0.06 kg/ha and 0.04 kg/ha for mini-catchments A and B, respectively.

Prior to event onset, SPM geochemistry at site A was dominated by high Ca concentrations (24-26%) and low concentrations of clay mineral and metal oxide associated elements, such as Al (7-8%), Mg (0.6-0.7%) and K (1.3-1.4%) (Figure 5.13). Such geochemistry is characteristic of material derived from deeper carbonate-rich sub-surface sources located within the chalky, flint-rich boulder clay deposits (Figure 5.6). The source apportionment model consequently estimated high median sediment contributions of 85-90% (60-99% at the 95% credible interval) from the combined channel bank and agricultural field drain subsurface source prior to event onset (Figure 5.13).

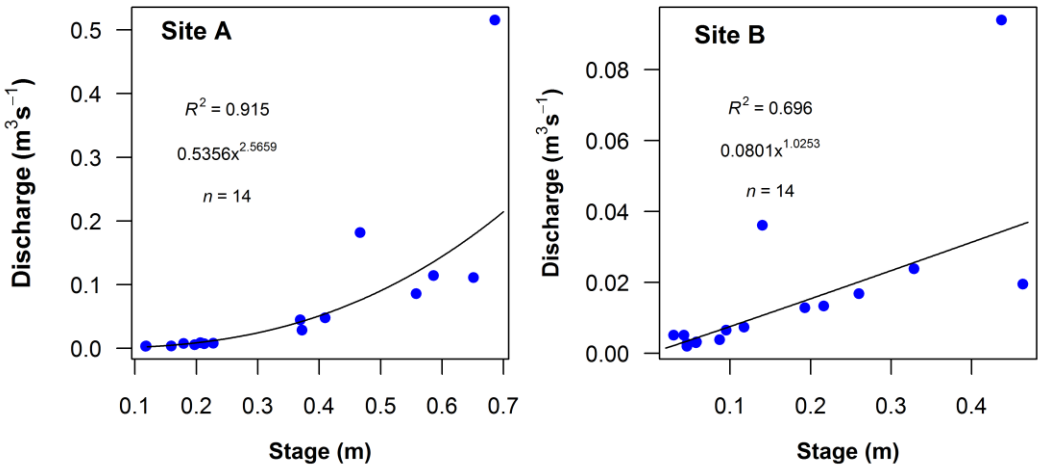

Figure 5.12: Stage-discharge rating curves for sites A and B. Points are manual flow-gauging measurements and the line is the regression.

As the weather front crossed mini-catchment A, heavy rainfall initiated surface runoff, dislodging and transporting fine-grained, carbonate depleted, surface source material to the river. This resulted in a rapid increase in the concentration of most metal oxide and clay mineral associated elements in SPM, mirrored by a rapid decline in the proportion of Ca. Elevated POC concentrations also indicated increased sediment input from organic matter rich surface sources (Jobbágy and Jackson, 2000). Accordingly, the mixing model estimated increased median contributions from both road verges (26-28%) and topsoils (21-29%) during the 2-3 hr period post-heaviest rainfall, with proportions from subsurface sources correspondingly declining and closely matching falling Ca concentrations (Figure 5.13). However, uncertainties around apportionment estimates increased as SPM shifted towards this more carbonate-depleted geochemistry, with topsoil and road verge contributions having wide 95% credible intervals of 2-58% and 1-95%, respectively. Essentially, similarity in the geochemistry of these two surface sources meant the mixing model struggled to identify a unique solution. NB: these uncertainties were predominantly due to variability in source area geochemistry rather than instrument precision, which is small in comparison.

As the event progressed, cessation of precipitation initiated a rapid return (within 1-2 hrs) towards pre-event geochemical conditions, with subsurface sources returning to being the major contributor of SPM (median 82-89%) in mini-catchment A. Such a rapid shift between surface and subsurface contributions strongly suggests that the catchment soils were relatively dry at this time, thus minimising the opportunities for soil saturation and prolonged surface runoff to occur.

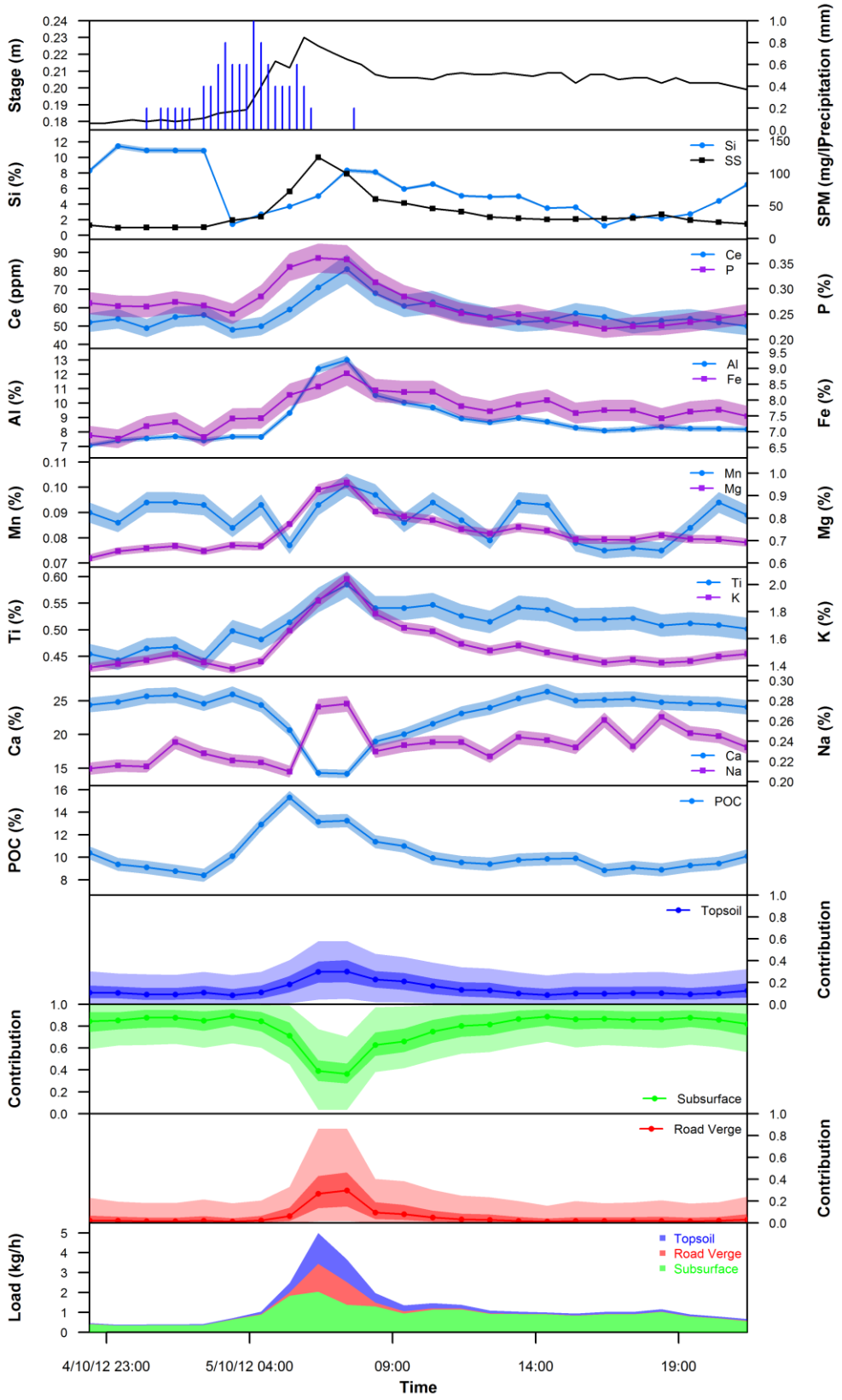

Figure 5.13: The October 2012 precipitation event at site A, showing changing SPM geochemistry (% by weight) and sediment source contributions at 60-min intervals over a 24 hr period. Shading around geochemical parameters represents instrumental precision (2 St. Dev.). Light and dark shading around median source apportionment estimates represent the 95% and 50% Bayesian credible intervals, respectively. Loads are based on median contribution estimates.

This event had the characteristics of a 'flashy' system, where surface sediments were rapidly delivered to the stream via impermeable surfaces whilst it was raining, with runoff ceasing very quickly after the rainfall stopped.

In contrast, response to the precipitation event at site B was considerably more muted, with SPM geochemistry changing very little over the 24 hr period (Figure 5.14). Inspection of the geochemical time-series reveals that whilst concentrations of Al, Fe, Ti, K and Al_{ox} did increase during the first 1-2 hrs of the event, these increases were relatively small and within the range of variability observed over the following 20 hrs. SPM concentrations peaked at just 35 mg/L shortly after the main period of rainfall ended, an increase of only 13 mg/L over pre-event conditions. Stage also increased by only 2 cm during the event, indicating most of the rainfall was absorbed by the soil. Soil conditions in mini-catchment B therefore appear to have been too dry prior to the event for any overland flow or accelerated soil through-flow to be initiated.

Consequently, the mixing model estimated negligible temporal variability in source apportionment for site B, with channel banks (median 42-47%) and field drains (median 23-26%) estimated to supply the majority of the sediment. These results support the findings of Russell *et al*. (2001) and Deasy *et al*. (2009) in confirming the importance of artificial agricultural drainage networks in the subsurface transfer of sediments from land to stream. The absence of any peak in either topsoil (median 8-9%) or road verge (median 17-19%) contribution, unlike that witnessed at site A, could have been due to the sandier soil texture in mini-catchment B, or due to differences in how road runoff from metalled roads was diverted into the stream channel. The surface source material that was transported during this event is thus likely to have been resuspended from bed sediment material deposited in the stream during previous events.

During this event, estimated median (95% credible interval) load weighted sediment contributions for site A were 22.1 kg (12.8-29.5 kg) from subsurfaces, 5.5 kg (0.4-12.7 kg) from topsoils and 3.2 kg (0.1-13.9 kg) from road verges. For site B, contributions were 2.6 kg (1.9-3.2 kg) from channel banks, 1.4 kg (0.6-2.5 kg) from field drains, 1.1 kg (0.3-2.1 kg) from road verges and 0.5 kg (0.1-1.5 kg) from topsoils.

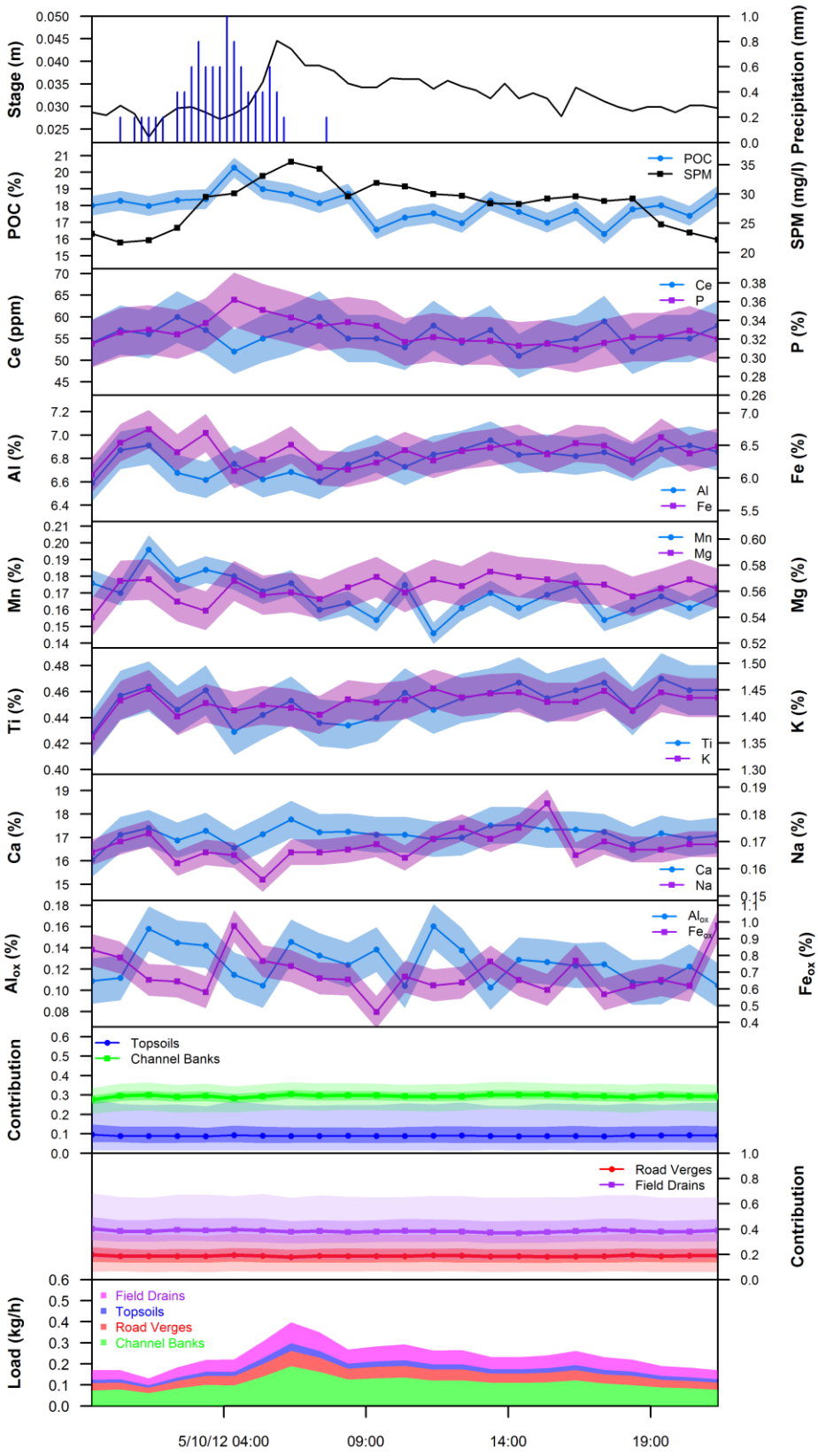

Figure 5.14: The October 2012 precipitation event at site B, showing changing SPM geochemistry (% by weight) and sediment source contributions at 60-min intervals over a 24 hr period. Shading around geochemical parameters represents instrumental precision. Light and dark shading around median source apportionment estimates represent the 95% and 50% Bayesian credible intervals, respectively. Loads are based on median contribution estimates.

5.3.5 High-flow Apportionment: November 2012

During a five day period in late November 2012, three consecutive precipitation events of 15.8 mm, 8.4 mm and 12.2 mm were captured in mini-catchments A and B, with an earlier fourth event of 8.4 mm captured only at site B (Figures 5.15 and 5.16). High-flow conditions were recorded at both sites during this period, with stage reaching 0.98 m at site A and 0.73 m at site B. As successive rainfall events passed across both mini-catchments, concentrations of most elements, excluding Ca, increased sharply over a period of 2-4 hrs, with particularly prominent increases recorded for Al, Mg and K. Based on our knowledge of source area geochemistry (Figures 5.6 and 5.7) the geochemical trends strongly indicate that surface runoff had been initiated. As with the October event, there were obvious declines in SPM Ca concentration during each pulse of rainfall, as well as a longer term decline across the entire monitoring period. This signified the reduced importance of channel bank sediment contributions across the succession of events. Consistent trends in compound concentrations were not quite as strong, with POC concentrations increasing following each rainfall event at site A, but displaying more variable behaviour at site B. Similarly, whilst Fe_{ox} concentrations at site B did increase during some of the events, Al_{ox} concentrations were much more variable with no obvious relationship with changing stage or SPM concentration.

These major geochemical trends were echoed by the source apportionment model for site A, with estimated subsurface contribution declining from a median 60% (44-76% at the 95% credible interval) just prior to the onset of the first precipitation event, to a low of 30% (15-46%) after the latter two events (Figure 5.15). However, it should be noted that whilst the proportions declined, actual masses of subsurface sediment increased during this time as the transport capacity of the stream increased (see the bottom panel of Figure 5.15). Pre-event median (95% credible interval) topsoil and road verge contributions of 16-24% (5-46%) and 22-31% (9-51%), respectively, were higher than observed in October as consequence of material still being in suspension from the prior 23rd November event. With each passing precipitation front, topsoil and road verge contributions increased, reaching highs of 32% (11-59%) and 38% (16-63%), respectively. Importantly, uncertainties around apportionment estimates were lower than that estimated for the October event at site A, indicating an improvement in the mixing model's ability to differentiate between sources under these particular geochemical conditions.

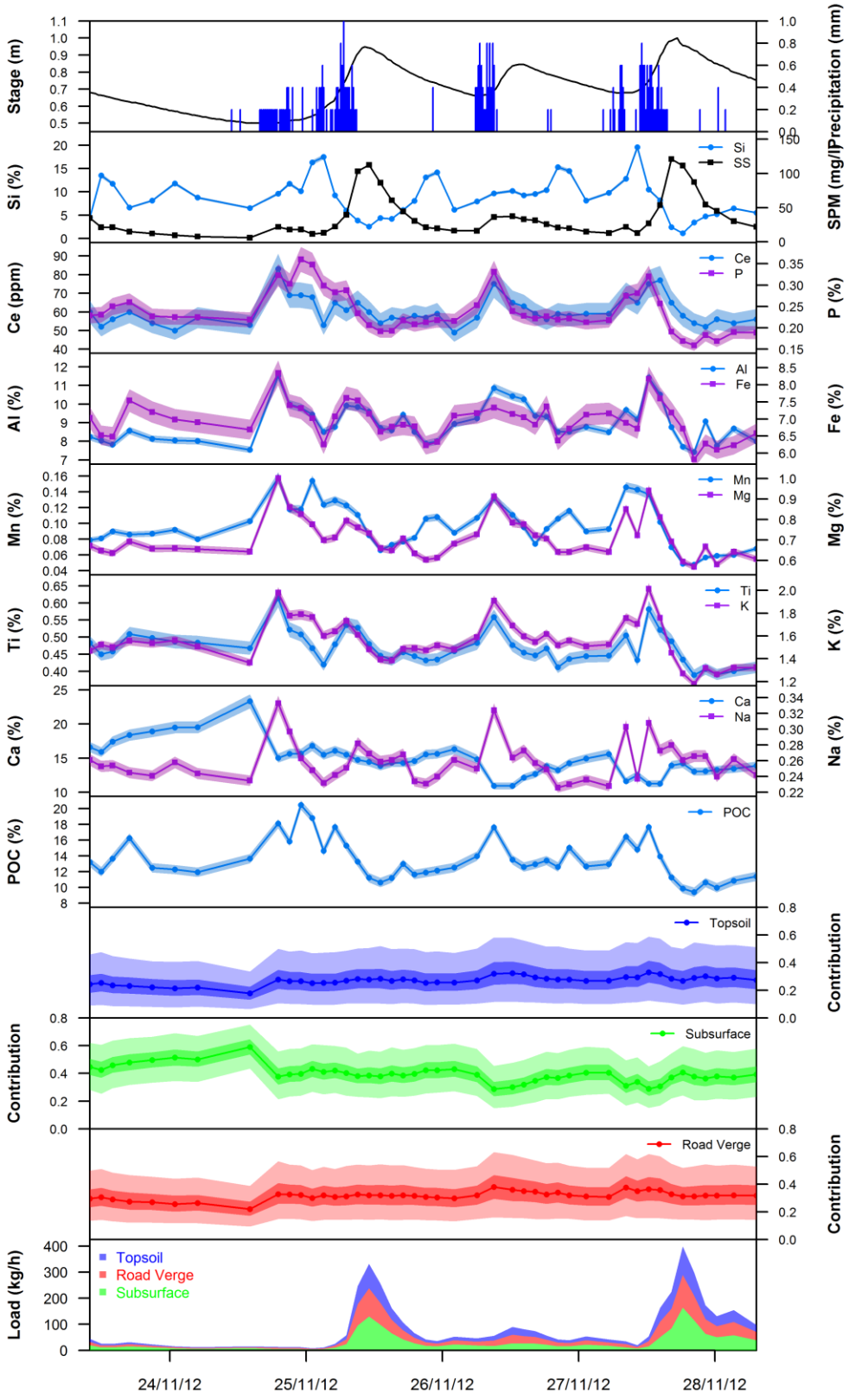

Figure 5.15: Time-series plots for three consecutive precipitation events in November 2012 at site A, showing changing SPM geochemistry (% by weight) and sediment source contributions at 120-min intervals over a 5 day period. Shading around geochemical parameters represents instrumental precision. Light and dark shading around median source apportionment estimates represent the 95% and 50% Bayesian credible intervals, respectively. Loads are based on median contribution estimates.

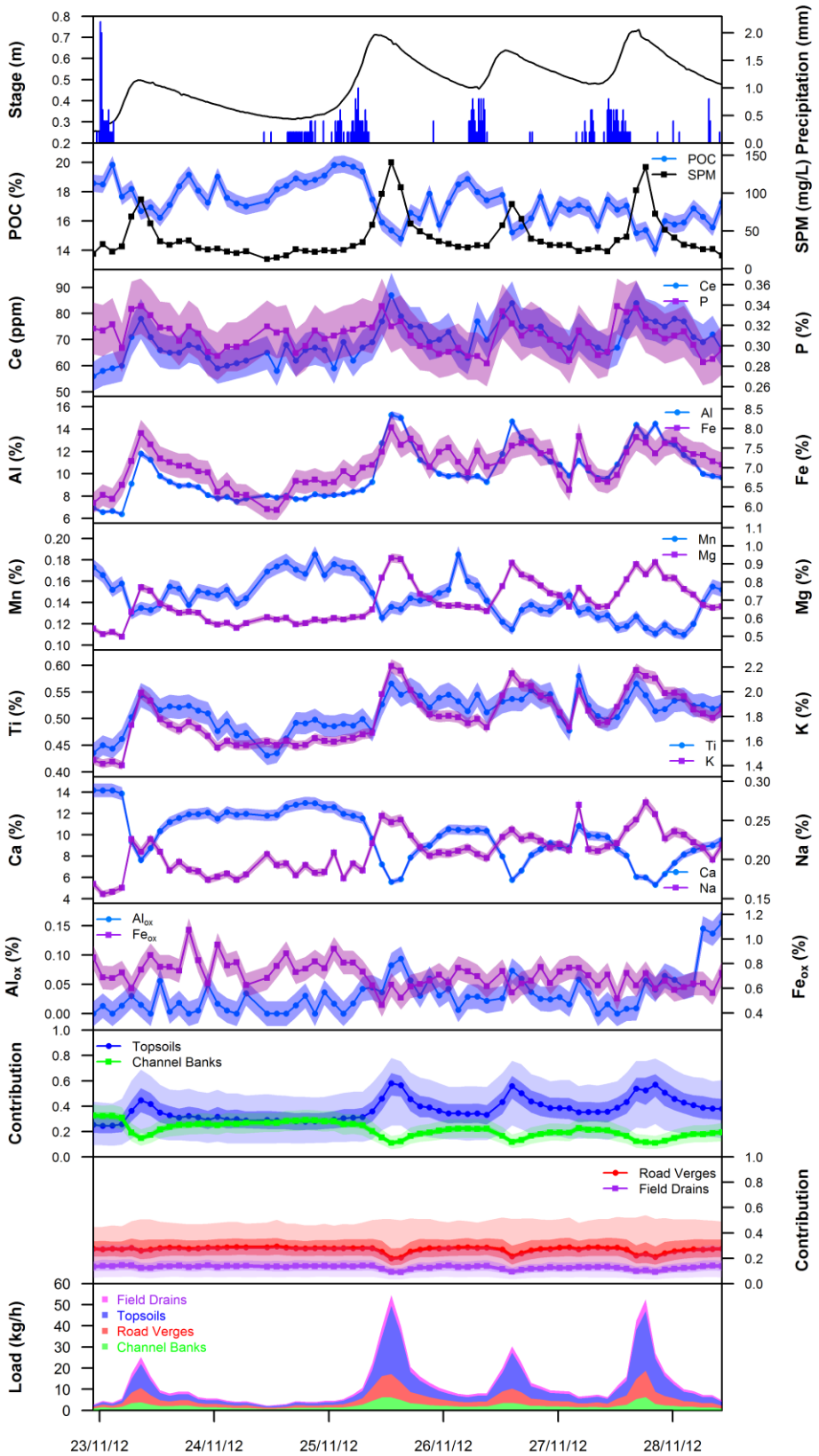

Figure 5.16: Time-series plots for four consecutive precipitation events in November 2012 at site B, showing changing SPM geochemistry (% by weight) and sediment source contributions at 120-min intervals over a 5 day period. Shading around geochemical parameters represents instrumental precision (2 St. Dev.). Light and dark shading around median source apportionment estimates represent the 95% and 50% Bayesian credible intervals, respectively. Loads are based on median contribution estimates.

For site B, topsoil was estimated to be the major contributor following the passing of each rainfall event, with median contributions rising up to 58% (25-78%) for periods of 2-6 hrs before contributions once more declined (Figure 5.16). The dominance of topsoil contribution resulted in the other three sources exhibiting declines in their relative contribution, although, as mentioned above, total loads of sediment delivered from all sources did increase during the events (see bottom panel of Figure 5.16).

Overall, these high-flow events resulted in the measured transport of 4030 kg and 840 kg of SPM from mini-catchments A and B, respectively. This equates to a catchment sediment loss of 7.5 kg/ha for A and 6.3 kg/ha for B. Median (95% credible interval) load weighted contributions for site A were 1584 kg (910-2337 kg) from subsurfaces, 1075 kg (362-2053 kg) from topsoils and 1304 kg (553-2224 kg) from road verges. Whilst for site B, load weighted sediment contributions were 366 kg (154-547 kg) from topsoils, 213 kg (86-423 kg) from road verges, 146 kg (93-202 kg) from channel banks and 99 kg (37-216 kg) from field drains.

5.3.6 Moderate Flow Apportionment: February 2013

The temporal trends observed during the moderate flows of the February 2013 event were very similar to that observed during the aforementioned November 2012 precipitation episodes (Figures 5.17 and 5.18). A total of 12.8 mm of rainfall fell over 10 hrs, resulting in stage rising up to 0.58 m at site A and 0.36 m at site B. Passage of the weather front across mini-catchment A was once again associated with an increase in concentrations of most elements (Al, Ce, Fe, K, Mg, Mn, Na, P and Ti) in SPM, with changes in geochemistry discernible approximately 90 min after event onset. These trends, combined with declines in Ca concentration, indicate material travelling downstream during the event had a composition more typical of surface rather than subsurface sources. The peak in SPM concentrations of 176 mg/L approximately 45 min after the most intense rainfall strongly suggests surface runoff was being generated, accelerating the land-to-river transfer of sediments.

The same geochemical trends were observed at site B, with sharp increases in clay mineral and metal oxide associated elements mirroring sharp declines in Ca concentrations. The difference here, however, was that the major shifts in SPM geochemistry did not occur until approximately 3 hrs after the onset of precipitation, some 2 hrs later than observed at site A. This implies that material was being delivered

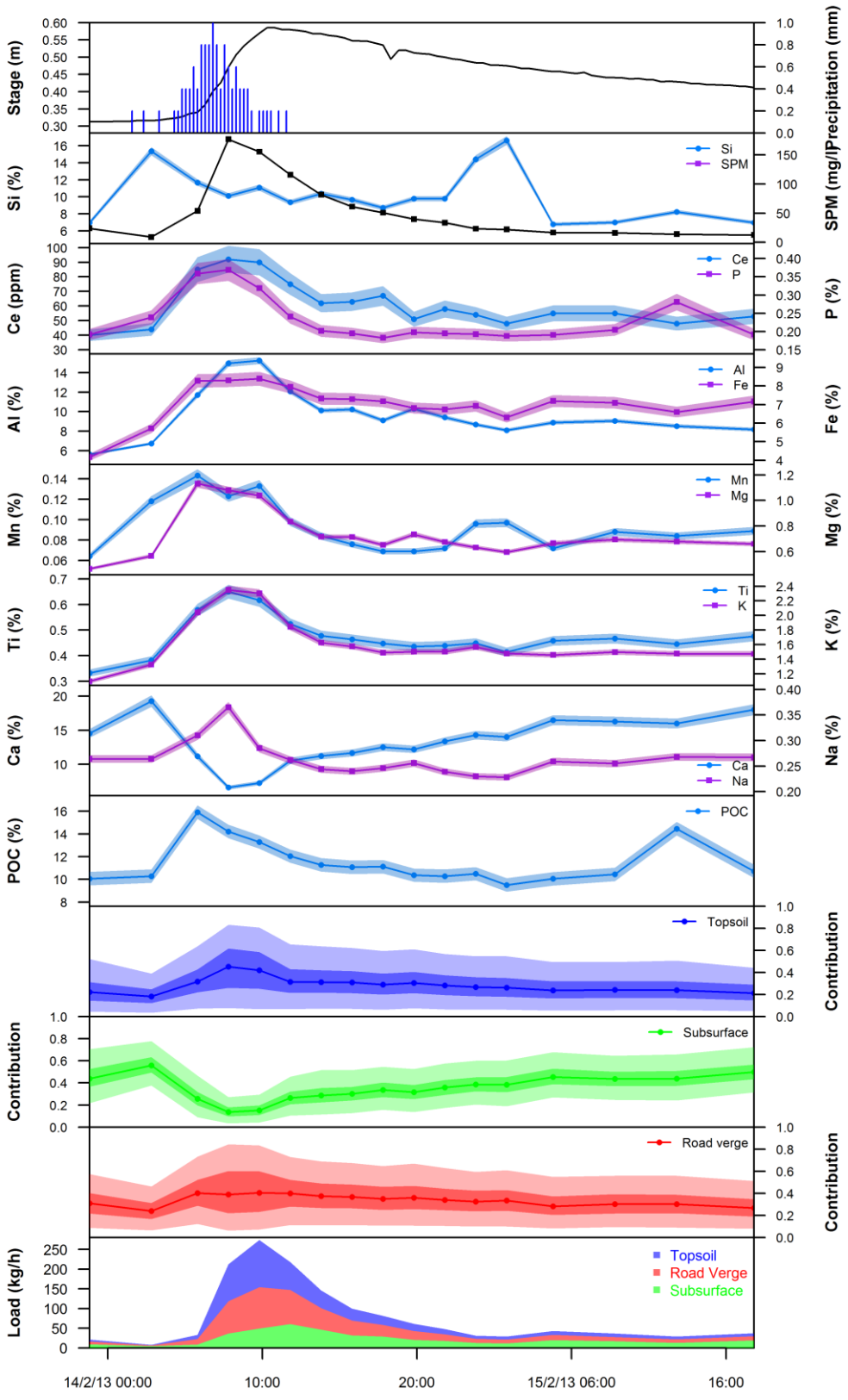

Figure 5.17: Time-series plots for the February 2013 precipitation event at site A, showing changing SPM geochemistry (% by weight) and sediment source contributions at 120-min intervals over a 48 hr period. Shading around geochemical parameters represents instrumental precision (2 St. Dev.). Light and dark shading around median source apportionment estimates represent the 95% and 50% Bayesian credible intervals respectively. Loads are based on median contribution estimates.

to the stream from sources a greater distance from the monitoring station in mini-catchment B than was the case in mini-catchment A. SPM concentrations at site B peaked at 592 mg/L, which was the highest concentration recorded over the 23-month monitoring period, highlighting a large amount of material was mobilised during this moderate flow event. Interestingly, whilst POC concentrations increased at both sites whilst it was raining, concentrations also increased again approximately 30 hrs later, indicating another pulse of organic material was moving downstream at this time (Figures 5.17 and 5.18). It is not clear why this POC increase occurred at both sites simultaneously, although SPM concentrations at this time had returned to lower baseflow levels (<20 mg/L) and therefore the masses of material involved were relatively small.

Topsoils were estimated to be the major contributing source of sediment (median 42-43%) over the 4 hr period towards the middle and later stages of the event at site A, although wide 95% credible intervals (8-78%) indicate high uncertainty. Median road verge contributions were estimated at between 37-40% during the peak in SPM concentrations, again with high uncertainty (7-81%), whilst median subsurface contributions of 16-27% (9-48%) were comparatively low. Peaking approximately 2 hrs later, median topsoil contributions at site B reached 82% (36-95%) and remained above 50% for the next 12 hrs, indicating a period of prolonged surface runoff. Uncertainty between topsoil and road verge contribution was again high during these periods of carbonate-depleted sediment input into the stream, further demonstrating that the mixing model had difficulty in differentiating between the topsoil and road verge sediment component.

Cessation of precipitation and the decline in stage were associated with an increase in relative sediment contributions from subsurface sources, as indicated by the gradual rise in the Ca concentration back to pre-event levels. As with the aforementioned events, the changing temporal contribution from subsurface sources mirrors that of Ca concentrations in SPM. Within 2 hrs of the cessation of precipitation, SPM geochemistry at site A had largely returned to pre-event concentrations and by the end of the monitoring period a median 51% (31-73%) contribution was derived from subsurface material, outweighing contributions of 26% (8-50%) from road verges and 20% (4-43%) from topsoils. SPM geochemistry at site B took considerably longer (approximately 18 hrs) to return to pre-event concentrations due to the prolonged supply of topsoil material. By the end of this period, the mixing model estimated 36% (8-59%) of SPM was still of topsoil origin, with a further 26% (9-56%) from road verges, 22% (11-29%) from channel banks and 13% (3-37%) from field drains.

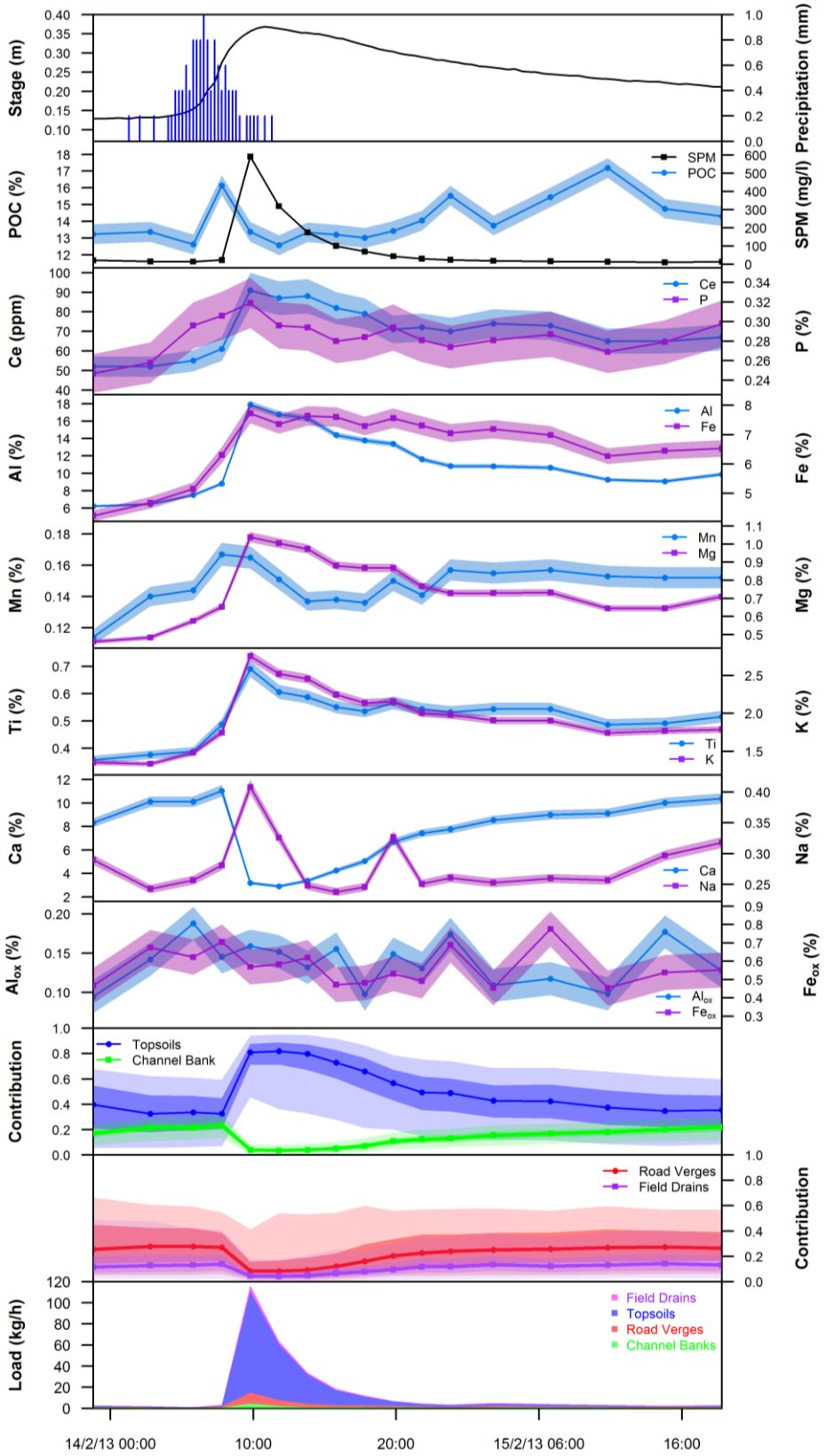

Figure 5.18: Time-series plots for the February 2013 precipitation event at site B, showing changing SPM geochemistry (% by weight) and sediment source contributions at 120-min intervals. Shading around geochemical parameters represents instrumental precision (2 St. Dev.). Light and dark shading around median source apportionment estimates represent the 95% and 50% Bayesian credible intervals, respectively. Loads are based on median contribution estimates.

In total, a measured 1444 kg and 295 kg of SPM were exported from mini-catchments A and B, respectively, during the monitoring period, equating to a sediment loss of 2.69 kg/ha and 2.21 kg/ha. Load weighted contributions for site A were 519 kg (139-1026 kg), 479 kg (101-938 kg) and 412 kg (178-699 kg) for road verges, topsoils and subsurface sources, respectively. At site B these were 218 kg (102-266 kg) from topsoils, 34 kg (6-146kg) from road verges, 18 kg (6-33kg) from channel banks and 18 kg (3-64kg) from field drains.

5.3.7 Omitting Fingerprints

The minimisation of Wilks-Lambda statistics revealed that inclusion of Fe, Na and Ti for site A, and Fe, Na and Mn for site B, did not statistically improve discrimination between sediment source groups (section 5.3.3). To explore what impact inclusion of these additional weak source discriminatory power fingerprints had on the source apportionment results, the mixing model was re-run for all five precipitation events from site A using a reduced suite of just five tracers (Al, Ca, Ce, K and Mg). Although not shown here, the resulting November 2012 and February 2013 apportionment estimates of the five fingerprint model were broadly similar to the eight fingerprint model. That said, median source contribution estimates still varied by up to 6.9% across all sources relative to the eight fingerprint model, whilst credible interval widths increased across all sources by up to 9.9%. Appointment results for the October 2012 event were, however, strongly impacted, with estimated median topsoil and road verge contribution during the 2-3 hr period post-heaviest rainfall declining by 11.5% and 17.8% respectively, relative to the eight fingerprint model (Figure 5.19). This was mirrored by a 28.3% increase in estimated median subsurface contribution. Uncertainty levels were similarly impacted, declining by 51%, 19.8% and 4% for road verge, subsurface and topsoil contributions, respectively. Such large changes demonstrate that whilst only five fingerprints were required to successfully differentiate the three source areas (Table 5.1), the additional three fingerprints still contained important information capable of significantly influencing source apportionment estimates. As previously reported (e.g. Parnell *et al*., 2010; Dutton *et al*., 2013), it is therefore advantageous to maximise the number of fingerprints incorporated into Bayesian mixing models as any tracer has the potential to assist with source mixing if the mixing processes for one particular tracer are different from the others. If additional fingerprints genuinely contributed limited information to aid source apportionment, they would exert only minor influence on the resulting posterior distributions.

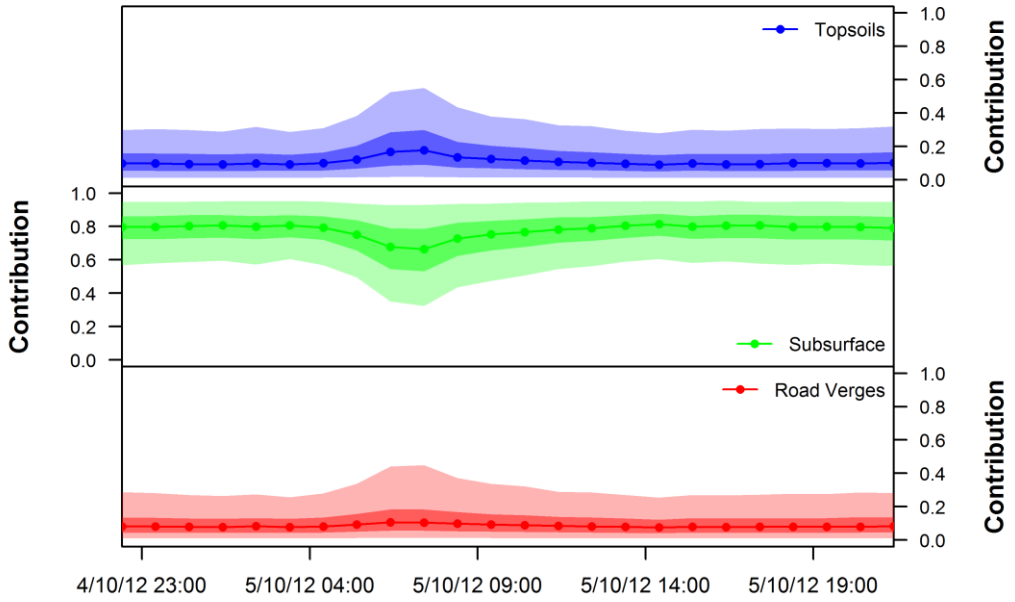

Figure 5.19: Source apportionment results for the October 2012 precipitation event at site A when employing a five fingerprint (Al, Ca, Ce, K, Mg) Bayesian mixing model. Light and dark shading around median source apportionment estimates represent the 95% and 50% Bayesian credible intervals, respectively.

Investigating this further, we explored the impact of removing the strongest source area discriminator, Ca, from the mixing model for the same October 2012 event at site A. Ca concentrations in SPM were very strongly correlated with subsurface sediment contribution (R^2 = 0.981) due to chalky boulder clay deposits forming the lower section of the stream channel banks. This made Ca an excellent discriminator of surface and subsurface sediments. Removing Ca resulted in the mixing model being unable to differentiate between the three sources, with estimated sediment contributions hardly varying from their initial starting values of 33.33% derived from each source (Figure 5.20). Surprisingly, this is in spite of the fact that the minimisation of Wilks-Lambda test is able successfully apportion 98.3% of source area samples when Ca is removed. This reinforces the point that as many viable fingerprints as possible should be included in the model and that selection and rejection of fingerprints should not rely too heavily upon the Wilks-Lambda test statistic. It also demonstrates that when applying this source apportionment technique to other catchments which do not have such a strong surface/subsurface geological contrast, a broader suite of fingerprints would need to be employed for successful source apportionment to be achieved.

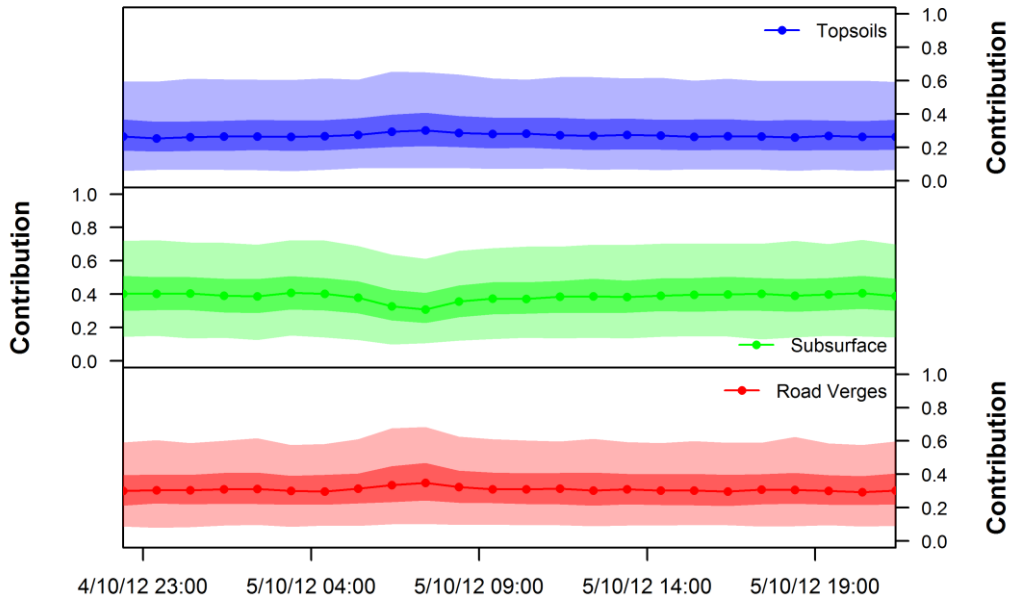

Figure 5.20: Sediment source apportionment results for the October 2012 precipitation event at site A when omitting Ca as a fingerprint. Light and dark shading around median source apportionment estimates represent the 95% and 50% Bayesian credible intervals respectively.

5.4 Discussion

5.4.1 Interpreting Apportionment Results

The temporal fluctuations observed in SPM geochemistry at sites A and B during all the precipitation events presented here indicate that lower flow, non-event conditions were characterised by subsurface erosion of the Mid-Pleistocene chalky, flint-rich boulder clays, with limited sediment input from surface sources. This situation was reversed during precipitation events, with SPM shifting towards the more organic matter and clay mineral-rich, Ca-depleted geochemistry characteristic of surface soils. The Bayesian mixing model was able to successfully translate these geochemical trends into estimated sediment volumes originating from each of the three or four source areas within a realistic uncertainty range. Importantly, by employing the direct spectroscopic analysis of sediment covered filter papers in conjunction with automatic water samplers, we are able to observe how this source apportionment varied at 60- to 120-min resolution during the progression of all these rainfall events. Encouragingly, the apportionment results also corresponded favourably with our knowledge of both catchment geology and connectivity of source areas to the stream channel.

However, due to sediment storage on the streambed over time, caution should be exercised when attempting to relate these high-resolution apportionment estimates directly to catchment erosion processes for a given event (Gellis and Noe, 2013). The instream retention of sediments is known to be spatially and temporally variable. Sediment eroded and mobilised during one season may be stored in the stream channel and subsequently remobilised and exported out of the catchment during later seasons (Evans *et al*., 2004; Demars and Harper, 2005; Walling *et al*., 2008). This is particularly true during low summer flows when flushing rates decline and sediment retention times increase allowing greater opportunity for biotic and abiotic mediated chemical and physical modification of the sediment (Bowes *et al*., 2003; Withers and Jarvie, 2008). When flow rates subsequently increase during the winter this transient sediment store is flushed out of the system with limited opportunities for further retention due to reduced residence times (Evans *et al*., 2004; Jarvie *et al*., 2005 & 2006; Ballantine *et al*., 2008). We see evidence of these processes occurring in the events presented here. For example, whilst sediment contributions from surface sources remained relatively high some 30 hrs after precipitation had ceased during the February 2013 event at site A (Figure 5.17), this does not imply that surface runoff was still occurring. Indeed, visual inspection of the catchment revealed it to have ceased many hours before. Instead, this reflects the continual resuspension of surface soils from the streambed, not just from this event, but previous events that occurred during the winter of 2012/13.

5.4.2 Critical Source Areas

Whilst the mixing model provides quantitative estimates of sediment volumes derived from all road verge and topsoil sources, visual observations suggested that sediments mobilised during rainfall events were dominantly transported to the river from a few CSAs (Thompson *et al*., 2012). These were the damaged field entrances, gateways, tramlines, narrow road sections and bridges that occupy relatively small areas of the catchment but, due to high antecedent soil moisture, abundant sediment supply and good hydrological connectivity, they contribute a significant proportion of the total land-to-river sediment transfer. In particular, peaks in estimated road verge contribution during most precipitation events indicate that land-to-river connectivity in both mini-catchments involved the transport of material along metalled roads which direct sediment-laden water into roadside ditches that discharge directly into the stream channel. In mini-catchment A, sediment concentrations in road runoff at a bridge crossing the stream have regularly been measured at between 400 and 1500 mg/L and flowing at rates exceeding

1.5 L/s. This issue surrounding the role of roads and roadside ditches in increasing the hydrological connectivity between agricultural fields and streams has previously been discussed by Buchanan *et al.* (2012) and Boardman (2013). Furthermore, the October and November precipitation events also coincided with the sugar beet harvest in mini-catchment A, during which time topsoil material was observed washing off heavily eroded field entrances and a concrete sugar beet storage area. This material was carried down metalled roads, picking up road verge material along the way, before draining into a roadside ditch at the bridge and discharging directly into the river (Figure 5.21).

Figure 5.21: Sediment mobilisation during the autumn 2012 sugar beet harvest in mini-catchment A. Tractors and other farm vehicles inadvertently transport soil from concreate sugar beet storage areas (A) and damaged field entrances (B) onto metalled roads (C). Surface runoff during precipitation events subsequently washes this soil, along with road verge material, off the road and into the stream via roadside ditches (D).

Visual observations of the increase in river turbidity upstream compared to downstream of this road bridge highlighted that road runoff at this location was a significant source of SPM in mini-catchment A during precipitation events. To quantitatively determine how much of this road runoff material was of topsoil or road verge origin, the Bayesian

mixing model was run for these two end members on 18 road runoff samples collected during rainfall events between May 2012 and March 2014. As with the SPM analysis, the Kruskal-Wallis *H*-test, the minimisation of Wilks-Lambda and PCA were conducted to determine which combination of fingerprints could successfully differentiate topsoil and road verge material. As can be seen in Table 5.3 and Figure 5.22, 100% of source area samples could be successfully differentiated by just four fingerprints (Al, Mg, Mn, Ca), although 10 elements were included in the mixing model. The strongest discriminator was Al which was capable of correctly classifying 96.6% of samples. PC1 also weighed most strongly on Al, with absolute Al concentrations in topsoil samples being approximately 4% higher than in road verge material.

Table 5.3: Assessing the ability of geochemical fingerprints to differentiate between road verge and topsoil sediments in mini-catchment A via the Kruskal-Wallis *H*-test and minimisation of Wilks-Lambda.

	Kruskal-Wallis		**Minimisation of Wilks-Lambda**			
Fingerprint property	***H*-value**	***p*-value**	**Selection step**	**Wilks-Lambda**	**Cumulative *p*-value**	**Cumulative % of source areas correctly classified**
Al	51.86	<0.001	1	0.2547	<0.001	96.6
Mg	39.23	<0.001	2	0.1616	<0.001	98.3
Mn	47.22	<0.001	3	0.1510	<0.001	98.3
Ca	30.50	<0.001	4	0.1399	<0.001	100.0
Ti	42.94	<0.001	5	0.1314	<0.001	100.0
Na	18.64	<0.001	6	0.1225	<0.001	100.0
Ce	4.75	0.092	7	0.1163	<0.001	100.0
P	21.10	<0.001	8	0.1157	<0.001	100.0
K	40.90	<0.001	9	0.1157	<0.001	100.0
Fe	24.20	<0.001	10	0.1156	<0.001	100.0

The results of the Bayesian source apportionment model revealed that road verge and topsoil contributions to road runoff sediments were highly variable, with median road verge contributions ranging from 44-100% (1-100% at the 95% credible interval) and topsoil contributions ranging from 0-56% (0-99%) (Figure 5.23). Whilst the low sampling resolution mean it is not possible to make a detailed assessment of how the relative contributions of these two sources varied temporally, it is interesting to note that some of the highest estimated topsoil contributions (median 38-40%) occurred on the 24th November 2012 during the sugar beet harvest. Contrast this with the 24th May 2012 when no harvest was occurring and estimated topsoil contribution was negligible (median 1%).

It is also worth noting that when the road runoff samples were collected on the 24th November 2012, topsoils and road verges were estimated to be contributing a median ~27% and ~32% of SPM, respectively (Figure 5.15). So, given that road runoff was composed of an estimated 60-62% road verge material and 38-40% topsoil material at this time (Figure 5.23), and that road verge material could only enter the stream as road runoff at this location, one can calculate that the majority (~75%) of topsoil material in the stream must have been being delivered by road runoff. This intuitively makes sense when one considers that the vast majority of the stream is bordered by grass buffer strips under the ELS stewardship scheme which should act to restrict direct field-to-river topsoil transfer in erosive surface flows (section 2.5). These results therefore confirm that metalled roads do indeed transport a significant amount of topsoil material into the river in mini-catchment A, and thus reducing the amount of topsoil deposited onto the road network should be a key goal for reducing sediment ingress into the river. Unfortunately, having not sampled road runoff from mini-catchment B, it is not possible to assess how much of the topsoil derived SPM measured at site B was associated with road runoff.

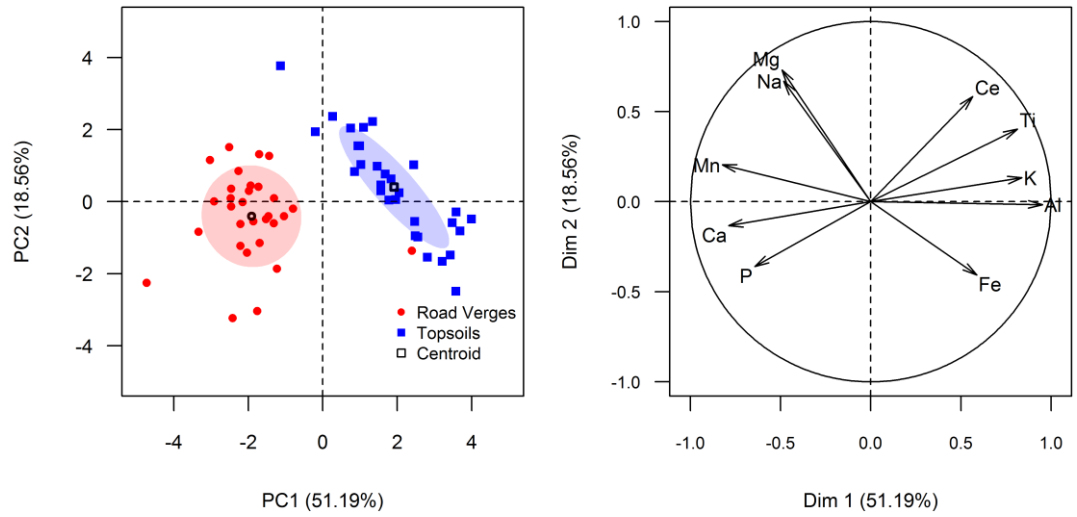

Figure 5.22: Principal component analysis plots of mini-catchment A road verge and topsoil sediments (left) and fingerprint loadings (right) for the first two components. Shaded ellipsoids cover 50% of the source area range.

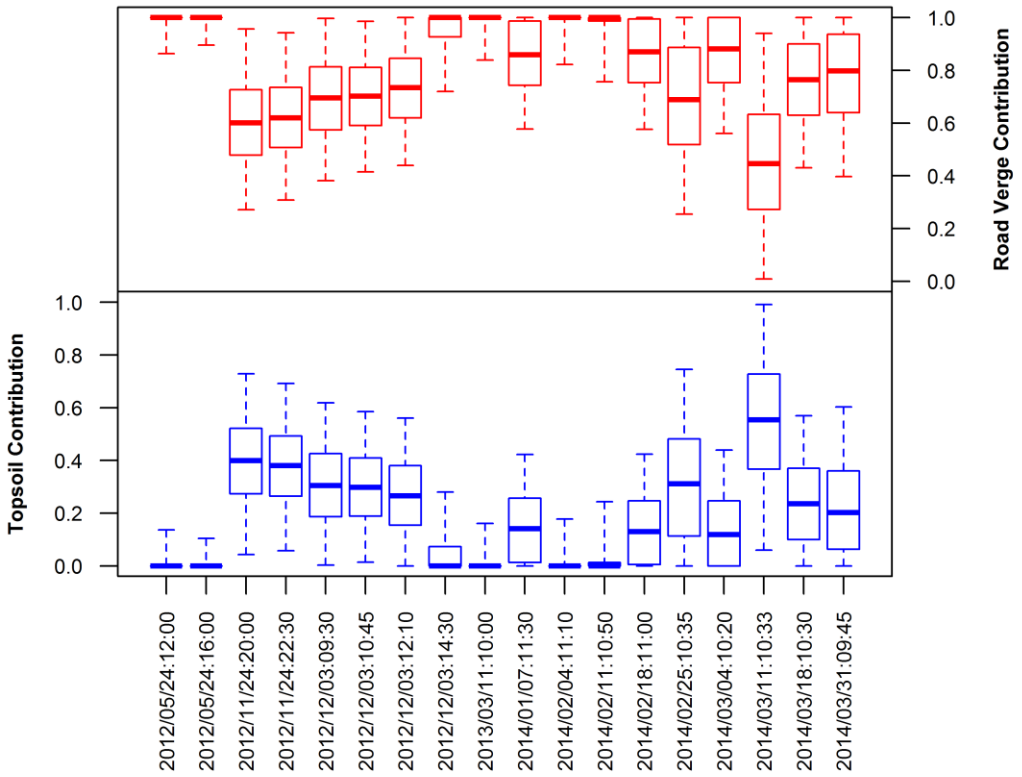

Figure 5.23: Estimated topsoil and road verge sediment contributions to road runoff material at the bridge in mini-catchment A. The solid central line and the end of the boxes and whiskers represent the median, 50% and 95% Bayesian credible intervals, respectively.

5.4.3 Hysteresis

Complementary supporting information for the mixing model source apportionment results can be obtained by examination of sediment-discharge relationships for each precipitation event. Hysteresis describes how sediment-discharge relationships are different on the rising limb of a hydrograph compared to that on the falling limb, with such hysteric behaviour having been extensively discussed in the literature (e.g. Asselman, 1999; Lefrançois *et al.*, 2007; Salant *et al.*, 2008; Oeurng *et al.*, 2010, 2011; Krueger *et al.*, 2009; Krueger *et al.*, 2012; Navratil *et al.*, 2012; Fan *et al.*, 2013). Sediment-discharge relationships can generally be grouped into one of three main classes (Williams, 1989):

Class 1 (symmetric hysteresis) – SPM concentration and discharge peak simultaneously and the concentration-discharge ratio is the same on the rising limb as it is on the falling limb. This situation is typically related to an abundant, unrestricted sediment supply.

Class 2 (clockwise hysteresis) – SPM concentrations are greater on the rising limb than on the recession limb, with SPM concentrations usually peaking before the peak in discharge. This behaviour is typically related to high energy systems with an initially unrestricted sediment supply in close proximity to the stream channel that quickly becomes exhausted by flushing and cannot easily be replaced.

Class 3 (anticlockwise hysteresis) – SPM concentrations are higher on the recession limb than discharge, with SPM tending to peak after maximum discharge. This situation is thought to occur when sediment sources are widely spread throughout the catchment and do not become easily exhausted, possibly as a consequence of sediment replenishment from channel bank collapse during the later stages of an event when soils become saturated.

Hysteresis curves the five precipitation events recorded at site A are presented in Figure 5.24. All events exhibited either clockwise or near symmetric hysteresis loops. This corresponds well with the notion of road runoff being a major sediment pathway in mini-catchment A. The road bridge where sediment ingress occurs is located just 670 m upstream of the monitoring station and surface runoff over the impermeable metalled road is generated rapidly after the onset of heavy precipitation. Once precipitation has ended, road runoff ceases shortly afterwards and does not recommence until the next rainfall period, hence generating the characteristic clockwise hysteric behaviour.

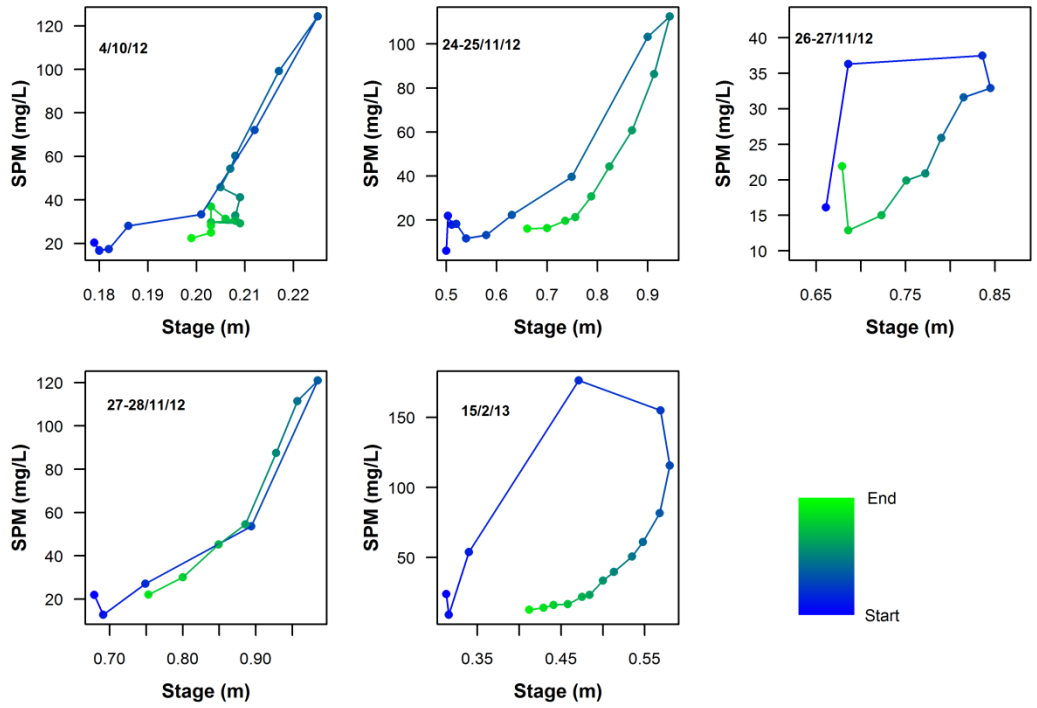

Figure 5.24: Hysteresis plots of SPM versus stage for the five monitored precipitation events at site A.

At site B the picture is more complex, with two of the six events displaying positive hysteresis, two negative hysteresis and two mixed (Figure 5.25). Road runoff was known to be an important source of sediment, particularly during the November 2012 events, as highlighted by the relatively high estimated road verge contribution to SPM (Figure 5.16). Therefore the two negative hysteresis curves for the 23/24th and 27/28th November could be explained by the greater distance between the monitoring station at site B and the main location of sediment ingress at the road 1.8 km upstream. In fact, sediment-rich road runoff from areas of the catchment some 2.5 km away from site B has been observed entering the stream channel and these distal sources could also help to explain the observed anti-clockwise hysteresis behaviour.

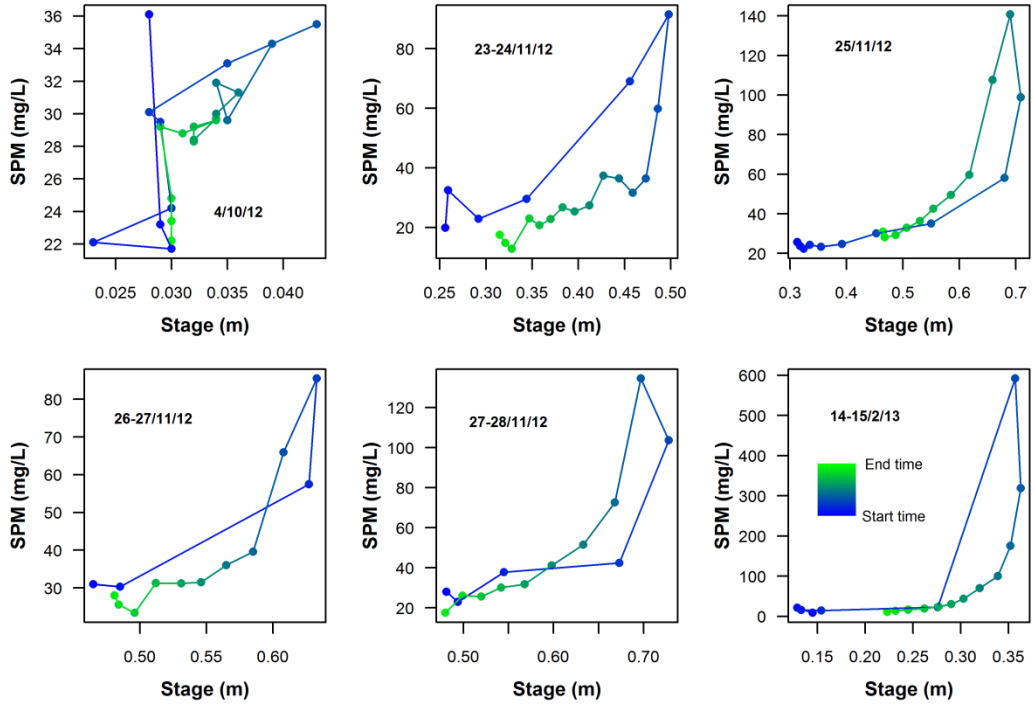

Figure 5.25: Hysteresis plots of SPM versus stage for the six monitored precipitation events at site B.

5.4.4 Implications for Catchment Management

The high-temporal resolution source appointment results presented in this chapter provide quantitative confirmation that precipitation events within the Blackwater catchment are associated with an increase in surface land-to-river sediment transfer. Considering their relatively small spatial extent, contributions from road verges are particularly significant CSAs of sediment, accounting for 13-59% and 8-50% of all SPM transported at sites A and B, respectively, during the events presented here based on the

95% credible intervals. This supports the findings of Collins *et al*. (2010, 2013b) on the importance of road verge derived sediment inputs on fluvial SPM concentrations. Previous research has demonstrated that it is more cost-effective to target mitigation efforts on these CSAs that may cover, for example, just 10% of the catchment area but are responsible for 90% of the sediment pollution, than to spread mitigation measure funds across the entire catchment (Dougherty *et al*., 2004; Heckrath *et al*., 2008). Therefore, mitigation measures targeted at reducing the connectivity of these CSAs, such as by installing roadside sediment traps, improving sugar beet storage practices and minimising agricultural machinery movement on and off fields during wet weather, would likely prove to be the most effective management techniques to reduce fluvial sediment ingress from the terrestrial environment. Additionally, a previous study by Rawlins *et al*. (2013) demonstrated that aggregates of topsoils across the Blackwater sub-catchment have lower stability in comparison to other agricultural soils in eastern England, in part due to the low organic matter content of the former. By applying organic amendments to increase the concentration of organic matter in topsoils, it may be possible to improve aggregate stability and limit the delivery of fine material to the channel network.

With a median 63% (44-80% at the 95% credible interval) of SPM derived from surface sources during the October, November and February events in mini-catchment A, up to 3386 kg (2442-4407 kg) of fine sediment could, theoretically, have been prevented from entering the stream with appropriately targeted mitigation measures. In mini-catchment B this proportion is even greater, with a median 73% (54-87%) of SPM derived from surface sources, equating to 835 kg (619-1000 kg) of fine sediments that could potentially have been kept out of the river. See Figure C1 (Appendix C) for the estimated SPM loads generated during all storm events captured between September 2012 and February 2014 at sites A and B.

5.4.5 Methodological Advantages

Although other studies have used infrared spectroscopy to analyse SPM-covered filter papers (e.g. Martínez-Carreras *et al.*, 2010b; Tremblay *et al*., 2011), the results presented in this chapter represents the first successful attempt at using direct XRFS analysis of SPM-covered filter papers to apportion sources of sediment during precipitation events. Because the method is non-destructive, cost-effective and time-efficient and can be used in conjunction with automatic samplers, the procedure is

conducive to this type of high-temporal resolution monitoring where large numbers of samples need to be analysed. Furthermore, because as little as 5 mg of sediment are required to yield accurate results for a wide array of elemental parameters (see Chapter 3), it is particularly beneficial in environments where SPM concentrations can be too low (<100 mg/L) for traditional analysis without bulking water samples. The result is that source apportionment estimates can be generated at a high-temporal resolution that is simply not possible when using time-integrated samplers or manual grab samples (e.g. Poulenard *et al.*, 2009).

A good example of how the temporal sampling resolution can affect resulting source apportionment estimates is by comparison with Collins *et al*. (2013a), who carried out a separate low-temporal resolution sediment fingerprinting procedure within the Wensum DTC area. In contrast to our high-resolution approach, Collins *et al*. (2013a) collected streambed sediment samples from three locations in the River Blackwater on a bimonthly basis. Whilst results are not directly comparable due to differences in the location of sediment sampling within the catchment, Collins *et al.* (2013a) estimated the topsoil contribution (~58-70%) to be much greater than that for channel banks (~19-30%) or road verges (~6-23%) during all months, with apportionment showing relatively little monthly variability. In contrast, our approach demonstrates significant variability in source contributions at 60- to 120-min intervals during the transition from low- to high-flow conditions, and emphasises that surface sediments are dominant sources for only a few hours during rainfall events when the highest sediment loads are recorded. This more precise knowledge of when, and for how long after rainfall, surfaces sources are dominant is beneficial when attempting to identify the locations of CSAs.

The other major advantage of the approach presented here arises from setting source apportionment within a Bayesian uncertainty framework. As discussed in Chapter 4, traditional fingerprinting studies often present uncertainties around apportionment estimates in *ad hoc* ways which do not fully and consistently represent the spatial variability in fingerprint properties across the catchment, uncertainties associated with instrumental precision, covariance between fingerprint properties, nor residual model error (Motha *et al.*, 2003; Wilkinson *et al.*, 2013). In contrast, the Bayesian mixing model results presented here represent full and coherent characterisation of all these factors. The resulting distributions, while often large, are nevertheless a realistic reflection of the often unavoidable uncertainties associated with sediment source apportionment estimates.

5.5 Conclusions

In this chapter, we have used the methodological advancements presented in Chapters 3 and 4 to address two key areas of sediment fingerprinting research. Namely, (i) how to improve the temporal resolution of source apportionment estimates during precipitation events and (ii) how to coherently quantify all perceived uncertainties associated with the mixing model procedure. By combining the direct XRFS and DRIFTS analysis of SPM-covered filter papers with automatic water samplers (Chapter 3), we have been able to observe temporal fluctuations in SPM geochemistry at 60- to 120-min resolution during the progression of five/six precipitation events in mini-catchments A and B. These high-resolution geochemical time-series reveal that SPM under lower flow, pre- and post-event conditions is dominated by high Ca concentrations, indicating erosion of the subsurface Mid-Pleistocene chalky, flint-rich boulder clays dominates during these periods, with limited sediment input from the weathered surface sources. This situation is reversed during precipitation events, with SPM shifting towards a more organic matter and clay mineral-rich, Ca-depleted geochemistry characteristic of more heavily weathered surface soils.

By employing the Bayesian mixing model procedure developed in Chapter 4, we have then been able to successfully translate these geochemical trends into quantitative estimates of sediment volumes originating from four main source areas; namely topsoils, road verges, channel banks and field drains. Importantly, the adoption of a Bayesian approach has allowed for full characterisation of spatial geochemical variability, instrument precision and residual error to yield a realistic and coherent assessment of the uncertainties associated with source apportionment estimates. During the five rainfall events monitored in mini-catchment A, 63% (44-80% at the 95% credible interval) of SPM was estimated to derive from surface sources, equating to a total land-to-river sediment transfer of 3386 kg (2442-4407 kg), with road verges (13-59%) in particular proving to be a highly important source. A similar situation was recorded in mini-catchment B, where 73% (54-87%) of SPM was derived from surface sources during six monitored events, equating to a total land-to-river sediment transfer of 835 kg (619-1000 kg).

The importance of maximising the number of tracers incorporated into Bayesian mixing models has been highlighted, with median source appointment estimates varying by up to 28.3% (51.4% at the 95% credible interval) depending on whether five or eight fingerprints were included in the model. We have also shown how source apportionment results are adversely affected by removal of the strongest source discriminating

fingerprint (Ca) from the mixing model, raising questions regarding how well such source apportionment procedures would work in other catchments lacking strong contrasts between surface and subsurface geochemistry. Overall, the results presented here demonstrate the benefits that high-resolution SPM monitoring and Bayesian uncertainty assessment bring to our understanding of catchment processes. Application of these source apportionment techniques in other locations will assist with the appropriate targeting of sediment pollution mitigation measures at a catchment level.

Chapter 6

APPORTIONING SOURCES OF ORGANIC MATTER IN STREAMBED SEDIMENTS: AN INTEGRATED MOLECULAR AND COMPOUND-SPECIFIC STABLE ISOTOPE APPROACH**

6.1 Chapter Summary

Organic matter is an important constituent of the particulate material transported in fluvial systems, yet techniques capable of quantitatively apportioning its origin have largely been overlooked by the sediment fingerprinting community. In this chapter, this deficiency is addressed through the novel application of a coupled molecular and compound-specific isotope analysis (CSIA) of long-chain leaf wax *n*-alkane biomarkers. Leaf wax extracts of 13 plant species were collected from across two environments (aquatic and terrestrial) and four plant functional types (trees, herbaceous perennials and C_3 and C_4 graminoids) from mini-catchment A during August and September 2013. Seven isotopic ($\delta^{13}C_{27}$, $\delta^{13}C_{29}$, $\delta^{13}C_{31}$, $\delta^{13}C_{27\text{-}31}$, $\delta^{2}H_{27}$, $\delta^{2}H_{29}$ and $\delta^{2}H_{27\text{-}29}$) and two *n*-alkane ratio (average chain length (ACL) and carbon preference index (CPI)) fingerprints were derived, which successfully differentiated 93% of individual plant specimens by plant functional type. The $\delta^{2}H$ values were the strongest discriminators of plants originating from different functional groups, with trees ($\delta^{2}H_{27\text{-}29}$ = -208‰ to -164‰) and C_3 graminoids ($\delta^{2}H_{27\text{-}29}$ = -259‰ to -221‰) providing the

** Chapter published as: Cooper RJ, Pedentchouk N, Hiscock KM, Disdle P, Krueger T, Rawlins BG. 2015b. Apportioning sources of organic matter in streambed sediments: An integrated molecular and compound-specific stable isotope approach. *Science of the Total Environment* **520**: 187-197. DOI: 10.1016/j.scitotenv.2015.03.058.

largest contrasts. The $\delta^{13}C$ values provided strong discrimination between C_3 ($\delta^{13}C_{27\text{-}31}$ = -37.5‰ to -33.8‰) and C_4 ($\delta^{13}C_{27\text{-}31}$ = -23.5‰ to -23.1‰) plants, but neither $\delta^{13}C$ nor $\delta^{2}H$ values could uniquely differentiate aquatic and terrestrial species, emphasising a stronger plant physiological/biochemical, rather than environmental, control over isotopic differences. ACL and CPI complemented isotopic discrimination, with significantly longer chain lengths recorded for trees and terrestrial plants compared with herbaceous perennials and aquatic species, respectively. The Bayesian mixing model developed in Chapter 4 was then applied to these data to quantitatively apportionment sources of organic matter in 18 streambed sediments collected between September 2013 and March 2014. Results revealed considerable temporal variability in organic matter sources, with median contributions ranging from 22-52% for trees, 29-50% for herbaceous perennials, 17-34% for C_3 graminoids and 3-7% for C_4 graminoids. The results presented in this chapter clearly demonstrate the effectiveness of an integrated molecular and stable isotope analysis for quantitatively apportioning, with uncertainty, plant-specific organic matter contributions to streambed sediments via a Bayesian mixing model approach.

6.2 Background

As discussed in Chapter 4, sediment fingerprinting has become a popular technique for apportioning the sources of deposited and suspended sediments across a range of aquatic environments via a mixing model approach (Mukundan *et al*., 2012; Guzmán *et al*., 2013; Walling, 2013). As the number and type of source apportionment studies have increased over recent years, there has been a shift in research focus towards re-evaluating and advancing existing fingerprinting procedures (e.g. Koiter *et al*., 2013; Cooper *et al*., 2014b; Smith and Blake, 2014; Laceby and Olley, 2014; Pulley *et al*., 2015). Because the majority of existing fingerprinting studies have focused solely on inorganic sediment provenance (e.g. Collins *et al*., 2013; Thompson *et al*., 2013; Wilkinson *et al*., 2013), the apportionment of organic matter in fluvial sediments in agricultural settings remains largely undeveloped. Understanding the origins of fluvial organic matter is important because organic material can constitute a significant percentage of the total sediment volume (e.g. Cooper *et al.*, 2015a; Chapter 5). Furthermore, elevated organic matter concentrations are associated with enhanced transport of nutrients and heightened biological oxygen demand, thus leading to the degradation of water quality (Evans *et al.*, 2004; Hilton *et al*., 2006; Withers and Jarvie, 2008). Whilst an understanding of the amount of organic material transported in fluvial systems can be achieved by monitoring the fluxes of dissolved (DOC) and particulate organic carbon (POC) at the catchment

outlet (Alvarez-Cobelas *et al*., 2012; Némery *et al*., 2013), such measurements are unable to yield quantitative information on the specific sources of this organic load.

Addressing this matter, compound-specific isotope analysis (CSIA) has the potential to facilitate the identification of organic matter contributions to riverine sediments by exploiting differences in the stable isotopic composition amongst different plants at either the species or plant functional type level (Marshall *et al*., 2007). Of particular interest in this study are the carbon ($\delta^{13}C$) and hydrogen ($\delta^{2}H$) stable isotopic compositions of plant *n*-alkanes. Although *n*-alkanes represent only a small fraction of total organic matter, these compounds have unique biological origins which allow them to be used as plant-specific biomarkers of organic matter contributions (Meyers, 1997). Compared with other plant biochemical components, such as carbohydrates, amino acids and lignin, long-chain *n*-alkanes also persist in the environment due to a high resistance to degradation (Bourbonniere and Meyers, 1996), thus making them suitable conservative fingerprints for sediment source apportionment. Variability in the carbon and hydrogen isotopic compositions of plant *n*-alkanes are driven by a complex combination of differences in plant physiology/biochemistry and a range of environmental factors, including temperature, humidity, light availability, salinity and the isotopic composition of water and CO_2 (O'Leary, 1988; Farquhar *et al.*, 1989; Sessions *et al*., 1999; Hou *et al*., 2007; Sachse *et al*., 2012). Importantly, this means the degree of isotopic fractionation is theoretically unique for each individual plant, thereby allowing distinct *n*-alkane isotopic signatures to develop that can be used to differentiate between different plant types.

A number of studies have previously been successful in using the $\delta^{13}C$ isotopic signatures of soils and sediments to identify fluvial sediment contributions derived from allochthonous and autochthonous sources (e.g. McConnachie and Petticrew, 2006; Schindler Wildhaber *et al*., 2012; Fu *et al*., 2014; Wang *et al*., 2015), or from different land-use types based on the dominant vegetation cover (e.g. Fox and Papanicolaou *et al*., 2007; Gibbs, 2008; Blake *et al*., 2012; Hancock and Revill, 2013; Laceby *et al*., 2014). Similarly, previous studies have used molecular ratios, such as the average chain length (ACL) and carbon preference index (CPI), to differentiate organic material of higher plant origin from algal or microbial contributions, or to identify petrogenic hydrocarbon inputs (e.g. Pancost and Boot, 2004; Jeng *et al*., 2006). However, to our knowledge, the usefulness of integrating both molecular ratios and compound-specific $\delta^{2}H$ and $\delta^{13}C$ values of individual organic compounds for quantifying organic matter source apportionment in stream sediments via a Bayesian mixing model approach has never been assessed. Therefore, the main objectives of this chapter were:

(i) to assess the effectiveness of δ^2H and $\delta^{13}C$ values of long-chain *n*-alkanes (C_{27}, C_{29}, C_{31}) in differentiating (a) plants derived from different functional types and (b) plants growing in aquatic and terrestrial environments;

(ii) to determine whether *n*-alkane ratios (ACL and CPI) can enhance discrimination between plant groups when used in combination with isotopic values;

(iii) to use these isotopic values and molecular ratios as fingerprints within a Bayesian mixing model to quantitatively apportion, with uncertainty, plant-specific organic matter contributions to streambed sediments.

This novel CSIA fingerprinting technique was applied to streambed sediments collected from mini-catchment A over a 7-month period between September 2013 and March 2014.

6.3 Methods

6.3.1 Sample Collection and Preparation

6.3.1.1 Streambed Sediments

Streambed sediments were collected at the outlet to mini-catchment A at approximately weekly intervals between September 2013 and March 2014, yielding a total of 18 samples for analysis. This autumn to spring period was chosen as it represents the most dynamic time with respect to catchment sediment mobilisation (e.g. Oeurng *et al*., 2011). Sediment volumes of 1 L were obtained from the streambed surface (approximately <50 mm depth) using a non-magnetic trowel that had been thoroughly washed in the stream prior to sampling. Sediments were transported back to the laboratory in sealed HDPE bottles, where they were immediately oven dried at 40^oC for 48-72 hrs. Dried sediments were lightly disaggregated using a pestle and mortar and sieved down to <63 µm to isolate the biochemically important clay-silt fraction (Horowitz, 2008), in keeping with common sediment fingerprinting practice (e.g. Walling, 2005; Chapter 5). These fine sediments were stored in the dark at room temperature in sealed polyethylene bags prior to analysis.

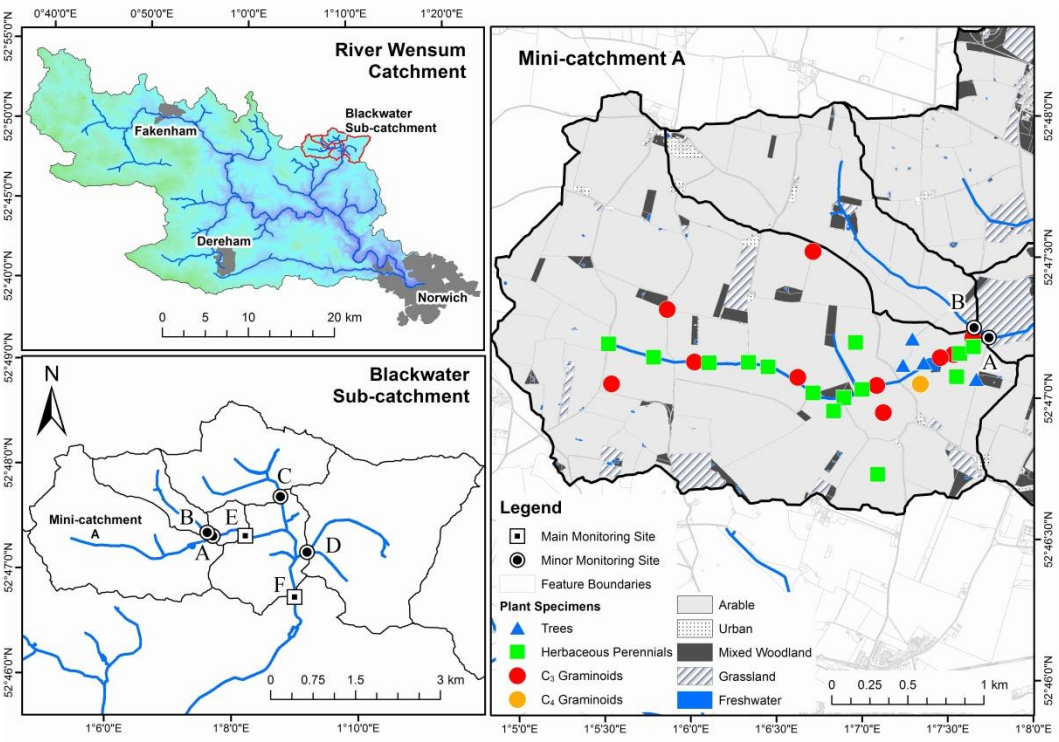

Figure 6.1: Map of the Blackwater sub-catchment showing the locations of tree, graminoid and herbaceous perennial plant collection within mini-catchment A.

6.3.1.2 Plant Specimens

Plant leaf samples were collected across mini-catchment A during August and September 2013 for the classification of organic matter source areas (Figure 6.1). A total of 30 individual plant specimens were collected from two environments (aquatic and terrestrial) and four plant functional types (trees, herbaceous perennials and C_3 and C_4 graminoids), and included a mixture of both cultivated and natural vegetation. For aquatic plants, 12 specimens were collected, all of which were emergent macrophytes owing to their dominance of stream biomass (Figure 6.2). These included the herbaceous perennials *Chamerion angustifolium* (rosebay willowherb), *Aegopodium podagraria* (ground elder), *Typha latifolia* (reed mace) and *Iris pseudacorus* (yellow flag iris), as well as three C_3 Poaceae graminoid specimens. For the terrestrial environment, 18 specimens were obtained, including the tree species *Crataegus monogyna* (hawthorn), *Carpinus betulus* (hornbeam), *Fraxinus excelsior* (ash) and *Acer campestre* (field maple), the herbaceous perennials *Typha latifolia* (reed mace), *Raphanus sativus* (oilseed radish) and *Phaseolus vulgaris* (spring beans), the C_4 graminoid *Zea mays* (maize), the C_3 graminoid *Triticum* sp. (wheat) and a further six natural C_3 Poaceae graminoids. For each plant specimen, ~10 g of leaves were collected to provide sufficient material for replicate

sample analysis. On return to the laboratory, samples were immediately frozen at -80^{o}C prior to being freeze-dried for 48 hrs and stored in the dark at room temperature in sealed polyethylene bags.

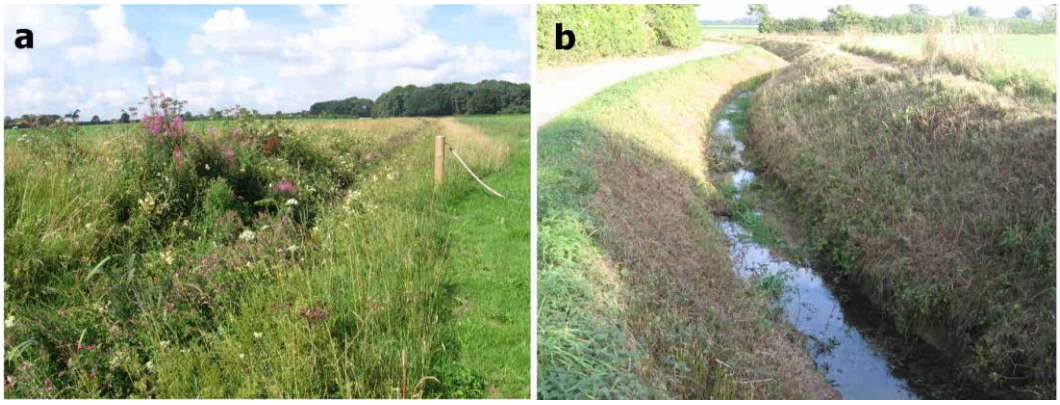

Figure 6.2: The River Blackwater in mini-catchment A, showing (a) the dominance of emergent macrophytes in August and (b) following vegetation clearance in October.

6.3.2 Particulate Organic Carbon

Particulate organic carbon (POC) concentrations for the 18 streambed sediments were determined by mixing 25 mg of the fine grained sediments into suspension with 1 L of Milli-Q water (Merck Millipore, Billerica, MA, USA), which was subsequently vacuum filtered onto QFF papers. Sediment covered filters were oven dried at 105^{o}C for 2 hrs, before being finely ground and the resulting powders analysed directly by DRIFTS following the procedures set out in Chapter 3.

6.3.3 *n*-Alkane Extraction

Two different techniques were required to extract aliphatic *n*-alkanes from streambed sediments and plant materials. For sediments requiring a more polar solvent to extract both the free and mineral-associated organic material, samples were mixed with Ottawa sand (SiO_2; 20-30 mesh) in a 4:1 sand-sediment ratio to improve volatilisation of material prior to being run through a Dionex Accelerated Solvent Extractor (ASE) 200^{TM} with HPLC grade dichloromethane solvent operated at 100^{o}C and 1500 psi. For plant specimens, alkanes were extracted by repeated sonication (3 x 10 min) of 2 g of leaf material in HPLC grade hexane. This procedure was duplicated for all 30 specimens using different leaves from the same plant to enable evaluation of isotopic variability

within individual plants. Extracts from both plants and sediments were concentrated down to 1 ml under nitrogen gas in a Caliper Life Sciences TurboVap Workstation™. Final concentration down to dryness was made under nitrogen gas and the residues were re-dissolved in 1 ml hexane. The *n*-alkane extracts were purified by elution with hexane during column chromatography through a silica gel (70-230 mesh) stationary phase, and the resulting eluate was concentrated down to 1 ml under nitrogen gas in preparation for molecular and stable isotope analyses.

6.3.4 *n*-Alkane Ratios

The distribution and abundance of *n*-alkanes C_{13}-C_{34} were identified using an Aglient Technologies 7820A gas chromatogram fitted with a flame ionisation detector (GC-FID). The GC oven temperature was initially set to 50°C for sample injection and was then ramped up at 20°C min^{-1} between 50°C and 150°C, and 8°C min^{-1} between 150°C to 320°C. The final temperature was held for 5 min. Individual *n*-alkanes were identified by comparison of elution times against a known *n*-C_{16} to *n*-C_{30} standard (A. Schimmelmann, Indiana University, USA). Chain length distributions were summarised by the carbon preference index (CPI; Equation 6.1):

$$\text{CPI} = \frac{1}{2}\left(\frac{C_{25} + C_{27} + C_{29} + C_{31} + C_{33}}{C_{24} + C_{26} + C_{28} + C_{30} + C_{32}} + \frac{C_{25} + C_{27} + C_{29} + C_{31} + C_{33}}{C_{26} + C_{28} + C_{30} + C_{32} + C_{34}}\right) \quad (6.1)$$

which expresses the odd-over-even *n*-alkane predominance. Larger CPI values typically indicate a higher vascular plant origin, whereas values close to zero typically indicate microbial or degraded organics (Zhang *et al*., 2006; Jeng *et al*., 2006). Distributions were also summarised by the average chain length (ACL) metric (Equation 6.2):

$$ACL = \frac{25(C_{25}) + 27(C_{27}) + 29(C_{29}) + 31(C_{31}) + 33(C_{33})}{C_{25} + C_{27} + C_{29} + C_{31} + C_{33}} \quad (6.2)$$

which provides a weighted average of the longer chained odd-numbered *n*-alkanes. Previous studies have found the ACL can be influenced by both plant physiology and climate (Jeng, 2006; Bush and McInerney, 2013).

6.3.5 *n*-Alkane Carbon and Hydrogen Isotope Analyses

Compound-specific δ^2H and $\delta^{13}C$ values were determined using a Thermo Scientific™ Delta V™ Advantage isotope ratio mass spectrometer (IRMS) coupled with

a GC-Isolink gas chromatograph. The GC oven temperature ramp was the same as that used for the GC-FID and reactor temperatures were set to 1000°C for carbon and 1400°C for hydrogen modes, respectively. All samples were run in duplicate and an *n*-alkane (C_{16} to *n*-C_{30}) standard was run at the beginning and end of every 16 run sequence. $^{13}C/^{12}C$ composition was expressed relative to the Vienna Pee-Dee belemnite (VPDB) standard, as follows (Equation 6.3):

$$(6.3) \quad \delta^{13}C\ (‰) = \{((^{13}C/^{12}C)_{sample} - (^{13}C/^{12}C)_{standard}) / (^{13}C/^{12}C)_{standard}\} \times 1000$$

$^{2}H/^{1}H$ isotopic composition was expressed relative to Vienna Standard Mean Ocean Water (VSMOW) (Equation 6.4):

$$(6.4) \quad \delta^{2}H\ (‰) = \{((^{2}H/^{1}H)_{sample} - (^{2}H/^{1}H)_{standard}) / (^{2}H/^{1}H)_{standard}\} \times 1000$$

Only compounds ubiquitous to all sediment samples and plant specimens were used as fingerprints for source apportionment. For $\delta^{13}C$, this meant the high-molecular weight *n*-alkanes C_{27}, C_{29} and C_{31}, whilst C_{27} and C_{29} where selected for $\delta^{2}H$. Poor reproducibility of C_{31} for $\delta^{2}H$ meant it was excluded from the analysis. Abundance weighted C_{27}-C_{31} values for $\delta^{13}C$ and C_{27}-C_{29} values for $\delta^{2}H$ were included as fingerprints to account for within plant variation in chain length abundance and were calculated as follows (Equation 6.5):

$$(6.5) \quad C_{27-29(31)}(‰) = \frac{\sum_{m=1}^{M}(\delta_m \times \alpha_m)}{\sum_{m=1}^{M}\alpha_m}$$

where δ is the isotopic value in ‰; α is the abundance in pico-volts (pV); *M* is the number of *n*-alkanes (three for $\delta^{13}C$, two for $\delta^{2}H$); and *m* is the alkane index. Mean absolute errors between replicate samples (precision) were 1.9‰ for $\delta^{2}H_{27}$, 1.1‰ for $\delta^{2}H_{29}$ and 0.1‰ for $\delta^{13}C_{27}$, $\delta^{13}C_{29}$ and $\delta^{13}C_{31}$. The mean absolute errors of the laboratory standard (accuracy) were 8‰ for $\delta^{2}H_{27}$, 10‰ for $\delta^{2}H_{29}$ and 0.6‰ for $\delta^{13}C_{27}$ and $\delta^{13}C_{29}$ (*n* = 49). The standard deviation of $\delta^{2}H$ reference gas pulses was 8‰. All isotopic measurements were corrected to account for standard inaccuracy and drift in reference gas values.

6.3.6 Statistical Source Discrimination and Bayesian Apportionment

Following on from Chapters 4 and 5, the Kruskal-Wallis one-way analysis of variance and stepwise LDA based on the minimisation of the Wilk's Lambda criterion were employed to quantitatively determine the proportion of source area samples that

could be correctly classified by selected isotopic values and molecular ratio fingerprints (Collins *et al*., 2012). PCA plots were also generated to visualise the mixing space geometry. Due to differences in plant physiology/biochemistry, the abundance of *n*-alkanes produced per unit of organic matter has been shown to vary between both species and different chain lengths within the same plant (Diefendorf *et al*., 2011; Bush and McInerney, 2013). Consequently, isotopic values and molecular ratios were weighted by relative *n*-alkane abundances (pV) when grouping fingerprints by source prior to running the Bayesian mixing model. This was done by passing the abundance weighted mean and covariance matrix for each source onto the Bayesian mixing model to quantitatively apportion *n*-alkane sources. The model, as presented in Chapter 4, was run in the open source software JAGS 3.3.0 (Just Another Gibbs Sampler; Plummer, 2003) within the R environment (R Development Core Team, 2014) using three parallel chains of 250,000 iterations each with a 100,000 sample burn-in and a 225 sample jump length to ensure model convergence and minimise autocorrelation between sample runs. A final correction was required to convert the mixing model *n*-alkane source apportionment results into contributions of organic matter and was applied as follows (Equation 6.6):

$$P_{OM} = \frac{\frac{P_k}{\alpha_k}}{\sum_{k=1}^{K}\left(\frac{P_k}{\alpha_k}\right)} \quad (6.6)$$

where P_{OM} is the corrected contribution of organic matter from each source; P is the mixing model estimated proportion of *n*-alkanes; α is the mean relative *n*-alkane abundance for each source; K is the number of sources; and k is the source index.

6.4 Results and Discussion

6.4.1 Isotopes for Discriminating Plant Functional Types

6.4.1.1 Hydrogen

CSIA of the 13 plant species collected from across mini-catchment A revealed that δ^2H provided strong discrimination between some plant functional groups (Figure 6.3; Table 6.1). Tree species (*Fraxinus excelsior*, *Carpinus betulus*, *Crataegus monogyna* and *Acer campestre*) exhibited the most ^2H-enriched composition, with $\delta^2H_{27\text{-}29}$ values ranging from -208‰ to -164‰, with an *n*-alkane abundance weighted mean of -185‰. This contrasted strongly with the C_3 graminoids which had the lowest $\delta^2H_{27\text{-}29}$ values, ranging from -259‰ to -221‰ with an abundance weighted mean of -246‰. This is

consistent with previous studies which have similarly recorded C_3 graminoids being isotopically depleted in ^2H relative to other plant types growing within the same environment (e.g. Hou *et al*., 2007; Eley *et al*., 2014). This has been linked to differences in leaf physiology between monocotyledonous graminoids and dicotyledonous trees and herbaceous plants (Helliker and Ehleringer, 2002).

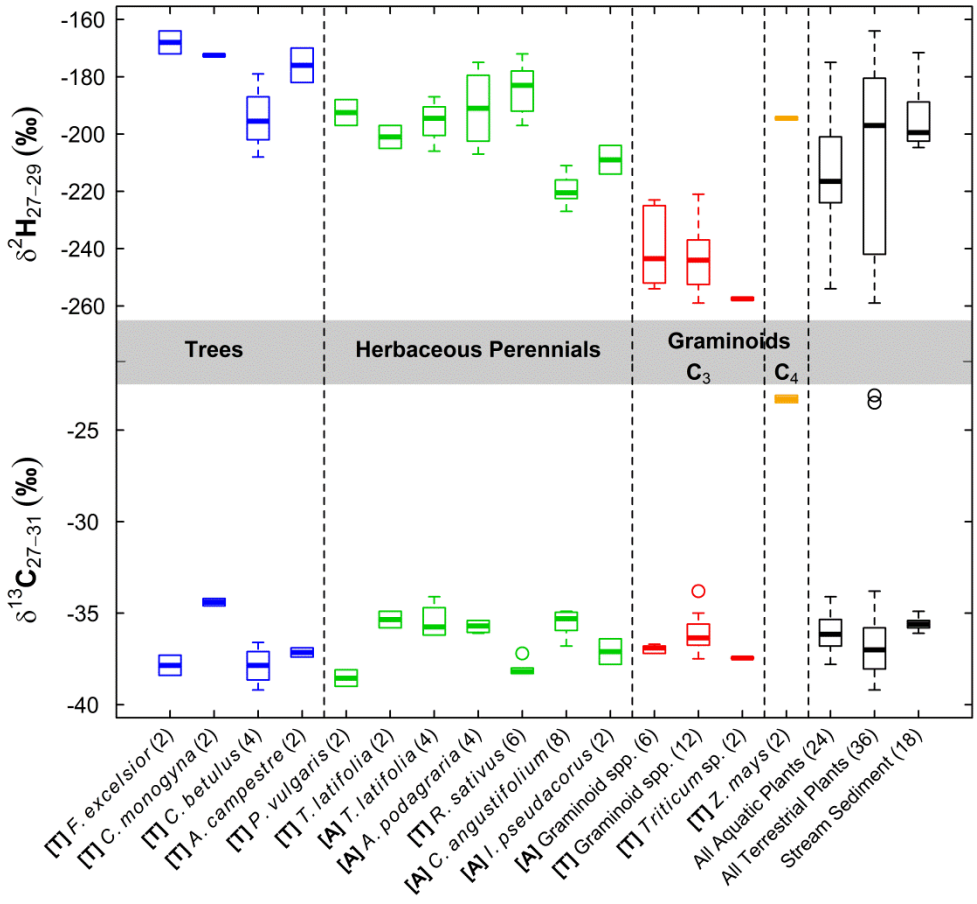

Figure 6.3: Distribution of δ^2H and $\delta^{13}C$ values (‰) for streambed sediments and individual plant species arranged by plant functional type. [A] and [T] refer to aquatic and terrestrial environments, respectively. Parentheses refer to the number of specimens for each species/sediment.

The majority of species representing the herbaceous perennials group ($\delta^2H_{27\text{-}29}$ =-223‰ to -172‰), which included both natural (*Typha latifolia*, *Aegopodium podagraria*, *Chamerion angustifolium* and *Iris pseudacorus*) and cultivated (*Phaseolus vulgaris* and *Raphanus sativus*) species, overlapped with trees, though some had $\delta^2H_{27\text{-}29}$ values closer to C_3 graminoids. Despite this, the herbaceous perennials, which had an abundance weighted mean of -216‰, were significantly (*t*-test p=0.002) different from both the tree and C_3 graminoid groups.

The C_4 graminoid *Zea mays* (-195‰), the only C_4 species in this study, was ^2H-enriched by ~50‰ relative to the C_3 graminoids, but overlapped with trees and herbaceous perennials. Previous studies have linked this ^2H-enrichment to shorter interveinal distances allowing for greater back diffusion of isotopically enriched water from the stomata into the veins in C_4 plants (Smith and Freeman, 2006). Overall, there existed a sizeable 94‰ range in $\delta^2H_{27\text{-}29}$ values across all 13 plant species with a clear distinction between C_3 graminoids and the other plant functional groups, thus confirming the suitability of δ^2H as an effective discriminator and fingerprint of different plant types.

Table 6.1: Summary *n*-alkane ratio and isotopic compositions for streambed sediments and plant species grouped by functional type and environment. ACL is the average chain length; CPI the carbon preference index; C_{max} the most abundant *n*-alkane; μ is the mean; σ is the standard deviation. Full results for individual plant specimens are presented in Appendix D.

Source/ Target	Stat	ACL	CPI	C_{max}	$\delta^{13}C_{27}$ (‰)	$\delta^{13}C_{29}$ (‰)	$\delta^{13}C_{31}$ (‰)	$\delta^{13}C_{27\text{-}31}$ (‰)	δ^2H_{27} (‰)	δ^2H_{29} (‰)	$\delta^2H_{27\text{-}29}$ (‰)
Streambed Sediments (*n* = 18)	μ	28.9	6.5	29	-34.7	-35.7	-36.0	-35.6	-178	-203	-195
	σ	0.1	1.1	0	0.5	0.3	0.3	0.3	9	10	9
Trees (*n* = 10)	μ	29.7	13.2	31	-35.5	-37.6	-37.2	-37.0	-158	-190	-181
	σ	0.5	6.2	1	1.2	1.2	1.7	1.6	13	14	14
Herbaceous Perennials (*n* = 28)	μ	28.7	12.2	29	-35.7	-36.7	-36.3	-36.4	-181	-209	-200
	σ	0.8	5.1	1	1.7	1.3	1.5	1.4	17	15	16
C_3 Graminoids (*n* = 20)	μ	29.0	20.8	29	-36.1	-36.5	-36.9	-36.5	-221	-251	-244
	σ	1.1	9.9	1	1.4	1.0	0.9	0.9	16	12	12
C_4 Graminoids (*n* = 2)	μ	30.4	13.4	31	-23.6	-23.7	-22.9	-23.3	-164	-200	-194
	σ	0.1	0.3	0	0.3	0.3	0.1	0.2	1	1	1
Aquatic Plants (*n* = 24)	μ	28.4	12.2	29	-35.4	-36.4	-36.1	-36.0	-200	-224	-215
	σ	0.8	4.8	1	1.0	1.1	1.2	0.9	23	20	21
Terrestrial Plants (*n* = 36)	μ	29.4	17.3	29	-35.4	-36.3	-36.2	-36.2	-184	-219	-209
	σ	0.8	9.2	1	3.5	3.4	3.6	3.5	30	31	31

6.4.1.2 Carbon

The dominant interspecies distinction in $\delta^{13}C_{27\text{-}31}$ values was the ~12‰ difference between the C_4 graminoid *Zea mays* and the other C_3 species (Figure 6.3). This is consistent with previous studies, which have recorded similar ^{13}C-enrichment of C_4 plants compared with C_3 species and attributed this to differences in plant physiology (e.g. Pancost and Boot, 2004). The range of $\delta^{13}C_{27\text{-}31}$ values for trees (-39.2‰ to -34.2‰), C_3 graminoids (-37.5‰ to -33.8‰) and herbaceous perennials (-39.0‰ to -34.1‰) are

comparable with the isotopic values recorded for long-chain *n*-alkanes from a variety of C_3 higher terrestrial plants in other studies (e.g. Collister *et al*., 1994; Lockheart *et al*., 1997; Chikaraishi and Naraoka, 2007). However, the substantial overlaps between functional groups means that there are no significant differences between trees, herbaceous perennials and C_3 grasses, thus preventing discrimination based solely upon the $\delta^{13}C$ values. This contrasts with past research that has identified differences in the $\delta^{13}C$ values between angiosperm and conifer species, for example (Pedentchouk *et al*., 2008). However, there remains relatively large intra-group variability that would allow individual species identification based on $\delta^{13}C_{27\text{-}31}$ values. For example, for herbaceous perennials where *P. vulgaris* (-38.6‰) is ^{13}C-depleted relative to the other herbaceous species (-38.3‰ to -34.1‰). The $\delta^{13}C_{27\text{-}31}$ values of the streambed sediments (-36.1‰ to -34.9‰) places them firmly within the isotopic range of the C_3 plant community, indicating limited input from C_4 plants. Because such C_3 versus C_4 discrimination cannot be obtained solely from δ^2H values, the results presented here clearly support a combined $\delta^2H/\delta^{13}C$ isotopic approach for apportioning sources of organic matter, particularly in catchments with a greater abundance of C_4 vegetation.

6.4.2 Isotopes for Discriminating Aquatic and Terrestrial Plants

The environment in which plants were growing exerted no obvious control over δ^2H or $\delta^{13}C$ values, as revealed by substantial overlap between the aquatic and terrestrial groups (Figure 6.3). $\delta^2H_{27\text{-}29}$ values were marginally more enriched in terrestrial plants (mean (μ) = -209‰; standard deviation (σ) = 31‰) compared with aquatic growing species (μ = -215‰; σ = 21‰), however this difference was not significant (*t*-test p=0.3). It is therefore not possible to differentiate terrestrial and aquatic plant groups based solely upon these isotopic values. The hydrogen isotopic composition of the streambed sediments placed them towards the terrestrial plant source group, although little can be inferred from this due to the poor source environment discrimination.

The absence of aquatic versus terrestrial discrimination implies that isotopic variability amongst the studied plants was principally driven by plant physiological and/or biochemical differences rather than the growing environment. Theoretically, one might have expected lower δ^2H values in aquatic plants compared to terrestrial species, because higher levels of humidity and water availability in aquatic environments reduce stomatal conductance and thus lower discrimination against ^2H during transpiration (Doucett *et al*., 2007; Sachse *et al*., 2012). Additionally, one might reasonably expect the δ^2H values of the stream water absorbed by aquatic plants to differ from the isotopic composition of the

soil water used by terrestrial species, with the former being supplied by groundwater and the latter by more recent precipitation. However, no evidence was observed for these mechanisms with the species collected here. This can probably be explained by the shallow nature of this headwater stream (mean stage = 0.25 m), where emergent macrophytes growing >1.5 m tall dominate aquatic primary productivity. In contrast to submerged macrophytes, emergent species will be exposed to similar environmental stressors as their terrestrial equivalents, thus weakening any environment driven differences. As a consequence, we cannot rule out δ^2H and $\delta^{13}C$ as potential discriminators between aquatic and terrestrial organic matter sources, but merely highlight that differences in growing environment, particularly in headwater streams, may not impart as large an isotopic fractionation signal as physiological differences linked to plant functional type. Because of these findings, plant functional type rather than environment was pursued as the main source group classification for Bayesian source apportionment

6.4.3 Molecular Ratios for Discriminating Plant Types and Environment

Figure 6.4 presents the *n*-alkane mixing space plots of ACL and CPI for plant species grouped by (a) plant functional type and (b) environment. Despite considerable scatter between individuals of the same group, tree species had significantly (*t*-test $p<0.001$) longer ACLs ($\mu = 29.7$; $\sigma = 0.5$; Table 6.1) than the herbaceous perennials ($\mu = 28.7$; $\sigma = 0.8$), whilst terrestrial plants ($\mu = 29.4$; $\sigma = 0.8$) had significantly (*t*-test $p<0.001$) longer ACLs than the aquatic growing plants ($\mu = 28.4$; $\sigma = 0.8$). Consequently, whilst overlap between the groups prevent ACL values being used on their own to uniquely identify sources, they nevertheless assist with source identification by contributing complimentary discrimination to that provided by the isotopic data. Similarly, although there is significant overlap in the CPI values, terrestrial plants ($\mu = 17.3$; $\sigma = 9.2$) do have significantly (*t*-test $p=0.006$) higher CPI values than aquatic plants ($\mu = 12.2$; $\sigma = 4.8$). There is also a clear distinction between terrestrial C_3 graminoids with CPI values >25 and aquatic C_3 graminoids with CPI values <15.

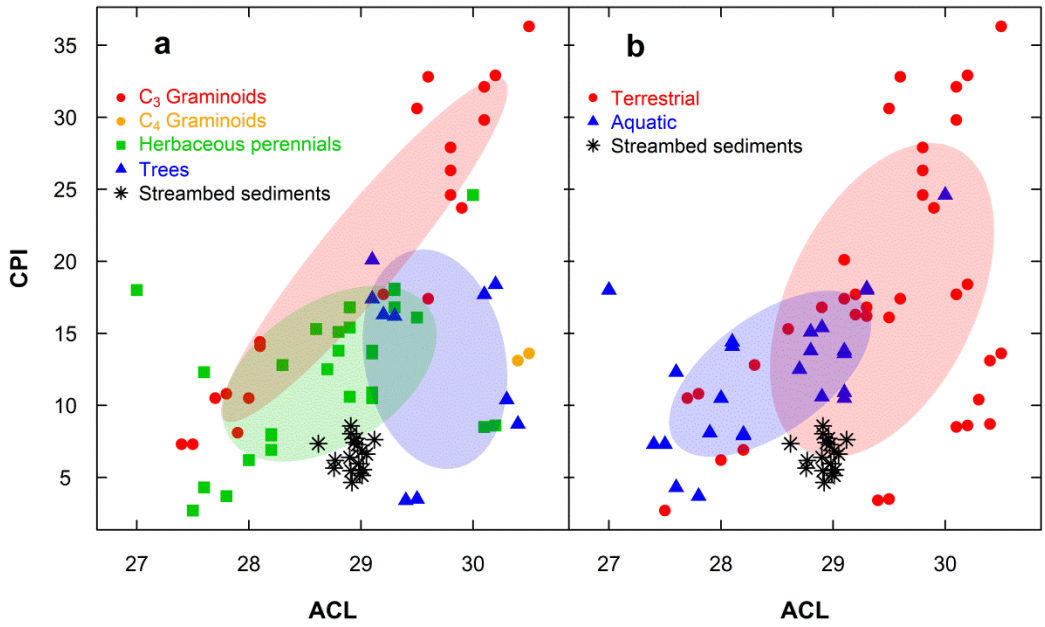

Figure 6.4: Average chain length (ACL) and carbon preference index (CPI) mixing space plots for streambed sediments and individual plant specimens grouped by (a) plant functional type and (b) environment. Shaded ellipsoids cover 50% of group range.

The ACL values for the 18 streambed sediments (range = 28.6 to 29.1) indicates higher plants were the dominant source of *n*-alkanes in this river system. In contrast, sediment CPI values (range = 4.7 to 8.6) are towards the lower end of the range observed across all source groups. Lower CPI values can be a sign of increased algal or microbial organic contributions (Jeng *et al.*, 2006; Zech *et al.*, 2011). However, a chromatogram of mean *n*-alkane chain length distributions for all 18 streambed samples (Figure 6.5) revealed sediments to be dominated by longer-chained *n*-alkanes with a strong odd-over-even predominance. Such distributions, coupled with large terrigenous-to-aquatic ratios (TAR_{HC}; range = 15.5 to 64.5), are indicative of higher terrestrial plant origins (Bourbonniere and Meyers, 1996; McDuffee *et al.*, 2004). This allows algae and bacteria to be excluded as major organic matter sources during this autumn to spring period. Low CPI values can also indicate contributions from ancient organic matter weathered out of the soil profile (Pancost and Boot, 2004). Depending on its age, this ancient material may reflect relic plant communities that bear little resemblance to the modern intensive arable system and would therefore not have been represented by the plants specimens collected here to classify source groups. Petroleum washed off metaled roads and transported into the stream during heavy rainfall events could also explain these low CPI values.

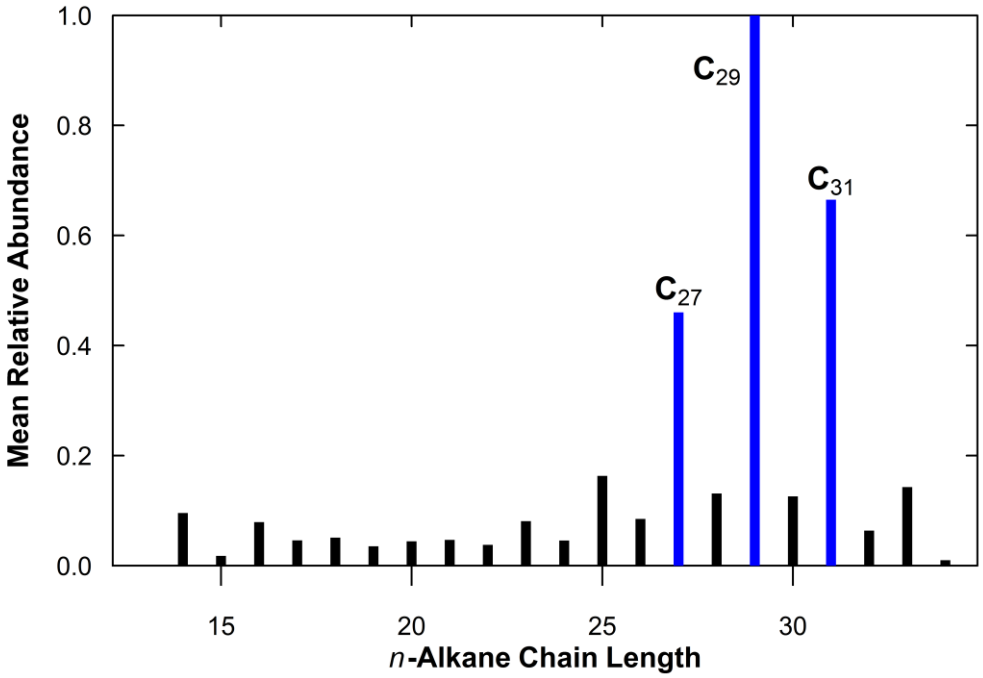

Figure 6.5: Chromatogram of the mean *n*-alkane chain length distribution for the 18 streambed sediment samples collected between September 2013 and March 2014 in mini-catchment A, expressed relative to C_{29}. High-molecular weight *n*-alkanes ubiquitous to all samples and selected as isotopic fingerprints are labelled.

6.4.4 Statistical Discrimination of Isotopic and Molecular Ratio Fingerprints

Principal component analysis (Figure 6.6) revealed that 95.1% of the variability between the plant species could be explained by the first three components when combining all nine of the measured isotopic and *n*-alkane ratio fingerprints ($\delta^{13}C_{27}$, $\delta^{13}C_{29}$, $\delta^{13}C_{31}$, $\delta^{13}C_{27\text{-}31}$, $\delta^{2}H_{27}$, $\delta^{2}H_{29}$, $\delta^{2}H_{27\text{-}29}$, ACL, CPI,). PC1, which explained 43.69% of data variance, weighed most heavily upon the four $\delta^{13}C$ fingerprints, with the more positive $\delta^{13}C$ values of C_4 graminoids providing the greatest distinction. The second principal component (33.92% of data variance) highlighted hydrogen isotope composition as a powerful discriminator between the ^{2}H-depleted C_3 graminoids and the comparatively ^{2}H-enriched herbaceous perennials and trees. In the third component (17.51% of variance), ACL was the dominant discriminator, with higher ACL values for trees helping to distinguish this group from the herbaceous perennials and C_3 graminoids. CPI was also an important distinguishing metric, with values increasing from herbaceous perennials ($\mu = 12.2$), to trees ($\mu = 13.2$) and finally C_3 graminoids ($\mu = 20.8$).

The Kruskal-Wallis one-way analysis of variance revealed that eight out of the nine fingerprints could successfully differentiate between plant functional types at the 95% significance level (Table 6.2). Whilst previous studies have used failure to pass this test as a fingerprint rejection criterion in traditional frequentist source apportionment studies (e.g. Collins *et al*., 2012; Evrard *et al*., 2013), other research has demonstrated that maximising the number of fingerprints used in Bayesian mixing models can help to significantly improve differentiation and reduce model uncertainties, provided the fingerprints contribute some discriminatory information (Parnell *et al*., 2010; Chapter 5). All nine fingerprints were therefore passed onto the Bayesian mixing model. In combination, the minimisation of Wilks-Lambda procedure revealed 93.1% of plant specimens could be correctly classified by plant functional type from these nine fingerprints, with $\delta^{13}C_{31}$ and $\delta^{2}H_{27\text{-}29}$ being the two most important discriminants (highest *F*-values; Table 6.2).

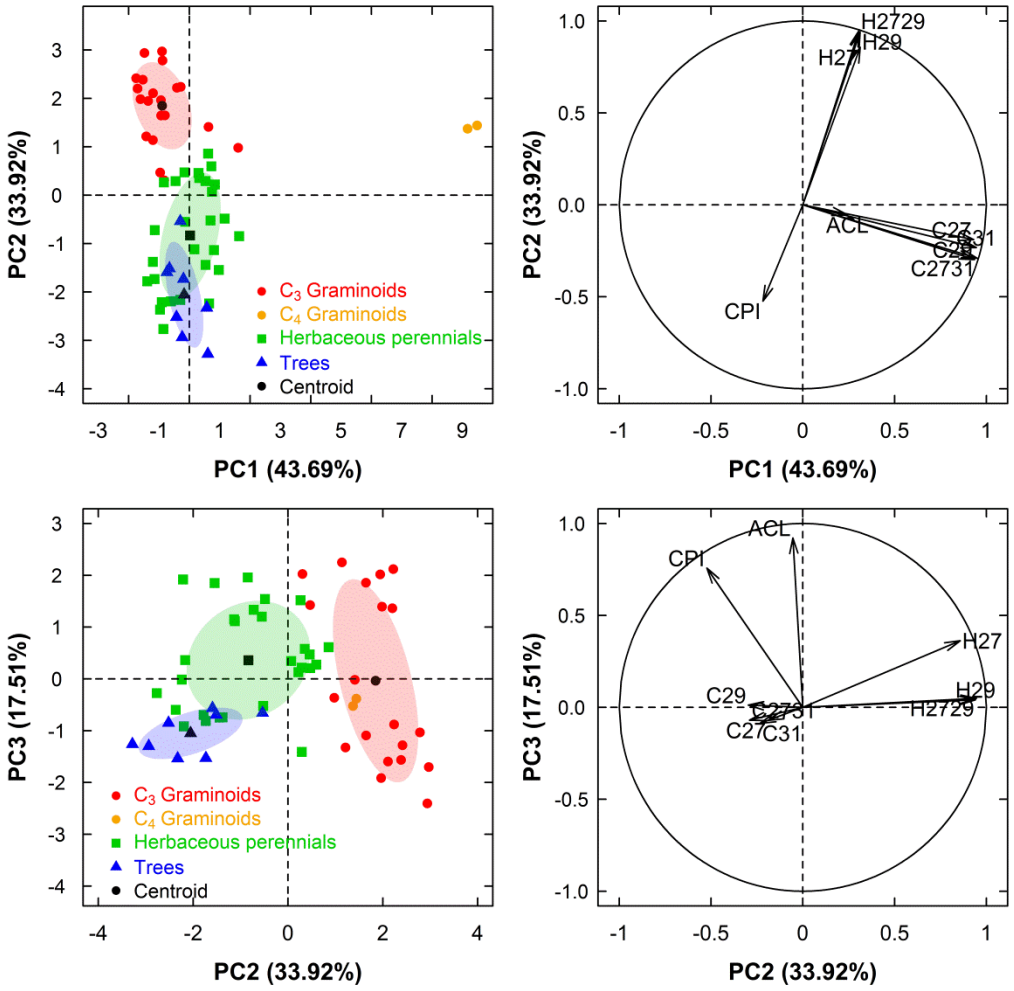

Figure 6.6: Principal component analysis of plant functional type sources (left) and fingerprint loadings (right) for the first three components. Shaded ellipsoids cover 50% of group range.

6.4.5 Application of the Bayesian Source Apportionment Mixing Model

The 7-month time-series of organic matter source contributions to streambed sediments, as estimated by the nine fingerprint Bayesian mixing model, are presented in Figure 6.7. Over the entire September 2013 to March 2014 period, POC concentrations varied between 3-7% of total sediment volume, which is considerably lower than the 10-13% recorded for suspended particulate matter (SPM) collected at the same time from the same site (see Chapter 7). Although *n*-alkanes represent only a small fraction of this total organic material, their conservative nature means we can work on the assumption that the sources of *n*-alkane biomarkers are representative of the sources of the entire organic matter content of the streambed sediments. In this regard, herbaceous perennials were estimated to account for a mean 39% (13-65% at the 95% credible interval) of sediment organic matter over this 7-month period, with a further 33% (12-54%) from trees , 26% (7-46%) from C_3 graminoids and just 4% (0-16%) from C_4 graminoids. The high contribution from herbaceous plants is consistent with the dominance of emergent herbaceous macrophytes in the stream channel during the summer months. Similarly, whilst only 1.5% of the catchment is deciduous woodland, significant tree contribution was not surprising given the proximity of deciduous trees to the stream. There is also an extensive network of *Crataegus monogyna* and *Acer campestre* hedgerows across the catchment, which most likely contributed significant quantities of tree derived organic material following autumn and winter leaf fall.

Table 6.2: Kruskal-Wallis one-way analysis of variance and minimisation of Wilks-Lambda fingerprint discrimination statistics.

	Kruskal-Wallis		**Minimisation of Wilks-Lambda**				
Fingerprint Property	***H*-value**	***p*-value**	**Selection step**	**Wilks-Lambda**	***F*-value**	**Cumulative *p*-value**	**Cumulative % of sources correctly classified**
$\delta^{13}C_{31}$	10.14	0.017	1	0.167	89.9	<0.001	51.7
$\delta^{2}H_{27\text{-}29}$	42.32	<0.000	2	0.043	68.0	<0.001	82.8
ACL	13.48	0.004	3	0.034	42.3	<0.001	84.5
$\delta^{13}C_{27}$	7.39	0.060	4	0.028	32.3	<0.001	89.7
$\delta^{2}H_{29}$	40.08	<0.000	5	0.024	26.4	<0.001	93.1
$\delta^{13}C_{27\text{-}31}$	8.24	0.041	6	0.021	22.6	<0.001	93.1
$\delta^{2}H_{27}$	41.95	<0.000	7	0.019	19.8	<0.001	93.1
$\delta^{13}C_{29}$	9.18	0.027	8	0.017	17.6	<0.001	93.1
CPI	8.34	0.039	9	0.016	15.5	<0.001	93.1

In spite of the relatively low precision of the proportional contributions, which arises as a consequence of the comprehensive Bayesian treatment of all perceived uncertainties (Chapter 4), temporal variability in apportionment estimates was still apparent. Median contributions from trees ranged from 22-52% (3-70% at the 95% credible interval), herbaceous perennials from 29-50% (2-67%) and C_3 graminoids from 17-34% (4-58%). By contrast, median C_4 graminoid contributions were consistently low across all 7-months at 3-7% (0-22%). As expected from the PC analysis (Figure 6.6), variability in sediment $\delta^2H_{27\text{-}29}$ values appeared to exert the dominant control over estimated source contributions. Increases in $\delta^2H_{27\text{-}29}$ values were generally associated with increases in tree contribution and declines in C_3 graminoid supply, reflecting the more positive δ^2H values of tree-derived organic material (Figure 6.3). None of the source contributions correlated with either stage or weekly precipitation totals.

Despite this variability in source apportionment estimates at a weekly timescale (Figure 6.7), there was no strong seasonality to estimated contributions, in contrast to what one might intuitively expect considering the strong seasonal nature of plant growth. Whilst tree contribution does increase by 17% during early October, which may relate to autumn leaf fall, this cannot directly explain the peak in tree contribution at 52% during mid-February 2014. Similarly, whilst herbaceous perennial contribution is marginally higher (median = 43%) during the September to November die-back of emergent macrophytes than during the December to March period (median = 38%), the trend is not significant within the 95% uncertainty intervals of the model.

Previous research has shown the δ^2H values of individual plant species can vary seasonally in response to environmental stressors (e.g. temperature) by up to 44‰ (Pedentchouk *et al.*, 2008; Eley *et al.*, 2014). Whilst we potentially see evidence for this seasonality here, with the most isotopically depleted sediment $\delta^2H_{27\text{-}29}$ values occurring during the colder winter months (~-200‰) and the most enriched values occurring in autumn and spring (~-185‰) (Figure 6.7), this does not translate into seasonality in apportionment estimates. On reflection, the lack of seasonal apportionment sensitivity most likely reflects the composition of deposited streambed sediments being inherently less dynamic and responsive to catchment processes than fine grained SPM, for example.

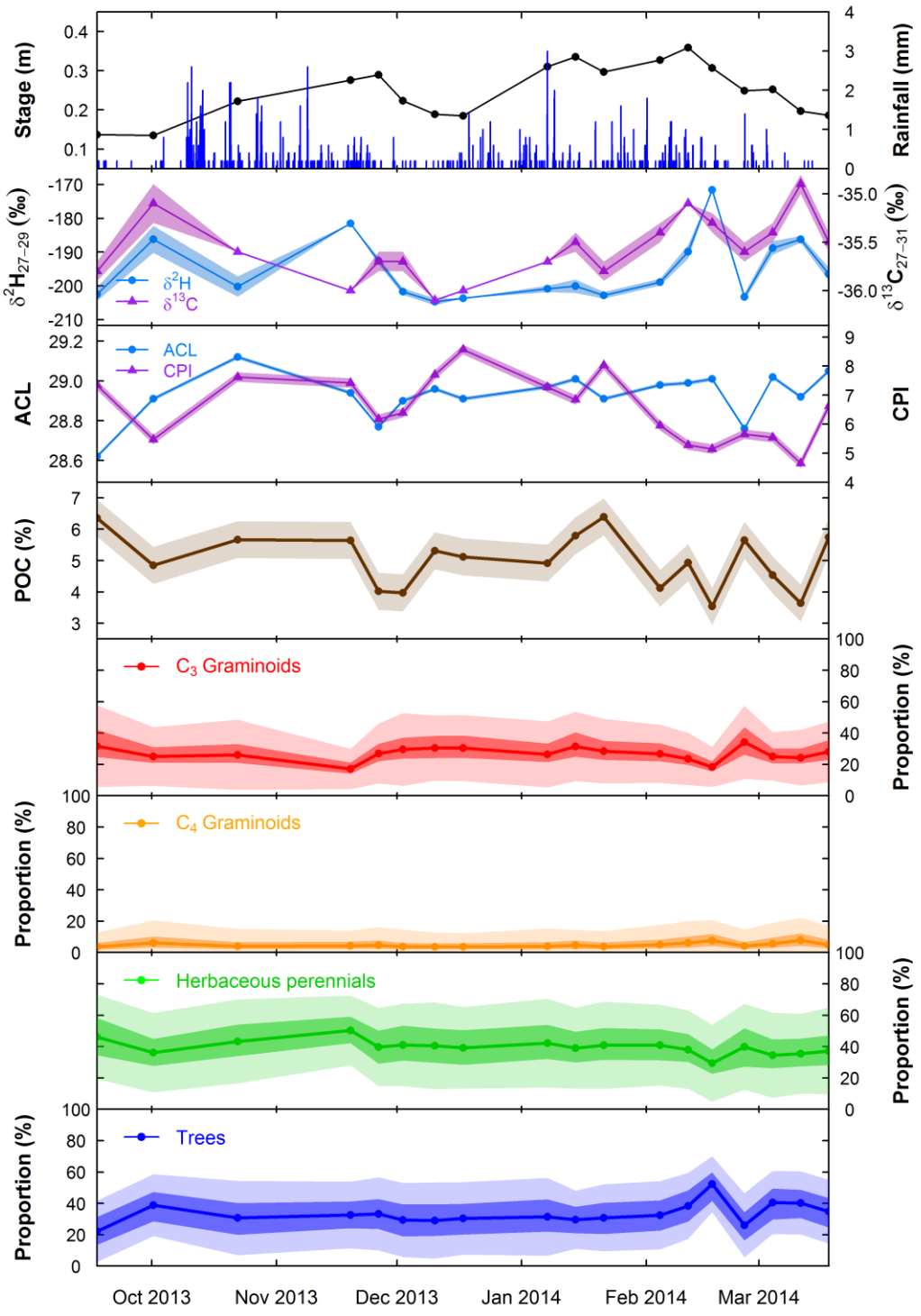

Figure 6.7: Time-series of organic matter source apportionment estimates and streambed sediment fingerprints for mini-catchment A during September 2013-March 2014. Dark and light shading around median source apportionment estimates represent the 50% and 95% Bayesian credible intervals, respectively. Shading around isotopic ratios and ACL, CPI and POC measurements represents instrument error.

Streambed sediments represent a cumulative composite of material deposited over a number of days, weeks or months. As such, the delivery of a pulse of δ^2H enriched autumn tree leaf litter to the river, which may be instantly detectable in SPM, would form just the most recent quantitatively insignificant addition to a larger pool of accumulated organic detritus deposited on the streambed. Additionally, autumn leaf litter may remain on the ground for a prolonged period of time before precipitation of sufficient intensity is capable of initiating surface runoff to entrain and transport this organic material to the stream channel.

6.4.6 Significance of Research

The novel data presented here clearly demonstrate that an integrated molecular and carbon and hydrogen CSIA of leaf wax *n*-alkanes is an effective approach for quantitatively apportioning plant-specific organic matter contributions to streambed sediments within a Bayesian uncertainty framework. In particular, the δ^2H values of leaf waxes proved to be an effective biomarker for differentiating between individual plant species based upon their broad functional type, whilst $\delta^{13}C$ values and *n*-alkane ratios provided complimentary discrimination based on C_3/C_4 physiological differences and different environments, respectively. In contrast to the commonly employed inorganic fingerprints, which have been used to discriminate sediment sources based on catchment geology and soil type in previous sediment source apportionment studies (e.g. Martínez-Carreras *et al.* 2010; D'Haen *et al.*, 2012; Chapters 4 and 5 of this thesis), these isotopic differences in *n*-alkane composition offer considerable potential to quantify land-use specific contributions to fluvial organic matter. Specifically, soils under particular plant types may be tagged with unique δ^2H and $\delta^{13}C$ signatures which would allow these isotopes to be used as direct land-use specific soil erosion tracers.

6.5 Conclusions

Organic matter is an important constituent of the particulate material transported in fluvial systems, yet techniques capable of quantitatively apportioning its origin have largely been overlooked by the sediment fingerprinting community. Addressing this deficiency in this chapter, we successfully demonstrate how a novel, combined molecular ratio and $\delta^{13}C$ and δ^2H compound-specific isotope analysis of *n*-alkane plant lipid extracts can be used to apportion plant-specific organic matter contributions to fine (<63

µm) streambed sediments in a lowland, arable catchment. From the lipid extracts of 18 streambed sediments and 30 individual plant specimens collected from across two environments (aquatic and terrestrial) and four plant functional types (trees, herbaceous perennials and C_3 and C_4 graminoids), seven isotopic values ($\delta^{13}C_{27}$, $\delta^{13}C_{29}$, $\delta^{13}C_{31}$, $\delta^{13}C_{27\text{-}31}$, $\delta^{2}H_{27}$, $\delta^{2}H_{29}$ and $\delta^{2}H_{27\text{-}29}$) and two *n*-alkane ratios (ACL and CPI) were derived, which were capable of successfully differentiating 93.1% of plant specimens by functional group. $\delta^{2}H_{27\text{-}29}$ proved to be the dominant discriminator of plants originating from different functional types, with the largest contrasts arising between trees (-208‰ to -164‰) and C_3 graminoids (259‰ to -221‰). $\delta^{13}C_{27\text{-}31}$ provided effective discrimination between the ^{13}C-enriched C_4 graminoids and C_3 plants. Neither $\delta^{2}H$ nor $\delta^{13}C$ could robustly differentiate aquatic and terrestrial plants, emphasising a stronger physiological rather than growing environment control over isotopic fractionation. The ACL and CPI were, however, more successful at differentiating terrestrial and aquatic plants, indicating such molecular ratios can complement source area identification when used in combination with isotopic values. Bayesian mixing model source apportionment results took full account of the uncertainties present whilst revealing considerable temporal variability in plant contributions to streambed sediments during the 7-month period between September 2013 and March 2014. Median contributions ranged from 22-52% for trees, 29-50% for herbaceous perennials, 17-34% for C_3 graminoids and 3-7% from C_4 graminoids, with apportionment exhibiting no apparent seasonality. The results of this study have clearly demonstrated the effectiveness of an integrated molecular and compound-specific carbon and hydrogen isotope analysis for identifying plant-specific contributions to streambed sediment organic matter via a Bayesian mixing model approach.

Chapter 7

INVESTIGATING ORGANO-MINERAL RELATIONSHIPS AND TEMPORAL TRENDS IN SPM COMPOSITION[††]

7.1 Chapter Summary

Exploring how the concentrations and relationships between various organic and geochemical constituents of SPM change under different flow conditions and over various temporal scales is important for understanding the processes that ultimately control SPM composition. Employing the analytical techniques developed in Chapter 3, we begin this chapter by investigating how SPM organo-mineral relationships change between baseflow and storm event conditions, with specific emphasis on the relationships between clay mineral associated elements, metal oxides, particulate organic carbon (POC) and particulate P (PP). Multiple linear regression models are then developed for the prediction of SPM P concentrations at sites A, B and E. These reveal association with Fe was the dominant control on the variation in PP concentration under baseflow conditions. In contrast, association with POC was the dominant control on PP during storm events. This pronounced transition in P control mechanism, which was consistent across the three study sites, is hypothesised to be driven by changes in SPM source area under differing hydrological conditions. An investigation of weekly baseflow SPM data over the 23-month monitoring period was then conducted to explore evidence of temporal trends in geochemistry. These revealed strong seasonal cycles in the majority of elements and phases, with seasonality in Fe-P and Al_{ox}-Al_{di} ratios indicating temporal variability in SPM P sorption capacity. In general, these time-series revealed SPM in winter to be dominated by higher concentrations of clay mineral associated elements,

[††] Chapter published as: Cooper RJ, Rawlins BG, Hiscock KM, Krueger T, Pedentchouk N. 2015c.Contrasting controls on the phosphorus concentration of suspended particulate matter under baseflow and storm event conditions in agricultural headwater streams. Under review at *Science of the Total Environment*.

metal oxides and Fe-P ratios, whilst SPM during the summer was typically richer in Ca, Fe, P and POC and had higher Al_{ox}-Al_{di} ratios. Employing the Bayesian source apportionment procedure of Chapter 4, these temporal geochemical trends were quantitatively apportioned to greater SPM inputs from Ca-rich subsurface sources during the summer, whilst contributions from clay mineral and metal oxide rich surface sources increased during the winter. Lastly, high-resolution (30 min) turbidity time-series from the bankside monitoring kiosks were explored and found to exhibit strong diel cycles, with increased night-time turbidity linked to the nocturnal feeding and burrowing habitats of fish and crayfish. Overall, the results presented in this chapter reveal significant variability in the concentrations, sources and relationships between organic and geochemical constituents of SPM under different flow conditions at diel-to-seasonal timescales.

7.2 Background

Diffuse phosphorus (P) pollution is a key factor behind the development of eutrophic conditions in agricultural catchments (Withers and Jarvie, 2008; Quinton *et al*., 2010). As a naturally limiting nutrient of plant growth in aquatic environments, dissolved P (DP) enrichment fuels blooms of phytoplankton, periphyton and neuro-toxin secreting cyanobacteria colonies, which can dramatically lower species diversity and lead to a fundamental breakdown of ecosystem functioning (Smith *et al*., 1999; Hilton *et al*., 2006). P is dominantly transported through rivers in particulate form, with sediment associated P variously estimated to account for up to 90% of total P (TP) load in rural UK catchments (e.g. He *et al*., 1995; Walling *et al*., 1997; Bowes *et al*., 2003). However, there exists a dynamic equilibrium between the quantity of labile P associated with mineral surfaces and the concentration of DP in both soil solution (Hartikainen *et al*., 2010) and in stream water (Palmer-Felgate *et al*., 2009) which is controlled by biogeochemical processes. Consequently, understanding the importance of sediment biogeochemistry in controlling particulate P (PP) concentrations is essential if DP enrichment is to be mitigated.

Previous research has shown that DP reacts strongly with clay minerals and metal oxyhydroxides, particularly iron (Fe) and aluminium (Al) oxide complexes in soils and stream sediments to form mineral-bearing PP phases. This occurs principally through the adsorption of phosphate ions onto solid phase mineral surfaces (non-occluded P), followed by the subsequent absorption of phosphate ions into the mineral itself (occluded P) (Walker and Syers, 1976; House and Denison, 2002; Evans *et al*., 2004). The rate at

which this sorption process occurs is a function of the availability of potential P binding sites on particulate surfaces. This in turn is determined by factors such as mineral surface ionisation, presence of organic matter (OM) complexes, competition from competing anions and the degree of oxyhydroxide coating on clay minerals (House *et al*., 1995; Withers and Jarvie, 2008; Palmer-Felgate *et al*., 2009). Furthermore, the physical and/or chemical form of P may change due to interactions with biota (e.g. uptake by algae) and inorganic constituents (e.g. co-precipitation with calcite) which cause P to partition between biologically available dissolved phases and less biologically available particulate and organic forms (Bowes *et al*., 2003)

Whilst much is known about how these processes affect the instream cycling of P, less is known about what controls various organic and geochemical associations of PP between high- and low-flow periods. Van der Perk *et al*. (2007) and Rawlins *et al*. (2011) developed regression models to demonstrate the importance of a range of elements (Al, Ca, Ce, Fe, K, Mn) and phases (Al/Fe oxyhydroxides, clay minerals, OM) in determining the P concentration of streambed sediments under baseflow conditions. Neither study, however, considered how these associations changed under differing flows. In fact, to our knowledge, no previous study has examined the geochemical associations between SPM and its P bearing phases under different hydrological conditions in agricultural headwater catchments. This represents a significant deficiency because the source apportionment results presented in Chapters 4 and 5 have demonstrated that there is a significant change in the sources of SPM under differing flow conditions; subsurface inputs (e.g. agricultural field drains and channel banks) are linked with baseflow sediment supply, whilst contributions from surface sources (e.g. topsoils and damaged road verges) increase during precipitation events. Therefore, if the sources of SPM change under different flow regimes, we can hypothesise that the organic and geochemical relationships between SPM and its P component may be similarly affected. Thus, two of the main objectives of this chapter were:

- **(i)** to compare and contrast SPM organo-mineral relationships under baseflow and storm events conditions in mini-catchments A, B and E;
- **(ii)** to develop multiple linear regression models to investigate the importance of various organic and inorganic phases in determining SPM P concentrations during low- and high-flows.

In addition, exploring how SPM geochemistry changes over various temporal scales is important for understanding the processes that ultimately control SPM composition. Whilst short-term, high-temporal resolution monitoring using automatic water samplers

can provide detailed information on changing SPM geochemistry during the progression of precipitation events (e.g. Chapter 5), sustained, lower resolution monitoring is required in order to detect any longer term trends. Thus, the third objective of this chapter was:

(iii) to examine evidence for seasonal cycles in both baseflow SPM geochemistry and SPM source apportionment over a 23-month period in mini-catchments A, B and E.

Lastly, from the examination of high-resolution turbidity time-series, previous research has found evidence of distinct diel cycles in fluvial SPM concentrations (Gillain, 2005; Loperfido *et al*., 2010). High turbidity values recorded during the night and low turbidity readings during the day have been attributed to instream bioturbation processes. Specifically, the feeding and burrowing activities of nocturnal fish, crayfish and other aquatic organisms are thought to stir up and entrain into suspension fine streambed sediments, resulting in peaks in night-time turbidity measurements (Harvey *et al*., 2014; Rice *et al*., 2014). There exists potential for similar such diel turbidity cycles to occur in the River Blackwater because, whilst no official population survey has been undertaken, observations over the past three years have revealed a significant crayfish population within the catchment. In particular, there appears to be a large population of the invasive Signal Crayfish (*Pacifastacus leniusculus*), which is known to have nocturnal burrowing habits. Therefore, the final objective of this chapter was:

(iv) to investigate evidence of diel cycles in high-resolution (30 min) turbidity data captured by the bankside monitoring kiosks at sites A, B and E.

7.3 Methods

7.3.1 SPM Sampling

Between May 2012 and March 2014, stream water grab samples (1-8 L depending on SPM concentration) were collected at 1-2 week intervals under baseflow conditions at the outlets to mini-catchments A, B and E, yielding 222 SPM samples in total. During the same period, the bankside automatic water samplers were remotely activated to capture a total of 721 grab samples (1 L) at 60- or 120-min resolution during 14 storm events at the same locations (where events are characterised by >8 mm of precipitation). All stream water samples were returned to the laboratory and vacuum filtered through Millipore quartz fibre filter (QFF) papers (Merck Millipore, Billerica,

MA, USA) with a retention rating of 99.1% at 0.7 µm to extract particulate matter. Sufficient water was filtered to obtain ~25 mg of SPM on each filter. The SPM-covered filters were subsequently oven dried at 105^{o}C for 2 hrs and weighed to determine sediment mass retention and instream SPM concentrations. Additionally, high-resolution (30 min) turbidity time-series for a 20-day period in April 2013 were obtained from the bankside kiosks at sites A, B and E and were used as a proxy for SPM concentration.

7.3.2 Spectroscopic Analysis

The geochemistry of all SPM-covered filter papers was analysed directly XRFS and DRIFTS following the methodology detailed in Chapter 3. The concentrations of 11 elements (Al, Ca, Ce, Fe, K, Mg, Mn, Na, P, Si, Ti) and five organic and inorganic phases (POC, Al_{di}, Fe_{di}, Al_{ox}, Fe_{ox}) were determined. Also calculated were Fe-P ratios, which are a useful indicator of P buffering capacity, and Al/Fe oxalate-dithionate ratios, which effectively quantify the proportion of reactive (amorphous) to less reactive (crystalline) oxide phases.

7.3.3 Statistical Analysis

The relationships between all measured SPM properties were initially assessed via correlation panel plots for both baseflow and storm event samples. Then, to obtain a more comprehensive understanding of PP control mechanisms, multiple linear regression analysis based on ordinary least squares (OLS) was performed for the prediction of SPM P under storm and baseflow conditions for each of the three sampling locations (A, B and E) in the R environment (R Development Core Team, 2014). Due to heteroscedasticity in the distribution of P values (based on inspection of histograms) these regression analyses were undertaken on log transformed P concentrations. Predictors for all six regression models were selected based on prior knowledge of their associations with P and included:

(i) Metal oxyhydroxides ($Al_{ox/di}$, $Fe_{ox/di}$) and elements associated with metal oxyhydroxides (Fe, Al, Mn);
(ii) Elements associated with clay minerals (K, Mg, Na);
(iii) Calcium (Ca) based on the co-precipitation of P with calcite (House, 2003);
(iv) Phases associated with organic material (POC);
(v) Elements strongly associated with particle size (Ti, Si) (Rawlins *et al*., 2009; Rawlins 2011);

(vi) Cerium (Ce) based in its enrichment in P-bearing apatite minerals (Rawlins, 2011);

(vii) Channel stage, because flow volumes influence both SPM transport capacity and its provenance.

A backwards elimination selection procedure was adopted, whereby an initial model including all of the aforementioned predictors was formulated and any statistically insignificant regressors (p >0.05) were then removed one by one until only significant predictors remained. Variance inflation factor (VIF) values were also calculated for each predictor as a measure of multicollinearity using the '*car*' package (Fox and Weisberg, 2013) in the R environment. Any predictor with VIF values >10 were considered to have high multicollinearity and were therefore removed from the model to minimise the risk of overfitting the regression. Once this final set of significant predictors had been identified, the relative importance of each regressor was estimated using the '*relaimpo*' package (Groemping, 2013).

Time-series for the full suite of geochemical data, including Fe-P and oxalate-dithionate ratios, were plotted and inspected for evidence of seasonality during the 23-month monitoring period. We used a 15 point, second order, Savitzky-Golay algorithm (Savitzky and Golay, 1964) to filter the time-series concentrations of selected SPM properties and overlaid these on the plots to aid their interpretation. The Bayesian source apportionment procedure of Chapter 4 was then employed to quantitatively apportion the changing sources of SPM over the 2-year monitoring period. Lastly, the high-resolution turbidity time-series were similarly smoothed with 15 point, second order Savitzky-Golay filters and were investigated for evidence of diel cycles in SPM concentration.

7.4 Results and Discussion

7.4.1 Baseflow Geochemistry

Figure 7.1 shows the correlation panel plots for baseflow SPM geochemistry at all three sites. Immediately apparent are the very strong positive correlations between Al and Mg (r = 0.95), Al and K (r = 0.92) and Mg and K (r = 0.84) which indicate the presence of clay minerals which contain significant amounts of all three cations. Strong positive correlations also exist between Al and Ti (r = 0.75), K and Ti (r = 0.77) and Na and Mg (r = 0.72), further supporting the presence of clay minerals within SPM, with 70% of kaolinite minerals reported to contain Ti (Dolcater *et al.*, 1970). Another notable

association is that between Fe and P (r = 0.71), which likely indicates P sorbing to the solid phase mineral surfaces of Fe-containing compounds. However, P is not correlated with the abundance of either Fe_{di} or Fe_{ox}. There is also no obvious association between P and Ce (r = 0.19), in contrast to the findings of Rawlins (2011) who demonstrated that variations in Ce could explain 10.4% of the variability in streambed sediment P concentrations in rivers across central England. This observation was attributed to the enrichment of Ce in naturally occurring P-bearing apatite minerals (Reynard *et al*., 1999).

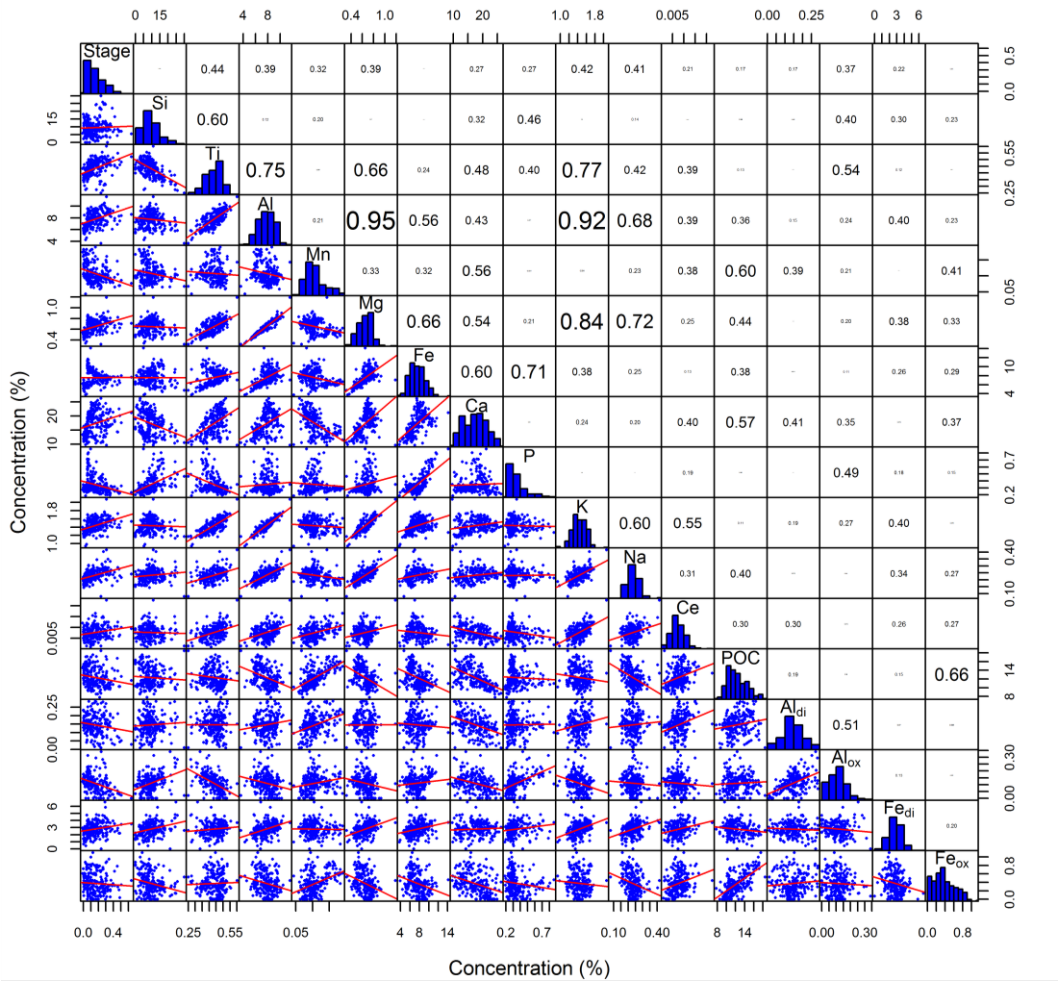

Figure 7.1: Panel plot of SPM geochemistry (% by weight) under baseflow conditions at sites A, B and E (n = 222). Stage is in metres. The upper right section displays Pearson's correlation coefficient with the text size proportional to correlation strength. The bottom left panel shows the SPM samples (points) and linear regression (line). Central histograms show the distribution of values for each parameter.

With respect to the organic fraction, POC exhibits negligible correlation with SPM P (r = 0.06) under baseflow conditions, suggesting a dominantly inorganic control on baseflow PP concentrations. Instead, POC correlates most strongly with Fe_{ox} (r = 0.66), which may

be explained by several mechanisms: (i) the stabilisation of OM through the formation of organo-Fe complexes; (ii) the sorption of POC onto the surfaces of Fe oxyhydroxides which - due to their large specific surface areas - commonly have sorption rates an order of magnitude greater than many common clay minerals; and (iii) physical protection from degradation afforded by POC aggregation with these metal oxyhydroxides (Kaiser and Guggenberger, 2003; Wagai and Mayer, 2007). Furthermore, it has been demonstrated that the amorphous Fe compounds tend to be more important than crystalline oxyhydroxides in this stabilisation process (Wilson *et al.*, 2013). Evidence for this can be seen here, with stronger linear correlations between POC and the amorphous Fe_{ox} (r = 0.66) than with crystalline Fe_{di} (r = 0.15). Note that the correlations between total Al/Fe and their respective dithionate/oxalate extractable oxides are generally weak (r <0.30) because total Al/Fe includes non-oxides bound up in clays and other minerals such as vivianite.

Table 7.1: Selected geochemistry data for SPM and source area sediments collected in mini-catchments A, B and E of the River Blackwater. μ is the mean; σ is the standard deviation.

SPM/ Source Area	Stat	Concentration (weight %)								Fe:P Ratio	Al_{ox}: Al_{di} Ratio	Fe_{ox}: Fe_{di} Ratio
		Al	Ca	Ce*	Fe	Mg	Mn	P	POC			
Baseflow SPM	μ	7.77	17.34	55	7.56	0.65	0.11	0.35	12.35	22.91	0.79	0.16
(n = 222)	σ	1.31	3.91	6	1.62	0.12	0.03	0.13	2.13	5.58	0.41	0.15
Storm Event SPM	μ	8.29	14.24	60	6.87	0.66	0.13	0.32	13.78	23.44	0.62	0.15
(n = 721)	σ	1.99	4.16	9	0.98	0.13	0.04	0.11	2.97	6.57	0.69	0.09
Channel Banks	μ	6.63	33.92	37	4.74	0.63	0.02	0.07	2.21	76.33	0.18	0.43
(n = 60)	σ	2.35	9.80	16	1.78	0.19	0.03	0.03	2.01	27.20	0.25	0.61
Field Drains	μ	6.66	14.25	60	6.88	0.53	0.19	0.27	7.89	33.67	1.00	0.42
(n = 48)	σ	2.96	10.75	28	4.59	0.27	0.26	0.26	3.61	15.04	0.67	0.78
Road Verges	μ	10.50	4.82	88	5.55	0.91	0.16	0.32	12.96	17.59	0.44	0.26
(n = 60)	σ	1.76	2.13	8	0.90	0.20	0.03	0.04	2.39	3.87	0.19	0.14
Topsoils	μ	14.23	3.18	94	6.53	0.84	0.12	0.29	10.22	23.90	0.63	0.25
(n = 60)	σ	1.91	3.29	11	0.83	0.11	0.02	0.07	2.30	6.71	0.14	0.16

*Ce concentration in ppm

7.4.2 Storm Event Geochemistry

Figure 7.2 presents the correlation plots for storm event SPM geochemistry. Strong, positive correlations are again apparent between Al and K (r = 0.93), Al and Mg

(r = 0.89) and K and Mg (r = 0.87), once more indicating that clay mineral composition likely dominates these geochemical associations. Strong correlations between Al and Ti (r = 0.82), K and Ti (r = 0.84) and Mg and Ti (r = 0.79), indicate Ti oxides in association with these clay minerals. Compared with baseflow conditions, linear correlations between Ce and K (r = 0.85), Ce and Al (r = 0.82) and Ce and Ti (r = 0.78) are substantially stronger, which may reflect the increased supply of Ce enriched topsoil and road verge sediments to the stream during heavy precipitation (see Chapter 5). This could also explain the stronger correlations between Fe and clay mineral-associated elements, with concentrations of both these components larger in surfaces sources than in subsurface channel banks (Table 7.1).

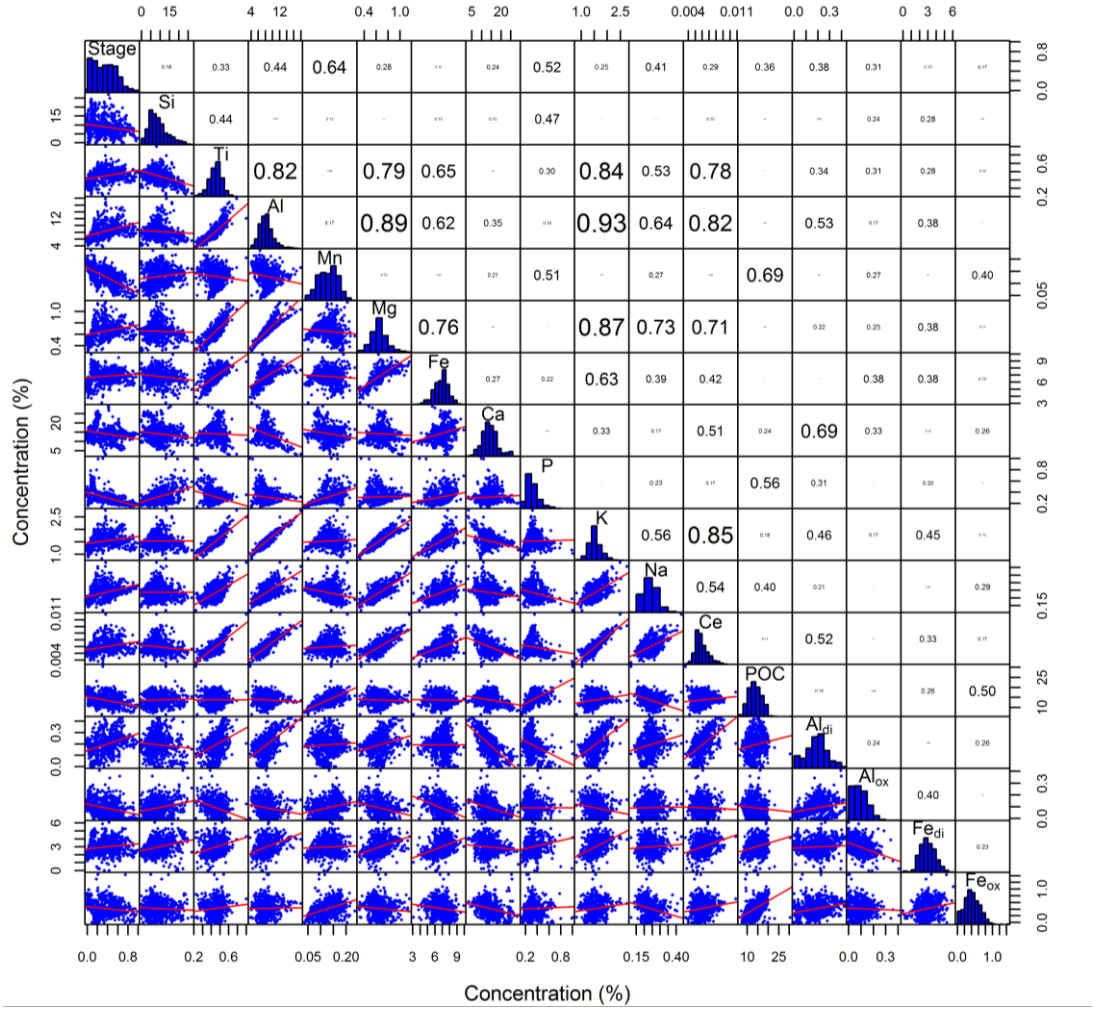

Figure 7.2: Panel plot of SPM geochemistry (% by weight) under storm event conditions at sites A, B and E (n = 721). Stage is in metres. The upper right section displays Pearson's correlation coefficient with the text size proportional to correlation strength. The bottom left panel shows the SPM samples (points) and linear regression (line). Central histograms show the distribution of values for each parameter.

Importantly, P has a strong positive correlation with POC during storm events (r = 0.56), in contrast to baseflow conditions. This is consistent with similar findings by Walling *et al*. (2001) for four other UK rivers (Seven, Avon, Exe and Dart) under storm event flows. However, the strongest positive correlation of POC is with Mn (r = 0.69). This can be explained the sorption of POC onto the surfaces of Mn oxyhydroxides as well as the supply of Mn from OM mineralisation reactions. This Mn-POC association may also explain the relatively strong P-Mn correlation (r = 0.50), although part of this probably relates to P sorption onto metal oxyhydroxide surfaces. As observed in other studies (e.g. Dawson *et al*., 2012; Cerro *et al*., 2014), POC, P and Mn concentrations are negatively correlated with channel stage, which could be attributed to an increase in inorganic mineral contribution from soil erosion during winter storms.

7.4.3 Determining Control Mechanisms of Particulate Phosphorus

7.4.3.1 Baseflow Regression Models

The baseflow multiple regression models are able to explain 76-96% of the variance in SPM P concentrations at each of the three sites based on between four and six geochemical predictors (Table 7.2). Variation in total Fe concentration is a consistently dominant predictor, explaining 37%, 12% and 38% of SPM P variability at sites A, B and E, respectively. The sorption of P onto the surfaces of Fe-oxides represents the most likely causal mechanism for this strong, positive Fe-P association. Similarly, sorption of P onto the surfaces of metal oxides would explain the significant association with Al_{ox} at site A (R^2 = 0.156) and with Mg at site A (R^2 = 0.048) and site E (R^2 = 0.112). Interestingly, neither K nor Na are significant predictors, suggesting that the quantity or type of clay minerals in SPM is not a dominant control of baseflow PP in these catchments.

A strong negative relationship with Ti is observed at site A (R^2 = 0.224) and site E (R^2 = 0.449), although it is not a significant predictor at site B. The most likely host for Ti is secondary Ti oxides, which tend to be fine-grained and form associations with other mineral phases. If the Ti in SPM is a secondary oxide, its strong linear correlations with Al, K and Mg (r >0.66; Figure 7.1) suggest it is closely associated with certain clay minerals which are less enriched in P than Fe-oxide phases, hence the negative association. At site B, Si is the dominant predictor of SPM P (R^2 = 0.445), with this strong, positive association contrasting strongly with the regression results for sites A and E. High SPM Si concentrations typically indicate a greater abundance of coarse quartz

material and thus a strong positive association with P, which tends to be enriched in fine sediment, would not intuitively be expected. However, Si is strongly and negatively associated with Ti (r = 0.60; Figure 7.1) and thus the association between P and Si at site B may be simply be a consequence of collinearity between these two predictors.

POC is a relatively weak predictor under baseflow conditions, explaining between 1% and 8% of the variability in PP concentrations at sites A, B and E. Similarly, Ce was a weak predictor at site B (R^2 = 0.062), whilst Ca was insignificant at all sites, thus implying that abiotically mediated co-precipitation of P with calcite is not an important control of SPM P concentrations. Overall, the results of these multiple regression models show that the abiotic sorption of P onto the surfaces of Fe-oxide complexes is a dominant control of baseflow SPM P concentrations in the River Blackwater.

Table 7.2: Multiple linear regression model results for the prediction of log-P in SPM under baseflow conditions at sites A (n = 74), B (n = 74) and E (n = 74) between May 2012 and March 2014. VIF is the variance inflation factor; VE is the variance explained.

Site A	**Predictor**	**Estimate**	**Std. Error**	***t*-value**	***p*- value**	**VIF**	**Proportion of VE (R^2)**
	Fe	0.147	0.010	15.29	<0.001	1.03	0.370
	Ti	-3.865	0.418	-9.24	<0.001	3.47	0.224
	Al_{ox}	1.357	0.310	4.37	<0.001	2.34	0.156
	POC	0.058	0.009	6.16	<0.001	1.15	0.078
	Mg	1.160	0.196	5.92	<0.001	2.47	0.048
	Al_{di}	-1.062	0.275	-3.86	<0.001	1.50	0.020
						Total R^2	0.895
Site B	**Predictor**	**Estimate**	**Std. Error**	***t*-value**	***p*- value**	**VIF**	**Proportion of VE (R^2)**
	Si	0.023	0.002	12.84	<0.001	1.45	0.445
	Fe	0.115	0.018	6.34	<0.001	3.64	0.123
	POC	0.017	0.005	3.36	<0.001	1.95	0.078
	Ce	-92.764	16.291	-5.69	<0.001	2.20	0.062
	Mn	0.955	0.268	3.57	<0.001	1.60	0.049
						Total R^2	0.757
Site E	**Predictor**	**Estimate**	**Std. Error**	***t*-value**	***p*- value**	**VIF**	**Proportion of VE (R^2)**
	Ti	-4.090	0.219	-18.69	<0.001	3.76	0.449
	Fe	0.131	0.008	17.39	<0.001	1.70	0.382
	Mg	0.880	0.181	4.86	<0.001	5.43	0.112
	POC	0.027	0.006	4.47	<0.001	1.62	0.014
						Total R^2	0.957

7.4.3.2 Storm Event Regression Models

The storm event multiple regression models explain 71-94% of the variance in SPM P concentrations across the three sites based on between four and eight predictors (Table 7.3). Importantly, the results reveal a clear shift in P association, from Fe-dominated under baseflow conditions to POC-dominated during storm events. Variability in POC concentrations are able explain 21%, 62% and 20% of the variance in PP at sites A, B and E, respectively, making it the strongest predictor at two of these locations. This P-POC association may relate to OM being a source of P through mineralisation reactions and soluble reactive phosphorus (SRP) sorbing onto the surfaces of OM in soils and sediments (White, 2006). However, organic molecules also liberate phosphate ions into solution by replacing them on clay mineral and metal oxyhydroxide surface binding sites, whilst also blocking the pore spaces of mineral aggregates and acting as a protective barrier around mineral surfaces (Kaiser and Guggenberger, 2003; Wagai *et al*., 2013). Despite these opposing processes, numerous studies have commented upon the link between P and OM in stream sediments, with most establishing similar positive associations to that observed here (e.g. Panuska *et al*., 2011; Rawlins, 2011; Krueger *et al*., 2012).

In further contrast with the baseflow regression models, Mn is a strong and significant predictor of P during storm events at site A (R^2 = 0.275) and site E (R^2 = 0.165). This likely reflects both Mn association with POC (r = 0.69; Figure 7.2) and the sorption of P onto the surfaces of metal oxides. Channel stage is also a strong and significant predictor at site A (R^2 = 0.182), indicating a dilution of SPM P concentrations under larger flows. Despite its much reduced importance, Fe remains a significant predictor of P during storm events at sites A (R^2 = 0.10) and E (R^2 = 0.06), confirming the sorption of P onto Fe oxyhydroxide complexes. Significant associations are again evident with Ti at sites A (R^2 = 0.043) and E (R^2 = 0.150), and with Si at sites B (R^2 = 0.038) and E (R^2 = 0.174), but these regressors are generally weaker predictors than that observed in the baseflow models. Overall, these multiple regression models reveal that storm event SPM P concentrations are dominantly associated with organic matter complexes.

Table 7.3: Multiple linear regression model results for the prediction of log-P in SPM under storm event conditions at sites A (n = 254), B (n = 251) and E (n = 216). VIF is the variance inflation factor; VE is the variance explained.

Site A	**Predictor**	**Estimate**	**Std. Error**	***t*-value**	***p*- value**	**VIF**	**Proportion of VE (R^2)**
	Mn	2.184	0.259	8.43	<0.001	3.73	0.275
	POC	0.042	0.003	13.65	<0.001	2.56	0.212
	Stage	-0.281	0.035	-8.01	<0.001	2.65	0.182
	Fe	0.117	0.010	11.55	<0.001	3.25	0.101
	K	0.557	0.062	8.95	<0.001	7.59	0.078
	Ti	-2.360	0.201	-11.76	<0.001	6.99	0.043
	Al_{di}	-0.844	0.094	-8.96	<0.001	2.01	0.031
	Fe_{di}	-0.046	0.007	-6.74	<0.001	1.38	0.013
						Total R^2	0.936
Site B	**Predictor**	**Estimate**	**Std. Error**	***t*-value**	***p*- value**	**VIF**	**Proportion of VE (R^2)**
	POC	0.074	0.003	24.53	<0.001	1.44	0.619
	Si	0.014	0.001	8.35	<0.001	1.19	0.038
	Fe_{di}	-0.076	0.009	-8.49	<0.001	1.99	0.037
	Al	0.021	0.003	6.62	<0.001	1.79	0.019
						Total R^2	0.714
Site E	**Predictor**	**Estimate**	**Std. Error**	***t*-value**	***p*- value**	**VIF**	**Proportion of VE (R^2)**
	POC	0.052	0.003	17.48	<0.001	1.68	0.200
	Si	0.019	0.002	9.84	<0.001	4.06	0.174
	Mn	1.527	0.255	6.00	<0.001	1.88	0.165
	Ti	-2.123	0.251	-8.45	<0.001	9.84	0.150
	Al_{di}	-0.957	0.078	-12.30	<0.001	1.44	0.130
	Fe	0.136	0.010	13.35	<0.001	1.91	0.055
	Mg	0.619	0.135	4.60	<0.001	5.39	0.035
	Fe_{di}	-0.055	0.009	-6.13	<0.001	1.68	0.031
						Total R^2	0.940

7.4.3.3 Interpreting Regression Results

The pronounced transition from Fe-P dominated associations under baseflow conditions to POC-P associations during storm events can most likely be explained by a change in SPM source area. The research presented in Chapters 4 and 5 demonstrated that baseflow SPM source contributions are dominated by subsurface inputs from channel

banks and agricultural field drains, which have comparatively low POC (μ = 2.2% and 7.9%) and high Fe (μ = 4.7% and 6.9%) concentrations, respectively, compared with surface soils (Table 7.1). This creates geochemical conditions conducive to the sorption of phosphate ions onto the surfaces of Fe-oxide complexes, hence the dominance of the Fe-P association during baseflow. This association may arise in either the stream, soil or field drains as a consequence of changing redox conditions initiating the precipitation of Fe-P complexes (Jarvie *et al*., 2008).

Conversely, during storm events, the provenance of SPM comprises a greater contribution from surficial sources (topsoils and road verges), which are comparatively enriched in POC (μ = 10.2% and 12.9%) compared with subsurface sediments (Table 7.1). This results in larger quantities of P being either transported with, or sorbed onto the surfaces of, OM-bearing complexes, hence the greater importance of the P-POC association observed in the storm event regression models. Whilst this change in association suggests that OM is the primary source of P, the stoichiometry of OM suggests otherwise. Under storm event conditions, the mean OM concentration of SPM is 23.8% and the mean PP concentration is 0.32% (Table 7.1; POC taken to be 58% of OM (Broadbent, 1953)). Assuming P comprises approximately 0.2% of dry plant matter (Schachtman *et al*., 1998), we can estimate a P concentration of 0.05% derived from OM (23.8% x 0.002), with the remainder (0.27% P) of inorganic origin. Thus, the ratio of organic to inorganic derived P is approximately 1:6. This confirms the idea that enhanced storm event POC-P association arises because both constituents are enriched in surface sources and are therefore delivered simultaneously to the stream and not because more P occurs within OM itself.

The data also suggest there is a third distinct source of Fe-enriched SPM that is mobilised during storm events. Evidence for this comes from examining the SPM Fe-P ratios, which increase during large storm events relative to baseflow conditions (Figure 7.3). Because surficial sediments have substantially lower Fe-P ratios than subsurface sediments (Table 7.1), this increase in SPM Fe-P ratio can be best explained by the storm event mobilisation of iron sulphide (FeS) which forms in the reducing conditions beneath the surface of streambeds.

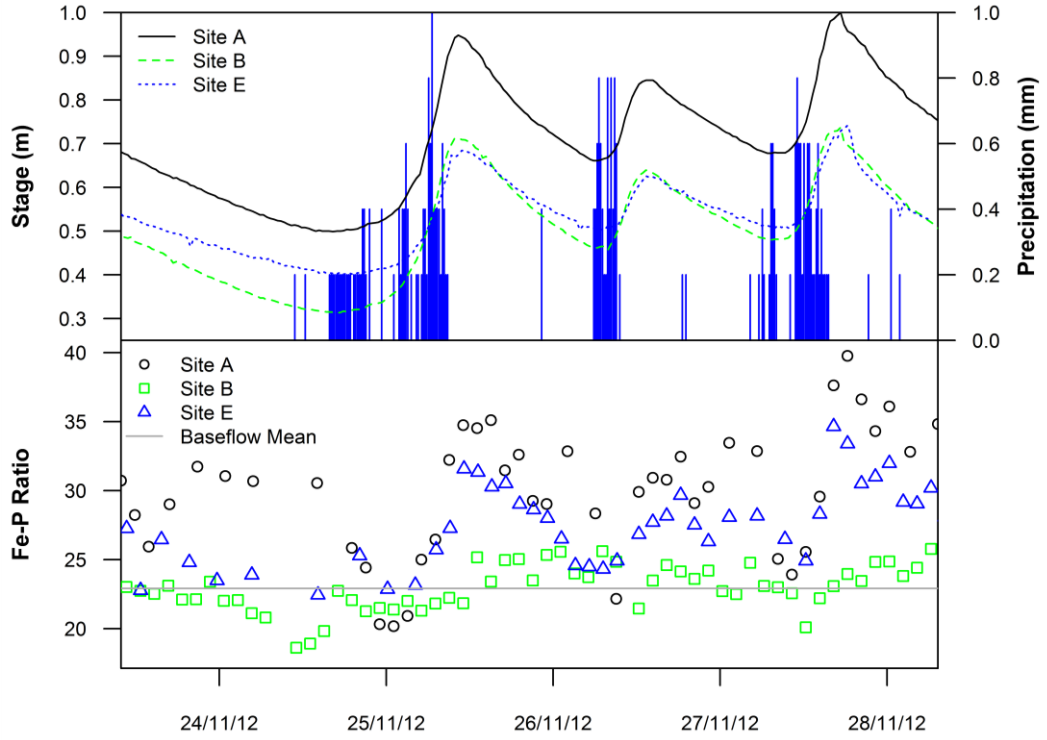

Figure 7.3: Time-series of SPM Fe-P ratios for sites A, B and E during three consecutive storm events in November 2012. Baseflow mean refers to the average for all three sites. See Chapter 5 for the Bayesian SPM source apportionment of this event at site A and B.

7.4.4 Seasonal Trends

7.4.4.1 Clay Mineral Associated Elements, Metal Oxides and Calcium

Figures 7.4-7.6 present time-series of baseflow SPM geochemistry at sites A, B and E between May 2012 and March 2014. Across all three sites, these time-series plots reveal strong seasonal cycles in geochemistry. Concentrations of metal oxides and clay mineral associated elements all increase during the autumn and winter period (approximately October to March) before declining again during the following summer (approximately April to September). Conversely, Ca concentrations exhibit the opposite response, with concentrations cycling between the highest values in summer and lowest values during the winter, a seasonal trend also observed in calcareous streams by Evans *et al*. (2004). Evans *et al*. (2004) similarly observed autumnal peaks in the concentrations of metals and organic matter in the Rivers Enborne and Lambourn (Berkshire, UK) and linked these to increases in surface runoff derived sediments with the onset of autumn storms and the breakdown of autochthonous macrophyte/periphyton material within the stream channel. Concentrations of Al_{di} and Fe_{di} appear to be higher in winter than in

summer, although the seasonal cycle is not as clearly defined as for the many of the elements. At all sites, Al_{ox} exhibits no seasonality, with concentrations falling to a minimum in November 2012, before rising almost continually to a maximum 12 months later in November 2013. Concentrations of Fe_{ox} also exhibit no obvious seasonal cycle.

7.4.4.2 Phosphorus

In contrast to most of the other geochemical parameters, P concentrations do not display consistent seasonality across the three sites (Figures 7.4a-7.6a). However, a very strong seasonal cycle is recorded at site E, with concentrations larger in the summer/autumn and smaller in the winter/spring. The timings of these peaks may be linked to a combination of (i) increased autochthonous P release as a consequence of growing season primary production; (ii) the development of P-rich biofilms around fine particulates which grow more vigorously during the summer; (iii) the enhanced bed sediment P sorption under low flows; or (iv) the increased P-rich SPM inputs from subsurface field drains. These summer/autumn P peaks correspond with similar findings by Walling *et al*. (2001), Stutter *et al*. (2007, 2008) and Ballantine *et al*. (2009) for a range of UK rivers under differing hydrological conditions.

Conversely, PP concentrations at site B exhibited three local minima in August 2012, July 2013 and January 2014 and a global maximum in April 2013, whilst concentrations at site A were small and stable between May 2012 and April 2013 before rising sharply during summer 2013. Previous studies have linked spatial intra-catchment variability in DP concentrations to differences in geology, land use and point sources of pollution, such as sewage treatment works (e.g. Ballantine *et al*., 2008). However, considering the short distance between sites A, B and E (600 m) and the absence of any sewage discharges between them, we can rule these out as explanatory factors. Instead, these spatial differences in P concentration are more likely related to localised instream primary production and inputs from agricultural field drains which may transport SRP from agricultural fertilisers directly into the stream channel. It is also worth noting that summer 2013 was warmer (mean monthly temperature 0.5^{o}C higher) and drier (mean monthly precipitation 45 mm lower) than summer 2012, conditions more conducive to vigorous instream primary productivity, which may partly explain the higher P peaks observed at all sites during 2013.

7.4.4.3 POC, Manganese and Iron

Like P, the temporal patterns in Mn concentrations are also different between sites. The two local winter maxima observed at site B were replaced by four local maxima at sites A and E in August 2012, January 2013, August 2013 and January 2014 (Figures 7.4a-7.6a). Four local maxima were also observed in POC concentrations during June 2012, January 2013, August 2013 and January 2014 at site A. Given that Mn is strongly correlated with POC under baseflow conditions (Figure 7.1), it is possible that the summer peaks in both Mn and POC were associated with the increased supply of autochthonous organic matter from macrophyte and algal growth. Similarly, the winter peaks may be related to increased allochthonous material from Mn and POC-rich surface runoff, as well from the breakdown of autochthonous plant material that had died off at the end of the growing season. Interestingly, variability in POC concentrations at site E does not correspond with either the obvious winter peaks in POC at site B, or the summer and winter peaks observed at site A. Considering that site E is downstream of A and B, this suggests POC concentrations at site E are more strongly influenced by autochthonous material within mini-catchment E rather than by material delivered from higher up the catchment.

As with POC and P, trends in SPM Fe concentration also appear to be unique to each mini-catchment, which may relate to the inherent geochemical variability of soil Fe concentrations across the catchments. Concentrations at site B were highest during the winter and lowest during the summer, whereas at both sites A and E maxima occurred during the summer and minima during the winter. These elevated summer Fe concentrations may have been due to the high Fe concentrations of sediments discharging from agricultural field drains in mini-catchment A (Figure 5.8) which have greater influence on SPM geochemistry during periods of low summer flow when surface runoff is negligible. Peaks in Fe concentration during the winter are likely due to increased surface sediment input.

7.4.4.4 Timing of Seasonal Cycles

Interestingly, the timing at which concentrations of most elements increase during the winter was not consistent between years. For example, at site B, K concentrations first rose above average in October 2012, but the following year concentrations did not rise above average again until December 2013, two months later (Figure 7.5a).

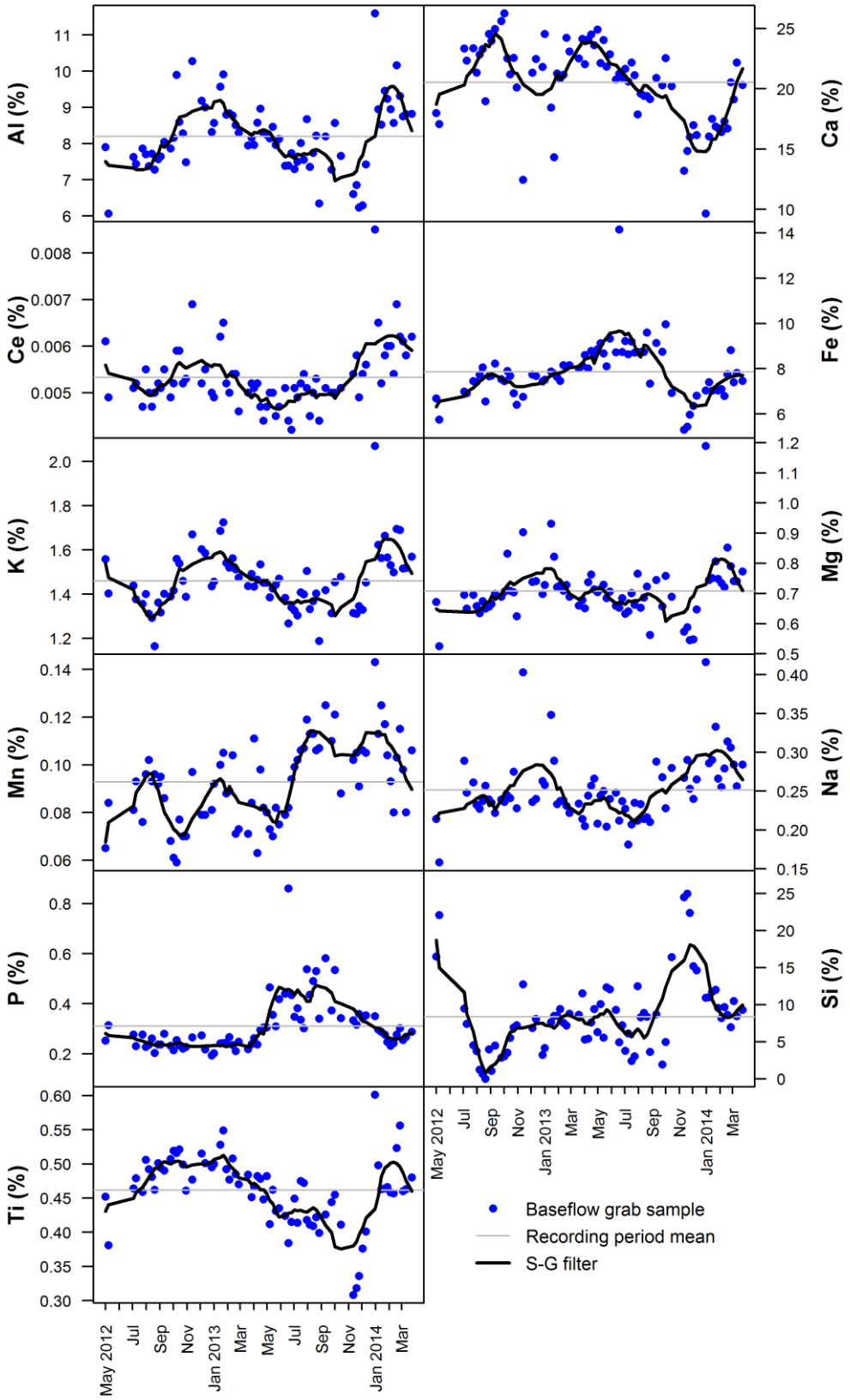

Figure 7.4a: Time-series of baseflow SPM geochemistry at site A, as recorded from 74 grab samples collected at 1-2 week intervals between May 2012 and March 2014. The smooth black line is a 15 point, 2nd order Savitzky-Golay filter.

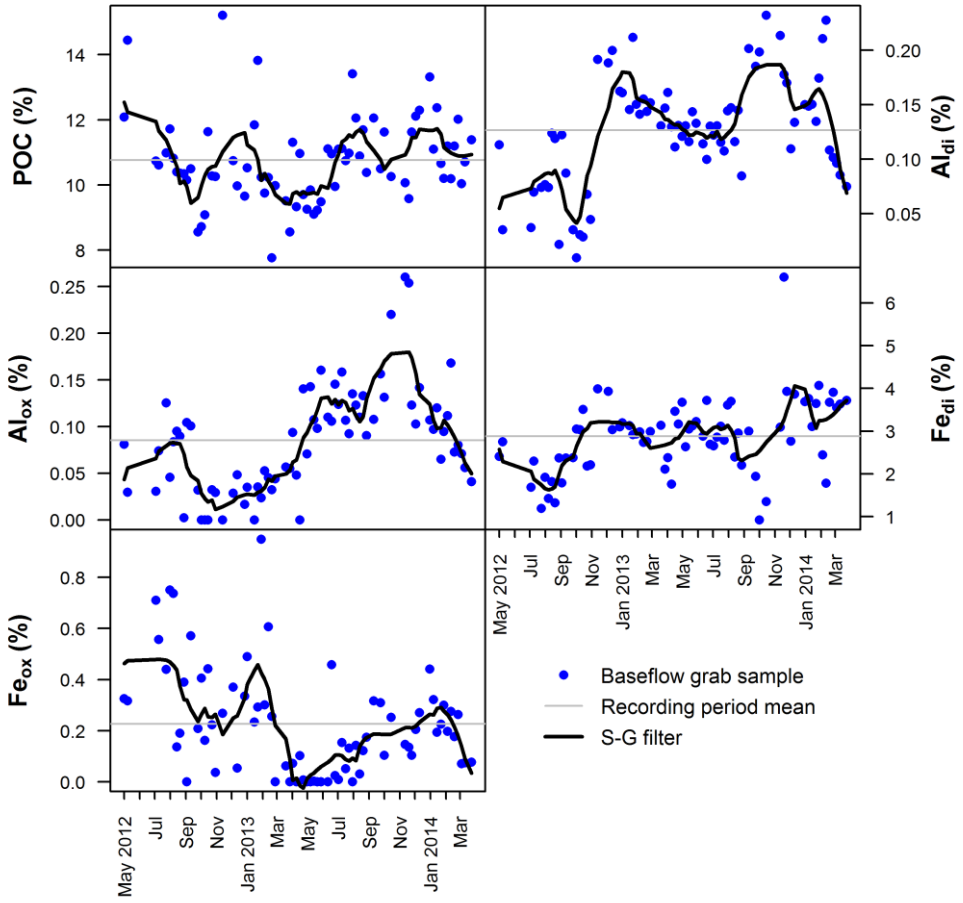

Figure 7.4b: Time-series of baseflow SPM organic and inorganic phases at site A, as recorded from 74 grab samples collected at 1-2 week intervals between May 2012 and March 2014. The smooth black line is a 15 point, 2nd order Savitzky-Golay filter.

Similarly, whilst the pronounced winter 2012/13 maxima in Al, Ce, Mg and Ti concentrations occurred in January 2013, the winter 2013/14 maxima did not occur until February 2014. This apparent delay is almost certainly a reflection of differences in both precipitation and agricultural practises between years. Higher rainfall totals were recorded in 2012 compared with 2013 (Figure 2.5), with the result that catchment soils were more susceptible to saturation and surface runoff generation earlier in the autumn, hence the increased transport of clay mineral and metal oxide-rich material into the stream. Furthermore, autumn/winter 2012 was also the time of sugar beet harvesting (Figure 5.21) and surface soils were left exposed and heavily disturbed for several months (October-February), thus making them more susceptible to erosion earlier in the year than might otherwise have been the case. This also explains the more pronounced peaks in clay mineral and metal oxide associated elements during winter 2012/13 than during winter 2013/14 when less sugar beet was being harvested in the catchment.

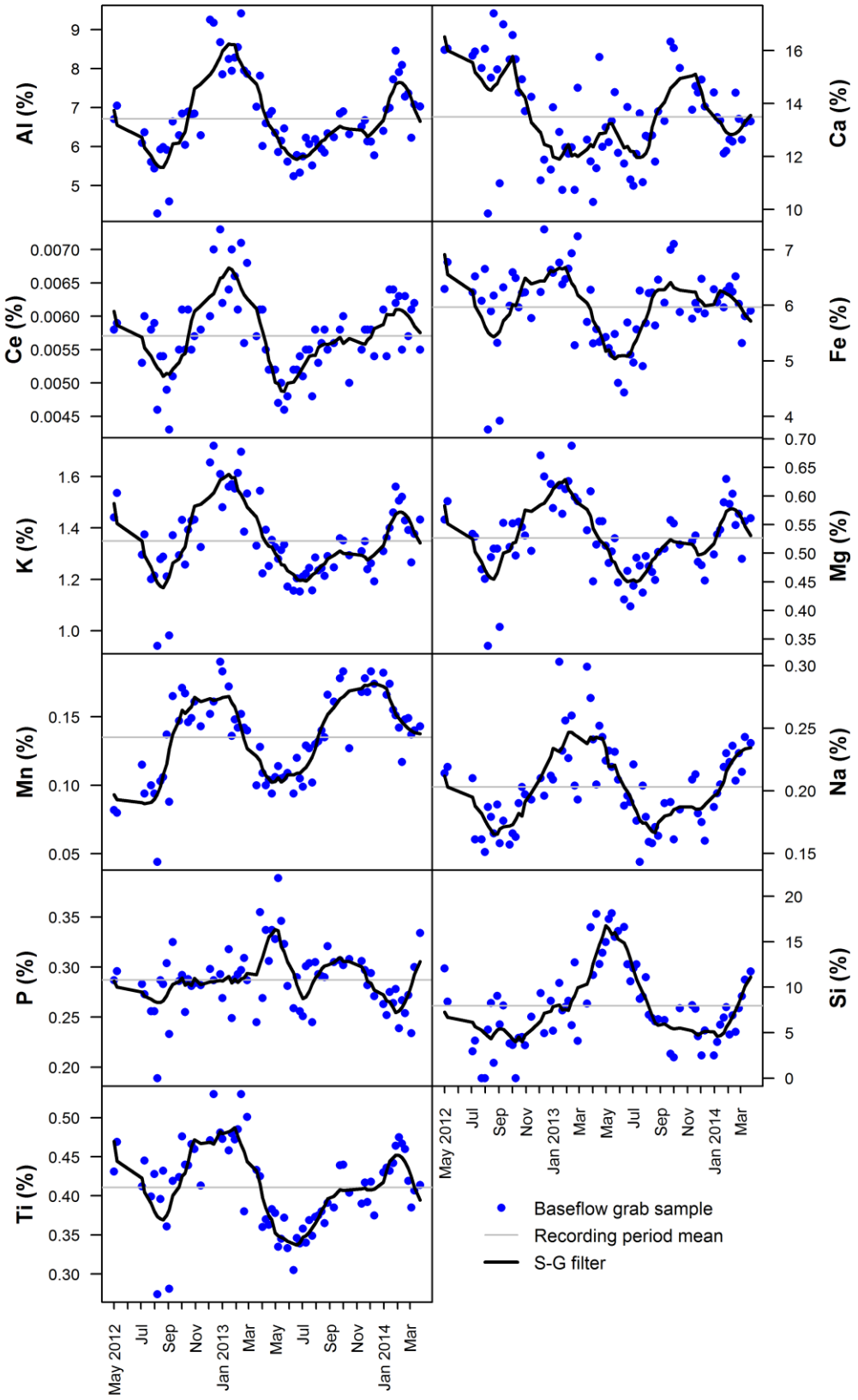

Figure 7.5a: Time-series of baseflow SPM geochemistry at site B, as recorded from 74 grab samples collected at 1-2 week intervals between May 2012 and March 2014. The smooth black line is a 15 point, 2nd order Savitzky-Golay filter.

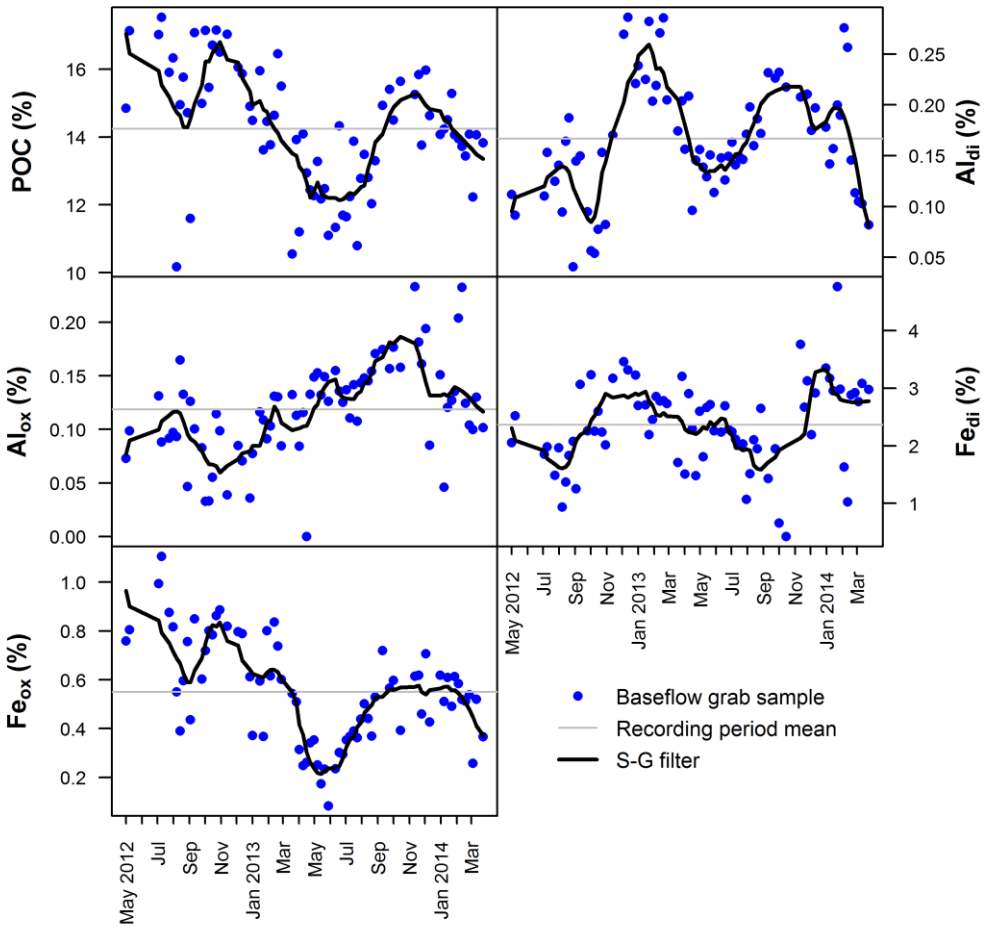

Figure 7.5b: Time-series of baseflow SPM organic and inorganic phases for site B, as recorded from 74 grab samples collected at 1-2 week intervals between May 2012 and March 2014. The smooth black line is a 15 point, 2nd order Savitzky-Golay filter.

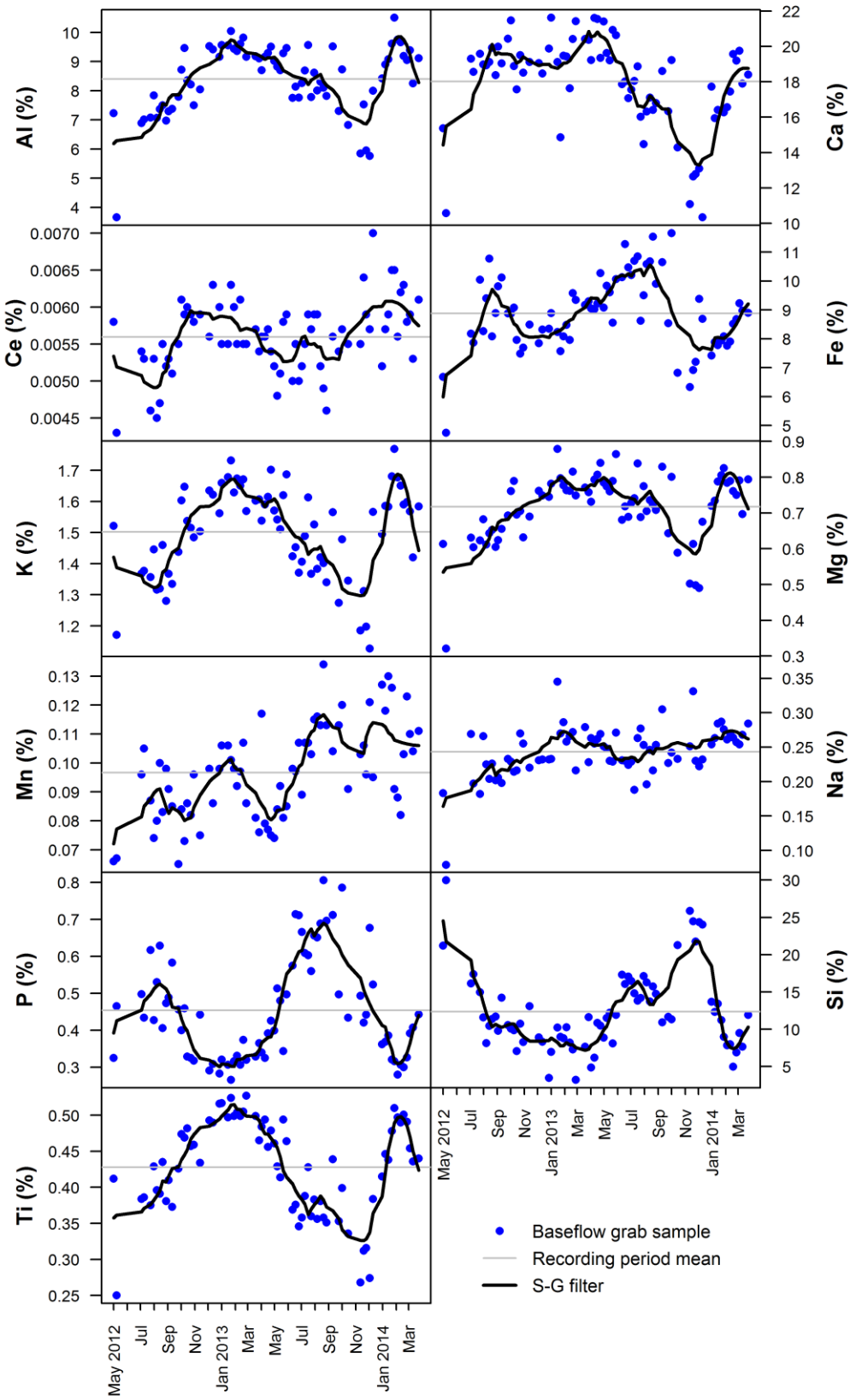

Figure 7.6a: Time-series of baseflow SPM geochemistry at site E, as recorded from 74 grab samples collected at 1-2 week intervals between May 2012 and March 2014. The smooth black line is a 15 point, 2nd order Savitzky-Golay filter.

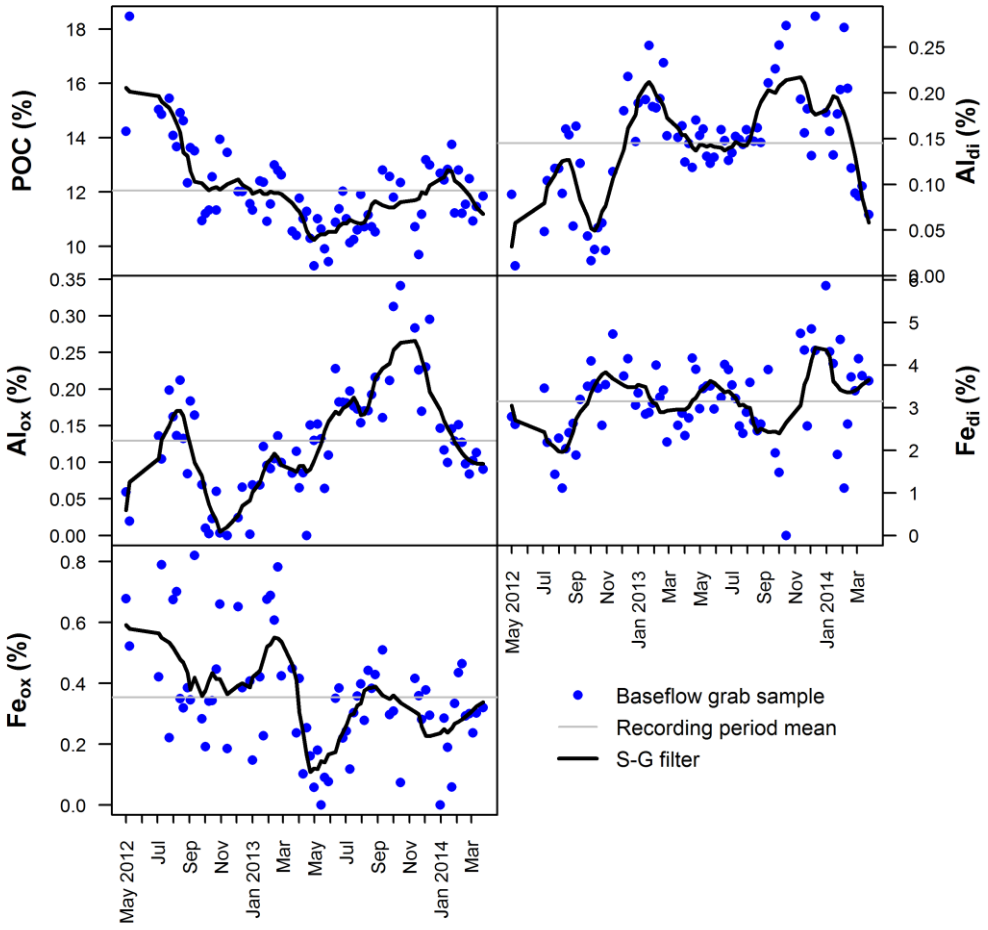

Figure 7.6b: Time-series of baseflow SPM organic and inorganic phases at site E, as recorded from 74 grab samples collected at 1-2 week intervals between May 2012 and March 2014. The smooth black line is a 15 point, 2nd order Savitzky-Golay filter.

7.4.4.5 Seasonality in SPM Concentrations

Previous research has described how the temporal dynamics of SPM concentration vary between phases of transient storage and mass flushing events which mobilise and transport large quantities of material out of the local stream system (e.g. Bowes *et al.*, 2003; Demars and Harper, 2005; Stutter *et al.*, 2008a; Ballantine *et al.*, 2009). Theoretically, instream sediment storage dominates during the low spring time flows as water levels decline due to rising evapotranspiration rates. Low summer flows are also usually dominated by instream sediment storage, although periodic storm events can facilitate the transient re-suspension of fine particulates which can significantly degrade stream ecology during this biologically sensitive period. The storage of sediment during these summer low-flows is known to be highly influential in determining SPM dynamics during the return to higher flows in autumn (Salant *et al.*, 2008). Rising water levels and

increased sediment flushing characterise this transition from dry summer to wet autumn conditions, whilst high stream flows, high flushing rates and minimal sediment storage theoretically characterise the cool, wet conditions of winter (Dorioz *et al*., 1998; Stutter *et al*., 2008a, b; Ballantine *et al*., 2009).

In the River Blackwater, baseflow SPM concentrations are generally below the 25 mg/L target threshold set out in the EU Freshwater Fisheries Directive (78/659/EEC; 2006/44/EC) for waters suitable for salmonid and cyprinid fish populations (Figures 7.7 and S7.1; Table 7.4). This finding is not unique, with previous research having shown chalk streams similar to the Blackwater having lower SPM concentrations than rivers draining less permeable catchments (Acornley and Sear, 1999; Heywood and Walling, 2003). At site A, baseflow SPM concentrations peaked at ~22 mg/L in September 2012 and subsequently declined over the following 18 months to ~6 mg/L, with no obvious seasonal trend. This was similar to site B, where SPM peaked in October 2012 at ~25 mg/L before declining throughout winter 2012/13 and spring 2013 prior to stabilising at ~8 mg/L for the rest of the monitoring period, again with no strong seasonal trend apparent.

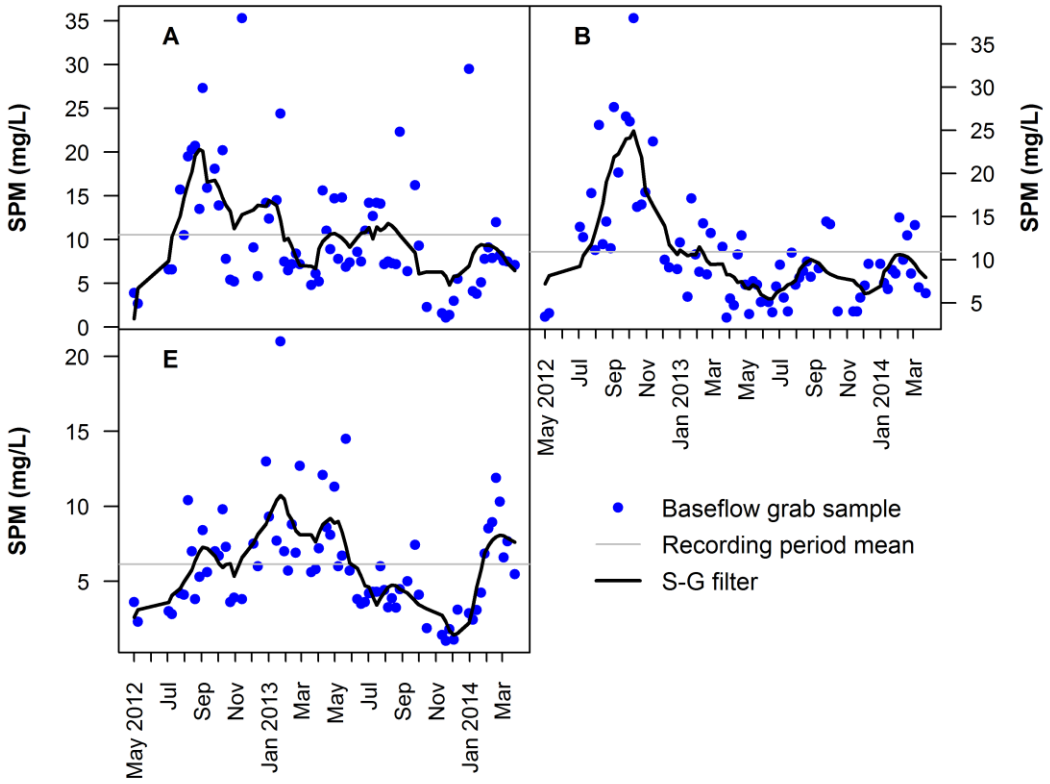

Figure 7.7: Time-series of weekly SPM concentrations at sites A, B and E between May 2012 and March 2014. The smooth black line is a 15 point, 2nd order Savitzky-Golay filter.

These higher SPM concentrations observed during late summer and early autumn 2012 are likely to relate to the increased frequency of rainfall events generating more surface runoff and initiating greater land-to-river sediment transfer compared with 2013. Furthermore, the autumn 2012 sugar beet harvest caused significant amounts of soil disturbance, further enhancing sediment transfers. During autumn 2013 an oilseed radish cover crop was grown across seven fields in mini-catchments A and B to help reduce surface runoff and nitrate leaching (Section 2.4). The protective action of these cover crops with respect to soil stabilisation, combined with the absence of sugar beet harvesting, probably contributed to the reduced SPM concentrations during autumn 2013 compared with the previous year.

Table 7.4: SPM concentrations (mg/L) recorded at sites A, B and E under baseflow (n = 222) and storm event (n = 721) conditions between May 2012 and March 2014. See Appendix E for plots of SPM exceedance frequency.

	Site A (mg/L)		**Site B (mg/L)**		**Site E (mg/L)**	
Flow	Baseflow	Storm	Baseflow	Storm	Baseflow	Storm
Min.	1.1	2.4	3.3	7.9	1.0	1.4
Median	7.9	29.7	9.3	28.3	5.7	19.1
Mean	10.5	44.9	10.9	42.6	6.1	38.4
Max.	35.3	266.5	38.0	592.0	21.0	387.0

Interestingly, at site E there was no peak in SPM concentrations in autumn 2012, with SPM instead peaking in January 2013 at ~12 mg/L. Average baseflow SPM concentrations of 6.1 mg/L at site E over the 23 months were also lower than that recorded at sites A (10.5 mg/L) or B (10.9 mg/L) (Table 7.4). Intuitively this may imply a dilution as flows increased downstream, however correlation of SPM with stage is low (r = -0.164). Instead, the channel morphology at site E is thought to have played a more important role. A bridge 50 m downstream of the monitoring station at site E caused the water to pond upstream, creating a pool of slower moving water from where sampling took place. This would certainly have enhanced sediment settling rates, thus explaining the lower SPM concentrations recorded. NB: the grab sampling location was not moved further upstream because the ISCO automatic water sampler intakes were also located in this zone of ponded water and both types of samples needed to be taken from the same location for consistency.

7.4.4.6 Seasonality in Oxalate-Dithionate Ratios

The ratio of oxalate-extractable (amorphous) to dithionate-extractable (crystalline) Fe and Al can be used as an index of the P sorption capacity of SPM (Hartikainen *et al*., 2010). The time-series data presented in Figure 7.8 reveal a clear seasonal cycle in the Al_{ox}-Al_{di} ratios at all sites, with a greater proportion of reactive amorphous material present during the summer months and less during the winter. This cycle is primarily driven by variation in the amorphous Al_{ox} fraction, which correlates strongly and positively with the Al_{ox}-Al_{di} ratios at sites A (r = 0.78), B (r = 0.53) and E (r = 0.57). This strongly suggests that SPM during the biologically sensitive summer season had a higher P adsorption capacity and thus greater ability to capture and transport SRP through the stream network. This conclusion is supported by the correlation between P and Al_{ox} under baseflow conditions (r = 0.49), which was the strongest association of the four Fe and Al oxyhydroxide compounds, and second only to total Fe (r = 0.71) for overall correlation with SPM P (Figure 7.2).

Examining the composition of sediment source areas (Table 7.1), we can hypothesise that field drains with enriched Al_{ox}-Al_{di} ratios supplied a greater proportion of Al_{ox} during the summer, whilst contributions from channel banks and road verges with lower Al_{ox}-Al_{di} ratios were more significant during the winter. Consequently, the SPM discharged by field drains appears to play an important role in determining the transport of PP during the growing season when streams are most sensitive to the detrimental effects of eutrophication. Furthermore, both the magnitude and timing of maxima and minima in Al_{ox}-Al_{di} ratios are different between years, with the winter 2012/13 minima occurring ~2 months earlier and being considerably more pronounced than during the corresponding winter 2013/14, for example. Again, this can likely be explained by a combination of larger total precipitation and different crop cultivation practices during autumn 2012 altering the sources of SPM compared with the following year.

Additionally, other processes may be contributing to the higher proportion of Al_{ox} observed during the summer months. For example, Violante and Violante (1980) demonstrated that higher concentrations of organic ligands slow down the crystallisation of Al oxides (i.e. the formation of Al_{di}). During the growing season, plants release larger quantities of organic acids into soil solution which would restrict the formation of Al_{di} and thus increase the proportion of Al_{ox}, thereby accounting for the higher Al_{ox}-Al_{di} ratios observed in SPM during the summer season.

Seasonality in the Fe_{ox}-Fe_{di} ratios is much less apparent than that observed for Al_{ox}-Al_{di} (Figure 7.8) and based on the overall weakness of these trends we cannot make any

conclusive statements regarding seasonality in these ratios. It is apparent though, that these Fe compounds, which had recording period mean Fe_{ox}-Fe_{di} ratios of between 0.10 and 0.27, were more crystalline in nature than the Al compounds which had mean Al_{ox}-Al_{di} ratios of between 0.67 and 0.92.

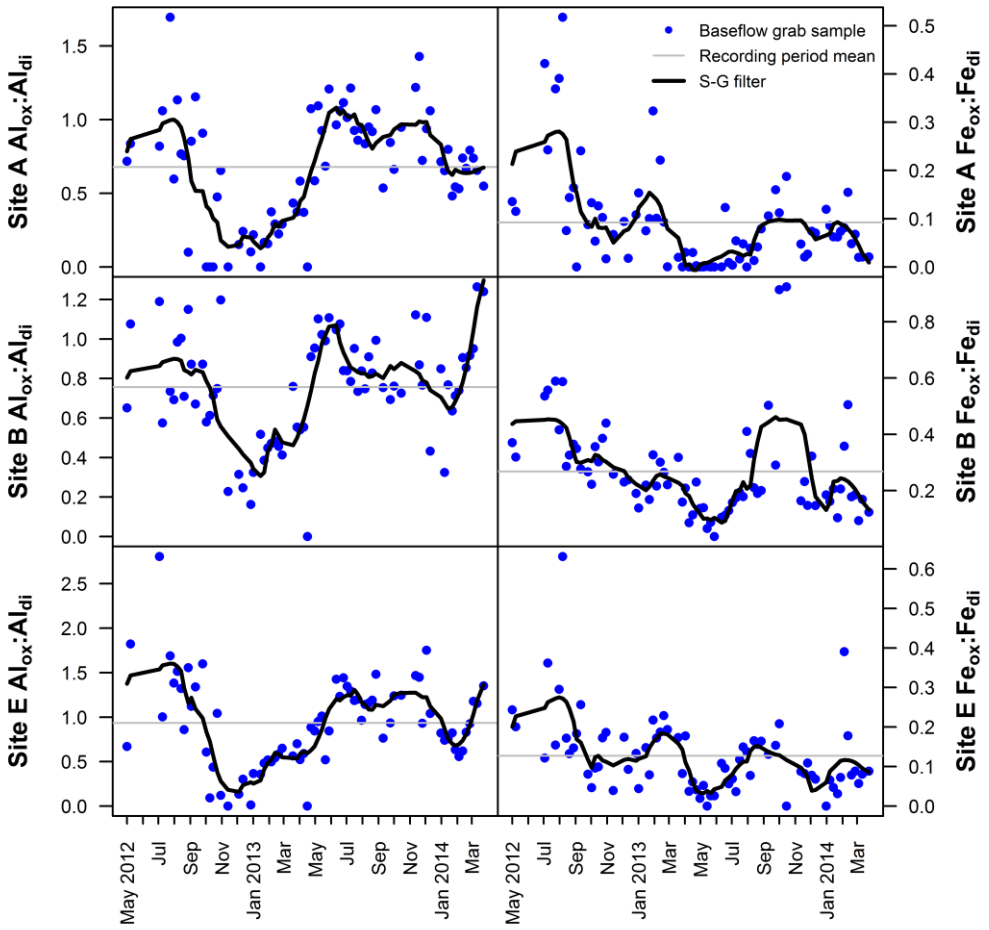

Figure 7.8: Ratios of oxalate vs. dithionate extractable Al and Fe in baseflow SPM at sites A, B and E between May 2012 and March 2014. The smooth black line is a 15 point, 2nd order Savitzky-Golay filter.

7.4.4.7 Seasonality in Iron-Phosphorus Ratios

Previous research has demonstrated that Fe-P ratios can be useful indicators of the P 'buffering capacity' of aquatic sediments (Jensen *et al*., 1992). Specifically, the higher the Fe-P ratio, the greater the potential for the adsorption of SRP onto the surfaces of Fe containing compounds within sediments. Thus, higher Fe-P ratios allow sediment to isolate SRP from uptake by biota and thereby minimise the risk of eutrophication.

In the River Blackwater, examination of the temporal variability in SPM Fe-P ratios under baseflow conditions reveal ratios during summer/autumn 2013 were approximately half that in the preceding winter/spring, particularly at sites A and E (Figure 7.9). This implies SPM had greater capacity to adsorb excess SRP outside of the growing season. Strong, negative, linear correlations between the Fe-P ratio and PP at sites A (r = -0.78), B (r = -0.56) and E (r = -0.84) indicate variation in SPM P concentration, not Fe, was the main driver behind variability in these ratios. For all sites, ratios observed across the seasons are within the range of values (1-290) reported by House and Denison (2002) for six British rivers and generally greater than 15, the value above which it has been shown sediments can moderate temporal SRP variability in lacustrine environments (Jensen *et al*., 1992).

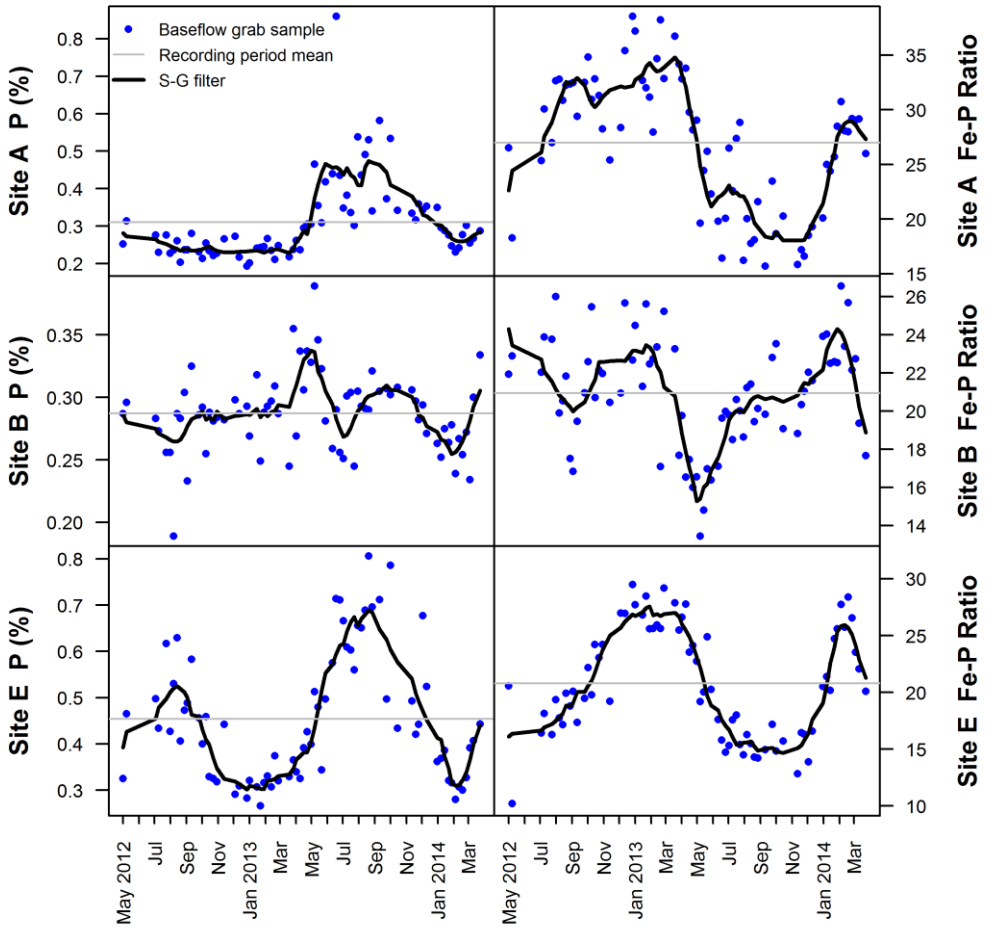

Figure 7.9: Fe-P ratios in SPM at sites A, B and E under baseflow conditions between May 2012 and March 2014. The smooth lines are 15 point, 2nd order Savitzky-Golay filters.

Interestingly, these winter peaks in the Fe-P ratio run counter to the idea of an increase in land surface-derived sources of SPM during the winter and subsurface derived sources during the summer. This is because the Fe-P ratios in surficial topsoil and road verge sediments are substantially lower than those in subsurface channel bank and field drain material (Table 7.1). The mobilisation of iron sulphide with high Fe-P ratios from the streambed during the more erosive winter flow conditions could explain this apparent anomaly by increasing the Fe-P ratio in SPM. Additionally, greater autochthonous P production during the growing season would lead to greater P sorption onto Fe-bearing sediments, thereby lowering Fe-P ratios during the summer months.

7.4.5 Seasonality in Baseflow SPM Source Apportionment

In general, the geochemical time-series presented in Figures 7.4-7.9 revealed SPM during the winter to be dominated by higher concentrations clay mineral associated elements, metal oxides and Fe-P ratios, whilst SPM during the summer was typically richer in Ca, Fe, P and POC, with higher Al_{ox}-Al_{di} ratios. Based on the findings of Chapter 5, such temporal geochemical trends suggest a greater proportion of SPM during the summer was derived from Ca-rich subsurface sources, whilst during the winter a higher contribution of SPM originated from surface sources rich in clay-associated elements. This is a logical assumption considering that higher antecedent soil moisture and bare arable fields in the winter increase the opportunities for surface runoff. Additionally, soil compaction by heavy machinery and soil destabilisation by ploughing expose fresh soil aggregates to surface flows, elevating erosion risk (Schelde *et al*., 2006; Archbold *et al*., 2007). During the summer, higher evapotranspiration rates and soil protection from actively growing crops reduces the risk of surface land-to-river sediment transfers, with subsurface sources dominating SPM supply. In order to quantitatively assess whether this was indeed how the sources of SPM changed over the seasons, the Bayesian sediment source apportionment mixing model was run for all 74 of the weekly baseflow SPM samples collected at sites A and B.

7.4.5.1 Site A

For site A, the three source (road verge, topsoil and subsurface sediment), eight fingerprint (Al, Ca, Ce, Fe, K, Mg, Na, Ti) mixing model presented in Chapter 5 was employed. The source apportionment results revealed strong evidence of a seasonal cycle in SPM sources (Figure 7.10). During summer 2012 and summer 2013, subsurface

sediment contribution dominated SPM supply with median apportionment of ~70% (55-85% at the 95% credible interval). This corresponds well with higher concentrations of Ca and lower concentrations of clay mineral and metal oxide associated elements during these periods. During the winter, estimated subsurface contributions declined to a low of 46% (21-76%) in January 2014, whilst contributions from topsoils and especially road verges increased considerably. Estimated median road verge contributions during the summer months were ~20% (8-35% at the 95% credible interval), but reached a high of 38% (14-70%) in January 2014, indicating an increase in road runoff generation during the colder, wetter winter conditions.

7.4.5.2 Site B

For site B, the four source (channel bank, field drain, road verge, topsoil), 11 fingerprint (Al, Ca, Ce, Fe, K, Mn, Mg, Na, Ti, Al_{ox}, Fe_{ox}) Bayesian mixing model of Chapter 5 was used. In contrast to site A, there was no strong seasonality to estimated source contributions (Figure 7.11). Channel bank contribution, the most variable of the four sources, did however, closely match the changing concentrations of Ca in SPM (R^2 = 0.963). High channel bank contributions of ~40% (31-50% at the 95% credible interval) were estimated during summer 2012 when high Ca concentrations were also recorded, with estimated contributions then declining in sync with Ca concentrations to ~30% (22-38%) during January and February 2013. Channel bank contribution was variable throughout summer 2013, as were Ca concentrations, but did increase back up to ~42% (33-51%) during the autumn, before declining once more down to ~32% (24-40%) with the onset of winter rainfall. In contrast, estimated topsoil and road verge contributions did not display the same seasonality as observed in most of the clay mineral associated elements. Whilst estimated topsoil contribution did increase up to ~28% (12-45%) in December 2012/January 2013 from ~20% (9-35%) during the previous summer and autumn, this increase was not as prominent as one might have expected when looking at the baseflow geochemical time-series (Figure 7.5a).

The reason for this can be explained by comparing the changes in geochemistry observed here with the changes witnessed during some of the storm events presented in Chapter 5 where large changes in topsoil contribution were estimated by the model. Under baseflow conditions at site B, Al concentrations increased during winter 2012/13 by just ~3% compared to summer 2012 values. Contrast this with the February 2013 storm event when Al concentrations increased by ~12%. The same is true for other elements such as Ce, whose concentrations increased during winter 2012/13 by only ~15 ppm compared to

~40 ppm during the February 2013 storm event. Thus, whilst there appeared to be a very strong seasonal cycle in SPM geochemistry at site B (Figure 7.5a), the actual changes in composition were relatively small compared to that witnessed during storm events. Large shifts in the estimated source contribution were therefore not required in order to model the temporal shifts in SPM composition, particularly when one considers that the source area distributions can be quite wide (see Chapter 4). Therefore, this explains the apparent 'flat-lining' of road verge and field drain contributions, in particular (Figure 7.11).

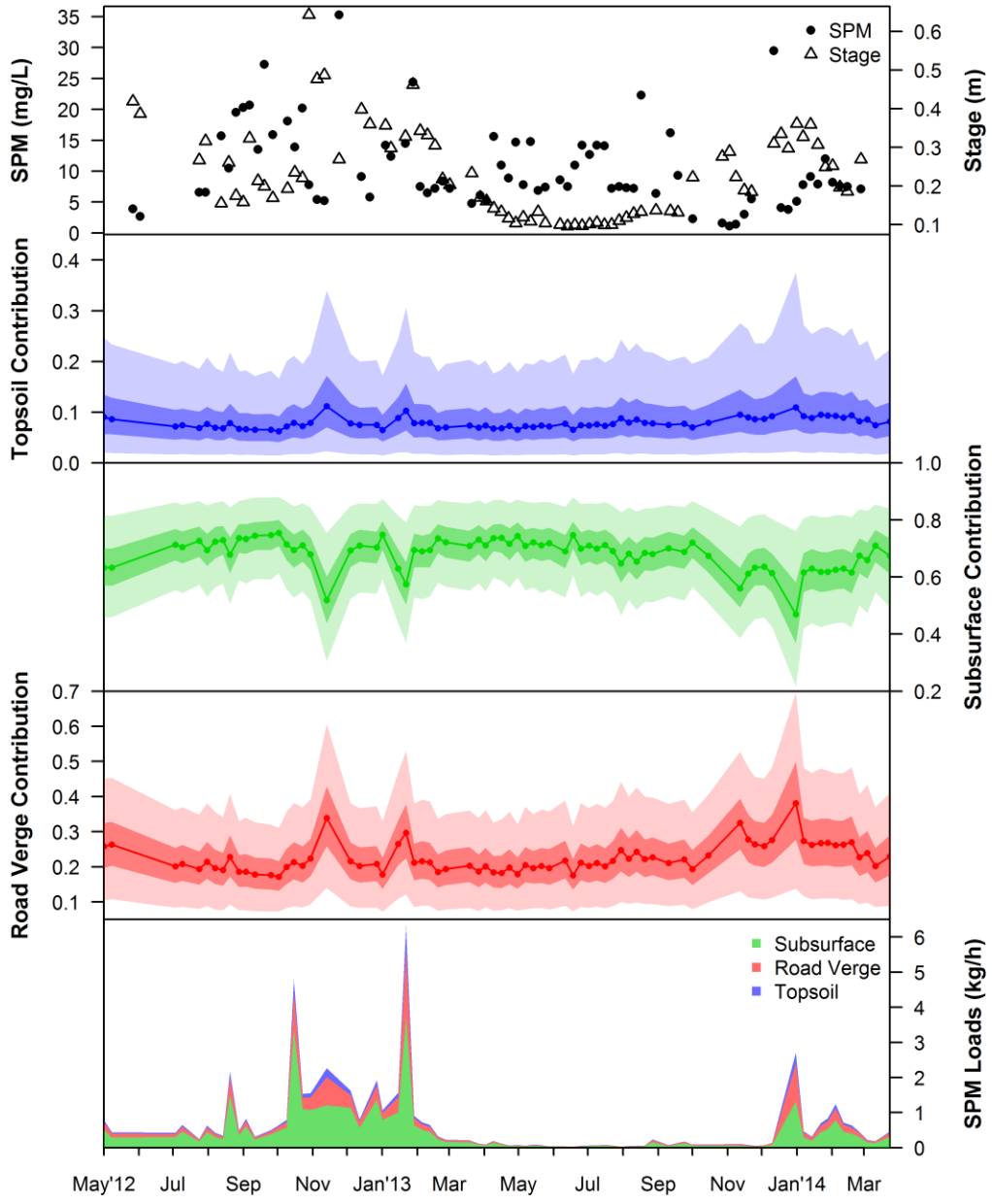

Figure 7.10: Time-series plots of baseflow SPM source apportionment at site A between May 2012 and March 2014, as derived from 74 weekly grab samples. Stacked SPM loads are based on estimated median source contribution. Light and dark shading around median source apportionment estimates represent the 95% and 50% Bayesian credible intervals, respectively.

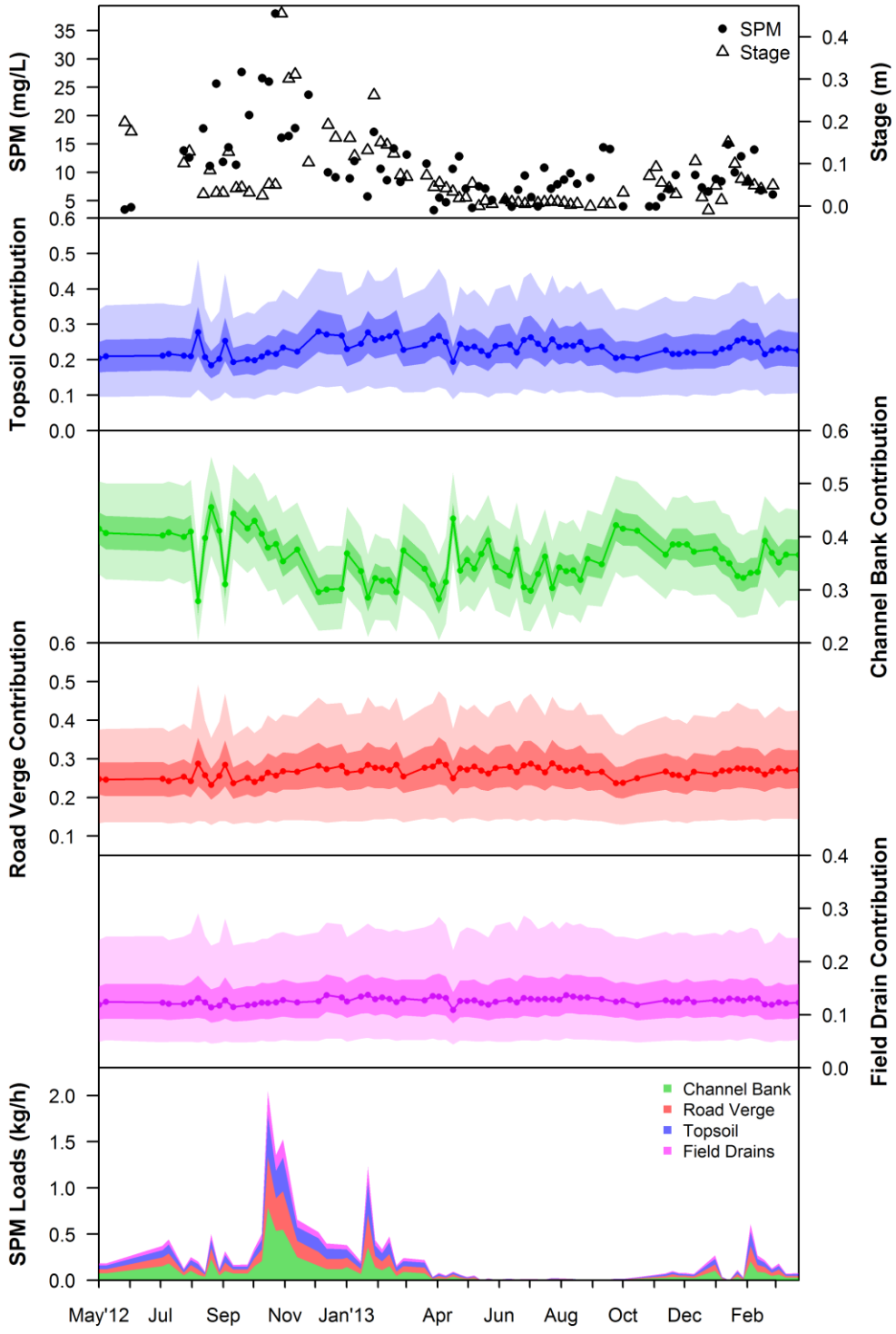

Figure 7.11: Time-series plots of baseflow SPM source apportionment at site B between May 2012 and March 2014, as derived from 74 weekly grab samples. Stacked loads are based on estimated median contributions. Light and dark shading around median source apportionment estimates represent the 95% and 50% Bayesian credible intervals, respectively.

7.4.6 Diel Cycles in SPM

To explore evidence for diel cycles in SPM concentration, an investigation was undertaken of 30-min resolution turbidity data obtained from YSI turbidity probes located in the bankside monitoring kiosks at sites A, B and E. These high-resolution turbidity measurements provide a robust proxy for SPM concentrations at all three sites (Figure E3; Appendix E). The turbidity time-series, shown here for the 10-29th April 2013, reveal clear evidence of strong diel cycles in turbidity measurements at sites A and E (Figure 7.12). The highest recorded turbidity values were generally reached sometime between 21:00 and 04:00 centring around midnight, with values then declining by ~10 nephelometric turbidity units (NTU) towards the lowest recorded values, which occurred between 10:00 and 14:00, centring on midday. Considering the timings of sunset (20:00) and sunrise (05:45) in mid-April, these turbidity peaks are consistent with the hypothesis that nocturnal bioturbation is responsible for generating these cycles. These timings are also consistent with the observations of Harvey *et al*. (2014) and Rice *et al*. (2014), who similarly found turbidity peaked at around midnight in the River Windrush, Oxfordshire and River Nene, Northamptonshire, respectively, with both studies linking these cycles to the nocturnal activities of Signal Crayfish. Whilst only shown here for a 20-day period in April 2013 (selected because this part of the turbidity record was less affected by noise), these diel turbidity cycles are present throughout much of the year at sites A and E. The cycles do, however, weaken during winter high-flows and precipitation events, when larger scale catchment-wide sediment mobilisation obscures these smaller diel fluctuations (e.g. turbidity typically rises by 100-200 NTU during storm events), an observation also made by Halliday *et al*. (2014).

At site B, diel turbidity cycles were less pronounced throughout most of the recording period than at the other two sites, suggesting a reduced impact from bioturbation. This can potentially be explained by the lower water levels and denser instream vegetation in mini-catchment B making it less accessible to larger aquatic fish and crayfish, thus reducing the incidences of bed sediment disturbance from nocturnal feeding and burrowing activities. Alternatively, differences in soil type between mini-catchment B and mini-catchments A and E, might mean crayfish found these channel banks less suitable for burrowing.

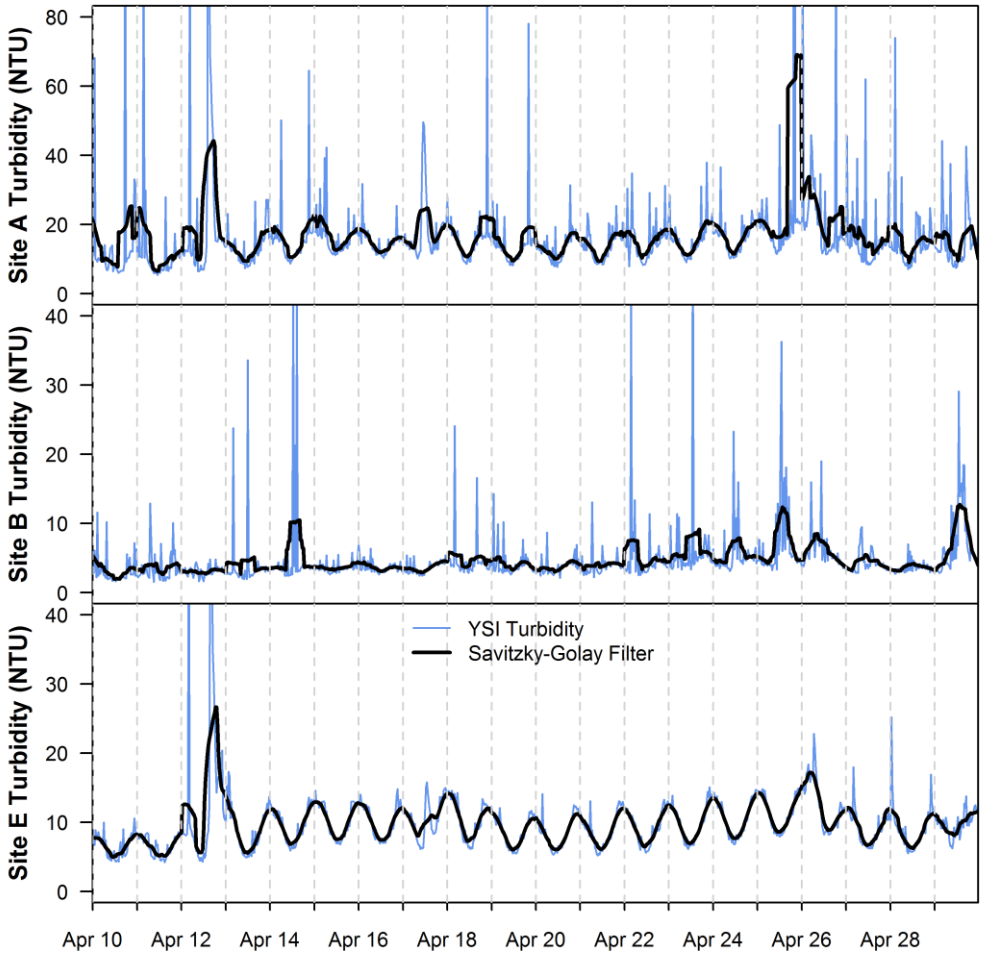

Figure 7.12: Time-series plots highlighting diurnal cycles in turbidity (NTU) at sites A, B and E over a 20-day period between 10/4/2013 and 30/4/2013. The smooth black line is a 15 point, 2nd order Savitzky-Golay filter. The YSI turbidity probe has an official accuracy of + 2%.

With such a strong and regular diel cycle observable in turbidity at sites A and E, it is important to rule out any potential instrument artefacts being responsible for inducing these trends if one is to have confidence in relating them to bioturbation. Firstly, it is important to recognise that turbidity is just a surrogate measure of SPM concentration and other factors, such as phytoplankton blooms, can lead to an increase in turbidity without the requirement for elevated SPM concentrations. Temperature is also known to affect turbidity measurements, with lower water temperatures leading to higher turbidity values and vice versa (Loperfido *et al.*, 2010). Thus, an instrumental anomaly in response to diurnal temperature variations could potentially yield the same diel pattern in turbidity as observed at sites A and E. However, as can be seen in Figure 7.13, temperature values at site A during April 2013 fell to a minimum just before dawn, several hours after the peak in turbidity around midnight. Additionally, correlation between temperature and

turbidity was weak (r = <0.01), implying no causal relationship exists between the two parameters.

Along with temperature, the influence of probe exposure to sunlight can also be ruled out as a potential driver of these cycles, because the turbidity probes used here were located inside the bankside monitoring kiosks and therefore kept in darkness. Additionally, comparison of turbidity values with an additional probe that was located instream at site A, revealed that both probes recorded very similar diel cycles in turbidity with respect to both timing and magnitude (data not shown). Correlation of turbidity with other parameters which display diel cycles, including stage (r = 0.02) and dissolved oxygen (r = 0.10), revealed that changes in these parameters were also unlikely to be causal factors as they do not align with the timings of the turbidity peaks (Figure 7.14).

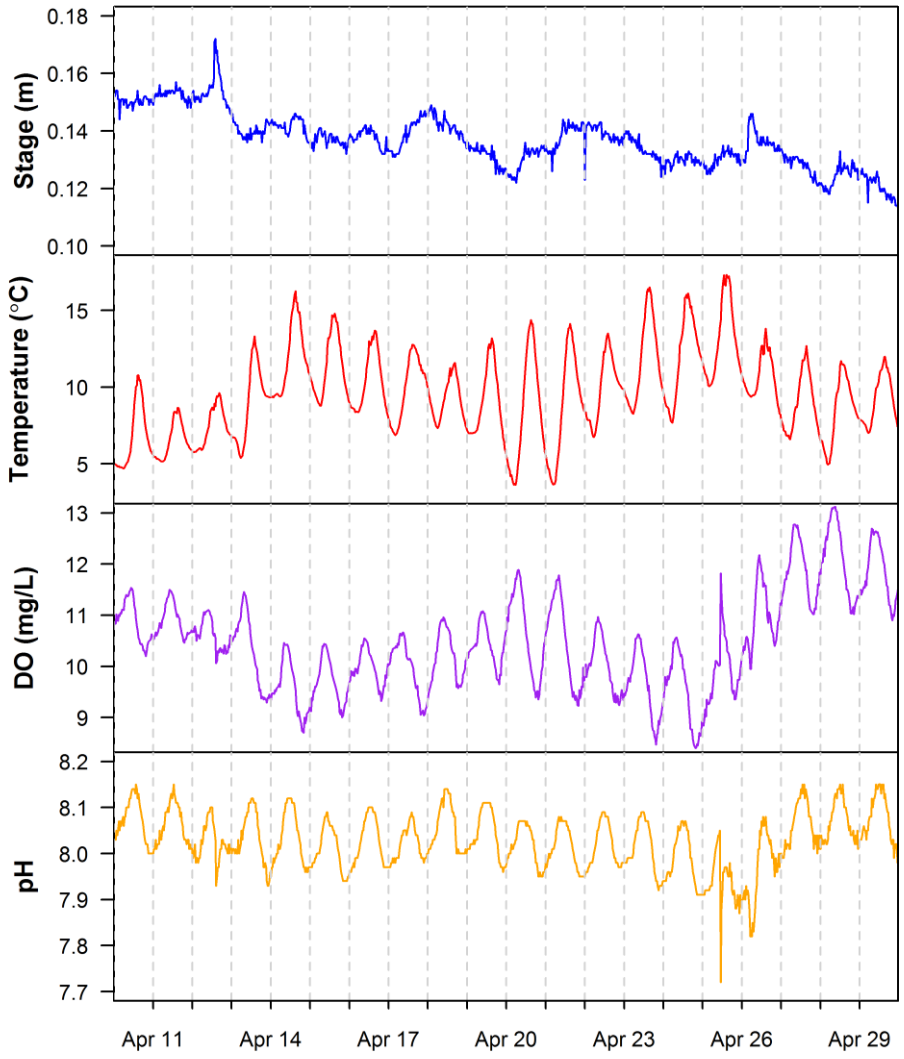

Figure 7.13: Time-series plots of diurnal variability in stage, water temperature, dissolved oxygen and pH at site A over a 20-day period during 10-29th April 2013.

However, diurnal cycles in pH, which peak at around midday and decline to a minimum around midnight, correspond more strongly with the turbidity trends. This daily pH variability relates to CO_2 consumption during photosynthesis by submergent macrophytes and algae during the day causing a decrease in acidity, and CO_2 release at night during respiration causing an increase in acidity (Nimick *et al.,* 2005). However, correlation between pH and turbidity is relatively weak (r = 0.23), and it is difficult to understand why a ~0.2 nocturnal decrease in pH would induce a ~10 NTU increase in turbidity, with the more acidic conditions favouring dissolution, not precipitation, of carbonate material (Loperfido *et al.*, 2010).

In conclusion, whilst it is not possible to conclusively prove that the diel turbidity cycles witnessed at sites A and E were caused by bioturbation, the evidence presented here, combined with that of previous studies, means this does provide a plausible casual mechanism.

7.4.7 Research Significance

In this chapter, through our analysis of large numbers of SPM samples collected under high- and low-flows at three adjacent catchment locations, we present clear evidence of a pronounced change in PP control mechanisms; from Fe-dominated associations under baseflow conditions, to greater POC associations during storm events. Because the most likely cause of this change is a shift in SPM source area under different hydrological conditions, this is likely to be a widespread phenomenon, but requires investigation in a range of different catchment settings. This finding has implications for mitigation measures aimed at reducing fluvial PP transfers, suggesting that different catchment source areas need to be targeted to reduce PP contributions under differing hydrological conditions. Furthermore, to our knowledge, this is the first study to demonstrate distinct seasonality in SPM Al_{ox}-Al_{di} ratios in an agricultural headwater catchment. This observation has important implications for (i) understanding the extent of P availability for exchange between dissolved and particulate forms and (ii) for the development of eutrophic conditions during the ecologically sensitive summer period. In particular, the enriched Al_{ox}-Al_{di} ratios of SPM derived from agricultural field drains indicates these subsurface drain networks are potentially important for controlling the instream concentration of reactive P. Consequently, mitigation measures aimed at reducing SPM discharges from field drains could decrease the amount of Al_{ox} associated P in agricultural headwater streams.

7.5 Conclusions

It is important to know how the relationships between various organic and geochemical constituents of SPM change under different flow conditions and over various temporal scales, as this information can help with our understanding of the processes that ultimately control SPM composition. In this chapter, investigation of SPM geochemical relationships revealed correlations between clay mineral associated elements to be the dominant associations under both baseflow and storm event conditions. However, there was a pronounced shift in P associations, from Fe-dominated under baseflow conditions to POC-dominated during storm events, for which it is hypothesised a change in the dominant SPM source area was the most likely causal mechanism. Examination of 23-month time-series of baseflow SPM geochemistry revealed strong seasonal cycles in the majority of elements, compounds and ratios. In general, these time-series revealed SPM during winter to be dominated by higher concentrations of clay mineral associated elements, metal oxides and Fe-P ratios, whilst SPM during the summer was typically richer in Ca, Fe, P and POC, with higher Al_{ox}-Al_{di} ratios. Using the Bayesian source apportionment mixing model these temporal trends were quantitatively apportioned to greater SPM inputs from Ca-rich subsurface sources during the summer, whilst contributions from clay mineral and metal oxide rich surface sources increased during the winter. Lastly, 30-min resolution turbidity time-series were found to have strong diel cycles, with increased night-time turbidity potentially the result of nocturnal feeding and burrowing habitats of fish and crayfish. Overall, the results presented in this chapter reveal significant variability in the concentrations, sources and relationships between organic and geochemical constituents of SPM under different flow conditions at diel-to-seasonal timescales.

Chapter 8

THESIS CONCLUSIONS AND FURTHER RESEARCH

8.1 Main Research Developments

Sediment fingerprinting is now a commonly employed technique for estimating sediment contributions from various eroding terrestrial sources to fluvial sediment load via a mixing model approach. However, there remained significant shortcomings in current fingerprinting practice which provided the motivation to advance sediment source apportionment procedures. The three main deficiencies identified as requiring further attention, along with the developments made in this thesis to address them, are discussed in turn.

8.1.1 High-Temporal Resolution SPM Monitoring

Deficiency: With the majority of fluvial sediments transported during short duration storm events, regular high-temporal resolution monitoring is essential in order to obtain a detailed understanding of the geochemical processes occurring in these dynamic high-flow periods. In particular, understanding how the provenance of SPM changes during the course of a storm event has the potential to yield important information for catchment managers looking to mitigate land-to-river sediment transfers. Until now, such investigations have been rare because many of the methods traditionally used for determining SPM geochemistry, both in the field (e.g. time-integrated samplers) and in the laboratory (e.g. acid digestion, ICP-MS/AES, LOI), are neither cost-effective nor time-efficient, thus making them prohibitive to long-term high-resolution monitoring.

Development: Addressing this limitation, a combined X-ray fluorescence spectroscopy (XRFS) and diffuse reflectance infrared Fourier transform spectroscopy (DRIFTS) approach was developed in Chapter 3 to rapidly, accurately and non-

destructively analyse SPM geochemistry for a range of elements (Al, Ca, Ce, Fe, K, Mg, Mn, Na, P, Si, Ti) and organic and inorganic phases (POC, Al_{di}, Al_{ox}, Fe_{di}, and Fe_{ox}) directly from sediment covered quartz fibre filter (QFF) papers at masses as low as 3 mg. Spectral pre-processing methods were shown to enhance the reproducibility of results for some compounds, whilst the importance of filter paper selection and homogeneous sample preparation in minimising spectral interference was emphasised. Additionally, the geochemical signal from sediment covered filters was demonstrated to be time stable, enabling SPM samples to be stored for several weeks prior to analysis.

8.1.2 Uncertainty in Source Apportionment Mixing Models

Deficiency: Whilst mixing models have become increasingly common tools for apportioning fluvial sediment load, the lack of a common method for incorporating uncertainty has resulted in a wide variety of Bayesian and frequentist modelling approaches being employed. Importantly, many of the commonly used frequentist models are inconsistent in their uncertainty representation and they lack the structural flexibility to coherently translate all sources of error into model results. Where Bayesian approaches have been adopted, there remained significant differences in the Bayesian frameworks used, specifically relating to the choice of priors, inclusion of covariance terms, incorporation of time-variant distributions and methods of proportion characterisation.

Development: Tackling this shortcoming, an improved Bayesian source apportionment mixing model was developed in Chapter 4 which allows for full characterisation of spatial geochemical variability, instrument precision and residual error, to yield a realistic and coherent assessment of the uncertainties associated with sediment fingerprinting estimates. Additionally, a one-factor-at-a-time (OFAT) sensitivity analysis was performed for 13 mixing models formulated with different error assumptions and model structural choices. This revealed varying degrees of sensitivity to changing priors, inclusion of covariance terms, incorporation of time-variant distributions and methods of proportion characterisation. Substantial differences in apportionment results were also demonstrated between full and empirical Bayesian approaches, and between Bayesian and frequentist frameworks.

8.1.3 Apportioning Sources of Fluvial Organic Matter

Deficiency: Organic matter forms an important component of the SPM transported by rivers. It can significantly influence dissolved oxygen concentrations and the transport of P and other contaminants which adsorb to its surface. However, techniques capable of quantitatively apportioning its origin have largely been overlooked by the sediment fingerprinting community, with the vast majority of studies using inorganic fingerprints to focus solely on the inorganic sediment fraction. Apportionment estimates which fail to account for this organic fraction may misrepresent the loads of organic material derived from each individual source, particularly if organic and inorganic material originates from difference sources.

Development: Addressing this deficiency, a novel application of a coupled molecular and compound-specific isotope analysis (CSIA) of leaf wax *n*-alkane biomarkers was conducted in Chapter 6 to apportion plant-specific organic matter contributions to streambed sediments. From the leaf wax extracts of 13 plant species collected from across two environments (aquatic and terrestrial) and four plant functional types (trees, herbaceous perennials and C_3 and C_4 graminoids), seven isotopic ($\delta^{13}C_{27}$, $\delta^{13}C_{29}$, $\delta^{13}C_{31}$, $\delta^{13}C_{27\text{-}31}$, $\delta^{2}H_{27}$, $\delta^{2}H_{29}$ and $\delta^{2}H_{27\text{-}29}$) and two *n*-alkane ratio (ACL and CPI) fingerprints were derived which successfully differentiated 93% of individual plant specimens by functional type. Hydrogen isotope values were the strongest discriminators of plants originating from different functional groups, whilst carbon isotopes provided strong discrimination between C_3 and C_4 plants. ACL and CPI complemented isotopic discrimination, with significantly longer chain lengths recorded for trees and terrestrial plants compared with herbaceous perennials and aquatic species, respectively. Using these molecular and isotopic fingerprints, quantitative Bayesian apportionment of streambed sediment organic matter sources was carried out, revealing considerable temporal variability in baseflow organic matter provenance over a 7-month, autumn to spring period.

8.1.4 Employing Thesis Advancements

Employing these developments in conjunction with automatic water samplers in Chapter 5, high-temporal resolution SPM source apportionment estimates were derived throughout the progression of numerous storm events in the lowland, agricultural River Blackwater catchment. This revealed significant temporal variability in SPM provenance at 60- and 120-min resolution. Ca-rich subsurface channel bank and field drain sources

dominated SPM supply before and after the event, whilst clay mineral and metal oxide rich contributions from topsoils and road verges increased in importance during the event itself. Lower resolution, weekly, baseflow sampling was also performed in Chapter 7, revealing distinct seasonal cycles in SPM geochemistry and sediment source apportionment over a 23-month period. In particular, higher concentrations of clay mineral associated elements during the winter highlighted increased sediment inputs from surface sources, whilst lower concentrations during the summer emphasised a greater abundance of Ca-rich subsurface material. Furthermore, distinct seasonality in the Fe-P and Al_{ox}-Al_{di} ratios of SPM indicated pronounced temporal variability in sediment P sorption capacity. A prominent shift in SPM P-control mechanism, from Fe dominated under baseflow conditions to POC associated during storm events, was also detected and attributed to a change in sediment source area under differing hydrological conditions.

Collectively, the developments presented in this thesis significantly advance sediment fingerprinting research by enabling organic and inorganic fluvial sediment fractions to be quantitatively apportioned at both low- and high-temporal resolution with realistic uncertainty estimates, thereby enhancing our understanding of sediment dynamics under a range of instream hydrological conditions.

8.2 Further Research

Whilst the developments in high-temporal resolution monitoring, mixing model uncertainty representation and apportionment of organic matter sources presented in this thesis represent a considerable improvement over existing sediment source apportionment techniques, there remains room to further advance fingerprinting research. Three areas that would benefit from increased attention are as follows:

(i) **Inclusion of an explicit temporal component in Bayesian mixing models:** In the benchmark Bayesian mixing model (M1) developed in Chapter 4, data were drawn from new source distributions (*S*) at each time-step, thereby enabling temporal variability in sediment source geochemistry to be incorporated into the model. This allowed the model to implicitly account for the erodability and connectivity of different locations within any given source classification (Fox and Papanicolaou *et al*., 2008), whilst also enabling the model to account for transient sediment storage within the fluvial system. However, other researchers outside of the sediment fingerprinting community (e.g. Brewer *et al.*, 2011; Parnell *et al*., 2013) have included more explicit temporal source components in

their mixing models, such as using splines to model autocorrelation within the dataset. These features can allow specific knowledge of temporal relationships to be incorporated into the model (e.g. specific bed sediment storage parameters). This aspect represents a highly promising area of Bayesian mixing model development and warrants further investigation to understand how inclusion of such features would influence sediment source apportionment results.

(ii) **Fingerprinting critical source areas:** The results presented in Chapter 5 demonstrated how fluvial SPM could be apportioned at high-temporal resolution to four broad source area categories (i.e. channel banks, field drains, road verges and topsoils). However, visual observations revealed most of this SPM originated from a few critical source areas, such as field entrances, narrow road sections and impervious sugar beet storage areas. Therefore, a useful development focus for future research would be to devise methods capable of quantitatively apportioning sediments derived from each of these critical sources to assist with the targeting of erosion mitigation measures. This would likely involve investigating the effectiveness of a different suite of tracers that are capable of resolving sediment sources with very similar surface soil geochemistry.

(iii) **Using $\delta^{2}H$ and $\delta^{13}C$ values as direct soil erosion tracers:** The novel results presented in Chapter 6 successfully demonstrated that an integrated carbon and hydrogen compound specific isotope analysis of leaf wax *n*-alkanes provides an effective approach for quantitatively apportioning plant-specific organic matter contributions to streambed sediments. A logical next step for future research would be to examine if soils under particular plant types are tagged with unique $\delta^{2}H$ and $\delta^{13}C$ signatures which would allow these isotopes to be used as direct land-use specific soil erosion tracers, as previously demonstrated for fatty acid $\delta^{13}C$ values by Blake *et al*. (2012). There would also be utility in applying these techniques to SPM collected at high-temporal resolution during precipitation events as a means of better understanding organic matter provenance and transport during dynamic high-flow conditions, as was achieved for inorganic sediments in Chapter 5.

REFERENCES

Acornley RM, Sear DA. 1999. Sediment transport and siltation of brown trout (*Salmo trutta* L.) spawning gravels in chalk streams. *Hydrological Processes* **13:** 447-458. DOI: 10.1002/(SICI)1099-1085(19990228)13:3<447::AID-HYP749>3.0.CO;2-G.

Aitchinson J. 1986. The statistical analysis of compositional data: Monographs on statistics and applied probability. *Chapman & Hall Ltd.*, London, pp. 416.

Alaoui G, Léger MN, Gagné J-P, Tremblay L. 2011. Assessment of estuarine sediment and sedimentary organic matter properties by infrared reflectance spectroscopy. *Chemical Geology* **286**: 290-300. DOI: 10.1016/j.chemgeo.2011.05.012.

Alvarez-Cobelas M, Angeler DG, Sánchez-Carrillo S, Almendros G. 2012. A worldwide view of organic carbon export from catchments. *Biogeochemistry* **107**: 275-293. DOI: 10.1007/s10533-010-9553-z.

Archbold M, Bruen M, Deakin J, Doody D, Flynn R, Kelly-Quinn M, Misstear B, Ofterdinger U. 2007. Contaminant movement and attenuation along pathways from the land surface to aquatic receptors – a review. STRIVE report (2007-WQ-CD-1-S1), EPA STRIVE programme 2007-2013, Environmental Protection Agency, Wexford, Ireland, pp. 35-52, 101-111.

Asselman NEM. 1999. Suspended sediment dynamics in a large drainage basin: the River Rhine. *Hydrological Processes* **13**: 1437-1450. DOI: 10.1002/(SICI)1099-1085(199907)13:10<1437::AID-HYP821>3.0.CO;2-J.

Ballantine DJ, Walling DE, Collins AL, Leeks GJL. 2008. The phosphorus content of fluvial suspended sediment in three lowland groundwater-dominated catchments. *Journal of Hydrology* **357**: 140-151. DOI: 10.1016/j.jhydrol.2008.05.011.

Ballantine DJ, Walling DE, Collins AL, Leeks GJL. 2009. The content and storage of phosphorus in fine-grained channel bed sediment in contrasting lowland agricultural catchments in the UK. *Geoderma* **151**: 141-149. DOI: 10.1016/j.geoderma.2009.03.021.

Barlow K, Nash D, Grayson R. 2004. Investigating phosphorus interactions with bed sediments in a fluvial environment using a recirculating flume and intact soil cores. *Water Research* **38**: 3420-3430. DOI: 10.1016/j.watres.2004.04.030.

Barnard J, McCulloch R, Meng X-L. 2000. Modelling covariance matrices in terms of standard deviations and correlations, with application to shrinkage. *Statistica Sinica* **10**: 1281-1311.

Barnhisel RI, Phillippe WR, Blevins RL. 1969. A simple X-ray fluorescence technique for the determination of iron and manganese in soils and concretion. *Soil Science Society of America Proceedings* **33**: 811-813.

Bilotta GS, Brazier RE, Haygarth PM. 2007. Processes affecting transfer of sediment and colloids with associated phosphorus from intensively farmed grasslands: erosion. *Hydrological Processes* **21**: 135-139. DOI: 10.1002/hyp.6600.

Bilotta GS, Brazier RE. 2008. Understanding the influence of suspended solids on water quality and aquatic biota. *Water Research* **42**: 2849-2861. DOI: 10.1016/j.watres.2008.03.018.

Bilotta GS, Krueger T, Brazier RE, Butler P, Freer J, Hawkins JMB, Haygarth PM, Macleod CJA, Quinton JN. 2010. Assessing catchment-scale erosion and yields of suspended solids form improved temperate grasslands. *Journal of Environmental Monitoring* **12**, 731-739. DOI: 10.1039/B921584K.

Bilotta GS, Burnside NG, Cheek L, Dunbar MJ, Grove MK, Harrison C, Joyce C, Peacock C, Davy-Bowker J. 2012. Developing environment-specific water quality guidelines for suspended particulate matter. *Water Research* **46**: 2324-2332. DOI: 10.1016/j.watres.2012.01.055.

Birgand F, Lefrançois J, Grimaldi C, Novince E, Gilliet N, Gascuel-odoux C. 2004. Mesure des flux et échantillonnage des matières en suspension sur de petits cours d'eau. *Ingénieries* **40**: 21–35.

Blake WH, Wallbrink PJ, Doerr SH, Shakesby RA, Humphreys GS. 2004. Sediment redistribution following wildfire in the Sydney region, Australia: a mineral magnetic tracing approach. In: Golosov V, Belayev V, Walling DE (eds). Sediment transfer through the fluvial system. *IAHS Publication* **288**: 52-59. ISBN 1-901502-67-8.

Blake WH, Wallbrink PJ, Wilkinson SN, Humphreys GS, Doerr SH, Shakesby RA, Tomkins KM. 2009. Deriving hillslope sediment budgets in wildfire-affected forests using fallout radionuclide tracers. *Geomorphology* **104**: 105-116. DOI: 10.1016/j.geomorph.2008.08.004.

Blake WH, Ficken KJ, Taylor P, Russell MA, Walling DE. 2012. Tracing crop-specific sediment sources in agricultural catchments. *Geomorphology* **139-140**: 322-329. DOI:10.1016/j.geomorph.2011.10.036.

Boardman J. 2013. The hydrological role of 'sunken lanes' with respect to sediment mobilization and delivery to watercourses with particular reference to West Sussex, southern England. *Journal of Soil and Sediments* **13**: 163-1644. DOI: 10.1007/s11368-013-0754-7.

Bourbonniere RA, Meyers PA. 1996. Sedimentary geolipid records of historical changes in the watersheds and productivities of lakes Ontario and Erie. *American Society of Limnology and Oceanography* **41**: 352-359.

Bowes MJ, House WA, Hodgkinson RA. 2003. Phosphorus dynamics along a river continuum. *Science of the Total Environment* **313**: 119–212. DOI: 10.1016/S0048-9697(03)00260-2.

Brewer MJ, Tetzlaff D, Malcolm IA, Soulsby C. 2011. Source distribution modelling for end-member mixing in hydrology. *Environmetrics* **22**: 921-932: DOI: 10.1002/env.1110.

Brimmer PJ, Griffiths PR. 1986. Effect of absorbing matrices on diffuse reflectance infrared spectra. *Analytical Chemistry* **58**: 2179-2184. DOI: 10.1021/ac00124a015.

Broadbent FE. 1953. The soil organic fraction. *Advances in Agronomy* **5**: 153-183.

Brouwer P. 2003. Theory of XRF: Getting acquainted with the principles. PANalytical BV, Almelo, Netherlands: 10-66.

Bruker. 2008. S4 Pioneer Spectrometry Solutions. Bruker AXS GmbH, Karlsruhe, Germany: 4-8.

Buchanan BP, Falbo K, Schneider RL, Easton ZM, Walter MT. 2012. Hydrological impact of roadside ditches in an agricultural watershed in central New York: implications for non-point source pollutant transport. *Hydrological Processes* **27**: 2422-2437. DOI: 10.1002/hyp.9305.

Bush RT, McInerney FA. 2013. Leaf wax *n*-alkane distributions in and across modern plants: Implications for paleoecology and chemotaxonomy. *Geochimica et Cosmochimica Acta* **117**: 161-179. DOI: 10.1016/j.gca.2013.04.016.

Cann JR, Winter CK. 1971. X-ray fluorescence analysis of suspended sediment in sea water. *Marine Geology* **11**: 33-37. DOI: 10.1016/0025-3227(71)90002-8.

Carlin BP, Louis TA. 1996. Bayes and empirical Bayes methods for data analysis. Chapman's & Hall, London, pp. 397. ISBN: 0-412-05611-9.

Cerro I, Sanchez-Perez JM, Ruiz-Romera E, Antigüedad I. 2014. Variability of particulate (SS, POC) and dissolved (DOC, NO_3) matter during storm events in the Alegria agricultural watershed. *Hydrological Processes* **28**: 2855-2867. DOI: 10.1002/hyp.9850.

Chikaraishi Y, Naraoka H. 2007. $\delta^{13}C$ and δD relationships among three *n*-alkyl compound classes (*n*-alkanoic acid, *n*-alkane and *n*-alkanol) of terrestrial higher plants. *Organic Geochemistry* **38**: 198-215. DOI: 10.1016/j.orggeochem.2006.10.003.

Christensen WF, Gunst RF. 2004. Measurement error models in chemical mass balance analysis of air quality data. *Atmospheric Environment* **38**: 733-744. DOI: 10.1016/j.atmosenv.2003.10.018.

Collins AL, Walling DE, Leeks GJL. 1997. Source type ascription for fluvial suspended sediment based on a quantitative composite fingerprinting technique. *Catena* **29**: 1-27. DOI: 10.1016/S0341-8162(96)00064-1.

Collins AL, Walling DE, Leeks GJL. 1998. Use of composite fingerprinting to determine the provenance of the contemporary suspended sediment load transported by rivers. *Earth Surface Processes and Landforms* **23**: 31-52. DOI: 10.1002/(SICI)1096-9837(199801)23:1<31::AID-ESP816>3.0.CO;2-Z.

Collins AL, Walling DE. 2004. Documenting catchment suspended sediment sources: problems, approaches and prospects. *Progress in Physical Geography* **28**: 159-196. DOI: 10.1191/0309133304pp409ra.

Collins AL, Walling DE. 2007. Sources of fine sediment recovered from the channel bed of lowland groundwater-fed catchments in the UK. *Geomorphology* **88**: 120-138. DOI: 10.1016/j.geomorph.2006.10.018.

Collins AL, Walling DE, Stroud RW, Robson M, Peet LM. 2010. Assessing damaged road verges as a suspended sediment source in the Hampshire Avon catchment, southern United Kingdom. *Hydrological Processes* **24**: 1106-1122. DOI: 10.1002/hyp.7573.

Collins AL, Zhang Y, Walling DE, Grenfell SE, Smith P, Grischeff J, Locke A, Sweetapple A, Brogden D. 2012. Quantifying fine-grained sediment sources in the River Axe catchment, southwest England: application of a Monte Carlo numerical modelling framework incorporating local and genetic algorithm optimisation. *Hydrological Processes* **26**: 1962-1983. DOI: 10.1002/hyp.8283.

Collins AL, Zhang YS, Hickinbotham R, Bailey G, Darlington S, Grenfell SE, Evans R, Blackwell M. 2013a. Contemporary fine-grained bed sediment sources across the River Wensum Demonstration Test Catchment, UK. *Hydrological Processes* **27**: 857-884. DOI: 10.1002/hyp.9654.

Collins AL, Zhang YS, Duethmann D, Walling DE, Black KS. 2013b. Using a novel tracing-tracking framework to source fine-grained sediment loss to watercourses at sub-catchment scale. *Hydrological Processes* **27**: 959-974. DOI: 10.1002/hyp.9652.

Collister JW, Rieley G, Stern B, Eglinton G, Fry B. 1994. Compound-specific $\delta^{13}C$ analyses of leaf lipids from plants with differing carbon dioxide metabolisms. *Organic geochemistry* **21**: 619-627.

Coombes, M., Curini, A., Howard-Keeble, A., Green, T. And Soar, P. 2007. River Wensum restoration strategy. Natural England research reports, Number 024.

Cooper RJ, Rawlins BG, Leze B, Krueger T, Hiscock KM. 2014a. Combining two filter paper-based analytical methods to monitor temporal variations in the geochemical properties of fluvial suspended particulate matter. *Hydrological Processes* **28**: 857-884. DOI: 10.1002/hyp.9945.

Cooper RJ, Krueger T, Hiscock KM, Rawlins BG. 2014b. Sensitivity of fluvial sediment source apportionment to mixing model assumptions: a Bayesian model comparison. *Water Resources Research* **50**: 9031-9047. DOI: 10.1002/2014WR016194.

Cooper RJ, Krueger T, Hiscock KM, Rawlins BG. 2015a. High-temporal resolution fluvial sediment source fingerprinting with uncertainty: a Bayesian approach. *Earth Surface Processes and Landforms* **40**: 78-92. DOI: 10.1002/esp.3621.

Cooper RJ, Pedentchouk N, Hiscock KM, Disdle P, Krueger T, Rawlins BG. 2015b. Apportioning sources of organic matter in streambed sediments: An integrated molecular and compound-specific stable isotope approach. *Science of the Total Environment* **520**: 187-197. DOI: 10.1016/j.scitotenv.2015.03.058.

Cooper RJ, Rawlins BG, Hiscock KM, Krueger T, Pedentchouk N. 2015c. Contrasting controls on the phosphorus content of suspended particulate matter under baseflow and storm event conditions in agricultural headwater streams. Under review at *Science of the Total Environment*.

Cordell D, Drangert J-O, White S. 2009. The story of phosphorus: Global food security and food for thought. *Global Environmental Change* **19**: 292-305. DOI: 10.1016/j.gloenvcha.2008.10.009.

D'Haen K, Verstraeten G, Dusar B, Degryse P, Haex J, Waelkens M. 2012. Unravelling changing sediment sources in a Mediterranean mountain catchment: a Bayesian fingerprinting approach. *Hydrological Processes* **27**: 896-910. DOI: 10.1002/hyp.9399.

D'Haen K, Dusar B, Verstraeten G, Degryse P, De Brue H. 2013. A sediment fingerprinting approach to understand the geomorphic coupling in an eastern Mediterranean mountainous river catchment. *Geomorphology* **197**: 64-75. DOI: 10.1016/j.geomorph.2013.04.038.

Darimont CT, Paquet PC, Relmchen TE. 2009. Landscape heterogeneity and marine subsidy generate extensive intrapopulation niche diversity in a large terrestrial vertebrate. *Journal of Animal Ecology* **78**: 126-133. DOI: 10.1111/j.1365-2656.2008.01473.x.

Dawson JJC, Adhikari YR, Soulsby C, Stutter MI. 2012. The biogeochemical reactivity of suspended particulate matter at nested sites in the Dee basin, NE Scotland. *Science of the Total Environment* **434**: 159-170. DOI: 10.1016/j.scitotenv.2011.08.048.

Deasy C, Brazier RE, Heathwaite AL, Hodgkinson R. 2009a. Pathways of runoff and sediment transfer in small agricultural catchments. *Hydrological Processes* **23**: 1349-1358. DOI: 10.1002/hyp.7257.

Deasy C, Quinton JN, Silgram M, Bailey AP, Jackson B, Stevens CJ. 2009b. Mitigation options for sediment and phosphorus loss from winter-sown arable crops. *Journal of Environmental Quality* **38**: 2121-2130. DOI: 10.2134/jeq2009.0028.

Deasy C, Quinton JN, Silgram M, Bailey AP, Jackson B, Stevens CJ. 2010. Contributing understanding of mitigation options for phosphorus and sediment to a review of the efficacy of contemporary agricultural stewardship measures. *Agricultural Systems* **103**: 105-109. DOI: 10.1016/j.agsy.2009.10.003.

Defra. 2011. Catchment Sensitive Farming. Department for Environment Food and Rural Affairs. http://www.defra.gov.uk/food-farm/land-manage/nitrates-watercourses/csf/. Last Accessed 1/12/11.

Demars BOL, Harper DM, Pitt J-A, Slaughter R. 2005. Impact of phosphorus control measures on in-river phosphorus retention associated with point source pollution. *Hydrology and Earth System Sciences Discussion* **2**: 37-72.

Demars BOL, Harper DM. 2005. Water column and sediment phosphorus in a calcareous lowland river and their differential response to point source control measures. *Water Air and Soil Pollution* **167**: 273–293. DOI: 10.1007/s11270-005-8862-7.

Demars BOL. 2008. Whole stream phosphorus cycling: testing methods to assess the effect of saturation of sorption capacity on nutrient uptake length measurements. *Water Research* **42**: 2507-2516. DOI: 10.1016/j.watres.2008.02.010.

Devereux OH, Prestegaard KL, Needelman BA, Gellis AC. 2010. Suspended-sediment sources in an urban watershed, northeast branch Anacostia River, Maryland. *Hydrological Processes* **24**: 1391-1403. DOI: 10.1002/hyp.7604.

Diefendorf AF, Freeman KH, Wing SL, Graham HV. 2011. Production of *n*-alkyl lipids in living plants and implications for the geologic past. *Geochimica et Cosmochimica Acta* **75**: 7478-7485. DOI: 10.1016/j.gca.2011.09.028.

Dilks DW, Canale RP, Meier PG. 1992. Development of Bayesian Monte Carlo techniques for water quality model uncertainty. *Ecological Modelling* **62**: 149-162.

Dismukes GC, Willigen RT. 2006. Manganese: The oxygen-evolving complex and models. *Encyclopaedia of Inorganic Chemistry*. DOI: 10.1002/0470862106.ia128.

Dolcater DL, Syers JK, Jackson ML. 1970. Titanium as free oxide and substituted forms in kaolinites and other soil minerals. *Clays and Clay Minerals* **18**: 71-79.

Dorioz JM, Cassell EA, Orand A, Eisenman KG. 1998. Phosphorus storage, transport and export dynamics in the Foron River watershed. *Hydrological Processes* **12**: 285-309. DOI: 10.1002/(SICI)1099-1085(199802)12:2<285::AID-HYP577>3.0.CO;2-H.

Doucett RR, Marks JC, Blinn DW, Caron M, Hungate BA. 2007. Measuring terrestrial subsides to aquatic food webs using stable isotopes of hydrogen. *Ecology* **88**: 1587-1592. DOI: 10.1890/06-1184.

Dougherty WJ, Fleming NK, Cox JW, Chittleborough DJ. 2004. Phosphorus transfer in surface runoff from intensive pasture systems at various scales: A review. *Journal of Environmental Quality* **33**: 1973-1988. DOI: 10.2134/jeq2004.1973.

Dutton C, Anisfeld SC, Ernstberger H. 2013. A novel sediment fingerprinting method using filtration: application to the Mara River, East Africa. *Journal of Soils and Sediments* **13**: 1708-1723. DOI: 10.1007/s11368-013-0725-z.

Edwards AC, Withers PJA. 1998. Soil phosphorus management and water quality: a UK perspective. *Soil Use and Management* **14**:124-130. DOI: 10.1111/j.1475-2743.1998.tb00630.x.

Egozcue J, Pawlowsky-Glahn V, Mateu-Figueras G, Barceló-Vidal C. 2003. Isometric log ratio transformations for compositional data analysis. *Mathematical Geology* **35**: 279-300. DOI: 10.1023/A:1023818214614.

Eley Y, Dawson L, Black S, Andrews J, Pedentchouk N. 2014. Understanding $^{2}H/^{1}H$ systematics of leaf wax *n*-alkanes in coastal plants at Stiffkey saltmarsh, Norfolk, UK. *Geochimica et Cosmochimica Acta* **128**: 13-28. DOI: 10.1016/j.gca.2013.11.045.

Ensign SH, Doyle MW. 2006. Nutrient spiralling in streams and river networks. *Journal of Geophysical Research* **111**: 1-13. DOI: 10.1029/2005JG000114.

Environment Agency. 2009. River Basin Management Plan, Anglian River Basin District. The Environment Agency, Bristol, UK. pp. 68.

Enzweiler J, Vendemiatto MA. 2004. Analysis of sediments and soils by X-ray fluorescence spectrometry using matrix corrections based on fundamental parameters. *Geostandards and Geoanalytical Research* **28**: 103-112. DOI: 10.1111/j.1751-908X.2004.tb01046.x.

Erhardt EB, Bedrick EJ. 2013. A Bayesian framework for stable isotope mixing models. *Environmental and Ecological Statistics* **20**: 377-397. DOI: 10.1007/s10651-012-0224-1.

Eusterhues K, Rumpel C, Kogel-Knabner I. 2005. Organo-mineral associations in sandy acid forest soils: importance of specific surface area, iron oxides and micropores. *European Journal of Soil Science* **56**: 753-763. DOI: 10.111/j.1365-2389.2005.00710.x.

Evans DJ, Johnes PJ, Lawrence DS. 2004. Physico-chemical controls on phosphorus cycling in two lowland streams. Part 2 – The sediment phase. *Science of the Total Environment* **329**: 165-182. DOI: 10.1016/j.scitotenv.2004.02.023.

Evrard O, Navratil O, Ayrault S, Ahmadi M, Némery J, Legout C, Lefèvre I, Poirel A, Bonté P, Esteves M. 2011. Combining suspended sediment monitoring and fingerprinting to determine the spatial origin of fine sediment in a mountainous river catchment. *Earth Surface Processes and Landforms* **36**: 1072-1089. DOI: 10.1002/esp.2133.

Evrard O, Poulenard J, Némery J, Ayrault S, Gratiot N, Duvert C, Prat C, Lefèvre I, Bonté P, Esteves M. 2013. Tracing sediment sources in a tropical highland catchment of central Mexico by using conventional and alterative fingerprinting methods. *Hydrological Processes* **27**: 911-922. DOI: 10.1002/hyp.9421.

Fan X, Shi C, Shao W, Zhou Y. 2013. The suspended sediment dynamics in the Inner-Mongolia reaches of the upper Yellow River. *Catena* **109**: 72-82. DOI: 10.1016/j.catena.2013.05.010.

Farquhar GD, Ehleringer JR, Hubick KT. 1989. Carbon isotope discrimination and photosynthesis. *Annual Review of Plant Physiology and Plant Molecular Biology* **40**: 503-537.

Fox JF, Papanicolaou AN. 2007. The use of carbon and nitrogen isotopes to study watershed erosion processes. *JAWRA Journal of the American Water Resources Association* **43**: 1047-1064. DOI: 10.1111/j.1752-1688.2007.00087.x.

Fox JF, Papanicolaou AN. 2008. An un-mixing model to study watershed erosion processes. *Advances in Water Resources* **31**: 96-108. DOI:10.1016/j.advwatres.2007.06.008.

Fox JF, Davis CM, Martin DK. 2010. Sediment source assessment in a lowland watershed using nitrogen stable isotopes. *Journal of the American Water Resources Association* **46**: 1192:1204. DOI: 10.1111/j.1752-1688.2010.00485.x.

Fox J, Weisberg S. 2013. R Package: *'car'*: Companion to applied regression.

Franco-Trecu V, Drago M, Riet-Sapriz FG, Parnell A, Frau R, Inchausti P. 2013. Bias in diet determination: incorporating traditional methods in Bayesian mixing models. *PLoS ONE* **8**: e80019. DOI:10.1371/journal.pone.0080019.

Franz C, Makeschin F, Weiß H, Lorz C. 2014. Sediments in urban river basins: Identification of sediment sources within the Lago Paranoá catchment, Brasilia DF, Brazil – using the fingerprint approach. *Science of the Total Environment* **466-467**: 513-523. DOI: 10.1016/j.scitotenv.2013.07.056.

Frey SK, Rudolph DL, Conant Jr B. 2012. Bromide and chloride tracer movement in macro-porous tile-drained agricultural soil during an annual climatic cycle. *Journal of Hydrology* **460-461**: 77-89. DOI: 10.1016/j.jhydrol.2012.06.041.

Fryirs K, Gore D. 2013. Sediment tracing in the upper Hunter catchment using elemental and mineralogical compositions: Implications for catchment-scale suspended sediment (dis)connectivity and management. *Geomorphology* **193**: 112-121. DOI: 10.1016/j.geomorph.2013.04.010.

Fu Y, Tang C, Li J, Zhao Y, Zhong W, Zeng X. 2014. Sources and transport of organic carbon from the Dongjiang River to the Humen outlet of the Pearl River, southern China. *Journal of Geographical Sciences* **24**: 143-158. DOI: 10.1007/s1142-014-1078-2.

Gellis AC, Noe GB. 2013. Sediment source analysis in the Linganore Creek watershed, Maryland, USA, using the sediment fingerprinting approach: 2008 to 2010. *Journal of Soils and Sediments* **13**: 1735-1753. DOI: 10.1007/s11368-013-0771-6.

Gibbs MM. 2008. Identifying source soils in contemporary estuarine sediments: A new compound-specific isotope method. *Estuaries and Coasts* **31**: 344-359. DOI: 10.1007/s12237-007-9012-9.

Gillain S. 2005. Diel turbidity fluctuations in streams in Gwinnett County, Georgia. Proceedings of the 2005 Georgia Water Resources Conference, April 25-27 2005, University of Georgia.

Gimbert LJ, Worsfold P, Haygarth PM. 2007. Processes affecting transfer of sediment and colloids, with associated phosphorus, from intensively farmed grasslands: colloid and sediment characterisation methods. *Hydrological Processes* **21**: 275-279: DOI: 10.1002/hyp.6599.

Granger SJ, Bol R, Butler PJ, Haygarth PM, Naden P, Old G, Owens PN, Smith BPG. 2007. Processes affecting transfer of sediment and colloids, with associated phosphorus, from intensively farmed grasslands: tracing sediment and organic matter. *Hydrological Processes* **21**: 417-422. DOI: 10.1002/hyp.6597.

Grieve N, Clarke S, Caswell B. 2002. Macrophyte Survey of the River Wensum SAC. Centre for Aquatic Plant Management, English Nature.

Groemping U. 2013. R Package: *'relaimpo'*: relative importance of regressors in linear models.

Gruszowski KE, Foster IDL, Lees JA, Charlesworth SM. 2003. Sediment sources and transport pathways in a rural catchment, Herefordshire, UK. *Hydrological Processes* **17**: 2665-2681. DOI: 10.1002/hyp.1296.

Guzmán G, Quinton JN, Nearing MA, Mabit L, Gómez JA. 2013. Sediment tracers in water erosion studies: current approaches and challenges. *Journal of Soils and Sediments* **13**, 816-833. DOI: 10.1007/s11368-013-0659-5.

Haddadchi A, Nosrati K, Ahmadi F. 2014. Differences between the source contribution of bed material and suspended sediments in a mountainous agricultural catchment of Western Iran. *Catena* **116**: 105-113. DOI: 10.1016/j.catena.2013.12.011.

Halliday SJ, Wade AJ, Skeffington RA, Neal C, Reynolds B, Rowland P, Neal M, Norris D. 2012. An analysis of long-term trends, seasonality and short-term dynamics in water quality data from Plynlimon, Wales. *Science of the Total Environment* **434**: 186-200. DOI: 10.1016/j.scitotenv.2011.10.052.

Halliday SJ, Skeffington RA, Bowes MJ, Gozzard E, Newman JR, Loewenthal M, Palmer-Felgate EJ, Jarvie HP, Wade AJ. 2014. The water quality of the River Enborne, UK: Observations form high-frequency monitoring in a rural, lowland river system. *Water* **6**: 150-180: DOI: 10.3390/w6010150.

Hancock GJ, Revill AT. 2013. Erosion source discrimination in a rural Australian catchment using compound-specific isotope analysis (CSIA). *Hydrological Processes* **27**: 923-932. DOI: 10.1002/hyp.9466.

Hartikainen H, Rasa K, Withers PJA. 2010. Phosphorus exchange properties of European soils and sediments derived from them. *European Journal of Soil Science* **6**: 1033-1042. DOI: 10.1111/j.1365-2389.2010.01295.x.

Harvey GL, Henshaw AJ, Moorhouse TP, Cliffod NJ, Holah H, Grey J, Macdonald DW. 2014. Invasive crayfish as drivers of fine sediment dynamics in rivers: field and laboratory evidence. *Earth Surface Processes and Landforms* **39**: 259-271. DOI: 10.1002/esp.3486.

Haygarth PM, Jarvis SC. 1999. Transfer of phosphorus from agricultural soil. *Advances in Agronomy* **66**: 195-249. DOI: 10.1016/S0065-2113(08)60428-9.

Haygarth PM, Bilotta GS, Bol R, Brazier RE, Butler PJ, Freer J, Gimbert LJ, Granger SJ, Krueger T, Macleod CJA, Naden P, Old G, Quinton JN, Smith B, Worsfold P. 2006. Processes affecting transfer of sediment and colloids, with associated phosphorus, from intensively farmed grasslands: an overview of key issues. *Hydrological Processes* **20**: 4407-4413. DOI: 10.1002/hyp.6598.

He ZL, Wilson MJ, Campbell CO, Edwards AC, Chapman SJ. 1995. Distribution of phosphorus in soil aggregate fractions and its significance with regard to phosphorus transport in agricultural runoff. *Water, Air and Soil Pollution* **83**: 69-84.

Heckrath G, Bechmann M, Ekholm P, Ulén B, Djodjic F, Andersen HE. 2008. Review of indexing tools for identifying high risk areas of phosphorus loss in Nordic catchments. *Journal of Hydrology* **349**: 68-87. DOI: 10.1016/j.jhydrol.2007.10.039.

Helliker BR, Ehleringer JR. 2002. Grass blades as tree rings: environmentally induced changes in the oxygen isotope ratio of cellulose along the length of grass blades. *New Phytology* **155**: 417–24. DOI: 10.1046/j.1469-8137.2002.00480.x.

Hens M, Merckx R. 2002. The role of colloidal particles in the speciation and analysis of "dissolved" phosphorus. *Water Research* **36**: 1483-1492. DOI: 10.1016/S0043-1354(01)00349-9.

Heywood MJT, Walling DE. 2003. Suspended sediment fluxes in chalk streams in the Hampshire Avon catchment, UK. *Hydrobiologia* **494**: 111-117. DOI: 10.1023/A:1025445711343.

Hilton J, O'Hare M, Bowes MJ, Jones JI. 2006. How green is my river? A new paradigm of eutrophication in rivers. *Science of the Total Environment* **365:** 66-83. DOI:10.1016/j.scitotenv.2006.02.055.

Hindell MA, Lydersen C, Hop H, Kovacs KM. 2013. Pre-partum diet of adult female bearded seals in years of contrasting ice conditions. *PLoS ONE* **7**: e38307. DOI: 10.1371/journal.pone.0038307.

Hiscock KM. 1993. The influence of pre-Devensian glacial deposits on the hydrogeochemistry of the chalk aquifer system of north Norfolk, UK. *Journal of Hydrology* **144**: 335-369. DOI: 10.1016/0022-1694(93)90179-D.

Hiscock KM, Dennis PF, Saynor PR, Thomas MO. 1996. Hydrochemical and stable isotope evidence for the extent and nature of the effective Chalk aquifer of north Norfolk, UK. *Journal of Hydrology* **180**: 79-107. DOI: 10.1016/0022-1694(95)02895-1.

Hiscock KM, Lister DH, Boar RR, Green FML. 2001. An integrated assessment of long-term changes in the hydrology of three lowland rivers in eastern England. *Journal of Environmental Management* **61**: 195-214. DOI: doi:10.1006/jema.2000.0405

Hopkins JB III, Ferguson JM. 2012. Estimating the diets of animals using stable isotopes and a comprehensive Bayesian mixing model. *PLoS ONE* **7**:e28478. DOI:10.1371/journal.pone.0028478.

Horowitz AJ, Elrick KA. 1987. The relation of stream sediment surface area, grain size and composition to trace element chemistry. *Applied Geochemistry* **2**: 437-451.

Horowitz AJ. 2008. Determining annual suspended sediment and sediment-associated trace elements and nutrient fluxes. *Science of the Total Environment* **400**: 315-343. DOI: 10.1016/j.scitotenv.2008.04.022.

Hou J, D'Andrea WJ, MacDonald D, Huang Y. 2007. Hydrogen isotopic variability in leaf waxes among terrestrial and aquatic plants around Blood Pond, Massachusetts (USA). *Organic Geochemistry* **38**: 977:984. DOI:10.1016/j.orggeochem.2006.12.009.

House WA, Denison FH, Armitage PD. 1995. Comparison of the uptake of inorganic phosphorus to a suspended and stream bed-sediment. *Water Research* **29**: 767-779. DOI: 10.1016/0043-1354(94)00237-2.

House WA, Jickells TD, Edwards AC, Praska KE, Denison FH. 1998. Reactions of phosphorus with sediments in fresh and marine waters. *Soil Use Management* **14**: 139-146. DOI: 10.1111/j.1475-2743.1998.tb00632.x.

House WA, Denison FH. 2002. Total phosphorus content of river sediments in relationship to calcium, iron and organic matter concentrations. *Science of the Total Environment* **282-283**: 341-351. DOI: 10.1016/S0048-9697(01)00923-8.

House WA. 2003. Geochemical cycling of phosphorus in rivers. *Applied Geochemistry* **18**: 739-748. DOI: 10.1016/S0883-2927(02)00158-0.

Howard PJA, Howard DM. 1990. Use of organic carbon and loss-on ignition to estimate soil organic matter in different soil types and horizons. *Biology and Fertility of Soils* **9**: 306-310.

Huisman NLH, Karthikeyan KG. 2012. Using radiometric tools to track sediment and phosphorus movement in an agricultural watershed. *Journal of Hydrology* **450-451**: 219-229. DOI: 10.1016/j.jhydrol.2012.05.007.

Jarvie HP, Jürgens MD, Williams RJ, Neal C, Davis JJL, Barrett C, White J. 2005. Role of river bed sediments as sources and sinks of phosphorus across two major eutrophic UK river basins: the Hampshire Avon and Herefordshire Wye. *Journal of Hydrology* **304**: 51-74. DOI: 10.1016/j.jhydrol.2004.10.002.

Jarvie HP, Neal C, Juergens MD, Sutton EJ, Neal M, Wickham HD, Hill LK, Harman SA, Davis JJL, Warwick A, Barrett C, Griffiths J, Binley A, Swannack N, McIntyre N. 2006. Within-river nutrient processing in Chalk streams: The Pang and Lambourn, UK. *Journal of Hydrology* **330**: 101–125. DOI: 10.1016/j.jhydrol.2006.04.014.

Jarvie HP, Haygarth PM, Neal C, Butler P, Smith B, Naden PS, Joynes A, Neal M, Wickham H, Armstrong L, Harman S, Palmer-Felgate EJ. 2008. Stream water chemistry and quality along an upland-lowland rural land-use continuum, south west England. *Journal of Hydrology* **350**: 215-231. DOI: 10.1016/j.jhydrol.2007.10.040.

Jeng W-L. 2006. Higher plant *n*-alkane average chain length as an indicator of petrogenic hydrocarbon contamination in marine sediments. *Marine Chemistry* **102**: 242-251. DOI: 10.1016/j.marchem.2006.05.001.

Jensen HS, Kristensen P, Jeppesen E, Skytthe A. 1992. Iron:phosphorus ratio in surface sediments as an indicator of phosphate release from aerobic sediments in shallow lakes. *Hydrobiologia* **235-236**: 731-743.

Jobbágy EG, Jackson RB. 2000. The vertical distribution of soil organic carbon and its relation to climate and vegetation. *Ecological Applications* **10**: 423-436. DOI: 10.1890/1051-0761(2000)010.

Johnes PJ, Hodgkinson RA. 1998. Phosphorus loss from agricultural catchments: pathways and implications for management. *Soil Use and Management* **14**: 175-185. DOI: 10.1111/j.1475-2743.1998.tb00637.x.

Johnson CC, Breward N, Ander EL, Ault L. 2005. G-BASE: baseline geochemical mapping of Great Britain and Northern Ireland. *Geochemistry: Exploration, Environment, Analysis* **5**: 347-357. DOI: 10.1144/1467-7873/05-070.

Jordan P, Arnscheidt A, McGrogan H, McCormick, S. 2007. Characterising phosphorus transfers in rural catchments using a continuous bank-side analyser. *Hydrology and Earth System Science* **11**: 372–381. DOI: 10.5194/hess-11-372-2007.

Kaiser K, Guggenberger G. 2003. Mineral surfaces and soil organic matter. *European Journal of Soil Science* **54**: 219-236. DOI: 10.1046/j.1365-2389.2003.00544.x.

Kim JK, Onda Y, Yang D-Y, Kim MS. 2013. Temporal variations of reservoir sediment sources in a small mountainous catchment in Korea. *Earth Surface Processes and Landforms* **38**: 1380-1392. DOI: 10.1002/esp.3379.

Koiter AJ, Owens PN, Petticrew EL, Lobb DA. 2013. The behavioural characteristics of sediment properties and their implications for sediment fingerprinting as an approach for identifying sediment sources in river basins. *Earth-Science Reviews* **125**: 24-42. DOI: 10.1016/j.earscirev.2013.05.009.

Krueger T, Quinton JN, Freer J, Macleod CJA, Bilotta GS, Brazier RE, Butler P, Haygarth PM. 2009. Uncertainties in data and models to describe event dynamics of agricultural sediment and phosphorus transfer. *Journal of Environmental Quality* **38**: 1137-1148. DOI: 10.2134/jeq2008.0179.

Krueger T, Quinton JN, Freer J, Macleod CJA, Bilotta GS, Brazier RE, Hawkins JMB, Haygarth PM. 2012. Comparing empirical models for sediment and phosphorus transfer from soils to water at field and catchment scale under data uncertainty. *European Journal of Soil Science* **63**: 211-223. DOI: 10.1111/j.1365-2389.2011.01419.x.

Kronvang B, Laubel A, Grant R. 1997. Suspended sediment and particulate phosphorus transport and delivery pathways in an arable catchment, Gelbaek Stream, Denmark. *Hydrological Processes* **11**: 627-642. DOI: 10.1002/(SICI)1099-1085(199705)11:6<627::AID-HYP481>3.0.CO;2-E.

Laceby JP, Olley J, Pietsch TJ, Sheldon F, Bunn SE. 2014. Identifying subsoil sediment sources with carbon and nitrogen stable isotope ratios. *Hydrological Processes*. DOI: 10.1002/hyp.10311.

Laceby JP, Olley J. 2014. An examination of geochemical modelling approaches to tracing sediment sources incorporating distribution mixing and elemental correlations. *Hydrological Processes*. DOI: 10.1002/hyp.10287.

Land M, Öhlander B, Ingri J, Thunberg J. 1999. Solid speciation and fractionation of rare earth elements in a spodosol profile from northern Sweden as revealed by sequential extraction. *Chemical Geology* **160**: 121-138. DOI: 10.1016/S0009-2541(99)00064-9.

Laubel A, Jacobsen OH, Kronvang B, Grant R, Andersen HE. 1999. Subsurface drainage loss of particles and phosphorus from field plot experiments and a tile-drained catchment. *Journal of Environmental Quality* **28**: 576–584. DOI: 10.2134/jeq1999.00472425002800020023x.

Lefrançois J, Grimaldi C, Gascuel-Odoux C, Gilliet N. 2007. Suspended sediment and discharge relationships to identify bank degradation as a main sediment source on small agricultural catchments. *Hydrological Processes* **21**: 2923-2933. DOI: 10.1002/hyp.6509.

Legout C, Poulenard J, Nemery J, Navratil O, Grangeon T, Evrard O, Esteves M. 2013. Quantifying suspended sediment sources during runoff events in headwater catchments using spectrocolorimetry. *Journal of Soils and Sediments* **13**: 1478-1492. DOI 10.1007/s11368-013-0728-9.

Lewis MA. 2011. Borehole drilling and sampling in the Wensum Demonstration Test Catchment. British Geological Survey Commissioned Report, CR/11/162, 38pp, National Environment Research Council, Nottingham, UK.

Lingwall JW, Christensen WF, Shane Reese C. 2008. Dirichlet based Bayesian multivariate receptor modelling. *Environmetrics* **19**: 618-629. DOI: 10.1002/env.902.

Lockheart MJ, Van Bergen PF, Evershed RP. 1997. Variations in the stable carbon isotope compositions of individual lipids from the leaves of modern angiosperms: implications for the study of higher land plant-derived sedimentary organic matter. *Organic Geochemistry* **26**: 137-153. DOI: 10.1016/S0146-6380(96)00135-0.

Loperfido JV, Just CL, Papanicolaou AN, Schnoor JL. 2010. In situ sensing to understand diel turbidity cycles, suspended solids, and nutrient transport in Clear Creek, Iowa. *Water Resources Research* **46**: W06525. DOI: 10.1029/2009WR008293.

Loveland P, Webb J. 2003. Is there a critical level of organic matter in the agricultural soils of temperate regions: a review. *Soil & Tillage Research* **70**: 1–18. DOI: 10.1016/S0167-1987(02)00139-3.

Lunn DJ, Thomas A, Best N, Spiegelhalter D. 2000. WinBUGS – A Bayesian modelling framework: Concepts, structure, and extensibility. *Statistics and Computing* **10**: 325-337. DOI: 10.1023/A:1008929526011.

Marshall JD, Brooks JR, Lajtha K. 2007. Sources of variation in the stable isotopic composition of plants. *In* Stable Isotopes in Ecology and Environmental Science (R. Michener and K. Lajtha, Eds.), Blackwell Publishing, pp. 22-60.

Martens H, Nielsen JP, Engelsen SB. 2003. Light scatting and light absorbance separated by extended multiplicative signal correction. Application to near-infrared transmission analysis of powder mixtures. *Analytical Chemistry* **75**: 394-404. DOI: 10.1021/ac020194w.

Martínez-Carreras N, Udelhoven T, Krein A, Gallart F, Iffly JF, Ziebel J, Hoffmann L, Pfister L, Walling DE. 2010a. The use of sediment colour measured by diffuse reflectance spectrometry to determine sediment sources: Application to the Attert River catchment (Luxembourg). *Journal of Hydrology* **382**: 49-63. DOI: 10.1016/j.jhydrol.2009.12.017.

Martínez-Carreras N, Krein A, Udelhoven T, Gallart F, Iffly JF, Hoffmann L, Pfister L, Walling DE. 2010b. A rapid spectral-reflectance-based fingerprinting approach for documenting suspended sediment sources

during storm runoff events. *Journal of Soils and Sediments* **10**: 400-413. DOI: 10.1007/s11368-009-0162-1.

Martínez-Carreras N, Krein A, Gallart F, Iffly JF, Hissler C, Pfister L, Hoffmann L, Owens PN. 2012. The influence of sediment sources and hydrologic events on the nutrient and metal content of fine-grained sediments (Attert River basin, Luxembourg). *Water, Air and Soil Pollution* **223**: 5685-5705. DOI: 10.1007/s11270-012-1307-1.

Marttila H, Saarinen T, Celebi A, Kløve B. 2013. Transport of particle-associated elements in two agriculture-dominated boreal river systems. *Science of the Total Environment* **461-462**: 693-705. DOI: 10.1016/j.scitotenv.2013.05.073.

Maruyama Y, Ogawa K, Okada T, Kato M. 2008. Laboratory experiments of particle size effect in X-ray fluorescence and implications to remote X-ray spectrometry of lunar regolith surface. *Earth, Planets and Space* **60**: 293-297. DOI: 10.1186/BF03352794.

Masserschmidt I, Cuelbas CJ, Poppi RJ, De Andrade JC, De Abreu CA, Davanzo CU. 1999. Determination of organic matter in soils by FTIR/Diffuse reflectance and multivariate calibration. *Journal of Chemometrics* **13**: 265-273. DOI: 10.1002/(SICI)1099-128X(199905/08)13:3/4<265::AID-CEM552>3.3.CO;2-5.

Massoudieh A, Gellis A, Banks WS, Wieczorek ME. 2012. Suspended sediment source apportionment in Chesapeake Bay watershed using Bayesian chemical mass balance receptor modelling. *Hydrological Processes* **27**: 3363-3374. DOI: 10.1002/hyp.9429.

McConnachie JL, Petticrew EL. 2006. Tracing organic matter sources in riverine suspended sediments: Implications for fine sediment transfers. *Geomorphology* **79**: 13-26. DOI:10.1016/j.geomorph.2005.09.011.

McDuffee KE, Eglinton TI, Sessions AL, Sylva S, Wagner T, Hayes JM. 2004. Rapid analysis of ^{13}C in plant-wax *n*-alkanes for reconstruction of terrestrial vegetation signals from aquatic sediments. *Geochemistry, Geophysics, Geosystems* **5** (10) Q10004. DOI:10.1029/2004GC000772.

McKeague JA, Day JH. 1966. Dithionite- and oxalate-extractable Fe and Al as aids in differentiating various classes of soils. *Canadian Journal of Soil Science* **46**: 13-22. DOI: 10.4141/cjss66-003.

Meteorological Office. 2013. UK climate averages: Reepham 1981-2010. Meteorological Office, Exeter. Online: http://www.metoffice.gov.uk/public/weather/climate/#?tab=climateTables.

Mevik B-J, Wehrens R, Liland KH. 2011. R Package: *'pls'*: Partial Least Squares and Principal Component regression.

Meyers PA. 1997. Organic geochemical proxies of paleoceanographic, paleolimnologic, and paleoclimatic processes. *Organic Geochemistry* **27**: 213-250. DOI: 10.1016/S0146-6380(97)00049-1.

Minasny B, Tranter G, McBratney AB, Brough DM, Murphy BW. 2009. Regional transferability of mid-infrared diffuse reflectance spectroscopic prediction for soil chemical properties. *Geoderma* **153**: 155-162. DOI: 10.1016/j.geoderma.2009.07.021.

Moore JW, Semmens BX. 2008. Incorporating uncertainty and prior information into stable isotope mixing models. *Ecology Letters* **11**: 470-480. DOI: 10.1111/j.1461-0248.2008.01163.x.

Motha JA, Wallbrink PJ, Hairsine PB, Grayson RB. 2002. Tracer properties of eroded sediment and source materials. *Hydrological Processes* **16**: 1983-2000. DOI: 10.1002/hyp.397.

Motha JA, Wallbrink PJ, Hairsine PB, Grayson RB. 2003. Determining the sources of suspended sediment in a forested catchment in southeastern Australia. *Water Resources Research* **39:** 1-14. DOI: 10.1029/2001WR000794.

Motha JA, Wallbrink PJ, Hairsine PB, Grayson RB. 2004. Unsealed roads as suspended sediment sources in an agricultural catchment in south-eastern Australia. *Journal of Hydrology* **286**: 1-18. DOI: 10.1016/j.hydrol.2003.07.006.

Mukundan R, Walling DE, Gellis AC, Slattery MC, Radcliffe DE. 2012. Sediment source fingerprinting: transforming from a research tool to a management tool. *Journal of the American Water Resources Association* **48**: 1241-1257. DOI: 10.1111/j.1752-1688.2012.00685.x.

Mulholland PJ, Marzolf ER, Webster JR, Hart DR, Hendricks SP. 1997. Evidence that hyporheic zones increase heterotrophic metabolism and phosphorus uptake in forest streams. *Limnology and Oceanography* **42**: 443–51.

Nakagawa S, Schielzeth H. 2013. A general and simple method for obtaining R2 from generalized linear mixed-effects models. Methods in Ecology and Evolution **4**: 133-142. DOI: 10.1111/j.2041-210x.2012.00261.x

Namduri H, Nasrazadani S. 2008. Quantitative analysis of iron oxides using Fourier transform infrared spectrophotometry. *Corrosion Science* **50**: 2493-2497. DOI: 10.1016/j.corsci.2008.06.034.

Navratil O, Evrard O, Esteves M, Legout C, Ayrault S, Némery J, Mate-Marin A, Ahmadi M, Lefèvre I, Poirel A, Bonté P. 2012. Temporal variability of suspended sediment sources in an alpine catchment combining river/rainfall monitoring and sediment fingerprinting. *Earth Surface Processes and Landforms* **37**: 828-846. DOI: 10.1002/esp.3201.

Némery J, Mano V, CoynelA, Etcheber H, Moatar F, Meybeck M, Belleudy P, Poirel A. 2013. Carbon and suspended sediment transport in an impounded alpine river (Isère, France). *Hydrological Processes* **27**: 2498-2508. DOI: 10.1002/hyp.9387.

Nimick DA, Cleasby, TE, McCleskey RB. 2005. Seasonality of diel cycles of dissolved trace-metal concentrations in a Rocky Mountain stream. *Environmental Geology* **47**: 603-614. DOI: 10.1007/s00254-004-1178-x.

Norrish K, Hutton JT. 1969. An accurate X-ray spectrographic method for the analysis of a wide range of geological samples. *Geochimica et Cosmochimica Acta* **33**: 431-453. DOI: 10.1016/0016-7037(69)90126-4.

Nosrati K, Govers G, Semmens BX, Ward EJ. 2014. A mixing model to incorporate uncertainty in sediment fingerprinting. *Geoderma* **217-218**: 173-180. DOI: 10.1016/j.geoderma.2013.12.002.

O'Leary MH. 1988. Carbon isotopes in photosynthesis. *BioScience* **38**: 328-336.

Oeurng C, Sauvage S, Sánchez-Pérez JM. 2010. Dynamics of suspended sediment transport and yield in a large agricultural catchment, southwest France. *Earth Surface Processes and Landforms* **35**: 1289-1301. DOI: 10.1002/esp.1971.

Oeurng C, Sauvage S, Coynel A, Maneux E, Etcheber H, Sánchez-Péez J-M. 2011. Fluvial transport of suspended sediments and organic matter during flood events in a large agricultural catchment in southwest France. *Hydrological Processes* **25**: 2365-2378. DOI: 10.1002/hyp.7999.

Ogden LJE, Hobson KA, Lank DB, Bittman S. 2005. Stable isotope analysis reveals that agricultural habitat provides an important dietary component for nonbreeding Dunlin. *Avian Conservation and Ecology* **1**: 1-19.

Olley J, Brooks A, Spenser J, Pietsch T, Borombovits D. 2013. Subsoil erosion dominates the supply of fine sediment to rivers draining into Princess Charlotte Bay, Australia. *Journal of Environmental Radioactivity* **124**: 121-129. DOI: 10.1016/j.jenvrad.2013.04.010

Outram FN, Lloyd CEM, Jonczyk J, Benskin CMH, Grant F, Perks MT, Deasy C, Burke SP, Collins AL, Freer J, Haygarth PM, Hiscock KM, Johnes PJ, Lovett AL. 2014. High-frequency monitoring of nitrogen and phosphorus response in three rural catchments to the end of the 2011-2012 drought in England. *Hydrology and Earth System Sciences* **18**: 3429-3448. DOI: 10.5194/hess-18-3429-2014.

Owens PN, Petticrew EL, van der Perk M. 2010. Sediment response to catchment disturbances. *Journal of Soils and Sediments* **10**: 591-596. DOI: 10.1007/s11368-010-0235-1.

Palmer MJ, Douglas GB. 2008. A Bayesian statistical model for end member analysis of sediment geochemistry, incorporating spatial dependences. *Applied Statistics* **57**: 313-327. DOI: 10.1111/j.1467-9876.2007.00615.x.

Palmer-Felgate EJ, Jarvie HP, Withers PJA, Mortimer RJG, Krom MD. 2009. Stream-bed phosphorus in paired catchments with different agricultural land use intensity. *Agriculture, Ecosystems and Environment* **134**: 53-66. DOI:10.1016/j.agee.2009.05.014.

Pancost RD, Boot CS. 2004. The palaeoclimatic utility of terrestrial biomarkers in marine sediments. *Marine Chemistry* **92**: 239-261. DOI:10.1016/j.marchem.2004.06.029.

Panuska JC, Good LW, Vadas PA, Busch DL, Ozkaynak A. 2011. Sediment and particulate phosphorus characteristics in grassed waterways from row crop corn and alfalfa fields collected by manual University of Exeter samplers and automatic sampling. *Hydrological Processes* **25**: 2329-2338. DOI: 10.1002/hyp.7987.

Parnell AC, Inger R, Bearhop S, Jackson AL. 2010. Source partitioning using stable isotopes: coping with too much variation. *PLoS ONE* **5**: e9672. DOI: 10.1371/journal.pone.0009672.

Parnell AC, Phillips DL, Bearhop S, Semmens BX, Ward EJ, Moore JW, Jackson AL, Inger R. 2013. Bayesian stable isotope mixing models. *Environmetrics* **24**: 387-399. DOI: 10.1002/env.2221.

Pawlowsky-Glahn V, Egozcue JJ. 2006. Compositional data and their analysis: an introduction. *Geological Society, London, Special Publications* **264**: 1-10. DOI: 10.1144/GSL.SP.2006.264.01.01.

Pedentchouk N, Sumner W, Tipple B, Pagani M. 2008. $\delta^{13}C$ and $\delta^{2}H$ compositions of *n*-alkanes from modern angiosperms and conifers: An experimental set up in central Washing State, USA. *Organic Geochemistry* **39**: 1066-1071. DOI: 10.1016/j.orggeochem.2008.02.005.

Perks MT, Warburton J, Bracken L. 2014. Critical assessment and validation of a time-integrating fluvial suspended sediment sampler. *Hydrological Processes* **28**: 4795-4807. DOI: 10.1002/hyp.9985.

Phillips DL, Gregg JW. 2001. Uncertainty in source partitioning using stable isotopes. *Ocecologia* **127**: 171-179. DOI: 10.1007/s004420000578.

Phillips JM, Russell MA, Walling DE. 2000. Time-integrated sampling of fluvial suspended sediment: a simple methodology for small catchments. *Hydrological Processes* **14**: 2589-2602. DOI: 10.1002/1099-1085(20001015)14:14<2589::AID-HYP94>3.0.CO;2-D

Pike Technologies. 2011. Diffuse Reflectance – Theory and Applications. Madison, USA; 39-40.

Pinheiro J, Bates D, DebRoy S, Sarkar D. 2012. R Package: '*nlme'*: Linear and nonlinear mixed effects models.

Plummer M. 2003. JAGS: A program for analysis of Bayesian graphical models using Gibbs sampling. Proceeding of the 3rd international workshop on distributed statistical computing, Vienna, Austria.

Plummer M, Best N, Cowles K, Vines K. 2006. R Package 'coda': convergence diagnosis and output analysis for MCMC.

Poulenard J, Perrette Y, Fanget B, Quetin P, Trevisan D, Dorioz JM. 2009. Infrared spectroscopy tracing of sediment sources in a small rural watershed (French Alps). *Science of the Total Environment* **407**: 2808-2819. DOI: 10.1016/j.scitotenv.2008.12.049.

Poulenard J, Legout C, Némery J, Bramorski J, Navratil O, Douchin A, Fanget B, Perrette Y, Evrard O, Esteves M. 2012. Tracing sediment sources during floods using Diffuse Reflectance Infrared Fourier Transform Spectrometry (DRIFTS): A case study in a highly erosive mountainous catchment (Southern French Alps). *Journal of Hydrology* **414-415**: 452-462. DOI: 10.1016/j.jhydrol.2011.11.022.

Pretty JN, Mason CF, Nedwell DB, Hine RE, Leaf S, Dils R. 2003. Environmental costs of freshwater eutrophication in England and Wales. *Environmental Science and Technology* **37:** 201-208. DOI**:** 10.1021/es020793k.

Pulley S, Foster I, Antunes P. 2015. The uncertainties associated with sediment fingerprinting suspended and recently deposited fluvial sediment in the Nene river basin. *Geomorphology* **228**: 303-319. DOI: 10.1016/j.geomorph.2014.09.016.

Puttock A, Dungait JAJ, Bol R, Dixon ER, Macleod CJA, Brazier RE. 2012. Stable carbon isotope analysis of fluvial sediment fluxes over two contrasting C_4-C_3 semi-arid vegetation transitions. *Rapid Communications in Mass Spectrometry* **26**: 2386-2392. DOI: 10.1002/rcm.6257.

Quinton JN, Govers G, Oost KV, Bardgett RD. 2010. The impact of agricultural soil erosion on biogeochemical cycling. *Nature Geoscience* **3**: 311-314. DOI: 10.1038/NGEO838.

R Development Core Team. 2014. R: A language and environment for statistical computing. R Foundation for Statistical Computing: Vienna, Austria. http://www.R-project.org.

Rawlins BG, Turner G, Mounteney I, Wildman G. 2010. Estimating specific surface area of fine stream bed sediments from geochemistry. *Applied Geochemistry* **25**: 1291-1300. DOI: 10.1016/j.apgeochem.2010.05.009.

Rawlins BG. 2011a. Controls on the phosphorus content of fine stream bed sediment in agricultural headwater catchments at the landscape scale. *Agriculture, Ecosystems and Environment* **144**: 352-363**.** DOI: 10.1016/j.agee.2011.10.002.

Rawlins BG. 2011b. A pilot study to assess soil spectroscopic methods for mapping key topsoil properties in the Blackwater sub-catchments (Wensum DTC). British Geological Survey, Climate Change Programme, Internal Report OR/11/053; 1-19, National Environment Research Council (NERC), Keyworth, UK.

Rawlins BG, Wragg J, Lark RM. 2013. Application of a novel method for soil aggregate stability measurement by laser granulometry with sonication. *European Journal of Soil Science* **64**: 92-103. DOI: 10.1111/ejss.12017.

Reynard B, Lécuyer C, Grandjean P. 1999. Crystal-chemical controls on rare-earth element concentrations in fossil biogenic apatites and implications for paleoenvironmental reconstructions. *Chemical Geology* **155**: 233-241. DOI: 10.1016/S0009-2541(98)00169-7.

Rice S, Johnson M, Extence C, Reeds J, Longstaff H. 2014. Diel patterns of suspended sediment flux and the zoogeomorphic agency of invasive crayfish. *Cuadernos de Investigación Geográfica* **40**: 7-26.

Riley N. 2010. River Wensum SSSI and Potter and Scarning Fens SSSI Diffuse Water Pollution Plan. Environment Agency report.

Rowan JS, Black S, Franks SW. 2011. Sediment fingerprinting as an environmental forensics tool explaining cyanobacteria blooms in lakes. *Applied Geography* **32:** 832-843. DOI:10.1016/j.apgeog.2011.07.004.

Russell MA, Walling DE, Webb BW, Bearne R. 1998. The composition of nutrient fluxes from contrasting UK river basins. *Hydrological Processes* **12**: 1461-1482. DOI: 10.1002/(SICI)1099-1085(199807)12:9<1461::AID-HYP650>3.0.CO;2-6.

Russell MA, Walling DE, Hodgkinson RA. 2001. Suspended sediment sources in two small lowland agricultural catchments in the UK. *Journal of Hydrology* **252**: 1-24. DOI: 10.1016/S0022-1694(01)00388-2.

Sachse D, Billault I, Bowen G, Chikaraishi Y, Dawson T, Feakins S, Freeman K, Magill C, McInerney F, van der Meer M, Polissar P, Robins R, Sachs J, Schmidt H, Sessions A, White J, West J, Kahmen A. 2012. Molecular paleohydrology: interpreting the hydrogen-isotopic composition of lipid biomarkers from photosynthesising organisms. *Annual Review of Earth and Planetary Sciences* **40**: 221–249. DOI: 10.1146/annurev-earth-042711-105535.

Salant NL, Hassan MA, Alonso CV. 2008. Suspended sediment dynamics at high and low storm flows in two small watersheds. *Hydrological Processes* **22**: 1573-1587. DOI: 10.1002/hyp.6743.

Savitzky A, Golay MJ. 1964. Smoothing and differentiation of data by simplified least square procedures. *Analytical Chemistry* **36**: 1627–1639. DOI: 10.1021/ac60214a047.

Schachtman DP, Reid RJ, Ayling SM. 1998. Phosphorus uptake by plants: from soil to cell. *Plant Physiology* **116**: 447-453. DOI: 10.1104.

Schelde K, de Jonge LW, Kjaergaard C, Laegdsmand M, Rubæk GH. 2006. Effects if manure application and ploughing on transport of colloids and phosphorus to tile drains. *Vadose Zone Journal* **5**: 445-458. DOI: 10.2136/vzj2005.0051.

Schindler Wildhaber Y, Liechti R, Alewell C. 2012a. Organic matter dynamics and stable isotope signature as tracers of the sources of suspended sediment. *Biogeosciences* **9**: 1985-1996. DOI: 1 0.5194/bg-9-1985-2012.

Schindler Wildhaber Y, Michel C, Burkhardt-Holm P, Bänninger D, Alewell C. 2012b. Measurement of spatial and temporal fine sediment dynamics in a small river. *Hydrology and Earth System Science* **16**: 1501-1515. DOI: 10.5194/hess-16-1501-2012.

Schmelter ML, Stevens DK. 2013. Traditional and Bayesian statistical models in fluvial sediment transport. *Journal of Hydraulic Engineering* **139**: 336-340. DOI: 10.1061/(ASCE)HY.1943-7900.0000672.

Schuller P, Walling DE, Iroumé A, Quilodrán C, Castillo A, Navas A. 2013. Using ^{137}Cs and $^{210}Pb_{ex}$ and other sediment source fingerprints to document suspended sediment sources in small forested catchments in south-central Chile. *Journal of Environmental Radioactivity* **124**: 147-159. DOI: 10.1016/j.jenvrad.2013.05.002.

Sear DA, Newson M, Old JC, Hill C. 2006. Geomorphological appraisal of the River Wensum Special Area of Conservation. English Nature Research Reports, No 685.

Semmens BX, Ward EJ, Moore JW, Darimont CT. 2009. Quantifying inter- and intra-population niche variability using hierarchical Bayesian stable isotope mixing models. *PLoS ONE* **4**: e6187. DOI:10.1371/journal.pone.0006187.

Sessions AL, Burgoyne TW, Schimmelmann A, Hayes JM. 1999. Fractionation of hydrogen isotopes in lipid biosynthesis. *Organic Geochemistry* **30**: 1193-1200. DOI: 10.1016/S0146-6380(99)00094-7.

Short T. 2011. R Package *'signal'*: Signal Processing.

Slimane AB, Raclot D, Evrard O, Sanaa M, Lefèvre I, Ahmadi M, Tounsi M, Rumpel C, Mammou AB, Le Bissonnais Y. 2013. Fingerprinting sediment sources in the outlet reservoir of a hilly cultivated catchment in Tunisia. *Journal of Soil and Sediments* **13**:801-815. DOI: 10.1007/s11368-012-0642-6.

Small IF, Rowan JS, Franks SW. 2002. Quantitative sediment fingerprinting using a Bayesian uncertainty estimation framework. In: The structure, function and management implications of fluvial sedimentary systems, edited by Dyer FJ, Thomas MC, Olley JM. *IAHS Publication* **276**: 443-450.

Smith AE, Ryan PB, Evans JS. 1992. The effect of neglecting correlations when propagating uncertainty and estimating the population distribution of risk. *Risk Analysis* **12**: 467-474. DOI: 10.1111/j.1539-6924.1992.tb00703.x.

Smith F, Freeman K. 2006. Influence of physiology and climate on δ^2H of leaf wax n-alkanes from $C_3$and C_4 grasses. *Geochimica et Cosmochimica Acta* **70**: 1172–1187. DOI: 10.1016/j.gca.2005.11.006.

Smith HG, Blake WH, Owens PN. 2013. Discriminating fine sediment sources and the application of sediment tracers in burned catchments: a review. *Hydrological Processes* **27**: 943:958. DOI: 10.1002/hyp.9537.

Smith HG, Blake WH. 2014. Sediment fingerprinting in agricultural catchments: A critical re-examination of source discrimination and data corrections. *Geomorphology* **204**: 177-191. DOI: 10.1016/j.geomorph.2013.08.003.

Smith VH, Tilman GD, Nekola JC. 1999. Eutrophication: impacts of excess nutrient inputs on freshwater, marine, and terrestrial ecosystems. *Environmental Pollution* **100:** 179-196. DOI:10.1016/S0269-7491(99)00091-3.

Stevens JC, Quinton JN. 2009a. Diffuse pollution swapping in arable agricultural systems. *Critical Reviews in Environmental Science and Technology* **39**: 478-520. DOI: 10.1080/10643380801910017.

Stevens JC, Quinton JN. 2009b. Policy implications of pollution swapping. *Physics and Chemistry of the Earth* **34**: 589-594. DOI:10.1016/j.pce.2008.01.001.

Stone M, Collins AL, Silins U, Emelko MB, Zhang YS. 2014. The use of composite fingerprints to quantify sediment sources in a wildfire impacted landscape, Alberta, Canada. *Science of the Total Environment* **473-474**: 642-650. DOI: 10.1016/j.scitotenv.2013.12.052.

Stumpe B, Weihermullerm L, Marschner B. 2011. Sample preparation and selection for qualitative and quantitative analyses of soil organic carbon with mid-infrared reflectance spectroscopy. *European Journal of Soil Science* **62**: 849-862. DOI: 10.1111/j.1365-2389.2011.01401.x

Stutter MI, Langan SJ, Demars BOL. 2007. River sediments provide a link between catchment pressures and ecological status in a mixed land use Scottish River system. *Water Research* **41**: 2803-2815. DOI: 10.1016/j.watres.2007.03.006.

Stutter MI, Langan SJ, Cooper RJ. 2008a. Spatial and temporal dynamics of stream water particulate and dissolved N, P and C forms along a catchment transect, NE Scotland. *Journal of Hydrology* **350**: 187-202. DOI: 10.1016/j.jhydrol.2007.10.048.

Stutter MI, Langan SJ, Cooper RJ. 2008b. Spatial contributions of diffuse inputs and within-channel processes to the form of stream water phosphorus over storm events. *Journal of Hydrology* **350**: 203-214. DOI: 10.1016/j.jhydrol.2007.10.045.

Stutter MI, Langan SJ, Lumsdon DG, Clark LM. 2009. Multi-element signatures of stream sediments and sources under moderate to low flow conditions. *Applied Geochemistry* **24**: 800-809. DOI: 10.1016/j.apgeochem.2009.01.005.

Sun D, Berger JO. 2006. Objective priors for the multivariate normal model. *Proc. Valencia / ISBA 8th World Meeting on Bayesian Statistics*, Benidorm, Spain, June 1st-6th 2006: 1-26.

Tarroux A, Bêty J, Gauthier G, Dominique B. 2012. The marine side of a terrestrial carnivore: intra-population variation in use of allochthonous resources by artic foxes. *PLoS ONE* **7**: e42427. DOI:10.1371/journal.pone.0042427.

Theuring P, Rode M, Behrens S, Kirchner G, Jha A. 2013. Identification of fluvial sediment sources in the Kharaa River catchment, Northern Mongolia. *Hydrological Processes* **27**: 845-856. DOI: 10.1002/hyp.9684.

Thompson J, Doody DG, Flynn R, Watson CJ. 2012. Dynamics of critical source areas: Does connectivity explain chemistry? *Science of the Total Environment* **435-436**: 499-508. DOI: 10.1016/j.scitotenv.2012.06.104.

Thompson J, Cassidy R, Doody DG, Flynn R. 2013. Predicting critical source areas of sediment in headwater catchments. *Agriculture, Ecosystems and Environment* **179**: 41-52. DOI: 10.1016/j.agee.2013.07.010.

Tiwari MK, Singh AK, Sawhney KJS. 2005. Sample preparation for evaluation of detection limits in X-ray florescence spectrometry. *Analytical Sciences* **21**: 143-147. DOI: 10.2116/analsci.21.143.

Toynton R. 1983. The relation between fracture patterns and hydraulic anisotropy in the Norfolk Chalk, England. *Quarterly Journal of Engineering Geology and Hydrogeology* **16**: 169-185.

Tremblay L, Gagné J-P. 2002. Fast Quantification of humic substances and organic matter by direct analysis of sediments using DRIFT spectroscopy. *Analytical Chemistry* **74**: 2985-2993. DOI: 10.1021/ac011043g.

Tremblay L, Alaoui G, Léger MN. 2011. Characterisation of aquatic particles by direct FT-IR analysis of filters and quantification of elemental and molecular compositions. *Environment, Science, and Technology* **45**: 9671-9679. DOI: 10.1021/ac011043g.

Tye AM, Robinson DA, Lark RM. 2013. Gradual and anthropogenic soil change for fertility and carbon on marginal sandy soils. *Geoderma* **207-208**: 35-48. 10.1016/j.geoderma.2013.05.004.

USEPA. 2001. Methods for Collection, Storage and Manipulation of Sediments for Chemical and Toxicological Analyses: Technical Manual. EPA 823-B-01-002. U.S. Environmental Protection Agency, Office of Water, Washington, DC; 1-16.

Van den Meersche K, Soetaert K, Middelbury JJ. 2008. A Bayesian compositional estimator for microbial taxonomy based on biomarkers. *Limnology and Oceanography: Methods* **6**: 190-199. DOI: 10.4319/lom.2008.6.190.

Van den Meersche K, Soetaert K, Van Oevelen D. 2009. xsample(): An R function for sampling linear inverse problems. *Journal of Statistical Software, Code Snippets* **30**: 1-15.

Van der Perk M, Owens PN, Deeks LK, Rawlins BG, Haygarth PM, Beven KJ. 2007. Controls on catchment-scale patterns of phosphorus in soil, streambed sediment, and stream water. *Journal of Environmental Quality* **36**: 694-708. DOI:10.2134/ jeq2006.0175.

Violante A, Violante P. 1980. Influence of pH, concentration, and chelating power of organic anions on the synthesis of aluminium hydroxides and oxyhydroxides. Clay and Clay Minerals **28**: 425-434.

Viscarra Rossel RA, Walvoort DJJ, McBrantney AB, Janik LJ, Skjemstad JO. 2006. Visible, near infrared, mid infrared or combined diffuse reflectance spectroscopy for simultaneous assessment of various soil properties. *Geoderma* **131**: 59-75. DOI: 10.1016/j.geoderma.2005.03.007.

Vogel H, Rosén P, Wagner B, Melles M, Persson P. 2008. Fourier transform infrared spectroscopy, a new cost-effective tool for quantitative analysis of biogeochemical properties in long sediment records. *Journal of Paleolimnology* **40**: 689-702. DOI: 10.1007/s10933-008-9193-7.

Wagai R, Mayer LM. 2007. Sorptive stabilization of organic matter in soils by hydrous iron oxides. *Geochimica et Cosmochimica Acta* **71**: 25:35. DOI: 10.1016/j.gca.2006.08.047.

Wagai R, Mayer LM, Kitayama K. 2009. Extent and nature of organic coverage of soil mineral surfaces assessed by a gas sorption approach. *Geoderma* **149**: 152-160. DOI: 10.1016/j.geoderma.2008.11.032.

Wagai R, Mayer LM, Kitayama K, Shirato Y. 2013. Association of organic matter with iron and aluminium across a range of soils determined via selective dissolution techniques coupled with dissolved nitrogen analysis. *Biogeochemistry* **112**: 95-109. DOI: 10.1007/s10533-011-9652-5.

Walker TW, Syers JK. 1986. The fate of phosphorus during pedogenesis. *Geoderma* **15**: 1-19.

Walling DE, Moorehead PW. 1989. The particle size characteristics of fluvial suspended sediment: an overview. *Hydrobiologia* **176-177**: 125-149. DOI: 10.1007/978-94-009-2376-8_12.

Walling DE, Webb BW, Russell MA. 1997. Sediment-associated nutrient transport in UK rivers. In: Webb B. (Ed.) Freshwater Contamination. IAHS Publication, pp. 69–81.

Walling DE, Russell MA, Webb BW. 2001. Controls on the nutrient content of suspended sediment transported by British rivers. *Science of the Total Environment* **266**: 113-123. DOI: 10.1016/S0048-9697(00)00746-4.

Walling DE, Collins AL, McMellin GK. 2003. A reconnaissance survey of the source of interstitial fine sediment recovered from salmonid spawning gravels in England and Wales. *Hydrobiologia* **497**: 91-108. DOI: 10.1023/A:1025413721647.

Walling DE. 2005. Tracing suspended sediment sources in catchments and river systems. *Science of the Total Environment* **344**: 159-184. DOI: 10.1016/j.scitotenv.2005.02.011.

Walling DE, Collins AL, Stroud RW. 2008. Tracing suspended sediment and particulate phosphorus sources in catchments. *Journal of Hydrology* **350:** 274-289. DOI:10.1016/j.jhydrol.2007.10.047.

Walling DE. 2013. The evolution of sediment source fingerprinting investigations in fluvial systems. *Journal of Soils and Sediments* **13**: 1658-1675. DOI: 10.1007/s11368-013-0767-2.

Wang Y, Yang H, Zhang J, Xu M, Wu C. 2015. Biomarker and stable carbon isotopic signatures for 100-200 year sediment record in the Chaihe catchment in southwest China. *Science of the Total Environment* **502**: 266-275. DOI: 10.1016/j.scitotenv.2014.09.017.

Ward EJ, Semmens BX, Schindler DE. 2010. Including source uncertainty and prior information in the analysis of stable isotope mixing models. *Environmental Science and Technology* **44**: 4645-4650. DOI: 10.1021/es100053v.

Wensum Alliance. 2014. River Wensum Demonstration Test Catchment Project. Online: www.wensumalliance.org.uk.

White RE. 2006. Principles and practice of soil science: the soil as a natural resource. 4th edition. Blackwell Publishing, Oxford, UK. ISBN: 978-0-632-06455-7.

Wilkinson BH. 2005. Humans as geologic agents: A deep-time perspective. *Geology* **33**: 161-164. DOI: 10.1130/G21108.1.

Wilkinson SN, Hancock GJ, Bartley R, Hawdon AA, Keen RJ. 2013. Using sediment tracing to assess processes and spatial patterns of erosion in grazed rangelands, Burdekin River basin, Australia. *Agriculture, Ecosystems and Environment* **180**: 90-102. DOI: 10.1016/j.agee.2012.02.002.

Williams GP. 1989. Sediment concentration versus water discharge during single hydrologic events in rivers. *Journal of Hydrology* **111**: 89-106. DOI: 10.1016/0022-1694(89)90254-0.

Wilson CA, Cloy JM, Graham MC, Hamlet LE. 2013. A microanalytical study of iron, aluminium and organic matter relationships in soils with contrasting hydrological regimes. *Geoderma* **202-203**: 71-81. DOI: 10.1016/j.geoderma.2013.03.020.

Withers PJA, Hodgkinson RA, Bates A, Withers CL. 2007. Soil cultivation effects on sediment and phosphorus mobilization in surface runoff from three contrasting soil types in England. *Soil and Tillage Research* **93**: 438-451. DOI: 10.1016/j.still.2006.06.004.

Withers PJA, Jarvie HP. 2008. Delivery and cycling of phosphorus in rivers: A review. *Science of the Total Environment* **400**: 379-395. DOI: doi:10.1016/j.scitotenv.2008.08.002.

Withers PJA, Jarvie HP, Hodgkinson RA, Palmer-Felgate EJ, Bates A, Neal M, Howells R, Withers CM, Wickham HD. 2009. Characterisation of phosphorus sources in rural watersheds. *Journal of Environmental Quality* **38**: 1998-2011. DOI: 10.2134/jeq2008.0096.

Yao Y, Zhang E, Kuhn N, Jones R, Langdon P, Shen J, Greenwood P. 2013. Sediment provenance in the Shudu Lake basin, northwest Yunnan Province, China, as revealed by composite fingerprinting. *DIE ERDE* **144**: 17-29. DOI: 10.12854/erde-144-2.

Zech M, Pedentchouk N, Buggle B, Leiber K, Kalbitz K, Marković SB, Glaser B. 2011. Effect of leaf litter degradation and seasonality on D/H isotope ratios of *n*-alkane biomarkers. *Geochimica et Cosmochimica Acta* **75**: 4917-4928. DOI: 10.1016/j.gca.2011.06.006.

Zhang XC, Friedrich JM, Nearing MA, Norton LD. 2001. Potential use of rare earth oxides as tracers for soil erosion and aggregation studies. *Soil Science Society of America Journal* **65**: 1508-1515. DOI: 10.2136/sssaj2001.6551508x.

Zhang Z, Zhao M, Eglinton G, Lu H, Huang C-Y. 2006. Leaf wax lipids as paleovegetational and paleoenvironmental proxies for the Chinese Loess Plateau over the last 170 kyr. *Quaternary Science Reviews* **25**: 575-594. DOI: 10.1016/j.quascirev.2005.03.009.

Appendix A

SUPPLEMENTARY MATERIAL FOR CHAPTER 2

Images of the Blackwater sub-catchment

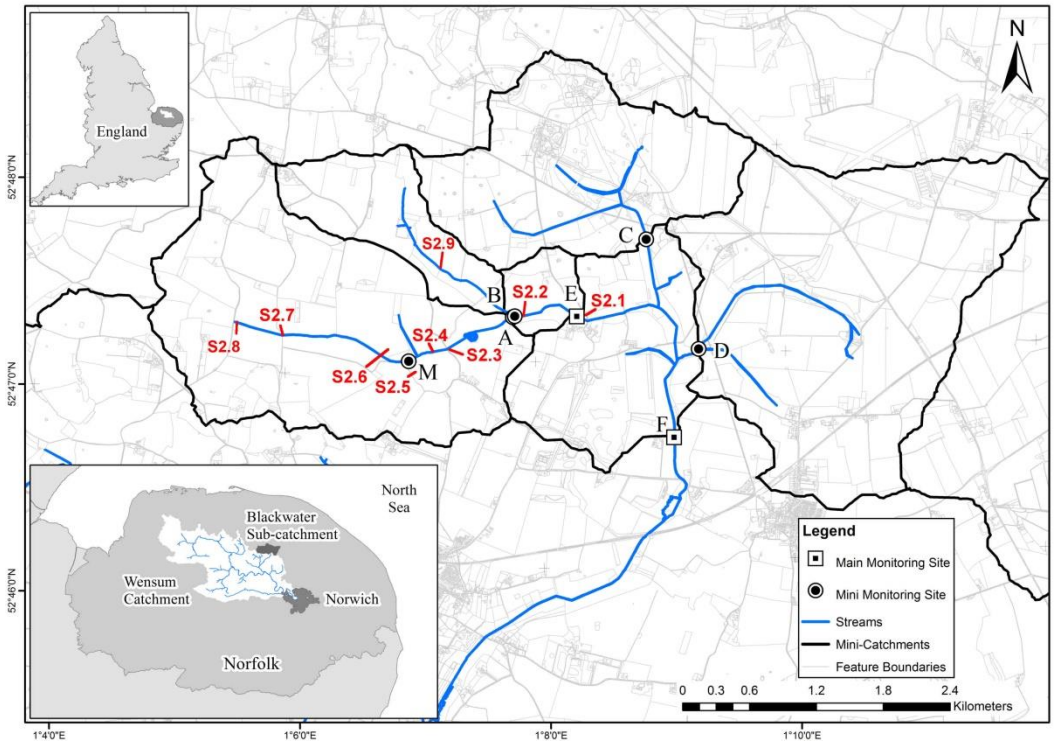

Figure A0: Map of the Blackwater sub-catchment showing the locations of the images presented below.

Figure A1: The River Blackwater at site E. March 2011. The intake for the bankside monitoring kiosk is visible in the centre of the channel.

Figure A2: The River Blackwater at the confluence of mini-catchments A and B. June 2012. The bankside monitoring station at site B is visible on the left hand side. The stream itself is hidden beneath dense emergent macrophyte growth.

Figure A3: The River Blackwater at the road bridge in mini-catchments A. May 2011. This road crossing is an important location for sediment ingress into the stream channel

Figure A4: The highly channelised morphology of the River Blackwater in mini-catchment A. February 2012.

Figure A5: An oilseed radish cover crop growing on Dunkirk field in mini-catchment A. October 2013.

Figure A6: Erosive surface runoff from a bare sugar beet field in mini-catchment A. May 2012.

Figure A7: The view downstream from the top of mini-catchment A. October 2013. The overgrown stream channel is visible in the centre of the image.

Figure A8: Elevated turbidity in the River Blackwater following the initiation of surface runoff during a prolonged period of heavy rainfall. May 2012.

Figure A9: The River Blackwater in mini-catchment B. May 2011. The stream runs through the foreground of the image.

Appendix B

SUPPLEMENTARY MATERIAL FOR CHAPTER 4

Benchmark Bayesian Model

Below is the code required to run the benchmark Bayesian mixing model (M1) of Chapter 4 through JAGS in the R environment.

```
## Benchmark Model 1

model {

# Target data likelihood
  for(i in 1:N) {
    Y[i,1:J] ~ dmnorm(mu[i,],OmegaresZ)
    mu[i,1:J] <- p[i,1:K]%*%s[1:K,1:J,i]
    }

  # s - sources
  for(i in 1:N) {
    for(k in 1:K) {
     s[k,1:J,i] ~ dmnorm(muS[,k],OmegaS[,,k])
    }
  }

  # s constraints
   for(i in 1:N) {
      for(k in 1:K) {
         for (j in 1:J) {
            positive[k,j,i] ~ dinterval(s[k,j,i], zero)
      }
   }
   }

    # p - proportions
  for(i in 1:N) {
    p[i,1:K] <- expphiV[i,1:K]/sum(expphiV[i,1:K])
    phiV[i,1:K] <- phi[i,1:(K-1)]%*%tV
    for(k in 1:K) {
      expphiV[i,k] <- exp(phiV[i,k])
    }
  }

  # phi
  for(i in 1:N) {
    for(k in 1:(K-1)) {
      phi[i,k] ~ dnorm(muphi[k],tauphi[k])
    }
    philast[i] <- -sum(phi[i,1:(K-1)])
  }

  # hyper-parameters for phi prior
  for(k in 1:(K-1)) {
     muphi[k] ~ dnorm(0,1)
     tauphi[k] ~ dgamma(2,1)
    sigma2phi[k] <- 1/tauphi[k]
  }

  # Prior on OmegaresZ
  # combined precision matrix of residual + measurement error
  OmegaresZ ~ dwish(Rres,kres)
  SigmaresZ <- inverse(OmegaresZ)
}
```

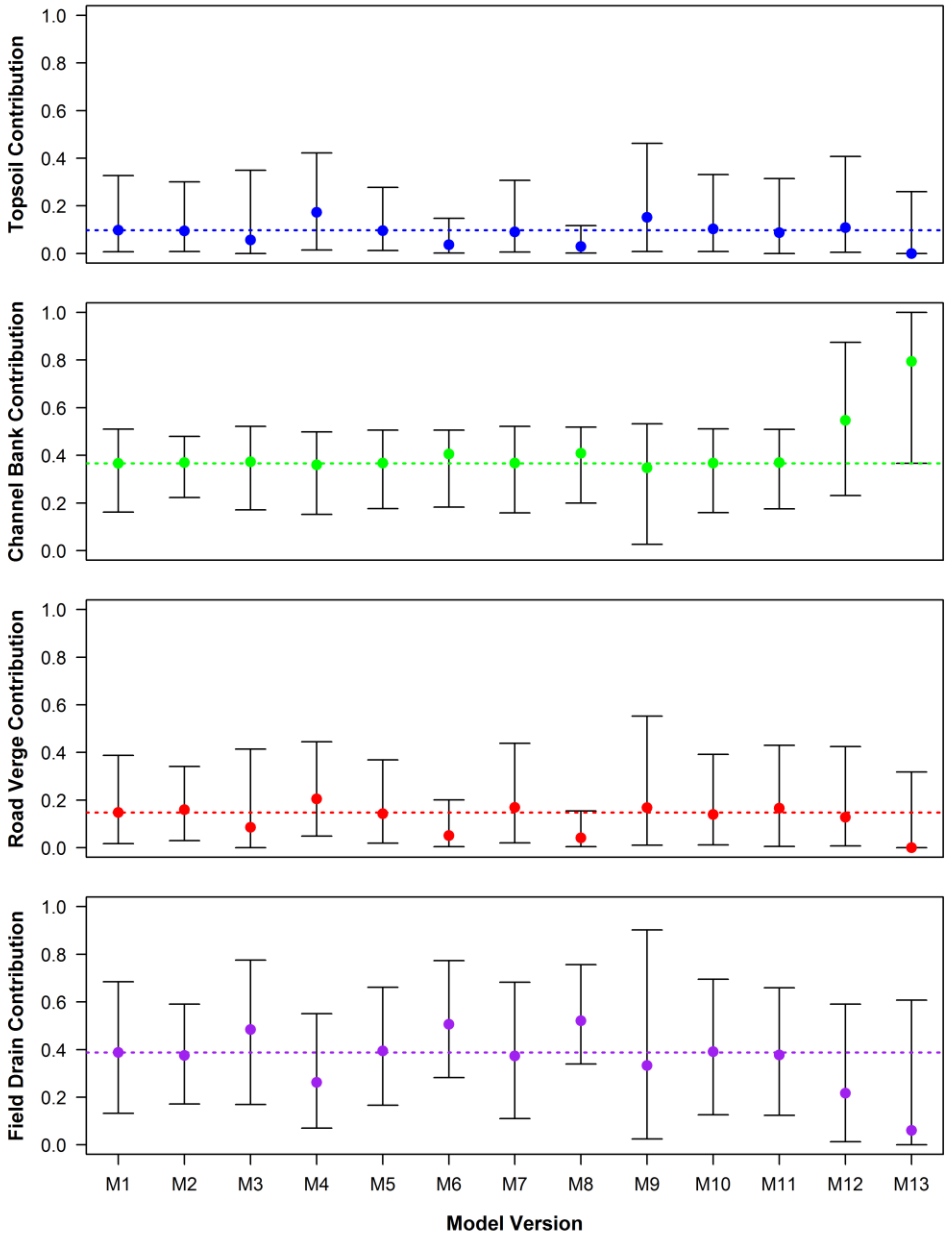

Figure B1: Comparison of SPM source apportionment for mini-catchment B as estimated by 13 four end-member mixing model versions. Results for each version are displayed as the temporal apportionment average across 10 baseflow SPM samples spanning May-September 2012. Points represent median contributions with associated 95% credible intervals, whilst dashed lines represent the median contribution estimated by M1. Note how the inter-model variability in median source apportionment and 95% credible interval width closely matches the trends observed with data from mini-catchment A (Figure 4.6).

Appendix C

SUPPLEMENTARY MATERIAL FOR CHAPTER 5

Table C1: Geochemistry for the 63 µm sieved source area sediments and SPM from mini-catchment A. σ is the standard deviation. SPM includes baseflow and storm event samples.

Source Areas	Stat.	Concentrations (weight %)														
		Al	**Ca**	**Ce***	**Fe**	**K**	**Mg**	**Mn**	**Na**	**P**	**Si**	**Ti**	**POC**	**Al_{di}**	**Al_{ox}**	**Fe_{di}**	**Fe_{ox}**
SPM (n = 328)	Min.	4.18	6.60	40	3.09	0.82	0.33	0.04	0.16	0.14	0.00	0.24	6.48	0.01	0.00	0.00	0.00
	Median	8.25	16.70	55	7.20	1.47	0.69	0.10	0.25	0.26	8.12	0.47	11.18	0.17	0.08	2.89	0.27
	Mean	8.53	17.55	57	7.26	1.52	0.71	0.11	0.26	0.29	8.59	0.46	11.76	0.16	0.08	2.88	0.29
	Max	15.24	28.85	108	14.14	2.50	1.19	0.22	0.43	0.86	24.94	0.80	23.08	0.40	0.41	6.60	1.44
	σ	1.44	4.52	10	1.03	0.21	0.12	0.03	0.04	0.10	4.58	0.06	2.47	0.07	0.06	0.86	0.21
Channel Banks (n = 30)	Mean	6.97	35.47	36	5.04	1.19	0.61	0.01	0.19	0.07	5.40	0.45	2.27	0.06	0.01	2.30	0.60
	σ	2.34	7.65	13	1.65	0.44	0.18	0.02	0.06	0.03	4.80	0.09	2.17	0.05	0.01	0.69	0.30
Field Drains (n = 30)	Mean	6.89	17.50	49	8.21	1.12	0.51	0.22	0.26	0.28	9.95	0.38	8.90	0.15	0.14	2.39	0.47
	σ	2.49	8.23	15	5.14	0.39	0.17	0.29	0.09	0.19	9.50	0.11	3.45	0.08	0.07	1.16	0.33
Road Verges (n = 30)	Mean	10.40	6.63	86	6.12	2.08	1.01	0.15	0.48	0.33	18.09	0.61	14.09	0.20	0.09	3.05	0.76
	σ	0.99	1.32	7	0.48	0.11	0.09	0.02	0.05	0.04	2.34	0.02	1.38	0.03	0.04	0.88	0.17
Topsoils (n = 30)	Mean	14.07	3.97	91	6.93	2.45	0.88	0.11	0.41	0.28	18.73	0.66	11.35	0.27	0.18	2.41	0.69
	σ	1.17	2.00	8	0.62	0.23	0.07	0.01	0.04	0.06	2.11	0.02	1.49	0.07	0.04	0.61	0.14

* Ce is measured in ppm

Table C2: Geochemistry for the 63 µm sieved source area sediments and SPM from mini-catchment B. σ is the standard deviation. SPM includes baseflow and storm event samples.

Source Areas	Stat.	Concentrations (weight %)															
		Al	**Ca**	**Ce***	**Fe**	**K**	**Mg**	**Mn**	**Na**	**P**	**Si**	**Ti**	**POC**	**Al_{di}**	**Al_{ox}**	**Fe_{di}**	**Fe_{ox}**
SPM (*n* = 325)	Min.	4.08	2.90	43	3.69	0.88	0.32	0.04	0.14	0.16	0.00	0.26	10.17	0.04	0.00	0.43	0.08
	Median	6.89	11.92	59	6.22	1.43	0.56	0.15	0.20	0.30	7.44	0.44	15.54	0.21	0.12	2.61	0.59
	Mean	7.76	12.01	61	6.17	1.50	0.58	0.15	0.21	0.30	7.95	0.44	15.36	0.22	0.12	2.74	0.59
	Max	17.91	18.55	91	8.03	2.76	1.04	0.21	0.41	0.50	21.05	0.69	20.32	0.43	0.28	6.07	1.11
	σ	2.40	3.18	9	0.86	0.30	0.12	0.03	0.04	0.05	4.15	0.07	2.37	0.08	0.06	0.94	0.17
Channel Banks (*n* = 20)	Mean	6.10	31.60	38	4.27	1.17	0.65	0.02	0.32	0.06	6.53	0.40	2.12	0.08	0.05	1.62	0.51
	σ	2.39	12.39	20	1.93	0.67	0.21	0.03	0.16	0.02	7.80	0.13	1.85	0.08	0.07	1.02	0.38
Field Drains (*n* = 18)	Mean	7.28	4.20	88	5.50	1.81	0.60	0.16	0.44	0.28	18.85	0.43	6.98	0.24	0.18	1.96	0.57
	σ	3.46	2.29	19	2.76	0.89	0.38	0.18	0.16	0.34	10.07	0.15	3.76	0.09	0.05	1.05	0.31
Road Verges (*n* = 30)	Mean	10.53	3.06	89	4.95	2.29	0.81	0.16	0.60	0.30	18.57	0.62	10.21	0.19	0.09	2.52	0.69
	σ	2.29	1.02	8	0.84	0.34	0.23	0.03	0.17	0.04	2.41	0.06	1.58	0.02	0.03	0.52	0.11
Topsoils (*n* = 30)	Mean	14.13	1.70	96	5.92	2.60	0.78	0.12	0.49	0.28	19.10	0.68	8.93	0.29	0.18	2.42	0.50
	σ	2.79	0.66	12	0.96	0.44	0.15	0.02	0.08	0.06	2.79	0.09	2.79	0.03	0.02	0.48	0.22

* Ce is measured in ppm

Table C3: Summary statistics for site E SPM geochemistry. Data includes baseflow and storm event samples. *N* = 290.

Statistic	Concentrations (weight %)															
	Al	**Ca**	**Ce***	**Fe**	**K**	**Mg**	**Mn**	**Na**	**P**	**Si**	**Ti**	**POC**	**Al_{di}**	**Al_{ox}**	**Fe_{di}**	**Fe_{ox}**
Min.	3.66	6.10	36	3.90	1.03	0.32	0.05	0.08	0.18	0.00	0.22	7.73	0.00	0.00	0.00	0.00
Median	8.21	15.11	57	7.50	1.52	0.67	0.11	0.24	0.35	10.15	0.44	12.89	0.16	0.09	3.25	0.36
Mean	8.22	15.38	58	7.65	1.51	0.68	0.12	0.24	0.39	11.12	0.43	13.21	0.16	0.09	3.22	0.35
Max.	15.86	21.63	91	11.66	2.36	1.04	0.24	0.35	1.00	29.99	0.64	30.43	0.38	0.34	5.86	0.86
Standard Deviation	1.50	2.91	8	1.20	0.19	0.10	0.03	0.04	0.15	6.09	0.07	2.48	0.09	0.07	0.90	0.17

*Ce is measured in ppm

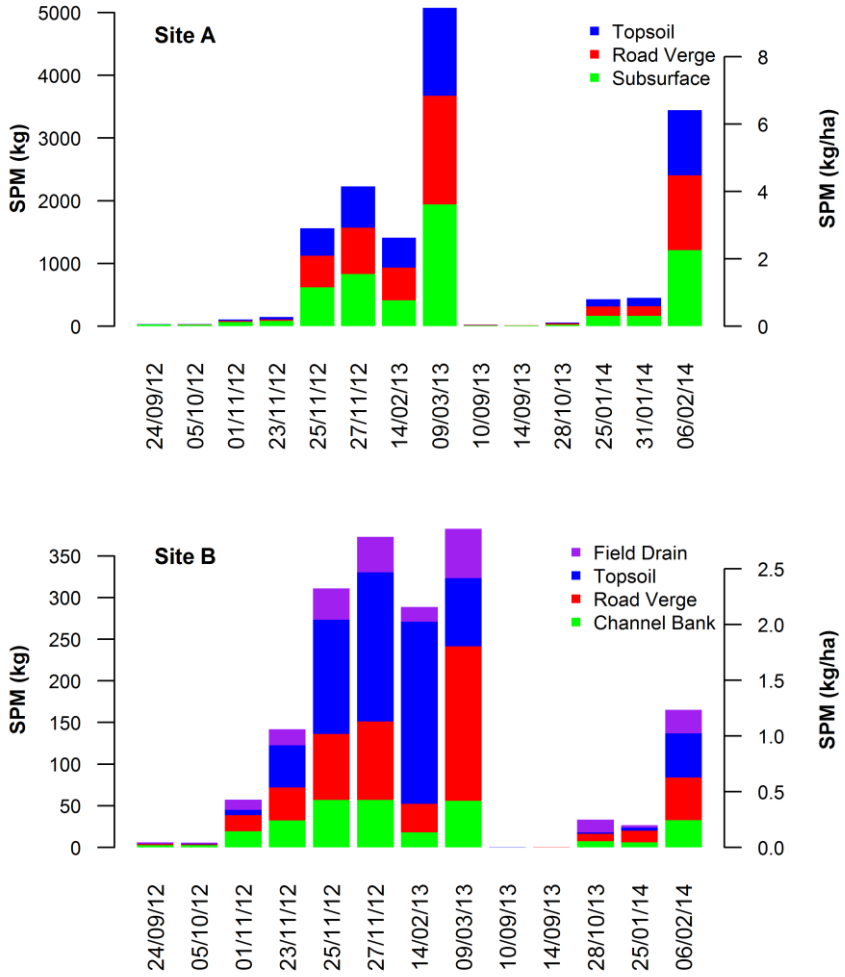

Figure C1: Estimated SPM export (kg) at sites A and B during 13-14 storm events captured between September 2012 and February 2014. Loads apportioned to specific sources are based on the median contributions estimated by the Bayesian mixing model.

Appendix D

SUPPLEMENTARY MATERIAL FOR CHAPTER 6

Table D1: All *n*-alkane chain length statistics and isotopic compositions for plant specimens arranged by plant functional type. ACL is the average chain length; CPI the carbon preference index; Cmax the most abundance n-alkane. Numbers in parentheses refer to error (±) based on duplicate measurements during isotope analysis.

Plant Functional Type	Species	Environment	ACL	CPI	C_{max}	$\delta^{13}C_{27}$ (‰)	$\delta^{13}C_{29}$ (‰)	$\delta^{13}C_{31}$ (‰)	$\delta^{13}C_{27-31}$ (‰)	$\delta^{2}H_{27}$ (‰)	$\delta^{2}H_{29}$ (‰)	$\delta^{2}H_{27-29}$ (‰)
C_3 Graminoids	*Triticum* sp.	Terrestrial	29.5	30.6	29	-37.2 (0.1)	-37.3 (0.0)	-37.9 (0.1)	-37.5 (0.1)	-210 (2)	-266 (2)	-258 (2)
	Triticum sp.	Terrestrial	29.6	32.8	29	-36.3 (0.1)	-37.4 (0.1)	-37.7 (0.2)	-37.4 (0.1)	-203 (1)	-265 (0)	-257 (0)
	Graminoid spp.	Aquatic	28.0	10.5	29	-36.2 (0.0)	-36.8 (0.1)	-38.2 (0.1)	-36.7 (0.1)	-217 (3)	-230 (1)	-225 (1)
	Graminoid spp.	Aquatic	27.9	8.1	29	-36.3 (0.1)	-36.9 (0.1)	-37.6 (0.1)	-36.8 (0.1)	-243 (2)	-259 (1)	-252 (1)
	Graminoid spp.	Aquatic	27.5	7.3	27	-36.5 (0.0)	-37.0 (0.0)	-36.8 (0.1)	-36.8 (0.0)	-217 (2)	-229 (1)	-223 (2)
	Graminoid spp.	Aquatic	27.4	7.3	27	-36.9 (0.0)	-37.1 (0.0)	-36.7 (0.0)	-37.0 (0.0)	-227 (1)	-250 (0)	-237 (1)
	Graminoid spp.	Aquatic	28.1	14.1	29	-36.6 (0.3)	-37.6 (0.2)	-37.5 (0.1)	-37.2 (0.2)	-242 (1)	-256 (1)	-250 (1)
	Graminoid spp.	Aquatic	28.1	14.4	29	-36.5 (0.3)	-37.6 (0.1)	-37.8 (0.1)	-37.2 (0.2)	-242 (5)	-263 (3)	-254 (4)
	Graminoid spp.	Terrestrial	29.8	26.3	31	-37.8 (0.1)	-37.6 (0.1)	-37.4 (0.0)	-37.5 (0.1)	-202 (0)	-243 (1)	-236 (1)
	Graminoid spp.	Terrestrial	29.8	24.6	31	-36.0 (0.0)	-36.3 (0.2)	-37.3 (0.0)	-36.8 (0.1)	-211 (2)	-248 (1)	-238 (1)
	Graminoid spp.	Terrestrial	27.7	10.5	27	-35.1 (0.1)	-35.6 (0.0)	-35.8 (0.2)	-35.4 (0.1)	-245 (1)	-255 (0)	-249 (0)
	Graminoid spp.	Terrestrial	27.8	10.8	27	-35.7 (0.0)	-36.7 (0.1)	-37.0 (0.2)	-36.3 (0.1)	-242 (2)	-244 (0)	-243 (1)
	Graminoid spp.	Terrestrial	29.6	17.4	31	-32.7 (0.1)	-33.8 (0.0)	-34.2 (0.0)	-33.8 (0.0)	-193 (4)	-230 (5)	-221 (5)
	Graminoid spp.	Terrestrial	29.2	17.7	29	-32.7 (0.1)	-34.1 (0.1)	-37.0 (0.5)	-35.0 (0.2)	-208 (2)	-240 (1)	-231 (2)
	Graminoid spp.	Terrestrial	29.8	27.9	29	-35.5 (0.1)	-36.5 (0.1)	-36.5 (0.0)	-36.4 (0.0)	-229 (2)	-262 (1)	-256 (1)
	Graminoid spp.	Terrestrial	29.9	23.7	29	-35.0 (0.0)	-35.9 (0.1)	-36.0 (0.0)	-35.8 (0.1)	-218 (1)	-254 (1)	-248 (1)
	Graminoid spp.	Terrestrial	30.1	29.8	31	-36.4 (0.1)	-37.3 (0.1)	-37.0 (0.0)	-37.1 (0.0)	-217 (1)	-253 (0)	-245 (0)
	Graminoid spp.	Terrestrial	30.1	32.1	29	-37.0 (0.3)	-36.4 (0.2)	-36.7 (0.1)	-36.6 (0.2)	-207 (1)	-250 (2)	-241 (2)
	Graminoid spp.	Terrestrial	30.2	32.9	31	-36.1 (0.1)	-36.4 (0.1)	-36.1 (0.1)	-36.3 (0.1)	-229 (6)	-261 (2)	-256 (3)
	Graminoid spp.	Terrestrial	30.5	36.3	31	-38.6 (0.1)	-36.4 (0.0)	-36.6 (0.1)	-36.7 (0.1)	-215 (9)	-269 (7)	-259 (4)
C_4 Graminoids	*Zea mays*	Terrestrial	30.5	13.6	31	-23.9 (0.1)	-24.0 (0.1)	-23.0 (0.0)	-23.5 (0.0)	-163 (0)	-201 (0)	-195 (0)
	Zea mays	Terrestrial	30.4	13.1	31	-23.3 (0.0)	-23.4 (0.0)	-22.8 (0.0)	-23.1 (0.0)	-165 (2)	-200 (0)	-194 (0)
Herbaceous Perennials	*Raphanus sativus*	Terrestrial	27.5	2.7	29	-37.9 (0.3)	-38.0 (0.1)	-37.6 (0.0)	-38.0 (0.1)	-182 (0)	-189 (1)	-187 (1)
	Raphanus sativus	Terrestrial	28.9	16.8	29	-39.5 (0.0)	-37.7 (0.0)	-37.7 (0.0)	-38.1 (0.0)	-152 (4)	-190 (1)	-178 (2)
	Raphanus sativus	Terrestrial	29.3	16.8	29	-38.4 (0.3)	-37.9 (0.6)	-38.7 (0.0)	-38.3 (0.4)	-163 (3)	-199 (0)	-192 (1)
	Raphanus sativus	Terrestrial	29.5	16.1	29	-38.1 (0.1)	-38.3 (0.1)	-38.4 (0.1)	-38.3 (0.1)	-172 (3)	-205 (2)	-197 (2)
	Raphanus sativus	Terrestrial	28.6	15.3	29	-37.7 (0.2)	-38.5 (0.0)	-38.3 (0.0)	-38.3 (0.0)	-151 (4)	-181 (1)	-172 (2)
	Raphanus sativus	Terrestrial	28.3	12.8	29	-37.0 (0.1)	-37.4 (0.0)	-37.1 (0.0)	-37.2 (0.1)	-164 (2)	-187 (1)	-179 (1)
	Aegopodium podagraria	Aquatic	29.3	18.1	31	-35.1 (0.0)	-35.5 (0.0)	-35.5 (0.0)	-35.4 (0.0)	-180 (0)	-206 (0)	-198 (0)

Table D1 continued

Plant Functional Type	Species	Environment	ACL	CPI	C_{max}	$\delta^{13}C_{27}$ (‰)	$\delta^{13}C_{29}$ (‰)	$\delta^{13}C_{31}$ (‰)	$\delta^{13}C_{27\text{-}31}$ (‰)	$\delta^{2}H_{27}$ (‰)	$\delta^{2}H_{29}$ (‰)	$\delta^{2}H_{27\text{-}29}$ (‰)
Herbaceous Perennials	*Aegopodium podagraria*	Aquatic	30.0	24.6	31	-35.2 (0.0)	-35.6 (0.0)	-35.3 (0.1)	-35.4 (0.1)	-191 (1)	-215 (0)	-207 (0)
	Aegopodium podagraria	Aquatic	29.3	18.0	31	-35.1 (0.0)	-36.4 (0.0)	-36.2 (0.1)	-36.1 (0.1)	-160 (1)	-198 (0)	-184 (0)
	Aegopodium podagraria	Aquatic	28.9	10.6	31	-36.4 (0.4)	-35.9 (0.1)	-36.0 (0.0)	-36.0 (0.1)	-154 (4)	-187 (1)	-175 (2)
	Chamerion angustifolium	Aquatic	29.1	10.9	29	-34.9 (0.0)	35.7 (0.3)	-35.8 (0.0)	-35.6 (0.2)	-202 (0)	-228 (0)	-222 (0)
	Chamerion angustifolium	Aquatic	29.1	10.5	29	-34.8 (0.1)	-34.7 (0.0)	-35.3 (0.0)	-34.9 (0.0)	-208 (0)	-232 (0)	-227 (0)
	Chamerion angustifolium	Aquatic	29.1	13.6	29	-33.9 (0.4)	-35.0 (0.2)	-35.6 (0.1)	-35.0 (0.2)	-200 (0)	-228 (0)	-219 (0)
	Chamerion angustifolium	Aquatic	29.1	13.8	29	-34.5 (0.1)	-34.8 (0.0)	-35.3 (0.1)	-34.9 (0.0)	-192 (2)	-221 (2)	-213 (2)
	Chamerion angustifolium	Aquatic	28.8	13.8	29	-34.2 (0.1)	-35.2 (0.0)	-35.6 (0.1)	-35.0 (0.1)	-187 (4)	-222 (2)	-211 (2)
	Chamerion angustifolium	Aquatic	28.7	12.5	29	-34.5 (0.0)	-36.1 (0.0)	-35.5 (0.1)	-35.6 (0.0)	-194 (5)	-230 (2)	-219 (3)
	Chamerion angustifolium	Aquatic	28.9	15.4	29	-35.0 (0.1)	-36.7 (0.1)	-36.2 (0.1)	-36.3 (0.1)	-196 (0)	-231 (1)	-223 (1)
	Chamerion angustifolium	Aquatic	28.8	15.1	29	-35.7 (0.1)	-37.3 (0.1)	-36.2 (0.0)	-36.8 (0.1)	-192 (0)	-232 (0)	-222 (0)
	Phaseolus vulgaris	Terrestrial	30.1	8.5	31	-38.0 (0.1)	-39.4 (0.1)	-38.9 (0.2)	-39.0 (0.2)	-173 (0)	-204 (0)	-197 (0)
	Phaseolus vulgaris	Terrestrial	30.2	8.6	31	-37.4 (0.1)	-38.2 (0.1)	-38.2 (0.0)	-38.1 (0.0)	-155 (5)	-198 (4)	-188 (4)
	Iris pseudacorus	Aquatic	27.6	12.3	27	-37.6 (0.0)	-38.4 (0.2)	-36.5 (0.0)	-37.8 (0.1)	-198 (2)	-212 (1)	-204 (2)
	Iris pseudacorus	Aquatic	27.0	18.0	27	-35.6 (0.2)	-37.0 (0.0)	-37.7 (0.3)	-36.4 (0.1)	-206 (2)	-225 (3)	-214 (2)
	Typha latifolia	Aquatic	28.2	8.0	27	-35.7 (0.0)	-37.1 (0.1)	-35.5 (0.2)	-36.2 (0.1)	-181 (1)	-209 (3)	-194 (2)
	Typha latifolia	Aquatic	28.2	7.9	27	-34.2 (0.1)	-37.8 (0.1)	-37.0 (0.2)	-36.2 (0.1)	-192 (4)	-219 (5)	-206 (4)
	Typha latifolia	Aquatic	27.8	3.7	29	-33.8 (0.2)	-34.6 (0.1)	-33.5 (0.2)	-34.1 (0.2)	-193 (0)	-197 (2)	-195 (1)
	Typha latifolia	Aquatic	27.6	4.3	29	-34.9 (0.0)	-36.4 (0.1)	-33.9 (0.1)	-35.3 (0.1)	-181 (3)	-192 (1)	-187 (2)
	Typha latifolia	Terrestrial	28.0	6.2	29	-33.2 (0.0)	-35.9 (0.1)	-34.1 (0.0)	-34.9 (0.0)	-184 (1)	-215 (0)	-205 (0)
	Typha latifolia	Terrestrial	28.2	6.9	29	-33.8 (0.1)	-37.0 (0.3)	-34.5 (0.3)	-35.8 (0.2)	-169 (4)	-210 (1)	-197 (2)
Trees	*Crataegus monogyna*	Terrestrial	29.5	3.5	31	-35.1 (0.5)	N/A	-33.8 (0.1)	-34.2 (0.2)	-172 (2)	N/A	-172 (2)
	Crataegus monogyna	Terrestrial	29.4	3.4	31	-34.8 (0.0)	N/A	-34.6 (0.4)	-34.6 (0.3)	-173 (1)	N/A	-173 (1)
	Carpinus betulus	Terrestrial	29.1	20.1	29	-36.5 (0.0)	-36.4 (0.0)	-37.2 (0.0)	-36.6 (0.0)	-170 (0)	-214 (0)	-208 (0)
	Carpinus betulus	Terrestrial	29.1	17.4	29	-37.2 (0.1)	-37.7 (0.0)	-37.7 (0.0)	-37.6 (0.0)	-158 (0)	-202 (0)	-196 (0)
	Carpinus betulus	Terrestrial	29.2	16.3	29	-36.0 (0.4)	-38.3 (0.1)	-38.2 (0.1)	-38.1 (0.2)	-147 (2)	-182 (0)	-179 (0)
	Carpinus betulus	Terrestrial	29.3	16.2	29	-33.3 (0.0)	-40.0 (0.1)	-38.2 (0.1)	-39.2 (0.1)	-169 (0)	-197 (0)	-195 (0)
	Fraxinus excelsior	Terrestrial	30.4	8.7	31	-35.8 (0.3)	-36.4 (0.1)	-37.8 (0.3)	-37.3 (0.2)	-137 (0)	-170 (0)	-164 (0)
	Fraxinus excelsior	Terrestrial	30.3	10.4	31	-36.3 (0.0)	-37.3 (0.2)	-39.2 (0.0)	-38.4 (0.1)	-147 (0)	-178 (0)	-172 (0)
	Acer campestre	Terrestrial	30.1	17.7	31	-34.0 (0.3)	-37.1 (0.0)	-37.6 (0.0)	-36.9 (0.1)	-150 (0)	-181 (0)	-170 (0)
	Acer campestre	Terrestrial	30.2	18.4	31	-36.1 (0.3)	-37.7 (0.3)	-37.6 (0.1)	-37.4 (0.2)	-165 (1)	-192 (0)	-182 (0)

Appendix E

SUPPLEMENTARY MATERIAL FOR CHAPTER 7

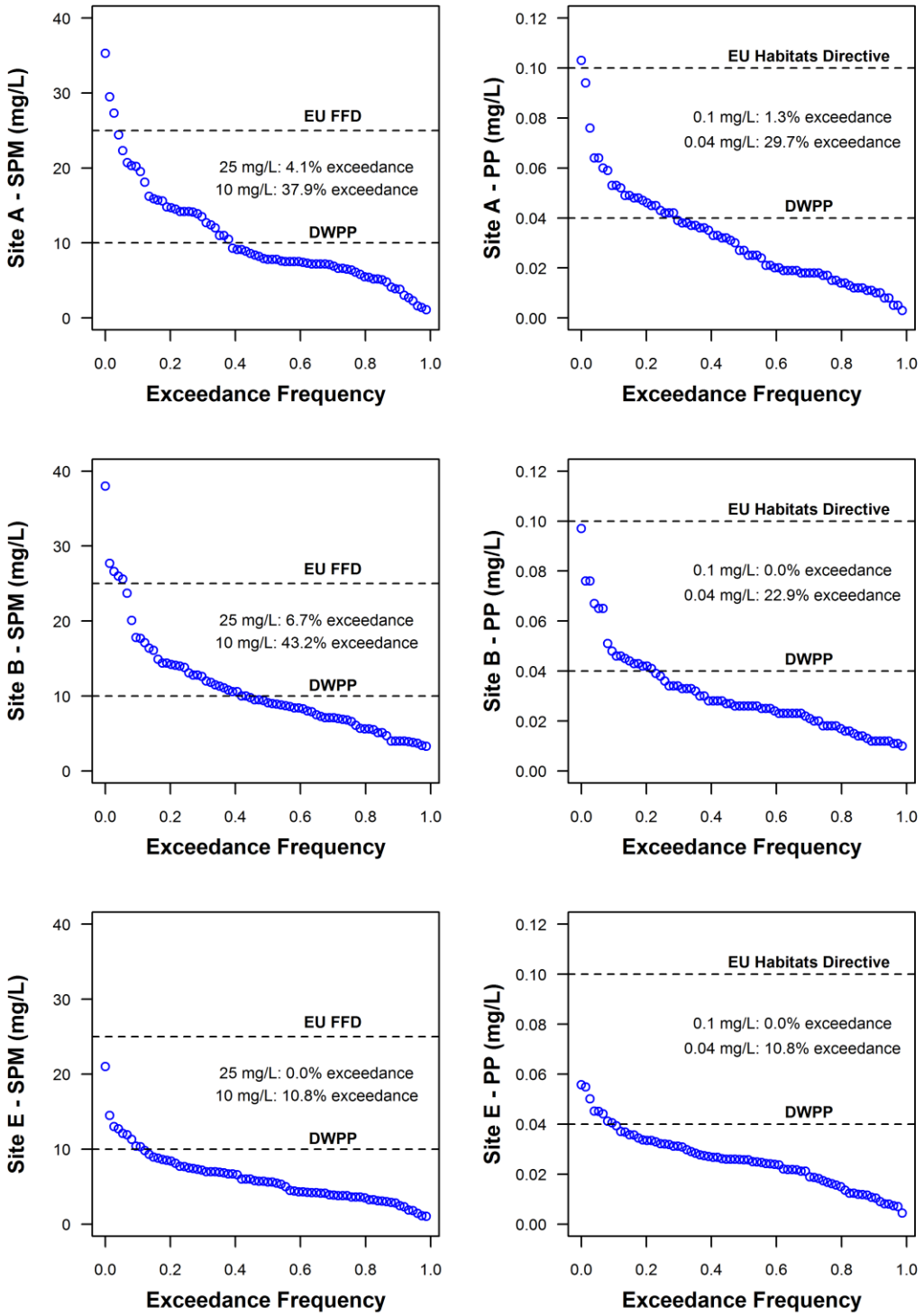

Figure E1: Baseflow exceedance frequency curves for SPM and PP concentration (mg/L) measured at sites A (n = 74), B (n = 74) and E (n = 74) between May 2012 and March 2014. Highlighted on the plots are the EU Freshwater Fisheries Directive (FFD) (78/659/EEC; 2006/44/EC) 25 mg/L SPM threshold; the River Wensum Diffuse Water Pollution Plan (DWPP) lower limit of 10 mg/L SPM for SSSI sites on the Wensum (Riley, 2010); the EU Habitats Directive (92/43/EC) target of 0.1 mg/L TP for headwater streams; and the DWPP lower target of 0.04 mg/L for SSSI sites on the River Wensum.

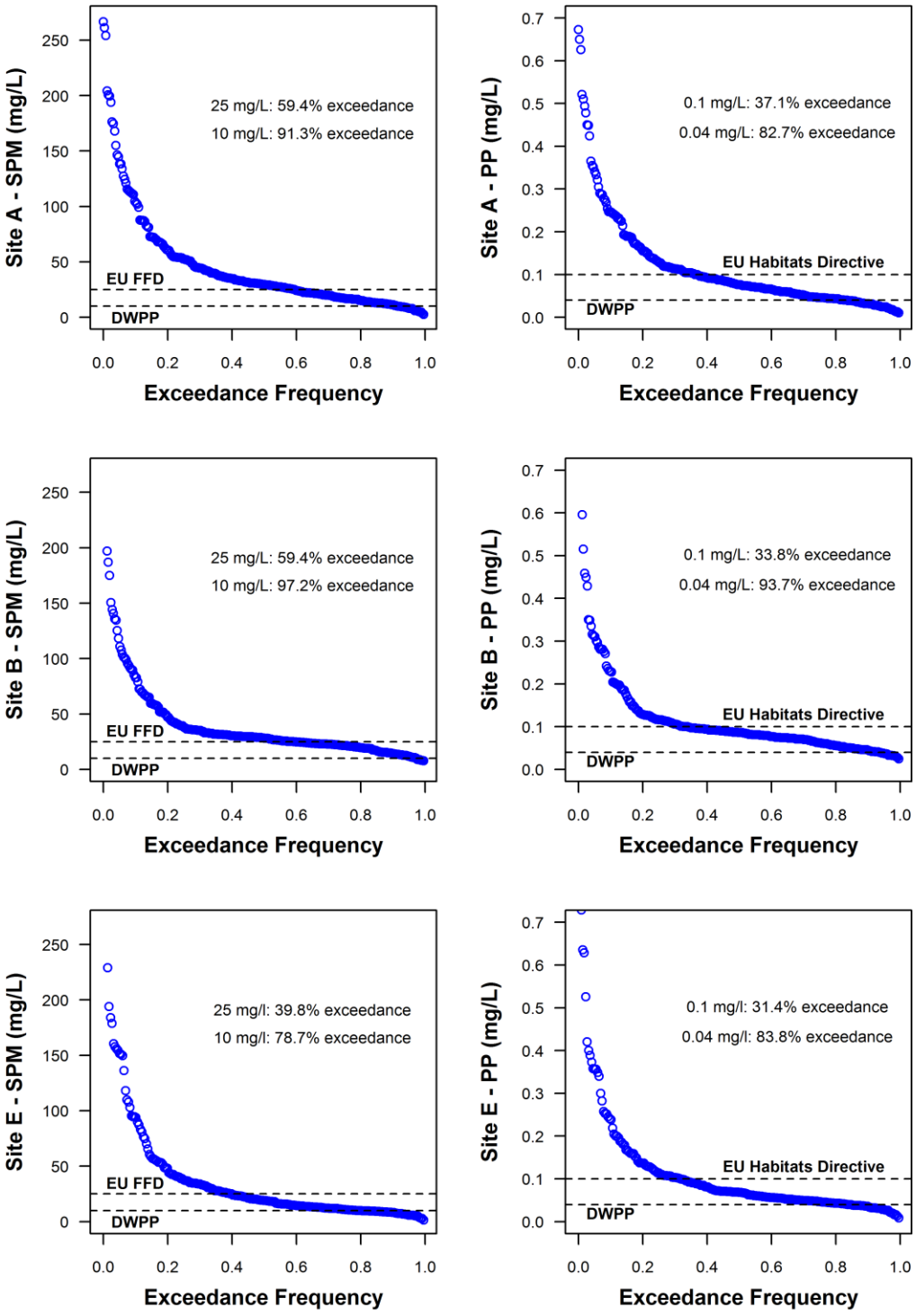

Figure E2: Storm event exceedance frequency curves for SPM and PP concentration (mg/L) measured at sites A (n = 254), B (n = 251) and E (n = 216) during 14 events between September 2012 and February 2014. Highlighted on the plots are the EU Freshwater Fisheries Directive (FFD) (78/659/EEC; 2006/44/EC) 25 mg/L SPM threshold; the River Wensum Diffuse Water Pollution Plan (DWPP) lower limit of 10 mg/L SPM for SSSI sites on the Wensum (Riley, 2010); the EU Habitats Directive (92/43/EC) target of 0.1 mg/L TP for headwater streams; and the DWPP lower target of 0.04 mg/L for SSSI sites on the River Wensum.

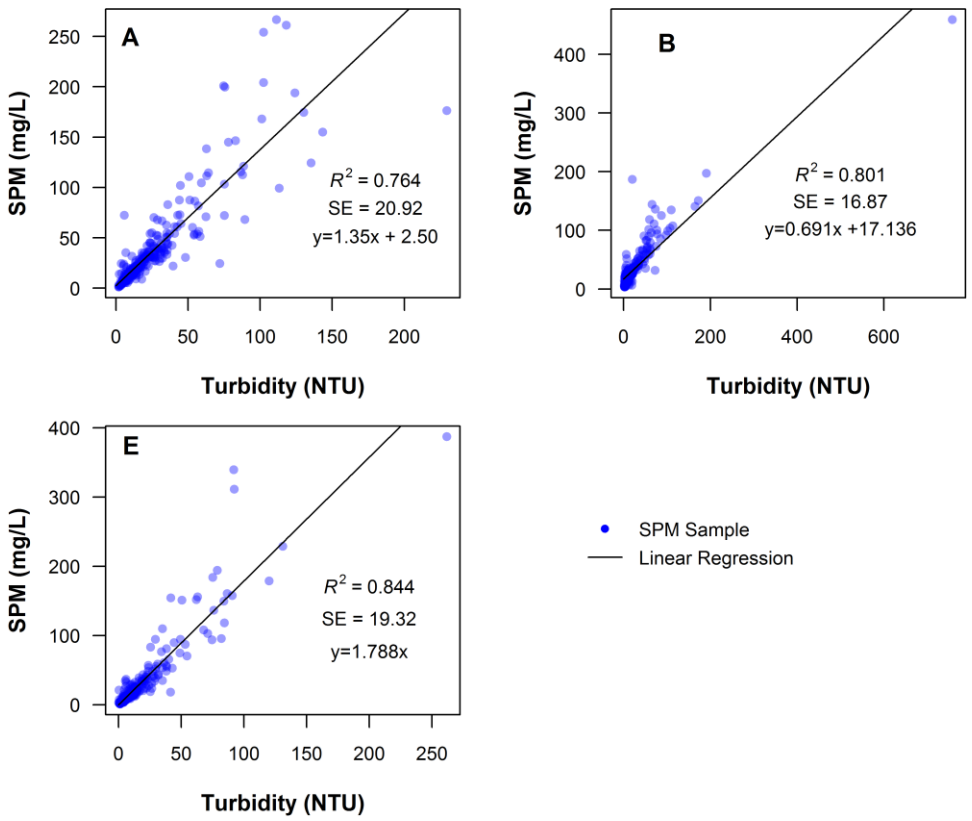

Figure E3: Calibration plots of measured SPM (mg/L) versus YSI optical turbidity measurements (NTU) for sites A (n = 297), B (n = 309) and E (n = 287).

Appendix F

RAW DATA: SPM GEOCHEMISTRY FOR SITES A, B AND E

Table F1: Raw geochemistry data for SPM collected at Site A (Swanhills A) between May 2012 and March 2014. *Ce is measured in ppm.

Sample ID	Flow Conditions	Date (yyyy/mm/dd:hh:mm)	Stage (m)	SPM (mg/L)	Concentration (weight %)															
					Al	Ca	Ce*	Fe	K	Mg	Mn	Na	P	Si	Ti	POC	Al_{di}	Al_{ox}	Fe_{di}	Fe_{ox}
120508A	Baseflow	2012/05/08:08:35	0.419	3.9	7.90	17.99	61	6.68	1.56	0.67	0.07	0.21	0.25	16.49	0.45	12.08	0.11	0.08	2.41	0.33
120515A	Baseflow	2012/05/15:08:18	0.387	2.7	6.06	17.06	49	5.74	1.40	0.53	0.08	0.16	0.31	22.06	0.38	14.44	0.04	0.03	2.75	0.32
120710A	Baseflow	2012/07/10:09:05	0.267	6.6	7.63	23.34	51	6.99	1.44	0.70	0.08	0.29	0.28	9.49	0.46	10.73	0.04	0.03	1.69	0.71
120716A	Baseflow	2012/07/16:08:35	0.316	6.6	7.43	22.32	52	6.92	1.38	0.65	0.09	0.25	0.23	7.40	0.48	10.61	0.07	0.07	2.29	0.56
120731A	Baseflow	2012/07/31:08:35	0.155	15.7	7.86	23.35	47	7.45	1.36	0.70	0.08	0.26	0.28	4.52	0.46	10.98	0.07	0.13	1.19	0.44
120807A	Baseflow	2012/08/07:08:35	0.261	10.5	7.70	21.33	55	7.41	1.40	0.66	0.10	0.23	0.23	3.73	0.51	11.72	0.08	0.05	1.92	0.75
120814A	Baseflow	2012/08/14:08:50	0.175	19.5	7.38	22.82	50	7.74	1.31	0.63	0.10	0.23	0.24	1.20	0.49	10.82	0.07	0.08	1.43	0.74
120821A	Baseflow	2012/08/21:08:35	0.158	20.3	7.72	23.29	47	8.05	1.29	0.67	0.09	0.24	0.26	0.62	0.48	10.40	0.12	0.10	1.82	0.14
120827A	Baseflow	2012/08/27:07:35	0.323	20.7	7.28	18.96	50	6.54	1.16	0.65	0.10	0.26	0.20	0.00	0.46	10.36	0.12	0.09	1.32	0.19
120904A	Baseflow	2012/09/04:08:20	0.213	13.5	7.57	24.53	52	7.66	1.36	0.66	0.09	0.24	0.24	3.97	0.50	10.34	0.02	0.00	2.37	0.39
120910A	Baseflow	2012/09/10:08:20	0.199	27.3	7.64	23.97	51	7.69	1.32	0.67	0.10	0.24	0.24	1.06	0.49	10.15	0.12	0.10	1.79	0.00
120918A	Baseflow	2012/09/18:08:20	0.169	15.9	8.04	24.95	55	8.23	1.40	0.70	0.09	0.22	0.28	4.47	0.49	10.50	0.09	0.10	2.37	0.57
120924A1	Storm Event	2012/09/23:13:35	0.170	17.9	7.07	22.40	51	7.02	1.37	0.62	0.13	0.21	0.33	11.32	0.42	10.90	0.03	0.02	2.59	0.05
120924A2	Storm Event	2012/09/23:14:35	0.171	16.2	7.81	24.70	54	7.76	1.46	0.68	0.13	0.22	0.33	10.74	0.46	9.87	0.03	0.04	3.43	0.05
120924A3	Storm Event	2012/09/23:15:35	0.173	17.4	8.42	25.66	51	8.10	1.54	0.74	0.13	0.23	0.35	8.17	0.49	11.44	0.05	0.06	2.68	0.13
120924A4	Storm Event	2012/09/23:16:35	0.176	22.0	7.61	24.19	53	7.74	1.42	0.67	0.12	0.21	0.30	5.66	0.48	11.12	0.05	0.09	2.18	0.00
120924A5	Storm Event	2012/09/23:17:35	0.194	31.8	7.57	23.89	52	7.51	1.32	0.67	0.10	0.22	0.28	0.84	0.47	10.84	0.03	0.05	2.07	0.25
120924A6	Storm Event	2012/09/23:18:35	0.192	40.0	8.11	23.02	55	7.65	1.45	0.72	0.11	0.22	0.29	3.96	0.49	11.25	0.06	0.05	2.54	0.00
120924A7	Storm Event	2012/09/23:19:35	0.192	37.0	8.31	22.71	56	8.02	1.54	0.74	0.12	0.23	0.31	5.28	0.50	12.21	0.04	0.03	1.97	0.00
120924A8	Storm Event	2012/09/23:20:35	0.200	43.5	8.21	23.32	54	7.83	1.48	0.73	0.12	0.24	0.31	3.84	0.50	12.12	0.04	0.04	2.49	0.00
120924A9	Storm Event	2012/09/23:21:35	0.208	33.5	8.06	21.77	57	7.43	1.52	0.73	0.11	0.23	0.31	8.27	0.47	12.63	0.04	0.03	3.11	0.03
120924A10	Storm Event	2012/09/23:22:35	0.212	35.3	8.05	21.56	52	7.31	1.53	0.71	0.11	0.21	0.31	8.31	0.47	12.38	0.04	0.04	2.52	0.00
120924A11	Storm Event	2012/09/23:23:35	0.233	38.3	7.95	23.53	52	7.42	1.49	0.71	0.10	0.25	0.31	5.38	0.48	11.79	0.03	0.03	2.76	0.04
120924A12	Storm Event	2012/09/24:00:35	0.245	39.2	8.17	22.47	54	7.27	1.52	0.73	0.11	0.24	0.30	6.52	0.48	11.72	0.04	0.03	3.00	0.07
120924A13	Storm Event	2012/09/24:01:35	0.229	35.1	8.24	22.45	58	7.29	1.51	0.73	0.11	0.23	0.30	7.04	0.48	11.93	0.03	0.00	2.70	0.00
120924A14	Storm Event	2012/09/24:02:35	0.222	30.5	8.10	23.60	52	7.14	1.47	0.73	0.10	0.26	0.30	6.61	0.47	11.21	0.01	0.02	3.04	0.26
120924A15	Storm Event	2012/09/24:03:35	0.234	27.0	7.71	23.80	51	7.17	1.42	0.69	0.09	0.25	0.27	5.36	0.47	10.57	0.02	0.03	2.25	0.04
120924A16	Storm Event	2012/09/24:04:35	0.239	30.8	7.68	23.89	50	7.41	1.42	0.67	0.10	0.24	0.27	4.30	0.49	10.97	0.02	0.01	2.69	0.04
120924A17	Storm Event	2012/09/24:05:35	0.244	37.6	7.54	23.62	52	7.31	1.38	0.66	0.09	0.24	0.26	1.99	0.49	11.44	0.04	0.05	2.58	0.19
120924A18	Storm Event	2012/09/24:06:35	0.246	32.8	7.65	24.48	51	7.39	1.39	0.66	0.10	0.22	0.26	2.60	0.49	11.02	0.01	0.02	2.60	0.17

Table F1 continued: Raw geochemistry data for SPM collected at Site A (Swanhills A) between May 2012 and March 2014. *Ce is measured in ppm.

Sample ID	Flow Conditions	Date (yyyy/mm/dd:hh:mm)	Stage (m)	SPM (mg/L)	Concentration (weight %)															
					Al	Ca	Ce*	Fe	K	Mg	Mn	Na	P	Si	Ti	POC	Al_{di}	Al_{ox}	Fe_{di}	Fe_{ox}
120924A19	Storm Event	2012/09/24:07:35	0.251	31.0	7.50	24.39	48	7.20	1.38	0.66	0.09	0.22	0.25	3.58	0.48	11.06	0.05	0.03	2.84	0.29
120924A20	Storm Event	2012/09/24:08:35	0.257	29.6	7.53	24.19	49	6.76	1.35	0.67	0.09	0.25	0.25	4.51	0.46	10.67	0.02	0.03	2.70	0.32
120924A21	Storm Event	2012/09/24:09:35	0.254	28.8	7.66	23.89	51	7.18	1.41	0.67	0.09	0.22	0.25	4.70	0.48	11.02	0.04	0.05	2.97	0.46
120924A22	Storm Event	2012/09/24:10:35	0.255	28.4	7.65	24.16	51	7.15	1.39	0.67	0.09	0.23	0.25	4.60	0.48	9.97	0.02	0.02	2.77	0.11
120924A23	Storm Event	2012/09/24:11:35	0.251	27.3	7.67	24.37	51	7.09	1.39	0.67	0.09	0.23	0.26	5.18	0.48	10.30	0.04	0.02	3.15	0.18
120924A24	Storm Event	2012/09/24:12:35	0.251	22.4	7.35	23.92	50	6.75	1.38	0.65	0.09	0.24	0.25	8.22	0.45	9.20	0.04	0.02	3.05	0.18
121002A	Baseflow	2012/10/02:08:35	0.193	18.1	7.86	25.61	49	7.54	1.39	0.69	0.07	0.24	0.23	2.86	0.51	8.55	0.04	0.03	2.38	0.21
121005A1	Storm Event	2012/10/04:22:24	0.179	20.4	7.09	24.39	52	6.88	1.39	0.62	0.09	0.21	0.27	8.30	0.46	10.40	0.08	0.05	2.73	0.47
121005A2	Storm Event	2012/10/04:23:24	0.180	16.6	7.42	24.83	54	6.78	1.41	0.65	0.09	0.22	0.27	11.45	0.44	9.37	0.10	0.06	3.27	0.64
121005A3	Storm Event	2012/10/05:00:24	0.180	16.7	7.58	25.69	49	7.18	1.44	0.67	0.09	0.22	0.27	10.91	0.47	9.11	0.06	0.02	2.78	1.30
121005A4	Storm Event	2012/10/05:01:24	0.180	16.9	7.70	25.83	55	7.30	1.48	0.68	0.09	0.24	0.27	10.90	0.47	8.76	0.09	0.04	2.67	0.33
121005A5	Storm Event	2012/10/05:02:24	0.182	17.4	7.43	24.60	56	6.83	1.42	0.65	0.09	0.23	0.27	10.85	0.44	8.40	0.09	0.06	3.01	0.20
121005A6	Storm Event	2012/10/05:03:24	0.186	28.1	7.69	25.96	48	7.41	1.38	0.68	0.08	0.22	0.25	1.44	0.50	10.11	0.07	0.04	2.68	0.64
121005A7	Storm Event	2012/10/05:04:24	0.201	33.4	7.67	24.37	50	7.43	1.43	0.68	0.09	0.22	0.29	2.71	0.48	12.92	0.06	0.01	2.97	0.95
121005A8	Storm Event	2012/10/05:05:24	0.212	72.1	9.33	20.67	59	8.16	1.66	0.77	0.08	0.21	0.34	3.70	0.51	15.31	0.09	0.04	2.85	0.25
121005A9	Storm Event	2012/10/05:06:24	0.225	124.3	12.38	14.30	71	8.43	1.88	0.93	0.09	0.27	0.36	5.05	0.56	13.17	0.20	0.07	2.73	0.51
121005A10	Storm Event	2012/10/05:07:24	0.217	99.2	13.00	14.17	81	8.85	2.04	0.96	0.10	0.28	0.36	8.32	0.59	13.27	0.20	0.07	3.48	0.83
121005A11	Storm Event	2012/10/05:08:24	0.208	60.3	10.56	18.94	68	8.31	1.79	0.83	0.10	0.23	0.31	8.12	0.54	11.39	0.13	0.08	3.47	0.63
121005A12	Storm Event	2012/10/05:09:24	0.207	54.3	10.04	20.04	61	8.25	1.68	0.81	0.09	0.24	0.29	5.96	0.54	11.00	0.16	0.09	2.88	0.53
121005A13	Storm Event	2012/10/05:10:24	0.205	45.9	9.71	21.60	63	8.26	1.65	0.79	0.09	0.24	0.27	6.59	0.55	9.93	0.12	0.07	3.20	0.52
121005A14	Storm Event	2012/10/05:11:24	0.209	41.2	8.96	23.14	58	7.81	1.56	0.75	0.09	0.24	0.25	5.06	0.53	9.55	0.10	0.05	2.74	0.94
121005A15	Storm Event	2012/10/05:12:24	0.208	32.9	8.69	23.99	55	7.65	1.51	0.73	0.08	0.23	0.24	4.92	0.52	9.39	0.10	0.07	3.06	1.04
121005A16	Storm Event	2012/10/05:13:24	0.208	31.0	8.98	25.37	52	7.86	1.55	0.76	0.09	0.24	0.25	5.01	0.54	9.76	0.07	0.01	3.40	1.44
121005A17	Storm Event	2012/10/05:14:24	0.209	29.2	8.72	26.36	53	8.00	1.50	0.74	0.09	0.24	0.24	3.49	0.54	9.86	0.15	0.07	2.80	0.29
121005A18	Storm Event	2012/10/05:15:24	0.203	29.7	8.31	25.01	57	7.59	1.46	0.71	0.08	0.23	0.23	3.60	0.52	9.91	0.13	0.06	2.86	0.43
121005A19	Storm Event	2012/10/05:16:24	0.208	30.4	8.10	25.16	55	7.68	1.42	0.71	0.08	0.26	0.22	1.24	0.52	8.83	0.12	0.09	2.15	0.34
121005A20	Storm Event	2012/10/05:17:24	0.206	31.3	8.20	25.28	51	7.67	1.44	0.70	0.08	0.24	0.23	2.45	0.52	9.09	0.13	0.03	2.63	0.03
121005A21	Storm Event	2012/10/05:18:24	0.203	36.9	8.37	24.78	53	7.42	1.42	0.72	0.08	0.26	0.23	2.17	0.51	8.89	0.10	0.06	2.82	0.32
121005A22	Storm Event	2012/10/05:19:24	0.203	28.2	8.24	24.61	54	7.63	1.43	0.71	0.08	0.25	0.23	2.74	0.51	9.27	0.13	0.10	2.82	0.22
121005A23	Storm Event	2012/10/05:20:24	0.203	25.0	8.24	24.51	52	7.69	1.47	0.71	0.09	0.25	0.24	4.40	0.51	9.46	0.11	0.07	2.14	0.00

Table F1 continued: Raw geochemistry data for SPM collected at Site A (Swanhills A) between May 2012 and March 2014. *Ce is measured in ppm.

Sample ID	Flow Conditions	Date (yyyy/mm/dd:hh:mm)	Stage (m)	SPM (mg/L)	Concentration (weight %)															
					Al	Ca	Ce*	Fe	K	Mg	Mn	Na	P	Si	Ti	POC	Al_{di}	Al_{ox}	Fe_{di}	Fe_{ox}
121005A24	Storm Event	2012/10/05:21:24	0.199	22.4	8.19	24.04	50	7.49	1.49	0.69	0.09	0.23	0.25	6.52	0.50	10.11	0.12	0.11	3.17	0.37
121009A	Baseflow	2012/10/09:08:35	0.235	13.9	8.16	26.25	52	7.45	1.42	0.71	0.06	0.24	0.21	3.02	0.52	8.72	0.01	0.00	3.05	0.41
121016A	Baseflow	2012/10/16:09:05	0.221	20.2	9.90	22.52	59	7.89	1.56	0.83	0.06	0.24	0.26	3.51	0.52	9.08	0.03	0.00	3.04	0.16
121022A	Baseflow	2012/10/22:14:00	0.643	7.8	8.60	21.19	59	7.68	1.54	0.71	0.08	0.24	0.23	5.50	0.52	11.63	0.03	0.00	3.51	0.44
121030A	Baseflow	2012/10/30:09:45	0.477	5.4	8.28	22.57	52	6.92	1.46	0.70	0.07	0.28	0.22	6.91	0.50	10.28	0.07	0.03	2.18	0.22
121101A5	Storm Event	2012/11/01:03:04	0.420	11.7	5.70	28.85	46	5.67	1.16	0.48	0.11	0.19	0.21	15.59	0.37	8.58	0.01	0.05	0.78	0.22
121101A6	Storm Event	2012/11/01:04:04	0.420	12.0	6.42	28.14	53	6.00	1.29	0.54	0.09	0.21	0.20	14.54	0.41	8.38	0.09	0.11	2.38	0.18
121101A7	Storm Event	2012/11/01:05:04	0.422	15.3	7.57	26.69	53	6.79	1.47	0.64	0.09	0.23	0.22	10.45	0.48	9.74	0.09	0.10	2.38	0.21
121101A8	Storm Event	2012/11/01:06:04	0.451	35.9	9.53	17.33	71	7.60	1.69	0.82	0.12	0.29	0.27	3.62	0.57	13.28	0.08	0.01	2.13	0.30
121101A9	Storm Event	2012/11/01:07:04	0.464	29.4	9.92	18.42	72	7.87	1.73	0.82	0.12	0.26	0.28	4.85	0.56	12.13	0.07	0.04	2.42	0.29
121101A10	Storm Event	2012/11/01:08:04	0.472	23.5	9.21	16.98	61	7.21	1.65	0.77	0.10	0.27	0.27	8.65	0.50	11.86	0.10	0.08	2.56	0.20
121101A11	Storm Event	2012/11/01:09:04	0.479	16.7	9.02	16.87	61	7.12	1.68	0.73	0.12	0.26	0.26	14.50	0.48	11.16	0.12	0.10	2.54	0.34
121101A12	Storm Event	2012/11/01:10:04	0.483	15.2	8.62	16.89	60	6.67	1.62	0.70	0.11	0.23	0.25	16.27	0.45	10.25	0.05	0.03	2.92	0.45
121101A13	Storm Event	2012/11/01:11:04	0.505	13.9	8.89	18.37	55	6.83	1.64	0.73	0.11	0.25	0.26	15.88	0.47	10.43	0.11	0.11	2.42	0.50
121101A14/15	Storm Event	2012/11/01:12:34	0.573	13.3	8.64	19.63	57	7.20	1.52	0.71	0.09	0.26	0.23	6.08	0.49	10.70	0.09	0.04	2.92	0.38
121101A16/17	Storm Event	2012/11/01:14:34	0.619	12.4	10.51	22.07	71	9.49	1.91	0.85	0.11	0.31	0.27	5.93	0.64	13.08	0.11	0.08	3.61	0.30
121101A18	Storm Event	2012/11/01:16:04	0.629	23.0	7.44	14.08	43	4.87	1.30	0.61	0.09	0.23	0.22	17.12	0.34	8.67	0.08	0.08	2.46	0.31
121101A19	Storm Event	2012/11/01:17:04	0.627	19.8	7.92	18.28	55	6.29	1.48	0.65	0.08	0.25	0.22	12.62	0.44	9.58	0.10	0.05	3.03	0.35
121101A20	Storm Event	2012/11/01:18:04	0.626	18.1	8.47	19.94	58	7.00	1.58	0.69	0.09	0.23	0.24	10.99	0.50	9.85	0.09	0.07	3.22	0.34
121101A21	Storm Event	2012/11/01:19:04	0.620	16.6	7.76	18.06	55	6.12	1.48	0.63	0.09	0.25	0.23	15.16	0.43	9.54	0.05	0.05	3.05	0.20
121101A22	Storm Event	2012/11/01:20:04	0.618	13.7	7.62	18.26	57	6.09	1.48	0.62	0.09	0.22	0.23	17.36	0.42	8.94	0.05	0.03	4.28	0.30
121101A23/24	Storm Event	2012/11/01:21:34	0.612	12.9	8.44	20.61	55	7.18	1.51	0.69	0.09	0.26	0.22	6.17	0.50	10.44	0.05	0.02	2.83	0.41
121106A	Baseflow	2012/11/06:08:00	0.487	5.2	7.48	20.11	53	6.41	1.39	0.62	0.07	0.23	0.23	7.23	0.46	10.26	0.05	0.03	2.21	0.04
121120A	Baseflow	2012/11/20:10:00	0.269	35.3	10.27	12.45	69	6.75	1.67	0.90	0.10	0.40	0.27	12.72	0.48	15.21	0.19	0.00	3.99	0.27
121123A1	Storm Event	2012/11/23:09:52	0.681	34.7	8.25	16.62	60	7.03	1.47	0.67	0.08	0.26	0.23	4.48	0.48	13.17	0.19	0.00	2.98	0.38
121123A2	Storm Event	2012/11/23:11:52	0.665	21.4	8.03	15.91	52	6.52	1.52	0.65	0.08	0.25	0.23	13.50	0.45	11.99	0.18	0.00	3.90	0.42
121123A3	Storm Event	2012/11/23:13:52	0.649	21.3	7.82	17.40	56	6.48	1.50	0.64	0.09	0.25	0.25	11.77	0.46	13.65	0.23	0.03	3.28	0.36
121123A4/A5	Storm Event	2012/11/23:16:52	0.626	14.9	8.58	18.38	60	7.54	1.56	0.69	0.09	0.25	0.26	6.61	0.51	16.25	0.18	0.00	4.29	0.21
121123A6/A7	Storm Event	2012/11/23:20:52	0.598	12.2	8.14	18.90	54	7.20	1.54	0.66	0.09	0.24	0.23	8.11	0.50	12.48	0.15	0.00	3.54	0.42

Table F1 continued: Raw geochemistry data for SPM collected at Site A (Swanhills A) between May 2012 and March 2014. *Ce is measured in ppm.

Sample ID	Flow Conditions	Date (yyyy/mm/dd:hh:mm)	Stage (m)	SPM (mg/L)	Concentration (weight %)															
					Al	Ca	Ce*	Fe	K	Mg	Mn	Na	P	Si	Ti	POC	Al_{di}	Al_{ox}	Fe_{di}	Fe_{ox}
121123A8/A9	Storm Event	2012/11/24:00:52	0.571	9.6	8.05	19.49	50	6.99	1.56	0.66	0.09	0.26	0.23	11.80	0.49	12.26	0.19	0.01	3.65	0.48
121123A10/A11	Storm Event	2012/11/24:04:52	0.545	7.8	8.02	19.51	57	6.90	1.51	0.66	0.08	0.24	0.23	8.75	0.48	11.93	0.17	0.00	3.72	0.32
121125A1/A2/A3/A4	Storm Event	2012/11/24:14:04	0.500	6.0	7.55	23.31	53	6.69	1.37	0.64	0.10	0.24	0.22	6.54	0.47	13.64	0.17	0.00	3.86	0.47
121125A5	Storm Event	2012/11/24:19:04	0.503	21.9	11.52	15.01	83	8.35	1.98	1.00	0.16	0.33	0.32	9.63	0.61	18.08	0.22	0.00	4.64	0.66
121125A6	Storm Event	2012/11/24:21:04	0.511	17.9	9.98	15.65	69	7.40	1.78	0.86	0.12	0.30	0.30	11.76	0.52	15.80	0.21	0.00	3.56	0.54
121125A7	Storm Event	2012/11/24:23:04	0.520	18.2	9.81	15.68	69	7.31	1.79	0.83	0.12	0.26	0.36	10.11	0.51	20.45	0.18	0.00	3.36	0.38
121125A8	Storm Event	2012/11/25:01:04	0.539	11.6	9.44	16.80	68	7.02	1.77	0.78	0.15	0.25	0.35	16.28	0.47	18.81	0.17	0.00	4.65	0.46
121125A9	Storm Event	2012/11/25:03:04	0.579	13.2	8.52	15.50	53	6.26	1.60	0.70	0.12	0.23	0.30	17.50	0.42	14.62	0.16	0.00	3.93	0.29
121125A10	Storm Event	2012/11/25:05:04	0.630	22.3	8.78	16.08	65	7.07	1.64	0.71	0.13	0.24	0.28	9.22	0.48	17.63	0.19	0.00	3.71	0.45
121125A11	Storm Event	2012/11/25:07:04	0.749	39.6	9.92	15.53	61	7.62	1.73	0.79	0.12	0.25	0.29	5.99	0.54	15.29	0.21	0.00	3.64	0.53
121125A12	Storm Event	2012/11/25:09:04	0.900	103.2	9.85	14.75	65	7.54	1.61	0.76	0.11	0.28	0.23	3.83	0.53	13.25	0.24	0.00	3.14	0.40
121125A13	Storm Event	2012/11/25:11:04	0.944	112.5	9.60	14.45	60	7.16	1.48	0.73	0.09	0.27	0.21	2.57	0.48	11.21	0.24	0.01	2.19	0.42
121125A14	Storm Event	2012/11/25:13:04	0.913	86.3	8.71	13.84	54	6.63	1.39	0.66	0.07	0.26	0.19	4.37	0.45	10.62	0.23	0.03	2.29	0.25
121125A15	Storm Event	2012/11/25:15:04	0.869	60.8	8.60	14.34	57	6.78	1.39	0.65	0.07	0.26	0.19	4.20	0.44	11.17	0.23	0.01	2.61	0.37
121125A16	Storm Event	2012/11/25:17:04	0.824	44.3	9.43	14.32	56	6.83	1.49	0.71	0.08	0.27	0.22	6.12	0.46	12.96	0.26	0.00	3.00	0.51
121125A17	Storm Event	2012/11/25:19:04	0.788	30.7	8.52	14.57	58	6.78	1.49	0.64	0.08	0.23	0.21	8.08	0.44	11.64	0.21	0.00	2.94	0.29
121125A18	Storm Event	2012/11/25:21:04	0.756	21.3	7.89	15.54	57	6.23	1.47	0.60	0.11	0.23	0.21	13.13	0.43	11.89	0.20	0.00	3.53	0.50
121125A19	Storm Event	2012/11/25:23:04	0.736	19.6	8.01	15.63	59	6.33	1.52	0.61	0.11	0.24	0.22	14.19	0.44	12.14	0.23	0.00	3.73	0.43
121125A20/A21	Storm Event	2012/11/26:02:04	0.700	16.3	8.94	16.31	49	7.10	1.48	0.68	0.09	0.26	0.22	6.13	0.46	12.51	0.26	0.02	2.67	0.39
121125A22/23	Storm Event	2012/11/26:06:04	0.661	16.1	9.23	14.85	57	7.17	1.59	0.73	0.11	0.25	0.25	7.93	0.48	13.97	0.21	0.00	3.07	0.48
121125A24	Storm Event	2012/11/26:09:04	0.686	36.3	10.86	10.96	75	7.33	1.91	0.91	0.13	0.32	0.33	9.66	0.56	17.59	0.25	0.00	3.75	0.66
121127A1	Storm Event	2012/11/26:12:19	0.836	37.5	10.43	10.93	65	7.15	1.69	0.78	0.11	0.26	0.24	10.21	0.48	13.49	0.28	0.01	3.73	0.40
121127A2	Storm Event	2012/11/26:14:19	0.845	32.9	10.26	12.16	63	7.05	1.60	0.78	0.10	0.27	0.23	9.23	0.46	12.58	0.27	0.00	3.64	0.46
121127A3	Storm Event	2012/11/26:16:19	0.815	31.6	9.38	12.67	59	6.83	1.55	0.72	0.07	0.26	0.22	9.51	0.45	12.94	0.27	0.00	3.82	0.58
121127A4	Storm Event	2012/11/26:18:19	0.790	25.9	9.33	13.80	56	7.37	1.62	0.71	0.09	0.25	0.23	10.40	0.47	13.41	0.24	0.00	4.14	0.45
121127A5	Storm Event	2012/11/26:20:19	0.772	20.9	8.52	13.24	59	6.37	1.52	0.64	0.11	0.23	0.22	15.30	0.41	12.59	0.24	0.00	3.97	0.30
121127A6	Storm Event	2012/11/26:22:19	0.751	19.9	8.53	14.28	58	6.72	1.56	0.64	0.12	0.23	0.22	14.48	0.44	14.99	0.23	0.00	5.27	1.43
121127A7/8	Storm Event	2012/11/27:01:19	0.723	15.0	8.77	14.94	59	7.13	1.51	0.66	0.09	0.24	0.21	8.14	0.44	12.67	0.25	0.00	3.76	0.34
121127A9/10	Storm Event	2012/11/27:05:19	0.686	12.9	8.50	15.62	59	7.16	1.53	0.64	0.09	0.23	0.22	9.79	0.45	12.94	0.26	0.00	3.90	0.25

Table F1 continued: Raw geochemistry data for SPM collected at Site A (Swanhills A) between May 2012 and March 2014. *Ce is measured in ppm.

Sample ID	Flow Conditions	Date (yyyy/mm/dd:hh:mm)	Stage (m)	SPM (mg/L)	Concentration (weight %)															
					Al	Ca	Ce*	Fe	K	Mg	Mn	Na	P	Si	Ti	POC	Al_{di}	Al_{ox}	Fe_{di}	Fe_{ox}
121127A11	Storm Event	2012/11/27:08:19	0.679	21.9	9.68	11.65	69	6.89	1.76	0.85	0.15	0.30	0.28	12.83	0.51	16.40	0.24	0.00	4.14	0.63
121127A12	Storm Event	2012/11/27:10:19	0.691	12.7	9.19	12.51	65	6.72	1.71	0.72	0.14	0.24	0.28	19.59	0.43	14.81	0.22	0.00	5.34	0.43
121127A13	Storm Event	2012/11/27:12:19	0.749	27.1	11.43	11.28	75	8.18	2.01	0.94	0.14	0.31	0.32	10.50	0.58	17.63	0.26	0.00	4.08	0.43
121127A14	Storm Event	2012/11/27:14:19	0.894	53.6	10.52	11.25	77	7.60	1.76	0.81	0.10	0.27	0.26	8.21	0.52	13.92	0.27	0.00	3.43	0.32
121127A15	Storm Event	2012/11/27:16:19	0.985	121.0	8.76	13.96	65	7.19	1.45	0.69	0.07	0.28	0.19	2.45	0.49	11.27	0.22	0.00	2.56	0.33
121127A16	Storm Event	2012/11/27:18:19	0.957	111.4	7.71	14.23	58	6.72	1.27	0.60	0.05	0.26	0.17	1.10	0.44	9.84	0.20	0.00	2.28	0.23
121127A17	Storm Event	2012/11/27:20:19	0.928	87.5	7.43	13.05	54	5.82	1.18	0.57	0.05	0.27	0.16	3.46	0.39	9.40	0.19	0.00	2.46	0.17
121127A18	Storm Event	2012/11/27:22:19	0.886	54.5	9.08	13.08	52	6.28	1.32	0.67	0.06	0.27	0.18	4.77	0.41	10.61	0.24	0.00	2.40	0.26
121127A19	Storm Event	2012/11/28:00:19	0.849	45.2	7.78	13.29	56	6.10	1.26	0.58	0.06	0.24	0.17	5.19	0.39	9.96	0.20	0.00	2.52	0.21
121127A20/21	Storm Event	2012/11/28:03:19	0.800	30.1	8.69	13.46	54	6.23	1.32	0.64	0.06	0.26	0.19	6.44	0.40	10.82	0.24	0.00	2.67	0.34
121127A22/23	Storm Event	2012/11/28:07:19	0.753	22.0	8.00	13.89	56	6.58	1.32	0.61	0.07	0.24	0.19	5.53	0.41	11.40	0.25	0.00	3.03	0.25
121211A	Baseflow	2012/12/11:09:50	0.398	9.1	9.18	21.33	52	7.74	1.60	0.74	0.08	0.24	0.27	6.84	0.52	10.74	0.19	0.03	3.93	0.37
121219A	Baseflow	2012/12/19:10:15	0.360	5.8	9.00	22.47	55	7.68	1.59	0.74	0.08	0.24	0.22	8.07	0.50	9.97	0.20	0.05	3.04	0.05
130103A	Baseflow	2013/01/03:12:45	0.357	14.2	8.32	21.80	50	7.44	1.44	0.70	0.08	0.26	0.19	3.22	0.50	9.65	0.16	0.02	3.10	0.34
130108A	Baseflow	2013/01/08:12:47	0.298	12.4	8.57	24.54	49	7.51	1.46	0.73	0.09	0.26	0.20	4.15	0.50	10.52	0.16	0.04	3.20	0.49
130122A	Baseflow	2013/01/22:10:05	0.328	14.5	9.57	18.44	62	7.87	1.69	0.93	0.10	0.35	0.24	7.61	0.53	11.84	0.15	0.00	3.13	0.23
130129A	Baseflow	2013/01/29:09:45	0.462	24.4	9.91	14.31	65	7.77	1.72	0.82	0.11	0.29	0.24	8.49	0.55	13.82	0.21	0.04	2.92	0.29
130205A	Baseflow	2013/02/05:10:10	0.343	7.5	8.80	21.25	52	7.63	1.54	0.72	0.09	0.23	0.25	8.51	0.49	10.24	0.15	0.02	2.93	0.95
130212A	Baseflow	2013/02/12:09:15	0.332	6.5	8.84	20.84	50	7.46	1.52	0.73	0.09	0.24	0.27	9.42	0.48	9.75	0.14	0.05	2.98	0.30
130214A1/2	Storm Event	2013/02/13:22:49	0.313	24.0	5.61	14.54	40	4.16	1.10	0.47	0.06	0.26	0.19	6.97	0.33	10.07	0.12	0.03	1.43	0.08
130214A3/4	Storm Event	2013/02/14:02:49	0.316	9.1	6.73	19.28	44	5.72	1.33	0.57	0.12	0.26	0.24	15.36	0.38	10.29	0.16	0.06	2.21	0.20
130214A5	Storm Event	2013/02/14:05:49	0.340	53.8	11.71	11.18	85	8.27	2.04	1.13	0.14	0.31	0.36	11.67	0.58	15.92	0.23	0.07	3.77	0.44
130214A6	Storm Event	2013/02/14:07:49	0.471	176.3	14.96	6.60	92	8.30	2.35	1.08	0.12	0.37	0.37	10.12	0.65	14.22	0.32	0.08	3.21	0.60
130214A7	Storm Event	2013/02/14:09:49	0.569	155.0	15.24	7.28	90	8.39	2.30	1.04	0.13	0.29	0.32	11.09	0.62	13.29	0.34	0.15	2.99	0.37
130214A8	Storm Event	2013/02/14:11:49	0.580	115.6	12.09	10.53	75	7.95	1.85	0.84	0.10	0.26	0.24	9.35	0.52	12.05	0.32	0.12	3.23	0.30
130214A9	Storm Event	2013/02/14:13:49	0.568	81.6	10.12	11.23	62	7.32	1.63	0.72	0.08	0.24	0.20	10.38	0.48	11.28	0.32	0.14	2.93	0.21
130214A10	Storm Event	2013/02/14:15:49	0.548	61.1	10.22	11.67	63	7.29	1.58	0.71	0.08	0.24	0.20	9.64	0.46	11.07	0.28	0.12	2.34	0.22
130214A11	Storm Event	2013/02/14:17:49	0.535	50.7	9.10	12.52	67	7.17	1.49	0.65	0.07	0.25	0.18	8.70	0.45	11.12	0.29	0.09	3.19	0.27
130214A12	Storm Event	2013/02/14:19:49	0.513	39.7	10.30	12.21	51	6.82	1.51	0.73	0.07	0.26	0.20	9.77	0.44	10.38	0.28	0.11	2.55	0.39

Table F1 continued: Raw geochemistry data for SPM collected at Site A (Swanhills A) between May 2012 and March 2014. *Ce is measured in ppm.

Sample ID	Flow Conditions	Date (yyyy/mm/dd:hh:mm)	Stage (m)	SPM (mg/L)	Concentration (weight %)															
					Al	Ca	Ce*	Fe	K	Mg	Mn	Na	P	Si	Ti	POC	Al_{di}	Al_{ox}	Fe_{di}	Fe_{ox}
130214A13	Storm Event	2013/02/14:21:49	0.500	33.5	9.41	13.38	58	6.74	1.50	0.68	0.07	0.24	0.20	9.79	0.44	10.29	0.27	0.11	2.80	0.25
130214A14	Storm Event	2013/02/14:23:49	0.484	23.3	8.68	14.29	54	6.92	1.57	0.63	0.10	0.23	0.19	14.43	0.45	10.50	0.26	0.11	3.27	0.41
130214A15	Storm Event	2013/02/15:01:49	0.475	22.0	8.09	14.01	48	6.31	1.48	0.60	0.10	0.23	0.19	16.61	0.41	9.51	0.25	0.14	2.87	0.34
130214A16/17	Storm Event	2013/02/15:04:49	0.458	16.7	8.88	16.48	55	7.19	1.46	0.67	0.07	0.26	0.19	6.78	0.46	10.05	0.25	0.10	2.35	0.22
130214A18/19	Storm Event	2013/02/15:08:49	0.441	16.2	9.05	16.27	55	7.09	1.50	0.70	0.09	0.26	0.21	6.99	0.47	10.44	0.24	0.12	2.52	0.37
130214A20/21	Storm Event	2013/02/15:12:49	0.429	14.1	8.52	16.00	48	6.60	1.48	0.68	0.08	0.27	0.28	8.22	0.45	14.46	0.20	0.07	2.75	0.11
130214A22/23/24	Storm Event	2013/02/15:17:49	0.412	12.7	8.17	18.04	53	7.16	1.47	0.66	0.09	0.27	0.19	6.98	0.48	10.71	0.22	0.08	2.49	0.19
130219A	Baseflow	2013/02/19:09:50	0.305	7.2	8.77	21.14	54	8.15	1.56	0.71	0.10	0.24	0.24	7.54	0.51	10.23	0.16	0.05	2.74	0.61
130226A	Baseflow	2013/02/26:11:50	0.218	8.4	8.50	24.22	54	8.06	1.51	0.73	0.07	0.23	0.21	7.17	0.49	7.76	0.14	0.03	2.76	0.26
130305A	Baseflow	2013/03/05:11:15	0.203	7.2	8.29	23.07	46	8.15	1.47	0.69	0.07	0.22	0.25	8.77	0.47	9.98	0.15	0.04	2.99	0.00
130309A1/2	Storm Event	2013/03/08:18:48	0.187	31.7	5.86	18.60	45	5.76	1.14	0.50	0.07	0.21	0.26	0.88	0.40	12.85	0.11	0.03	2.08	0.00
130309A4	Storm Event	2013/03/08:23:48	0.204	193.8	14.07	10.69	84	8.51	2.18	1.14	0.13	0.41	0.35	10.46	0.60	12.80	0.18	0.12	2.74	0.35
130309A5	Storm Event	2013/03/09:01:48	0.210	174.6	13.74	10.07	84	8.30	2.22	1.12	0.13	0.39	0.36	11.77	0.61	13.79	0.21	0.07	4.77	0.38
130309A6	Storm Event	2013/03/09:03:48	0.221	87.5	11.79	15.10	72	8.32	1.96	0.97	0.11	0.35	0.31	10.73	0.57	12.01	0.19	0.05	3.95	0.27
130309A7	Storm Event	2013/03/09:05:48	0.245	110.7	10.75	16.09	69	8.34	1.88	0.90	0.11	0.34	0.32	8.12	0.56	12.87	0.14	0.04	2.76	0.04
130309A8	Storm Event	2013/03/09:07:48	0.333	204.2	8.90	16.66	64	7.82	1.63	0.74	0.10	0.30	0.26	4.08	0.54	11.57	0.15	0.05	1.92	0.15
130309A9	Storm Event	2013/03/09:09:48	0.467	261.1	7.59	15.86	57	6.66	1.37	0.63	0.08	0.28	0.18	2.64	0.48	9.76	0.16	0.09	1.75	0.12
130309A10	Storm Event	2013/03/09:11:48	0.627	266.5	7.04	14.15	55	5.76	1.22	0.56	0.05	0.29	0.16	3.15	0.42	8.00	0.13	0.09	1.37	0.08
130309A11	Storm Event	2013/03/09:13:48	0.716	254.1	8.58	13.28	60	6.02	1.47	0.68	0.07	0.32	0.20	7.71	0.48	8.81	0.16	0.07	2.09	0.09
130309A12	Storm Event	2013/03/09:15:48	0.795	199.6	7.84	13.06	56	5.95	1.35	0.62	0.06	0.30	0.18	6.54	0.45	8.83	0.18	0.09	1.88	0.13
130309A13	Storm Event	2013/03/09:17:48	0.900	200.8	7.63	12.86	56	5.72	1.29	0.59	0.04	0.30	0.17	7.18	0.42	8.34	0.19	0.10	1.63	0.02
130309A14	Storm Event	2013/03/09:19:48	0.913	138.4	7.85	13.37	50	5.94	1.28	0.59	0.04	0.28	0.17	6.24	0.42	8.19	0.18	0.07	1.75	0.06
130309A15	Storm Event	2013/03/09:21:48	0.912	114.4	7.34	13.17	53	5.79	1.28	0.55	0.05	0.27	0.16	7.85	0.41	8.25	0.17	0.08	1.76	0.05
130309A16	Storm Event	2013/03/09:23:48	0.904	101.9	6.83	12.91	49	5.53	1.18	0.51	0.04	0.28	0.15	6.83	0.39	7.73	0.20	0.13	1.66	0.10
130309A17	Storm Event	2013/03/10:01:48	0.893	82.9	7.28	13.83	52	5.91	1.26	0.55	0.05	0.28	0.17	8.06	0.41	7.76	0.19	0.09	2.01	0.06
130309A18	Storm Event	2013/03/10:03:48	0.871	66.9	7.70	13.60	50	5.65	1.22	0.58	0.04	0.27	0.17	7.53	0.39	7.75	0.19	0.09	1.81	0.08
130309A19	Storm Event	2013/03/10:05:48	0.848	67.7	6.62	13.93	49	5.71	1.13	0.50	0.04	0.25	0.15	4.53	0.37	7.58	0.18	0.10	2.00	0.01
130309A20	Storm Event	2013/03/10:07:48	0.824	55.0	7.10	13.46	51	5.57	1.19	0.53	0.04	0.25	0.16	7.58	0.37	8.16	0.19	0.09	2.06	0.07
130309A21	Storm Event	2013/03/10:09:48	0.777	54.0	6.74	12.73	50	5.53	1.18	0.52	0.05	0.25	0.16	8.48	0.37	8.06	0.17	0.08	2.08	0.04

Table F1 continued: Raw geochemistry data for SPM collected at Site A (Swanhills A) between May 2012 and March 2014. *Ce is measured in ppm.

Sample ID	Flow Conditions	Date (yyyy/mm/dd:hh:mm)	Stage (m)	SPM (mg/L)	Concentration (weight %)															
					Al	Ca	Ce*	Fe	K	Mg	Mn	Na	P	Si	Ti	POC	Al_{di}	Al_{ox}	Fe_{di}	Fe_{ox}
130309A22	Storm Event	2013/03/10:11:48	0.745	44.4	6.78	13.74	47	5.46	1.21	0.51	0.06	0.24	0.16	11.18	0.38	8.29	0.21	0.13	2.33	0.00
130309A23/24	Storm Event	2013/03/10:14:48	0.698	35.3	7.20	14.10	51	5.98	1.26	0.55	0.05	0.27	0.17	7.89	0.40	8.51	0.20	0.10	2.12	0.07
130326A	Baseflow	2013/03/26:10:30	0.233	4.8	7.95	22.51	50	8.01	1.44	0.66	0.07	0.23	0.22	8.64	0.48	9.51	0.13	0.06	3.13	0.06
130403A	Baseflow	2013/04/03:09:30	0.170	6.1	8.16	24.13	52	8.13	1.49	0.68	0.08	0.21	0.24	11.51	0.45	8.55	0.15	0.06	2.11	0.00
130409A	Baseflow	2013/04/09:09:45	0.161	5.2	7.96	22.03	51	8.60	1.43	0.65	0.11	0.21	0.26	5.30	0.47	11.31	0.16	0.09	2.38	0.07
130416A	Baseflow	2013/04/16:10:10	0.142	15.6	8.58	24.08	52	8.01	1.46	0.74	0.06	0.24	0.24	5.39	0.48	9.33	0.13	0.05	1.76	0.00
130423A	Baseflow	2013/04/23:09:35	0.133	11.0	8.96	24.50	47	8.78	1.53	0.76	0.10	0.26	0.30	7.57	0.48	10.96	0.11	0.00	3.46	0.10
130430A	Baseflow	2013/04/30:09:08	0.116	8.9	8.29	23.60	44	8.59	1.45	0.71	0.08	0.27	0.31	9.42	0.45	9.70	0.13	0.14	3.17	0.01
130507A	Baseflow	2013/05/07:09:55	0.104	14.7	8.24	24.90	47	8.86	1.45	0.70	0.08	0.21	0.31	6.29	0.48	9.25	0.12	0.07	3.68	0.00
130514A	Baseflow	2013/05/14:09:33	0.119	7.8	8.14	22.12	50	9.12	1.39	0.71	0.07	0.24	0.47	10.08	0.41	9.85	0.13	0.14	2.64	0.00
130521A	Baseflow	2013/05/21:09:40	0.108	14.8	8.46	24.04	50	8.67	1.43	0.73	0.07	0.25	0.36	5.55	0.46	9.10	0.12	0.11	3.05	0.00
130528A	Baseflow	2013/05/28:10:10	0.133	6.9	7.96	21.82	45	8.10	1.44	0.68	0.08	0.20	0.31	12.32	0.43	9.22	0.14	0.10	3.12	0.00
130604A	Baseflow	2013/06/04:09:55	0.104	7.4	8.12	22.86	47	9.32	1.47	0.71	0.08	0.24	0.42	12.09	0.44	9.48	0.13	0.16	3.23	0.00
130618A	Baseflow	2013/06/18:10:15	0.100	8.6	7.39	20.76	51	8.72	1.38	0.66	0.08	0.25	0.44	9.28	0.42	11.11	0.11	0.11	2.88	0.00
130625A	Baseflow	2013/06/25:10:11	0.096	7.5	7.39	21.23	44	14.14	1.27	0.65	0.08	0.21	0.86	4.92	0.38	10.95	0.10	0.11	3.72	0.46
130702A	Baseflow	2013/07/02:09:25	0.099	11.0	7.73	20.95	42	8.73	1.34	0.68	0.09	0.24	0.44	7.23	0.42	9.95	0.13	0.15	2.69	0.03
130709A	Baseflow	2013/07/09:09:35	0.097	14.2	7.29	21.65	51	9.22	1.33	0.63	0.10	0.23	0.35	3.79	0.45	11.10	0.12	0.12	2.65	0.01
130716A	Baseflow	2013/07/16:09:50	0.101	12.7	7.50	20.60	49	8.63	1.30	0.64	0.10	0.18	0.38	6.11	0.41	11.12	0.13	0.16	2.86	0.15
130723A	Baseflow	2013/07/23:09:50	0.105	14.2	8.01	22.18	52	9.20	1.41	0.70	0.11	0.21	0.34	2.39	0.48	10.74	0.12	0.11	3.11	0.05
130730A	Baseflow	2013/07/30:09:55	0.099	14.1	7.55	21.11	54	8.71	1.40	0.66	0.11	0.24	0.30	3.05	0.47	10.97	0.11	0.09	2.78	0.13
130806A	Baseflow	2013/08/06:10:20	0.100	7.2	8.67	17.86	51	8.73	1.51	0.77	0.12	0.21	0.54	12.48	0.42	13.41	0.14	0.14	3.61	0.00
130813A	Baseflow	2013/08/13:10:25	0.110	7.5	7.35	19.61	45	8.73	1.33	0.65	0.11	0.23	0.44	8.28	0.41	12.05	0.15	0.12	3.70	0.14
130820A	Baseflow	2013/08/20:08:55	0.118	7.3	7.74	19.42	50	8.73	1.37	0.69	0.11	0.21	0.49	8.90	0.41	10.89	0.12	0.11	2.39	0.03
130827A	Baseflow	2013/08/27:09:35	0.128	7.2	8.22	19.38	53	9.59	1.40	0.72	0.11	0.22	0.53	8.35	0.42	11.69	0.15	0.13	2.95	0.12
130903A	Baseflow	2013/09/03:09:35	0.133	22.3	6.34	19.13	44	7.34	1.19	0.56	0.11	0.21	0.34	3.61	0.40	10.38	0.09	0.09	2.20	0.17
130910A1	Storm Event	2013/09/09:19:21	0.132	19.0	6.53	17.96	40	7.29	1.47	0.61	0.20	0.18	0.67	10.48	0.35	19.64	0.13	0.07	2.14	0.00
130910A2	Storm Event	2013/09/09:21:21	0.163	70.0	6.90	20.65	51	8.56	1.31	0.62	0.18	0.23	0.35	0.00	0.47	13.88	0.16	0.09	2.25	0.30
130910A3	Storm Event	2013/09/09:23:21	0.149	42.5	9.63	16.15	62	7.94	1.73	0.89	0.19	0.31	0.45	7.72	0.49	14.70	0.14	0.06	3.16	0.05
130910A4	Storm Event	2013/09/10:01:21	0.137	35.5	11.41	14.66	70	8.47	1.92	1.03	0.18	0.30	0.48	8.99	0.52	14.98	0.18	0.07	3.71	0.08

Table F1 continued: Raw geochemistry data for SPM collected at Site A (Swanhills A) between May 2012 and March 2014. *Ce is measured in ppm.

Sample ID	Flow Conditions	Date (yyyy/mm/dd:hh:mm)	Stage (m)	SPM (mg/L)	Concentration (weight %)															
					Al	Ca	Ce*	Fe	K	Mg	Mn	Na	P	Si	Ti	POC	Al_{di}	Al_{ox}	Fe_{di}	Fe_{ox}
130910A5	Storm Event	2013/09/10:03:21	0.134	30.0	10.56	16.13	65	8.95	1.91	0.93	0.19	0.32	0.47	8.93	0.52	14.68	0.21	0.10	4.24	0.08
130910A6	Storm Event	2013/09/10:05:21	0.137	24.3	9.53	16.58	59	8.52	1.78	0.83	0.21	0.28	0.48	9.92	0.48	15.82	0.17	0.08	3.51	0.22
130910A7	Storm Event	2013/09/10:07:21	0.150	25.6	7.90	19.20	53	8.16	1.50	0.69	0.20	0.21	0.42	7.41	0.45	15.35	0.16	0.10	3.33	0.15
130910A8	Storm Event	2013/09/10:09:21	0.156	13.1	6.92	16.77	51	6.90	1.35	0.64	0.15	0.24	0.45	17.67	0.33	16.90	0.15	0.16	3.67	0.36
130910A9	Storm Event	2013/09/10:11:21	0.148	14.6	7.40	16.74	49	7.26	1.48	0.68	0.17	0.25	0.45	16.26	0.36	16.47	0.16	0.14	3.36	0.26
130910A10	Storm Event	2013/09/10:13:21	0.147	21.1	7.77	17.59	51	7.38	1.52	0.72	0.17	0.29	0.45	13.05	0.40	17.11	0.17	0.15	3.05	0.30
130910A11	Storm Event	2013/09/10:15:21	0.178	26.5	7.95	16.79	53	7.42	1.51	0.71	0.16	0.21	0.39	11.93	0.41	16.51	0.18	0.14	3.08	0.24
130910A12	Storm Event	2013/09/10:17:21	0.175	52.6	10.80	14.04	69	8.21	1.96	0.98	0.16	0.35	0.41	9.72	0.53	15.58	0.21	0.11	3.51	0.15
130910A13	Storm Event	2013/09/10:19:21	0.171	56.2	10.60	13.41	72	7.67	1.86	0.96	0.17	0.37	0.40	9.76	0.49	13.98	0.18	0.08	3.11	0.16
130910A14	Storm Event	2013/09/10:21:21	0.173	44.0	9.81	14.38	71	7.61	1.79	0.89	0.16	0.34	0.41	10.87	0.48	14.57	0.20	0.10	3.20	0.16
130910A15	Storm Event	2013/09/10:23:21	0.163	31.0	9.35	16.26	59	8.02	1.77	0.85	0.15	0.32	0.42	10.14	0.48	14.19	0.16	0.11	3.10	0.22
130910A16	Storm Event	2013/09/11:01:21	0.169	26.1	8.50	16.25	59	7.29	1.60	0.77	0.15	0.31	0.40	11.06	0.43	14.50	0.14	0.05	3.44	0.15
130910A17	Storm Event	2013/09/11:03:21	0.150	20.8	8.41	17.34	55	7.38	1.56	0.76	0.19	0.32	0.43	10.36	0.43	13.27	0.13	0.09	3.06	0.32
130910A18	Storm Event	2013/09/11:05:21	0.145	19.7	8.36	18.49	53	7.87	1.58	0.75	0.19	0.29	0.44	9.78	0.44	13.55	0.14	0.08	3.12	0.17
130910A19/20	Storm Event	2013/09/11:08:21	0.140	13.0	7.52	17.91	50	7.91	1.45	0.68	0.20	0.26	0.48	10.79	0.40	13.97	0.17	0.12	3.02	0.23
130910A21/22	Storm Event	2013/09/11:12:21	0.138	6.9	6.99	16.68	44	7.93	1.42	0.64	0.22	0.23	0.57	16.55	0.36	14.37	0.17	0.18	4.32	0.21
130910A23/24	Storm Event	2013/09/11:16:21	0.137	8.6	7.44	18.07	44	7.92	1.45	0.68	0.18	0.25	0.53	12.92	0.38	13.58	0.13	0.09	2.89	0.20
130914A1	Storm Event	2013/09/13:18:46	0.136	16.1	7.60	20.53	51	8.35	1.58	0.70	0.21	0.27	0.58	10.59	0.42	15.18	0.17	0.08	2.59	0.18
130914A2	Storm Event	2013/09/13:20:46	0.137	17.6	7.51	20.48	48	7.77	1.44	0.68	0.18	0.20	0.45	10.18	0.41	13.93	0.19	0.10	2.35	0.34
130914A3	Storm Event	2013/09/13:22:46	0.181	51.3	8.12	21.66	53	8.70	1.45	0.70	0.14	0.21	0.34	0.00	0.50	11.57	0.18	0.08	2.28	0.12
130914A4	Storm Event	2013/09/14:00:46	0.192	70.8	11.60	13.48	81	8.60	1.99	1.01	0.16	0.36	0.41	5.56	0.57	13.28	0.20	0.07	2.59	0.22
130914A5	Storm Event	2013/09/14:02:46	0.175	40.0	9.88	16.70	68	8.52	1.76	0.85	0.16	0.25	0.38	5.90	0.53	13.18	0.20	0.06	2.46	0.19
130914A6	Storm Event	2013/09/14:04:46	0.189	30.6	9.25	17.34	60	8.01	1.66	0.80	0.14	0.28	0.38	6.18	0.48	13.20	0.16	0.04	2.61	0.18
130914A7	Storm Event	2013/09/14:06:46	0.178	20.1	8.42	18.05	57	7.69	1.60	0.74	0.14	0.26	0.38	11.17	0.44	13.21	0.17	0.05	2.76	0.15
130914A8/9	Storm Event	2013/09/14:09:46	0.164	10.7	8.29	17.54	56	8.23	1.55	0.72	0.16	0.20	0.45	10.09	0.43	14.83	0.18	0.09	2.67	0.08
130914A10/11	Storm Event	2013/09/14:13:46	0.154	8.9	7.60	18.19	56	8.08	1.47	0.67	0.16	0.24	0.46	12.73	0.41	13.41	0.17	0.12	2.25	0.23
130914A12/13	Storm Event	2013/09/14:17:46	0.148	11.8	8.20	21.17	58	8.91	1.52	0.72	0.16	0.22	0.41	5.49	0.48	13.10	0.15	0.06	2.37	0.26
130914A14/15	Storm Event	2013/09/14:21:46	0.143	14.1	8.06	20.95	55	8.25	1.45	0.71	0.15	0.23	0.42	5.55	0.47	12.49	0.14	0.04	3.21	0.33
130914A16/17	Storm Event	2013/09/15:01:46	0.140	10.6	7.94	21.00	52	8.69	1.47	0.70	0.15	0.23	0.45	7.32	0.45	12.65	0.14	0.06	2.47	0.22

Table F1 continued: Raw geochemistry data for SPM collected at Site A (Swanhills A) between May 2012 and March 2014. *Ce is measured in ppm.

Sample ID	Flow Conditions	Date (yyyy/mm/dd:hh:mm)	Stage (m)	SPM (mg/L)	Concentration (weight %)															
					Al	Ca	Ce*	Fe	K	Mg	Mn	Na	P	Si	Ti	POC	Al_{di}	Al_{ox}	Fe_{di}	Fe_{ox}
130914A18/19	Storm Event	2013/09/15:05:46	0.139	9.4	8.04	19.45	46	8.13	1.45	0.72	0.15	0.27	0.50	10.42	0.41	12.25	0.15	0.08	2.98	0.30
130914A20/21/22	Storm Event	2013/09/15:10:46	0.142	5.9	7.84	20.53	51	8.83	1.43	0.71	0.13	0.26	0.52	11.51	0.41	12.09	0.17	0.09	2.46	0.26
130917A	Baseflow	2013/09/17:09:35	0.137	6.4	8.19	20.89	51	9.13	1.42	0.74	0.13	0.29	0.58	8.72	0.43	12.05	0.20	0.11	3.00	0.32
131001A	Baseflow	2013/10/01:09:20	0.135	16.2	7.28	20.29	50	8.75	1.31	0.66	0.11	0.27	0.37	1.93	0.44	10.50	0.19	0.16	1.94	0.31
131008A	Baseflow	2013/10/08:09:05	0.132	9.3	8.57	22.54	50	9.96	1.45	0.76	0.12	0.23	0.53	4.96	0.46	11.62	0.20	0.13	0.92	0.10
131022A	Baseflow	2013/10/22:09:20	0.222	2.3	7.65	20.22	51	6.93	1.48	0.69	0.09	0.28	0.34	16.40	0.41	10.26	0.23	0.22	1.35	0.25
131028A1/2/3	Storm Event	2013/10/27:23:21	0.184	4.8	5.29	13.42	45	5.35	1.43	0.52	0.14	0.16	0.80	18.17	0.28	23.08	0.17	0.12	0.49	0.12
131028A4/5	Storm Event	2013/10/28:04:21	0.201	7.9	6.61	17.52	52	6.56	1.42	0.59	0.14	0.23	0.40	14.83	0.39	14.35	0.25	0.22	0.42	0.19
131028A6	Storm Event	2013/10/28:07:21	0.239	12.6	8.26	9.94	61	6.39	1.68	0.68	0.13	0.24	0.41	22.30	0.39	16.15	0.39	0.41	0.24	0.21
131028A7/8	Storm Event	2013/10/28:10:21	0.300	13.3	8.87	10.15	68	7.04	1.68	0.74	0.15	0.28	0.36	16.39	0.45	18.99	0.23	0.08	5.88	0.66
131028A9/10	Storm Event	2013/10/28:14:21	0.435	18.6	7.87	15.18	58	7.46	1.42	0.65	0.13	0.24	0.30	3.65	0.44	13.29	0.26	0.23	2.54	0.19
131028A11/12	Storm Event	2013/10/28:18:21	0.473	9.8	7.38	14.55	53	6.52	1.47	0.60	0.13	0.22	0.33	14.93	0.39	13.94	0.25	0.14	2.55	0.36
131028A13/14/15	Storm Event	2013/10/28:23:21	0.429	5.1	7.26	13.83	47	6.22	1.47	0.58	0.11	0.22	0.36	18.62	0.36	13.26	0.23	0.19	0.00	0.26
131028A16/17/18/19	Storm Event	2013/10/29:06:21	0.382	3.4	6.74	13.44	51	5.80	1.39	0.55	0.13	0.21	0.41	20.45	0.34	15.72	0.22	0.20	0.92	0.33
131028A20/21/22/23/24	Storm Event	2013/10/29:15:21	0.337	2.4	7.04	15.77	53	6.12	1.46	0.61	0.13	0.25	0.39	19.45	0.37	14.15	0.23	0.16	0.00	0.35
131119A	Baseflow	2013/11/19:10:35	0.276	1.6	6.60	13.19	54	5.29	1.31	0.57	0.10	0.27	0.33	24.45	0.31	10.07	0.21	0.26	3.09	0.15
131126A	Baseflow	2013/11/26:11:15	0.289	1.1	6.85	14.83	58	5.43	1.31	0.59	0.11	0.29	0.32	24.94	0.32	9.58	0.18	0.25	6.60	0.14
131202A	Baseflow	2013/12/02:10:35	0.223	1.4	6.23	16.01	49	5.97	1.35	0.55	0.09	0.25	0.36	22.37	0.34	11.62	0.17	0.12	3.93	0.10
131210A	Baseflow	2013/12/10:10:35	0.189	3.0	6.29	16.97	54	6.35	1.33	0.55	0.11	0.24	0.34	15.18	0.38	12.11	0.11	0.10	2.77	0.21
131217A	Baseflow	2013/12/17:11:15	0.185	5.5	7.42	16.15	56	6.81	1.45	0.65	0.11	0.27	0.35	14.61	0.40	12.29	0.13	0.14	3.87	0.27
140107A	Baseflow	2014/01/07:10:15	0.310	29.5	11.60	9.64	85	7.03	2.07	1.19	0.14	0.42	0.35	10.92	0.60	13.32	0.15	0.11	3.69	0.44
140114A	Baseflow	2014/01/14:10:10	0.335	4.1	8.94	16.04	65	7.40	1.62	0.74	0.11	0.29	0.30	10.99	0.50	11.10	0.15	0.10	3.76	0.32
140121A	Baseflow	2014/01/21:10:20	0.297	3.8	8.52	17.51	52	7.02	1.56	0.75	0.13	0.29	0.29	11.71	0.46	12.37	0.15	0.12	3.11	0.19
140125A1/2	Storm Event	2014/01/24:23:11	0.323	11.3	6.62	14.26	46	4.98	1.32	0.61	0.14	0.25	0.34	13.34	0.35	12.81	0.16	0.18	1.80	0.25
140125A3/4	Storm Event	2014/01/25:03:11	0.328	9.3	7.81	16.14	61	6.37	1.49	0.68	0.13	0.26	0.29	12.53	0.43	12.55	0.18	0.16	3.09	0.32
140125A5/6	Storm Event	2014/01/25:07:11	0.330	7.9	6.91	15.68	52	5.72	1.38	0.60	0.13	0.26	0.36	15.34	0.37	14.70	0.11	0.13	2.45	0.20
140125A7/8	Storm Event	2014/01/25:11:11	0.331	5.0	6.67	13.10	51	5.16	1.31	0.58	0.15	0.27	0.27	22.96	0.32	10.72	0.13	0.19	4.20	0.35
140125A9/10	Storm Event	2014/01/25:15:11	0.344	5.7	7.17	14.73	53	5.61	1.38	0.62	0.15	0.27	0.28	20.29	0.36	10.07	0.13	0.19	3.43	0.45
140125A11	Storm Event	2014/01/25:18:11	0.364	68.0	12.10	10.93	108	8.91	2.50	1.16	0.21	0.43	0.35	8.06	0.80	17.63	0.20	0.12	4.28	0.71

Table F1 continued: Raw geochemistry data for SPM collected at Site A (Swanhills A) between May 2012 and March 2014. *Ce is measured in ppm.

Sample ID	Flow Conditions	Date (yyyy/mm/dd:hh:mm)	Stage (m)	SPM (mg/L)	Concentration (weight %)															
					Al	Ca	Ce*	Fe	K	Mg	Mn	Na	P	Si	Ti	POC	Al_{di}	Al_{ox}	Fe_{di}	Fe_{ox}
140125A12	Storm Event	2014/01/25:20:11	0.365	17.3	9.30	14.46	67	7.10	1.76	0.82	0.15	0.29	0.29	12.28	0.51	13.79	0.22	0.20	2.91	0.27
140125A13/14	Storm Event	2014/01/25:23:11	0.368	14.2	7.24	17.01	55	6.36	1.35	0.62	0.12	0.24	0.33	4.74	0.43	15.19	0.15	0.11	3.67	0.18
140125A15/16	Storm Event	2014/01/26:03:11	0.377	9.8	7.96	16.46	55	6.49	1.50	0.68	0.13	0.26	0.25	11.68	0.44	10.58	0.19	0.14	2.43	0.24
140125A17/18	Storm Event	2014/01/26:07:11	0.385	10.0	7.74	16.93	58	6.26	1.46	0.66	0.14	0.27	0.25	11.92	0.43	10.08	0.18	0.17	2.68	0.33
140125A19/20	Storm Event	2014/01/26:11:11	0.398	8.1	7.62	16.19	55	6.09	1.49	0.65	0.15	0.27	0.25	15.22	0.42	10.61	0.21	0.22	2.30	0.29
140125A21	Storm Event	2014/01/26:14:11	0.427	44.9	9.60	11.83	81	7.29	1.86	0.93	0.16	0.36	0.30	6.73	0.58	14.03	0.21	0.13	3.09	0.47
140125A22	Storm Event	2014/01/26:16:11	0.454	34.9	8.92	13.48	67	7.20	1.59	0.76	0.12	0.29	0.26	4.91	0.50	11.21	0.19	0.12	2.05	0.32
140125A23	Storm Event	2014/01/26:18:11	0.497	52.0	8.76	14.04	58	6.80	1.41	0.71	0.09	0.27	0.22	2.45	0.46	10.05	0.20	0.16	2.38	0.30
140125A24	Storm Event	2014/01/26:20:11	0.531	52.4	7.82	14.28	57	6.56	1.28	0.63	0.09	0.26	0.19	0.79	0.43	9.22	0.18	0.08	1.91	0.38
140125A25	Storm Event	2014/01/27:13:35	0.476	11.3	8.84	17.16	56	7.17	1.53	0.71	0.11	0.26	0.23	6.64	0.48	10.27	0.21	0.17	3.32	0.37
140129A	Baseflow	2014/01/29:10:45	0.361	5.1	9.45	16.87	58	7.10	1.66	0.81	0.12	0.33	0.28	12.00	0.46	10.66	0.14	0.07	3.65	0.23
140131A1/2	Storm Event	2014/01/31:15:51	0.327	20.1	5.83	13.91	44	5.02	1.15	0.47	0.11	0.22	0.22	6.93	0.35	10.69	0.15	0.06	2.34	0.22
140131A3	Storm Event	2014/01/31:17:21	0.336	27.7	7.38	13.93	55	5.74	1.37	0.68	0.14	0.27	0.25	11.06	0.42	11.93	0.14	0.09	3.36	0.32
140131A4	Storm Event	2014/01/31:18:21	0.341	87.6	10.83	10.31	81	6.99	1.95	1.07	0.19	0.36	0.35	8.84	0.58	16.04	0.15	0.07	2.45	0.44
140131A5	Storm Event	2014/01/31:19:21	0.348	57.7	10.85	11.08	78	7.25	1.93	0.99	0.17	0.34	0.33	8.85	0.56	14.99	0.20	0.06	5.30	0.65
140131A6	Storm Event	2014/01/31:20:21	0.352	65.8	10.89	10.68	76	7.19	1.90	0.94	0.16	0.32	0.37	7.86	0.53	14.93	0.20	0.07	3.69	0.37
140131A7	Storm Event	2014/01/31:21:21	0.358	44.8	10.24	11.92	72	7.30	1.84	0.89	0.14	0.30	0.35	8.72	0.53	13.92	0.22	0.18	3.61	0.42
140131A8	Storm Event	2014/01/31:22:21	0.361	26.3	10.21	15.22	74	8.73	1.87	0.85	0.15	0.29	0.35	7.20	0.56	14.56	0.20	0.10	3.75	0.28
140131A9	Storm Event	2014/01/31:23:21	0.366	25.7	8.42	14.26	60	7.03	1.52	0.70	0.13	0.28	0.29	9.70	0.44	12.06	0.23	0.16	3.14	0.34
140131A10	Storm Event	2014/02/01:00:21	0.375	28.6	7.16	14.26	55	6.05	1.39	0.58	0.11	0.23	0.31	8.56	0.41	13.03	0.16	0.16	2.37	0.08
140131A11	Storm Event	2014/02/01:01:21	0.381	27.4	7.64	14.31	55	6.52	1.41	0.62	0.11	0.23	0.26	9.05	0.42	12.69	0.20	0.11	3.71	0.21
140131A12	Storm Event	2014/02/01:02:21	0.387	27.4	7.28	14.49	59	5.94	1.38	0.59	0.12	0.24	0.23	11.12	0.41	9.84	0.20	0.11	3.73	0.26
140131A13	Storm Event	2014/02/01:03:21	0.395	29.2	7.40	16.13	60	6.38	1.41	0.60	0.11	0.25	0.23	8.49	0.44	10.63	0.17	0.08	2.48	0.31
140131A14	Storm Event	2014/02/01:04:21	0.421	51.9	7.44	16.02	61	6.63	1.42	0.62	0.10	0.27	0.22	4.44	0.47	10.53	0.17	0.03	2.23	0.28
140131A15	Storm Event	2014/02/01:05:21	0.471	138.4	10.48	9.95	82	7.20	1.92	0.91	0.15	0.34	0.33	6.84	0.58	14.22	0.29	0.10	3.67	0.34
140131A16	Storm Event	2014/02/01:06:21	0.527	127.4	9.22	12.31	66	7.09	1.53	0.70	0.09	0.28	0.23	4.13	0.48	10.57	0.22	0.09	2.89	0.28
140131A17	Storm Event	2014/02/01:07:21	0.572	134.0	10.10	12.61	65	7.05	1.60	0.75	0.08	0.27	0.22	5.57	0.49	9.24	0.24	0.14	3.01	0.29
140131A18	Storm Event	2014/02/01:08:21	0.594	113.3	9.23	13.94	65	7.34	1.47	0.69	0.08	0.26	0.20	2.58	0.48	9.77	0.23	0.09	3.11	0.30
140131A19	Storm Event	2014/02/01:09:21	0.594	87.3	9.00	14.11	63	7.32	1.47	0.67	0.08	0.25	0.20	3.49	0.47	9.36	0.24	0.09	2.71	0.22

Table F1 continued: Raw geochemistry data for SPM collected at Site A (Swanhills A) between May 2012 and March 2014. *Ce is measured in ppm.

Sample ID	Flow Conditions	Date (yyyy/mm/dd:hh:mm)	Stage (m)	SPM (mg/L)	Concentration (weight %)															
					Al	Ca	Ce*	Fe	K	Mg	Mn	Na	P	Si	Ti	POC	Al_{di}	Al_{ox}	Fe_{di}	Fe_{ox}
140131A20	Storm Event	2014/02/01:10:21	0.580	81.0	8.90	14.11	64	7.06	1.45	0.68	0.08	0.27	0.20	4.50	0.47	10.42	0.21	0.07	1.55	0.27
140131A21	Storm Event	2014/02/01:11:21	0.578	68.1	8.87	13.86	69	7.01	1.47	0.66	0.09	0.29	0.20	4.87	0.46	10.41	0.25	0.09	2.99	0.31
140131A22	Storm Event	2014/02/01:12:21	0.570	54.1	9.27	14.76	59	7.64	1.55	0.69	0.09	0.27	0.21	5.17	0.49	10.91	0.28	0.16	3.65	0.28
140131A23	Storm Event	2014/02/01:13:21	0.560	42.4	9.18	14.26	57	7.13	1.49	0.69	0.09	0.26	0.21	6.45	0.45	10.78	0.28	0.10	3.47	0.26
140131A24	Storm Event	2014/02/01:14:21	0.548	47.6	8.14	13.82	58	6.76	1.30	0.63	0.08	0.25	0.19	2.83	0.42	10.06	0.19	0.11	2.86	0.07
140204A	Baseflow	2014/02/04:10:10	0.327	7.8	9.24	16.72	60	7.03	1.57	0.75	0.10	0.27	0.25	9.57	0.47	10.20	0.17	0.10	4.07	0.30
140206A1	Storm Event	2014/02/06:15:04	0.288	72.3	4.18	9.61	42	3.09	0.82	0.33	0.05	0.23	0.14	13.10	0.24	6.48	0.10	0.11	1.04	0.16
140206A2	Storm Event	2014/02/06:17:04	0.297	50.6	11.46	11.16	83	7.55	2.01	1.10	0.16	0.38	0.33	8.02	0.61	15.94	0.19	0.08	2.81	0.82
140206A3	Storm Event	2014/02/06:19:04	0.316	72.4	10.45	11.10	82	7.42	1.85	0.98	0.16	0.32	0.34	5.14	0.56	15.76	0.19	0.10	3.37	0.47
140206A4	Storm Event	2014/02/06:21:04	0.344	64.0	11.74	10.03	77	7.20	2.00	0.99	0.15	0.32	0.40	7.92	0.55	17.02	0.26	0.09	4.80	0.48
140206A5	Storm Event	2014/02/06:23:04	0.377	36.2	10.31	13.25	69	7.53	1.72	0.81	0.12	0.28	0.28	5.72	0.51	11.72	0.23	0.14	3.21	0.36
140206A6	Storm Event	2014/02/07:01:04	0.404	32.3	9.02	14.67	59	7.05	1.58	0.71	0.11	0.27	0.23	6.80	0.47	10.75	0.23	0.14	3.52	0.41
140206A7	Storm Event	2014/02/07:03:04	0.429	42.0	9.33	14.16	63	7.14	1.63	0.76	0.12	0.29	0.25	6.23	0.50	11.90	0.19	0.19	3.45	0.48
140206A8	Storm Event	2014/02/07:05:04	0.480	54.0	10.66	12.65	69	7.86	1.79	0.80	0.12	0.27	0.28	7.09	0.52	12.49	0.26	0.17	3.32	0.28
140206A9	Storm Event	2014/02/07:07:04	0.625	144.8	10.35	13.48	72	7.00	1.64	0.77	0.09	0.29	0.23	6.36	0.50	9.94	0.11	0.03	3.02	0.33
140206A10	Storm Event	2014/02/07:09:04	0.734	168.0	9.30	13.19	59	7.05	1.50	0.70	0.07	0.28	0.19	4.82	0.48	9.45	0.21	0.08	3.26	0.33
140206A11	Storm Event	2014/02/07:11:04	0.716	146.5	9.53	12.49	59	6.80	1.44	0.69	0.07	0.26	0.19	5.49	0.44	9.33	0.25	0.21	1.86	0.17
140206A12	Storm Event	2014/02/07:13:04	0.710	104.5	9.21	12.70	60	6.71	1.42	0.66	0.08	0.26	0.18	6.50	0.44	9.65	0.28	0.11	2.59	0.33
140206A13	Storm Event	2014/02/07:15:04	0.667	72.8	8.91	12.76	56	6.73	1.40	0.64	0.07	0.26	0.18	6.51	0.43	9.75	0.31	0.13	3.47	0.24
140206A14	Storm Event	2014/02/07:17:04	0.636	62.5	8.67	12.81	54	6.44	1.35	0.63	0.08	0.25	0.18	5.82	0.41	11.39	0.40	0.36	1.20	0.38
140206A15	Storm Event	2014/02/07:19:04	0.609	48.6	8.72	13.40	54	6.87	1.38	0.63	0.06	0.25	0.18	5.32	0.42	9.55	0.23	0.17	2.32	0.38
140206A16	Storm Event	2014/02/07:21:04	0.587	41.7	8.34	13.56	49	6.43	1.36	0.61	0.08	0.24	0.18	7.44	0.40	9.65	0.26	0.11	2.16	0.37
140206A17	Storm Event	2014/02/07:23:04	0.569	33.2	8.18	14.18	53	6.73	1.43	0.60	0.07	0.22	0.18	10.27	0.41	10.18	0.34	0.16	2.78	0.20
140206A18	Storm Event	2014/02/08:01:04	0.554	29.2	7.96	13.74	52	6.33	1.42	0.58	0.08	0.22	0.18	12.34	0.40	9.54	0.27	0.16	3.59	0.35
140206A19	Storm Event	2014/02/08:03:04	0.544	27.4	8.16	14.19	55	6.53	1.46	0.61	0.10	0.23	0.20	11.93	0.42	11.26	0.16	0.10	0.56	0.19
140206A20	Storm Event	2014/02/08:05:04	0.531	25.2	7.93	13.69	50	6.18	1.44	0.58	0.09	0.22	0.19	14.74	0.39	11.38	0.29	0.13	3.50	0.35
140206A21	Storm Event	2014/02/08:07:04	0.519	23.7	8.25	14.69	52	6.42	1.47	0.62	0.08	0.25	0.20	14.08	0.40	10.43	0.24	0.15	3.87	0.45
140206A22	Storm Event	2014/02/08:09:04	0.507	21.8	8.07	14.23	49	6.10	1.45	0.60	0.09	0.23	0.20	16.19	0.39	15.97	0.25	0.11	4.17	0.35
140206A23/24	Storm Event	2014/02/08:12:04	0.497	19.8	8.66	14.46	56	6.86	1.45	0.68	0.08	0.26	0.20	6.17	0.45	7.19	0.14	0.13	1.59	0.35

Table F1 continued: Raw geochemistry data for SPM collected at Site A (Swanhills A) between May 2012 and March 2014. *Ce is measured in ppm.

Sample ID	Flow Conditions	Date (yyyy/mm/dd:hh:mm)	Stage (m)	SPM (mg/L)	Concentration (weight %)															
					Al	Ca	Ce*	Fe	K	Mg	Mn	Na	P	Si	Ti	POC	Al_{di}	Al_{ox}	Fe_{di}	Fe_{ox}
140211A	Baseflow	2014/02/11:10:10	0.359	9.1	8.95	16.41	60	7.10	1.53	0.73	0.09	0.26	0.23	8.17	0.46	11.19	0.21	0.11	2.44	0.20
140218A	Baseflow	2014/02/18:10:10	0.307	7.9	8.57	17.29	54	6.79	1.50	0.72	0.08	0.28	0.24	9.67	0.46	10.19	0.23	0.17	1.78	0.28
140225A	Baseflow	2014/02/25:09:50	0.249	12.0	10.16	16.69	69	7.75	1.69	0.85	0.10	0.31	0.28	8.63	0.52	11.19	0.11	0.07	3.68	0.18
140304A	Baseflow	2014/03/04:09:40	0.252	8.2	9.31	20.52	62	8.81	1.69	0.79	0.12	0.31	0.30	6.95	0.56	12.02	0.10	0.08	3.91	0.26
140311A	Baseflow	2014/03/11:09:38	0.197	7.6	8.75	19.12	61	7.40	1.52	0.74	0.10	0.28	0.26	10.46	0.46	10.04	0.10	0.07	3.55	0.07
140318A	Baseflow	2014/03/18:09:40	0.186	7.5	8.81	22.16	58	7.81	1.52	0.74	0.08	0.26	0.27	8.44	0.46	10.71	0.09	0.06	3.63	0.07
140331A	Baseflow	2014/03/31:08:50	0.269	7.1	8.82	20.29	62	7.46	1.57	0.77	0.11	0.28	0.29	9.31	0.48	11.38	0.08	0.04	3.72	0.08

Table F2: Raw geochemistry data for SPM collected at Site B (Swanhills B) between May 2012 and March 2014. *Ce is measured in ppm.

Sample ID	Flow Conditions	Date (yyyy/mm/dd:hh:mm)	Stage (m)	SPM (mg/L)	Concentration (weight %)															
					Al	Ca	Ce*	Fe	K	Mg	Mn	Na	P	Si	Ti	POC	Al_{di}	Al_{ox}	Fe_{di}	Fe_{ox}
120508B	Baseflow	2012/05/08:08:40	0.198	3.4	6.70	16.02	58	6.29	1.44	0.56	0.08	0.21	0.29	12.06	0.43	14.85	0.11	0.07	2.05	0.76
120515B	Baseflow	2012/05/15:08:27	0.176	3.8	7.05	16.08	59	6.78	1.54	0.59	0.08	0.22	0.30	8.43	0.47	17.13	0.09	0.10	2.52	0.81
120710B	Baseflow	2012/07/10:09:15	0.101	13.8	6.09	15.80	53	6.24	1.30	0.53	0.12	0.21	0.28	2.97	0.41	17.02	0.11	0.13	1.85	0.99
120716B	Baseflow	2012/07/16:08:45	0.129	12.6	6.37	15.97	60	6.52	1.38	0.53	0.09	0.16	0.27	4.12	0.45	17.53	0.15	0.09	1.98	1.11
120731B	Baseflow	2012/07/31:08:45	0.028	17.7	5.61	15.34	58	6.08	1.20	0.47	0.10	0.16	0.26	0.00	0.40	15.90	0.13	0.09	1.49	0.88
120807B	Baseflow	2012/08/07:08:45	0.085	11.1	5.44	16.07	59	6.65	1.21	0.46	0.09	0.15	0.26	0.00	0.43	16.33	0.14	0.10	1.96	0.82
120814B	Baseflow	2012/08/14:08:55	0.031	25.6	4.28	9.85	46	3.76	0.94	0.34	0.04	0.19	0.19	5.34	0.27	10.17	0.10	0.09	0.94	0.55
120821B	Baseflow	2012/08/21:08:40	0.031	11.8	5.93	14.98	54	5.89	1.28	0.49	0.10	0.18	0.29	8.26	0.40	14.95	0.16	0.17	1.37	0.39
120827B	Baseflow	2012/08/27:07:45	0.128	14.4	5.98	17.40	54	6.18	1.29	0.51	0.11	0.17	0.28	1.70	0.43	15.76	0.19	0.13	1.83	0.60
120904B	Baseflow	2012/09/04:08:30	0.042	11.3	5.91	15.29	49	5.33	1.21	0.51	0.14	0.19	0.30	9.04	0.36	14.71	0.04	0.05	2.08	0.76
120910B	Baseflow	2012/09/10:08:30	0.044	27.7	4.59	10.99	43	3.92	0.98	0.37	0.09	0.16	0.23	5.90	0.28	11.60	0.14	0.13	1.25	0.44
120918B	Baseflow	2012/09/18:08:30	0.032	20.1	6.64	16.98	51	6.32	1.37	0.55	0.17	0.18	0.33	7.98	0.42	17.08	0.15	0.10	3.07	0.85
120924B7	Storm Event	2012/09/23:19:35	0.029	22.9	6.32	16.89	58	6.07	1.36	0.54	0.15	0.17	0.39	5.07	0.41	19.59	0.07	0.08	3.18	0.85
120924B8	Storm Event	2012/09/23:20:35	0.029	20.0	6.46	17.09	50	5.97	1.40	0.57	0.17	0.21	0.41	6.84	0.40	18.23	0.13	0.14	1.93	0.76
120924B9	Storm Event	2012/09/23:21:35	0.028	20.0	6.49	16.85	54	5.96	1.39	0.56	0.17	0.16	0.43	6.90	0.40	18.94	0.14	0.14	2.37	0.59
120924B10	Storm Event	2012/09/23:22:35	0.030	21.0	6.48	16.70	53	5.97	1.41	0.56	0.16	0.17	0.42	7.51	0.41	19.42	0.15	0.12	1.64	0.59
120924B11	Storm Event	2012/09/23:23:35	0.037	21.8	6.51	17.15	60	5.91	1.42	0.58	0.16	0.18	0.44	7.98	0.40	18.28	0.13	0.15	1.91	0.54
120924B12	Storm Event	2012/09/24:00:35	0.052	22.8	6.61	17.70	52	6.15	1.43	0.58	0.17	0.16	0.42	7.39	0.41	19.90	0.18	0.15	2.72	0.58
120924B13	Storm Event	2012/09/24:01:35	0.038	27.3	6.05	17.77	52	5.85	1.33	0.53	0.15	0.16	0.37	4.96	0.40	17.74	0.13	0.14	1.97	0.55
120924B14	Storm Event	2012/09/24:02:35	0.041	25.8	6.22	16.44	52	5.92	1.35	0.53	0.16	0.16	0.37	5.21	0.41	16.92	0.12	0.12	2.06	0.50
120924B15	Storm Event	2012/09/24:03:35	0.046	30.4	5.92	15.10	51	5.55	1.34	0.51	0.17	0.18	0.44	3.98	0.39	19.11	0.12	0.08	2.17	0.50
120924B16	Storm Event	2012/09/24:04:35	0.050	31.0	5.95	17.52	53	6.09	1.29	0.51	0.15	0.16	0.31	0.76	0.43	16.26	0.12	0.09	2.01	0.65
120924B17	Storm Event	2012/09/24:05:35	0.054	31.7	6.18	16.88	51	5.98	1.33	0.53	0.14	0.19	0.33	2.13	0.42	16.15	0.14	0.12	1.75	0.60
120924B18	Storm Event	2012/09/24:06:35	0.057	31.5	6.02	17.70	54	5.95	1.28	0.52	0.14	0.18	0.31	1.39	0.41	16.51	0.12	0.11	1.88	0.43
120924B19	Storm Event	2012/09/24:07:35	0.061	28.8	6.19	17.56	49	5.82	1.33	0.53	0.13	0.18	0.32	4.21	0.42	15.94	0.12	0.10	1.89	0.52
120924B20	Storm Event	2012/09/24:08:35	0.067	25.3	6.31	17.11	51	5.88	1.36	0.53	0.15	0.16	0.33	5.57	0.42	16.11	0.14	0.12	2.34	0.49
120924B21	Storm Event	2012/09/24:09:35	0.064	24.4	6.45	17.74	53	5.95	1.37	0.55	0.15	0.17	0.33	5.74	0.43	15.85	0.11	0.09	2.79	0.59
120924B22	Storm Event	2012/09/24:10:35	0.060	24.9	6.57	18.37	52	6.02	1.38	0.56	0.15	0.17	0.33	5.21	0.43	15.35	0.10	0.09	1.92	0.48
120924B23	Storm Event	2012/09/24:11:35	0.062	23.1	6.49	16.95	51	5.71	1.35	0.55	0.14	0.17	0.34	7.15	0.41	15.75	0.10	0.06	2.74	0.71

Table F2 continued: Raw geochemistry data for SPM collected at Site B (Swanhills B) between May 2012 and March 2014. *Ce is measured in ppm.

Sample ID	Flow Conditions	Date (yyyy/mm/dd:hh:mm)	Stage (m)	SPM (mg/L)	Concentration (weight %)															
					Al	Ca	Ce*	Fe	K	Mg	Mn	Na	P	Si	Ti	POC	Al_{di}	Al_{ox}	Fe_{di}	Fe_{ox}
120924B24	Storm Event	2012/09/24:12:35	0.061	25.3	6.47	18.55	54	5.90	1.35	0.56	0.14	0.17	0.32	5.28	0.42	15.25	0.12	0.12	1.64	0.48
121002B	Baseflow	2012/10/02:08:45	0.025	26.6	6.29	15.66	55	5.99	1.29	0.51	0.15	0.16	0.29	3.82	0.42	14.99	0.10	0.08	2.26	0.60
121005B1	Storm Event	2012/10/04:22:22	0.028	36.1	5.57	13.83	50	5.39	1.22	0.46	0.15	0.17	0.27	2.91	0.39	15.37	0.17	0.14	2.09	0.61
121005B2	Storm Event	2012/10/04:23:22	0.029	23.2	6.59	16.03	54	6.05	1.36	0.54	0.18	0.17	0.32	5.70	0.43	18.00	0.19	0.11	2.29	0.83
121005B3	Storm Event	2012/10/05:00:22	0.030	21.7	6.87	17.11	57	6.54	1.43	0.57	0.17	0.17	0.33	4.93	0.46	18.30	0.22	0.11	2.61	0.79
121005B4	Storm Event	2012/10/05:01:22	0.023	22.1	6.91	17.40	56	6.75	1.45	0.57	0.20	0.17	0.33	4.85	0.46	17.99	0.24	0.16	1.89	0.65
121005B5	Storm Event	2012/10/05:02:22	0.030	24.2	6.68	16.88	60	6.39	1.40	0.55	0.18	0.16	0.33	5.02	0.45	18.33	0.25	0.15	2.07	0.64
121005B6	Storm Event	2012/10/05:03:22	0.029	29.5	6.62	17.29	57	6.69	1.43	0.55	0.18	0.17	0.34	3.31	0.46	18.40	0.24	0.14	1.93	0.58
121005B7	Storm Event	2012/10/05:04:22	0.028	30.1	6.75	16.56	52	6.11	1.41	0.57	0.18	0.17	0.36	5.84	0.43	20.28	0.23	0.12	2.27	0.98
121005B8	Storm Event	2012/10/05:05:22	0.035	33.1	6.62	17.14	55	6.28	1.42	0.56	0.17	0.16	0.35	5.02	0.44	18.99	0.20	0.11	2.86	0.77
121005B9	Storm Event	2012/10/05:06:22	0.043	35.5	6.68	17.77	57	6.51	1.42	0.56	0.18	0.17	0.34	3.59	0.45	18.70	0.20	0.15	1.94	0.74
121005B10	Storm Event	2012/10/05:07:22	0.039	34.3	6.61	17.23	60	6.16	1.40	0.55	0.16	0.17	0.33	4.67	0.44	18.16	0.22	0.13	2.35	0.66
121005B11	Storm Event	2012/10/05:08:22	0.035	29.6	6.75	17.25	55	6.13	1.43	0.56	0.16	0.17	0.34	6.70	0.43	18.72	0.23	0.12	2.62	0.66
121005B12	Storm Event	2012/10/05:09:22	0.034	31.9	6.84	17.12	55	6.24	1.43	0.57	0.15	0.17	0.33	5.47	0.44	16.59	0.20	0.14	1.84	0.46
121005B13	Storm Event	2012/10/05:10:22	0.036	31.3	6.73	17.12	53	6.43	1.43	0.56	0.18	0.16	0.32	4.08	0.46	17.30	0.22	0.10	2.61	0.67
121005B14	Storm Event	2012/10/05:11:22	0.034	30.0	6.83	16.93	58	6.27	1.45	0.57	0.15	0.17	0.32	5.55	0.45	17.55	0.22	0.16	2.10	0.62
121005B15	Storm Event	2012/10/05:12:22	0.034	29.7	6.88	16.99	54	6.41	1.44	0.56	0.16	0.18	0.32	4.87	0.46	16.96	0.23	0.14	2.75	0.64
121005B16	Storm Event	2012/10/05:13:22	0.032	28.4	6.96	17.52	57	6.47	1.44	0.58	0.17	0.17	0.32	5.08	0.46	18.30	0.19	0.10	2.36	0.76
121005B17	Storm Event	2012/10/05:14:22	0.032	28.3	6.83	17.53	51	6.54	1.45	0.57	0.16	0.18	0.31	3.97	0.47	17.63	0.21	0.13	2.58	0.65
121005B18	Storm Event	2012/10/05:15:22	0.032	29.2	6.85	17.33	54	6.36	1.43	0.57	0.17	0.18	0.32	4.89	0.46	16.99	0.19	0.13	1.97	0.59
121005B19	Storm Event	2012/10/05:16:22	0.034	29.6	6.82	17.33	55	6.53	1.43	0.57	0.18	0.17	0.31	3.66	0.46	17.69	0.21	0.12	2.13	0.77
121005B20	Storm Event	2012/10/05:17:22	0.031	28.8	6.85	17.23	59	6.50	1.45	0.57	0.15	0.17	0.32	4.68	0.47	16.31	0.20	0.13	2.57	0.57
121005B21	Storm Event	2012/10/05:18:22	0.029	29.2	6.76	16.71	52	6.28	1.41	0.56	0.16	0.17	0.32	4.80	0.45	17.78	0.19	0.11	2.31	0.62
121005B22	Storm Event	2012/10/05:19:22	0.030	24.8	6.88	17.17	55	6.62	1.45	0.56	0.17	0.17	0.32	3.83	0.47	18.03	0.20	0.11	2.75	0.65
121005B23	Storm Event	2012/10/05:20:22	0.030	23.4	6.91	16.96	55	6.38	1.44	0.57	0.16	0.17	0.33	4.69	0.46	17.40	0.16	0.12	2.84	0.62
121005B24	Storm Event	2012/10/05:21:22	0.030	22.2	6.86	17.09	58	6.48	1.44	0.56	0.17	0.17	0.32	4.56	0.46	18.62	0.15	0.11	3.03	0.98
121009B	Baseflow	2012/10/09:08:40	0.051	26.0	6.85	16.59	61	6.60	1.43	0.55	0.17	0.17	0.29	3.64	0.48	17.14	0.06	0.03	3.23	0.72
121016B	Baseflow	2012/10/16:09:10	0.050	38.0	6.04	15.68	55	6.49	1.26	0.50	0.17	0.16	0.26	0.00	0.44	15.46	0.05	0.03	2.25	0.80
121022B	Baseflow	2012/10/22:14:30	0.455	16.1	6.89	14.42	61	5.96	1.39	0.56	0.15	0.19	0.29	4.43	0.44	16.71	0.08	0.06	2.60	0.78

Table F2 continued: Raw geochemistry data for SPM collected at Site B (Swanhills B) between May 2012 and March 2014. *Ce is measured in ppm.

Sample ID	Flow Conditions	Date (yyyy/mm/dd:hh:mm)	Stage (m)	SPM (mg/L)	Concentration (weight %)															
					Al	Ca	Ce*	Fe	K	Mg	Mn	Na	P	Si	Ti	POC	Al_{di}	Al_{ox}	Fe_{di}	Fe_{ox}
121030B	Baseflow	2012/10/30:09:50	0.301	16.4	6.82	14.92	55	6.22	1.43	0.55	0.15	0.20	0.28	4.51	0.47	17.15	0.15	0.12	2.24	0.86
121101B5	Storm Event	2012/11/01:03:04	0.242	26.7	6.18	14.33	56	6.03	1.35	0.49	0.17	0.16	0.27	4.07	0.44	15.35	0.14	0.07	2.64	0.70
121101B6	Storm Event	2012/11/01:04:04	0.242	29.7	6.07	14.62	56	6.11	1.32	0.49	0.17	0.17	0.27	2.55	0.45	15.82	0.10	0.07	2.70	0.77
121101B7	Storm Event	2012/11/01:05:04	0.246	34.3	6.06	13.71	60	5.95	1.32	0.48	0.17	0.16	0.27	2.80	0.44	14.91	0.10	0.05	2.29	0.74
121101B8	Storm Event	2012/11/01:06:04	0.273	35.6	6.21	14.43	55	5.77	1.35	0.50	0.16	0.19	0.28	4.20	0.44	14.50	0.13	0.12	2.18	0.75
121101B9	Storm Event	2012/11/01:07:04	0.285	35.7	6.40	14.53	55	6.28	1.43	0.51	0.16	0.16	0.29	4.33	0.46	17.01	0.16	0.09	3.32	0.77
121101B10	Storm Event	2012/11/01:08:04	0.292	30.4	6.56	14.77	58	6.17	1.43	0.52	0.17	0.17	0.30	5.35	0.46	15.86	0.10	0.08	2.64	0.76
121101B11	Storm Event	2012/11/01:09:04	0.300	28.9	6.59	14.32	57	5.81	1.42	0.54	0.15	0.20	0.29	6.51	0.43	15.52	0.10	0.07	3.01	0.88
121101B12	Storm Event	2012/11/01:10:04	0.321	26.5	6.85	14.44	58	6.01	1.45	0.55	0.15	0.21	0.30	7.32	0.44	14.73	0.11	0.11	3.07	0.77
121101B13	Storm Event	2012/11/01:11:04	0.346	67.5	6.15	13.45	55	5.87	1.39	0.50	0.17	0.19	0.34	2.32	0.44	18.25	0.11	0.07	2.50	0.55
121101B14	Storm Event	2012/11/01:12:04	0.376	39.5	6.49	13.67	58	6.25	1.42	0.52	0.16	0.20	0.31	2.41	0.45	16.63	0.12	0.07	2.77	0.71
121101B15	Storm Event	2012/11/01:13:04	0.402	35.6	7.14	12.32	59	6.06	1.55	0.55	0.15	0.17	0.35	4.77	0.46	19.25	0.14	0.07	3.01	0.60
121101B16	Storm Event	2012/11/01:14:04	0.426	29.8	7.47	11.81	53	5.84	1.54	0.57	0.15	0.21	0.38	5.71	0.43	18.30	0.13	0.08	3.11	0.58
121101B17	Storm Event	2012/11/01:15:04	0.438	25.7	7.45	12.07	56	6.06	1.56	0.56	0.16	0.17	0.36	5.63	0.44	18.59	0.16	0.07	3.09	0.53
121101B18	Storm Event	2012/11/01:16:04	0.443	24.4	7.54	12.88	61	6.10	1.56	0.58	0.17	0.22	0.35	6.50	0.45	16.09	0.13	0.08	2.91	0.68
121101B19	Storm Event	2012/11/01:17:04	0.444	24.8	7.14	13.02	55	6.28	1.53	0.54	0.17	0.17	0.33	4.49	0.47	16.05	0.15	0.14	2.98	0.57
121101B20	Storm Event	2012/11/01:18:04	0.439	22.5	7.78	12.87	59	6.23	1.59	0.58	0.15	0.20	0.39	6.24	0.46	15.86	0.12	0.09	2.72	0.62
121101B21	Storm Event	2012/11/01:19:04	0.436	22.4	7.13	13.13	55	5.91	1.48	0.55	0.14	0.21	0.31	7.28	0.44	14.96	0.11	0.09	3.04	0.80
121101B22	Storm Event	2012/11/01:20:04	0.433	19.6	7.24	13.52	59	6.22	1.55	0.56	0.17	0.21	0.33	8.34	0.46	15.40	0.09	0.10	2.70	0.87
121101B23	Storm Event	2012/11/01:21:04	0.429	19.1	7.04	12.75	61	5.78	1.49	0.54	0.13	0.17	0.32	9.99	0.44	14.30	0.15	0.09	3.33	0.65
121101B24	Storm Event	2012/11/01:22:04	0.425	17.3	7.38	13.62	57	6.23	1.57	0.57	0.15	0.18	0.34	9.97	0.46	15.56	0.13	0.11	3.48	0.62
121106B	Baseflow	2012/11/06:08:00	0.311	17.8	6.84	13.72	57	6.24	1.43	0.53	0.16	0.20	0.28	3.61	0.46	16.50	0.08	0.10	2.02	0.89
121120B	Baseflow	2012/11/20:10:05	0.103	23.7	6.29	14.25	58	5.77	1.33	0.50	0.14	0.19	0.28	6.74	0.41	17.03	0.17	0.04	3.17	0.82
121123B1	Storm Event	2012/11/22:22:40	0.256	19.9	6.94	14.17	56	6.10	1.45	0.54	0.17	0.17	0.32	7.90	0.44	18.58	0.20	0.00	3.95	0.85
121123B2	Storm Event	2012/11/23:00:40	0.259	32.5	6.57	14.16	58	6.30	1.42	0.51	0.17	0.16	0.32	4.08	0.45	18.51	0.21	0.01	3.47	0.69
121123B3	Storm Event	2012/11/23:02:40	0.292	22.9	6.67	14.15	59	6.20	1.43	0.52	0.15	0.16	0.32	5.21	0.44	19.84	0.16	0.00	4.48	0.68
121123B4	Storm Event	2012/11/23:04:40	0.344	29.6	6.40	13.86	60	6.56	1.40	0.50	0.16	0.16	0.30	1.40	0.46	17.67	0.21	0.01	3.15	0.73
121123B5	Storm Event	2012/11/23:06:40	0.456	69.0	9.10	9.32	71	7.17	1.73	0.64	0.13	0.23	0.34	5.01	0.50	18.20	0.32	0.03	4.31	0.60
121123B6	Storm Event	2012/11/23:08:40	0.498	91.5	11.81	7.63	78	7.88	1.99	0.77	0.14	0.21	0.34	6.18	0.54	16.67	0.35	0.02	4.32	0.75

Table F2 continued: Raw geochemistry data for SPM collected at Site B (Swanhills B) between May 2012 and March 2014. *Ce is measured in ppm.

Sample ID	Flow Conditions	Date (yyyy/mm/dd:hh:mm)	Stage (m)	SPM (mg/L)	Concentration (weight %)															
					Al	Ca	Ce*	Fe	K	Mg	Mn	Na	P	Si	Ti	POC	Al_{di}	Al_{ox}	Fe_{di}	Fe_{ox}
121123B7	Storm Event	2012/11/23:10:40	0.486	59.8	11.25	8.74	71	7.59	1.93	0.75	0.13	0.23	0.33	6.07	0.54	16.94	0.32	0.00	5.01	0.87
121123B8	Storm Event	2012/11/23:12:40	0.473	36.4	9.80	10.35	66	7.23	1.78	0.68	0.14	0.21	0.32	6.06	0.52	16.23	0.31	0.06	3.87	0.78
121123B9	Storm Event	2012/11/23:14:40	0.459	31.6	9.30	11.20	65	7.14	1.73	0.66	0.16	0.19	0.32	5.32	0.52	17.11	0.28	0.00	4.22	0.77
121123B10	Storm Event	2012/11/23:16:40	0.444	36.4	8.92	11.56	65	7.05	1.69	0.63	0.15	0.20	0.31	4.09	0.52	18.36	0.29	0.02	3.97	0.74
121123B11	Storm Event	2012/11/23:18:40	0.427	37.4	8.98	11.92	68	7.05	1.75	0.64	0.14	0.19	0.32	7.06	0.52	19.15	0.26	0.00	6.07	1.07
121123B12	Storm Event	2012/11/23:20:40	0.412	27.4	8.82	11.95	67	6.90	1.71	0.63	0.15	0.19	0.31	5.73	0.52	18.07	0.26	0.01	4.42	0.83
121123B13	Storm Event	2012/11/23:22:40	0.396	25.3	8.09	12.07	63	6.88	1.64	0.58	0.15	0.17	0.29	4.95	0.51	17.26	0.25	0.05	3.30	0.64
121123B14	Storm Event	2012/11/24:00:40	0.383	26.7	7.81	11.51	59	6.38	1.55	0.56	0.15	0.18	0.29	5.05	0.48	19.03	0.27	0.02	3.98	0.96
121123B15	Storm Event	2012/11/24:02:40	0.370	22.8	7.93	12.13	60	6.60	1.60	0.58	0.15	0.18	0.30	6.71	0.50	17.58	0.23	0.01	4.92	0.79
121123B16	Storm Event	2012/11/24:04:40	0.358	20.7	7.52	11.89	61	6.31	1.57	0.55	0.14	0.17	0.30	8.82	0.47	17.21	0.24	0.00	4.50	0.81
121123B17	Storm Event	2012/11/24:06:40	0.347	23.0	7.80	11.97	62	6.30	1.57	0.57	0.14	0.18	0.30	7.43	0.47	17.01	0.24	0.04	4.32	0.63
121125B1	Storm Event	2012/11/24:11:04	0.328	12.8	8.08	11.79	65	5.94	1.60	0.61	0.17	0.21	0.32	15.86	0.43	17.35	0.22	0.00	4.50	0.69
121125B2	Storm Event	2012/11/24:13:04	0.321	14.8	7.86	11.86	58	5.92	1.57	0.59	0.17	0.19	0.31	14.21	0.44	18.17	0.23	0.00	4.60	0.78
121125B3	Storm Event	2012/11/24:15:04	0.315	17.5	8.03	12.59	68	6.24	1.60	0.60	0.18	0.20	0.32	10.32	0.46	18.41	0.21	0.00	4.30	0.88
121125B4	Storm Event	2012/11/24:17:04	0.313	25.7	7.74	12.81	62	6.66	1.56	0.57	0.17	0.18	0.29	4.32	0.49	18.90	0.27	0.01	3.29	0.73
121125B5	Storm Event	2012/11/24:19:04	0.318	23.7	7.77	12.97	66	6.62	1.57	0.57	0.17	0.19	0.30	5.05	0.49	18.63	0.28	0.03	3.62	0.76
121125B6	Storm Event	2012/11/24:21:04	0.324	22.3	8.17	12.94	67	6.70	1.62	0.59	0.19	0.18	0.32	5.92	0.50	18.81	0.22	0.00	4.08	0.82
121125B7	Storm Event	2012/11/24:23:04	0.335	24.3	8.02	12.57	66	6.60	1.60	0.59	0.17	0.18	0.31	5.15	0.49	19.11	0.29	0.04	3.98	0.76
121125B8	Storm Event	2012/11/25:01:04	0.355	23.3	8.10	12.59	59	6.63	1.60	0.60	0.18	0.21	0.31	6.05	0.49	19.81	0.27	0.02	3.75	0.92
121125B9	Storm Event	2012/11/25:03:04	0.392	24.8	8.17	11.96	69	6.91	1.61	0.59	0.17	0.18	0.31	5.03	0.49	19.88	0.25	0.00	4.36	0.81
121125B10	Storm Event	2012/11/25:05:04	0.453	30.1	8.39	11.79	62	6.73	1.63	0.61	0.17	0.20	0.32	5.16	0.49	19.70	0.27	0.02	3.89	0.81
121125B11	Storm Event	2012/11/25:07:04	0.550	35.1	8.55	11.54	67	7.00	1.66	0.61	0.16	0.19	0.32	4.49	0.50	19.37	0.30	0.04	3.61	0.74
121125B12	Storm Event	2012/11/25:09:04	0.680	58.1	9.28	9.61	69	7.07	1.67	0.65	0.15	0.22	0.32	3.17	0.48	17.48	0.33	0.05	3.43	0.63
121125B13	Storm Event	2012/11/25:11:04	0.709	98.9	12.76	7.22	77	7.40	1.98	0.82	0.13	0.26	0.34	7.11	0.53	15.91	0.35	0.04	3.84	0.47
121125B14	Storm Event	2012/11/25:13:04	0.690	140.7	15.27	5.57	87	8.03	2.21	0.93	0.14	0.25	0.32	8.32	0.57	15.37	0.43	0.08	4.27	0.63
121125B15	Storm Event	2012/11/25:15:04	0.659	107.6	15.03	5.84	79	7.58	2.17	0.93	0.13	0.25	0.32	9.29	0.55	14.80	0.42	0.09	3.98	0.53
121125B16	Storm Event	2012/11/25:17:04	0.618	59.7	13.03	7.85	75	7.74	2.01	0.83	0.14	0.23	0.31	6.31	0.55	16.57	0.40	0.06	3.50	0.62
121125B17	Storm Event	2012/11/25:19:04	0.585	49.5	11.25	8.76	75	7.51	1.90	0.73	0.14	0.22	0.30	5.90	0.54	16.18	0.37	0.03	4.20	0.64
121125B18	Storm Event	2012/11/25:21:04	0.554	42.5	10.70	8.98	69	7.02	1.82	0.71	0.14	0.21	0.30	6.70	0.52	17.87	0.39	0.06	3.39	0.66

Table F2 continued: Raw geochemistry data for SPM collected at Site B (Swanhills B) between May 2012 and March 2014. *Ce is measured in ppm.

Sample ID	Flow Conditions	Date (yyyy/mm/dd:hh:mm)	Stage (m)	SPM (mg/L)	Concentration (weight %)															
					Al	Ca	Ce*	Fe	K	Mg	Mn	Na	P	Si	Ti	POC	Al_{di}	Al_{ox}	Fe_{di}	Fe_{ox}
121125B19	Storm Event	2012/11/25:23:04	0.530	36.3	10.01	9.90	70	7.40	1.80	0.67	0.15	0.21	0.29	4.62	0.54	15.75	0.33	0.03	3.35	0.71
121125B20	Storm Event	2012/11/26:01:04	0.507	32.9	9.77	10.51	73	7.52	1.81	0.67	0.15	0.21	0.29	4.60	0.55	17.25	0.34	0.04	3.94	0.65
121125B21	Storm Event	2012/11/26:03:04	0.487	29.2	9.90	10.49	66	7.15	1.79	0.67	0.19	0.21	0.30	5.51	0.53	18.51	0.34	0.01	4.40	0.77
121125B22	Storm Event	2012/11/26:05:04	0.468	28.1	9.64	10.40	63	6.88	1.75	0.66	0.16	0.22	0.29	5.63	0.51	18.87	0.33	0.03	4.24	0.74
121125B23	Storm Event	2012/11/26:07:04	0.465	31.0	9.81	10.45	77	7.43	1.78	0.66	0.16	0.21	0.29	3.72	0.55	17.98	0.34	0.03	3.02	0.70
121125B24	Storm Event	2012/11/26:09:04	0.485	30.3	9.27	10.36	70	7.03	1.71	0.64	0.14	0.20	0.28	4.67	0.51	17.41	0.30	0.02	3.70	0.62
121127B1	Storm Event	2012/11/26:12:19	0.627	57.5	11.79	7.97	79	7.16	1.97	0.78	0.12	0.23	0.33	8.45	0.53	17.78	0.36	0.03	4.77	0.74
121127B2	Storm Event	2012/11/26:14:19	0.633	85.5	14.67	5.75	84	7.56	2.15	0.91	0.12	0.24	0.32	9.76	0.54	15.22	0.43	0.07	4.21	0.57
121127B3	Storm Event	2012/11/26:16:19	0.608	65.9	13.27	6.65	75	7.63	2.06	0.84	0.13	0.23	0.31	9.04	0.54	15.62	0.41	0.06	4.58	0.64
121127B4	Storm Event	2012/11/26:18:19	0.585	39.6	12.65	8.10	74	7.68	2.05	0.82	0.14	0.23	0.32	7.99	0.55	16.19	0.36	0.04	4.33	0.66
121127B5	Storm Event	2012/11/26:20:19	0.565	36.0	11.85	8.63	75	7.37	1.97	0.78	0.13	0.22	0.31	8.64	0.54	17.65	0.36	0.03	4.55	0.77
121127B6	Storm Event	2012/11/26:22:19	0.546	31.5	11.10	9.19	70	7.41	1.94	0.74	0.13	0.22	0.31	7.35	0.55	15.83	0.32	0.02	4.66	0.64
121127B7	Storm Event	2012/11/27:00:19	0.531	31.2	10.81	8.89	68	6.81	1.83	0.73	0.14	0.22	0.30	8.84	0.51	17.16	0.36	0.03	4.50	0.74
121127B8	Storm Event	2012/11/27:02:19	0.512	31.3	9.83	8.78	67	6.44	1.71	0.66	0.15	0.21	0.29	9.15	0.48	16.78	0.33	0.02	4.37	0.77
121127B9	Storm Event	2012/11/27:04:19	0.496	23.4	11.17	10.83	73	7.80	2.01	0.77	0.13	0.27	0.32	7.94	0.58	17.09	0.33	0.06	4.87	0.77
121127B10	Storm Event	2012/11/27:06:19	0.484	25.6	10.29	9.93	69	6.99	1.85	0.70	0.13	0.21	0.30	7.86	0.52	16.84	0.32	0.04	4.54	0.71
121127B11	Storm Event	2012/11/27:08:19	0.481	28.0	9.62	9.88	67	6.69	1.75	0.66	0.13	0.21	0.29	8.00	0.51	15.68	0.27	0.00	3.78	0.63
121127B12	Storm Event	2012/11/27:10:19	0.494	23.0	9.57	9.77	65	6.63	1.75	0.67	0.13	0.22	0.29	9.41	0.50	17.46	0.29	0.02	4.24	0.71
121127B13	Storm Event	2012/11/27:12:19	0.545	37.8	10.84	8.66	67	6.81	1.88	0.73	0.12	0.22	0.34	8.97	0.50	16.78	0.29	0.00	4.33	0.52
121127B14	Storm Event	2012/11/27:14:19	0.673	42.4	12.33	8.06	77	7.39	2.03	0.82	0.12	0.24	0.33	10.00	0.53	17.05	0.35	0.01	4.91	0.72
121127B15	Storm Event	2012/11/27:16:19	0.728	103.7	14.37	6.06	84	7.78	2.18	0.90	0.13	0.25	0.34	8.55	0.57	15.18	0.36	0.01	3.69	0.62
121127B16	Storm Event	2012/11/27:18:19	0.697	134.5	13.23	6.01	78	7.64	2.13	0.84	0.12	0.27	0.32	12.67	0.54	15.39	0.40	0.06	5.12	0.72
121127B17	Storm Event	2012/11/27:20:19	0.668	72.6	14.49	5.29	77	7.36	2.11	0.91	0.11	0.26	0.31	12.47	0.51	14.10	0.38	0.04	3.91	0.60
121127B18	Storm Event	2012/11/27:22:19	0.633	51.5	12.87	6.33	75	7.62	1.99	0.82	0.12	0.23	0.31	9.80	0.52	16.01	0.40	0.07	4.30	0.66
121127B19	Storm Event	2012/11/28:00:19	0.598	41.1	12.62	7.35	78	7.71	1.99	0.82	0.11	0.24	0.31	8.61	0.53	15.76	0.39	0.06	4.14	0.59
121127B20	Storm Event	2012/11/28:02:19	0.568	31.8	11.69	8.14	77	7.48	1.96	0.76	0.11	0.23	0.31	9.31	0.54	15.91	0.33	0.05	4.11	0.61
121127B21	Storm Event	2012/11/28:04:19	0.542	30.1	11.07	8.54	71	7.35	1.86	0.73	0.12	0.22	0.30	6.72	0.52	16.86	0.39	0.05	3.97	0.64
121127B22	Storm Event	2012/11/28:06:19	0.520	25.7	9.99	8.85	69	7.32	1.82	0.67	0.14	0.22	0.28	8.95	0.53	16.29	0.38	0.15	3.65	0.64
121127B23	Storm Event	2012/11/28:08:19	0.499	26.1	9.79	9.01	72	7.16	1.79	0.66	0.16	0.20	0.29	7.98	0.52	15.57	0.35	0.14	3.86	0.56

Table F2 continued: Raw geochemistry data for SPM collected at Site B (Swanhills B) between May 2012 and March 2014. *Ce is measured in ppm.

Sample ID	Flow Conditions	Date (yyyy/mm/dd:hh:mm)	Stage (m)	SPM (mg/L)	Concentration (weight %)															
					Al	Ca	Ce*	Fe	K	Mg	Mn	Na	P	Si	Ti	POC	Al_{di}	Al_{ox}	Fe_{di}	Fe_{ox}
121127B24	Storm Event	2012/11/28:10:19	0.480	17.5	9.67	9.48	66	7.08	1.86	0.67	0.15	0.22	0.30	13.32	0.52	17.26	0.36	0.16	4.08	0.73
121211B	Baseflow	2012/12/11:09:50	0.192	10.0	9.25	11.10	60	6.24	1.66	0.67	0.15	0.21	0.30	9.36	0.47	16.06	0.27	0.09	3.46	0.80
121219B	Baseflow	2012/12/19:10:15	0.162	9.1	9.18	11.88	70	7.37	1.72	0.63	0.16	0.20	0.29	4.96	0.53	15.87	0.29	0.07	3.31	0.79
130103B	Baseflow	2013/01/03:12:55	0.161	8.9	8.68	11.51	73	6.64	1.61	0.62	0.19	0.21	0.29	8.51	0.48	14.90	0.22	0.04	3.23	0.61
130108B	Baseflow	2013/01/08:12:55	0.118	12.0	7.85	13.86	62	6.59	1.48	0.58	0.18	0.21	0.27	5.23	0.47	14.49	0.24	0.08	2.70	0.37
130122B	Baseflow	2013/01/22:10:10	0.132	5.7	8.24	12.93	64	6.77	1.56	0.62	0.17	0.30	0.32	10.47	0.46	15.95	0.23	0.12	2.71	0.60
130129B	Baseflow	2013/01/29:09:50	0.262	17.1	7.95	10.75	70	6.38	1.57	0.57	0.14	0.23	0.25	7.44	0.48	13.62	0.28	0.11	2.19	0.37
130205B	Baseflow	2013/02/05:10:05	0.151	10.6	8.28	12.35	66	6.47	1.55	0.61	0.15	0.26	0.29	7.85	0.47	14.46	0.20	0.09	2.45	0.80
130212B	Baseflow	2013/02/12:09:25	0.145	8.6	8.55	12.11	61	6.66	1.61	0.63	0.14	0.23	0.29	8.52	0.49	13.77	0.22	0.10	2.85	0.62
130214B1/2	Storm Event	2013/02/13:22:48	0.129	21.4	6.22	8.33	52	4.24	1.35	0.46	0.11	0.29	0.25	11.67	0.36	13.24	0.26	0.10	2.05	0.47
130214B3/4	Storm Event	2013/02/14:02:48	0.133	15.4	6.44	10.11	52	4.68	1.33	0.48	0.14	0.24	0.26	13.93	0.38	13.38	0.26	0.14	1.93	0.68
130214B5	Storm Event	2013/02/14:05:48	0.154	14.1	7.49	10.12	55	5.15	1.48	0.58	0.14	0.26	0.30	21.05	0.39	12.63	0.26	0.19	2.66	0.62
130214B6	Storm Event	2013/02/14:07:48	0.276	23.0	8.82	11.04	61	6.30	1.75	0.65	0.17	0.28	0.31	11.48	0.49	16.15	0.28	0.15	2.76	0.71
130214B7	Storm Event	2013/02/14:09:48	0.357	592.0	17.91	3.18	91	7.72	2.76	1.04	0.17	0.41	0.32	13.43	0.69	13.38	0.41	0.16	3.90	0.57
130214B8	Storm Event	2013/02/14:11:48	0.363	318.9	16.78	2.90	87	7.36	2.52	1.01	0.15	0.33	0.30	16.35	0.61	12.58	0.40	0.15	3.98	0.58
130214B9	Storm Event	2013/02/14:13:48	0.352	175.0	16.32	3.37	88	7.64	2.46	0.97	0.14	0.25	0.29	16.49	0.59	13.35	0.41	0.13	4.13	0.62
130214B10	Storm Event	2013/02/14:15:48	0.339	100.4	14.39	4.25	82	7.60	2.25	0.88	0.14	0.24	0.28	17.39	0.55	13.21	0.42	0.16	3.97	0.47
130214B11	Storm Event	2013/02/14:17:48	0.320	70.0	13.79	5.04	79	7.29	2.14	0.87	0.14	0.25	0.28	15.43	0.54	13.02	0.35	0.10	3.66	0.48
130214B12	Storm Event	2013/02/14:19:48	0.303	43.8	13.38	6.69	71	7.56	2.16	0.87	0.15	0.33	0.29	13.70	0.57	13.43	0.34	0.15	3.26	0.53
130214B13	Storm Event	2013/02/14:21:48	0.290	30.5	11.61	7.43	72	7.31	2.00	0.77	0.14	0.25	0.28	12.77	0.54	14.05	0.37	0.13	3.86	0.49
130214B14	Storm Event	2013/02/14:23:48	0.277	24.0	10.83	7.75	70	7.05	1.98	0.73	0.16	0.26	0.27	15.01	0.53	15.54	0.35	0.17	4.02	0.69
130214B15/16	Storm Event	2013/02/15:02:48	0.262	18.9	10.81	8.55	74	7.19	1.91	0.73	0.16	0.25	0.28	10.52	0.54	13.76	0.33	0.11	2.72	0.46
130214B17/18	Storm Event	2013/02/15:06:48	0.245	16.4	10.66	9.00	73	6.99	1.90	0.73	0.16	0.26	0.29	10.33	0.54	15.44	0.32	0.12	3.18	0.78
130214B19/20	Storm Event	2013/02/15:10:48	0.232	13.4	9.26	9.13	65	6.27	1.74	0.64	0.15	0.26	0.27	13.80	0.49	17.19	0.32	0.10	3.77	0.46
130214B21/22	Storm Event	2013/02/15:14:48	0.223	10.8	9.08	10.01	65	6.45	1.77	0.65	0.15	0.30	0.28	15.69	0.49	14.76	0.34	0.18	3.59	0.54
130214B23/24	Storm Event	2013/02/15:18:48	0.212	13.9	9.90	10.37	67	6.53	1.79	0.71	0.15	0.32	0.30	10.60	0.52	14.32	0.28	0.13	2.69	0.55
130219B	Baseflow	2013/02/19:09:55	0.124	14.2	9.42	12.35	71	6.94	1.70	0.69	0.15	0.26	0.30	5.81	0.53	14.64	0.27	0.13	2.78	0.84
130226B	Baseflow	2013/02/26:11:55	0.073	8.3	7.95	10.75	56	5.28	1.39	0.60	0.14	0.20	0.31	12.72	0.38	16.45	0.29	0.13	2.78	0.74
130305B	Baseflow	2013/03/05:11:25	0.069	13.1	7.87	14.60	68	7.24	1.53	0.59	0.14	0.19	0.29	4.09	0.50	15.50	0.21	0.08	2.73	0.60

Table F2 continued: Raw geochemistry data for SPM collected at Site B (Swanhills B) between May 2012 and March 2014. *Ce is measured in ppm.

Sample ID	Flow Conditions	Date (yyyy/mm/dd:hh:mm)	Stage (m)	SPM (mg/L)	Concentration (weight %)															
					Al	Ca	Ce*	Fe	K	Mg	Mn	Na	P	Si	Ti	POC	Al_{di}	Al_{ox}	Fe_{di}	Fe_{ox}
130309B1	Storm Event	2013/03/08:17:48	0.060	28.8	6.15	10.35	54	4.84	1.36	0.47	0.14	0.27	0.25	10.92	0.39	10.98	0.17	0.15	2.03	0.51
130309B2	Storm Event	2013/03/08:19:48	0.060	46.9	7.47	14.96	66	7.42	1.50	0.60	0.14	0.23	0.25	1.45	0.51	13.30	0.20	0.16	1.72	0.53
130309B3	Storm Event	2013/03/08:21:48	0.061	28.0	6.51	11.49	55	5.51	1.42	0.50	0.14	0.22	0.27	8.54	0.42	13.15	0.19	0.16	2.24	0.40
130309B4/5	Storm Event	2013/03/09:00:48	0.064	22.7	7.33	13.24	65	6.50	1.50	0.56	0.17	0.25	0.27	4.82	0.48	14.29	0.16	0.15	1.77	0.53
130309B6	Storm Event	2013/03/09:03:48	0.068	23.4	8.05	13.04	64	6.62	1.64	0.61	0.15	0.28	0.28	8.58	0.50	13.71	0.19	0.17	2.72	0.52
130309B7	Storm Event	2013/03/09:05:48	0.077	32.6	7.89	12.44	63	6.66	1.57	0.60	0.16	0.28	0.26	4.36	0.49	13.26	0.19	0.18	2.50	0.48
130309B8	Storm Event	2013/03/09:07:48	0.146	66.9	8.04	10.73	67	6.60	1.58	0.62	0.16	0.27	0.27	3.13	0.49	14.28	0.24	0.18	2.02	0.40
130309B9	Storm Event	2013/03/09:09:48	0.255	90.3	8.54	10.08	69	6.60	1.68	0.64	0.16	0.26	0.27	5.98	0.51	13.91	0.24	0.16	2.66	0.51
130309B10	Storm Event	2013/03/09:11:48	0.397	144.2	7.25	8.50	65	5.68	1.45	0.53	0.14	0.27	0.22	5.02	0.45	11.81	0.21	0.14	1.54	0.43
130309B11	Storm Event	2013/03/09:13:48	0.480	118.3	9.09	7.89	66	5.75	1.61	0.66	0.13	0.31	0.25	8.74	0.46	11.06	0.22	0.15	2.23	0.43
130309B12	Storm Event	2013/03/09:15:48	0.544	135.9	8.58	7.83	68	5.86	1.63	0.61	0.14	0.30	0.23	8.77	0.46	11.92	0.22	0.18	2.00	0.41
130309B13	Storm Event	2013/03/09:17:48	0.637	125.3	8.42	7.74	71	6.14	1.63	0.59	0.14	0.29	0.23	8.64	0.47	11.92	0.25	0.15	2.38	0.38
130309B14	Storm Event	2013/03/09:19:48	0.643	110.8	10.14	6.80	68	6.09	1.71	0.70	0.12	0.32	0.25	11.12	0.47	11.47	0.27	0.14	2.58	0.29
130309B15	Storm Event	2013/03/09:21:48	0.647	101.3	9.55	6.52	63	5.90	1.59	0.65	0.11	0.31	0.23	11.12	0.42	10.91	0.29	0.23	1.23	0.34
130309B16	Storm Event	2013/03/09:23:48	0.646	82.6	9.26	6.50	62	5.82	1.53	0.63	0.10	0.30	0.23	12.06	0.41	10.48	0.29	0.20	1.62	0.32
130309B17	Storm Event	2013/03/10:01:48	0.636	65.0	8.96	6.79	68	5.90	1.55	0.61	0.10	0.28	0.22	12.24	0.41	11.60	0.29	0.17	1.81	0.31
130309B18	Storm Event	2013/03/10:03:48	0.621	55.9	10.28	6.58	64	6.12	1.52	0.70	0.10	0.29	0.23	10.11	0.39	10.85	0.28	0.17	2.18	0.31
130309B19	Storm Event	2013/03/10:05:48	0.601	52.0	9.24	6.68	63	5.94	1.50	0.63	0.10	0.28	0.22	10.40	0.40	10.94	0.29	0.18	2.12	0.24
130309B20	Storm Event	2013/03/10:07:48	0.569	47.1	8.59	6.90	65	5.86	1.49	0.58	0.12	0.27	0.21	10.58	0.39	11.11	0.28	0.17	2.01	0.23
130309B21	Storm Event	2013/03/10:09:48	0.534	35.3	9.19	7.71	61	6.19	1.61	0.63	0.12	0.28	0.23	12.75	0.42	12.05	0.28	0.19	2.32	0.39
130309B22	Storm Event	2013/03/10:11:48	0.502	31.9	8.57	7.54	62	5.78	1.55	0.59	0.12	0.27	0.23	14.38	0.40	12.06	0.27	0.19	2.71	0.32
130309B23	Storm Event	2013/03/10:13:48	0.473	29.7	8.30	7.82	62	5.65	1.54	0.58	0.12	0.27	0.23	14.68	0.41	12.40	0.27	0.18	2.31	0.33
130309B24	Storm Event	2013/03/10:15:48	0.448	25.2	7.01	7.95	57	4.91	1.45	0.50	0.12	0.23	0.22	19.35	0.38	10.85	0.24	0.17	2.72	0.35
130326B	Baseflow	2013/03/26:10:30	0.072	11.5	7.02	12.64	57	5.70	1.33	0.54	0.10	0.30	0.25	8.19	0.43	10.55	0.17	0.13	1.71	0.54
130403B	Baseflow	2013/04/03:09:30	0.045	3.3	7.82	11.81	61	6.28	1.55	0.61	0.13	0.27	0.36	16.58	0.43	13.92	0.20	0.11	3.20	0.51
130409B	Baseflow	2013/04/09:09:40	0.055	5.5	6.02	10.28	61	5.32	1.22	0.45	0.11	0.24	0.27	11.36	0.36	11.20	0.16	0.08	1.51	0.31
130416B	Baseflow	2013/04/16:10:10	0.042	4.7	6.60	11.56	55	5.57	1.39	0.52	0.10	0.21	0.34	18.07	0.37	14.09	0.21	0.12	2.90	0.25
130423B	Baseflow	2013/04/23:09:40	0.034	10.6	6.81	15.76	52	5.34	1.25	0.56	0.10	0.25	0.31	12.54	0.36	12.94	0.10	0.00	2.30	0.26
130430B	Baseflow	2013/04/30:09:15	0.019	12.8	6.91	12.37	52	5.39	1.35	0.56	0.09	0.24	0.34	13.79	0.38	12.44	0.15	0.13	1.48	0.34

Table F2 continued: Raw geochemistry data for SPM collected at Site B (Swanhills B) between May 2012 and March 2014. *Ce is measured in ppm.

Sample ID	Flow Conditions	Date (yyyy/mm/dd:hh:mm)	Stage (m)	SPM (mg/L)	Concentration (weight %)															
					Al	Ca	Ce*	Fe	K	Mg	Mn	Na	P	Si	Ti	POC	Al_{di}	Al_{ox}	Fe_{di}	Fe_{ox}
130507B	Baseflow	2013/05/07:10:05	0.020	7.1	6.35	13.11	52	5.43	1.33	0.51	0.11	0.22	0.33	14.96	0.38	12.27	0.16	0.15	2.60	0.35
130514B	Baseflow	2013/05/14:10:05	0.053	3.7	5.86	12.54	47	5.23	1.28	0.48	0.11	0.23	0.39	17.49	0.34	13.28	0.14	0.15	1.81	0.25
130521B	Baseflow	2013/05/21:09:50	0.000	7.5	6.15	13.35	50	5.12	1.31	0.50	0.11	0.22	0.35	18.13	0.35	12.17	0.13	0.13	2.66	0.17
130528B	Baseflow	2013/05/28:10:15	0.012	7.1	6.46	14.43	46	5.48	1.34	0.53	0.11	0.23	0.32	15.52	0.37	12.48	0.15	0.15	2.71	0.24
130604B	Baseflow	2013/06/04:09:51	0.005	5.1	5.61	12.14	48	4.61	1.17	0.45	0.11	0.21	0.28	16.17	0.33	11.10	0.11	0.13	2.26	0.08
130618B	Baseflow	2013/06/18:10:20	0.015	5.1	5.24	11.73	52	4.43	1.16	0.42	0.09	0.19	0.26	16.61	0.31	11.33	0.15	0.16	2.24	0.24
130625B	Baseflow	2013/06/25:10:20	0.009	3.9	5.78	13.87	52	5.69	1.20	0.47	0.12	0.20	0.29	12.52	0.35	14.33	0.13	0.14	2.69	0.30
130702B	Baseflow	2013/07/02:09:35	0.008	6.9	5.33	11.13	54	5.12	1.15	0.41	0.11	0.19	0.26	10.63	0.34	11.69	0.15	0.13	2.28	0.29
130709B	Baseflow	2013/07/09:09:45	0.005	9.4	5.75	10.89	51	4.97	1.21	0.44	0.10	0.22	0.25	12.07	0.36	11.64	0.16	0.14	2.24	0.35
130716B	Baseflow	2013/07/16:09:55	0.008	5.6	6.22	12.10	55	5.57	1.22	0.49	0.13	0.18	0.30	12.52	0.34	12.24	0.14	0.11	2.11	0.37
130723B	Baseflow	2013/07/23:09:55	0.007	4.0	6.07	13.63	55	6.26	1.24	0.48	0.13	0.14	0.30	8.73	0.37	13.87	0.15	0.14	2.01	0.39
130730B	Baseflow	2013/07/30:10:10	0.009	10.8	5.51	11.03	48	4.90	1.16	0.43	0.10	0.20	0.25	9.00	0.35	10.79	0.15	0.11	2.03	0.36
130806B	Baseflow	2013/08/06:10:35	0.011	7.1	6.19	12.78	58	5.68	1.29	0.50	0.13	0.18	0.31	11.09	0.37	12.78	0.17	0.14	1.07	0.44
130813B	Baseflow	2013/08/13:10:35	0.010	7.9	6.05	12.72	53	6.22	1.24	0.48	0.13	0.16	0.29	6.97	0.38	13.49	0.20	0.15	1.51	0.50
130820B	Baseflow	2013/08/20:08:45	0.008	8.7	5.94	12.80	56	6.23	1.24	0.47	0.14	0.16	0.29	6.62	0.38	12.81	0.16	0.15	2.10	0.44
130827B	Baseflow	2013/08/27:09:40	0.003	9.8	5.85	11.81	58	5.64	1.21	0.45	0.14	0.17	0.29	6.26	0.37	12.03	0.19	0.15	1.95	0.37
130903B	Baseflow	2013/09/03:09:20	0.005	8.0	6.34	13.70	55	6.46	1.29	0.50	0.17	0.16	0.32	6.49	0.39	13.30	0.17	0.17	2.65	0.53
130910B1	Storm Event	2013/09/09:19:21	0.000	32.5	5.05	10.79	52	4.92	1.13	0.41	0.19	0.18	0.36	8.92	0.32	16.02	0.19	0.06	1.75	0.56
130910B2/3	Storm Event	2013/09/09:22:21	0.000	10.8	5.40	12.77	45	5.50	1.25	0.47	0.21	0.20	0.50	10.33	0.33	20.32	0.21	0.15	2.41	0.88
130910B4/5	Storm Event	2013/09/10:02:21	0.000	11.2	5.57	11.81	49	5.47	1.24	0.46	0.20	0.16	0.43	11.53	0.34	18.30	0.21	0.10	1.90	0.63
130910B6/7	Storm Event	2013/09/10:06:21	0.000	13.1	5.59	12.72	55	5.79	1.24	0.46	0.20	0.17	0.39	7.51	0.35	17.57	0.19	0.12	1.21	0.60
130910B8/9	Storm Event	2013/09/10:10:21	0.000	10.3	5.35	11.74	49	5.26	1.20	0.45	0.19	0.16	0.42	13.42	0.32	18.70	0.19	0.13	1.60	0.62
130910B10/11	Storm Event	2013/09/10:14:21	0.001	13.2	5.28	12.80	46	5.41	1.21	0.45	0.18	0.16	0.43	10.76	0.32	18.88	0.21	0.10	2.31	0.77
130910B11/12	Storm Event	2013/09/10:16:21	0.002	15.7	5.19	12.22	47	4.84	1.16	0.45	0.17	0.16	0.45	12.07	0.31	18.82	0.24	0.16	2.37	0.70
130910B13	Storm Event	2013/09/10:19:21	0.006	18.9	5.17	11.04	49	4.55	1.19	0.45	0.18	0.17	0.46	16.20	0.29	18.96	0.22	0.12	1.68	0.70
130910B14	Storm Event	2013/09/10:21:21	0.006	29.5	5.55	10.51	46	4.57	1.20	0.46	0.15	0.19	0.36	11.82	0.32	15.91	0.22	0.11	1.62	0.61
130910B15	Storm Event	2013/09/10:23:21	0.004	20.3	6.24	11.59	53	5.41	1.36	0.51	0.18	0.18	0.41	12.90	0.36	18.26	0.24	0.12	1.90	0.62
130910B16	Storm Event	2013/09/11:01:21	0.004	19.5	5.83	10.91	48	5.02	1.28	0.48	0.17	0.18	0.39	15.47	0.32	17.33	0.23	0.15	1.81	0.66
130910B17/18	Storm Event	2013/09/11:04:21	0.003	15.7	5.90	11.32	53	5.11	1.21	0.48	0.17	0.17	0.36	8.89	0.33	16.29	0.23	0.13	1.80	0.58

Table F2 continued: Raw geochemistry data for SPM collected at Site B (Swanhills B) between May 2012 and March 2014. *Ce is measured in ppm.

Sample ID	Flow Conditions	Date (yyyy/mm/dd:hh:mm)	Stage (m)	SPM (mg/L)	Concentration (weight %)															
					Al	Ca	Ce*	Fe	K	Mg	Mn	Na	P	Si	Ti	POC	Al_{di}	Al_{ox}	Fe_{di}	Fe_{ox}
130910B19/20	Storm Event	2013/09/11:08:21	0.000	11.7	5.71	12.19	51	5.36	1.24	0.47	0.20	0.18	0.36	11.89	0.35	17.18	0.23	0.12	1.44	0.51
130910B21/22/23	Storm Event	2013/09/11:13:21	0.000	9.1	5.59	12.67	51	5.69	1.22	0.45	0.20	0.16	0.35	7.97	0.36	17.51	0.22	0.09	1.84	0.45
130914B1/2	Storm Event	2013/09/13:19:46	0.000	12.7	5.96	13.76	55	6.05	1.29	0.49	0.20	0.18	0.36	6.91	0.38	16.42	0.23	0.15	2.19	0.55
130914B3/4	Storm Event	2013/09/13:23:46	0.002	15.4	5.90	13.27	49	5.54	1.27	0.49	0.18	0.16	0.39	8.32	0.36	17.58	0.21	0.13	1.54	0.55
130914B5	Storm Event	2013/09/14:02:46	0.010	22.2	5.75	11.82	53	5.14	1.29	0.48	0.16	0.19	0.38	14.09	0.34	17.69	0.21	0.08	2.16	0.58
130914B6	Storm Event	2013/09/14:04:46	0.006	26.4	6.58	12.03	58	5.99	1.42	0.52	0.17	0.20	0.34	9.23	0.40	16.06	0.23	0.12	2.00	0.55
130914B7	Storm Event	2013/09/14:06:46	0.008	23.9	6.28	12.82	52	5.56	1.35	0.51	0.18	0.18	0.33	11.30	0.37	15.48	0.23	0.09	2.32	0.52
130914B8/9	Storm Event	2013/09/14:09:46	0.005	15.4	6.66	13.13	57	5.96	1.35	0.53	0.18	0.21	0.33	5.93	0.39	16.59	0.25	0.13	2.01	0.57
130914B10/11	Storm Event	2013/09/14:13:46	0.002	12.8	6.59	15.03	59	6.28	1.38	0.54	0.17	0.18	0.32	6.48	0.42	15.68	0.24	0.13	1.99	0.46
130914B12/13	Storm Event	2013/09/14:17:46	0.000	11.1	6.50	14.84	52	6.37	1.39	0.53	0.19	0.18	0.34	7.99	0.41	16.31	0.22	0.08	2.28	0.55
130914B14/15	Storm Event	2013/09/14:21:46	0.000	8.9	6.80	14.62	55	6.32	1.41	0.56	0.19	0.20	0.36	11.13	0.40	16.49	0.22	0.09	2.32	0.59
130914B16/17	Storm Event	2013/09/15:01:46	0.000	7.9	6.34	13.78	52	5.73	1.32	0.53	0.17	0.19	0.41	14.08	0.36	16.98	0.22	0.11	2.42	0.58
130914B18/19	Storm Event	2013/09/15:05:46	0.000	8.4	6.62	14.53	48	6.10	1.37	0.56	0.16	0.21	0.37	12.36	0.38	15.50	0.23	0.11	1.78	0.83
130914B20/21/22	Storm Event	2013/09/15:10:46	0.001	8.0	6.52	14.17	50	6.14	1.32	0.52	0.18	0.18	0.35	7.58	0.39	16.40	0.22	0.11	1.78	0.48
130917B	Baseflow	2013/09/17:09:45	0.001	9.0	6.24	13.34	56	6.05	1.25	0.51	0.16	0.19	0.31	6.39	0.39	14.93	0.23	0.18	1.43	0.72
131001B	Baseflow	2013/10/01:09:35	0.005	14.4	6.85	16.33	58	7.00	1.36	0.56	0.18	0.19	0.31	2.68	0.44	15.40	0.23	0.16	1.95	0.57
131008B	Baseflow	2013/10/08:09:15	0.004	14.1	6.90	16.10	60	7.10	1.35	0.55	0.18	0.16	0.30	2.30	0.44	14.50	0.23	0.18	0.65	0.60
131022B	Baseflow	2013/10/22:09:15	0.032	4.0	6.32	15.35	50	5.88	1.29	0.52	0.13	0.19	0.31	7.69	0.40	15.64	0.22	0.16	0.43	0.39
131028B1/2	Storm Event	2013/10/27:22:21	0.018	21.1	4.08	9.19	52	3.81	0.97	0.33	0.19	0.19	0.24	11.25	0.28	11.20	0.14	0.18	2.00	0.38
131028B3/4	Storm Event	2013/10/28:02:21	0.022	13.8	4.80	11.15	51	4.79	1.13	0.38	0.21	0.17	0.30	11.43	0.33	13.87	0.17	0.11	1.79	0.49
131028B5/6	Storm Event	2013/10/28:06:21	0.045	14.8	4.77	11.12	50	4.57	1.12	0.39	0.19	0.19	0.31	11.00	0.32	14.60	0.15	0.18	2.93	0.51
131028B7/8	Storm Event	2013/10/28:10:21	0.107	14.7	5.59	10.42	51	4.58	1.21	0.45	0.16	0.20	0.35	11.58	0.32	14.57	0.13	0.20	2.64	0.38
131028B9	Storm Event	2013/10/28:13:21	0.230	43.3	6.30	9.73	61	5.57	1.27	0.48	0.17	0.22	0.27	4.46	0.38	13.73	0.22	0.18	2.68	0.27
131028B10/11	Storm Event	2013/10/28:16:21	0.279	20.8	5.75	10.66	56	5.10	1.16	0.44	0.17	0.19	0.27	3.30	0.36	13.38	0.19	0.16	1.99	0.48
131028B12/13	Storm Event	2013/10/28:20:21	0.245	17.1	5.50	11.69	56	5.27	1.19	0.43	0.19	0.18	0.27	4.49	0.37	13.78	0.20	0.15	1.89	0.42
131028B14/15	Storm Event	2013/10/29:00:21	0.209	16.2	5.09	10.90	55	4.68	1.13	0.39	0.17	0.17	0.27	7.75	0.33	13.27	0.20	0.12	2.31	0.58
131028B16/17	Storm Event	2013/10/29:04:21	0.181	19.1	4.23	10.10	47	4.33	0.98	0.33	0.18	0.14	0.24	3.49	0.30	15.70	0.19	0.11	2.20	0.61
131028B18/19	Storm Event	2013/10/29:08:21	0.157	13.7	5.35	11.28	52	4.79	1.18	0.42	0.17	0.18	0.28	9.20	0.35	14.06	0.21	0.12	2.57	0.57
131028B20/21	Storm Event	2013/10/29:12:21	0.139	14.2	5.43	11.31	59	4.68	1.19	0.42	0.16	0.19	0.28	9.02	0.35	14.35	0.18	0.16	2.95	0.63

Table F2 continued: Raw geochemistry data for SPM collected at Site B (Swanhills B) between May 2012 and March 2014. *Ce is measured in ppm.

Sample ID	Flow Conditions	Date (yyyy/mm/dd:hh:mm)	Stage (m)	SPM (mg/L)	Concentration (weight %)															
					Al	Ca	Ce*	Fe	K	Mg	Mn	Na	P	Si	Ti	POC	Al_{di}	Al_{ox}	Fe_{di}	Fe_{ox}
131028B22/23/24	Storm Event	2013/10/29:17:21	0.115	12.5	5.45	11.15	55	4.83	1.15	0.42	0.16	0.19	0.26	4.62	0.35	11.75	0.15	0.19	1.77	0.42
131119B	Baseflow	2013/11/19:10:45	0.071	4.0	6.51	13.76	55	5.76	1.31	0.52	0.17	0.21	0.31	8.03	0.39	15.25	0.21	0.23	3.76	0.61
131126B	Baseflow	2013/11/26:11:25	0.092	4.0	6.68	14.66	58	6.04	1.35	0.53	0.18	0.21	0.30	7.62	0.42	15.84	0.21	0.18	2.67	0.62
131202B	Baseflow	2013/12/02:10:45	0.055	5.6	6.13	14.42	58	5.93	1.24	0.49	0.17	0.18	0.28	4.61	0.39	13.76	0.21	0.16	3.13	0.46
131210B	Baseflow	2013/12/10:10:45	0.042	7.0	6.13	14.90	58	6.48	1.26	0.48	0.18	0.18	0.29	2.49	0.42	15.97	0.18	0.19	2.19	0.71
131217B	Baseflow	2013/12/17:11:25	0.028	9.5	5.78	13.89	54	5.85	1.19	0.45	0.17	0.16	0.27	5.25	0.38	14.63	0.20	0.09	2.91	0.43
140107B	Baseflow	2014/01/07:10:15	0.106	9.5	6.40	14.42	61	6.29	1.31	0.50	0.18	0.19	0.26	2.51	0.43	14.07	0.18	0.15	3.35	0.62
140114B	Baseflow	2014/01/14:10:20	0.021	7.3	6.95	13.48	54	6.06	1.36	0.53	0.17	0.20	0.25	3.99	0.44	14.23	0.14	0.05	3.17	0.51
140121B	Baseflow	2014/01/21:10:35	0.000	6.6	6.99	13.36	64	6.19	1.40	0.54	0.17	0.21	0.28	5.88	0.43	14.51	0.16	0.12	2.95	0.61
140125B1	Storm Event	2014/01/24:22:11	0.015	186.9	4.08	9.34	55	5.17	0.88	0.32	0.18	0.16	0.16	0.00	0.31	11.19	0.19	0.16	1.91	0.44
140125B2	Storm Event	2014/01/25:00:11	0.018	89.5	4.42	10.50	56	5.35	1.00	0.34	0.19	0.16	0.18	0.00	0.35	13.91	0.20	0.14	2.42	0.56
140125B3	Storm Event	2014/01/25:02:11	0.018	58.7	4.41	10.17	53	4.99	0.98	0.33	0.18	0.14	0.19	0.04	0.34	12.08	0.17	0.20	2.21	0.46
140125B4	Storm Event	2014/01/25:04:11	0.020	40.4	4.69	10.52	56	4.94	1.03	0.36	0.18	0.17	0.20	2.56	0.34	12.54	0.18	0.16	1.40	0.47
140125B5	Storm Event	2014/01/25:06:11	0.021	51.6	4.30	9.69	52	4.71	0.93	0.33	0.17	0.18	0.18	0.75	0.31	10.83	0.17	0.22	1.69	0.52
140125B6	Storm Event	2014/01/25:08:11	0.021	26.8	5.30	11.00	54	5.00	1.17	0.40	0.17	0.18	0.23	9.44	0.35	13.51	0.22	0.23	1.96	0.52
140125B7	Storm Event	2014/01/25:10:11	0.021	22.7	4.64	9.88	53	4.15	1.05	0.36	0.15	0.18	0.22	17.59	0.29	10.87	0.19	0.24	2.37	0.52
140125B8	Storm Event	2014/01/25:12:11	0.024	21.5	4.69	10.03	49	4.10	1.06	0.37	0.15	0.20	0.22	18.73	0.29	10.75	0.14	0.18	2.68	0.55
140125B9	Storm Event	2014/01/25:14:11	0.029	21.4	4.71	10.58	52	4.24	1.07	0.38	0.16	0.21	0.22	18.04	0.29	11.62	0.10	0.21	1.87	0.51
140125B10/11	Storm Event	2014/01/25:17:11	0.043	27.8	4.81	10.41	53	5.17	0.99	0.37	0.16	0.15	0.20	0.00	0.34	16.71	0.13	0.13	2.59	0.79
140125B12	Storm Event	2014/01/25:20:11	0.053	31.5	6.13	11.39	58	5.35	1.26	0.46	0.16	0.19	0.24	5.63	0.39	13.80	0.19	0.19	3.57	0.50
140125B13	Storm Event	2014/01/25:22:11	0.053	30.0	6.31	11.76	61	5.71	1.29	0.48	0.17	0.21	0.24	5.27	0.41	13.91	0.20	0.20	2.18	0.53
140125B14	Storm Event	2014/01/26:00:11	0.056	25.2	6.29	12.18	63	5.74	1.33	0.48	0.16	0.21	0.25	7.58	0.41	14.78	0.21	0.26	2.40	0.49
140125B15	Storm Event	2014/01/26:02:11	0.060	24.5	6.00	11.47	59	5.14	1.25	0.46	0.16	0.20	0.24	9.70	0.37	14.41	0.20	0.23	2.57	0.42
140125B16	Storm Event	2014/01/26:04:11	0.064	25.0	5.51	10.36	54	4.63	1.18	0.42	0.15	0.19	0.23	12.56	0.33	12.52	0.21	0.27	2.01	0.47
140125B17	Storm Event	2014/01/26:06:11	0.069	19.3	6.22	11.35	56	4.94	1.27	0.49	0.15	0.22	0.26	14.41	0.36	11.63	0.19	0.21	3.06	0.67
140125B18	Storm Event	2014/01/26:08:11	0.074	20.3	5.88	11.43	56	5.04	1.25	0.46	0.16	0.21	0.24	13.20	0.36	14.74	0.20	0.23	2.51	0.39
140125B19	Storm Event	2014/01/26:10:11	0.080	23.2	4.96	8.97	48	3.69	1.04	0.39	0.13	0.18	0.21	19.62	0.26	11.37	0.17	0.17	3.20	0.51
140125B20	Storm Event	2014/01/26:12:11	0.085	15.4	5.61	10.44	54	4.37	1.17	0.45	0.16	0.22	0.24	20.33	0.31	11.49	0.20	0.27	3.00	0.62
140125B21	Storm Event	2014/01/26:14:11	0.106	19.1	5.69	10.01	53	4.44	1.21	0.44	0.15	0.20	0.24	17.27	0.32	12.43	0.16	0.19	2.29	0.65

Table F2 continued: Raw geochemistry data for SPM collected at Site B (Swanhills B) between May 2012 and March 2014. *Ce is measured in ppm.

Sample ID	Flow Conditions	Date (yyyy/mm/dd:hh:mm)	Stage (m)	SPM (mg/L)	Concentration (weight %)															
					Al	Ca	Ce*	Fe	K	Mg	Mn	Na	P	Si	Ti	POC	Al_{di}	Al_{ox}	Fe_{di}	Fe_{ox}
140125B22	Storm Event	2014/01/26:16:11	0.132	45.3	8.88	9.99	78	6.65	1.74	0.63	0.17	0.27	0.30	7.73	0.50	16.14	0.26	0.25	3.12	0.37
140125B23	Storm Event	2014/01/26:18:11	0.173	51.6	8.67	10.26	72	6.69	1.66	0.63	0.16	0.26	0.29	6.12	0.48	15.55	0.23	0.21	3.36	0.67
140125B24	Storm Event	2014/01/26:20:11	0.204	35.3	7.95	10.85	69	6.36	1.53	0.58	0.17	0.23	0.27	6.18	0.47	14.63	0.21	0.24	2.57	0.58
140125B25	Storm Event	2014/01/27:13:40	0.149	8.7	8.73	12.16	66	6.62	1.64	0.65	0.18	0.24	0.28	7.16	0.49	15.20	0.18	0.20	2.56	0.47
140129B	Baseflow	2014/01/29:10:45:00	0.048	8.8	7.73	12.12	64	5.96	1.46	0.59	0.16	0.22	0.26	6.68	0.44	15.28	0.20	0.13	4.76	0.49
140204B	Baseflow	2014/02/04:10:20:00	0.014	8.4	8.46	12.21	62	6.27	1.56	0.63	0.15	0.23	0.28	7.81	0.46	14.06	0.19	0.14	2.99	0.61
140206B1/2	Storm Event	2014/02/06:15:34:00	0.083	11.9	7.20	12.63	59	5.71	1.44	0.55	0.17	0.24	0.28	8.08	0.44	13.33	0.24	0.20	1.78	0.63
140206B3/4	Storm Event	2014/02/06:17:34:00	0.089	14.9	7.04	13.34	65	6.57	1.44	0.53	0.18	0.20	0.25	3.26	0.47	14.62	0.27	0.18	2.31	0.57
140206B5	Storm Event	2014/02/06:19:04:00	0.103	19.0	7.56	12.79	62	6.12	1.54	0.57	0.17	0.21	0.28	10.20	0.45	16.61	0.31	0.20	2.70	0.63
140206B6	Storm Event	2014/02/06:20:04:00	0.111	20.7	8.14	12.24	64	6.24	1.60	0.61	0.17	0.23	0.29	9.46	0.47	15.19	0.34	0.28	1.52	0.48
140206B7	Storm Event	2014/02/06:21:04:00	0.132	41.0	9.97	10.93	73	7.10	1.88	0.69	0.17	0.28	0.30	7.31	0.54	16.10	0.34	0.20	2.64	0.63
140206B8	Storm Event	2014/02/06:22:04:00	0.146	50.2	11.05	9.42	78	7.02	1.94	0.76	0.18	0.28	0.34	8.09	0.54	14.63	0.30	0.19	2.26	0.43
140206B9	Storm Event	2014/02/06:23:04:00	0.161	39.3	10.27	10.13	80	7.36	1.81	0.72	0.17	0.26	0.30	5.87	0.54	16.23	0.38	0.17	2.12	0.43
140206B10	Storm Event	2014/02/07:00:04:00	0.174	32.9	9.46	10.26	73	7.04	1.68	0.68	0.15	0.26	0.27	5.18	0.51	14.11	0.28	0.17	2.00	0.42
140206B11	Storm Event	2014/02/07:01:04:00	0.185	26.6	9.44	10.68	70	6.76	1.69	0.68	0.16	0.25	0.28	7.11	0.50	13.99	0.23	0.19	2.56	0.48
140206B12	Storm Event	2014/02/07:02:04:00	0.192	23.7	9.26	11.63	69	6.86	1.71	0.68	0.16	0.25	0.28	7.51	0.51	14.71	0.30	0.21	2.03	0.44
140206B13	Storm Event	2014/02/07:03:04:00	0.206	21.4	9.27	11.61	70	6.64	1.69	0.68	0.15	0.25	0.28	8.60	0.50	14.36	0.30	0.16	3.28	0.51
140206B14	Storm Event	2014/02/07:04:04:00	0.230	32.9	9.72	10.62	71	6.66	1.79	0.69	0.16	0.27	0.28	7.67	0.52	14.35	0.27	0.17	1.79	0.51
140206B15	Storm Event	2014/02/07:05:04:00	0.259	79.1	12.82	7.17	88	7.10	2.20	0.84	0.19	0.32	0.36	10.49	0.57	14.25	0.37	0.22	3.19	0.53
140206B16	Storm Event	2014/02/07:06:04:00	0.338	458.9	6.82	10.92	70	6.39	1.42	0.50	0.16	0.24	0.23	2.02	0.46	12.09	0.28	0.13	1.36	0.49
140206B17	Storm Event	2014/02/07:07:04:00	0.400	197.0	11.86	8.03	86	7.31	2.02	0.77	0.17	0.33	0.30	7.54	0.57	12.96	0.33	0.18	2.46	0.40
140206B18	Storm Event	2014/02/07:08:04:00	0.465	150.5	12.08	7.81	84	7.38	2.05	0.79	0.17	0.31	0.31	9.20	0.57	12.58	0.34	0.20	2.71	0.46
140206B19	Storm Event	2014/02/07:09:04:00	0.491	93.7	12.25	8.61	84	7.44	2.00	0.81	0.15	0.30	0.29	9.02	0.56	12.02	0.32	0.20	3.11	0.47
140206B20	Storm Event	2014/02/07:10:04:00	0.495	72.1	12.30	8.58	78	7.26	1.92	0.81	0.15	0.27	0.28	8.48	0.54	12.58	0.32	0.07	3.37	0.46
140206B21	Storm Event	2014/02/07:11:04:00	0.484	58.5	11.71	9.44	75	7.54	1.92	0.78	0.13	0.27	0.27	8.42	0.56	13.66	0.27	0.07	2.06	0.39
140206B22	Storm Event	2014/02/07:12:04:00	0.480	82.9	9.48	9.50	69	7.08	1.67	0.65	0.15	0.25	0.24	4.23	0.52	13.45	0.33	0.15	1.79	0.38
140206B23	Storm Event	2014/02/07:13:04:00	0.472	95.7	7.83	9.65	67	5.85	1.45	0.55	0.12	0.26	0.21	5.68	0.45	11.70	0.27	0.12	1.37	0.40
140206B24	Storm Event	2014/02/07:14:04:00	0.447	65.0	7.87	9.34	66	5.98	1.46	0.55	0.11	0.25	0.21	5.59	0.44	11.72	0.30	0.23	1.97	0.27
140211B	Baseflow	2014/02/11:10:20:00	0.150	14.9	7.91	12.65	63	6.34	1.51	0.59	0.14	0.22	0.24	4.80	0.48	13.95	0.28	0.20	1.63	0.58

Table F2 continued: Raw geochemistry data for SPM collected at Site B (Swanhills B) between May 2012 and March 2014. *Ce is measured in ppm.

Sample ID	Flow Conditions	Date (yyyy/mm/dd:hh:mm)	Stage (m)	SPM (mg/L)	Concentration (weight %)															
					Al	Ca	Ce*	Fe	K	Mg	Mn	Na	P	Si	Ti	POC	Al_{di}	Al_{ox}	Fe_{di}	Fe_{ox}
140218B	Baseflow	2014/02/18:10:20:00	0.100	10.0	8.09	12.56	55	6.25	1.52	0.60	0.12	0.24	0.27	6.91	0.47	13.72	0.26	0.23	1.03	0.52
140225B	Baseflow	2014/02/25:10:05:00	0.064	12.8	7.28	14.41	63	6.52	1.43	0.55	0.15	0.21	0.25	5.10	0.46	13.44	0.15	0.12	2.88	0.51
140304B	Baseflow	2014/03/04:09:50:00	0.058	8.4	7.36	13.42	57	6.03	1.39	0.57	0.15	0.23	0.27	7.68	0.42	14.08	0.11	0.10	2.92	0.54
140311B	Baseflow	2014/03/11:09:50:00	0.049	14.0	6.22	12.63	61	5.32	1.27	0.49	0.14	0.22	0.23	9.01	0.39	12.23	0.11	0.10	2.76	0.26
140318B	Baseflow	2014/03/18:09:50:00	0.040	6.8	7.08	13.27	62	5.81	1.38	0.56	0.14	0.24	0.30	10.82	0.41	14.06	0.10	0.13	3.08	0.52
140331B	Baseflow	2014/03/31:08:55:00	0.049	6.1	7.03	13.33	55	5.90	1.43	0.56	0.14	0.24	0.33	11.74	0.41	13.83	0.08	0.10	2.98	0.37

Table F3: Raw geochemistry data for SPM collected at Site E (Stinton Hall Farm) between May 2012 and March 2014. *Ce is measured in ppm.

Sample ID	Flow Conditions	Date (yyyy/mm/dd:hh:mm)	Stage (m)	SPM (mg/L)	Concentration (weight %)															
					Al	Ca	Ce*	Fe	K	Mg	Mn	Na	P	Si	Ti	POC	Al_{di}	Al_{ox}	Fe_{di}	Fe_{ox}
120508EE	Baseflow	2012/05/08:09:05	0.237	3.6	7.23	15.38	58	6.68	1.52	0.61	0.07	0.18	0.33	21.21	0.41	14.24	0.09	0.06	2.79	0.68
120515EE	Baseflow	2012/05/15:09:02	0.235	2.3	3.66	10.58	43	4.74	1.17	0.32	0.07	0.08	0.47	29.99	0.25	18.47	0.01	0.02	2.60	0.52
120710EE	Baseflow	2012/07/10:08:45	0.156	3.0	6.89	19.30	54	8.18	1.37	0.63	0.10	0.27	0.50	16.16	0.38	15.04	0.05	0.14	3.46	0.42
120716EE	Baseflow	2012/07/16:09:06	0.219	2.8	7.01	18.56	53	7.87	1.38	0.60	0.11	0.20	0.43	17.37	0.39	14.86	0.10	0.10	2.18	0.79
120731EE	Baseflow	2012/07/31:09:10	0.090	4.2	7.07	19.58	46	10.05	1.36	0.62	0.09	0.18	0.62	14.97	0.38	15.45	0.12	0.20	1.44	0.22
120807EE	Baseflow	2012/08/07:09:05	0.220	4.1	7.84	18.97	53	8.26	1.45	0.68	0.07	0.27	0.43	11.60	0.43	14.08	0.12	0.16	2.29	0.68
120814EE	Baseflow	2012/08/14:09:20	0.102	10.4	7.07	18.93	45	9.40	1.32	0.61	0.08	0.23	0.53	8.15	0.40	13.67	0.09	0.14	1.11	0.70
120821EE	Baseflow	2012/08/21:09:05	0.073	7.0	7.37	19.12	47	10.78	1.32	0.64	0.10	0.20	0.63	10.44	0.39	14.92	0.16	0.21	2.04	0.35
120827EE	Baseflow	2012/08/27:08:00	0.243	3.8	7.50	19.93	55	8.09	1.46	0.65	0.08	0.23	0.41	11.36	0.44	14.62	0.15	0.13	2.41	0.32
120904EE	Baseflow	2012/09/04:08:45	0.113	5.3	6.97	18.38	52	8.89	1.28	0.61	0.10	0.20	0.47	11.70	0.38	12.34	0.05	0.09	2.63	0.39
120910EE	Baseflow	2012/09/10:08:45	0.085	8.4	7.29	19.99	53	9.82	1.37	0.62	0.09	0.21	0.49	9.79	0.41	13.63	0.16	0.18	1.89	0.35
120918EE	Baseflow	2012/09/18:08:45	0.062	5.6	7.38	19.04	51	10.12	1.34	0.66	0.09	0.20	0.58	14.24	0.37	13.51	0.12	0.17	3.20	0.82
120924EE1/2	Storm Event	2012/09/23:14:12	0.063	7.2	6.18	16.78	41	8.53	1.25	0.57	0.12	0.18	0.70	15.81	0.32	15.47	0.02	0.09	3.85	0.46
120924EE3	Storm Event	2012/09/23:15:42	0.066	6.7	6.75	13.79	61	7.17	1.25	0.60	0.13	0.20	0.78	22.98	0.29	12.97	0.00	0.06	4.48	0.86
120924EE4	Storm Event	2012/09/23:16:42	0.071	8.2	5.57	14.33	43	6.63	1.16	0.49	0.11	0.18	0.60	23.22	0.28	11.65	0.03	0.11	3.95	0.60
120924EE5	Storm Event	2012/09/23:17:42	0.075	6.3	6.28	13.23	48	7.04	1.12	0.55	0.10	0.21	0.63	24.47	0.25	12.85	0.03	0.15	4.08	0.69
120924EE6	Storm Event	2012/09/23:18:42	0.078	8.6	6.69	15.84	47	7.64	1.29	0.60	0.12	0.23	0.61	21.18	0.31	11.99	0.05	0.17	3.67	0.55
120924EE7	Storm Event	2012/09/23:19:42	0.091	8.7	6.02	14.63	45	6.70	1.26	0.54	0.14	0.18	0.60	22.11	0.29	13.85	0.01	0.08	4.35	0.54
120924EE8	Storm Event	2012/09/23:20:42	0.098	10.0	6.20	15.14	48	6.86	1.29	0.55	0.12	0.17	0.58	20.85	0.32	14.14	0.03	0.11	4.62	0.48
120924EE9	Storm Event	2012/09/23:21:42	0.098	12.1	6.86	14.31	54	7.28	1.45	0.61	0.13	0.19	0.67	17.88	0.38	17.88	0.04	0.12	4.21	0.58
120924EE10	Storm Event	2012/09/23:22:42	0.111	13.7	6.74	13.75	51	7.14	1.45	0.60	0.14	0.19	0.64	17.19	0.37	16.10	0.03	0.05	3.69	0.53
120924EE11	Storm Event	2012/09/23:23:42	0.122	13.1	7.33	15.14	54	7.39	1.52	0.65	0.13	0.20	0.58	17.16	0.38	16.96	0.02	0.06	4.45	0.39
120924EE12	Storm Event	2012/09/24:00:42	0.127	13.7	6.95	14.78	51	6.96	1.46	0.62	0.12	0.18	0.52	18.91	0.37	15.98	0.05	0.09	4.43	0.19
120924EE13	Storm Event	2012/09/24:01:42	0.131	14.1	7.07	16.45	57	7.33	1.50	0.62	0.12	0.19	0.49	18.18	0.38	15.23	0.03	0.07	3.59	0.16
120924EE14	Storm Event	2012/09/24:02:42	0.143	15.8	7.08	17.69	56	7.63	1.51	0.62	0.12	0.19	0.47	15.54	0.40	14.94	0.04	0.03	3.66	0.08
120924EE15	Storm Event	2012/09/24:03:42	0.134	14.9	7.31	16.84	58	7.32	1.53	0.65	0.11	0.20	0.47	17.04	0.40	13.82	0.05	0.08	3.66	0.13
120924EE16	Storm Event	2012/09/24:04:42	0.137	13.0	7.23	17.01	57	7.24	1.51	0.64	0.12	0.20	0.48	18.02	0.39	13.52	0.05	0.07	3.81	0.08
120924EE17	Storm Event	2012/09/24:05:42	0.140	14.1	7.01	17.85	56	7.38	1.47	0.62	0.11	0.20	0.48	16.15	0.39	13.59	0.04	0.10	3.74	0.10
120924EE18	Storm Event	2012/09/24:06:42	0.145	11.5	7.33	18.28	59	7.17	1.52	0.65	0.11	0.21	0.49	19.18	0.38	12.79	0.03	0.08	3.37	0.22

Table F3 continued: Raw geochemistry data for SPM collected at Site E (Stinton Hall Farm) between May 2012 and March 2014. *Ce is measured in ppm.

Sample ID	Flow Conditions	Date (yyyy/mm/dd:hh:mm)	Stage (m)	SPM (mg/L)	Concentration (weight %)															
					Al	Ca	Ce*	Fe	K	Mg	Mn	Na	P	Si	Ti	POC	Al_{di}	Al_{ox}	Fe_{di}	Fe_{ox}
120924EE19	Storm Event	2012/09/24:07:42	0.150	9.2	7.36	17.44	56	6.88	1.48	0.66	0.11	0.20	0.48	20.84	0.37	13.05	0.02	0.05	4.72	0.20
120924EE20	Storm Event	2012/09/24:08:42	0.150	9.6	6.57	16.84	54	6.23	1.38	0.57	0.11	0.18	0.43	22.20	0.33	11.82	0.04	0.05	3.32	0.08
120924EE21	Storm Event	2012/09/24:09:42	0.158	10.2	6.25	17.62	60	6.50	1.34	0.54	0.11	0.18	0.41	19.70	0.41	12.78	0.02	0.06	3.49	0.13
120924EE22	Storm Event	2012/09/24:10:42	0.161	9.9	6.57	17.02	58	6.20	1.37	0.58	0.09	0.19	0.43	21.84	0.34	12.11	0.02	0.08	4.33	0.19
120924EE23	Storm Event	2012/09/24:11:42	0.162	8.4	7.29	19.43	59	7.32	1.52	0.63	0.11	0.21	0.44	21.21	0.38	11.10	0.03	0.08	4.95	0.11
120924EE24	Storm Event	2012/09/24:12:42	0.158	7.4	7.27	18.16	64	7.03	1.49	0.62	0.10	0.21	0.44	22.43	0.38	10.27	0.04	0.08	4.65	0.09
121002EE	Baseflow	2012/10/02:09:05	0.103	7.0	7.79	20.44	55	8.88	1.44	0.69	0.07	0.23	0.46	10.57	0.43	10.94	0.04	0.07	3.50	0.28
121005EE1/2	Storm Event	2012/10/04:22:52	0.092	9.6	6.93	18.10	46	8.17	1.48	0.62	0.12	0.20	0.57	10.00	0.39	17.45	0.00	0.04	2.92	0.00
121005EE3/4	Storm Event	2012/10/05:00:52	0.090	7.8	6.72	18.00	49	7.83	1.38	0.62	0.13	0.19	0.63	14.00	0.36	16.68	0.00	0.02	2.67	0.60
121005EE5/6	Storm Event	2012/10/05:02:52	0.094	8.5	6.85	17.99	51	8.59	1.44	0.61	0.15	0.20	0.59	11.27	0.41	14.42	0.00	0.04	3.41	0.42
121005EE7/8	Storm Event	2012/10/05:04:52	0.097	9.4	7.15	17.75	51	8.69	1.47	0.63	0.16	0.19	0.63	8.10	0.42	17.06	0.00	0.07	2.93	0.50
121005EE9	Storm Event	2012/10/05:06:22	0.119	12.0	7.36	18.33	47	7.11	1.46	0.69	0.11	0.27	0.54	16.46	0.36	13.55	0.00	0.00	3.50	0.61
121005EE10	Storm Event	2012/10/05:07:22	0.140	12.2	7.71	18.52	60	7.58	1.57	0.69	0.12	0.20	0.48	16.36	0.40	13.70	0.02	0.03	4.38	0.02
121005EE11	Storm Event	2012/10/05:08:22	0.142	23.5	10.77	12.67	64	7.87	1.95	0.86	0.14	0.20	0.63	12.93	0.45	19.90	0.03	0.00	5.30	0.00
121005EE12	Storm Event	2012/10/05:09:22	0.139	35.1	12.11	10.69	71	8.29	2.01	0.89	0.11	0.27	0.48	13.73	0.50	15.59	0.14	0.07	4.26	0.11
121005EE13	Storm Event	2012/10/05:10:22	0.131	30.7	11.28	12.27	76	8.74	1.95	0.85	0.12	0.25	0.43	13.29	0.51	13.64	0.13	0.07	4.35	0.03
121005EE14	Storm Event	2012/10/05:11:22	0.131	20.2	9.93	15.84	65	9.04	1.82	0.79	0.11	0.21	0.44	11.26	0.49	13.88	0.11	0.07	5.01	0.11
121005EE15	Storm Event	2012/10/05:12:22	0.130	16.3	9.02	16.48	62	8.23	1.71	0.74	0.11	0.21	0.42	15.11	0.46	12.32	0.05	0.03	4.29	0.16
121005EE16	Storm Event	2012/10/05:13:22	0.130	13.7	8.46	17.26	60	7.92	1.64	0.71	0.12	0.21	0.41	16.67	0.44	12.50	0.03	0.01	4.61	0.22
121005EE17	Storm Event	2012/10/05:14:22	0.132	11.5	8.34	18.58	68	7.99	1.64	0.71	0.12	0.22	0.42	17.48	0.44	10.94	0.02	0.04	4.89	0.07
121005EE18/19	Storm Event	2012/10/05:15:52	0.132	10.4	8.23	19.53	58	8.65	1.59	0.71	0.11	0.20	0.42	9.53	0.46	12.61	0.01	0.02	3.30	0.03
121005EE20/21	Storm Event	2012/10/05:17:52	0.127	11.0	8.20	20.41	60	9.07	1.57	0.71	0.11	0.21	0.41	7.22	0.48	11.81	0.00	0.00	2.60	0.23
121005EE22/23	Storm Event	2012/10/05:19:52	0.126	9.5	8.44	20.11	54	8.87	1.61	0.72	0.12	0.21	0.43	9.52	0.47	12.56	0.00	0.00	3.70	0.65
121009EE	Baseflow	2012/10/09:09:05	0.152	6.7	8.72	21.47	61	8.87	1.60	0.76	0.08	0.23	0.40	10.08	0.47	11.20	0.02	0.01	4.10	0.19
121016EE	Baseflow	2012/10/16:09:20	0.135	9.8	9.47	18.88	59	9.08	1.65	0.79	0.07	0.21	0.46	9.86	0.47	11.33	0.03	0.00	3.56	0.34
121022EE	Baseflow	2012/10/22:13:30	0.509	7.3	8.35	17.58	60	7.96	1.54	0.70	0.09	0.22	0.33	7.07	0.48	12.56	0.05	0.02	3.46	0.34
121030EE	Baseflow	2012/10/30:10:15	0.371	3.6	8.21	19.51	59	7.49	1.52	0.71	0.08	0.27	0.33	10.76	0.46	11.33	0.06	0.06	2.59	0.45
121101E4/5	Storm Event	2012/11/01:02:40	0.324	9.4	7.38	19.66	55	7.22	1.45	0.62	0.11	0.23	0.33	9.13	0.44	11.68	0.02	0.04	2.91	0.26
121101E6/7	Storm Event	2012/11/01:04:40	0.330	10.7	7.07	18.48	46	7.10	1.51	0.62	0.12	0.20	0.46	7.08	0.44	17.45	0.00	0.00	3.19	0.00

Table F3 continued: Raw geochemistry data for SPM collected at Site E (Stinton Hall Farm) between May 2012 and March 2014. *Ce is measured in ppm.

Sample ID	Flow Conditions	Date (yyyy/mm/dd:hh:mm)	Stage (m)	SPM (mg/L)	Concentration (weight %)															
					Al	Ca	Ce*	Fe	K	Mg	Mn	Na	P	Si	Ti	POC	Al_{di}	Al_{ox}	Fe_{di}	Fe_{ox}
121101E8/9	Storm Event	2012/11/01:06:40	0.339	11.2	7.92	19.37	55	7.76	1.53	0.66	0.11	0.23	0.34	5.88	0.49	12.12	0.03	0.03	2.57	0.35
121101E10/11	Storm Event	2012/11/01:08:40	0.364	11.9	9.25	15.60	62	7.53	1.71	0.76	0.12	0.25	0.36	9.86	0.49	13.33	0.06	0.03	2.88	0.20
121101EE12	Storm Event	2012/11/01:10:10	0.382	14.1	8.27	16.09	56	6.97	1.63	0.70	0.11	0.27	0.36	15.29	0.43	12.72	0.05	0.05	3.40	0.43
121101E13/14	Storm Event	2012/11/01:11:40	0.406	12.6	8.51	17.38	60	8.07	1.63	0.69	0.11	0.22	0.34	6.48	0.49	14.12	0.09	0.04	3.09	0.24
121101E15/16	Storm Event	2012/11/01:13:40	0.458	19.7	7.56	17.90	54	7.80	1.45	0.63	0.10	0.21	0.30	1.49	0.47	13.29	0.07	0.02	2.41	0.46
121101E17/18	Storm Event	2012/11/01:15:40	0.507	15.8	8.39	17.48	55	7.51	1.57	0.69	0.14	0.25	0.32	5.71	0.48	14.23	0.08	0.02	2.76	0.34
121101EE19	Storm Event	2012/11/01:17:10	0.520	16.6	8.15	17.51	57	7.38	1.61	0.68	0.11	0.26	0.33	12.04	0.47	11.99	0.07	0.04	3.56	0.43
121101E20/21	Storm Event	2012/11/01:18:40	0.523	13.7	8.15	17.49	57	7.64	1.54	0.66	0.10	0.22	0.30	6.31	0.48	12.08	0.10	0.07	2.77	0.24
121101E22/23	Storm Event	2012/11/01:20:40	0.519	10.6	8.20	17.93	57	7.61	1.56	0.68	0.10	0.25	0.31	8.81	0.47	12.13	0.06	0.01	2.65	0.45
121101EE24	Storm Event	2012/11/01:22:10	0.515	9.1	7.91	15.83	47	6.32	1.52	0.64	0.08	0.27	0.31	20.75	0.39	9.41	0.09	0.11	2.41	0.41
121106E	Baseflow	2012/11/06:08:00	0.417	3.9	7.50	18.52	58	7.70	1.48	0.63	0.10	0.26	0.32	8.30	0.46	13.94	0.03	0.00	3.54	0.66
121120E	Baseflow	2012/11/20:09:30	0.207	3.8	8.05	19.12	59	8.49	1.50	0.69	0.08	0.22	0.44	13.10	0.43	13.46	0.11	0.00	4.73	0.19
121123EE1/2	Storm Event	2012/11/22:23:41	0.371	12.4	7.85	16.66	55	7.42	1.53	0.68	0.12	0.23	0.39	5.72	0.48	16.24	0.14	0.00	4.23	0.58
121123EE3/4	Storm Event	2012/11/23:03:41	0.400	18.9	10.34	14.32	62	7.51	1.75	0.88	0.12	0.30	0.37	6.00	0.53	16.10	0.18	0.00	3.65	0.60
121123EE5	Storm Event	2012/11/23:06:41	0.475	48.5	9.44	15.24	69	8.08	1.72	0.77	0.12	0.25	0.35	3.93	0.53	15.65	0.17	0.00	2.95	0.15
121123EE6	Storm Event	2012/11/23:08:41	0.537	42.5	9.56	15.30	62	8.08	1.71	0.75	0.11	0.25	0.32	4.83	0.53	16.02	0.22	0.00	4.51	0.56
121123EE7	Storm Event	2012/11/23:10:41	0.531	29.8	9.33	15.17	68	8.45	1.70	0.72	0.12	0.25	0.31	4.70	0.53	15.26	0.28	0.00	3.90	0.42
121123EE8	Storm Event	2012/11/23:12:41	0.523	19.0	9.16	14.95	62	7.42	1.68	0.72	0.11	0.24	0.33	12.00	0.47	14.38	0.26	0.00	4.54	0.40
121123EE9/10	Storm Event	2012/11/23:15:41	0.506	16.1	8.79	15.89	64	8.01	1.53	0.70	0.12	0.22	0.30	3.43	0.49	15.24	0.23	0.00	3.63	0.48
121123EE11/12	Storm Event	2012/11/23:19:41	0.485	13.2	9.17	16.97	61	8.09	1.64	0.73	0.13	0.25	0.33	5.27	0.51	15.29	0.24	0.00	3.61	0.50
121123EE13/14	Storm Event	2012/11/23:23:41	0.468	10.3	8.50	16.66	56	7.47	1.61	0.69	0.11	0.26	0.32	9.85	0.47	14.66	0.22	0.00	3.88	0.46
121123EE15/16/17	Storm Event	2012/11/24:04:41	0.441	8.2	8.45	17.09	63	7.72	1.57	0.69	0.12	0.24	0.32	6.74	0.49	14.91	0.23	0.00	3.60	0.41
121125EE1/2/3/4	Storm Event	2012/11/24:14:11	0.411	5.3	7.60	18.54	52	6.98	1.42	0.64	0.12	0.24	0.31	9.63	0.43	14.63	0.17	0.00	3.78	0.38
121125EE5/6	Storm Event	2012/11/24:20:11	0.404	11.8	9.10	14.91	65	7.94	1.68	0.76	0.13	0.25	0.31	8.95	0.51	15.57	0.22	0.00	3.90	0.41
121125EE7/8	Storm Event	2012/11/25:00:11	0.415	12.9	8.60	15.41	63	8.00	1.63	0.70	0.16	0.22	0.35	5.44	0.49	18.99	0.18	0.00	4.01	0.41
121125EE9/10	Storm Event	2012/11/25:04:11	0.452	16.0	8.83	15.25	62	7.41	1.55	0.73	0.12	0.26	0.32	3.92	0.47	16.19	0.20	0.00	3.20	0.49
121125EE11	Storm Event	2012/11/25:07:11	0.534	34.7	7.96	15.89	59	7.64	1.46	0.65	0.12	0.23	0.30	1.71	0.47	16.14	0.22	0.00	2.82	0.43
121125EE12	Storm Event	2012/11/25:09:11	0.629	95.4	9.01	15.37	64	8.07	1.59	0.72	0.13	0.26	0.30	1.64	0.52	15.29	0.19	0.00	3.28	0.49
121125EE13	Storm Event	2012/11/25:11:11	0.684	118.2	8.65	15.00	64	7.99	1.44	0.69	0.10	0.24	0.25	0.00	0.48	12.57	0.23	0.00	2.68	0.27

Table F3 continued: Raw geochemistry data for SPM collected at Site E (Stinton Hall Farm) between May 2012 and March 2014. *Ce is measured in ppm.

Sample ID	Flow Conditions	Date (yyyy/mm/dd:hh:mm)	Stage (m)	SPM (mg/L)	Concentration (weight %)															
					Al	Ca	Ce*	Fe	K	Mg	Mn	Na	P	Si	Ti	POC	Al_{di}	Al_{ox}	Fe_{di}	Fe_{ox}
121125EE14	Storm Event	2012/11/25:13:11	0.671	102.9	9.47	13.77	62	7.84	1.50	0.71	0.09	0.24	0.25	1.00	0.48	13.18	0.29	0.03	2.87	0.34
121125EE15	Storm Event	2012/11/25:15:11	0.651	70.2	10.25	14.09	65	7.99	1.64	0.75	0.09	0.25	0.26	4.05	0.51	13.69	0.27	0.00	3.83	0.46
121125EE16	Storm Event	2012/11/25:17:11	0.620	56.4	8.80	14.42	57	7.63	1.50	0.66	0.09	0.23	0.25	3.44	0.48	13.87	0.26	0.00	3.16	0.32
121125EE17	Storm Event	2012/11/25:19:11	0.596	41.6	8.85	14.86	59	7.52	1.53	0.67	0.09	0.22	0.26	4.86	0.48	13.54	0.28	0.00	3.79	0.35
121125EE18	Storm Event	2012/11/25:21:11	0.574	34.2	8.53	15.58	59	7.56	1.50	0.66	0.10	0.23	0.26	4.46	0.47	15.05	0.26	0.00	4.11	0.57
121125EE19	Storm Event	2012/11/25:23:11	0.557	27.7	8.16	15.59	56	7.31	1.49	0.63	0.10	0.22	0.26	6.49	0.46	13.87	0.23	0.00	3.99	0.37
121125EE20	Storm Event	2012/11/26:01:11	0.540	23.0	8.30	15.70	56	7.18	1.55	0.64	0.10	0.23	0.27	9.26	0.47	13.35	0.23	0.00	3.48	0.45
121125EE21	Storm Event	2012/11/26:03:11	0.526	20.3	7.97	15.15	51	6.68	1.52	0.62	0.09	0.22	0.27	11.97	0.44	13.04	0.22	0.00	3.73	0.48
121125EE22	Storm Event	2012/11/26:05:11	0.509	18.3	8.21	15.76	61	7.03	1.58	0.65	0.09	0.23	0.29	12.52	0.45	13.13	0.18	0.00	3.77	0.45
121125EE23	Storm Event	2012/11/26:07:11	0.504	19.4	7.80	15.07	57	6.71	1.53	0.61	0.09	0.22	0.28	13.05	0.44	14.03	0.24	0.00	3.90	0.50
121125EE24	Storm Event	2012/11/26:09:11	0.513	23.2	9.09	13.75	68	7.52	1.69	0.72	0.10	0.24	0.30	9.58	0.50	15.53	0.24	0.00	4.26	0.55
121127EE1	Storm Event	2012/11/26:12:19	0.605	33.9	10.71	11.83	69	7.78	1.76	0.80	0.12	0.24	0.29	8.94	0.51	14.35	0.30	0.08	3.64	0.49
121127EE2	Storm Event	2012/11/26:14:19	0.624	44.1	9.72	11.85	64	7.37	1.62	0.71	0.10	0.24	0.27	7.79	0.47	13.20	0.29	0.07	3.39	0.42
121127EE3	Storm Event	2012/11/26:16:19	0.607	38.8	9.62	12.73	61	7.46	1.61	0.71	0.10	0.23	0.27	7.38	0.48	12.28	0.31	0.12	2.65	0.38
121127EE4	Storm Event	2012/11/26:18:19	0.587	35.1	8.67	12.86	65	7.36	1.51	0.66	0.09	0.23	0.25	6.15	0.46	13.01	0.29	0.10	2.52	0.36
121127EE5	Storm Event	2012/11/26:20:19	0.573	27.0	8.29	13.22	61	6.99	1.52	0.63	0.10	0.23	0.25	9.61	0.45	12.83	0.27	0.12	2.65	0.37
121127EE6	Storm Event	2012/11/26:22:19	0.557	22.0	8.48	13.75	54	6.87	1.56	0.65	0.11	0.22	0.26	12.24	0.45	12.59	0.27	0.10	3.36	0.31
121127EE7/8	Storm Event	2012/11/27:01:19	0.539	20.2	8.41	13.61	51	6.99	1.46	0.64	0.10	0.22	0.25	6.50	0.45	12.90	0.28	0.09	2.79	0.50
121127EE9/10	Storm Event	2012/11/27:05:19	0.518	18.0	8.39	14.64	53	7.21	1.49	0.64	0.09	0.23	0.26	6.22	0.45	12.52	0.27	0.09	2.68	0.38
121127EE11/12	Storm Event	2012/11/27:09:19	0.512	15.9	8.80	13.58	62	7.31	1.57	0.69	0.11	0.24	0.28	8.73	0.46	14.18	0.28	0.07	3.59	0.37
121127EE13	Storm Event	2012/11/27:12:19	0.544	20.5	8.35	12.26	63	6.88	1.61	0.66	0.12	0.23	0.28	14.67	0.45	12.95	0.28	0.10	3.09	0.37
121127EE14	Storm Event	2012/11/27:14:19	0.640	94.5	8.51	14.02	66	7.22	1.49	0.66	0.10	0.25	0.26	3.59	0.48	11.36	0.24	0.09	2.43	0.35
121127EE15	Storm Event	2012/11/27:16:19	0.715	157.7	8.52	14.99	63	7.83	1.44	0.68	0.08	0.25	0.23	0.00	0.50	11.32	0.24	0.05	2.23	0.37
121127EE16	Storm Event	2012/11/27:18:19	0.741	93.8	10.59	14.38	64	7.78	1.63	0.79	0.08	0.25	0.23	3.93	0.52	11.12	0.27	0.07	2.69	0.28
121127EE17	Storm Event	2012/11/27:20:19	0.643	107.8	8.31	13.36	57	6.74	1.34	0.63	0.06	0.24	0.22	2.16	0.43	10.68	0.25	0.06	2.20	0.31
121127EE18	Storm Event	2012/11/27:22:19	0.609	74.7	7.72	13.44	56	6.76	1.32	0.58	0.06	0.23	0.22	2.92	0.43	10.62	0.24	0.05	2.62	0.24
121127EE19	Storm Event	2012/11/28:00:19	0.581	58.7	7.57	13.42	58	6.68	1.31	0.58	0.05	0.23	0.21	2.60	0.42	10.68	0.22	0.03	2.25	0.27
121127EE20	Storm Event	2012/11/28:02:19	0.563	48.2	7.64	13.10	52	6.27	1.32	0.58	0.06	0.24	0.22	5.02	0.41	11.12	0.25	0.08	2.42	0.43
121127EE21	Storm Event	2012/11/28:04:19	0.541	40.5	7.96	13.28	53	6.48	1.35	0.60	0.06	0.24	0.22	5.09	0.42	11.07	0.23	0.04	3.06	0.31

Table F3 continued: Raw geochemistry data for SPM collected at Site E (Stinton Hall Farm) between May 2012 and March 2014. *Ce is measured in ppm.

Sample ID	Flow Conditions	Date (yyyy/mm/dd:hh:mm)	Stage (m)	SPM (mg/L)	Concentration (weight %)															
					Al	Ca	Ce*	Fe	K	Mg	Mn	Na	P	Si	Ti	POC	Al_{di}	Al_{ox}	Fe_{di}	Fe_{ox}
121127EE22	Storm Event	2012/11/28:06:19	0.522	33.2	7.33	13.88	56	6.73	1.39	0.56	0.07	0.23	0.22	6.86	0.43	11.94	0.25	0.06	2.99	0.49
121127EE23	Storm Event	2012/11/28:08:19	0.506	23.1	7.83	14.39	55	6.72	1.51	0.60	0.07	0.22	0.24	12.01	0.44	11.99	0.23	0.05	3.61	0.46
121127EE24	Storm Event	2012/11/28:10:19	0.491	18.0	8.34	13.98	59	6.78	1.62	0.65	0.09	0.24	0.26	15.34	0.45	12.87	0.27	0.09	4.79	0.41
121211E	Baseflow	2012/12/11:10:10	0.232	7.5	9.53	19.05	56	7.85	1.64	0.76	0.10	0.23	0.29	8.91	0.49	12.02	0.18	0.02	3.74	0.65
121219E	Baseflow	2012/12/19:10:35	0.197	6.0	9.42	18.47	63	8.32	1.62	0.75	0.09	0.23	0.31	8.32	0.49	12.02	0.22	0.07	4.15	0.39
130103E	Baseflow	2013/01/03:13:35	0.174	13.0	9.17	19.88	60	8.35	1.56	0.75	0.10	0.23	0.28	3.49	0.52	11.57	0.15	0.00	3.06	0.41
130108E	Baseflow	2013/01/08:12:25	0.158	9.3	9.57	21.63	55	8.89	1.66	0.78	0.11	0.23	0.32	6.95	0.52	11.33	0.19	0.07	3.34	0.15
130122E	Baseflow	2013/01/22:10:40	0.182	7.7	9.56	19.11	55	8.23	1.68	0.88	0.11	0.35	0.31	10.23	0.50	12.41	0.19	0.07	2.85	0.42
130129E	Baseflow	2013/01/29:10:15	0.285	21.0	10.05	14.86	63	7.57	1.73	0.80	0.10	0.27	0.27	8.99	0.52	12.36	0.25	0.12	2.89	0.23
130205E	Baseflow	2013/02/05:10:45	0.186	7.0	9.43	19.47	60	8.09	1.63	0.78	0.10	0.29	0.32	8.78	0.50	10.92	0.19	0.10	3.11	0.68
130212E	Baseflow	2013/02/12:09:45	0.183	5.7	9.36	19.43	55	8.48	1.67	0.76	0.09	0.26	0.33	10.27	0.50	11.56	0.18	0.09	4.00	0.69
130214EE1/2	Storm Event	2013/02/13:22:49	0.165	21.3	6.49	15.06	50	5.57	1.35	0.54	0.13	0.23	0.29	6.76	0.40	14.48	0.20	0.07	1.87	0.16
130214EE3/4	Storm Event	2013/02/14:02:49	0.171	9.9	7.63	17.82	49	6.44	1.48	0.64	0.14	0.27	0.32	15.23	0.41	13.55	0.23	0.13	3.59	0.39
130214EE5	Storm Event	2013/02/14:05:49	0.190	14.3	8.36	14.27	59	6.27	1.57	0.71	0.12	0.30	0.34	19.54	0.42	11.82	0.29	0.22	3.12	0.42
130214EE6	Storm Event	2013/02/14:07:49	0.277	178.8	11.49	10.99	84	8.14	1.99	1.04	0.14	0.31	0.35	7.00	0.60	14.83	0.25	0.07	2.47	0.38
130214EE7	Storm Event	2013/02/14:09:49	0.374	387.0	15.86	6.10	91	8.11	2.36	1.04	0.16	0.33	0.33	10.94	0.64	12.50	0.35	0.15	2.86	0.58
130214EE8	Storm Event	2013/02/14:11:49	0.389	228.9	14.23	7.76	80	8.11	2.19	0.93	0.13	0.27	0.28	11.56	0.60	12.53	0.38	0.17	4.05	0.45
130214EE9	Storm Event	2013/02/14:13:49	0.381	136.2	12.36	8.81	72	7.48	1.84	0.83	0.10	0.25	0.26	10.44	0.51	12.51	0.38	0.14	3.10	0.26
130214EE10	Storm Event	2013/02/14:15:49	0.373	87.3	11.47	10.01	66	7.35	1.77	0.78	0.09	0.25	0.22	10.94	0.49	11.38	0.36	0.15	3.07	0.28
130214EE11	Storm Event	2013/02/14:17:49	0.353	52.9	12.47	12.45	75	8.95	1.98	0.86	0.11	0.27	0.24	7.93	0.58	13.16	0.38	0.18	3.14	0.20
130214EE12	Storm Event	2013/02/14:19:49	0.339	51.6	11.02	11.01	61	6.95	1.62	0.78	0.09	0.26	0.22	8.78	0.46	11.36	0.35	0.14	2.73	0.25
130214EE13	Storm Event	2013/02/14:21:49	0.324	37.1	10.02	12.71	65	7.49	1.69	0.72	0.11	0.26	0.22	10.43	0.49	11.72	0.33	0.16	3.09	0.18
130214EE14	Storm Event	2013/02/14:23:49	0.316	33.0	9.04	12.55	57	6.71	1.61	0.66	0.10	0.26	0.22	13.27	0.45	11.08	0.31	0.13	2.68	0.23
130214EE15/16	Storm Event	2013/02/15:02:49	0.306	25.2	9.24	13.37	59	6.96	1.54	0.68	0.10	0.26	0.22	8.26	0.47	11.57	0.29	0.09	3.02	0.24
130214EE17/18	Storm Event	2013/02/15:06:49	0.258	19.2	8.96	15.03	63	7.33	1.59	0.68	0.10	0.27	0.22	7.94	0.49	11.26	0.27	0.12	2.58	0.21
130214EE19/20	Storm Event	2013/02/15:10:49	0.276	15.4	8.87	14.81	57	7.09	1.62	0.69	0.10	0.26	0.24	11.15	0.48	12.05	0.25	0.07	3.49	0.41
130214EE21/22	Storm Event	2013/02/15:14:49	0.264	13.3	8.85	15.80	58	6.98	1.64	0.70	0.12	0.28	0.25	12.40	0.48	11.56	0.23	0.08	2.73	0.24
130214EE23/24	Storm Event	2013/02/15:18:49	0.253	15.9	8.65	16.54	56	7.24	1.62	0.69	0.10	0.28	0.24	9.21	0.49	12.06	0.22	0.07	3.00	0.40
130219E	Baseflow	2013/02/19:10:40	0.164	8.8	9.61	17.63	61	7.96	1.65	0.76	0.10	0.27	0.31	8.22	0.50	13.00	0.19	0.11	3.24	0.61

Table F3 continued: Raw geochemistry data for SPM collected at Site E (Stinton Hall Farm) between May 2012 and March 2014. *Ce is measured in ppm.

Sample ID	Flow Conditions	Date (yyyy/mm/dd:hh:mm)	Stage (m)	SPM (mg/L)	Concentration (weight %)															
					Al	Ca	Ce*	Fe	K	Mg	Mn	Na	P	Si	Ti	POC	Al_{di}	Al_{ox}	Fe_{di}	Fe_{ox}
130226E	Baseflow	2013/02/26:10:20	0.105	6.9	9.82	20.42	55	9.59	1.67	0.82	0.11	0.27	0.37	7.29	0.51	12.80	0.23	0.14	3.41	0.78
130305E	Baseflow	2013/03/05:10:45	0.100	12.7	9.16	21.42	55	9.34	1.57	0.75	0.09	0.22	0.32	3.22	0.53	12.63	0.15	0.10	2.19	0.43
130326E	Baseflow	2013/03/26:10:05	0.125	5.6	9.18	20.41	57	9.18	1.60	0.77	0.08	0.28	0.33	7.66	0.50	10.55	0.15	0.09	2.59	0.45
130403E	Baseflow	2013/04/03:09:05	0.086	5.8	9.11	20.37	54	9.30	1.61	0.76	0.08	0.23	0.37	11.61	0.47	10.40	0.16	0.12	2.87	0.24
130409E	Baseflow	2013/04/09:09:15	0.087	7.2	8.70	19.23	56	9.05	1.54	0.73	0.12	0.26	0.34	4.88	0.48	11.77	0.12	0.07	2.35	0.42
130416E	Baseflow	2013/04/16:09:35	0.074	12.1	9.16	21.60	56	9.02	1.59	0.79	0.08	0.26	0.33	6.19	0.49	11.02	0.15	0.09	2.76	0.10
130423E	Baseflow	2013/04/23:09:05	0.068	8.6	9.30	21.54	57	9.22	1.62	0.81	0.08	0.26	0.39	10.85	0.46	11.29	0.12	0.00	4.16	0.25
130430E	Baseflow	2013/04/30:08:35	0.058	8.1	9.51	19.34	54	10.28	1.70	0.84	0.08	0.27	0.43	10.50	0.48	10.29	0.17	0.15	3.90	0.16
130507E	Baseflow	2013/05/07:09:25	0.064	11.3	9.02	21.41	52	9.08	1.57	0.79	0.07	0.25	0.40	8.88	0.46	9.28	0.15	0.13	2.97	0.06
130514E	Baseflow	2013/05/14:09:23	0.056	6.0	8.83	19.63	48	9.84	1.54	0.77	0.08	0.25	0.51	11.52	0.43	11.02	0.16	0.15	3.45	0.18
130521E	Baseflow	2013/05/21:09:20	0.054	6.7	8.70	19.21	51	9.61	1.51	0.76	0.09	0.23	0.48	12.20	0.41	10.64	0.13	0.13	3.51	0.00
130528E	Baseflow	2013/05/28:09:25	0.077	14.5	9.29	20.93	58	8.56	1.62	0.79	0.08	0.23	0.34	8.08	0.49	9.91	0.12	0.06	3.51	0.09
130604E	Baseflow	2013/06/04:09:15	0.062	5.7	9.47	20.63	59	10.07	1.69	0.86	0.09	0.27	0.50	11.91	0.46	9.44	0.13	0.11	2.96	0.08
130618E	Baseflow	2013/06/18:09:45	0.053	3.8	7.75	17.87	50	10.13	1.42	0.68	0.10	0.23	0.58	17.32	0.37	10.88	0.16	0.23	3.24	0.35
130625E	Baseflow	2013/06/25:09:35	0.052	3.5	8.14	18.02	55	11.28	1.45	0.72	0.10	0.23	0.71	16.08	0.38	11.38	0.15	0.18	4.01	0.38
130702E	Baseflow	2013/07/02:08:44	0.052	3.6	7.77	17.07	50	10.47	1.37	0.69	0.11	0.22	0.71	17.07	0.35	12.03	0.13	0.18	3.89	0.22
130709E	Baseflow	2013/07/09:09:10	0.058	4.2	8.26	17.56	52	10.20	1.41	0.73	0.09	0.23	0.67	16.48	0.36	11.02	0.13	0.18	3.53	0.24
130716E	Baseflow	2013/07/16:09:20	0.061	4.3	8.70	18.04	55	10.70	1.49	0.74	0.11	0.19	0.61	14.82	0.39	10.13	0.15	0.20	3.22	0.12
130723E	Baseflow	2013/07/23:09:40	0.058	4.3	9.57	18.87	59	10.85	1.61	0.84	0.11	0.26	0.60	13.83	0.43	10.25	0.15	0.18	2.57	0.30
130730E	Baseflow	2013/07/30:09:20	0.057	6.0	7.79	16.02	57	8.63	1.37	0.69	0.10	0.28	0.56	14.19	0.36	10.60	0.14	0.17	2.39	0.36
130806E	Baseflow	2013/08/06:09:19	0.070	4.4	8.62	14.48	59	9.51	1.53	0.78	0.12	0.25	0.66	17.13	0.38	11.91	0.16	0.15	2.89	0.40
130813E	Baseflow	2013/08/13:09:20	0.061	3.3	8.01	16.32	59	10.59	1.38	0.71	0.12	0.20	0.65	16.28	0.36	10.72	0.15	0.17	3.59	0.28
130820E	Baseflow	2013/08/20:08:25	0.062	3.9	8.31	17.11	52	10.68	1.42	0.74	0.11	0.25	0.69	13.71	0.38	11.16	0.15	0.17	2.68	0.44
130827E	Baseflow	2013/08/27:09:15	0.066	3.2	8.10	16.42	49	11.53	1.40	0.72	0.13	0.22	0.81	15.73	0.36	10.72	0.16	0.19	2.46	0.38
130903E	Baseflow	2013/09/03:09:05	0.063	4.5	7.82	16.80	46	9.90	1.34	0.71	0.11	0.25	0.70	14.76	0.35	10.53	0.15	0.22	2.61	0.43
130910EE1	Storm Event	2013/09/09:19:22	0.064	34.6	4.69	15.58	39	5.51	1.05	0.44	0.15	0.17	0.46	11.57	0.27	18.35	0.09	0.06	1.85	0.43
130910EE2	Storm Event	2013/09/09:21:22	0.065	26.6	5.80	17.38	45	7.20	1.24	0.52	0.18	0.16	0.51	7.99	0.36	16.08	0.16	0.09	2.98	0.40
130910EE3	Storm Event	2013/09/09:23:22	0.089	32.5	5.83	17.70	46	7.30	1.23	0.52	0.17	0.17	0.42	7.43	0.37	15.03	0.10	0.06	2.72	0.51
130910EE4	Storm Event	2013/09/10:01:22	0.075	28.8	6.06	18.07	48	7.49	1.30	0.54	0.16	0.18	0.45	8.53	0.37	14.12	0.11	0.08	3.42	0.33

Table F3 continued: Raw geochemistry data for SPM collected at Site E (Stinton Hall Farm) between May 2012 and March 2014. *Ce is measured in ppm.

Sample ID	Flow Conditions	Date (yyyy/mm/dd:hh:mm)	Stage (m)	SPM (mg/L)	Concentration (weight %)															
					Al	Ca	Ce*	Fe	K	Mg	Mn	Na	P	Si	Ti	POC	Al_{di}	Al_{ox}	Fe_{di}	Fe_{ox}
130910EE5	Storm Event	2013/09/10:03:22	0.067	27.6	6.71	17.88	45	8.05	1.40	0.60	0.17	0.22	0.45	8.37	0.41	13.99	0.13	0.09	2.79	0.45
130910EE6	Storm Event	2013/09/10:05:22	0.067	23.9	6.67	16.43	53	7.55	1.39	0.58	0.15	0.19	0.46	10.61	0.39	14.62	0.12	0.05	2.86	0.40
130910EE7	Storm Event	2013/09/10:07:22	0.067	22.1	6.07	16.27	48	7.22	1.32	0.54	0.16	0.18	0.48	12.45	0.36	16.20	0.15	0.12	3.16	0.49
130910EE8	Storm Event	2013/09/10:09:22	0.074	11.9	5.74	13.04	44	6.02	1.23	0.52	0.15	0.18	0.50	22.24	0.28	15.92	0.08	0.09	4.03	0.45
130910EE9	Storm Event	2013/09/10:11:22	0.077	8.8	5.54	11.73	53	6.09	1.17	0.50	0.16	0.21	0.50	24.47	0.26	15.16	0.10	0.17	3.62	0.56
130910EE10	Storm Event	2013/09/10:13:22	0.077	10.1	5.14	11.39	52	5.70	1.07	0.49	0.12	0.23	0.55	23.64	0.23	16.08	0.09	0.13	4.81	0.84
130910EE11	Storm Event	2013/09/10:15:22	0.085	9.9	5.32	11.95	43	6.02	1.12	0.51	0.15	0.22	0.53	22.89	0.24	18.43	0.12	0.20	4.84	0.81
130910EE12	Storm Event	2013/09/10:17:22	0.104	13.0	5.98	11.66	45	6.14	1.28	0.53	0.15	0.16	0.47	21.59	0.29	19.44	0.10	0.12	5.07	0.52
130910EE13	Storm Event	2013/09/10:19:22	0.107	23.4	8.40	13.30	63	7.95	1.65	0.75	0.15	0.24	0.46	10.30	0.44	18.68	0.18	0.12	3.79	0.41
130910EE14	Storm Event	2013/09/10:21:22	0.103	23.9	9.13	10.69	56	7.17	1.69	0.81	0.15	0.28	0.45	13.77	0.40	18.33	0.17	0.10	2.36	0.38
130910EE15	Storm Event	2013/09/10:23:22	0.107	18.7	8.44	12.09	57	7.05	1.66	0.76	0.14	0.29	0.50	16.66	0.39	17.10	0.18	0.10	3.05	0.53
130910EE16	Storm Event	2013/09/11:01:22	0.099	18.5	7.90	15.06	56	7.53	1.56	0.69	0.16	0.21	0.46	12.36	0.41	17.13	0.15	0.08	3.36	0.34
130910EE17	Storm Event	2013/09/11:03:22	0.096	14.3	7.32	12.77	53	6.55	1.49	0.64	0.14	0.21	0.47	18.43	0.35	16.65	0.17	0.09	3.63	0.28
130910EE18/19	Storm Event	2013/09/11:06:22	0.082	9.3	7.38	13.79	51	7.61	1.46	0.64	0.17	0.20	0.53	14.33	0.36	18.46	0.17	0.07	2.98	0.37
130910EE20/21	Storm Event	2013/09/11:10:22	0.074	5.8	6.98	12.83	50	7.52	1.40	0.60	0.16	0.17	0.65	19.84	0.32	15.85	0.18	0.12	2.40	0.42
130910EE22/23/24	Storm Event	2013/09/11:15:22	0.076	11.8	7.05	16.64	53	8.64	1.37	0.63	0.16	0.22	0.57	10.22	0.37	14.76	0.15	0.08	2.32	0.47
130914EE1/2	Storm Event	2013/09/13:19:46	0.070	13.3	6.51	16.42	48	8.05	1.35	0.57	0.24	0.19	0.52	6.08	0.38	15.80	0.16	0.11	2.34	0.34
130914EE3	Storm Event	2013/09/13:22:46	0.085	12.2	6.32	13.61	42	6.64	1.32	0.57	0.22	0.23	0.57	18.41	0.32	14.25	0.15	0.17	3.42	0.59
130914EE4	Storm Event	2013/09/14:00:46	0.130	15.5	6.84	15.91	49	7.11	1.43	0.62	0.18	0.24	0.51	14.32	0.37	14.98	0.12	0.11	3.31	0.58
130914EE5	Storm Event	2013/09/14:02:46	0.117	27.8	10.05	12.12	65	7.69	1.75	0.86	0.18	0.28	0.46	8.36	0.46	14.36	0.17	0.07	3.31	0.44
130914EE6	Storm Event	2013/09/14:04:46	0.129	21.0	8.81	14.81	63	8.28	1.70	0.75	0.20	0.22	0.47	9.42	0.46	15.84	0.18	0.11	3.70	0.34
130914EE7	Storm Event	2013/09/14:06:46	0.127	14.8	8.46	13.83	55	7.38	1.63	0.72	0.18	0.26	0.46	16.15	0.40	13.76	0.17	0.12	4.39	0.33
130914EE8/9	Storm Event	2013/09/14:09:46	0.110	9.7	8.11	13.68	55	7.68	1.56	0.69	0.18	0.24	0.49	13.64	0.39	14.91	0.16	0.13	3.60	0.35
130914EE10/11	Storm Event	2013/09/14:13:46	0.095	7.3	7.21	14.18	58	7.63	1.43	0.61	0.18	0.19	0.54	17.41	0.36	14.25	0.15	0.07	3.42	0.40
130914EE12/13	Storm Event	2013/09/14:17:46	0.088	6.4	6.99	14.36	51	7.62	1.40	0.61	0.17	0.25	0.56	18.42	0.33	13.36	0.16	0.08	2.85	0.38
130914EE14/15	Storm Event	2013/09/14:21:46	0.082	9.7	7.42	16.98	46	8.10	1.38	0.64	0.19	0.21	0.50	12.04	0.39	13.07	0.17	0.14	3.07	0.33
130914EE16/17	Storm Event	2013/09/15:01:46	0.076	6.9	7.38	16.53	56	8.92	1.46	0.65	0.19	0.24	0.56	14.59	0.39	13.20	0.17	0.12	3.20	0.45
130914EE18/19	Storm Event	2013/09/15:05:46	0.077	5.8	7.67	16.54	51	9.22	1.47	0.68	0.17	0.25	0.63	15.91	0.38	12.90	0.18	0.10	3.35	0.54
130914EE20/21/22	Storm Event	2013/09/15:10:46	0.076	3.8	7.20	16.13	50	9.92	1.46	0.64	0.19	0.25	0.69	16.85	0.37	14.28	0.17	0.12	3.02	0.51

Table F3 continued: Raw geochemistry data for SPM collected at Site E (Stinton Hall Farm) between May 2012 and March 2014. *Ce is measured in ppm.

Sample ID	Flow Conditions	Date (yyyy/mm/dd:hh:mm)	Stage (m)	SPM (mg/L)	Concentration (weight %)															
					Al	Ca	Ce*	Fe	K	Mg	Mn	Na	P	Si	Ti	POC	Al_{di}	Al_{ox}	Fe_{di}	Fe_{ox}
130917E	Baseflow	2013/09/17:09:15	0.070	5.0	9.52	18.61	56	10.65	1.57	0.83	0.10	0.31	0.71	10.91	0.44	12.81	0.21	0.16	3.89	0.51
131001E	Baseflow	2013/10/01:09:05	0.057	7.4	7.31	16.34	54	8.54	1.27	0.64	0.11	0.23	0.50	11.67	0.35	12.57	0.23	0.21	1.94	0.30
131008E	Baseflow	2013/10/08:08:50	0.059	4.1	8.73	19.22	57	11.66	1.48	0.80	0.12	0.24	0.79	11.33	0.40	11.80	0.25	0.31	1.48	0.31
131022E	Baseflow	2013/10/22:09:05	0.237	1.9	6.83	14.29	55	6.82	1.35	0.59	0.09	0.23	0.43	21.29	0.34	12.35	0.27	0.34	0.00	0.07
131028EE1/2	Storm Event	2013/10/27:22:21	0.213	7.2	4.48	11.13	38	4.83	1.17	0.48	0.17	0.20	0.99	19.40	0.25	20.62	0.22	0.23	0.25	0.13
131028EE3/4/5/6	Storm Event	2013/10/28:04:21	0.229	3.0	5.49	12.12	54	6.11	1.22	0.50	0.17	0.21	0.65	21.26	0.29	18.11	0.28	0.17	1.51	0.05
131028EE7/8/9	Storm Event	2013/10/28:11:21	0.344	5.8	8.03	8.18	67	6.68	1.64	0.66	0.13	0.23	0.55	22.03	0.37	18.32	0.24	0.13	2.25	0.17
131028EE10/11	Storm Event	2013/10/28:16:21	0.509	9.0	7.92	9.62	59	6.39	1.54	0.62	0.16	0.22	0.42	20.11	0.36	15.15	0.24	0.23	3.48	0.18
131028EE12/13/14	Storm Event	2013/10/28:21:21	0.476	5.0	6.82	10.61	53	6.03	1.40	0.54	0.17	0.22	0.45	21.35	0.33	13.79	0.19	0.19	4.52	0.13
131028EE15/16/17/18	Storm Event	2013/10/29:04:21	0.442	2.9	6.05	9.51	51	5.30	1.25	0.48	0.16	0.20	0.45	24.95	0.28	15.51	0.17	0.34	3.87	0.13
131028EE19/20/21/22/23/24	Storm Event	2013/10/29:14:21	0.417	1.4	5.50	7.96	56	4.97	1.16	0.46	0.16	0.20	0.59	27.02	0.24	15.38	0.15	0.26	2.32	0.16
131119E	Baseflow	2013/11/19:10:10	0.260	1.4	5.85	11.09	55	6.33	1.19	0.50	0.10	0.25	0.49	25.86	0.27	10.72	0.19	0.28	4.74	0.42
131126E	Baseflow	2013/11/26:10:45	0.295	1.0	7.53	12.64	64	6.92	1.31	0.61	0.11	0.33	0.42	24.46	0.31	9.69	0.16	0.23	4.35	0.36
131202E	Baseflow	2013/12/02:10:25	0.223	1.8	5.95	12.79	59	7.20	1.20	0.50	0.10	0.23	0.44	21.75	0.32	11.18	0.18	0.17	2.57	0.28
131210E	Baseflow	2013/12/10:10:15	0.174	1.1	5.76	13.10	57	9.39	1.13	0.49	0.12	0.22	0.68	24.35	0.27	13.18	0.13	0.23	4.84	0.38
131217E	Baseflow	2013/12/17:10:50	0.168	3.1	8.00	10.35	70	8.69	1.57	0.68	0.10	0.23	0.52	24.03	0.38	13.00	0.28	0.30	4.34	0.30
140107E	Baseflow	2014/01/07:10:00	0.294	2.9	8.42	17.72	52	7.43	1.50	0.72	0.13	0.25	0.36	13.68	0.42	12.69	0.18	0.15	5.86	0.00
140114E	Baseflow	2014/01/14:09:50	0.308	2.4	8.90	15.95	57	7.89	1.59	0.73	0.12	0.26	0.37	12.32	0.45	12.44	0.16	0.12	4.32	0.29
140121E	Baseflow	2014/01/21:10:05	0.261	3.1	9.08	16.42	59	7.78	1.58	0.79	0.13	0.28	0.39	13.42	0.44	12.83	0.13	0.10	4.03	0.19
140125EE1/2	Storm Event	2014/01/24:23:11	0.286	11.9	6.55	14.20	53	6.08	1.38	0.57	0.16	0.22	0.38	9.41	0.38	15.94	0.11	0.14	2.87	0.27
140125EE3/4	Storm Event	2014/01/25:03:11	0.291	11.0	7.90	14.25	59	7.05	1.52	0.70	0.16	0.30	0.34	9.35	0.44	13.91	0.15	0.14	4.35	0.37
140125EE5/6	Storm Event	2014/01/25:07:11	0.294	8.5	7.53	14.87	58	6.89	1.50	0.64	0.17	0.25	0.35	12.77	0.41	13.18	0.15	0.14	3.25	0.34
140125EE7/8	Storm Event	2014/01/25:11:11	0.296	5.7	6.94	13.06	53	6.00	1.40	0.60	0.15	0.29	0.36	20.00	0.35	12.36	0.22	0.24	5.25	0.37
140125EE9/10	Storm Event	2014/01/25:15:11	0.304	9.6	3.77	9.84	36	3.90	1.03	0.35	0.14	0.12	1.00	13.12	0.22	30.43	0.11	0.00	4.15	0.15
140125EE11/12	Storm Event	2014/01/25:19:11	0.324	18.2	8.97	13.20	71	7.26	1.68	0.79	0.16	0.29	0.38	5.31	0.50	14.65	0.17	0.05	2.97	0.05
140125EE13/14	Storm Event	2014/01/25:23:11	0.326	13.0	8.60	15.03	66	7.73	1.62	0.73	0.15	0.26	0.31	5.43	0.51	15.25	0.13	0.06	3.78	0.27
140125EE15/16	Storm Event	2014/01/26:03:11	0.335	10.3	7.88	15.04	55	7.07	1.53	0.66	0.16	0.25	0.30	9.72	0.45	13.39	0.22	0.22	1.94	0.35
140125EE17/18	Storm Event	2014/01/26:07:11	0.343	9.1	7.94	15.32	57	6.86	1.54	0.67	0.14	0.27	0.30	11.58	0.44	12.88	0.15	0.13	4.50	0.39
140125EE19/20	Storm Event	2014/01/26:11:11	0.354	5.1	7.69	13.55	67	6.17	1.47	0.65	0.15	0.27	0.32	20.15	0.38	11.68	0.22	0.29	5.00	0.26

Table F3 continued: Raw geochemistry data for SPM collected at Site E (Stinton Hall Farm) between May 2012 and March 2014. *Ce is measured in ppm.

Sample ID	Flow Conditions	Date (yyyy/mm/dd:hh:mm)	Stage (m)	SPM (mg/L)	Concentration (weight %)															
					Al	Ca	Ce*	Fe	K	Mg	Mn	Na	P	Si	Ti	POC	Al_{di}	Al_{ox}	Fe_{di}	Fe_{ox}
140125EE21	Storm Event	2014/01/26:14:11	0.374	14.6	8.68	11.85	65	6.17	1.66	0.82	0.16	0.32	0.32	16.57	0.45	14.43	0.21	0.14	5.23	0.39
140125EE22	Storm Event	2014/01/26:16:11	0.396	30.8	10.00	11.92	74	7.42	1.85	0.85	0.16	0.30	0.35	9.06	0.53	14.93	0.21	0.11	3.90	0.34
140125EE23	Storm Event	2014/01/26:18:11	0.427	40.0	9.61	14.06	65	7.87	1.70	0.77	0.15	0.27	0.28	4.27	0.52	12.54	0.23	0.12	3.28	0.36
140125EE24	Storm Event	2014/01/26:20:11	0.452	42.6	8.96	15.61	59	7.85	1.63	0.70	0.13	0.25	0.26	3.97	0.51	10.15	0.20	0.13	3.73	0.20
140125EE25	Storm Event	2014/01/27:12:45	0.415	9.6	9.82	14.91	61	7.11	1.68	0.84	0.11	0.30	0.29	10.23	0.48	11.24	0.20	0.13	2.92	0.39
140129E	Baseflow	2014/01/29:10:30	0.312	4.2	9.61	16.39	65	7.94	1.68	0.81	0.13	0.29	0.32	11.23	0.48	13.75	0.18	0.15	1.90	0.06
140131EE1	Storm Event	2014/01/31:15:22	0.277	36.7	6.06	13.28	54	5.60	1.22	0.50	0.11	0.23	0.28	7.90	0.36	12.45	0.06	0.04	2.16	0.38
140131EE2	Storm Event	2014/01/31:16:22	0.281	19.1	6.85	14.97	58	6.06	1.37	0.58	0.12	0.28	0.29	14.87	0.39	11.66	0.04	0.00	4.01	0.37
140131EE3	Storm Event	2014/01/31:17:22	0.283	20.4	7.30	15.60	56	6.41	1.43	0.60	0.12	0.25	0.30	12.23	0.42	11.70	0.07	0.01	3.48	0.32
140131EE4	Storm Event	2014/01/31:18:22	0.288	29.9	7.81	16.34	61	7.38	1.51	0.66	0.12	0.26	0.28	6.26	0.48	13.09	0.07	0.02	3.43	0.58
140131EE5	Storm Event	2014/01/31:19:22	0.294	60.7	10.39	11.77	73	7.27	1.84	0.99	0.15	0.35	0.34	7.14	0.55	15.59	0.10	0.02	3.66	0.48
140131EE6	Storm Event	2014/01/31:20:22	0.301	53.4	10.31	12.90	76	7.76	1.84	0.91	0.15	0.32	0.33	6.22	0.55	14.61	0.08	0.02	3.81	0.49
140131EE7	Storm Event	2014/01/31:21:22	0.306	54.8	10.35	12.28	75	7.58	1.86	0.88	0.13	0.31	0.37	6.91	0.54	14.55	0.12	0.05	3.61	0.54
140131EE8	Storm Event	2014/01/31:22:22	0.309	40.8	9.66	12.86	72	7.74	1.74	0.82	0.13	0.29	0.34	4.80	0.52	15.66	0.13	0.07	3.21	0.31
140131EE9	Storm Event	2014/01/31:23:22	0.317	33.8	9.08	14.11	71	7.85	1.66	0.74	0.12	0.27	0.32	4.35	0.51	15.01	0.12	0.07	3.27	0.41
140131EE10	Storm Event	2014/02/01:00:22	0.321	27.9	8.31	14.27	58	7.39	1.57	0.67	0.13	0.24	0.29	5.55	0.48	13.62	0.11	0.04	3.31	0.37
140131EE11	Storm Event	2014/02/01:01:22	0.327	25.1	8.15	14.30	59	7.13	1.53	0.66	0.13	0.23	0.29	7.42	0.46	13.20	0.10	0.04	3.94	0.37
140131EE12	Storm Event	2014/02/01:02:22	0.336	25.6	8.39	15.03	62	7.25	1.55	0.69	0.13	0.26	0.28	6.61	0.47	12.76	0.11	0.07	3.30	0.31
140131EE13	Storm Event	2014/02/01:03:22	0.343	25.5	7.85	14.95	64	7.09	1.51	0.63	0.13	0.24	0.28	7.35	0.46	12.56	0.08	0.03	3.13	0.35
140131EE14	Storm Event	2014/02/01:04:22	0.356	32.2	7.50	14.47	64	7.03	1.44	0.61	0.13	0.24	0.28	3.70	0.46	13.42	0.11	0.08	2.98	0.34
140131EE15	Storm Event	2014/02/01:05:22	0.394	57.0	8.79	14.77	71	7.54	1.64	0.76	0.14	0.29	0.28	4.75	0.53	13.24	0.11	0.02	3.50	0.34
140131EE16	Storm Event	2014/02/01:06:22	0.440	160.4	11.23	10.64	86	7.93	1.98	0.83	0.14	0.32	0.33	5.80	0.60	13.01	0.17	0.06	2.82	0.41
140131EE17	Storm Event	2014/02/01:07:22	0.483	149.6	9.76	12.62	71	7.60	1.67	0.72	0.11	0.27	0.26	4.41	0.52	11.23	0.16	0.10	3.03	0.29
140131EE18	Storm Event	2014/02/01:08:22	0.508	184.0	7.79	12.68	62	7.18	1.32	0.61	0.09	0.25	0.22	0.00	0.44	9.83	0.15	0.12	2.22	0.27
140131EE19	Storm Event	2014/02/01:09:22	0.513	155.7	7.77	12.94	63	6.83	1.29	0.60	0.09	0.25	0.22	0.83	0.43	9.30	0.12	0.10	1.94	0.21
140131EE20	Storm Event	2014/02/01:10:22	0.511	151.0	8.00	13.83	61	7.00	1.34	0.62	0.11	0.25	0.25	2.77	0.43	10.50	0.14	0.09	2.37	0.33
140131EE21	Storm Event	2014/02/01:11:22	0.503	154.3	6.98	13.82	56	6.83	1.27	0.55	0.09	0.24	0.23	2.16	0.42	11.11	0.13	0.11	2.28	0.16
140131EE22	Storm Event	2014/02/01:12:22	0.495	109.8	7.32	13.54	57	6.92	1.30	0.57	0.09	0.25	0.23	2.44	0.43	10.46	0.11	0.07	2.52	0.26
140131EE23	Storm Event	2014/02/01:13:22	0.487	94.5	7.37	12.58	55	6.23	1.23	0.57	0.08	0.25	0.21	2.45	0.40	10.38	0.13	0.08	2.46	0.37

Table F3 continued: Raw geochemistry data for SPM collected at Site E (Stinton Hall Farm) between May 2012 and March 2014. *Ce is measured in ppm.

Sample ID	Flow Conditions	Date (yyyy/mm/dd:hh:mm)	Stage (m)	SPM (mg/L)	Concentration (weight %)															
					Al	Ca	Ce*	Fe	K	Mg	Mn	Na	P	Si	Ti	POC	Al_{di}	Al_{ox}	Fe_{di}	Fe_{ox}
140131EE24	Storm Event	2014/02/01:14:22	0.478	83.0	7.47	13.35	58	6.39	1.29	0.58	0.08	0.25	0.23	3.25	0.41	10.55	0.15	0.08	2.15	0.24
140204E	Baseflow	2014/02/04:09:50	0.281	6.9	10.51	16.27	65	8.09	1.77	0.83	0.09	0.28	0.32	8.98	0.51	11.23	0.20	0.13	4.60	0.33
140206EE1/2	Storm Event	2014/02/06:16:07	0.243	14.8	6.82	12.99	49	5.71	1.33	0.57	0.14	0.24	0.31	9.70	0.37	12.51	0.19	0.11	2.92	0.35
140206EE3	Storm Event	2014/02/06:19:07	0.260	36.8	10.07	13.93	70	7.64	1.83	0.88	0.13	0.31	0.33	7.36	0.55	13.09	0.22	0.06	1.80	0.52
140206EE4	Storm Event	2014/02/06:21:07	0.290	65.4	11.07	11.20	74	7.46	2.00	0.95	0.14	0.32	0.39	7.73	0.57	16.48	0.23	0.12	1.00	0.65
140206EE5	Storm Event	2014/02/06:23:07	0.324	48.5	10.20	12.17	70	7.28	1.79	0.80	0.13	0.27	0.33	7.10	0.51	12.48	0.21	0.12	2.95	0.43
140206EE6	Storm Event	2014/02/07:01:07	0.350	37.6	9.22	14.33	62	7.51	1.66	0.73	0.11	0.27	0.27	6.06	0.50	11.39	0.18	0.12	1.69	0.37
140206EE7	Storm Event	2014/02/07:03:07	0.371	38.9	8.45	14.55	57	7.08	1.54	0.67	0.10	0.27	0.24	5.08	0.48	10.23	0.20	0.08	2.15	0.38
140206EE8	Storm Event	2014/02/07:05:07	0.413	81.0	10.08	11.49	71	6.89	1.76	0.75	0.12	0.30	0.30	7.19	0.52	12.00	0.26	0.12	2.28	0.59
140206EE9	Storm Event	2014/02/07:07:07	0.517	339.3	7.55	12.28	59	6.31	1.30	0.58	0.09	0.26	0.23	2.11	0.42	10.17	0.20	0.13	1.14	0.23
140206EE10	Storm Event	2014/02/07:09:07	0.615	311.3	7.92	13.92	63	7.11	1.38	0.61	0.08	0.28	0.23	2.38	0.47	9.25	0.23	0.15	1.89	0.31
140206EE11	Storm Event	2014/02/07:11:07	0.617	194.1	8.70	13.57	62	7.01	1.44	0.65	0.07	0.27	0.22	3.50	0.46	9.49	0.22	0.15	1.84	0.15
140206EE12	Storm Event	2014/02/07:13:07	0.596	151.7	9.28	12.35	58	6.76	1.47	0.67	0.07	0.26	0.24	3.49	0.45	9.76	0.20	0.09	2.14	0.26
140206EE13	Storm Event	2014/02/07:15:07	0.570	89.8	8.82	12.66	60	6.82	1.45	0.64	0.06	0.26	0.20	4.47	0.45	9.31	0.30	0.24	2.22	0.24
140206EE14	Storm Event	2014/02/07:17:07	0.545	76.4	8.26	12.85	58	6.52	1.41	0.61	0.06	0.28	0.20	6.05	0.43	9.24	0.25	0.16	2.02	0.27
140206EE15	Storm Event	2014/02/07:19:07	0.524	55.5	8.32	11.46	56	6.01	1.29	0.62	0.05	0.26	0.18	4.48	0.38	7.73	0.23	0.15	1.91	0.18
140206EE16	Storm Event	2014/02/07:21:07	0.508	53.6	8.22	11.47	56	5.93	1.29	0.60	0.05	0.25	0.19	4.76	0.39	7.94	0.23	0.17	1.53	0.23
140206EE17	Storm Event	2014/02/07:23:07	0.493	43.2	8.04	12.81	54	6.41	1.37	0.60	0.06	0.25	0.20	5.22	0.41	9.51	0.25	0.17	1.78	0.15
140206EE18/19	Storm Event	2014/02/08:02:07	0.479	34.6	8.19	11.66	51	5.71	1.27	0.60	0.06	0.25	0.19	5.61	0.38	8.94	0.23	0.16	1.65	0.21
140206EE20/21	Storm Event	2014/02/08:06:07	0.460	26.4	8.36	14.04	62	7.09	1.45	0.63	0.08	0.25	0.21	3.24	0.46	10.68	0.23	0.08	2.32	0.22
140206EE22	Storm Event	2014/02/08:09:07	0.444	26.3	7.96	13.70	55	6.40	1.48	0.60	0.09	0.25	0.23	11.05	0.42	9.52	0.24	0.17	1.74	0.46
140206EE23/24	Storm Event	2014/02/08:12:07	0.430	22.3	8.53	13.75	59	6.82	1.48	0.66	0.09	0.25	0.22	5.87	0.45	11.09	0.23	0.13	2.53	0.27
140211E	Baseflow	2014/02/11:10:15	0.301	8.5	9.76	16.57	56	7.76	1.68	0.78	0.09	0.26	0.28	7.83	0.50	12.81	0.27	0.15	1.11	0.44
140218E	Baseflow	2014/02/18:09:55	0.245	8.9	9.66	17.44	62	7.90	1.65	0.79	0.08	0.27	0.31	7.98	0.49	11.21	0.21	0.13	2.61	0.46
140225E	Baseflow	2014/02/25:09:45	0.182	11.9	9.20	19.57	63	8.52	1.59	0.76	0.10	0.26	0.30	4.97	0.50	11.55	0.12	0.10	3.72	0.29
140304E	Baseflow	2014/03/04:09:25	0.180	10.3	9.05	19.19	58	8.69	1.60	0.75	0.12	0.26	0.33	6.90	0.49	12.49	0.09	0.08	3.40	0.30
140311E	Baseflow	2014/03/11:09:25	0.129	6.6	9.39	19.76	59	9.23	1.57	0.79	0.11	0.25	0.39	9.50	0.45	10.93	0.09	0.10	4.15	0.24
140318E	Baseflow	2014/03/18:09:25	0.116	7.7	8.25	17.90	53	8.98	1.42	0.70	0.10	0.27	0.41	7.66	0.44	11.46	0.10	0.11	3.75	0.30
140331E	Baseflow	2014/03/31:08:40	0.254	5.5	9.12	18.40	61	8.90	1.58	0.79	0.11	0.28	0.44	11.93	0.44	11.85	0.07	0.09	3.63	0.32

Appendix G

RAW DATA: SEDIMENT SOURCE AREA GEOCHEMISTRY FOR MINI-CATCHMENTS A AND B

Table G1: Raw geochemistry data for topsoils collected in mini-catchment A. *Ce is measured in ppm.

Sample ID	Date (yyyy/mm/dd)	Concentration (weight %)															
		Al	Ca	Ce*	Fe	K	Mg	Mn	Na	P	Si	Ti	POC	Al_{di}	Al_{ox}	Fe_{di}	Fe_{ox}
TS01A	2013/04/15	15.42	3.10	95	5.60	2.00	0.90	0.09	0.36	0.25	19.77	0.63	12.80	0.29	0.23	2.36	0.72
TS02A	2013/04/15	15.91	2.97	96	6.61	2.91	1.02	0.13	0.42	0.38	17.43	0.70	12.13	0.24	0.12	2.14	0.81
TS03A	2013/04/15	14.40	4.17	86	6.42	2.62	0.90	0.10	0.43	0.36	18.94	0.67	12.35	0.25	0.20	2.47	0.80
TS04A	2013/04/15	13.79	1.89	92	6.38	2.50	0.88	0.12	0.41	0.27	21.00	0.65	11.32	0.23	0.18	2.61	0.60
TS05A	2013/04/15	15.38	2.35	93	7.00	2.80	0.96	0.10	0.41	0.23	19.41	0.70	10.47	0.30	0.23	2.81	0.67
TS06A	2013/04/15	12.94	7.71	83	7.58	2.52	0.88	0.11	0.34	0.30	16.29	0.63	12.38	0.21	0.14	1.97	0.87
TS07A	2013/04/15	15.30	3.11	98	6.81	2.53	0.98	0.09	0.35	0.17	20.98	0.67	8.25	0.26	0.21	1.59	0.48
TS08A	2013/04/15	15.71	1.57	100	6.71	2.69	1.03	0.14	0.42	0.28	21.42	0.69	9.30	0.24	0.17	1.51	0.51
TS09A	2013/04/15	14.76	1.60	90	6.32	2.47	0.96	0.11	0.43	0.24	20.53	0.69	12.54	0.29	0.20	3.06	0.54
TS10A	2013/04/15	8.82	24.08	47	8.55	1.65	0.73	0.08	0.25	0.19	10.64	0.49	9.44	0.09	0.10	1.70	0.61
TS11A	2013/04/15	13.24	6.03	81	7.63	2.40	0.90	0.13	0.38	0.27	19.32	0.63	10.43	0.22	0.14	1.85	0.74
TS12A	2013/04/15	13.87	5.37	89	6.60	2.47	0.86	0.11	0.38	0.25	20.58	0.66	8.92	0.24	0.17	2.80	0.53
TS13A	2013/04/15	12.41	8.71	79	6.85	2.42	0.83	0.12	0.42	0.37	18.63	0.64	9.28	0.20	0.14	2.38	0.46
TS14A	2013/04/15	14.88	4.24	81	6.39	2.53	0.95	0.14	0.38	0.34	20.54	0.65	12.19	0.28	0.23	3.19	0.77
TS15A	2013/04/15	13.48	3.13	95	6.76	2.67	0.86	0.13	0.41	0.35	21.91	0.68	10.59	0.23	0.13	2.37	0.59
TS16A	2013/04/15	15.06	2.70	103	8.29	2.80	0.91	0.14	0.40	0.27	20.96	0.72	9.58	0.31	0.23	3.47	0.69
TS17A	2013/04/15	13.85	2.18	101	6.61	2.71	0.84	0.12	0.46	0.33	20.85	0.68	9.92	0.29	0.16	2.45	0.63
TS18A	2013/04/15	13.09	5.89	81	7.49	2.50	0.87	0.13	0.40	0.34	17.13	0.66	12.39	0.24	0.16	2.61	0.81
TS19A	2013/04/15	12.40	5.67	86	8.18	2.22	0.82	0.12	0.42	0.32	17.82	0.62	11.46	0.21	0.13	2.62	0.83
TS20A	2013/04/15	12.32	7.23	82	7.61	2.19	0.79	0.12	0.40	0.35	17.44	0.64	12.22	0.25	0.20	2.25	0.78
TS21A	2013/04/15	11.30	6.82	76	7.08	2.18	0.76	0.13	0.35	0.46	15.59	0.60	14.55	0.21	0.11	2.68	0.93
TS22A	2013/04/15	13.27	4.57	80	6.74	2.04	0.78	0.11	0.45	0.24	18.02	0.66	11.40	0.23	0.16	1.98	0.77
TS23A	2013/04/15	13.63	3.29	91	7.21	2.18	0.82	0.11	0.44	0.27	18.76	0.65	11.98	0.30	0.19	2.28	0.78
TS24A	2013/04/15	14.06	2.23	89	6.37	2.15	0.77	0.11	0.49	0.23	19.70	0.65	12.47	0.30	0.19	2.26	0.69
TS25A	2013/10/08	13.06	4.69	89	7.99	2.19	0.80	0.10	0.39	0.34	14.03	0.63	14.05	0.33	0.25	1.98	1.02
TS26A	2013/10/08	13.87	4.40	93	7.39	2.32	0.86	0.09	0.37	0.25	14.21	0.66	12.60	0.37	0.26	0.81	0.88
TS27A	2013/10/08	14.86	5.27	103	7.24	2.64	0.93	0.07	0.37	0.22	15.20	0.68	11.69	0.38	0.23	3.83	0.71
TS28A	2013/10/08	15.60	1.90	105	6.35	2.53	0.96	0.08	0.44	0.25	17.97	0.69	11.52	0.47	0.17	2.82	0.49
TS29A	2013/10/08	14.67	1.68	99	6.28	2.59	0.86	0.09	0.52	0.23	18.92	0.70	11.36	0.40	0.16	3.00	0.62
TS30A	2013/10/08	15.41	1.67	108	6.38	2.57	0.91	0.11	0.50	0.19	18.82	0.70	11.15	0.40	0.23	2.68	0.54

Table G2: Raw geochemistry data for road verge sediments collected in mini-catchment A. *Ce is measured in ppm.

Sample ID	Date (yyyy/mm/dd)	Concentration (weight %)															
		Al	Ca	Ce*	Fe	K	Mg	Mn	Na	P	Si	Ti	POC	Al_{di}	Al_{ox}	Fe_{di}	Fe_{ox}
RV01A	2013/04/15	11.19	5.82	79	6.28	2.06	0.89	0.14	0.45	0.33	21.09	0.59	13.27	0.27	0.14	3.14	0.70
RV02A	2013/04/15	12.68	4.41	87	6.84	2.13	0.86	0.14	0.40	0.36	21.23	0.60	13.43	0.25	0.13	2.82	0.77
RV03A	2013/04/15	10.47	6.55	88	6.13	2.13	0.98	0.16	0.52	0.36	19.96	0.63	15.02	0.20	0.11	3.55	0.79
RV04A	2013/04/15	10.60	6.83	77	6.35	2.03	0.93	0.18	0.42	0.37	19.41	0.58	14.84	0.20	0.11	4.07	0.89
RV05A	2013/04/15	10.98	5.73	79	6.11	2.09	1.00	0.14	0.48	0.35	20.23	0.59	13.60	0.17	0.09	2.46	0.88
RV06A	2013/04/15	10.45	5.77	79	5.74	2.17	1.09	0.15	0.56	0.34	20.50	0.63	13.98	0.18	0.11	3.94	0.68
RV07A	2013/04/15	10.00	5.43	75	5.69	1.98	0.98	0.17	0.43	0.36	20.42	0.56	14.99	0.19	0.07	3.18	0.92
RV08A	2013/04/15	9.31	6.62	77	5.40	2.00	0.98	0.16	0.50	0.33	20.16	0.60	13.84	0.17	0.05	3.80	0.78
RV09A	2013/04/15	9.64	5.66	83	5.39	2.05	0.99	0.17	0.46	0.35	18.72	0.61	15.46	0.19	0.08	3.37	0.96
RV10A	2013/04/15	11.20	5.44	82	5.89	2.12	0.98	0.13	0.47	0.35	19.99	0.58	14.52	0.19	0.06	2.93	0.72
RV11A	2013/04/15	11.24	6.61	91	6.42	2.15	0.99	0.14	0.48	0.33	18.68	0.63	12.74	0.16	0.06	3.21	0.77
RV12A	2013/04/15	10.47	6.54	82	6.25	2.04	0.96	0.17	0.44	0.38	18.52	0.60	15.51	0.19	0.12	3.78	0.94
RV13A	2013/04/15	10.91	7.03	92	6.60	2.10	0.96	0.14	0.47	0.32	19.49	0.64	13.01	0.18	0.11	3.24	0.74
RV14A	2013/04/15	10.42	6.07	80	5.92	2.06	1.01	0.14	0.49	0.32	20.00	0.60	13.91	0.21	0.09	3.17	0.63
RV15A	2013/04/15	11.10	6.32	85	6.36	2.10	0.96	0.14	0.50	0.34	18.98	0.62	14.05	0.21	0.11	3.91	0.83
RV16A	2013/04/15	10.82	6.64	84	6.37	2.07	1.01	0.14	0.51	0.30	19.58	0.63	14.17	0.21	0.06	3.75	0.73
RV17A	2013/04/15	9.56	8.19	87	5.71	2.10	1.19	0.14	0.64	0.27	20.24	0.66	11.75	0.20	0.10	2.74	0.57
RV18A	2013/04/15	10.33	7.64	90	6.34	2.08	1.05	0.17	0.49	0.37	16.31	0.63	16.16	0.17	0.09	3.21	0.87
RV19A	2013/04/15	10.71	7.16	88	6.31	2.08	1.00	0.14	0.50	0.31	16.91	0.64	13.62	0.20	0.06	3.12	0.72
RV20A	2013/04/15	10.55	10.49	80	6.85	2.05	1.02	0.14	0.48	0.30	17.15	0.63	12.02	0.17	0.08	2.99	0.34
RV21A	2013/04/15	11.21	8.03	91	6.69	2.17	1.10	0.17	0.50	0.35	17.52	0.65	13.68	0.21	0.10	3.45	0.69
RV22A	2013/04/15	10.63	7.43	85	6.31	2.13	1.13	0.16	0.53	0.31	18.99	0.64	13.46	0.22	0.06	3.70	0.57
RV23A	2013/04/15	11.40	6.92	92	6.31	2.30	1.12	0.16	0.54	0.35	18.87	0.66	12.95	0.22	0.09	2.91	0.49
RV24A	2013/04/15	9.50	8.18	84	5.78	1.99	1.07	0.17	0.53	0.35	16.88	0.60	14.65	0.17	0.07	3.67	0.62
RV25A	2013/10/08	8.47	6.02	85	5.49	1.89	0.86	0.16	0.47	0.28	15.22	0.58	13.66	0.21	0.19	2.74	0.78
RV26A	2013/10/08	10.36	7.85	97	6.22	2.21	1.14	0.18	0.59	0.28	16.18	0.66	12.66	0.25	0.00	2.41	0.60
RV27A	2013/10/08	8.64	8.21	99	5.77	1.91	1.28	0.27	0.46	0.39	12.93	0.60	17.43	0.21	0.17	1.90	1.14
RV28A	2013/10/08	9.83	5.14	93	5.97	2.16	1.02	0.16	0.44	0.33	14.21	0.61	16.70	0.27	0.17	0.00	1.12
RV29A	2013/10/08	8.12	5.65	100	5.22	1.86	0.89	0.18	0.40	0.36	11.57	0.59	16.02	0.25	0.21	0.81	0.90
RV30A	2013/10/08	13.20	3.05	111	7.57	2.42	1.00	0.11	0.45	0.21	16.63	0.63	11.89	0.31	0.07	3.81	0.66

Table G3: Raw geochemistry data for channel bank sediments collected in mini-catchment A. *Ce is measured in ppm.

Sample ID	Date (yyyy/mm/dd)	Depth (cm)	Concentration (weight %)															
			Al	Ca	Ce*	Fe	K	Mg	Mn	Na	P	Si	Ti	POC	Al_{di}	Al_{ox}	Fe_{di}	Fe_{ox}
CB01 10A	2013/04/22	10	7.48	36.10	30	4.67	1.12	0.63	0.01	0.16	0.05	0.25	0.46	1.38	0.07	0.00	1.80	0.67
CB01 30A	2013/04/22	30	7.02	35.33	31	5.06	1.08	0.59	0.02	0.17	0.06	3.44	0.45	1.49	0.02	0.00	2.28	0.97
CB01 50A	2013/04/22	50	12.89	14.99	73	7.06	2.01	0.89	0.10	0.27	0.19	15.11	0.59	9.21	0.19	0.05	4.01	0.59
CB02 10A	2013/04/22	10	8.62	31.97	38	4.62	1.43	0.71	0.01	0.18	0.06	3.72	0.52	2.02	0.09	0.00	2.40	0.48
CB02 30A	2013/04/22	30	9.01	32.56	41	4.78	1.45	0.73	0.02	0.19	0.07	5.05	0.53	2.46	0.08	0.00	2.32	0.62
CB02 50A	2013/04/22	50	11.01	24.47	61	6.67	1.83	0.82	0.05	0.29	0.13	10.24	0.63	6.03	0.13	0.00	3.88	0.45
CB03 10A	2013/04/22	10	9.22	29.55	45	7.15	1.76	0.98	0.01	0.36	0.09	6.16	0.57	1.58	0.09	0.00	2.87	0.56
CB03 30A	2013/04/22	30	9.28	28.82	49	8.37	1.83	0.98	0.05	0.33	0.11	7.62	0.57	1.60	0.08	0.00	2.91	0.29
CB03 50A	2013/04/22	50	9.80	28.52	51	7.94	1.92	1.04	0.04	0.35	0.10	6.71	0.60	1.95	0.09	0.00	2.64	0.18
CB04 10A	2013/04/22	10	6.83	33.35	38	4.65	1.29	0.59	0.00	0.18	0.06	10.84	0.46	2.05	0.07	0.02	1.93	0.93
CB04 30A	2013/04/22	30	7.59	33.03	39	5.14	1.43	0.63	0.02	0.18	0.07	8.57	0.50	2.03	0.10	0.01	2.58	0.71
CB04 50A	2013/04/22	50	4.39	44.36	21	3.15	0.63	0.48	0.00	0.13	0.04	0.00	0.28	0.91	0.01	0.00	1.63	0.77
CB05 10A	2013/04/22	10	4.33	44.62	20	3.52	0.62	0.46	0.00	0.12	0.05	0.00	0.31	1.35	0.00	0.00	1.82	0.91
CB05 30A	2013/04/22	30	3.96	45.21	21	3.83	0.59	0.43	0.00	0.12	0.06	0.00	0.29	1.64	0.00	0.00	1.95	1.46
CB05 50A	2013/04/22	50	10.02	26.25	51	7.72	1.53	0.79	0.11	0.24	0.20	7.49	0.53	9.65	0.11	0.00	3.22	0.54
CB06 10A	2013/04/22	10	3.77	46.13	18	3.88	0.61	0.40	0.00	0.13	0.05	0.00	0.35	1.03	0.00	0.00	1.90	0.90
CB06 30A	2013/04/22	30	4.24	46.99	20	3.87	0.69	0.44	0.00	0.15	0.05	0.00	0.40	1.08	0.00	0.00	1.68	1.23
CB06 50A	2013/04/22	50	5.69	43.05	32	3.68	0.92	0.51	0.02	0.14	0.06	0.93	0.42	1.71	0.03	0.00	1.79	0.86
CB07 10A	2013/04/22	10	8.01	29.02	40	4.85	1.58	0.65	0.02	0.19	0.06	14.51	0.52	2.29	0.09	0.00	2.49	0.23
CB07 30A	2013/04/22	30	8.67	28.48	47	4.62	1.69	0.70	0.02	0.20	0.06	12.45	0.55	3.02	0.16	0.06	2.89	0.26
CB07 50A	2013/04/22	50	8.08	26.98	50	6.51	1.51	0.63	0.04	0.23	0.06	16.26	0.54	2.66	0.13	0.04	3.20	0.30
CB08 10A	2013/04/22	10	7.15	33.79	38	8.11	1.29	0.62	0.02	0.19	0.08	7.44	0.46	1.91	0.09	0.00	2.76	0.25
CB08 30A	2013/04/22	30	5.67	38.77	29	3.89	0.97	0.51	0.00	0.16	0.05	5.09	0.40	0.93	0.01	0.00	2.31	0.62
CB08 50A	2013/04/22	50	5.51	41.10	33	4.72	0.93	0.48	0.01	0.18	0.06	3.89	0.44	1.67	0.03	0.00	2.27	0.60
CB09 10A	2013/04/22	10	5.65	39.87	30	2.60	0.97	0.52	0.00	0.17	0.04	3.79	0.43	1.26	0.02	0.00	1.77	0.67
CB09 30A	2013/04/22	30	4.76	41.46	23	4.29	0.81	0.45	0.00	0.16	0.05	3.16	0.38	1.23	0.04	0.00	1.25	0.35
CB09 50A	2013/04/22	50	5.75	38.83	31	3.82	0.96	0.52	0.00	0.19	0.05	2.76	0.44	1.15	0.05	0.00	1.62	0.45
CB10 10A	2013/04/22	10	4.45	41.42	23	3.00	0.76	0.43	0.00	0.17	0.04	2.69	0.38	0.70	0.00	0.00	1.40	0.43
CB10 30A	2013/04/22	30	4.56	42.03	24	3.29	0.76	0.44	0.00	0.16	0.05	1.85	0.37	0.97	0.03	0.00	1.58	0.56
CB10 50A	2013/04/22	50	5.83	37.16	27	5.91	0.93	0.52	0.01	0.18	0.06	2.19	0.41	1.36	0.04	0.00	2.02	0.44

Table G4: Raw geochemistry data for field drain sediments collected in mini-catchment A. *Ce is measured in ppm.

Sample ID	Date (yyyy/mm/dd)	SPM (mg/L)	Concentration (weight %)															
			Al	Ca	Ce*	Fe	K	Mg	Mn	Na	P	Si	Ti	POC	Al_{di}	Al_{ox}	Fe_{di}	Fe_{ox}
FD01A	2012/09/24	5.8	9.31	14.54	51	6.45	1.53	0.65	0.23	0.18	0.18	11.83	0.44	9.10	0.19	0.17	1.71	0.30
FD02A	2012/12/03	2.4	7.72	12.11	53	8.24	1.29	0.57	0.17	0.23	0.26	11.45	0.39	15.22	0.20	0.04	3.70	0.71
FD03A	2012/12/03	3.0	9.34	9.52	47	15.83	1.31	0.80	0.11	0.22	0.58	12.09	0.34	16.65	0.24	0.12	4.29	1.34
FD04A	2012/12/03	1.4	7.77	13.99	55	6.49	1.33	0.54	0.09	0.23	0.22	10.92	0.43	12.64	0.24	0.09	3.07	0.64
FD05A	2012/12/03	0.5	5.51	12.83	35	11.70	1.04	0.39	0.11	0.14	0.76	17.36	0.27	14.06	0.22	0.14	3.90	1.08
FD06A	2013/03/26	0.6	7.90	8.00	58	5.93	1.33	0.56	0.13	0.24	0.37	27.00	0.31	10.56	0.17	0.10	3.60	0.34
FD07A	2013/05/14	1.5	1.67	16.25	23	1.50	0.34	0.13	0.08	0.14	0.14	35.72	0.08	4.87	0.09	0.16	0.69	0.32
FD08A	2013/05/21	1.9	7.78	14.96	53	5.65	1.33	0.52	0.12	0.24	0.17	23.54	0.36	5.15	0.16	0.17	3.47	0.28
FD09A	2013/05/28	1.5	2.93	16.79	33	2.35	0.59	0.20	0.09	0.17	0.12	31.54	0.15	4.64	0.13	0.16	3.01	0.39
FD10A	2013/10/31	10.9	10.73	8.54	69	13.34	1.55	0.79	0.30	0.35	0.33	7.72	0.48	9.23	0.23	0.22	2.94	1.00
FD11A	2013/10/31	11.3	6.49	15.33	58	5.13	1.03	0.48	0.19	0.30	0.15	7.40	0.43	5.99	0.15	0.08	1.24	0.05
FD12A	2013/10/31	36.4	11.64	9.41	82	10.24	1.76	0.86	0.30	0.31	0.32	7.42	0.57	9.91	0.31	0.19	1.04	0.60
FD13A	2013/10/31	67.7	5.83	14.17	56	4.52	0.98	0.43	0.16	0.44	0.11	11.75	0.48	3.91	0.19	0.26	0.39	0.15
FD14A	2013/10/31	3.9	6.95	10.06	58	4.74	1.36	0.48	0.18	0.37	0.25	16.42	0.43	11.13	0.25	0.19	1.47	0.33
FD15A	2013/10/31	1.7	10.19	12.82	73	6.88	1.65	0.73	0.19	0.35	0.31	15.29	0.50	12.62	0.26	0.12	1.36	0.47
FD16A	2013/10/31	4.3	4.64	29.95	31	3.82	0.55	0.36	0.00	0.21	0.07	0.00	0.37	6.02	0.06	0.07	0.80	0.11
FD17A	2013/10/31	10.3	5.73	21.46	32	4.21	0.91	0.46	0.10	0.17	0.24	1.50	0.31	11.57	0.12	0.09	0.85	0.29
FD18A	2013/10/31	57.2	4.82	14.64	57	3.65	1.00	0.36	0.08	0.43	0.11	13.23	0.53	3.84	0.04	0.05	1.68	0.25
FD19A	2013/10/31	21.4	1.83	32.06	16	18.93	0.38	0.19	0.22	0.22	0.49	0.00	0.24	5.46	0.00	0.17	1.77	0.73
FD20A	2013/10/31	7.4	4.75	33.86	33	4.52	0.72	0.39	0.25	0.21	0.13	0.00	0.38	7.70	0.02	0.10	2.81	0.09
FD21A	2013/10/31	48.1	7.26	26.00	31	22.51	0.71	0.60	0.24	0.19	0.55	0.00	0.28	7.65	0.14	0.17	3.14	0.88
FD22A	2013/10/31	39.0	8.85	17.37	57	6.42	1.35	0.65	0.09	0.31	0.16	6.82	0.49	6.56	0.14	0.14	2.45	0.34
FD23A	2013/10/31	16.2	8.01	14.84	58	8.60	1.49	0.63	0.12	0.46	0.17	8.42	0.52	7.65	0.15	0.13	3.50	0.47
FD24A	2013/10/31	14.2	3.92	31.78	27	3.20	0.62	0.35	0.03	0.12	0.28	1.07	0.24	13.97	0.00	0.00	1.52	0.16
FD25A	2013/10/31	30.5	8.57	8.82	63	16.09	1.48	0.63	0.65	0.35	0.76	2.34	0.46	9.27	0.17	0.15	3.28	0.88
FD26A	2013/10/31	5.5	6.92	20.91	55	6.13	1.14	0.50	0.12	0.32	0.14	4.65	0.47	7.47	0.05	0.04	1.24	0.16
FD27A	2013/10/31	36.2	8.27	8.30	64	14.79	1.41	0.61	0.64	0.36	0.71	2.43	0.44	9.60	0.19	0.22	3.13	0.96
FD28A	2013/10/31	23.0	7.77	23.36	50	9.52	1.28	0.60	0.15	0.25	0.26	4.04	0.47	10.19	0.23	0.37	2.57	0.60
FD29A	2013/10/31	29.7	9.26	16.32	59	8.66	1.58	0.72	0.10	0.36	0.19	6.77	0.50	8.23	0.21	0.20	4.40	0.25
FD30A	2013/10/31	35.7	4.68	36.06	37	6.30	0.75	0.39	1.61	0.17	0.12	0.00	0.34	6.18	0.11	0.13	2.94	0.13

Table G5: Raw geochemistry data for topsoils collected in mini-catchment B. *Ce is measured in ppm.

Sample ID	Date (yyyy/mm/dd)	Concentration (weight %)															
		Al	Ca	Ce*	Fe	K	Mg	Mn	Na	P	Si	Ti	POC	Al_{di}	Al_{ox}	Fe_{di}	Fe_{ox}
TS01B	2013/08/30	18.72	1.18	97	7.72	2.94	1.05	0.09	0.39	0.17	17.75	0.71	6.42	0.39	0.20	3.07	0.37
TS02B	2013/08/30	15.49	1.16	117	7.23	2.86	0.85	0.14	0.52	0.31	20.01	0.73	7.06	0.34	0.20	2.65	0.27
TS03B	2013/08/30	15.67	1.20	98	6.03	2.87	0.88	0.10	0.56	0.28	21.19	0.72	6.82	0.31	0.20	2.50	0.32
TS04B	2013/08/30	16.53	1.05	116	6.46	3.06	0.91	0.12	0.52	0.23	20.28	0.79	7.22	0.34	0.22	2.46	0.24
TS05B	2013/08/30	15.35	1.15	111	5.84	2.98	0.81	0.15	0.59	0.21	22.88	0.79	6.82	0.33	0.19	2.46	0.26
TS06B	2013/08/30	16.39	1.44	94	5.86	2.98	0.89	0.12	0.52	0.32	20.01	0.74	8.11	0.31	0.23	1.90	0.41
TS07B	2013/08/30	15.50	1.72	99	6.41	3.04	0.85	0.19	0.57	0.34	20.55	0.74	6.35	0.24	0.15	3.00	0.60
TS08B	2013/08/30	15.15	1.36	93	5.51	2.82	0.75	0.11	0.54	0.26	23.47	0.77	6.78	0.28	0.18	2.52	0.41
TS09B	2013/08/30	16.40	1.47	100	6.35	3.16	0.86	0.13	0.51	0.28	19.43	0.79	6.72	0.32	0.22	2.17	0.42
TS10B	2013/08/30	16.25	1.33	102	5.90	3.21	0.91	0.14	0.49	0.35	20.28	0.76	7.30	0.32	0.20	3.16	0.42
TS11B	2013/08/30	15.79	2.39	105	7.09	2.88	0.90	0.12	0.49	0.25	18.22	0.73	7.15	0.27	0.19	2.74	0.55
TS12B	2013/08/30	15.81	1.64	104	6.42	2.88	0.98	0.13	0.55	0.30	18.56	0.72	8.12	0.29	0.21	2.76	0.55
TS13B	2013/08/30	11.52	1.59	88	4.73	1.93	0.67	0.08	0.50	0.18	22.07	0.56	8.26	0.25	0.21	1.81	0.47
TS14B	2013/08/30	9.94	3.65	87	5.04	1.99	0.54	0.08	0.49	0.31	16.77	0.58	11.02	0.23	0.17	2.43	0.83
TS15B	2013/08/30	12.56	1.21	98	4.96	2.49	0.66	0.14	0.55	0.35	20.97	0.60	10.62	0.30	0.16	2.53	0.52
TS16B	2013/08/30	12.08	2.15	98	4.83	2.51	0.70	0.16	0.55	0.33	20.04	0.63	9.67	0.26	0.20	1.61	0.78
TS17B	2013/08/30	14.69	2.18	97	5.83	2.08	0.81	0.09	0.44	0.24	15.37	0.67	12.23	0.27	0.17	2.75	0.79
TS18B	2013/08/30	11.36	2.30	94	7.29	1.95	0.58	0.11	0.43	0.43	13.16	0.58	15.72	0.30	0.17	2.21	1.01
TS19B	2013/08/30	9.40	2.53	79	5.38	2.15	0.55	0.12	0.37	0.47	12.99	0.50	14.47	0.28	0.19	2.38	0.82
TS20B	2013/08/30	15.01	1.59	101	6.02	2.42	0.83	0.09	0.51	0.18	19.16	0.70	8.63	0.32	0.18	3.17	0.38
TS21B	2013/08/30	17.04	1.77	100	6.24	2.64	0.99	0.10	0.51	0.23	19.17	0.74	6.67	0.31	0.22	1.90	0.32
TS22B	2013/08/30	14.50	1.19	102	5.71	2.86	0.81	0.12	0.61	0.28	21.73	0.73	7.11	0.30	0.15	2.68	0.27
TS23B	2014/04/09	13.57	1.22	100	5.53	2.58	0.78	0.14	0.62	0.26	22.58	0.71	10.15	0.26	0.10	5.30	0.40
TS24B	2014/04/09	12.85	2.60	94	6.34	2.70	0.82	0.15	0.46	0.34	19.08	0.65	10.87	0.22	0.07	5.71	0.58
TS25B	2014/04/09	13.90	1.19	79	5.43	2.67	0.68	0.11	0.52	0.36	20.80	0.73	11.43	0.28	0.13	5.07	0.45
TS26B	2014/04/09	12.85	2.59	94	6.35	2.71	0.83	0.16	0.46	0.34	19.08	0.65	8.25	0.24	0.11	4.09	0.34
TS27B	2014/04/09	18.40	1.78	92	6.88	2.97	0.99	0.10	0.38	0.35	18.75	0.74	10.36	0.31	0.12	5.63	0.50
TS28B	2014/04/09	14.99	1.13	103	6.49	2.70	0.85	0.15	0.54	0.30	21.86	0.70	9.85	0.29	0.08	5.79	0.36
TS29B	2014/04/09	15.07	1.38	108	6.46	2.77	0.81	0.14	0.55	0.28	18.85	0.76	10.65	0.29	0.14	4.93	0.44
TS30B	2014/04/09	14.45	1.56	98	6.03	2.55	0.80	0.12	0.60	0.25	18.78	0.73	11.80	0.28	0.12	4.52	0.41

Table G6: Raw geochemistry data for road verge sediments collected in mini-catchment B. *Ce is measured in ppm.

Sample ID	Date (yyyy/mm/dd)	Concentration (weight %)															
		Al	Ca	Ce*	Fe	K	Mg	Mn	Na	P	Si	Ti	POC	Al_{di}	Al_{ox}	Fe_{di}	Fe_{ox}
RV01B	2013/08/30	12.82	4.64	96	6.54	2.71	0.94	0.12	0.62	0.32	18.75	0.72	9.28	0.25	0.15	2.48	0.57
RV02B	2013/08/30	11.53	6.22	87	5.53	2.58	1.32	0.15	0.67	0.36	18.25	0.64	10.02	0.16	0.06	2.71	0.56
RV03B	2013/08/30	12.00	1.61	89	5.58	2.45	0.75	0.10	0.56	0.20	20.47	0.63	7.96	0.22	0.13	2.30	0.56
RV04B	2013/08/30	11.85	2.19	95	4.90	2.70	0.76	0.12	0.63	0.30	23.51	0.68	8.24	0.23	0.14	2.27	0.60
RV05B	2013/08/30	8.47	2.90	89	4.30	2.14	0.55	0.20	0.41	0.29	17.13	0.58	13.14	0.18	0.07	2.22	0.77
RV06B	2013/08/30	6.42	3.32	89	3.63	1.47	0.48	0.16	0.31	0.27	14.46	0.49	11.76	0.15	0.04	1.57	0.69
RV07B	2013/08/30	11.12	2.71	103	5.13	2.22	0.68	0.22	0.78	0.38	16.98	0.60	11.91	0.18	0.08	2.42	0.88
RV08B	2013/08/30	9.85	2.95	86	4.67	2.12	0.72	0.18	0.92	0.39	18.36	0.57	11.91	0.16	0.08	2.71	0.85
RV09B	2013/08/30	12.01	2.60	96	5.39	2.43	0.68	0.15	0.52	0.36	16.70	0.63	10.92	0.19	0.11	2.65	0.85
RV10B	2013/08/30	12.32	2.37	104	5.19	2.20	0.70	0.18	0.86	0.42	18.64	0.57	11.32	0.20	0.10	3.06	0.82
RV11B	2013/08/30	12.85	2.39	92	5.56	2.41	0.80	0.15	0.59	0.34	17.05	0.67	12.02	0.22	0.13	1.97	0.80
RV12B	2013/08/30	12.91	3.22	102	5.83	2.67	0.98	0.16	0.64	0.30	18.34	0.72	9.35	0.18	0.06	2.34	0.71
RV13B	2013/08/30	11.90	2.73	90	5.29	2.50	0.89	0.14	0.61	0.32	19.18	0.65	9.84	0.22	0.13	2.31	0.65
RV14B	2013/08/30	13.33	2.11	99	5.83	2.79	0.88	0.12	0.67	0.29	20.32	0.71	8.29	0.23	0.14	2.40	0.62
RV15B	2013/08/30	14.04	2.52	99	6.29	2.83	1.02	0.16	0.66	0.29	18.72	0.75	8.05	0.23	0.14	2.87	0.54
RV16B	2013/08/30	13.01	2.75	97	5.87	2.63	1.02	0.16	0.66	0.33	18.10	0.69	9.37	0.18	0.07	2.61	0.69
RV17B	2013/08/30	13.43	2.80	96	5.53	2.28	1.02	0.15	0.89	0.39	18.70	0.62	10.99	0.19	0.09	4.12	0.79
RV18B	2013/08/30	11.45	3.00	87	5.02	2.40	1.38	0.22	0.85	0.30	19.08	0.61	9.35	0.16	0.04	2.44	0.54
RV19B	2014/04/09	6.71	1.80	75	3.25	1.90	0.40	0.19	0.47	0.29	25.71	0.53	10.88	0.16	0.09	2.24	0.63
RV20B	2014/04/09	6.30	4.14	78	3.68	1.78	0.73	0.19	0.79	0.27	14.64	0.53	16.92	0.04	0.00	2.68	0.92
RV21B	2014/04/09	10.93	2.57	91	4.72	2.66	0.86	0.21	0.63	0.28	21.00	0.70	11.74	0.19	0.06	4.40	0.57
RV22B	2014/04/09	8.99	2.71	86	4.25	2.15	0.84	0.17	0.56	0.28	19.81	0.62	13.71	0.14	0.00	3.65	0.62
RV23B	2014/04/09	10.43	3.00	98	5.42	2.33	0.71	0.14	0.37	0.28	13.88	0.63	17.31	0.20	0.07	3.86	0.95
RV24B	2014/04/09	8.99	3.12	88	4.57	1.99	0.67	0.19	0.41	0.34	16.97	0.56	16.60	0.17	0.08	3.81	0.83
RV25B	2014/04/09	6.13	2.91	73	3.05	1.60	0.46	0.15	0.39	0.25	19.06	0.50	15.14	0.15	0.04	3.00	0.64
RV26B	2014/04/09	9.97	2.37	74	5.03	2.19	0.60	0.14	0.35	0.28	16.94	0.57	14.91	0.22	0.07	4.43	0.80
RV27B	2014/04/09	8.47	2.37	72	4.00	1.91	0.55	0.13	0.38	0.31	17.77	0.53	15.03	0.17	0.03	3.48	0.86
RV28B	2014/04/09	8.83	5.25	85	5.10	2.36	1.16	0.15	0.78	0.24	20.77	0.60	12.05	0.12	0.00	4.54	0.44
RV29B	2014/04/09	9.34	4.04	86	4.83	2.16	0.86	0.19	0.52	0.31	17.83	0.62	13.83	0.17	0.06	3.73	0.74
RV30B	2014/04/09	9.63	4.66	96	4.79	2.30	1.05	0.21	0.70	0.29	20.03	0.68	12.78	0.13	0.06	3.50	0.68

Table G7: Raw geochemistry data for channel bank sediments collected in mini-catchment B. *Ce is measured in ppm.

Sample ID	Date (yyyy/mm/dd)	Depth (cm)	Concentration (weight %)														
			Al	Ca	Ce*	Fe	K	Mg	Mn	Na	P	Si	Ti	POC	Al_{di}	Al_{ox}	Fe_{di}	Fe_{ox}
CB01 10B	2014/02/19	10	3.51	45.06	23	3.88	0.56	0.42	0.00	0.13	0.05	1.59	0.23	0.52	0.06	0.00	2.46	0.37
CB01 30B	2014/02/19	30	3.62	42.90	19	3.65	0.52	0.43	0.00	0.22	0.05	0.00	0.29	0.44	0.00	0.00	1.01	0.66
CB01 50B	2014/02/19	50	3.97	42.24	22	4.07	0.53	0.47	0.00	0.18	0.05	0.00	0.28	0.72	0.00	0.00	1.18	0.61
CB02 10B	2014/02/19	10	4.13	38.58	22	2.69	0.65	0.48	0.00	0.29	0.04	0.00	0.33	0.66	0.00	0.00	1.30	0.91
CB02 30B	2014/02/19	30	4.09	40.98	25	2.77	0.61	0.49	0.00	0.19	0.04	0.00	0.29	0.66	0.00	0.00	0.56	0.91
CB02 50B	2014/02/19	50	3.94	42.15	22	2.53	0.57	0.48	0.00	0.18	0.04	0.00	0.27	0.93	0.00	0.00	0.39	1.19
CB03 10B	2014/02/19	10	5.60	22.36	45	3.53	1.37	0.56	0.04	0.42	0.05	16.83	0.45	2.14	0.14	0.02	1.46	0.17
CB03 30B	2014/02/19	30	7.38	28.39	43	3.80	1.48	0.77	0.00	0.34	0.06	10.60	0.49	1.04	0.13	0.05	1.16	0.36
CB03 50B	2014/02/19	50	9.30	26.22	56	5.10	1.65	0.75	0.03	0.27	0.10	6.19	0.58	5.78	0.20	0.12	1.32	0.27
CB06 10B	2014/02/19	10	4.67	38.77	16	11.06	0.59	0.59	0.13	0.18	0.05	0.00	0.25	1.36	0.06	0.00	1.60	0.80
CB06 30B	2014/02/19	30	5.23	39.23	26	3.78	0.86	0.61	0.01	0.24	0.05	0.00	0.37	0.62	0.05	0.03	0.29	0.90
CB06 50B	2014/02/19	50	7.47	13.31	57	3.57	1.81	0.80	0.01	0.62	0.05	22.21	0.48	1.56	0.14	0.05	2.42	0.03
CB08 10B	2014/02/19	10	8.76	14.40	66	6.22	1.99	0.88	0.03	0.58	0.07	16.04	0.54	2.04	0.20	0.18	2.61	0.00
CB08 30B	2014/02/19	30	10.68	16.59	72	6.36	2.36	1.11	0.02	0.55	0.07	14.28	0.65	1.64	0.23	0.17	2.33	0.03
CB09 10B	2014/02/19	10	3.62	46.84	16	2.34	0.46	0.48	0.00	0.14	0.03	0.00	0.25	0.40	0.00	0.00	0.01	0.85
CB09 30B	2014/02/19	30	4.29	42.33	23	3.06	0.63	0.48	0.00	0.21	0.05	0.00	0.35	3.57	0.05	0.01	1.02	0.62
CB09 50B	2014/02/19	50	5.19	42.02	32	3.76	0.75	0.52	0.02	0.20	0.08	0.00	0.39	4.77	0.01	0.26	1.78	1.04
CB10 10B	2014/02/19	10	9.44	20.26	64	4.85	2.12	1.05	0.02	0.53	0.06	13.54	0.57	2.63	0.20	0.05	2.77	0.00
CB10 30B	2014/02/19	30	8.95	16.45	66	4.49	2.03	0.90	0.05	0.47	0.11	13.41	0.55	5.15	0.15	0.06	4.07	0.19
CB10 50B	2014/02/19	50	8.22	12.96	63	3.93	1.93	0.77	0.06	0.53	0.12	16.10	0.52	5.72	0.16	0.10	2.77	0.37

Table G8: Raw geochemistry data for field drain sediments collected in mini-catchment B. *Ce is measured in ppm.

Sample ID	Date (yyyy/mm/dd)	Concentration (weight %)															
		Al	Ca	Ce*	Fe	K	Mg	Mn	Na	P	Si	Ti	POC	Al_{di}	Al_{ox}	Fe_{di}	Fe_{ox}
FD01B	2012/12/03	4.50	6.18	58	9.34	0.90	0.30	0.26	0.19	0.87	3.11	0.27	9.24	0.18	0.11	1.71	0.96
FD02B	2012/12/03	3.00	4.14	76	1.92	1.08	0.18	0.11	0.47	0.11	36.52	0.45	5.10	0.15	0.11	1.24	0.39
FD03B	2014/02/19	2.39	7.77	67	6.87	0.77	0.21	0.06	0.16	0.70	20.54	0.22	14.62	0.08	0.17	0.22	0.46
FD04B	2014/02/19	2.56	4.32	96	12.54	0.44	0.15	0.19	0.19	1.31	0.00	0.18	4.66	0.09	0.17	0.56	0.80
FD05B	2014/02/19	3.42	2.54	92	6.38	0.77	0.22	0.56	0.33	0.36	11.18	0.20	6.26	0.15	0.19	1.48	0.62
FD06B	2014/02/19	4.89	2.62	87	4.14	1.24	0.31	0.21	0.29	0.15	12.21	0.36	9.36	0.24	0.12	1.95	0.59
FD07B	2014/02/19	5.93	2.27	100	4.89	1.48	0.41	0.22	0.35	0.18	15.74	0.39	11.04	0.32	0.25	1.68	1.14
FD08B	2014/02/19	3.99	3.46	119	10.30	0.89	0.27	0.70	0.31	0.51	3.12	0.28	8.75	0.21	0.16	1.53	0.99
FD09B	2014/02/19	8.95	0.98	118	2.64	2.08	0.61	0.01	0.61	0.12	31.61	0.46	3.69	0.35	0.26	2.54	0.35
FD10B	2014/02/19	9.95	1.20	119	3.02	2.26	0.70	0.05	0.60	0.11	25.24	0.48	6.66	0.39	0.29	2.00	0.36
FD11B	2014/02/19	9.28	3.30	113	4.93	1.96	0.56	0.10	0.36	0.21	13.75	0.55	14.87	0.37	0.27	2.16	1.19
FD12B	2014/02/19	12.60	7.69	83	5.21	3.35	1.38	0.05	0.61	0.08	20.28	0.67	2.86	0.33	0.17	1.79	0.16
FD13B	2014/02/19	11.95	5.69	79	4.35	3.21	1.29	0.05	0.61	0.08	23.42	0.61	2.77	0.28	0.19	1.77	0.35
FD14B	2014/02/19	6.91	3.69	60	3.21	2.10	0.70	0.07	0.54	0.08	28.62	0.42	3.18	0.25	0.10	3.01	0.39
FD15B	2014/02/19	9.99	6.84	79	4.04	2.66	0.94	0.06	0.63	0.06	24.41	0.59	3.40	0.28	0.23	3.04	0.22
FD16B	2014/02/19	10.54	3.75	82	4.46	2.73	0.96	0.07	0.62	0.08	25.30	0.57	4.75	0.30	0.20	4.86	0.49
FD17B	2014/02/19	10.27	1.42	81	5.38	2.56	0.88	0.09	0.61	0.10	23.88	0.55	8.23	0.15	0.18	0.96	0.54
FD18B	2014/02/19	9.96	7.88	75	5.42	2.13	0.85	0.10	0.52	0.11	20.43	0.55	6.16	0.26	0.23	2.87	0.36

INDEX